SCCER SoE

SWISS COMPETENCE CENTER for ENERGY RESEARCH
SUPPLY of ELECTRICITY

SCCER-SoE Science Report

2019

Supported by:

Schweizerische Eidgenossenschaft
Confédération suisse
Confederazione Svizzera
Confederaziun svizra

Swiss Confederation

Innosuisse – Swiss Innovation Agency

Imprint

Editor
Swiss Competence Center for Energy Research – Supply of Electricity (SCCER-SoE)

Address
SCCER-SoE
Gianfranco Guidati & Ueli Wieland
c/o ETH Zurich
Sonneggstrasse 5
8092 Zurich

Website
www.sccer-soe.ch

Date of Issue
10 September 2019

Content

Editorial

The Swiss Competence Center for Energy Research – Supply of Electricity (SCCER-SoE) has been established in 2013 to ensure that the academic community works closely with industry to provide the required research advancement, develop innovative technologies and robust solutions, and ultimately ensure the future provision of electricity and energy to the Swiss country and the transition to a competitive carbon-free economy.

The specific targets are geo-energies and hydropower, the two resources identified by the Energy Strategy 2050 to provide a substantial band-electricity contribution to enable the exit from nuclear power, with the target of up to 7 % electricity production from deep geothermal energy and a 10 % increase of hydropower production.

The SCCER-SoE initiated in 2017 its second implementation phase. More than 200 scientists, engineers, researchers, doctoral and master students and professors are now associated to the SCCER-SoE, working together in inter-disciplinary projects to realize the identified innovation roadmap. Among these, over 70 doctoral students are now carrying out their research in the SCCER-SoE, providing a substantial component of the future capacity building of Switzerland.

The SCCER-SoE Annual Conference 2019, held on 3 and 4 September at the EPFL in Lausanne, aimed at providing a comprehensive overview of the R&D conducted by the SCCER-SoE and its associated projects, and to confront the scientific agenda with the needs and views of stakeholders from industry, public institutions, federal offices and policy makers.

Following with the tradition established in past conferences in 2015 Neuchatel, 2016 Sion, 2017 Birmensdorf and 2018 Horw, the 2019 report will consist of nearly 120 posters, covering all aspects of the scientific portfolio of the SCCER-SoE. These posters are collected in this volume and presented according to the work packages and tasks to which they are associated.

These are exciting times for energy research in Switzerland. The Energy Law 2016 has been confirmed by the public referendum, providing the basis for the implementation of the Energy Strategy 2050. The new CO_2 law is currently under discussion in the parliament. The SCCER-SoE will continue with the development of integrative solutions, testing and installation of innovative technologies, technology assessment and scenario modelling.

In the second phase, we expanded the overall R&D portfolio and increased our focus on pilot and demonstration projects, conducted with industry partners, to validate the technologies and proposed solutions. Seven pilot and demonstration projects are now pursued, covering the whole portfolio of technologies and energy sources of the SCCER-SoE. The Flexstor project successfully demonstrated a package of technologies that will help to make hydro power plants fit for the future. In geoenergy we just started research in the new Bedretto Underground Laboratory for Geoenergies which will bring us another step closer to the generation of electricity from the deep underground.

The Annual Conference 2019 shows a vibrant and integrated scientific community, and the scientific level of the presentations proves that we are on the good way to complete the implementation of the geo-energy and hydropower R&D roadmaps. We are soon entering the final year of our programme and we trust that our excellent results will form a solid basis for a continuation of energy research in the years after 2020.

Domenico Giardini
Head of the SCCER-SoE

Work Package 1: Geo-energies

Geoscience can contribute in various ways to reach the objectives of the Energy Strategy 2050. The first option is to generate baseload electricity, which helps to compensate the future lack of nuclear generation. Alternatively, the extraction and/or seasonal storage of thermal energy can help to reduce emissions from the heating sector, having also a positive impact on the electricity sector. Last but not least, the geological storage of CO_2 can enable near-emission-free fossil power generation or the production of hydrogen for the transport and industrial sector. All three options are being tackled within the SCCER-SoE, especially in a series of demonstration projects, that are reported under Work Package 5, later in this report.

Highlights 2019

Resource exploration, characterization and simulation

The interpretation of borehole geophysical data from the GDP1 borehole on the Grimsel Pass was completed. GDP1 was drilled in the framework of NRP70 to explore and characterize a hydro-thermically active shear/fracture zone. Initial steps towards a generic petrophysical workflow for characterizing fractured crystalline rocks were developed. A comprehensive suite of borehole log data was acquired in the exploratory boreholes at the new Bedretto Underground Laboratory for Geoenergies. These data will be used to continue the development of the aforementioned petrophysical workflow.
A novel approach to estimate the mechanical fracture compliance from full-waveform sonic log data was developed. An inversion algorithm to estimate the effective hydraulic aperture and mechanical compliance of fractures from hydrophone vertical seismic profiling (VSP) was developed. Both new approaches will be applied to one of the stimulation boreholes at the Grimsel Test Site.
New approaches to measure stress in deep boreholes using simultaneous displacement measurement during injection experiments and to evaluate wellbore stability have been developed. Work is also ongoing on the characterization of fault systems and their role on deep-seated fluid flow and in-situ stresses, with the ultimate objectives to better assess fault stability and adequacy to host geothermal projects. Multi-parameter studies allow the development of favorability maps (fairways) for geothermal exploration and projecting targeting.

Enable geological sequestration of CO_2

The experimental characterization of shale caprock materials has been carried out. Opalinus clay core samples extracted from the underground laboratory in Mont Terri have been tested. The analysis focused on two aspects: (1) the evaluation sealing capacity, and (2) the assessment of the influence of CO_2 injection on the material's geomechanical properties.

1. A systematic experimental methodology has been established to evaluate the sealing capacity in terms of capillary entry-pressure. The procedure foresees the injection of CO_2 in fully water saturated sample under stress condition. The tested Opalinus clay samples exhibited capillary entry pressure in the order of few megapascals.
2. Long-term exposure of Opalinus Clay samples to CO_2 has been performed in laboratory experiments. The exposure has been performed by injecting both pure CO_2 and CO_2-rich water for several months. Geomechanical properties have been measured both before and after the exposure. Permeability resulted to be slightly affected by the injection of CO_2, as well as the compressibility.

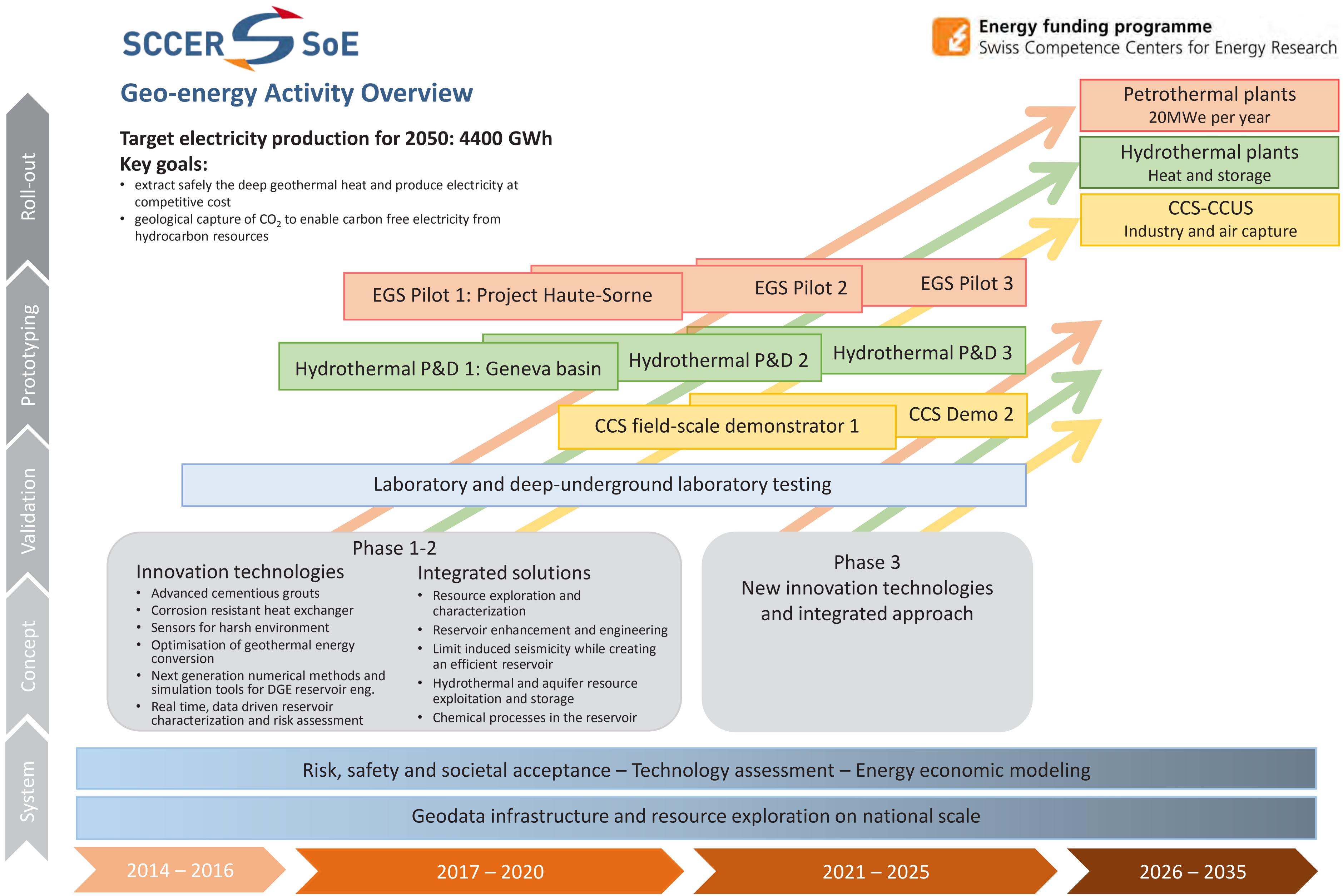
SCCER SoE
Energy funding programme
Swiss Competence Centers for Energy Research
Geo-energy Activity Overview
Target electricity production for 2050: 4400 GWh
Key goals:
• extract safely the deep geothermal heat and produce electricity at competitive cost
• geological capture of CO_2 to enable carbon free electricity from hydrocarbon resources
Roll-out
Prototyping
Validation
Concept
System
Petrothermal plants
20MWe per year
Hydrothermal plants
Heat and storage
CCS-CCUS
Industry and air capture
EGS Pilot 1: Project Haute-Sorne
EGS Pilot 2
EGS Pilot 3
Hydrothermal P&D 1: Geneva basin
Hydrothermal P&D 2
Hydrothermal P&D 3
CCS field-scale demonstrator 1
CCS Demo 2
Laboratory and deep-underground laboratory testing
Phase 1-2
Innovation technologies
• Advanced cementious grouts
• Corrosion resistant heat exchanger
• Sensors for harsh environment
• Optimisation of geothermal energy conversion
• Next generation numerical methods and simulation tools for DGE reservoir eng.
• Real time, data driven reservoir characterization and risk assessment
Integrated solutions
• Resource exploration and characterization
• Reservoir enhancement and engineering
• Limit induced seismicity while creating an efficient reservoir
• Hydrothermal and aquifer resource exploitation and storage
• Chemical processes in the reservoir
Phase 3
New innovation technologies and integrated approach
Risk, safety and societal acceptance – Technology assessment – Energy economic modeling
Geodata infrastructure and resource exploration on national scale
2014 – 2016
2017 – 2020
2021 – 2025
2026 – 2035

Task 1.1

Title

Resource exploration and characterization

Projects (presented on the following pages)

Wireline logging of Bedretto stress measurement boreholes – preliminary results
Eva Caspari, Andrew Greenwood, Ludovic Baron, Klaus Holliger

Numerical simulation of seismic wave dispersion and attenuation due to squirt flow
Yury Alkhimenkov, Eva Caspari, Nicolás D. Barbosa, Beatriz Quintal

Regional-scale flow models of the orogenic hydrothermal system at Grimsel Pass, Switzerland
Peter Alt-Epping, Larryn W. Diamond, Christoph Wanner

Reliability of calibration and prediction of borehole failure models
Asmae Dahrabou, Benoît Valley, Philip Brunner, Andres Alcolea ,Peter Meier

Application of Chemostratigraphy and petrology to characterize the Reservoirs of The Mesozoic sequence crossed by the Geo-01 well: potential for direct heat production and heat-storage
G. Ferreira De Oliveira, A. De Haller, L. Guglielmetti, Y. Makhlou, A. Moscariello

Hydraulic Characterization of the Bedretto Underground Laboratory
Nima Gholizadeh Doonechaly, Nathan Dutler, Bernard Brixel, Marian Hertrich, Simon Loew

Monitoring and Flow Path Reconstruction of Saline Tracer Tests with GPR
Peter-Lasse Giertzuch, Joseph Doetsch, Mohammadreza Jalali, Alexis Shakas, Cédric Schmelzbach, Hansruedi Maurer

Borehole radar and full waveform sonic measurements of the Bedretto stressmeasurement boreholes
Andrew Greenwood, Eva Caspari, Ludovic Baron, Klaus Holliger

Geochemical Characterization of Geothermal Waters Circulation in Carbonatic Geothermal Reservoirs of the Geneva Basin (GB)
L. Guglielmetti, F. Eichinger, A. Moscariello

Bayesian inversion of tube waves to estimate fracture aperture and compliance: Application to a real dataset
Jürg Hunziker, Andrew Greenwood, Shohei Minato, Nicolas Barbosa, Eva Caspari, Klaus Holliger

In-situ stress estimation from fault slip triggered during fluid injection
Maria Kakurina, Yves Guglielmi, Christophe Nussbaum, Benoît Valley

Rock mechanics properties for fractured limestone hydrothermal system
Morgane Koumrouyan, Reza Sohrabi, Benoît Valley

Determine fault criticality using seismic monitoring and fluid pressure analysis
Léa Perrochet, Giona Preisig, Benoît Valley

SCCER SoE

SWISS COMPETENCE CENTER for ENERGY RESEARCH
SUPPLY of ELECTRICITY

UNIL | Université de Lausanne

SCCER-SoE Annual Conference 2019

Supported by:

Schweizerische Eidgenossenschaft
Confédération suisse
Confederazione Svizzera
Confederaziun svizra

Swiss Confederation

Innosuisse – Swiss Innovation Agency

Wireline logging of Bedretto stress measurement boreholes - preliminary results

Eva Caspari, Andrew Greenwood, Ludovic Baron and Klaus Holliger

Summary

A set of geophysical wireline logs, comprising optical and acoustic televiewer data (OTV and ATV), full waveform sonic (FWS), normal resisitivity (N08, N16, N32, N64), fluid temperature and conductivity (FTC), natural gamma (NG), spectral gamma (SGR), and borehole radar (BHR) were collected in 6 stress measurements boreholes in the Bedretto underground laboratory. The laboratory is situated in the crystalline basement of the Gotthard massif and the prevailing rock type is the Rotondo granite. The purpose of the logging campaign was twofold:

1) characterization of the rock mass in preparation for mini-frac and hydraulic shearing stress measurements and associated induced fractures
2) in-depth analysis of the petrophysical properties of the rock mass

Here, we show a selection of the log data which will be utilized for the petrophysical analysis.

The sketch shows the location of the stress measurement boreholes and slip surfaces of fracture planes mapped along the tunnel. (Courtesy Xiaodong Ma)

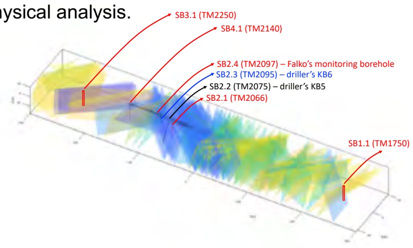

FWS - velocities

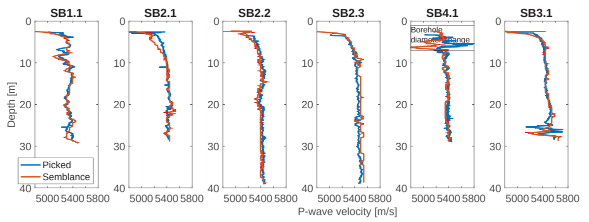

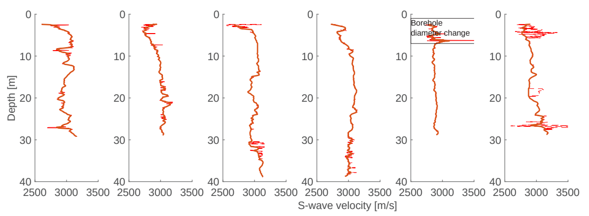

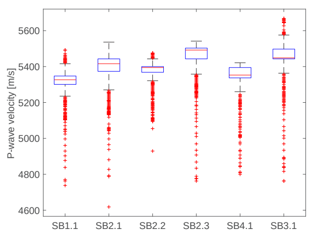

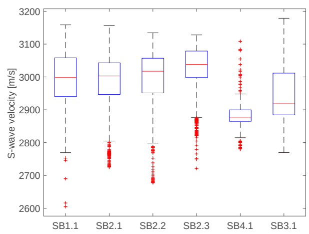

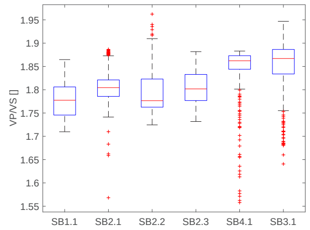

The average P- and S-wave velocities are in the expected range for a granitic formation. Some of the erratic variations, especially in the S-wave velocities, are due to automatic picking in the semblance algorithm and still have to be corrected. These erroneous values are also reflected in the Vp/Vs ratio.

Natural gamma

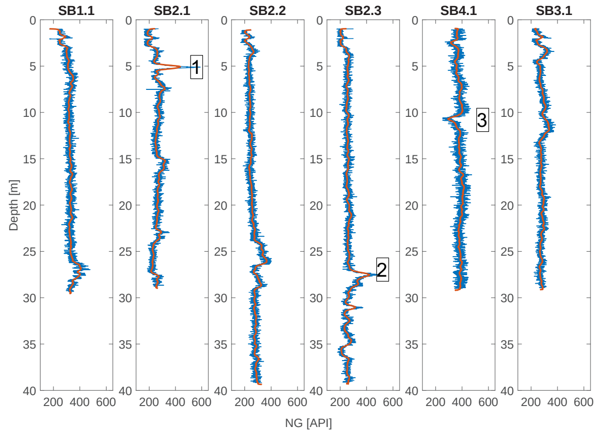

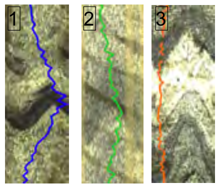

Strong variations in the natural gamma logs are likely to be associated with variations in Biotite content (1 and 2) and Quartz veins (3).

The highest average natural gamma readings as indicated by the boxplots are observed in borehole SB1.1 and SB 4.1, which are otherwise relative homogeneous.

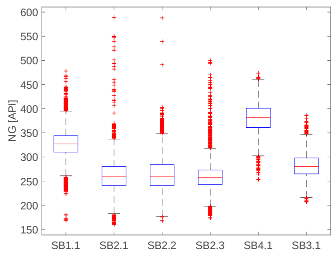

Fluid conductivity

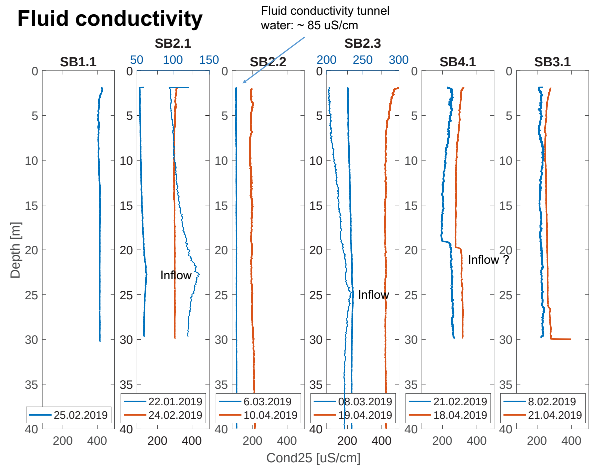

All boreholes were flushed after drilling with tunnel water, which originates from in-flow through fault zones. The fluid conductivity of the tunnel water is ~ 85 uS/m, which is considerably different with regard to the fluid conductivity measured in all boreholes after some equilibration time. At the time these measurements were taken, SB1.1 and SB2.3 were probably closest to their natural ambient state.

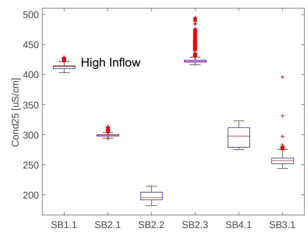

Acknowledgement: We thank Benoît Valley from the University of Neuchatel for providing logging equipment and support and the BULG team for their support.

SCCER SoE
SWISS COMPETENCE CENTER for ENERGY RESEARCH
SUPPLY of ELECTRICITY

Numerical simulation of seismic wave dispersion and attenuation due to squirt flow

Yury Alkhimenkov[1,2]*, Eva Caspari[1], Nicolás D. Barbosa[3], Beatriz Quintal[1]
[1] *Institute of Earth Sciences, University of Lausanne, Switzerland,* [2] *Swiss Geocomputing Centre, University of Lausanne, Switzerland,* [3] *University of Geneve, Switzerland*

Unil | Université de Lausanne
Swiss Geocomputing Centre

Introduction

One of the major causes of seismic wave attenuation and velocity dispersion in fluid-saturated porous media is the local flow induced by a passing wave. Local flow at the microscopic scale is referred to as squirt flow and occurs in very compliant pores such as grain contacts or microcracks which are connected to other less compliant pores [1, 2].

In this study, we perform a 3D numerical simulation of squirt flow using a finite element approach. We obtain frequency-dependent effective properties of a porous medium and calculate dispersion and attenuation due to fluid flow from a compliant crack to a stiff pore. We compare our numerical simulation with an existing analytical squirt flow model [3].

Theory

We consider a two phase medium composed by a solid phase (grains) and a fluid-saturated pore space. Grains are described as a linear isotropic elastic material for which the conservation of momentum is

$$\nabla \cdot \boldsymbol{\sigma} = 0, \tag{1}$$

where $\boldsymbol{\sigma}$ is the stress tensor. The stress-strain relation is written as

$$\boldsymbol{\sigma} = \mathbf{C} : \boldsymbol{\epsilon}, \tag{2}$$

where $\boldsymbol{\epsilon}$ is the strain tensor and $\mathbf{C}$ is the isotropic stiffness tensor, whose components are fully described by bulk K and shear μ moduli.

A fluid phase is described by the quasi-static linearised compressible Navier-Stokes momentum equation [4]:

$$-\nabla p + \eta \nabla^2 v + \frac{1}{3} \eta \nabla (\nabla \cdot v) = 0, \tag{3}$$

where v is the particle velocity and η is the shear viscosity. Equation (3) is valid for the laminar flow of a Newtonian fluid. In our simulation the energy dissipation is caused only by fluid pressure diffusion because inertial effects are neglected [5].

Acknowledgements

This research is funded by the Swiss National Science Foundation. Yury Alkhimenkov thanks Dr. J.Hunziker for technical support, Dr. B. Gurevich and Dr. S. Glubokovskikh for stimulating discussions and Dr. M. Klepikova for the template.

Numerical methodology

In this study, we consider a 3D numerical model of a flat cylinder whose edges are connected with a torus. Topologically these two geometries represent one domain.

Figure 1: (Left) Sketch illustrating a flat cylinder representing a crack whose edges are connected with a torus (a stiff pore). The blue region represents the pore space saturated with a fluid, the transparent gray area corresponds to the solid grain material; (Right) Sketch showing a quarter of the model.

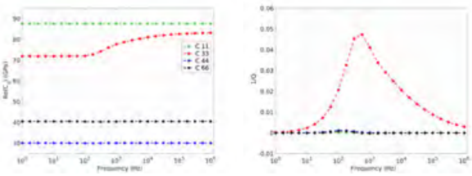

Figure 2: Numerical results for the Cij components: (left) Real part of the Cij components and (right) dimensionless attenuation for the corresponding Cij components.

Comparison to an analytical model

Z_nQ—Z_tQ model: the difference between "*a torus embedded into the solid grain material (VTI_1)*" compliance tensor and "a crack embedded into a medium described by the VTI_1" compliance tensor.
Z_nD—Z_tD model: the difference between the VTI_1 compliance tensor and "*a torus connected with a crack embedded into the grain material*" compliance tensor.

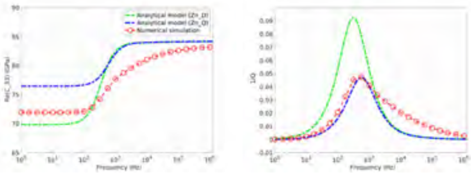

Figure 3: Real part of the C33 component and dimensionless attenuation for the C33 component.

Conclusion

We calculated the frequency-dependent effective properties of a fluid-saturated porous medium due to squirt fluid flow. While our numerical results are consistent with the current physical understanding of the squirt flow impact on the velocity dispersion and wave attenuation, some new features have been found. We confirmed that the attenuation is controlled by the length of a fluid path but dispersion is controlled by the combined compliances of the crack connected to the stiffer pore which hasn't been taken into account in analytical models. However, the observed discrepancy between the analytical and numerical solutions tends to become smaller as the aspect ratio of the crack and the minor radius of the torus (representing spherical pores) is decreased.

References

[1] William F Murphy, Kenneth W Winkler, and Robert L Kleinberg. Acoustic relaxation in sedimentary rocks: Dependence on grain contacts and fluid saturation. *Geophysics*, 51(3):757–766, 1986.

[2] Boris Gurevich, Dina Makarynska, Osni Bastos de Paula, and Marina Pervukhina. A simple model for squirt-flow dispersion and attenuation in fluid-saturated granular rocks. *Geophysics*, 75(6):N109–N120, 2010.

[3] Olivia Collet and Boris Gurevich. Frequency dependence of anisotropy in fluid saturated rocks–part i: aligned cracks case. *Geophysical Prospecting*, 64(4):1067–1084, 2016.

[4] LD Landau and EM Lifshitz. *Course of theoretical physics. vol. 6: Fluid mechanics.* London, 1959.

[5] Beatriz Quintal, J Germán Rubino, Eva Caspari, and Klaus Holliger. A simple hydromechanical approach for simulating squirt-type flow. *Geophysics*, 81(4):D335–D344, 2016.

SCCER SoE
SWISS COMPETENCE CENTER for ENERGY RESEARCH
SUPPLY of ELECTRICITY

u^b
UNIVERSITÄT BERN

SCCER-SoE Annual Conference 2019

Regional-scale flow models of the orogenic hydrothermal system at Grimsel Pass, Switzerland

Supported by:
Schweizerische Eidgenossenschaft
Confédération suisse
Confederazione Svizzera
Confederaziun svizra
Swiss Confederation
Innosuisse – Swiss Innovation Agency

Peter Alt-Epping, Larryn W. Diamond & Christoph Wanner
Rock-Water Interaction, Institute of Geological Sciences, University of Bern

1) Introduction

Thermal waters at temperatures ranging between 17 - 28 °C discharge at a rate of ≤ 10 L/min into a tunnel underneath Grimsel Pass (2164 m) in the Central Alps. Fluid discharge occurs at the intersection with a brecciated fault zone (Grimsel Breccia Fault (GBF)), a late Neogene exhumed strike-slip fault (Belgrano et al., 2016). The chemical composition of the water sampled in the tunnel shows that the water is a mixture of old geothermal water and younger cold water. Both components have meteoric isotope signatures, but the thermal water is derived from a higher altitude. Residence times of the old and young waters are ≤30 ky and ~7 years, respectively (Waber et al., 2017).

Results from Na-K geothermometry on present-day fluid samples indicate the maximum temperature at depth could be as high as 250 °C. Given the local geothermal gradient this corresponds to a circulation depth of meteoric water to at least 9 km (Diamond et al., 2018). These results imply that little or no fluid-rock interaction or fluid mixing occurred during the ascent of the hot fluid.

The breccia in the GBF has a sub-vertical, pipe-like structure in 3D, and constitutes a permeable linkage zone between parallel segments of the main shear-zone. Another such linkage zone exists in the Sidelhorn area to the west (Belgrano et al., 2016). Thus, it can be expected that these permeable linkage zones are common structural features along the fault.

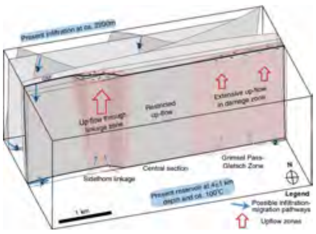

Conceptual model of structures and fluid pathways. Sub-vertical brecciated linkage zones connecting shear zone segments constitute permeable pathways for fluids (from Belgrano et al., 2016).

2) Numerical model

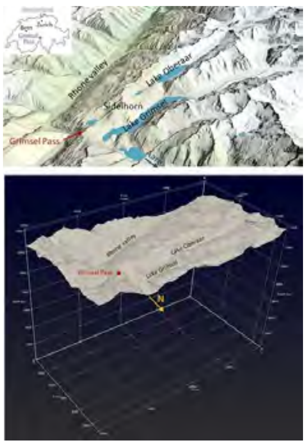

We use numerical modelling to better understand the regional flow system in the Grimsel area that leads to discharge of thermal water at Grimsel Pass. The model incorporates the topography of the region as its top boundary and extends to a depth of 12.5 km. The upflow zone at Grimsel Pass is incorporated as a vertical permeable conduit (k = 1e-13 m^2) within a low permeability granitic rock (k = 3e-20 m^2).
The model is composed of 3.9 Mio. cells. Simulations were carried out with the high performance reactive transport code PFLOTRAN (www.pflotran.org) on UBELIX, the HPC cluster at the University of Bern

3) Results

- *What is the role of the GBF in generating upflow under Grimsel Pass?*

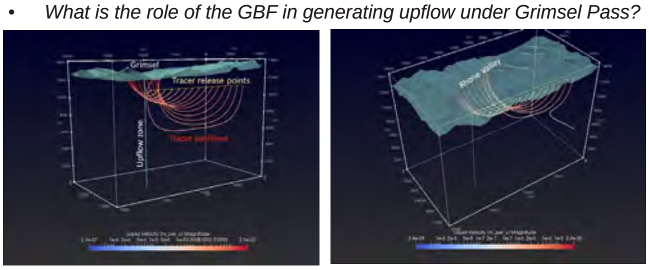

The GBF, if represented as an unconfined, permeable vertical plane extending into the high mountains towards the west and to a depth of 12.5 km, sustains hydrothermal upflow at Grimsel Pass. Without the GBF, deep groundwater discharges into the Rhone Valley.

Results cont'd

- *Can topography drive meteoric water to a depth > 9 km?*

Homogeneous fault permeability 1e-15 m^2

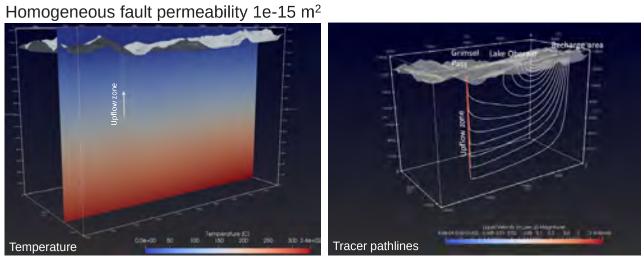

Homogeneous fault permeability 1e-14 m^2

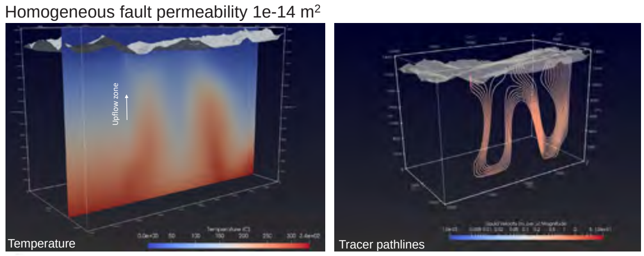

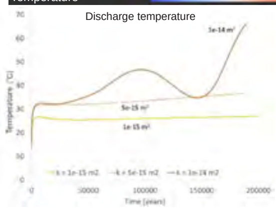

Simulations show that deep infiltration of meteoric water into the fault plane to a depth > 9 km, solely driven by topography and without permeability forcing, is possible. Models calibrated to match discharge rates and temperatures at the thermal springs suggest permeabilities of the GBF between 1e-15 m^2 and 1e-14 m^2 (fault width 100 m).

At permeabilities > 5e-15 m^2, the flow system in the fault becomes unstable and convection cells form which induce transient flow and transient temperature conditions at the discharge site.
Under stable flow conditions significant fluid mixing along the upflow conduit occurs, which is inconsistent with geochemical evidence. Some permeability forcing is needed to focus flow into the deeper section of the upflow zone.

- *What controls focused flow in the deep fault zone*

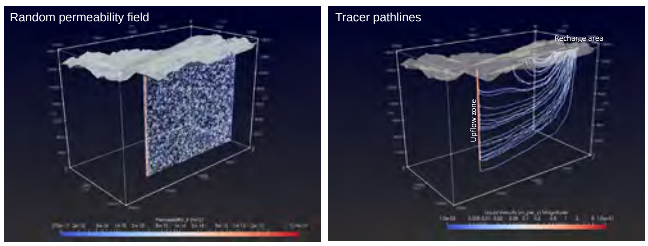

Heterogeneity due to random permeability perturbations leads to flow channelling. It is possible that an (unknown) permeability distribution in the fault causes focused inflow into the deep section of the upflow zone.

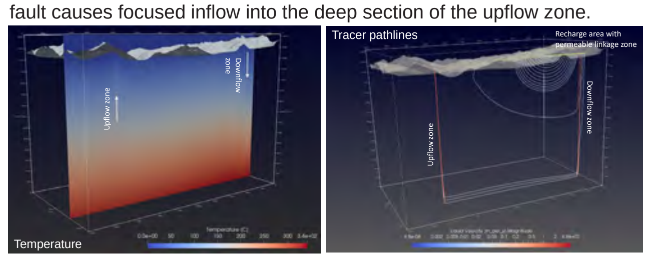

Alternatively, permeable linkage zones causing upflow may also occur at higher altitude, inducing focused downflow and focused flow at depth.

REFERENCES
Belgrano, T.M., Herwegh, M. & Berger, A., 2016: Inherited structural controls on fault geometry, architecture and hydrothermal activity, an example from Grimsel Pass, Switzerland, Swiss J. Geosci., 109, 345-364
Diamond, L.W., Wanner, C. & Alt-Epping, P. 2018: Penetration depth of meteoric water in orogenic geothermal systems. Geology, 46, 1063-1066
Waber, H.N., Schneeberger, R., Mäder, U.K., Wanner, C., 2017, Constraints on evolution and residence time of geothermal water in granitic rock at Grimsel (Switzerland), 15th Water-Rock Interaction Symposium, WRI-15, Procedia Earth and Planetary Science 17, 774-777

SCCER SoE
SWISS COMPETENCE CENTER for ENERGY RESEARCH
SUPPLY of ELECTRICITY

unine
UNIVERSITÉ DE NEUCHÂTEL

SCCER-SoE Annual Conference 2019

GEO ENERGIE SUISSE

In cooperation with the CTI
Energy
Swiss Competence Centers for Energy Research
Commission for Technology and Innovation CTI

Reliability of calibration and prediction of borehole failure models

Asmae Dahrabou(1), Benoît Valley(1), Philip Brunner(1) ,Andres Alcolea(2) ,Peter Meier(2)
(1) Centre for Hydrogeology and Geothermics, University of Neuchâtel,Emile-Argand 11, 2000-Neuchâtel, Switzerland.
(2) Geo-Energie Suisse AG, Reitergasse 11, 8004 Zürich, Switzerland.

I- Project context and objectives

In the frame of a CTI-project, the CHYN and Geo-Energie Suisse AG are developing a workflow and associated software tools that allow a fast decision-making process for selecting an optimal well trajectory while drilling deep inclined wells for EGS-projects. The goal is to minimize borehole instabilities as it enhances drilling performance and maximize the intersection with natural fractures because it increases overall productivity or injectivity of the well. The specificity of the workflow is that it applies to crystalline rocks and includes an uncertainty and risk assessment framework.

II- Calibration study by using inverse problem method

The main challenge in these analyses is that the strength and stress profiles are unknown independently. Calibration of a geomechanical model on the observed borehole failure has been performed using data from the Basel Geothermal well BS-1 and inverse problem method (PEST: Parameter ESTimation software).

2.1- Parameters distribution before and after calibration

- We use breakout data from the BS1 borehole to develop and test our approach
- We calibrate on observations data (breakout width and length) between 3000 m and 3600 m depth
- We use Kirsch solution to compute breakout width by looking at the stress conditions at the borehole wall and comparing them to Mohr-Coulomb failure criteria
- The unknown stress profiles that need to be calibrated are the one for SHmax and Shmin. We consider that these profiles are simple linear functions of depth.

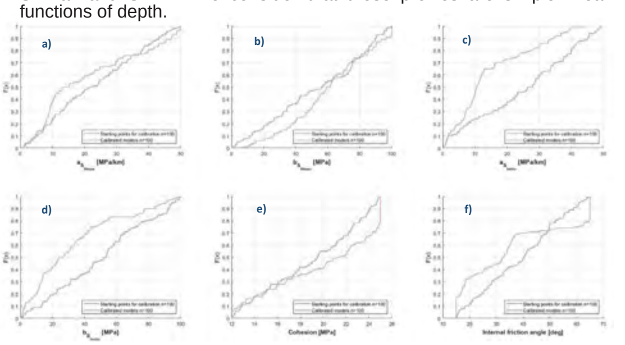

Figure 1. Distribution of initial and calibrated parameters (a) slope of S_{hmax}, (b) intercept of S_{hmax}, (c) slope of S_{hmin}, (d) intercept of S_{hmin}, (e) cohesion, (f) internal angle of friction for n = 100 starting points

2.2- Calibrated breakout width and length

The calibrated breakout width and length profiles for n = 100 starting points as well as the 25 observations are plotted below between 3000m and 3600m. Some of the curves fit the data well while some of them diverge for both breakout width and length.

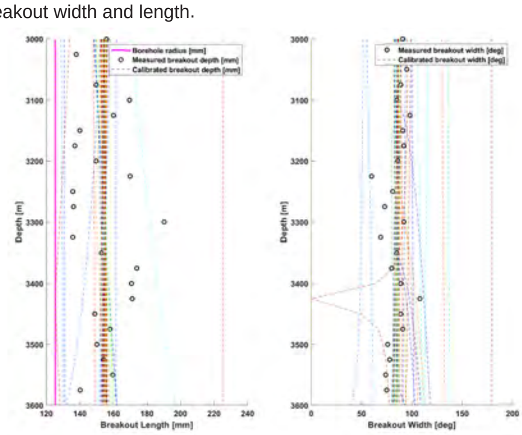

Figure 2. left: Measured breakout penetration (black circles) and calibrated breakout penetration profiles (dashed lines) for n = 100 different starting points, right: Measured breakout width (black circles) and calibrated breakout width profiles (dashed lines) for n = 100 different starting points

2.3- Failure prediction results

We predict failure from 3.6km to 5km depth by calculating the breakout width and length based on previous calibrated models. At the end of the process, we keep only 15 calibrated models that predict well the failure.

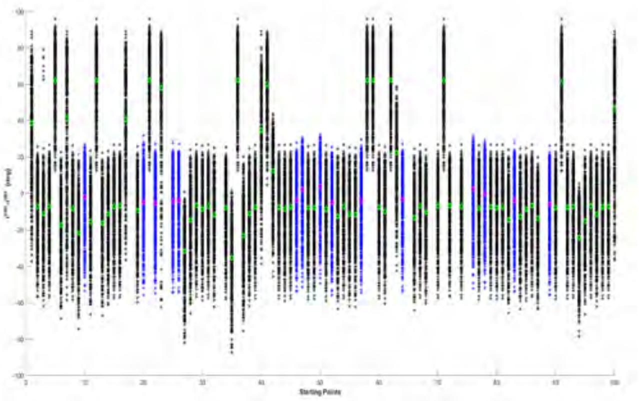

Figure 3. The difference l(calc)-l(obs) Vs. the calibrated models.The models in blue predict the failure well from 3.6km to 5km as their median (in magenta) is close to zero.

2.4.- Final «good» calibrated models

The final 15 calibrated models were used to calculate breakout width and length from 2.6km to 5km. Results are shown below:

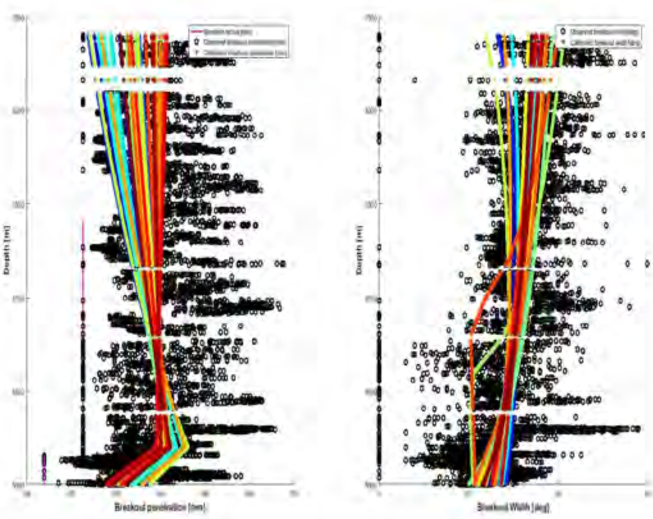

Figure 4. (left) calibrated breakout penetration (mm) and (right) calibrated breakout width from 2.6km to 5km

III- Conclusions

- Calibrated cohesion and friction angle tend to be high when using Mohr-Coulomb failure criterion
- Sensitivity to used failure critirion should be taken into consideration
- The calibrations are still not «perfect» and not unique but uncertainties should be quantified.
- Variability of the calibrated parameters should be integrated.

SCCER-SoE Annual Conference 2019

Application of Chemostratigraphy and petrology to characterize the Reservoirs of The Mesozoic sequence crossed by the Geo-01 well: potential for direct heat production and heat-storage.

Ferreira De Oliveira G.1, De Haller A. 1, Guglielmetti L. 1, Makhloufi Y. 1, Moscariello A1.
1: University of Geneva – Earth Sciences Department. Rue des Maraîchers 13, 1205 Geneva (Switzerland)
gustavo.ferreira@etu.unige.ch

1.Introduction

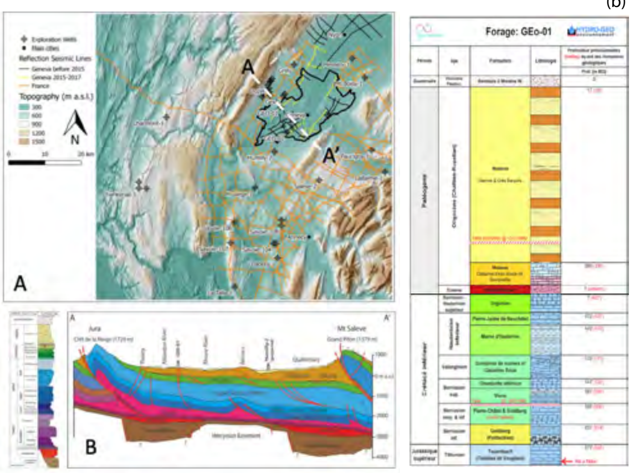

The Satigny well is the first medium-depth exploration well of the GEothermie 2020 program. This pilot project will make it possible to specify the geothermal potential available and to confront the concrete realities on the subsurface.
The purpose of GEo-01 is to explore the Mesozoic units and to identify and characterize the geological and hydrogeological conditions of the subsurface units. GEo-01 went through 407 meters of Tertiary Molasse, 241 meters of Cretaceous limestones and reached the Tithonian limestones at a final depth of 745 meters. Hot water was found at different depths. This water naturally rises to the surface at a temperature of 33 °C with a flow rate of more than 50 litres / second.

A) The Geneva Basin and surrounding region with location of main boreholes and 2D seismic lines acquired to date. The main wells used in this project (Geo-01, Crozet, Grilly, Humilly-2 and Thônex-1) are also indicated;
B) Simplified stratigraphic columns and NW-SE geological cross-section (AA') showing the principal stratigraphic and tectonic features of the GB (drawings modified from Moscariello et al., 2020)

2. Metodology

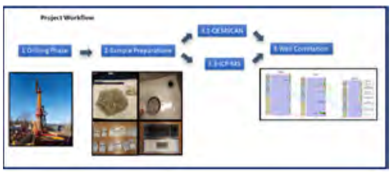

Fluxogram showing the methodology steps.

To realize this project several samples were provided by the GEothermie 2020 project. The cutting samples were taken during the GEo-01 drilling phase.
A complete petrographic and mineralogical characterization has been done using QEMSCAN analysis and optical microscopy. This is aimed to have a better understanding of the composition and repartition of the sedimentary facies and to help correlate the stratigraphy of GEo-01 with other reference wells in the GGB (HU2; TH1; GRY1; CRO1).

3. Results

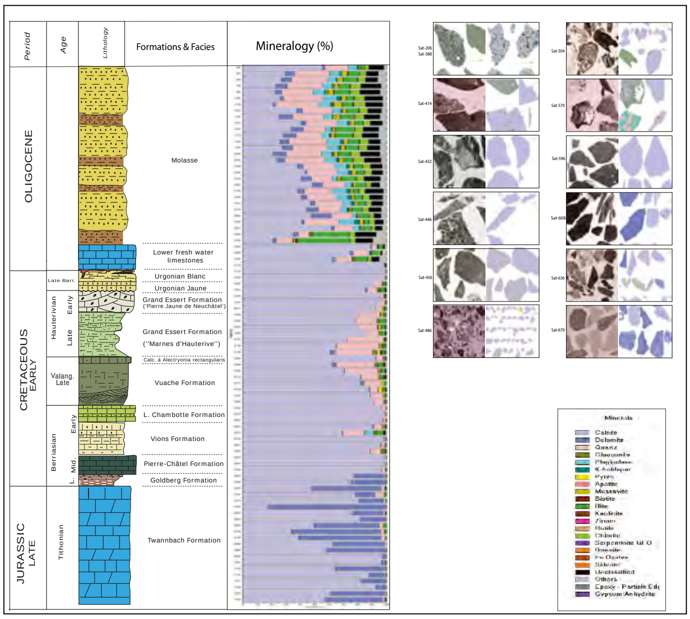

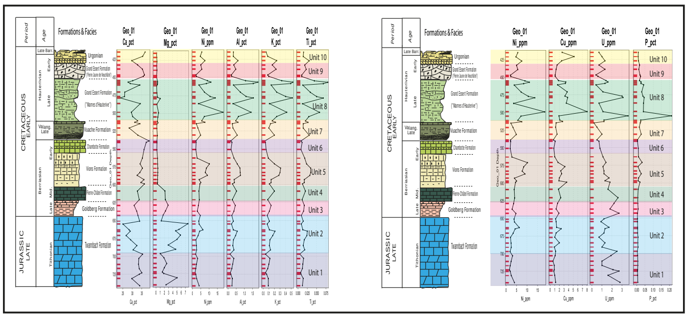

4. Discussion

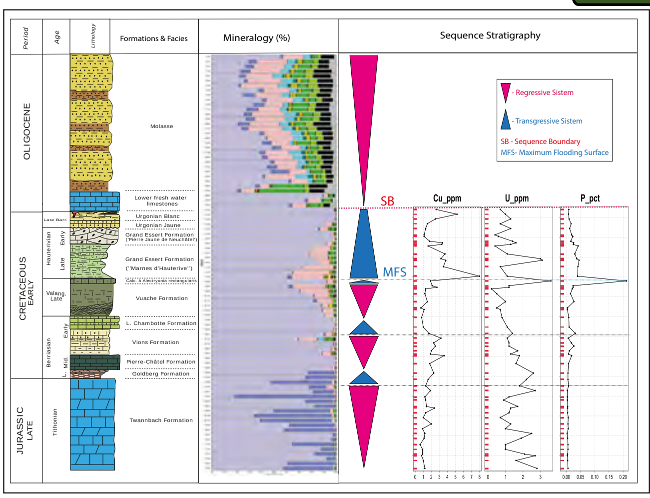

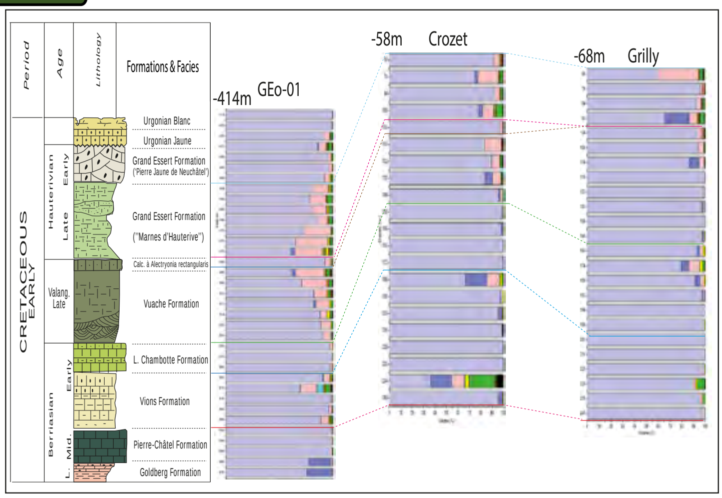

Bibliography:
PGG (2011). Evaluation du potentiel géothermique du canton de Genève – Vol. 1:Rapport final. Technical report, Service cantonal de l'énergie-Services Industriels de Genève.
RUSILLON, Elme. Characterisation and rock typing of deep geothermal reservoirs in the Greater Geneva Basin (Switzerland & France). Université de Genève.
www.geothermie2020.ch

GE RGBA GROUP
Geo Energy / Reservoir Geology and Basin Analysis

5. Conclusions

- The geochemical and petrological analysis of the sedimentary sequences traversed by the Geo-01, Crozet and Grilly wells allows us to recognize and characterize the main sedimentary facies in the subsurface of the GGB.

- With the new data generated by this type of study it is possible to correlate wells present in the same geological context and to check the lateral continuity and thickness of the sedimentary packages along the basin.

SCCER SoE

SWISS COMPETENCE CENTER for ENERGY RESEARCH
SUPPLY of ELECTRICITY

SCCER-SoE Annual Conference 2019

Supported by:

Schweizerische Eidgenossenschaft
Confédération suisse
Confederazione Svizzera
Confederaziun svizra

Swiss Confederation

Innosuisse – Swiss Innovation Agency

Hydraulic Characterization of the Bedretto Underground Laboratory

Nima Gholizadeh Doonechaly[a], Nathan Dutler[b], Bernard Brixel[a], Marian Hertrich[a] and Simon Loew[a]
[a]:Department of Earth Sciences, ETH Zuerich, CH-8092, Zuerich
[b]:Centre for Hydrogeology and Geothermics, University of Neuchâtel, CH-2000, Neuchâtel

Introduction

Bedretto underground research laboratory in the Bedretto Adit of the Furka Base Tunnel (BUL) is a multi-disciplinary collaborative project of the Swiss Competence Centre for Supply of Energy. Completion and inauguration of this test facility operated by the Department of Earth Sciences at ETH was carried out on May 18, 2019. The first large scale experiments carried out in this lab are related to enhanced geothermal systems and will include drilling of a large number of long (250-300m) injection and monitoring boreholes. A hydrogeological model of the test volume is a fundamental component of this multi-disciplinary project and will be developed from a combination of measurements carried out during the drilling operations, and during a special characterization phase following the drilling phase. The long boreholes will also be monitored using pressure sensors over longer term after the hydraulic characterization phase. Prior to the main characterization phase of the project on the long boreholes, several short boreholes are already drilled in the BUL and used for preliminary analysis of the system.

Permeability Estimation

Based on the observed fracture map in the short boreholes, hydraulic characterization is carried out by packer testing of individual fractures to obtain the permeability value and water discharge (if any) from each individual fracture.

The permeability value measurement is carried out using pressure pulse test with applying a high short pulse by injection at a high pressure and monitoring the transient pressure decline. The diffusivity equation is then used as a basis to estimate the fracture permeability value. The results for the pulse pressure testing of the single fracture at the depth of 20.7m at the SB1.1 borehole in BUL is presented in Figure 2. The packer interval's pressure is increased to 46.01bar over approximately 4 seconds. The interval's pressure was then monitored for a duration of 30 minutes while recovering towards formation pressure. The pressure decay into the interval containing the single fracture is presented in Figure 2.

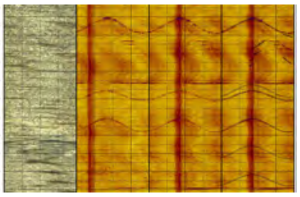

Figure 1: Selected interval of the OTV and ATV of wellbore SB1.1 before and after mini-fracture experiment.

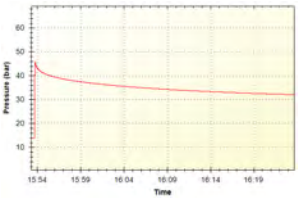

Figure 2: Pressure decline curve for the single fracture at the depth of 20.7m after applying a pressure pulse.

The analysis of the pressure decline curve is analysed using the curve fitting to analytical solution for diffusivity equation. Based on the obtained pressure data, and assumption of fracture aperture of 1um, the fracture permeability is estimated as 5E-13 m^2. The flow rate from the borehole SB1.1 is also monitored and recorded at 0.12L/min.

Characterization of Long Boreholes

In the next phase of the experiment, the long boreholes (which are currently being drilled (Figure 3)) in the BUL will be analysed with a comprehensive hydro-geological analysis, including, flow measurement while drilling, heat dilution test, pulse test, cross hole test and tracer tests. After the hydraulic characterizations, the long boreholes will be equipped by a network of multi-disciplinary monitoring devices, such as microseismic, pressure, fiber-optics strain and temperature sensors so as to provide the required data for the design, execution and evaluation of the hydraulic stimulation.

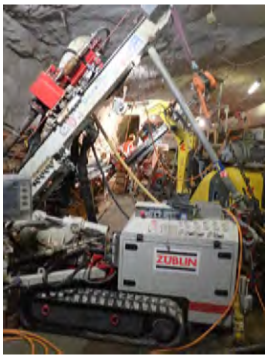

Figure 3: Ongoing operation for drilling of the long boreholes in BUL.

Flow Measurement While Drilling

The initial estimate of the major flowing zones in the boreholes will be identified from the flow measurements during drilling (Figure 4). For this purpose, a side flow line is connected to the blowout preventer to directly measure the flow discharge from the borehole. The borehole flow is fully directed towards an electromagnetic flow meter and recorded continuously. Also several times a day, during the drilling breaks, borehole will be shut in and $_a$ pressure sensor is used to monitor the pressure build up within the borehole. Such tests, gives us first hand estimate of the flowing intervals within a boreholes as well as an estimate of the permeability of corresponding intervals.

Figure 4: Flow measurement during drilling operation.

Fluid Flow Logging using Heat Dilution Test

The major flowing zones (fractures) of boreholes will be qualitatively identified using heat dissipation-tests. Hybrid heating cable and fiber optic distributed temperature sensing (FO-DTS) will be implemented in the corresponding boreholes, individually, to measure the wellbores' response to artificially induced temperature disturbances using a heating cable. The heating cable will be used to heat up the wellbore to a temperature of ~20˚C above the formation temperature in a relatively short period of time. After heating the borehole, the borehole fluid temperature profile will be continuously monitored with the installed FO cable while the wellbore can flow freely at natural conditions. The transient temperature profile will be continuously monitored until stabilized condition is reached. Then the obtained data will be analyzed to identify the flowing zones along the borehole length. The above-mentioned procedure will be repeated for all boreholes.

Hydraulic Tomography

After identifying the major flowing zones in the boreholes (identified from heat dilution test), packer testing will be carried out to test the permeability of the transmissive fractures in corresponding flow zones. Then Hydraulic tomography will be carried out to reconstruct the heterogeneity and directional properties of the system. For this purpose, the cross hole well testing will be carried out followed by injecting three different fluorescent dye tracers in transmissive intervals. The inversion will be carried out using both numerical and analytical techniques.

Discussion & Conclusions

The preliminary results from the short boreholes shows the influence of the hydraulic fractures on creating the connected flow path in the borehole. The results also show shows the heterogenous nature of the hydraulic properties of the system, even within the same well. Therefore, large scale characterization using tracer and cross hole test in long boreholes play major role in understanding the hydraulic characteristics of the system.

References

- Cooper Jr, H.H., Bredehoeft, J.D. and Papadopulos, I.S., 1967. Response of a finite-diameter well to an instantaneous charge of water. Water Resources Research, 3(1), pp.263-269.
- Papadopulos, S.S., Bredehoeft, J.D. and Cooper Jr, H.H., 1973. On the analysis of 'slug test'data. Water Resources Research, 9(4), pp.1087-1089.
- Masset, O. and Loew, S., 2013. Quantitative hydraulic analysis of pre-drillings and inflows to the Gotthard Base Tunnel (Sedrun Lot, Switzerland). Engineering geology, 164, pp.50-66.
- Renard, P., 2017. Hytool: an open source matlab toolbox for the interpretation of hydraulic tests using analytical solutions. J. Open Source Software, 2(19), p.441.
- https://escholarship.org/uc/item/03q0365v
- Jalali, M., Klepikova, M., Doetsch, J., Krietsch, H., Brixel, B., Dutler, N., Gischig, V. and Amann, F., 2018, November. A Multi-Scale Approach to Identify and Characterize the Preferential Flow Paths of a Fractured Crystalline Rock. In 2nd International Discrete Fracture Network Engineering Conference. American Rock Mechanics Association.

SCCER SoE
SWISS COMPETENCE CENTER for ENERGY RESEARCH
SUPPLY of ELECTRICITY

SCCER-SoE Annual Conference 2019

Supported by:
Schweizerische Eidgenossenschaft
Confédération suisse
Confederazione Svizzera
Confederaziun svizra

Swiss Confederation

Innosuisse – Swiss Innovation Agency

Monitoring and Flow Path Reconstruction of Saline Tracer Tests with GPR

Peter-Lasse Giertzuch[1], Joseph Doetsch[1], Mohammadreza Jalali[2], Alexis Shakas[1], Cédric Schmelzbach[1], Hansruedi Maurer[1]

[1]Department of Earth Sciences, ETH Zurich, Switzerland; [2]RWTH Aachen University, Chair of Engineering Geology and Hydrogeology, Germany

1 Introduction

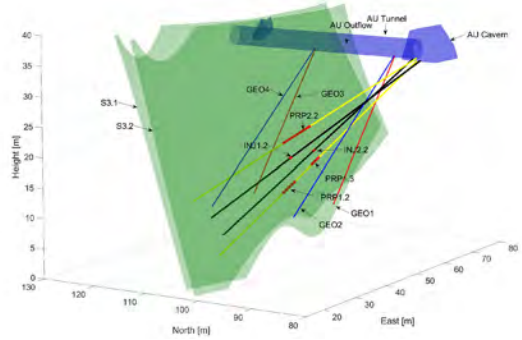

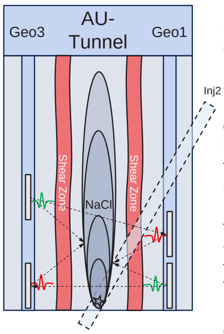

In two experiments at the Grimsel Test Site (GTS) in Switzerland, 100 L and 200 L of salt water were injected at a rate of 2 L/min in INJ2 in between the S3 shear zones, and time-lapse Ground Penetrating Radar (GPR) reflection data were recorded in GEO3 and GEO1 in the respective tests. Simultaneously, transmission data was recorded by using a 4-channel system and two 250 MHz borehole antenna sets. The temporal resolutions were ~10 min and ~30 min for the reflection and transmission acquisition, respectively. The upper figure shows the GTS with INJ, GEO and PRP boreholes, as well as the S3 shear zones. On the left the GPR survey schematic is shown.

2 Difference Attenuation Tomography

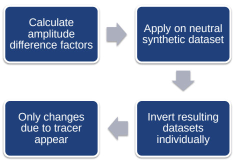

The transmission data is analyzed by a Difference Attenuation Approach. This approach allows to invert for changes due to the tracer only, disregarding all geological information in the GPR data (top). The time-lapse datasets are inverted individually and show clearly the tracer injection, build up and signal decrease in the tomography plane over time.

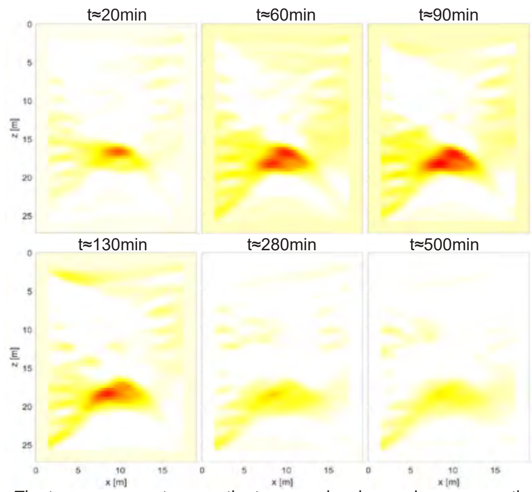

The tracer appears to cross the tomography plane only once near the injection point and is not resolved towards shallower borehole depths.

3 Difference Reflection Imaging

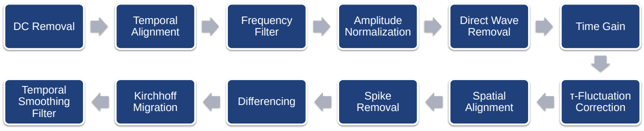

The concept of Difference Reflection Imaging relies on subtracting a reference profile that was recorded prior to tracer injection from all of the following time-lapse monitoring profiles. Only changes due to the salt tracer remain. The necessary processing steps are shown above. Special attention needed the fluctuation of the sampling rate during data acquisition. The developed correction is based on resampling and cross-correlation to reconstruct compatible waveforms. The process is described in [1].

Below: Four differenced profiles from the two experiments at different times after tracer injection and measured breakthrough curves in different borehole intervals. Symbols represent the calculated reflection positions of the different borehole intervals. The tracer first appears around the injection point, appears to split up and propagates towards PRP13 and the AU tunnel outflow. The tracer reflection are in good accordance with the measured breakthrough curves at the different positions. Note that the PRP2 curve is clipped.

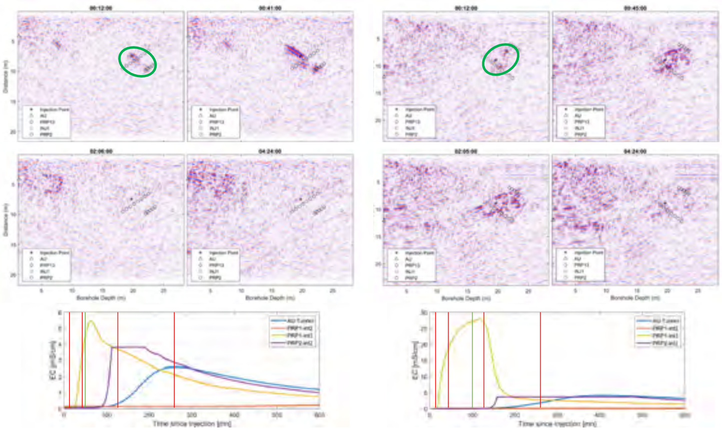

[1]: Giertzuch et. al. (*in review*), GEOPHYSICS

4 3D Flow Path Reconstruction

Single-hole reflection GPR data does not allow for actual localization, as the antennas show a radial symmetry, but this can be overcome by combining the two datasets. After migration, a tube shaped form contains the possible reflection locations (right top). The data from the GEO1 and the GEO3 surveys are combined by calculating the intersections of those shapes and thereby allow for a 3D localization of the tracer flow path in blue (right middle).
Combined with the difference attenuation results it is possible to further constrain the flowpath (bottom). The tracer splits close to the injection point, one part propagates though the tomography plane towards PRP13, the other part seems to stay below the plane propagating towards the AU outflow. The view from below is presented at the right bottom.

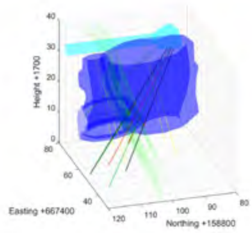

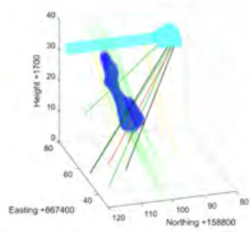

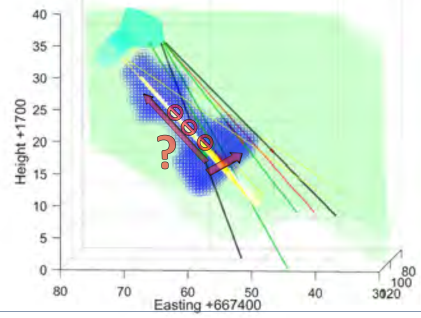

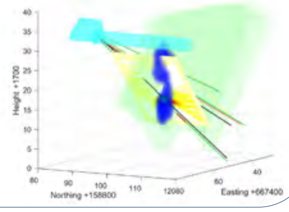

peter-lasse.giertzuch@erwd.ethz.ch

SWISS COMPETENCE CENTER for ENERGY RESEARCH
SUPPLY of ELECTRICITY

UNIL | Université de Lausanne

SCCER-SoE Annual Conference 2019

Supported by:
Schweizerische Eidgenossenschaft
Confédération suisse
Confederazione Svizzera
Confederaziun svizra
Swiss Confederation
Innosuisse – Swiss Innovation Agency

Borehole radar and full waveform sonic measurements of the Bedretto stress-measurement boreholes

Andrew Greenwood, Eva Caspari, Ludovic Baron and Klaus Holliger.

Abstract: High-quality and high-resolution wireline logging has been completed in the Bedretto Underground Laboratory stress-measurement boreholes (SB) to assist determination of the local stress field and characterise the rock mass.
Here we present preliminary results of borehole radar (BHR) and full-waveform sonic (FWS) data with particular emphasis on the method's ability to locate and map hydraulically open fractures.

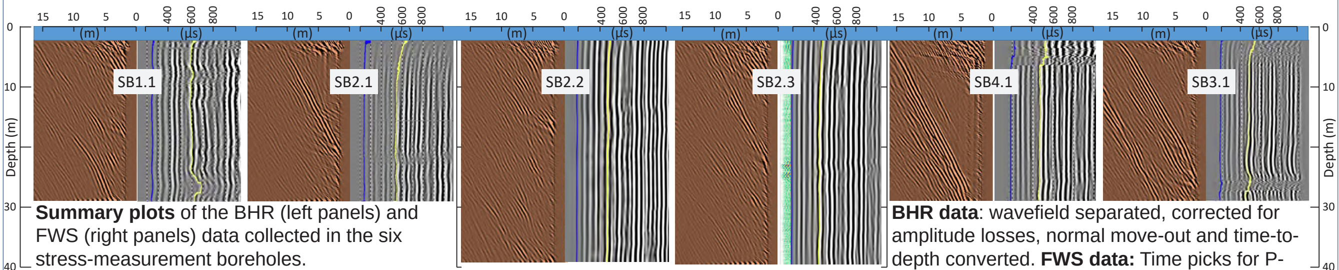

Summary plots of the BHR (left panels) and FWS (right panels) data collected in the six stress-measurement boreholes.

BHR data: wavefield separated, corrected for amplitude losses, normal move-out and time-to-depth converted. **FWS data:** Time picks for P- (blue) and S-wave (yellow) arrivals.

Fracture detection and mapping

Fluid-filled fractures within crystalline rocks can be detected by their high-contrasting conductivity in BHR data, and in borehole acoustic methods, such as FWS, when a hydraulically open fracture intersects a fluid-filled borehole.

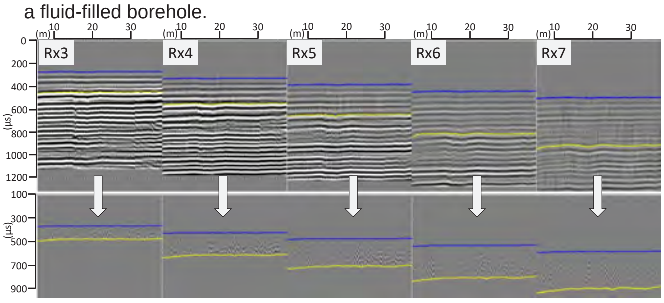

Above Top: Raw FWS data collected with 5 receivers (Rx) at a frequency of 25kHz and transmitter-to-receiver spacings of 3 to 7 feet. **Bottom:** Data after removal of head-wave modes which reveals tube-waves generated at hydraulically open fractures by passing acoustic waves. These are observed as chevrons within the wavefield-separated profiles. Blue and yellow lines are P- and S-wave arrival travel-times, respectively.

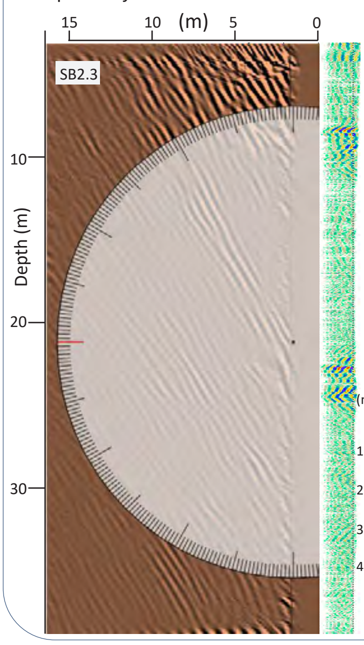

Left: Time-to-depth converted, wavefield-separated 100 MHz BHR data and the tube-wave profile (green section) from Rx5 above. Analysis of vertical radar profiles (**below**) were used to determine an accurate radar velocity for the Bedretto (Rotondo) granite. This enables an accurate time-to-depth conversion and accurate estimation of fracture plane orientation with respect to the borehole axis.

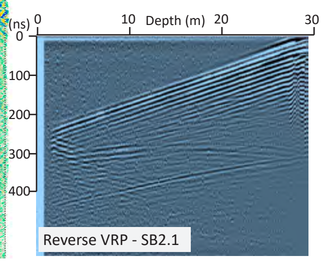

Velocity comparison

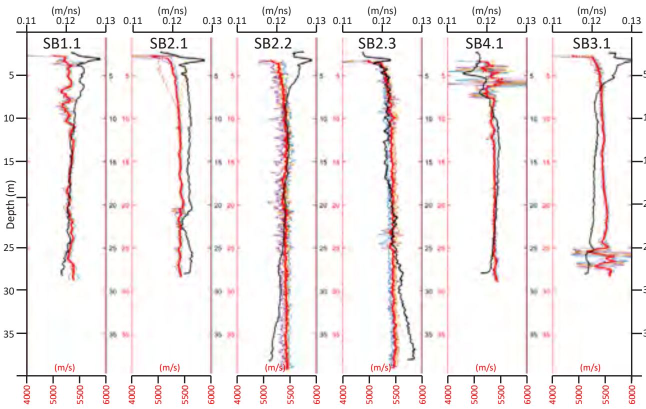

Above: BHR interval velocity profiles (black) are shown overlying P-wave velocity (red) determined from the average of each FWS transmitter-receiver pair (colours). Despite the two methods measuring different wave propagation, namely electromagnetic and acoustic, and effective rock mass volumes, similar variances can been seen in the velocity profiles. Large variations occur near the top of the boreholes where the borehole collar and radius changes have greater effect.

Summary and outlook

We have collected high-quality full wave form sonic and borehole radar data in the six SB boreholes. This combination accurately locates open fractures by identifying tube-waves and infers the orientation and extent of the fracture plane away from the borehole.

It is possible to determine fracture compliance from the amplitude ratio between the onset acoustic wave and the corresponding generated tube wave. We intend to modify the inversion scheme of Hunziker (2019) to invert for fracture compliance from multi-receiver FWS data. Having multiple receivers allows for higher precision estimation of acoustic velocities and attenuation, and allows for a more robust inversion due to the additional offset tube-wave-profiles.

Reference:

Hunziker, J., A. Greenwood, S. Minato, N. Barbosa, E. Caspari and K. Holliger., 2019. Bayesian Full-Waveform Tube-Wave Inversion for Effective Hydraulic Fracture Aperture and Mechanical Fracture Compliance. 81st EAGE Conference and Exhibition, London, 2019,

Acknowledgement:
We thank the BULG team for their support.

SCCER SoE
SWISS COMPETENCE CENTER for ENERGY RESEARCH
SUPPLY of ELECTRICITY

SCCER-SoE Annual Conference 2019

UNIVERSITÉ DE GENÈVE
FACULTY OF SCIENCES
Department of Earth Sciences

GE-RGBA
GEOENERGY RESERVOIR GEOLOGY AND BASIN ANALYSIS GROUP

Supported by:
Schweizerische Eidgenossenschaft
Confédération suisse
Confederazione Svizzera
Confederaziun svizra
Swiss Confederation
Innosuisse – Swiss Innovation Agency

Geochemical Characterization of Geothermal Waters Circulation in Carbonatic Geothermal Reservoirs of the Geneva Basin (GB)

Guglielmetti L., Eichinger F.**. Moscariello A.*,*

This study focuses on the interpretation of geochemical data collected at springs and at two deep geothermal exploration wells located on the edges and within the Geneva Basin (GB Canton of Geneva, Switzerland).

The sampling sites have been selected across one North-South trending sections following the main groundwater flow from the recharge zone to the deep geothermal reservoirs in the Mesozoic carbonatic units.

These formations have been drilled by two geothermal exploration wells; the 745 m deep GEO-01 well, where water with a temperature of 34˚C and an artesian flow rate of 50l/s is encountered, and at the 2530 m deep Thonex-01 well, which produces app. 0.1 l/s by artesian flow at reservoir temperature of 80˚C.

Major ions, trace elements, stable isotopes of Oxygen and Hydrogen, Tritium, Sulphur and Carbon isotopes as well as noble gas samples have been collected and analysed. The analyses aim at characterizing the fluid circulation in terms of recharge zone, origin of the water, mean residence times, reservoir temperature, and water-rock interactions.

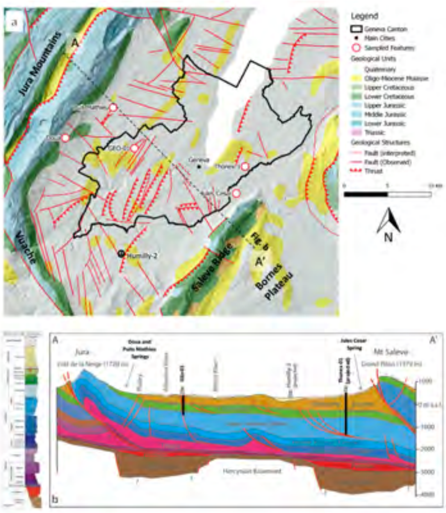

RESULTS

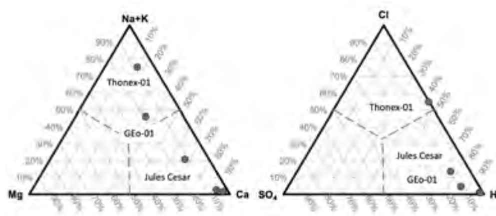

Ternary plots of the analysed samples

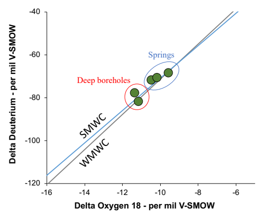

Stable isotopes of Oxygen and Hydrogen showing the meteoric origin of the sampled waters

Saturation Index						
	Puits Matthieu	Doua Spring	GEo-01 Well	Thonex-01 Well (wellhead)	Thonex-01 Well (bottomhole at 88˚C)	Jules Cesar Spring
Temperature	8.6	9.5	29.8	14.6	88.0	12.1
pH	7.5	7.3	7.5	7.7	7.5	7.3
Calcite	-0.054	-0.073	-0.072	0.346	0.944	-0.011
Aragonite	-0.209	-0.229	-0.215	0.191	0.836	-0.164
Dolomite	-1.258	-1.695	-0.075	0.514	1.931	-0.627
Gypsum	-3.041	-3.025	-2.611	-4.150	-4.162	-1.801
Anhydrite	-3.534	-3.509	-2.910	-4.626	-3.850	-2.252
Amorphous Silica	-2.111	-1.818	-1.255	-0.803	-1.366	-1.311
Chalcedony	-1.213	-0.923	-0.417	0.089	-0.702	-0.426
Quartz	-0.730	-0.443	0.010	0.568	-0.435	0.044

Elevation estimation based on of δ^2H and $\delta^{18}O$ isotopes

Sample Name	Na-K-Ca	Measured Temperature
Puits Matthieu	-	
Source de la Doua	-	
GEo-01 Well	36	34
Thonex-01 Well	84	88
Source Jules Cesar	21	

Reservoir temperature (˚C) estimated by Na-K-Ca and measured after drilling

CONCEPTUAL MODEL

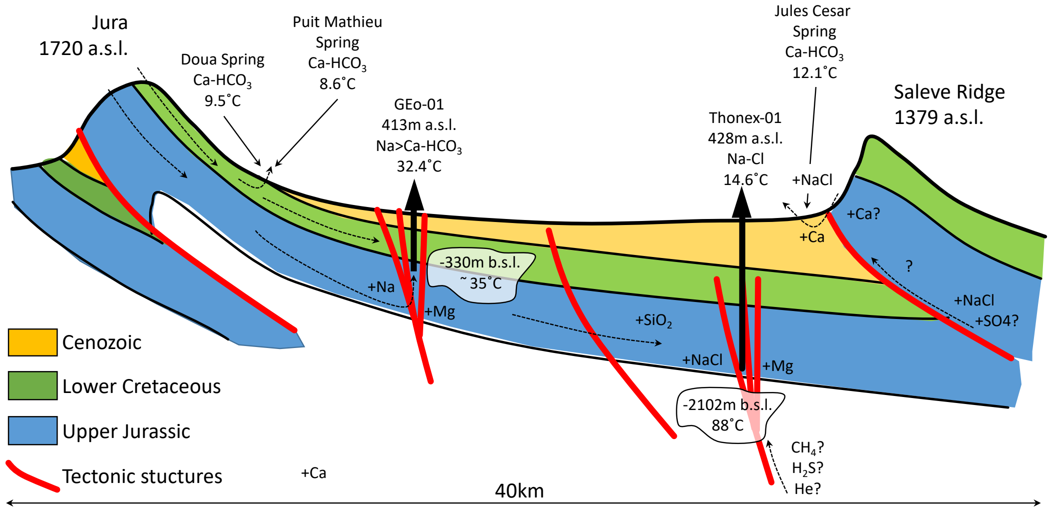

CONCLUSIONS: The interpretations show that the geothermal waters have a meteoric origin with the main recharge zone being located in the Jura Mountains towards the North.
The infiltration is dominated by secondary porosity controlled by intense fracture conditions.
Infiltrating water circulates in the Mesozoic Units and the groundwater flow direction is controlled by the geometry of these formations, which gently dip towards south with a 3˚ average dip.
Fracture zones associated to sub-vertical strike-slip faults represent the main corridors where waters as well as hydrocarbons and dissolved gas rise towards the surface. Moreover, the highly porous and permeable karstified horizons at the Lower Cretaceous level and the reef complex in the Upper Jurassic represent very promising potential geothermal reservoirs across the whole Geneva Canton for heat production with temperatures ranging from about 30˚C to more than 110˚C.

*Department of Earth Sciences, University of Geneva. Rue des maraichers 13, 1205 Geneve (Switzerland)
**Hydroisotop GmbH. Woelkestr. 9, D-85301 Schweitenkirchen (Germany)

luca.guglielmetti@unige.ch

AKNOWLEDGEMENTS
The authors would like to thank Services Industriels de Genève for funding this research and providing access to the well sites, and HydroGeo Environement Sarl for the fruitful support and dialogues in selecting the sampling sites

SCCER SoE

SWISS COMPETENCE CENTER for ENERGY RESEARCH
SUPPLY of ELECTRICITY

SCCER-SoE Annual Conference 2019

Unil UNIL | Université de Lausanne

UNIVERSITÉ DE GENÈVE

TUDelft Delft University of Technology

Supported by:
Schweizerische Eidgenossenschaft
Confédération suisse
Confederazione Svizzera
Confederaziun svizra

Swiss Confederation

Innosuisse – Swiss Innovation Agency

Bayesian inversion of tube waves to estimate fracture aperture and compliance: Application to a real dataset

Jürg Hunziker, Andrew Greenwood, Shohei Minato, Nicolas Barbosa, Eva Caspari and Klaus Holliger

Introduction

We propose to estimate the effective hydraulic aperture of fractures as well as their mechanical compliance, through a Bayesian full-waveform inversion of tube waves. Tube waves are created when a seismic body wave encounters a fluid-filled fracture which is connected to a borehole. When such a fracture is deformed by the passing body wave, fluid is squeezed into the borehole. This creates an acoustic disturbance known as a tube wave, which propagates along the borehole wall. Usually, tube waves are considered as noise in the processing of vertical seismic profiling (VSP) data, but here we profit from the fact that the characteristics of tube waves depend on the displaced fluid volume to infer the effective hydraulic aperture and the mechanical compliance of fractures.

Method

Considering the small parameter space and the strong non-linearity of the inverse problem, we chose to use a stochastic instead of a deterministic inversion approach. This has the following advantages:

- Our Bayesian inversion does not infer only one single model that explains the data, but rather an entire ensemble allowing to sample the posterior probability density function and, thus, providing a measure of uncertainty.
- The algorithm is able to leave local minima. It is therefore sufficient to draw random models from the prior probability density function to initialize the inversion.

We sample the posterior probability density function using the DREAM(ZS) algorithm (ter Braak and Vrugt, 2008; Laloy and Vrugt, 2012), which is a Markov chain Monte Carlo (MCMC) approach using multiple interacting chains and a database of past models for fast convergence.

As a forward solver, to simulate the tube-wave data during the inversion process, we use the semi-analytic algorithm of Minato and Ghose (2017) and Minato et al. (2017) with the following extensions:

- Geometrical spreading for body waves
- Transmission losses of body waves across fractures
- Variable source-depth to accommodate velocity changes above the borehole section under consideration
- Separate effective isotropic shear moduli for the body waves and for the tube waves to take anisotropy into account

Results: modelspace

We apply our inversion algorithm to zero-offset VSP data from the Grimsel test site in Switzerland. The inversion was run three times with each run consisting of three interactive Markov chains. The development of the estimates of the aperture and mechanical compliance for two fractures, which are separated from each other by only 0.4 m vertical distance, are plotted below.

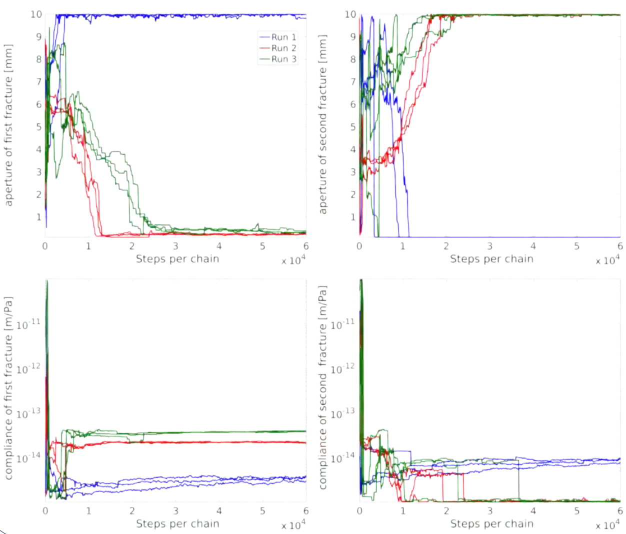

Results: dataspace

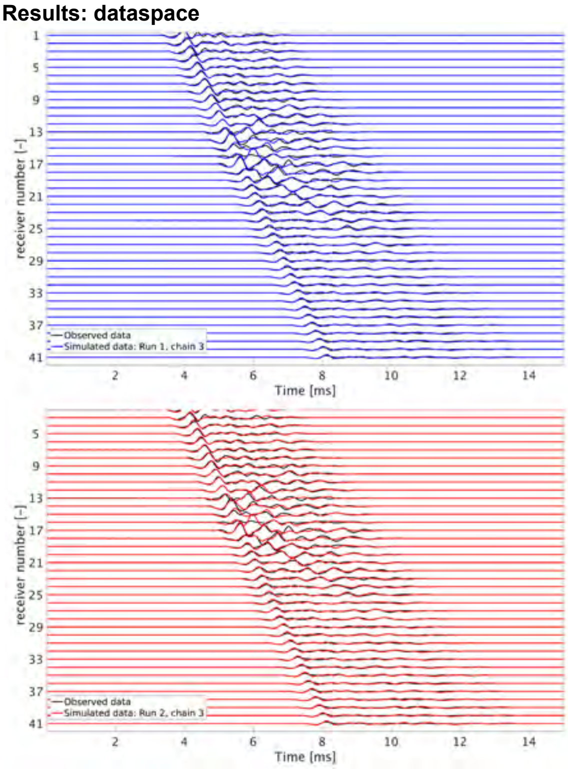

These results show that our Bayesian inversion approach discovered two equally probably modes: Either the first fracture has a large aperture and a relatively small compliance while the second fracture has a small aperture and a relatively large compliance (as discovered by run 1) or vice versa (run 2 and 3).

Conclusions

- We have developed a stochastic full-waveform inversion approach for tube waves and applied it to a field dataset from the Grimsel test site in Switzerland. The method allows to explain the data well.
- Our Bayesian tube-wave inversion is able to determine that one of the two fractures has a larger aperture than the other. The identification of these two equally probable models nicely illustrates one of the key advantages of Bayesian inversion compared to a deterministic approach, which would have converged only to one of these solutions.
- Optical televiewer data and a study based on the attenuation analysis of full-waveform sonic log data (Barbosa et al., 2019) support the solution proposed by the 2nd and 3rd run.

References

- Barbosa, N. D., Caspari, E., Rubino, J. G., Greenwood, A., Baron, L. and Holliger, K. [2019] Estimation of fracture compliance from attenuation and velocity analysis of full-waveform sonic log data, Journal of Geophysical Research: Solid Earth, 124, 2738-2761.
- ter Braak, C.J.F. and Vrugt, J.A. [2008] Differential evolution Markov Chain with snooker updater and fewer chains. Statistics and Computing, 18(4), 435–446.
- Laloy, E. and Vrugt, J.A. [2012] High-dimensional posterior exploration of hydrologic models using multiple-try DREAM (ZS) and high-performance computing. Water Resources Research, 48, WO1526.
- Minato, S. and Ghose, R. [2017] Low-frequency guided waves in a fluid-filled borehole: Simultaneous effects of generation and scattering due to multiple fractures. Journal of Applied Physics, 121(10), 104902.
- Minato, S., Ghose, R., Tsuji, T., Ikeda, M. and Onishi, K. [2017] Hydraulic properties of closely spaced dipping open fractures intersecting a fluid-filled borehole derived from tube wave generation and scattering. Journal of Geophysical Research: Solid Earth, 122, 8003–8020.

SCCER SoE
SWISS COMPETENCE CENTER for ENERGY RESEARCH
SUPPLY of ELECTRICITY

SCCER-SoE Annual Conference 2019

Supported by:
Schweizerische Eidgenossenschaft
Confédération suisse
Confederazione Svizzera
Confederaziun svizra
Swiss Confederation
Innosuisse – Swiss Innovation Agency

In-situ stress estimation from fault slip triggered during fluid injection

Maria Kakurina[1], Yves Guglielmi[2], Christophe Nussbaum[3] and Benoît Valley[1]

(1)University of Neuchâtel, CHYN, Neuchâtel, Switzerland, (2) Lawrence Berkeley National Laboratory, Berkeley CA, United States, (3) Swisstopo, Wabern, Switzerland

Introduction

Standard **in situ stress measurement** methods using fluid injection in deep boreholes are based on the analyses of pressure, flowrate and pre- and post-injection fracture mapping. Here we apply a **new methodology** to improve the estimation of the in situ stress by adding the record of **three-dimensional (3D) displacement** in the pressured interval measured continuously during the injection. We use the displacement-flowrate-pressure data from a **fault reactivation** experiments conducted in shale rocks at the Mont Terri rock laboratory, Switzerland. The experiment consisted in fluid injections into the fault damage zone in order to reactivate the fault planes and to measure the slip during the injection. The experiment protocol followed the step-rate injection method for fracture in situ properties (SIMFIP) developed by Guglielmi et al. (2013).

Input data

Stress orientations and **magnitudes** are estimated using the data of (Table 1):

1) Geology of the injected interval
2) Measured slip orientation (Figure 1)
3) Normal stress (σ_n) on the reactivated fracture (ISIP)
4) Vertical stress (σ_v) on the reactivated fracture ($\sigma_v = \sum_{i=1}^{n} \rho_i \, g \, \Delta z$)

Table 1. Summary of the input data

Potentially activated fractures		Slip direction		Projected slip		Normal stress, MPa	Vertical stress, MPa
Dip Direction	Dip Angle	Dip Direction	Dip Angle	Dip Direction	Dip Angle		
130	55	75	25	75	39	4.4±0.2	7.2±0.2
130	46				31		
131	65				50		
130	37				23		

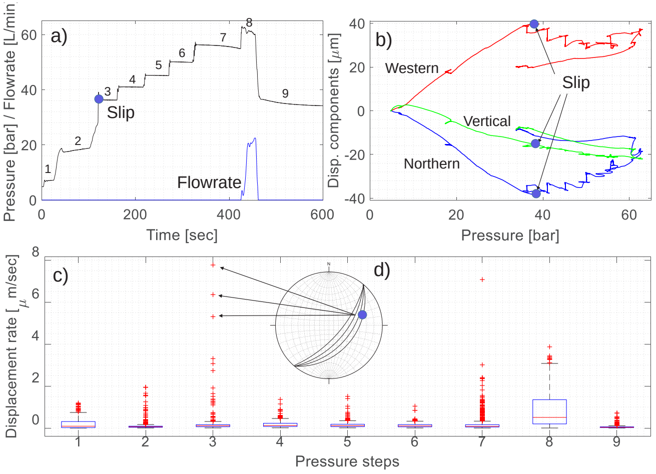

Figure 1. a) Pressure, flowrate and b) 3 components of displacement monitored during the step-rate test and indication when slip occurs, c) Box plot of displacement rate at each pressure step used to identify slip events, d) Stereoplot with the slip direction of identified slip events and fractures in the interval.

Protocol of estimation the complete stress tensor

(1) Grid search over all possible reduced stress tensor (orientation and stress ratio R) in order to identify the ones compatible with observed slip orientation (good FIT value) (Figure 2)

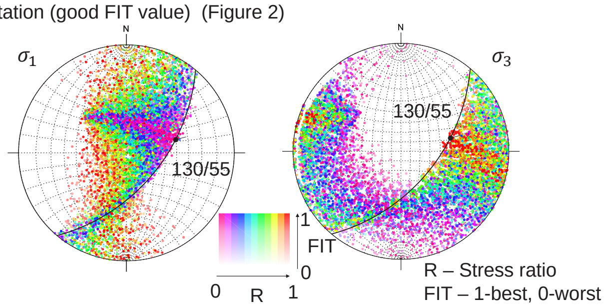

Figure 2. All possible stress combinations and their fit to the fracture slip. Example: fracture oriented 130°/55°

(2) Sorting of the possible reduced stress tensor keeping only those with a FIT > 90% , i.e. allowing for a max misfit angle between measured and calculated slip of 5.7° or less.

(3) Calculating absolute principal stress magnitude values $\sigma_1, \sigma_2, \sigma_3$ by considering the accepted reduced stress tensor and estimations of the vertical and fracture normal stress. This is done by solving the following system of equations:

$$\begin{cases} R = \dfrac{\sigma_2 - \sigma_3}{\sigma_1 - \sigma_3} \\ \sigma_n = l_1^2\sigma_1 + m_1^2\sigma_2 + n_1^2\sigma_3 \\ \sigma_v = l_2^2\sigma_1 + m_2^2\sigma_2 + n_2^2\sigma_3 \end{cases}$$

where *l* , *m* and *n* are the direction cosines of the normal of the fracture with respect to the principal stress axes

(4) Reducing the number of possible solutions by insuring that only solutions showing high slip tendency on the considered fracture are kept and insuring acceptable bound on the principal stress magnitudes ($\sigma_1, \sigma_2, \sigma_3$>1.5 MPa and $\sigma_1, \sigma_2, \sigma_3$<8 MPa) (Figure 3)

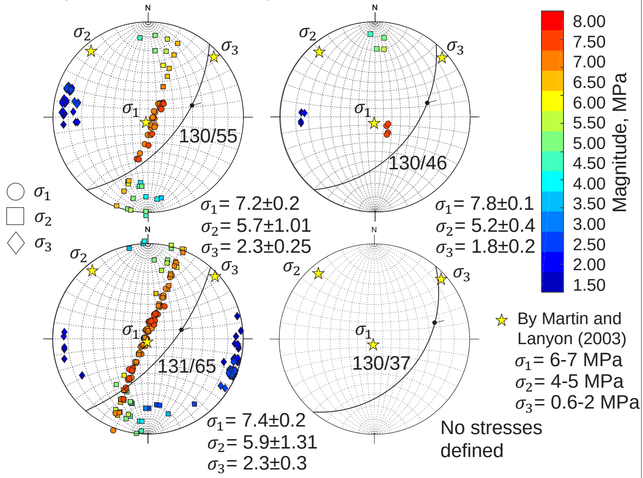

Figure 3. Orientations and magnitudes of the in situ stresses for potentially activated fractures

Conclusions

- The presented methodology allow estimating the full stress tensor from a single set of fracture activation measurements. Some uncertainties remains concerning what exact fracture is activated but this doesn't affect the robustness of the stress estimation.
- Estimation of the stress orientation and magnitudes is consistent with the state of stress, estimated in Mont Terri by Martin and Lanyon (2003):

References

Guglielmi, Y., Cappa, F., Lançon, H., Janowczyk, J. B., Rutqvist, J., Tsang, C. F., & Wang, J. S. Y. (2013). ISRM suggested method for step-rate injection method for fracture in-situ properties (SIMFIP): Using a 3-components borehole deformation sensor. In The ISRM Suggested Methods for Rock Characterization, Testing and Monitoring: 2007-2014 (pp. 179-186). Springer International Publishing.

SCCER-SoE Annual Conference 2019

Rock mechanics properties for fractured limestone hydrothermal system

Morgane Koumrouyan, Reza Sohrabi, Benoît Valley

Centre for Hydrogeology and Geothermics (CHYN), University of Neuchâtel, Switzerland

morgane.koumrouyan@unine.ch

Motivation

This research aims at constraining the geomechanical properties of a fractured limestone hydrothermal system in the Geneva basin (Switzerland). This region is characterised by strike-slip and thrust faults [1] that increase locally the permeability. These structures are targeted by geothermal projects. We analyse logging data collected during drilling operations, especially optical and acoustic televiewers, and full-waveform sonic data. The study focusses on the assessment of fracture distribution, mechanical characteristics and stress state of the limestone surrounding the exploration well GEo-01.

Methods

Wellbore images analyses

We identify the fractures (Figure 1) and determine their orientation, dip angle and aperture based on the optical and acoustic images of the well. Transit time measurements recorded by the acoustic tool are converted into radius to analyse the well shape.

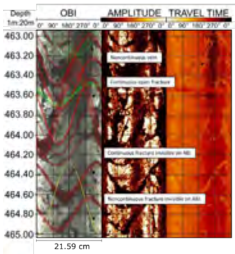

Figure 1: Fractures displayed on optical and acoustic televiewers.

Rock mechanical properties

From the full-waveform sonic data, we extract estimations of the P-wave and S-wave velocities of the formation using a semblance analysis [2]. We combine with density log to calculate the Poisson's ratio (ν), and the Young's modulus (*E*) of the rock assuming a linear elastic and isotropic rock:

$$\upsilon = \frac{V_p^2 - 2V_s^2}{2(V_p^2 - V_s^2)} \quad ; \quad E = \frac{\rho {V_s}^2(3{V_p}^2 - 4{V_s}^2)}{{V_p}^2 - {V_s}^2} \qquad \text{Eq. 1}$$

Stress state

An estimation of the expected vertical stress magnitude is obtained by the integration of density data (Eq. 2). Bounds on allowable horizontal stresses is calculate by considering purely frictional stability (Eq. 3) for a coefficient of friction μ of 0.6 and 1.0 (Figure 2).

$$S_v = \int_0^z \rho(z) g dz \qquad \text{Eq. 2}$$

$$\frac{\sigma_1 - P_p}{\sigma_3 - P_p} = [(\mu^2 + 1)^{\frac{1}{2}} + \mu]^2 \qquad \text{Eq. 3}$$

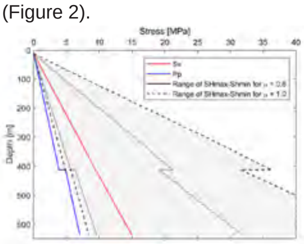

Figure 2: Ranges of SHmax, Shmin, Sv and Pore pressure expected in the well.

We further constrain the horizontal stress magnitudes by estimating the impact of stiffness contrast between the various layers of our sedimentary column determined from the sonic logging data. We apply a displacement boundary mimicking tectonic loading to a finite element stress model consisting of 14 layers. Stiffer layers attract larger stress magnitude (Figure 3).

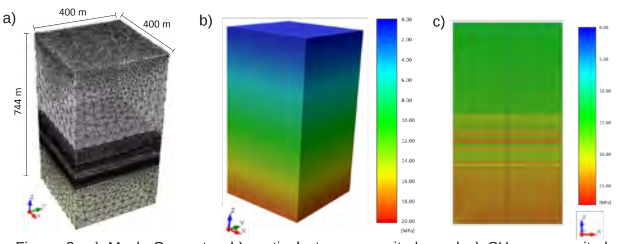

Figure 3: a) Mesh Geometry, b) vertical stress magnitude and c) SHmax magnitude variations induced by displacement.

Fracture slip tendency

Having measurements for the fractures orientations and an estimate of the in-situ stress state, we can compute the slip tendency (*Ts*) on the fractures defined as the ratio of shear (τ) to normal tractions (σ_n) resolved on the fracture planes (Eq. 4). Fractures with larger slip tendency are closer to shear failure [3] and are often considered as the active flow paths in the fractured rock mass [4].

$$T_s = \frac{\tau}{\sigma_n} \qquad \text{Eq. 4}$$

Results

A synthesis of our stress and fracture data are presented in Fig. 4. An important clockwise rotation of the fracture orientation is observed according to depth (Figure 4). Between 460.0 and 480.0 meters deep, steeper dip angles and highly fractured carbonates highlight interaction of the wellbore with a faulted zone. It induces local stress heterogeneities in the vicinity of the well and stimulate the development of fractured networks.

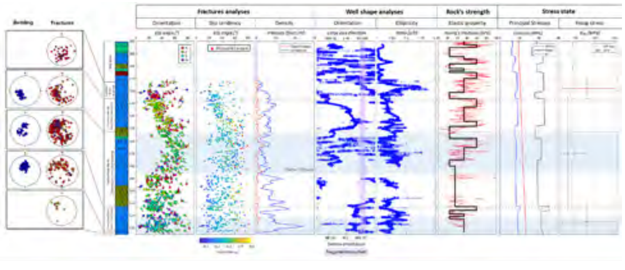

Figure 4: Fractures characterisation, borehole shape analyses, rock's strength evaluation and stress state estimation along the GEo-01 borehole.

Sections characterised by water inflows present critically stressed open fractures. The latter might enhance the permeability of the fracture limestone reservoir and significantly contribute to fluid circulations by creating important hydraulic conduits.
According to shale content variations, large stiffness contrasts appear at stratigraphic limits and could be responsible for important variations of the in situ stress magnitude and of the fracture orientation.

Conclusions

These rock physical analyses highlight that the presence of a faulted zone crossing the borehole related to a flower structure in a strike-slip fault oriented NNW-SSE contributes significantly to water inflows. Contrasting Young's modulus values are noticed along the well, influencing the stress accumulation into stiffer layers. The assessment of fracture distribution and rock mechanical properties provide thus good characterisation of the rocks surrounding a geothermal borehole.

Acknowledgements

This work is developed in collaboration with the Industrial Services of Geneva (SIG) and HydroGéo Environnement SA. It takes part in the framework of the European Project HEATSTORE (170153-4401) under the GEOTHERMICA-ERA NET Grant (N° 731117) supported by the the European Commission, RVO (the Netherlands), DETEC (Switzerland), FZJ-PtJ (Germany), ADEME (France), EUDP (Denmark), Rannis (Iceland), VEA (Belgium), FRCT (Portugal), and MINECO (Spain).

References

[1] Clerc, N., Rusillon, E., Moscariello, A., Renard, P., Paolacci, S., and Meyer, M. (2015). Detailed Structural and Reservoir Rock Typing Characterization of the Greater Geneva Basin, Switzerland for Geothermal Resource Assessment, Proceedings World Geothermal Congress 2015, Melbourne, Australia.

[2] Valley, B., Bewick, R. P., and Hudson, R. (2011). Rock and rock mass characterization for deep mining using sonic data. In 45th US Rock Mechanics/Geomechanics Symposium. American Rock Mechanics Association.

[3] Morris, A., Ferrill, D.A., Brent Henderson, D.B.(1996). Slip-tendency analysis and fault reactivation. Geology 24, 275.

[4] Barton, CA, MD Zoback, and D Moos. (1995). Fluid Flow along Potentially Active Faults in Crystalline Rock. Geology 23 (8): 683–86.

SCCER-SoE Annual Conference 2019

SCCER SoE
SWISS COMPETENCE CENTER for ENERGY RESEARCH
SUPPLY of ELECTRICITY

unine
UNIVERSITÉ DE NEUCHÂTEL

Supported by:
Schweizerische Eidgenossenschaft
Confédération suisse
Confederazione Svizzera
Confederaziun svizra
Swiss Confederation
Innosuisse – Swiss Innovation Agency
swisstopo

Determine fault criticality using seismic monitoring and fluid pressure analysis

Léa Perrochet, Giona Preisig, Benoît Valley

Centre for Hydrogeology and Geothermics (CHYN), University of Neuchâtel

Setting, Motivations & Objectives

Better understanding fault criticality, the proximity of a fault to shear failure, is of primary interest when planning underground projects. Stress perturbations in the surroundings of a critically stressed fault, resulting from human activities, can affect the fault's stability - and eventually lead to a forced interruption of projects due to seismic risk.

Changes in the stress state also occur naturally. It has been observed [1] that in karstic regions, an increase in groundwater pressure following significant recharge (precipitations and/or seasonal snowmelt) can result in a fault re-activation, inducing microseismicity.

The aim of this study is to combine the natural microseismicity and groundwater level fluctuations observations to estimate the fault criticality.

To this end, the objectives are to :

- **Monitor microseismicity** of several strike-slip fault in the Jura Mountains;
- Have continuous **spring discharge** and water table **measurements** of the major karstic springs in the vicinity of the faults;
- Determine **relations** between increasing **spring discharge** rates and **low magnitude earthquakes**;
- Develop a **straightforward methodology** to assess fault criticality.
- Generate stress models of the shallow earth's crust based on field data

Theoretical Background

A) In a mature **karst aquifer**, channeling effects allows large and rapid water table fluctuation resulting in a **rapid and important increase in fluid pressure**. This has a direct **effect on discharge rates** at karstic springs.

B) An **increasing fluid pressure** in the deep aquifers and in the fault zone changes the stress-regime by **reducing the effective normal stress**, leading to the shifting of the Mohr circle towards the Coulomb **failure** envelope.

C) Fault slip affects the fault's transmisivity leading to **fluid flow changes**

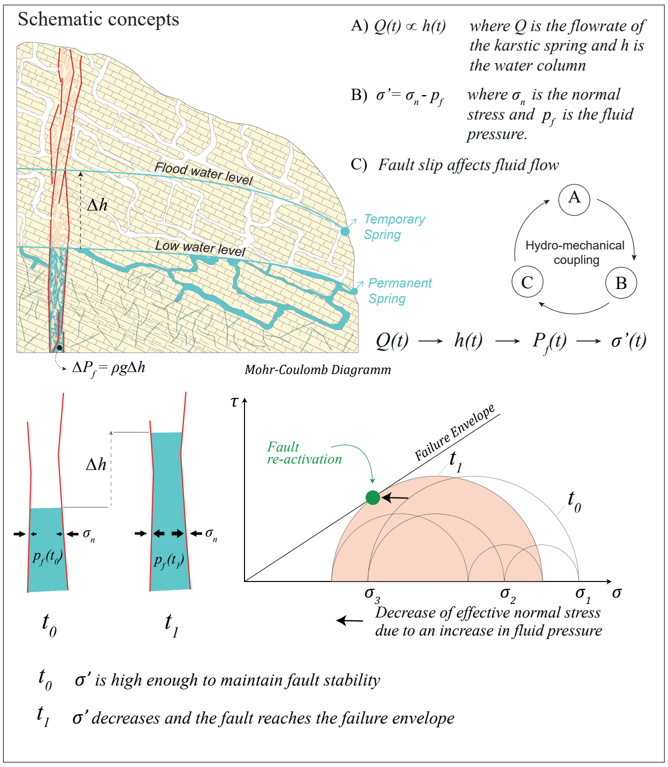

Figure 1 Schematic concept of how karst channeling can influence fluid pressure and consequently the effective normal stress, which can lead to failure and affect the fault's transmisivity and change fluid flow.

Research site, Methods & Data aquisition

The research is carried out on two major strike-slip faults on the northern shore of lake Neuchâtel - La Lance Fault and La Ferrière Fault. Data aquisition mainly consists in (1) hydrogeologic and (2) seismic monitoring.

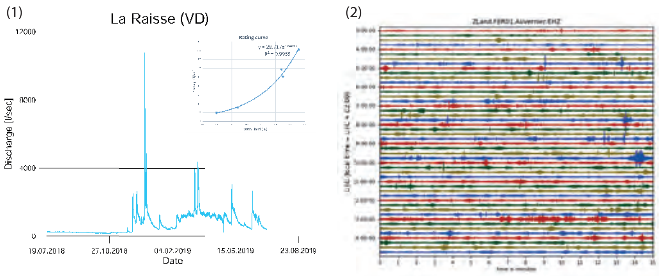

Figure 2 **(1)** 1-year high resolution discharge ratios of the La Raisse Spring near Vaumarcus and the rating curve. **(2)** 12-hours (16.07.2019) recording plot of a 3-Channel geophone installed in Auvernier.

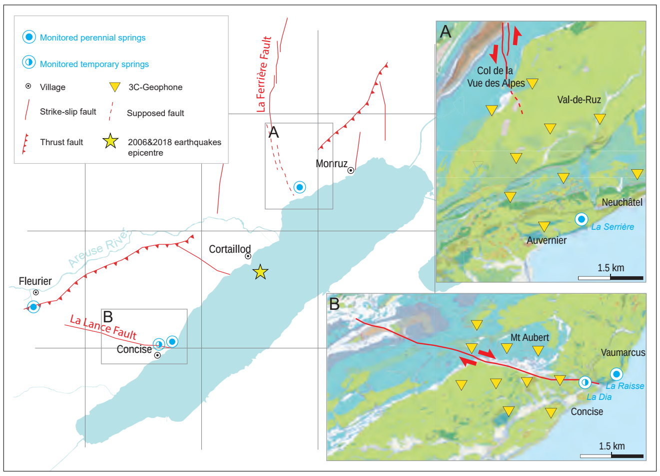

Figure 3 Situation map of the research area. Showing major strike-slip and thrust faults in red, monitored karstic springs and future position of the 3C-geophones. Also shown, epicentre of 2006 and 2018 events (see next section). Data from the geologic and hydrogeologic map [2].

Project Status & Future work

- The hydrogeologic and part of the seismic monitoring stations are in place and **data acquisition on-going**
- **First observations** on historical data [3] revealed two earthquakes with **M_L= 3.2 (2006) and M_L= 1.1 (2018)** occuring during **flowrates** of 1-year return period for the Areuse River **(60-70 m³/s)**. Both events have same epicentre and source (according to waveform similarity theory [4]). Future data will allow more correlation.
- Correlation of seismic patterns with specific flowrates will be used to **develop a quantitative knowledge of what pressure change is affecting fault stability**. This will allow to better constrain the stresses in the Neuchâtel Jura.

Aknowledgments

The project is financially supported by swisstopo and the Swiss Federal Office of Energy.

References

[1] Miller S.A. (2008) *Note on rain-triggered earthquakes and their dependence on karst geology*, Geophysical Journal International, Volume 173, Issue 1, pages 334-338

[2] *https://map.geo.admin.ch Geocover and hydrogeologic map.*

[3] Swiss Seismological Service (SED). *http://www.seismo.ethz.ch*

[4] Geller R. & Mueller C. (1980) *Four similar earthquakes in Central California*, Geophysical Research Letters, 7, 821-824

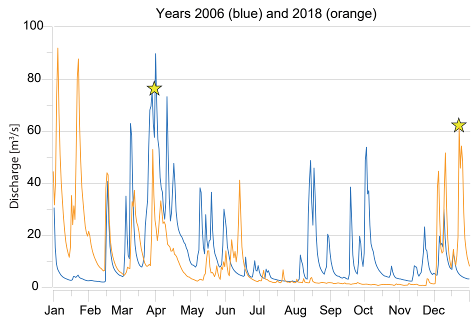

Figure 4 Areuse discharge ratios for 2006 and 2018. Yellow star = earthquake

SCCER-SoE Annual Conference 2019

SCCER SoE
SWISS COMPETENCE CENTER for ENERGY RESEARCH
SUPPLY of ELECTRICITY

Supported by:
Schweizerische Eidgenossenschaft
Confédération suisse
Confederazione Svizzera
Confederaziun svizra
Swiss Confederation
Innosuisse – Swiss Innovation Agency

Anomalous Vp/Vs in pressurized reservoirs: Does it exist and what does it entail?

Lucas Pimienta[1], Beatriz Quintal[2], Eva Caspari[2], & Marie Violay[1]
[1]Laboratory of Experimental Rock Mechanics, EPFL, Lausanne, Switzerland
[2]University of Lausanne, Lausanne, Switzerland

Motivation

Either for prospection or monitoring purposes, one needs to understand the reservoir rocks at depths and its evolution, i.e. the realm of geophysical methods. Field seismics is one main tool that allows enhanced understanding of reservoir rocks at depths. One infers rocks, fluids and their pressure states from the measured seismic attributes: P- and S-wave velocities and attenuations. However, the method relies on a full understanding of the intrinsic elastic properties of fluid saturated rocks and their seismic signature at depth.

P- to S-wave velocity ratio is an attractive property that directly links to rocks Poisson's ratio, an intrinsic property. However, this property is heavily affected by the frequency of measurements (Pimienta et al., 2016; 2017). Thus, the exact same fluid-saturated rock will exhibit very different Vp/Vs if measured with different methods. In the low frequency range relevant to the field scale, Vp/Vs was shown to reach anomalous values of above 2.5 (Pimienta et al., 2018). Here, we aim at investigating the Vp/Vs expected for different reservoir rocks, from the non-porous granites to the high-porosity sandstones.

Project:
- ***PROGRESS:*** *PROspection and PROduction of Geothermal RESservoirS*

Understand the links between physical properties in geothermal reservoir rocks, & get insights for properties at the field scale.

Principle & Method

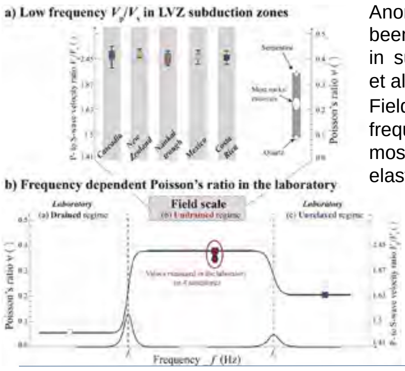

Anomalously high Vp/Vs have been observed in nature (***Fig. a***), in subduction zones (e.g. Audet et al., 2009).

Field's measurements are at a frequency of about 1-100 Hz, mostly relevant to the undrained elastic regime (***Fig. b***).

In isotropic rocks, Vp/Vs links to Poisson's ratio when strain amplitudes are small.

Results : Non-porous rocks

Within the framework of the stress-strain methods, the Poisson's ratio is measured, as a function of frequency, as the ratio of radial-to-axial strains.

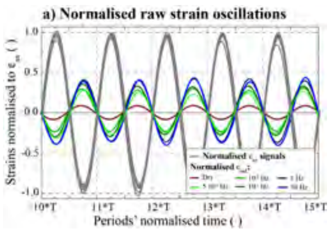

Here, for normalized axial strain, radial strain increases as frequency increases.

Measured Poisson's ratio at a given pressure is inferred from each oscillations, at frequencies relevant to the undrained regime.

From measuring rocks, either dry or undrained, one gets:
- Under dry conditions: Slight dependence on Terzaghi effective pressure.
- Under water-saturated undrained conditions:
  - "Intact" rock: Slight effect of pressures
  - "Cracked" rock: Large decrease with increasing effective pressure (by decreasing pore fluid pressure), starting from values above 0.4 although of different initial Poisson's ratio!

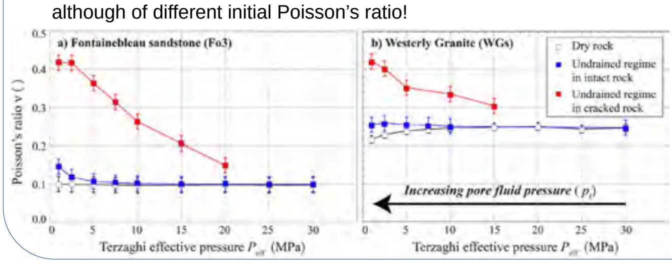

For **non-porous rocks**, consistent with inclusions models for effective medium theory:

Independent of the mineral matrix, Poisson's ratio increases as the concentration of cracks opened by high pore fluid pressure increases.

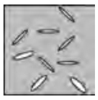

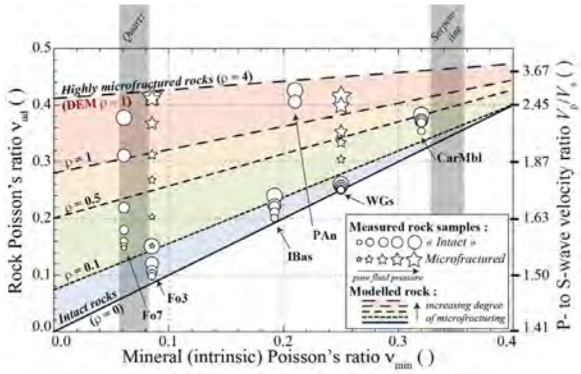

Discussion: High-porosity rocks

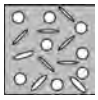

For current strategies to both enhance geothermal systems and heat fluids, tracking seismic Vp/Vs might give insights on the fracture networks and whether they are open or closed.

However, because they would bear much larger permeability, attractive reservoirs rocks for geothermal energy applications need to be porous. It is then of interest to question which Vp/Vs one would get in heavily microcracked rocks. Indeed, owing to their genesis, many sandstones naturally bear open microcracks or grain contacts.

From existing inclusion models of effective medium theories, the effect of two families of pores on the bulk modulus and Poisson's ratio can be predicted for fluids of different compressibility (air, water or glycerine). As the amount of spherical pores (i.e. "porosity") increases, large decreases are expected for both properties.

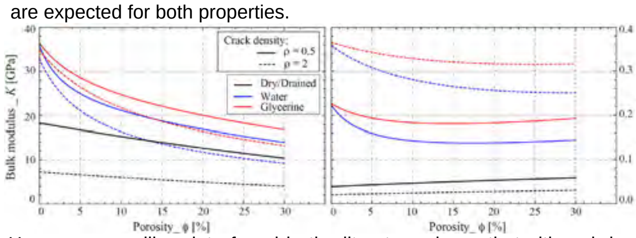

However, compiling data found in the literature shows that although large decrease in bulk moduli are indeed observed, no clear variations in Poisson's ratio can be inferred. Moreover, no effect of fluid compressibility is observed either, implying deviations from standard theories. **A possible explanation is the anisotropic stress solicitation applied on the poroelastic material, similar to that induced by P-waves.**

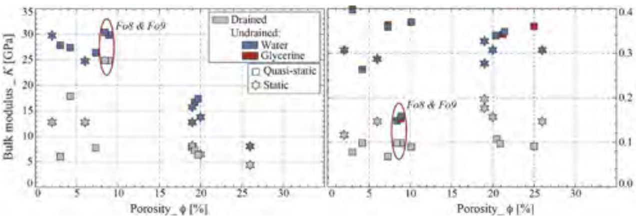

References

- Audet, P., Bostock, M. G., Christensen, N. I., & Peacock, S. M. (**2009**): Seismic evidence for overpressured subducted oceanic crust and megathrust fault sealing, *Nature*, **457**(7225), 76–78.
- Pimienta, L., Fortin, J., & Guéguen, Y. (**2016**): Effect of fluids and frequencies on the Poisson ratio of sandstones, *Geophysics*, **81**(2), D35-D47.
- Pimienta, L., Borgomano, J.V.M., Fortin, J., & Guéguen, Y. (**2017**): Elastic Dispersions and Attenuations in fully saturated sandstones: Role of mineral content, porosity and pressures, *Journal of Geophysical Research*, **122**(12), 2169-9356 .
- Pimienta, L., Schubnel, A., Violay, M., Fortin, J., Guéguen, Y. & Lyon Caen, H., (**2018**): Anomalous Vp/Vs ratios at seismic frequencies might evidence highly damaged rocks in subduction zones, *Geophysical Research Letters*, **45**.

SCCER-SoE Annual Conference 2019

Effects of fracture connectivity on Rayleigh wave dispersion

Gabriel Quiroga, J. Germán Rubino, Santiago Solazzi, Nicolás Barbosa, and Klaus Holliger

Introduction

Passive seismic sensing is widely used in the monitoring of hydrothermal reservoirs to assess the risks that may derive from their exploitation and stimulation (Taira et. al., 2018; Obermann et. al., 2015). One key factor in geothermal reservoirs is fracture connectivity. Changes in this parameter have effects on seismic attenuation, anisotropy, and velocity (Rubino et. al. 2016). In this work, we studied the effects of fracture connectivity on Rayleigh wave dispersion accounting for frequency-dependent poroelastic effects. This may allow the use of seismic data for a better evaluation of geothermal reservoirs.

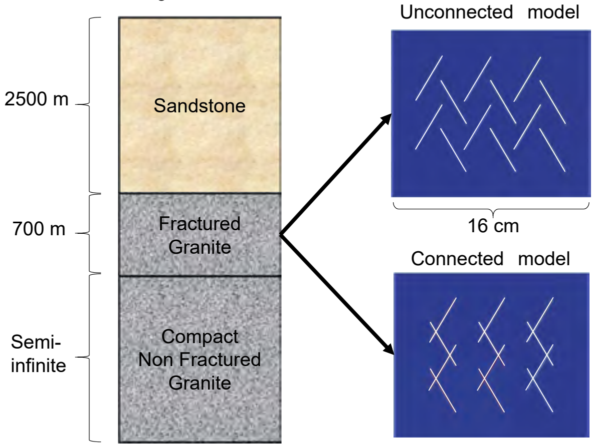

Figure 1. Schematic illustration of the considered three-layer model. The panels on the right show representative samples associated with the fractured reservoir models analyzed in this work.

Methodology and results

We used an upscaling approach based on Biot's poroelasticity theory (Rubino et. al. 2016, Hunziker et. al. 2018) to determine the effective properties of a water-saturated granite with an unconnected and a connected fracture network (Figure 1). This procedure is used to obtain body wave velocities taking into account fluid pressure diffusion effects (Figure 2).

Using the body wave velocities obtained with the upscaling procedure we implement two reservoir models (Table 1). To obtain the Rayleigh wave dispersion for these models (Figure 3) we used the Geopsy software, which is based on a propagation matrix method (Wathelet 2005, 2011).

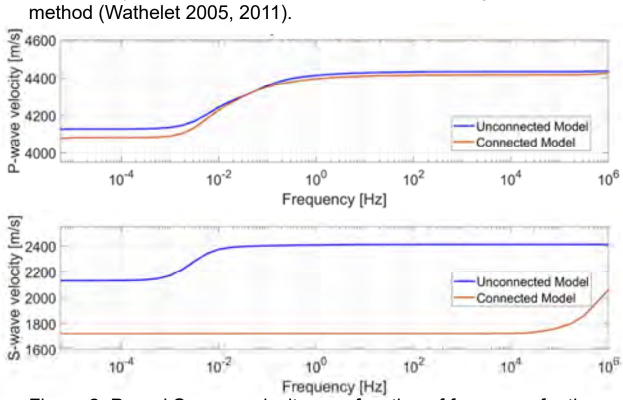

Figure 2. P- and S-wave velocity as a function of frequency for the connected and unconnected granite samples. The frequency range of interest for the Rayleigh wave analysis is highlighted in yellow. It can be appreciated that the relative velocity variation in this region is smaller than 5%, thus allowing the use of constant P- and S- wave velocity values.

Unconnected model			
Layer thickness [m]	Vp [m/s]	Vs [m/s]	Density [kg/m³]
2500	3500	2000	2500
700	4430	2410	2750
Infinite	5040	2620	2770
Connected model			
Layer thickness [m]	Vp [m/s]	Vs [m/s]	Density [kg/m³]
2500	3500	2000	2500
700	4310	1720	2750
Infinite	5040	2620	2770

Table 1. Parameters used for the Rayleigh wave dispersion analysis. Values for the second layer result from the upscaling procedure illustrated in Figure 2.

Conclusions

The Rayleigh wave dispersion exhibits a significant sensitivity to fracture connectivity and thus could be used to monitor fracture connectivity as well as related properties of reservoirs.

For different rock types and fracture models, poroelastic attenuation peaks might fall in the frequency range of interest for Rayleigh wave analysis. In these cases, it would be necessary to consider a non-elastic model for the analysis.

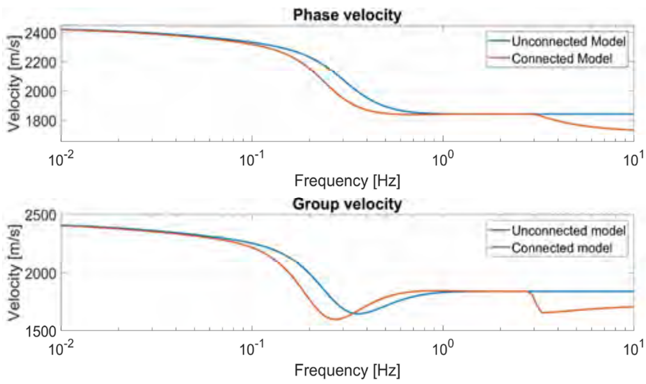

Figure 3. Rayleigh wave dispersion for the connected and unconnected models as functions of frequency. The curves were generated using the GPDC program of the Geopsy applications.

References

Hunziker, J., Favino, M., Caspari, E., Quintal, B., Rubino, J. G., Krause, R., & Holliger, K. (2018). Seismic attenuation and stiffness modulus dispersion in porous rocks containing stochastic fracture networks. *Journal of Geophysical Research: Solid Earth*, *123*(1) , 125-143.

Obermann, A., Kraft, T., Larose, E., & Wiemer, S. (2015). Potential of ambient seismic noise techniques to monitor the St. Gallen geothermal site (Switzerland). *Journal of Geophysical Research: Solid Earth*, 4301-4316.

Rubino, J. G., Caspari, E., Müller, T. M., Milani, M., Barbosa, N. D., & Holliger, K. (2016). Numerical upscaling in 2-D heterogeneous poroelastic rocks: Anisotropic attenuation and dispersion of seismic waves. *Journal of Geophysical Research: Solid Earth*, *121*(9) , 6698-6721.

Taira, T., Nayak, A., Brenguier, F., & Manga, M. (2018). Monitoring reservoir response to earthquakes and fluid extraction, Salton Sea geothermal field, California. *Science Advances*, *4*(1), e1701536.

Wathelet, M. (2005). Array recordings of ambient vibrations: surface-wave inversion. Phd. Thesis, Faculté des Sciences Appliquées, Université de Liège

Wathelet, M. (2011). Geopsy project. Software, LGIT, Grenoble, Fr.

SCCER SoE
SWISS COMPETENCE CENTER for ENERGY RESEARCH
SUPPLY of ELECTRICITY

SCCER-SoE Annual Conference 2019

UNIL | Université de Lausanne
Faculté des géosciences et de l'environnement

Supported by:
Schweizerische Eidgenossenschaft
Confédération suisse
Confederazione Svizzera
Confederaziun svizra
Swiss Confederation
Innosuisse – Swiss Innovation Agency

Seismic signatures of porous rocks containing partially saturated fracture networks

Santiago G. Solazzi, Jürg Hunziker, Eva Caspari, Marco Favino, and Klaus Holliger

Motivation

A great variety of problems and applications throughout the Earth, environmental, and engineering sciences are concernd with detecting and monitoring the displacement of immiscible fluid phases in fractured geological formations. Given that seismic waves tend to be significantly affected by the presence of hydraulic and mechanical heterogeneities, the seismic method may permit to better characterize partially saturated and fractured environments. In this work, we explore the behaviour of seismic attenuation and phase velocity dispersion due to mesoscopic wave-induced pore fluid pressure diffusion in a brine-saturated porous rock containing a fracture network. We analyse these seismic signatures before and after a CO_2 invasion process. Our results suggest that information about the presence and, more importantly, about the spatial distribution of the CO_2 plume can be retrieved based on the analysis of time-lapse seismic data.

Methodology

- We consider a porous medium that contains an anisotropic stochastic fracture network with a backbone, that is, a connected path for fluid flow (Hunziker et al., 2017). Fracture dip is limited to angles between 30º and 150º, where 0º denotes a vertical fracture and 90º a horizontal one.
- An invasion percolation procedure is employed to simulate the CO_2 displacement through the initially brine-saturated fractured medium (Masson & Pride, 2004). We perform a Monte Carlo analysis of the resulting fluid distribution considering pseudo-random invasion potentials within the fractures.
- We use a numerical upscaling procedure based on poroelasticity theory to obtain the seismic attenuation and phase velocity dispersion of a sub-sample of the medium for different frequencies (Rubino et al., 2016).

Results

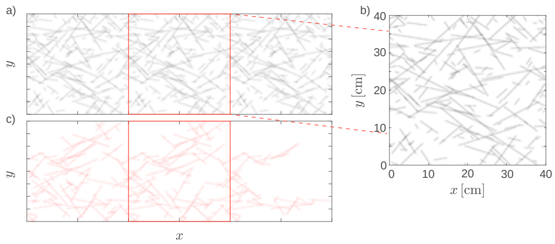

Figure 1: (a) Fracture network considered in the flow simulations and (b) sub-sample considered when exploring the seismic signatures. (c) CO_2-invaded fractures (red) resulting from a single invasion percolation realization.

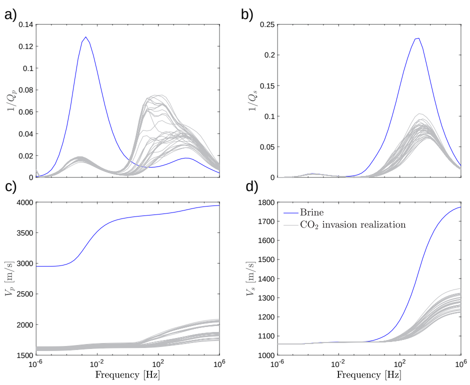

Figure 2: Inverse quality factor and phase velocity as functions of frequency for (a) and (c) P- and (b) and (d) S-waves travelling in the *y*-direction. We illustrate the fully brine-saturated scenario (blue line), which represents the seismic response prior to the invasion, and 32 curves associated with different invasion percolation realizations (grey lines).

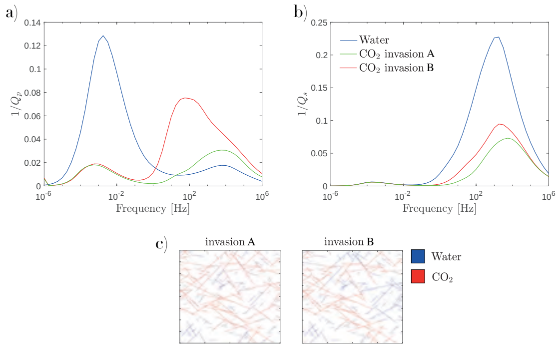

Figure 3: Inverse quality factor as a function of frequency for (a) P- and (b) S-waves for the bine-saturated scenario (blue line) and after two invasion percolation realizations with contrasting characteristics, invasions A (green line) and B (red line). Panel (c) illustrates the fluid distributions associated with the considered models.

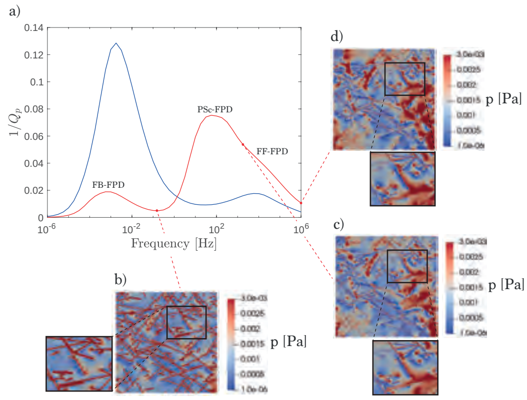

Figure 4: (a) Inverse quality factor as a function of frequency for the fully brine-saturated scenario (blue line) as compared to the partially saturated scenario generated by invasion B (red line). Labels over the attenuation peaks refer to the prevailing fluid pressure diffusion process (FPD), namely, fracture-to-background (FB), partially saturated clustering (PSc), and fracture-to-fracture (FF) flow. Panels (b), (c), and (d) illustrate the pressure fields associated with 0.1 Hz, 1E3 Hz and 1E6 Hz.

Conclusions

In this work, we have analysed the effects partial saturation on a porous rock containing a fracture network. Our results show that the presence of CO_2 in fractures can significantly reduce the phase velocity, particularly for P-waves. We also note that, for P-waves, dissipation levels due to fracture-to-background are reduced and the corresponding effects due to fracture-to-fracture flow are enhanced when compared to the brine saturated scenario. Conversely, we observe a reduction in the attenuation levels due to fracture-to-fracture flow after CO_2 invasion for S-waves. Interestingly, information regarding the fluid distribution within the fracture network is also present in the seismic signatures. Particularly, when CO_2 is not evenly distributed throughout the probed rock sample, P-waves are affected by a new fluid pressure diffusion process taking place between partially saturated and brine saturated zones.

References

Hunziker, J., Favino, M., Caspari, E., Quintal, B., Rubino, J. G., Krause, R., & Holliger, K. (2018). Seismic attenuation and stiffness modulus dispersion in porous rocks containing stochastic fracture networks. *J. Geophys. Res*, *123*(1), 125-143.

Masson, Y & Pride, S. R. (2014). A fast algorithm for invasion percolation, *Transp. Porous Med.*, 102(2), 301-312.

Rubino, J. G., Caspari, E., Müller, T. M., Milani, M., Barbosa, N. D., & Holliger, K. (2016), Numerical upscaling in 2D heterogeneous poroelastic rocks: Anisotropic attenuation and dispersion of seismic waves, *J. Geophys. Res.*, 121, 6698-6721.

SCCER SoE
SWISS COMPETENCE CENTER for ENERGY RESEARCH
SUPPLY of ELECTRICITY

SCCER-SoE Annual Conference 2019

Supported by:
Schweizerische Eidgenossenschaft
Confédération suisse
Confederazione Svizzera
Confederaziun svizra
Swiss Confederation
Innosuisse – Swiss Innovation Agency

CONICET

UNIL | Université de Lausanne
Institut des sciences de la Terre

Poroelastic effects of the damaged zone on fracture reflectivity

UNIVERSITÉ DE GENÈVE

Edith Sotelo, Santiago G. Solazzi, J. Germán Rubino, Nicolás D. Barbosa, Klaus Holliger

Motivation

Studies show evidence of a zone of microfractures surrounding fractures and faults.

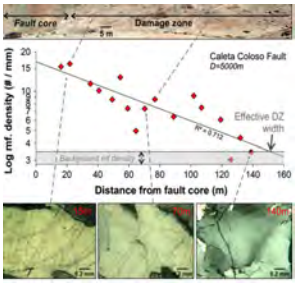

Figure 1. Microfracture density versus distance from fault core and thin sections below. Modified from Mitchell and Faulkner (2012).

Hydraulic changes of the damaged zone can promote fluid pressure diffusion from the fracture as seismic waves travel through the system. This process, together with the damaged zone mechanical weakening are expected to affect the reflectivity of the system.

Methodology

a) Reference model

b) Model with damaged zone

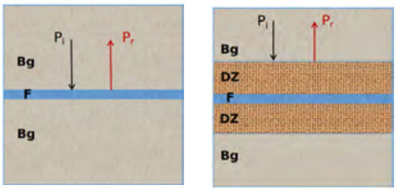

Figure 2. Reference model and model with damaged zone.

- P_i is the normally incident fast P-wave. P_r is the reflected P-wave.

- **Bg** is the background rock, **DZ** is the damaged zone and **F** is the fracture.

We compute the reflection coefficients at the F-Bg interface (Figure 2a) and the DZ-Bg interface (Figure 2b), respectively.

To find amplitudes, we formulate a system of equations by setting continuity of traction and pressure as well as continuity of solid and relative fluid displacements at each interface.

Following Barbosa et al. (2016), we use Biot's theory (Biot, 1962) to formulate pressures, tractions, and displacements since it accounts for fluid pressure diffusion effects.

Results

Property	Background	Fracture
Permeability (D)	10^{-6}	100
Grain bulk modulus (GPa)	36	36
Grain density (g/cm³)	2.7	2.7
Porosity	0.15	0.8
Frame bulk modulus (GPa)	9	0.056
Frame shear modulus (GPa)	7	0.033
Tortuosity	3	1
Thickness (m)	-	0.001
Fluid density (g/cm³)	1	
Fluid bulk modulus (GPa)	2.25	
Fluid viscosity (P)	0.01	

Table 1. Reference model properties according to Barbosa et al. (2016)

Unless stated otherwise, the properties of the damaged zone are the same as those of the background except for permeability.

Sensitivity to permeability and thickness of the damaged zone

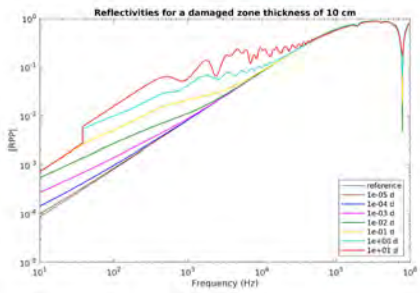

Figure 3. P-wave reflectivity for a model with a damaged zone of 10 cm thicknes and with different values of permeability.

Reverberations at high frequencies can be associated with scattering within the damaged zone and the fracture.

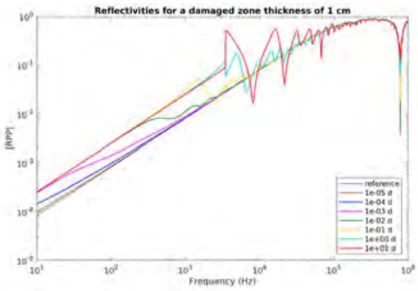

Figure 4. P-wave reflectivity for a model with a damaged zone of 1 cm thickness and with different values of permeability.

Effect of decreasing the damaged zone mechanical properties

We decrease the frame bulk and shear moduli of the damaged zone by 20%, 50%, and 80% with respect to its reference values (background, Table 1). The thickness of the damaged zone is 10 cm.

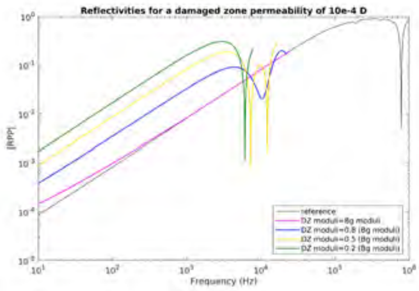

Figure 5. P-wave reflectivity for models with weaker damaged zones, and with a permeability of 10^{-4} D.

The truncation of curves is associated with numerical issues in the matrix inversion.

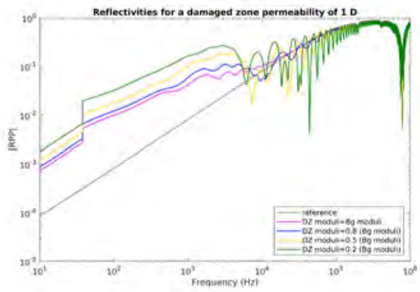

Figure 6. P-wave reflectivity for models with weaker damaged zones, and with a permeability of 1 D.

Jumps at lower frequencies may suggest a background-damaged zone fluid interaction, but further investigation is needed to explain this behavior.

Discussion and Conclusions

As shown in Figures 3 and 4, accounting only for the permeability enhancement associated with the damaged zone increases the reflectivity. This effect is explained by the increase of fracture compliance when fluid pressure diffusion occurs from the fracture to the damaged zone.

As shown in Figures 5 and 6, mechanical weakening of the damaged zone increases the reflectivity, thus showing the effect of enhancing the mechanical contrast with the background.

Further studies are needed to fully asses the presence of reverberations at higher frequencies, jumps at lower frequencies, and of other local features in the reflectivity curves.

Reference

Barbosa, Nicolás D., et al. (2016) "Fluid pressure diffusion effects on the seismic reflectivity of a single fracture." The Journal of the Acoustical Society of America 140(4), 2554-2570.

Biot, M. A. (1962). "Mechanics of deformation and acoustic propagation in porous media." Journal Applied Physics 33, 1482–1498.

Mitchell, T. M., and D. R. Faulkner (2012). "Towards quantifying the matrix permeability of fault damage zones in low porosity rocks." Earth and Planetary Science Letters 339, 24-31.

SCCER-SoE Annual Conference 2019

SCCER SoE
SWISS COMPETENCE CENTER for ENERGY RESEARCH
SUPPLY of ELECTRICITY

Supported by: Schweizerische Eidgenossenschaft, Confédération suisse, Confederazione Svizzera, Confederaziun svizra. Swiss Confederation. Innosuisse – Swiss Innovation Agency

Where are the favorable locations for deep geothermal in Switzerland ?

Benoît Valley & Stephen A. Miller

Centre for Hydrogeology and Geothermics (CHYN), University of Neuchâtel, Switzerland

benoit.valley@unine.ch

Motivation

We know conceptually what features constitute favorable targets for geothermal projects (Fig. 1), however optimally targeting projects remains challenging. Numerous data sets have been compiled over the last few years to assist geothermal exploration.

- How can we combine these data to identify favorable locations for geothermal projects ?
- What limitations exists in our data and method to successfully target deep geothermal projects ?

The objective of this contribution is to answer these questions by an attempt to compute a geothermal favorability index for the Swiss plateau based on the currently available data.

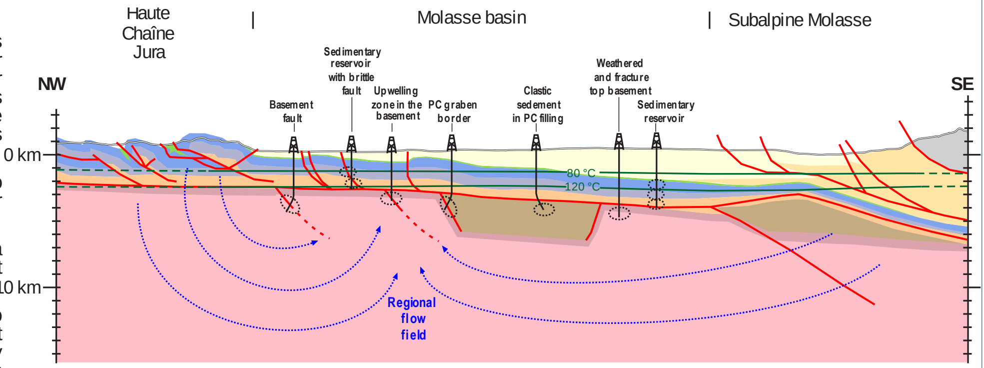

Figure 1: Cross-section through the swiss plateau after Burkhard and Sommaruga (1998) with a representation of the conceptual targets for deep geothermal.

Data set

In this work we compiled and combined the following data sets and information:

- Hydrostratigraphy (Chevalier et al. 2010)
- Mechanical stratigraphy (Hergert et al., 2015)
- Geomol horizon model (swisstopo)
- Geomol fault model (swisstopo)
- Geomol temperature model (swisstopo)
- Heat fllow map (swisstopo)
- Spring and thermal spring locations (Hydr. Atlas of CH, Sonney and Vuataz; 2008)
- Evaluation of regional flow pattern
- Stress field estimation with a Swiss-scale finite element stress simulation
- Earthquake catalog of Switzerland (download from SED website)

We defined 11 favorability criteria computed from one or a combination of the datasets listed above. For each criteria a favorability index ranging from 0 (=unfavorable) to 1 (= favorable) was computed. We performed our analyses on a 1km x 1km grid covering the extend of the geomol model. In addition, we focus on two specific temperature levels: 80°C and 120°C, being the typical minimum temperature level for direct use and electricity production, respectively. We show here the results of the computation for the 80°C temperature target.

Criteria 1: depth to target temperature
We give higher favorability when the target temperature of 80°C is reached at shallower depth.

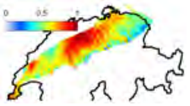

Criteria 2: heat flow
High heatflow is indicative of enhanced heat transport through advection and thus area with higher heat flow are rated with a higher favorability index

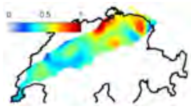

Criteria 3: Seismic event density
Higher seismic density are associated with damage in the crust and fluid flow. We give thus higher favorability for area with higher seismic events density. We recognize that seismic risk must be assessed separately

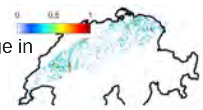

Criteria 4: Lithogical control
Impervious lithologies (aquicludes) are unfavorable while aquifer formation favorability are rated according to the aquifer thickness (thick aquifer are most favorable).

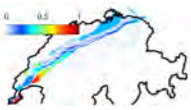

Criteria 5: distance to faults
Faults enhance rock mass damage favoring permeability. Location close to faults are rated favorably.

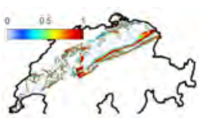

Acknowledgements
We acknowledge the support from R. Reynolds and R. Allenbach from swisstopo in providing the geomol structural and temperature datasets. B. Valley is supported by the Swiss Competence Center for Energy Research (SCCER-SoE).

Criteria 6: Slip tendency
Critically stressed faults with high slip tendency are considered favorable to host deep seated fluid flow. We combined here the stress model and the fault data to give higer favorability to location close to faults with high slip tendency.

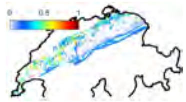

Criteria 7: Dilation tendency
Location close to faults with low normal stress (high dilation tendency) are rated favorably.

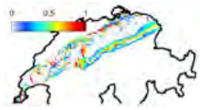

Criteria 8: Von Mises stress
Stiff formation attracting stresses will be more fractured and thus are rated more favorably. We derive this index from the stress model results.

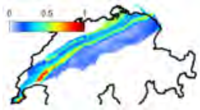

Criteria 9: Regional flow pattern
Regional high recharge area (downward flow) are rated less favorably than regional discharge areas.

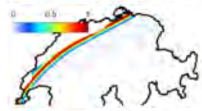

Criteria 10: Regional springs
The proximity of regional spring a indicative of water flow pathways and thus rated as favorable

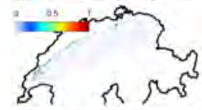

Criteria 11: Thermal springs
Thermal springs denote up flow area and are indicative of favorable conditions for geothermal projects.

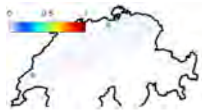

Combined favorability index
The combination of all criteria is shown on Fig. 2. Sharp contrast in favorability can be highlighted on the swiss plateau and these contrasts can guide exploration. However, this as to be considered as a preliminary approach and also at a scale that is not appropriate for local scale exploration planning. Future approaches will include a more careful analyses of the elements leading to the combined favorability map. Another important element will be to include data from exploration projects in order to based the weighting scheme on a more robust ground. The methodology and results presented here are bound to evolve when more data becomes available.

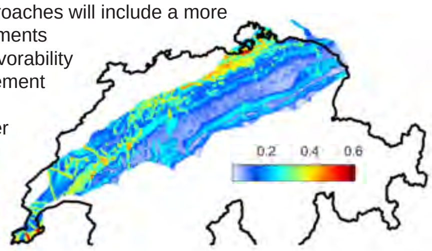

Figure 2: Combined favorability index for 80°C geothermal targets.

References

Burkhard M, Sommaruga A (1998) Evolution of the western Swiss Molasse basin: structural relations with the Alps and the Jura belt. Geol Soc Lond Spec Publ 134:279–298. doi: 10.1144/GSL.SP.1998.134.01.13

Chevalier G, Diamond LW, Leu W (2010) Potential for deep geological sequestration of CO2 in Switzerland: a first appraisal. Swiss J Geosci 103:427–455. doi: 10.1007/s00015-010-0030-4

Hergert T, Heidbach O, Reiter K, et al (2015) Stress field sensitivity analysis in a sedimentary sequence of the Alpine foreland, northern Switzerland. Solid Earth 6:533–552. doi: 10.5194/se-6-533-2015

Sonney R, Vuataz F-D (2008) Properties of geothermal fluids in Switzerland: a new interactive database. Geothermics 37:496–509

SCCER SoE

SWISS COMPETENCE CENTER for ENERGY RESEARCH
SUPPLY of ELECTRICITY

SCCER-SoE Annual Conference 2019

Supported by:

Schweizerische Eidgenossenschaft
Confédération suisse
Confederazione Svizzera
Confederaziun svizra

Swiss Confederation

Innosuisse – Swiss Innovation Agency

Geochemical evidence for large-scale and long-term topography-driven groundwater flow in orogenic crystalline basements

Christoph Wanner[1], H. Niklaus Waber[1], Kurt Bucher[2]

[1]Rock–Water Interaction, Institute of Geological Sciences, University of Bern
[2]Mineralogy and Petrology, University of Freiburg, Germany

Motivation

Orogenic belts without active igneous activity are recognized as plays for geothermal energy. In these systems, meteoric water circulation is typically expressed by thermal springs discharging at temperatures up to 70 °C from deep-reaching faults. The hydraulic gradients that drive circulation arise from the conjunction of high orographic precipitation, mountainous topography and permeable faults that link topographic highs with valley floors via the hot bedrock. Since the bedrock geotherm is the only source of heat for the circulating water, its maximum depth of penetration defines the maximum temperature attainable by surface springs and their upflow zones, thereby setting limits on their potential for geothermal energy exploitation. In the framework of the SCCER-SoE Task 1.1 we have conducted large-scale (20 x 10 x 9 km) thermal-hydraulic-chemical (THC) simulations of meteoric water circulation within a selected domain of the Aar Massif hosting the Gotthard railbase tunnel in the Central Alps, Switzerland, to better understand THC processes in orogenic crystalline basements and to assess their role in generating exploitable heat anomalies.

Geological and hydrogeochemical constraints

- Study relates to the Amsteg section of the Gotthard railbase tunnel with steeply dipping granitic rock units and fracture systems
- 122 groundwater samples were collected during tunnel construction (2003–2006) and subsequently analyzed (Bucher et al., 2012)
- Stable water-isotope analyses reveal a meteoric fluid origin
- Water samples collected beneath the only major valley of the section, the Maderaner Valley, are supersaturated with respect to chalcedony
- This is a typical feature of ascending thermal waters and indicates that these samples have infiltrated into the tunnel from below
- A distinct salinity peak (e.g. [Cl]) appears at ca.10 km along the tunnel, roughly consistent with the identified upflow zone
- Matrix porewater (i.e. remnants of ancient hydrothermal fluids) is the most likely Cl source. [Cl] may thus operate as a residence time tracer
- Low [Cl] beneath major mountain peaks (e.g. Chrüzlistock) suggest short residence times and hence infiltration into the tunnel from above
- The postulated up- and downflow zones are consistent with the occurrence of two distinct water types along the tunnel (see Fig. 1f)
- Water temperatures correlate with over-burden and do not show any anomalies

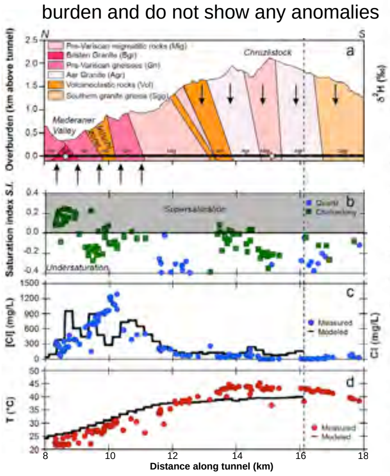

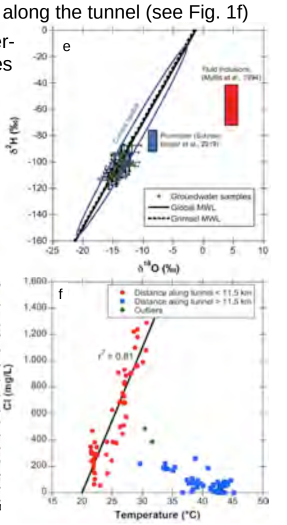

*Fig. 1: Profiles along the Amsteg section of the Gotthard railbase tunnel. **(a)** Geological units and flow zones inferred form geochemical constraints. **(b)** Saturation indices of quartz (pH>9.5) and chalcedony (pH<9.5) in groundwater samples. **(c)** Measured and computed [Cl] of groundwater samples. **(d)** Measured and computed temperatures of groundwater samples. **(e)** Stable O-H isotope signatures of 30 groundwater samples. **(f)** [Cl] of all 122 groundwater samples plotted against their discharge temperature.*

Model setup

- Horizontal extent constrained by the catchment of the Maderaner Valley
- Upper model boundary specified based on digital elevation model
- Fixed *P* and *T* at upper model boundary (1 bar, 4 °C)
- Initial conductive temperature distribution considering a geothermal gradient of 25 °C/km; initial hydrostatic *P* distribution
- Depth dependent permeability and porosity (Stober & Bucher, 2015)
- Uptake of Cl abstracted by defining a hypothetical $NaCl_{(s)}$ source with a fixed dissolution rate ($NaCl_{(s)} = Na^+ + Cl^-$)

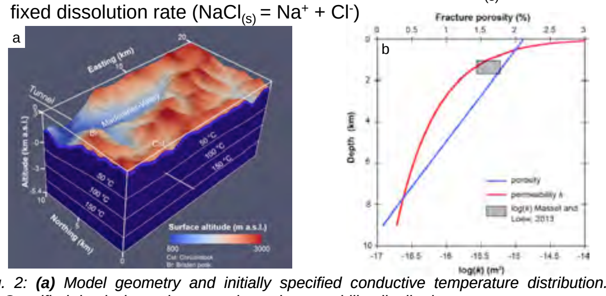

*Fig. 2: **(a)** Model geometry and initially specified conductive temperature distribution. **(b)** Specified depth-dependent porosity and permeability distribution.*

Results and discussion

- Model predicts downflow (v_z<0) of meteoric water at high altitude, and upflow (v_z>0) beneath major valleys (Fig. 4a)
- Meteoric water infiltrating at the surface reaches the lower model boundary and hence attains *T* > 150 °C (Fig. 4b)
- Despite such deep circulation, the model predicts only a minor *T* anomaly beneath the Maderaner Valley (see 50 °C isotherm)
- The model is able to capture observed [Cl] and temperatures, as well as up- and downflow zones identified from geochemical constraints (Fig. 1)
- The model predicts slow upflow rates below 2 m/year. Such low water fluxes, is the likely reason major thermal anomalies are absent
- Slow water circulation also results in residence times that may exceed 100'000 years (Fig. 3)

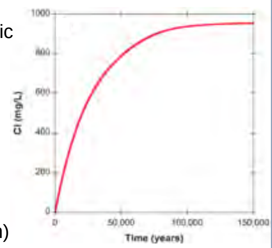

Fig. 3: Simulated Cl breakthrough below the Maderaner Valley.

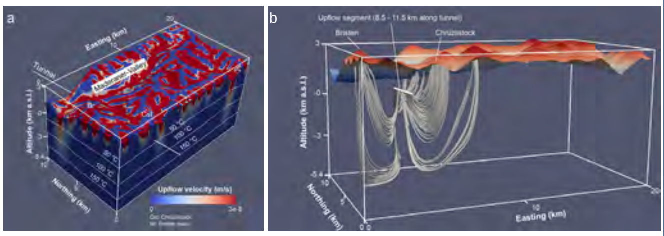

*Fig. 4: **(a)** Upflow velocity distribution (i.e. positive z-component of the computed flow vectors) and steady state isotherms. **(b)** Streamlines of meteoric water infiltrating at the upper model boundary and discharging into the tunnel along the identified upflow zone (Fig. 1a)*

Implications for exploration for orogenic geothermal systems

- Surface topography and meteoric water infiltration form the main controls on fluid flow in orogenic geothermal systems
- Down to 9 km depth, penetration of meteoric water is not limited by the decrease in permeability typical of granitic basement rocks
- Temperature anomalies and hence exploitable geothermal systems preferably form when steeply-dipping, major faults zones with elevated permeability intersect with valley floors

References: Bucher K., Stober I. & Seelig U. (2012). Chem. Geol. 334, 240-253**.** Masset O. & Loew S. (2013) Eng. Geol. 164, 50-66. Schneeberger R., Kober F., et al. (2019) NTB 19-01. Mullis J., Dubessy J., et al. (1994) Geochim. Cosmochim. Acta 58, 2239-2267. Stober I. & Bucher K. (2015) Geofluids 15, 161-178.

Task 1.2

Title

Reservoir stimulation and engineering

Projects (presented on the following pages)

SCCER-SoE Annual Conference 2019

A true triaxial frame for hydraulic stimulation

Thomas Blum, Dmitry Loginov, Brice Lecampion
Geo-Energy Laboratory - Gaznat chair on Geo-energy, EPFL, Lausanne, Switzerland

Elastic wave monitoring system

- 64 piezoelectric transducers arranged in 32 sources and 32 receivers (800 kHz)
- Both longitudinal and shear transducers in order to use both P- and S-waves
- Sequential excitation of all 32 sources up to every few seconds for snapshots of the mechanical properties during fracture propagation, using the following arrivals:

R – reflected signal → fluid content of the fracture
D – diffracted signal → position of the fracture tip
T – transmitted signal → fracture thickness

Piezo transducer schematic

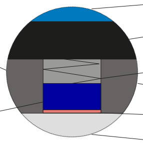

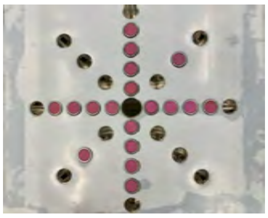

Piezo transducers array

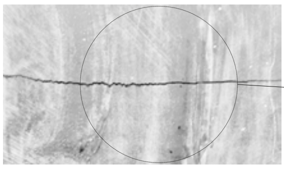

Visible fracture on one side of the block

Top-view photo inside the reaction frame, with flat-jacks and platen on the sides of the specimen, and platen with piezo transducers on top.

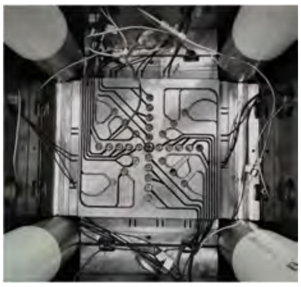

Experimental setup characteristics

- Cubic geologic specimen, 250 x 250 x 250 mm
- Reaction frame: confining stresses of up to 25 MPa along each axis
- Independently controlled pairs of flat-jacks to apply confining stresses
- High-pressure injection pump: flow rate from 1 μL/s to 100 mL/s
- 51 MPa maximum injection pressure
- Notch at the bottom of the wellbore for localized initiation
- Experiment duration on the order of minutes to a few hours

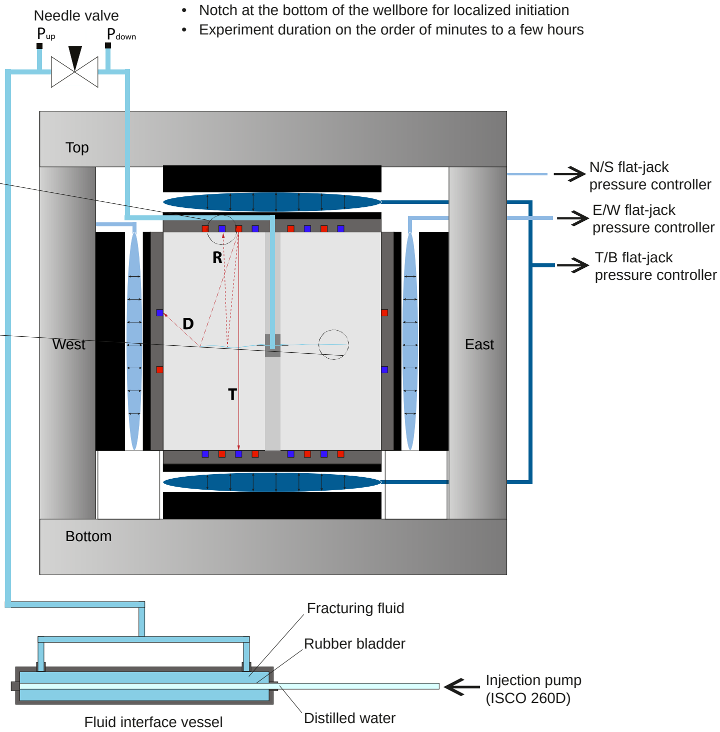

Examples of elastic wave data

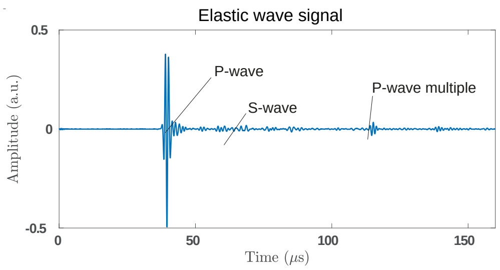

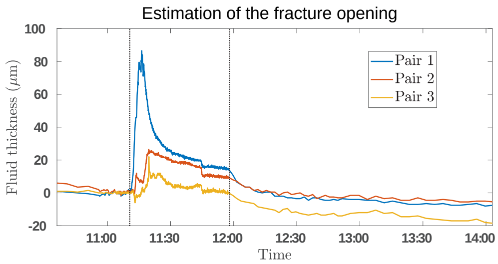

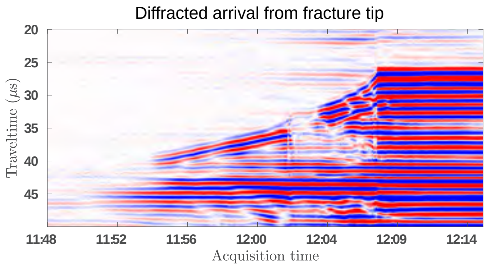

HF propagation in a Carmen slate specimen

- Applied stresses: 0.5 MPa vertical, 20 MPa perpendicular to bedding, 2 MPa in remaining horizontal direction
- Injection performed with Glycerol (μ = 0.6 Pa·s), flow rate = 0.6 mL/min
- Toughness-dominated regime of propagation

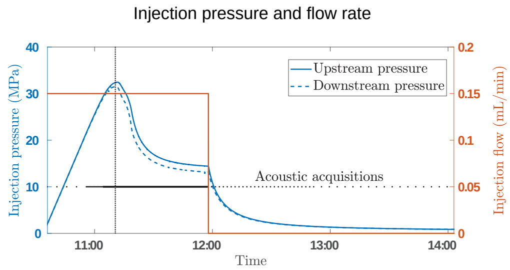

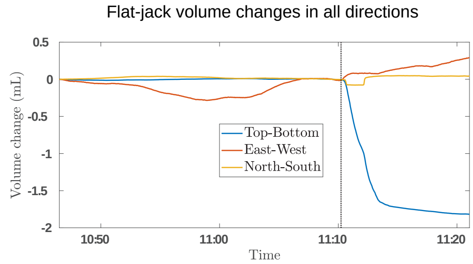

Post-mortem photos of the fractured specimen

Part of the fluid-driven fracture surface (perpendicular to bedding)

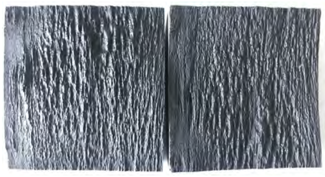

SCCER-SoE Annual Conference 2019

EPFL

FNSNF Fonds national suisse · Schweizerischer Nationalfonds · Fondo nazionale svizzero · Swiss National Science Foundation

Schweizerische Eidgenossenschaft
Confédération suisse
Confederazione Svizzera
Confederaziun svizra

Swiss Federal Office of Energy SFOE

Fluid induced aseismic slip in a Discrete Fracture Network: marginally pressurized vs critically stressed case

Federico Ciardo, Brice Lecampion

Geo-Energy Laboratory - Gaznat chair on Geo-energy, EPFL, Lausanne, Switzerland

Research context and motivation

Under the **2050 Swiss Energy Strategy**, nuclear power is to be replaced by renewables. In this context, **deep geothermal energy** represents an attractive source of of energy.
A better understanding of **hydro-shearing stimulation** of enhanced geothermal systems is required in relation to **induced seismicity**. To this end, we aim at:
- providing robust numerical tools to simulate hydraulic stimulation of fractured rock masses
- getting insight into the physical governing phenomena, with the ultimately goal of helping engineers during operational decisions.

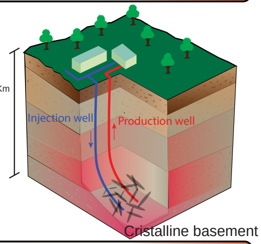

Model assumptions

- Homogenous, isotropic and linear elastic host medium
- Plane strain conditions
- Fractures permeability (constant) way larger than host medium permeability
- No thermal effects and no shear-induced dilatancy
- Neutral friction condition
- Pressure control type of injection (moderate scenario)

Numerical framework

- Displacement discontinuity method for elasticity (BEM)
- Finite volume scheme for fluid flow
- Hierarchical matrix technique combined with Adaptive Cross Approximation
- One-way coupled HM problem solved with a fully implicit scheme
- Adaptive time stepping based on crack velocity

DFN generation & dimensionless governing parameters

- Power law distribution for fracture length with cut-off for min. and max. fracture lenghts
- Uniform distribution for fracture location and orientation within the characteristic area

Stress criticality: $\Lambda = \frac{\kappa - 1}{f}\frac{\mathrm{Cot}(\theta)}{(\kappa \mathrm{Cot}(\theta)^2+1)}$ Normalized over-pressure at injected fracture k_{inj} : $\frac{\Delta P}{t'^{,k_{inj}}_{n,o}}$

Observations & future perspectives

- For a marginally pressurized DFN, the slipping patch is driven by fluid flow diffusion whose front is located well ahead the slipping patch front.
- On the contrary, for a critically stressed DFN, the fast expansion of slipping patch is mainly driven by stress interaction between fractures. The fluid front is located well inside the slipping patch.
- At which scale a macroscopic fault (shear) zone is created upon fluid injection?

MARGINALLY PRESSURIZED DFN

$\frac{\Delta P}{t'^{,k_{inj}}_{n,o}} = 0.5$

$f = 0.6$

$\kappa = \frac{\sigma'_{xx}}{\sigma'_{yy}} = 2$

$(x_{inj}, y_{inj}) = (1, 1)$

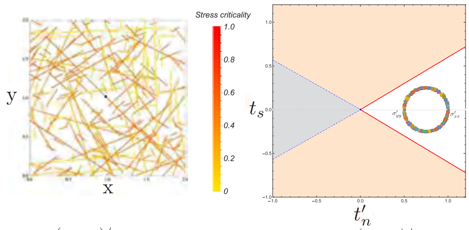

OVER-PRESSURE

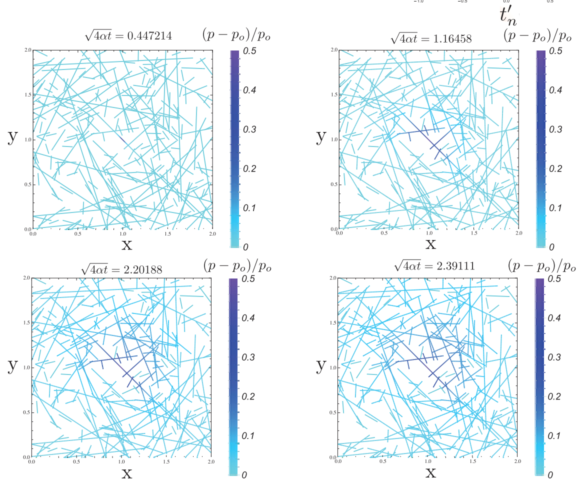

ASEISMIC SLIPPING PATCH

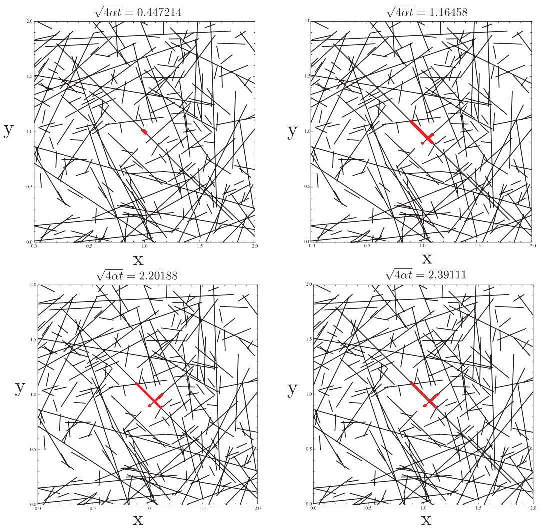

CRITICALLY STRESSED DFN

$\frac{\Delta P}{t'^{,k_{inj}}_{n,o}} = 0.5$

$f = 0.6$

$\kappa = \frac{\sigma'_{xx}}{\sigma'_{yy}} = 3.082$

$(x_{inj}, y_{inj}) = (1, 1)$

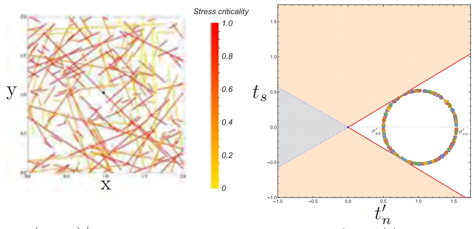

OVER-PRESSURE

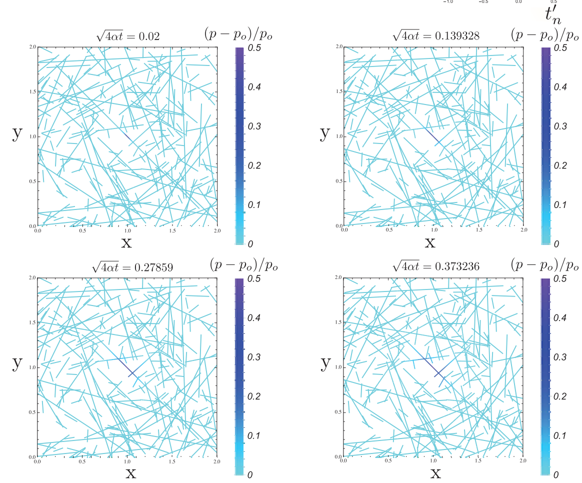

ASEISMIC SLIPPING PATCH

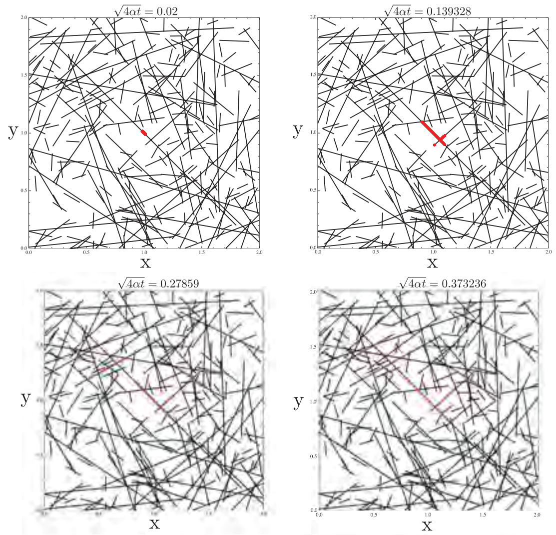

SCCER-SoE Annual Conference 2019

Effect of dilatancy on the transition from aseismic to seismic slip due to fluid injection in a fault

Federico Ciardo, Brice Lecampion

Geo-Energy Laboratory - Gaznat chair on Geo-energy, EPFL, Lausanne, Switzerland

FNSNF Fonds national suisse Schweizerischer Nationalfonds Fondo nazionale svizzero Swiss National Science Foundation

Schweizerische Eidgenossenschaft Confédération suisse Confederazione Svizzera Confederaziun svizra Swiss Federal Office of Energy SFOE

Model and problem formulation

Plane strain

Impermeable medium

$\tau_p = f_p \sigma'_o$
$\tau_r = f_r \sigma'_o$

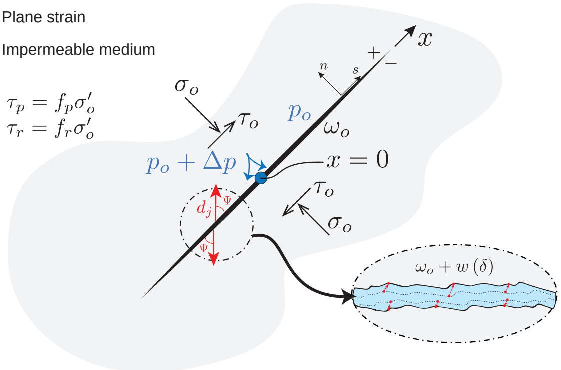

Friction weakening

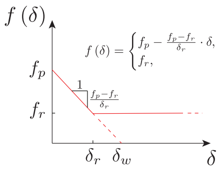

Slip induced dilatancy

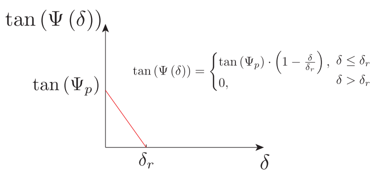

- Linear elastic equilibrium (quasi-static formulation)

$$t_i(x,t) = t_i^o(x) + \int_{-a}^{a} K_{ij}(\xi, x) \cdot d_j(\xi, t) \mathrm{d}\xi, \quad \text{for} \quad i,j = n,s$$

- Shear weakening Mohr-Coulomb yield criterion

$$F(\tau, \sigma'_n) = |\tau| - f(\delta) \cdot \sigma' \le 0$$

- Non-associated flow rule / Dilatancy

$$\dot{d}_i = \lambda \cdot \frac{\partial G}{\partial t'_i}, \qquad G(\tau, \sigma'_n) = |\tau| - \tan(\psi(\delta))\sigma', \quad \Rightarrow \quad \dot{d}_s = \dot{\delta} = \lambda \cdot \mathrm{sign}(\tau), \quad \dot{d}_n = \dot{w} = \lambda \cdot \tan(\psi(\delta))$$

- Fluid flow ($\alpha = k_f / \mu\beta$ fault hydraulic diffusivity)

$$w_h \beta \frac{\partial p}{\partial t} + \frac{\partial w(\delta)}{\partial \delta}\frac{\partial \delta}{\partial t} + \frac{\partial q}{\partial x} = 0, \quad q = -\frac{w_h \cdot k_f(\delta)}{\mu}\frac{\partial (p - p_o)}{\partial x}$$

- Constant pressure injection condition

$$p(x = 0, t) = p_o + \Delta P$$

Fault undrained response

The width averaged fluid mass conservation equation under undrained conditions leads to a pore pressure drop:

$$\boxed{w_o \beta \Delta p_u + \Delta w = 0 \rightarrow \Delta p_u = -\frac{\Delta w}{w_o \beta} = -\frac{\epsilon_d}{\beta}}$$

which leads to a local shear strengthening.

Small scale yielding & ultimate stability

When the half crack length a is much larger than $a_w = \delta_w E' / 2\tau_p$, all the strength weakening occur in a small zone near crack tips. The stress intensity factor at complete weakening is thus:

$$K_{II} = (\tau_o - \tau_r)\sqrt{\pi a} + f_r \sqrt{\frac{a}{\pi}} \int_{-a}^{a} \frac{\Delta p(x,t)}{\sqrt{a^2 - x^2}} \mathrm{d}x$$

When $a \gg a_w, a \gg \sqrt{4\alpha t}$ & $\dot{a} \gg 0$:

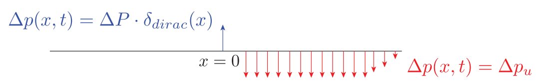

$$\Rightarrow K_{II} \simeq \left(\tau_o - \tau_r + \tau_r \frac{\Delta p_u}{\sigma'_o}\right)\sqrt{\pi a} + f_r \frac{\Delta P}{\sqrt{\pi a}}$$

Taking the limit when $a \rightarrow \infty$, a dilatant fault is stable when

$$\boxed{\tau_o < \tau_r^u = \tau_r \left(1 - \frac{\Delta p_u}{\sigma'_o}\right) \quad \text{Undrained shear strength}}$$

Alternatively, this provides a minimum value of dilatancy for a fault stabilization (for a set of in-situ conditions and residual strength)

$$\boxed{\epsilon_d^c = \beta \sigma'_o \left(\frac{\tau_o}{\tau_r} - 1\right) \quad \text{Critical dilatancy value}}$$

Numerics

- Displacement discontinuity method for elasticity (BEM)
- Finite volume scheme for fluid flow
- Coupled problem solved with a fully implicit scheme
- Adaptive time stepping based on crack velocity

Results - otherwise unstable fault

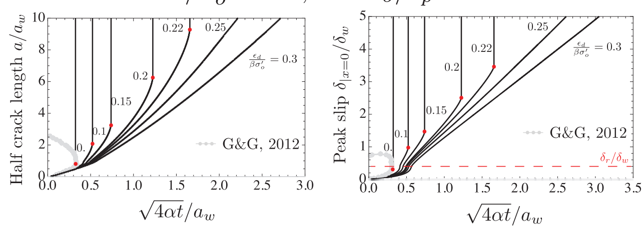

Normalized half crack length a/a_w and peak slip δ/δ_w as function of dimensionless time for an otherwise unstable fault ($\tau_o/\tau_p = 0.75, f_r/f_p = 0.6$), subjected to a moderate over-pressure $\Delta P/\sigma'_o = 0.5$.
Effect of the dimensionless dilatancy parameter $\epsilon_d/\beta\sigma'_o$ below and above the critical stabilizing value ($\epsilon_d^c/\beta\sigma'_o = 0.25$ for this case).

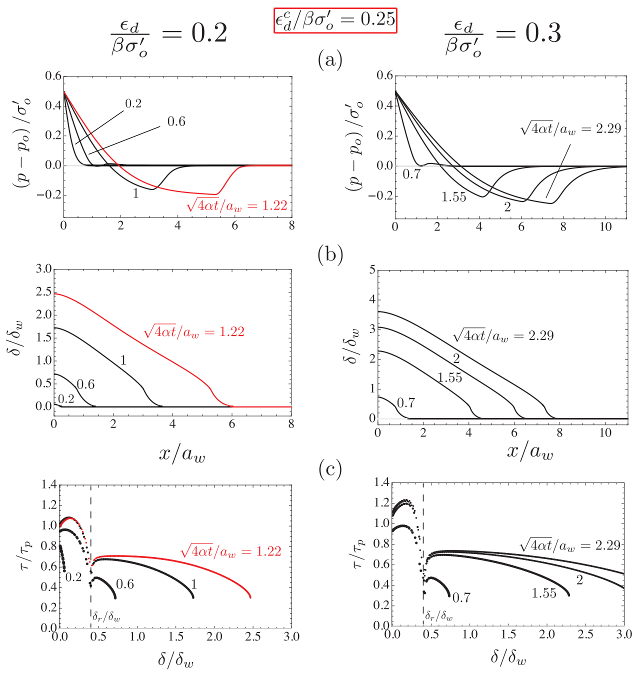

Corresponding spatial profiles of normalized (a) pore pressure changes and (b) slip at different time, below (left) and above (right) the critical value of dilatancy ($\epsilon_d^c/\beta\sigma'_o = 0.25$). Sub-figures (c) show the corresponding evolution of normalized shear strength with slip.

Conclusions

- Dilatancy above a critical value inhibits nucleation of a dynamic rupture for injection pressure sufficient to reach residual friction.
- Dilatancy delays the onset of a dynamic rupture (if occcuring) and slows down aseismic crack growth.
- Additional numerical results (not shown here) show that a fault permeability increases with slip accelerate aseismic crack growth but does not affect the stabilizing effect above critical dilatancy.

Reference

Ciardo, F., and Lecampion, B. (2019). Effect of dilatancy on the transition from aseismic to seismic slip due to fluid injection in a fault. *Journal of Geophysical Research: Solid Earth*, 124, 3724-3743.

SCCER-SoE Annual Conference 2019

ÉCOLE POLYTECHNIQUE FÉDÉRALE DE LAUSANNE

Schweizerische Eidgenossenschaft
Confédération suisse
Confederazione Svizzera
Confederaziun svizra

Swiss Federal Office of Energy SFOE

Critically-stressed reservoir stimulation direction via stress preconditioning

Barnaby Fryer, Xiaodong Ma, Gunter Siddiqi, Lyesse Laloui

barnaby.fryer@epfl.ch

Motivation

The ability to direct a stimulation treatment in an Enhanced Geothermal System (EGS) well would be a significant advancement for the EGS industry because it would allow for a higher assurance of connectivity (also allowing for larger well separation) and would help avoid known faults.

Previous work has looked at the positive effects of stimulating two wells at the same time (Baria et al., 2004), with a focus on the effect of an elevated pore pressure. Other works have shown the influence of poroelastic effects during stimulation (Jacquey et al., 2018). In this work, these two concepts will be combined and an attempt will be made to guide a stimulation treatment using poroelastic effects from a previous stimulation.

Methods

A sequentially coupled 2-D plane strain poroelastic simulator is emplyed. A fully implicit finite flow model based on the conservation of mass,

$$\frac{\partial(\phi\rho)}{\partial t} - \nabla\cdot\left(\frac{k}{\mu}\rho\left(\nabla P - \nabla(\rho g z)\right)\right) = q,$$

is used in combination with a finite element mechanical model based on the conservation of momentum,

$$\nabla\cdot\sigma' + \nabla(\alpha P) = -f,$$

and the linear theory of poroelasticity,

$$S_{ij} - \alpha P\delta_{ij} = \frac{E}{(1+\nu)}\epsilon_{ij} + \frac{E\nu}{(1+\nu)(1-2\nu)}\epsilon_{kk}\delta_{ij},$$

The permeability model is based on Miller, 2015 and assumes an orientation of pre-existing potential shear plane in each finite volume cell. Based on this orientation and the stress state, it can be determined if slip is expected. In the event of shear failure, the permeability of cell is assumed to permanently increase by a factor of 200. The reservoir is initially assumed to be critically stressed, such that a Coulomb stress change of 0.1 MPa is enough to induce shear failure.

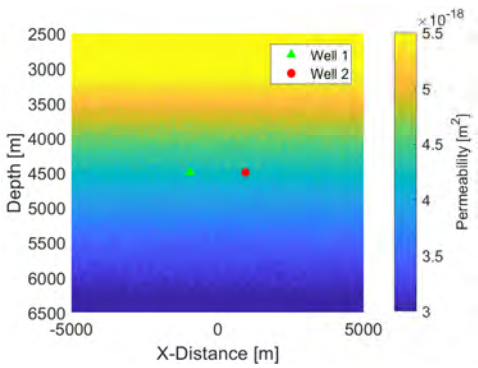

Figure 1: The initial permeability field used. The heterogeneity is due to the randomness associated with the permeability model (Miller, 2015).

Results

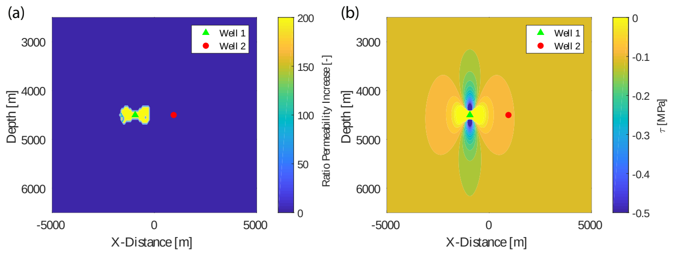

Figure 2: The result of the stimulation of well 1 in the reverse faulting stress regime case. (a) The permeability enhancement associated with the stimulation treatment (t=3 days). (b) The Coulomb stress changes resulting from the stimulation treatment (t=3 days).

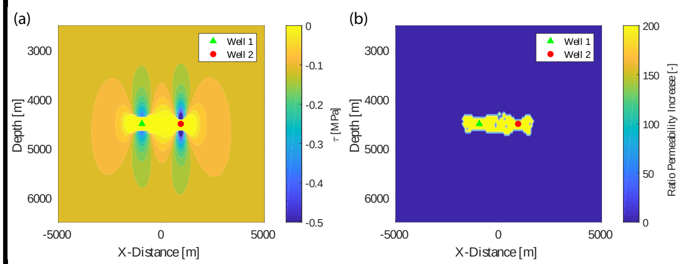

Figure 3: (a) The Coulomb stresses after the stimulation of the second well (t=6 days). (b) The permeability enhancement at the end of the entire procedure (t=6 days). The stimulated zone of each well extends and average 761m away from the other doublet well and 942m towards it.

Conclusion

1) It is suggested that shear stimulation treatments in EGS reservoirs can be directed.

2) Injection-induced poroelastic stress changes are significant in a critically-stressed crust.

3) A methodology which directs shear stimulation treatments in critically-stressed reservoirs using poroelastic stress changes is developed here for all three stress regimes.

References & Funding

[1] Baria, R., Michelet, S., Baumgaertner, J., et al., (2004), Microseismic monitoring of the World's largest potential HDR reservoir.
[2] Jacquey, A., Urpi, L., Cacace, M., Blöcher, G., Zimmermann, G., Scheck-Wenderoth, M. (2018), Far field poroelastic response of geothermal reservoirs to hydraulic stimulation treatment: Theory and application at the Gross Schönebeck geothermal research facility, International Journal of Rock Mechanics and Mining Sciences, 110, 316-327.
[3] Miller, S. (2015), Modeling enhanced geothermal systems and the essential nature of large-scale changes in permeability at the onset of slip, Geofluids, 15, 338-349.

This work has been funded by a research grant (SI/500963-01) of the Swiss Federal Office of Energy. Xiaodong Ma received funding from the Swiss Competence Center for Energy Research - Supply of Electricity and Swiss Science Foundation Grant No. 182150.

SCCER SoE
SWISS COMPETENCE CENTER for ENERGY RESEARCH
SUPPLY of ELECTRICITY

SCCER-SoE Annual Conference 2019

Supported by:
Schweizerische Eidgenossenschaft
Confédération suisse
Confederazione Svizzera
Confederaziun svizra
Swiss Confederation
Innosuisse – Swiss Innovation Agency

Geomechanical response of carbonate-rich Opalinus clay to CO2

Taeheon Kim, Alberto Minardi and Lyesse Laloui

Objective of the research

This research is carried out at the Laboratory of Soil Mechanics at the EPFL within the phase 24 of the CS-C project with the objective of better understanding the caprock material.
Opalinus Clay (OPA) is often used for studying the behaviour of caprocks as it demonstrates the traits of a proper caprock material for geological CO_2 storage. The OPA samples cored from Mont terri URL contained a thin section of highly concentrated carbonates. Clay-rich OPA was reported to be chemically inert to CO_2, however, since carbonate minerals are highly reactive to acid, the geomechanical response of carbonate-rich OPA (CAR-OPA) to CO_2 was investigated.
To observe the effect of CO_2 on the CAR-OPA, evolution of permeability with CO_2 exposure and spontaneous displacement during CO_2 injection was monitored.

[Experimental scheme]

❑ Apparatus:

High pressure Oedometer cell

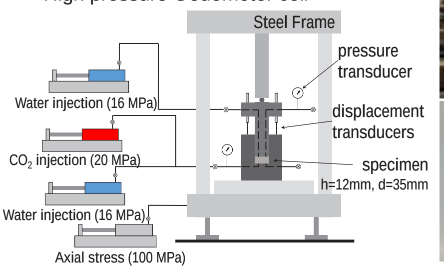

❑ Experimental procedure:

- Pre-exposure phase

1) Saturation of the sample under constant stress state
2) Loading to σ_a = 2.1, 4.3, 8.6 MPa of total axial stress with pore pressure of 1.0 MPa
3) Constant head permeability test each stress state

- CO_2 exposure phase

1) Short-term exposure followed by constant head permeability test
2) Long-term exposure followed by constant head permeability test
3) Injection of CO_2 under σ_a=4.3 MPa

- Post-exposure phase

1) Reloading-unloading cycles from 4.3 to 8.6 MPa

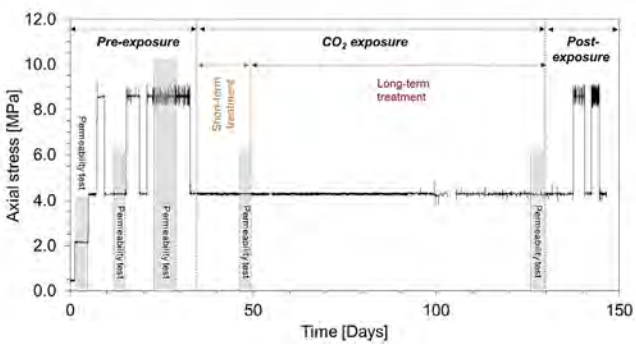

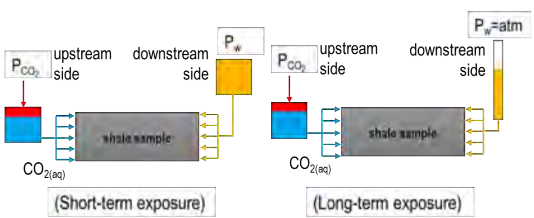

[Results]

❑Displacement measured during long-term injection

- Compaction continued until the sample flushing stage
- Total compaction 14μm (irreversible)
- Recorded displacement responds sensitive to temperature

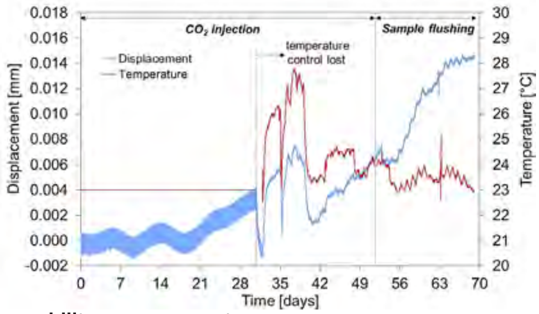

❑Permeability measurement

- Slight decrease in permeability measurements, using deaerated water, after each treatment
- Permeability measured during the long-term CO_2 injection stage is much lower (fluid is carbonated water)

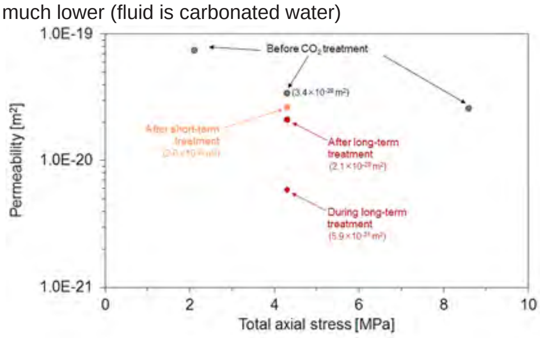

❑Compression curve pre and post-exposure

- Slightly larger compaction after CO_2 exposure

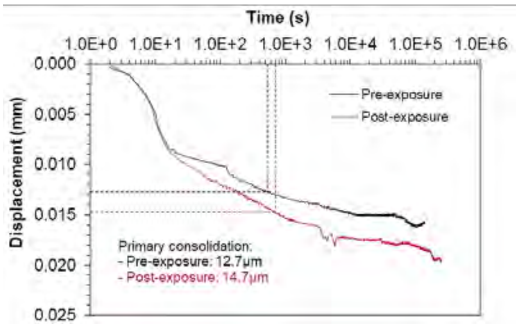

[Discussion]

❑ Permeability measured during the long-term injection can be due to the difference in physical properties (density and viscosity) which the values were unable to measure during the experiment.
❑ The response to temperature may be the response of the sample itself or the system compliance

[Summary]

❑ Permeability was not significantly affected by the CO_2 injection
❑ Irreversible displacement was monitored
❑ Slightly larger compaction after CO_2 exposure
❑ The experiment reacts sensitive to the surrounding temperature

SCCER SoE

SWISS COMPETENCE CENTER for ENERGY RESEARCH
SUPPLY of ELECTRICITY

SCCER-SoE Annual Conference 2019

Supported by:

Schweizerische Eidgenossenschaft
Confédération suisse
Confederazione Svizzera
Confederaziun svizra

Swiss Confederation

Innosuisse – Swiss Innovation Agency

On the seismo-hydro-mechanical response of a shear zone during hydraulic stimulation

H. Krietsch[1], L. Villiger[1], J. Doetsch[1], V. Gischig[2], M.R. Jalali[3] and F. Amann[3]
[1]ETH Zurich, [2]CSD Ingenieure Bern & [3]RWTH Aachen (hannes.krietsch@sccer-soe.ethz.ch)

1. Introduction and monitoring

The experiment was conducted in the framework of the decameter-scale In-situ Stimulation and Circulation (ISC) project in the crystalline rocks at the Grimsel Test Site (GTS), Switzerland. The vertical overburden at the test volume is ~480 m. A comprehensive monitoring system consisting of pressure, strain and seismic monitoring was installed along various boreholes inside the test volume. The here presented hydraulic stimulation experiment targeted a brittle-ductile shear zone (hosted within a meta-basic dyke) for the high pressure fluid injection. The injection volume was 1211 m^3.

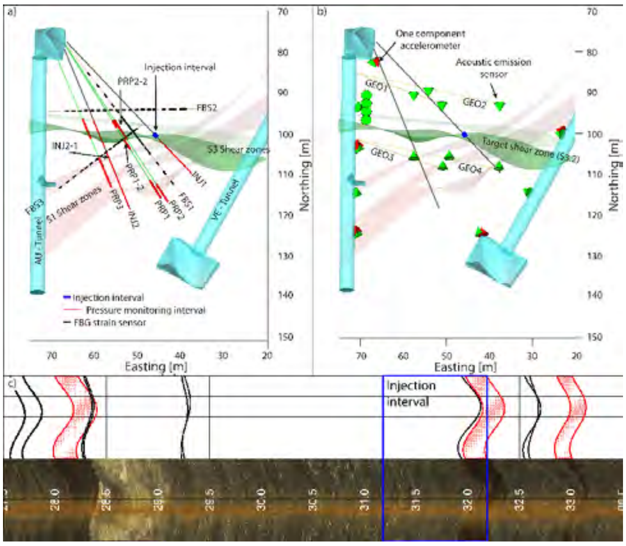

Geological model of ISC test volume with pressure and strain monitoring (a), and seismic array (b). The target shear zone is marked in dark green. The geology of the injection interval is visualized in c).

2. Injection parameters & relation to stress field

The injection consisted of four injection cycles (also see 3. a). The comparison of linear relationships between flow rate and pressure observed for low pressure injection steps during injection cycles 2 and 4 indicate that in-situ injectivity was not increased. Thus, we argue that this stimulation was not successful at the injection well. Nevertheless, hydro-mechanically coupled deformations were dominant at the injection well above 6.1 MPa at the injection well. In addition, injection pressure was limited to ~8 MPa while flow rate was constantly increased. This indicates normal opening (mode I) of the target structures.

Prior to the stimulation experiments the in-situ stress close ('perturbed tensor') to the target shear zone has been characterized. Based on this characterization and geological mapping, stresses across and along the target structures were calculated.

This analysis indicates that there is a higher likelihood for the target shear zone to experience normal opening during high pressure injections at PRP2-2 compared to shear dislocation at PRP1-2.

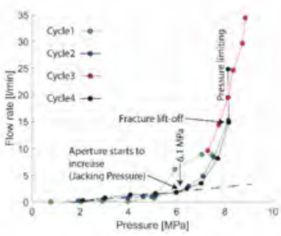

Injection flow rate versus pressure for all four injection cycles.

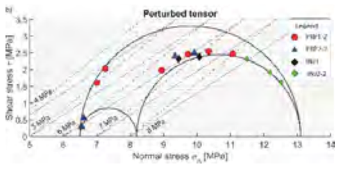

Mohr-Coulomb diagrams for the perturbed stress tensor (b). Potential failure criteria for different fracture fluid pressures and stress state for the corresponding fractures.

3. Hydraulic and seismic rock mass response

The four injection cycles were followed by shut-in phases and venting, during which all pressure lines connected to the test volume were opened. During the first two injection cycles, only minor pressure perturbations and seismicity were detected. The main injection cycle (C3) induced a high pressure perturbation with a steep pressure front in the interval PRP2-2. This pressure perturbation occurred relatively aseismically around this monitoring interval. Most of the seismic events appeared towards the interval PRP1-2 during C3. With ongoing stimulation (C4), the seismic front propagated continuously towards PRP1-2 and away from the injection interval INJ1-2. Additionally, a high pressure perturbation arrived at the interval PRP1-2, while interval PRP2-2 was not pressurized again.

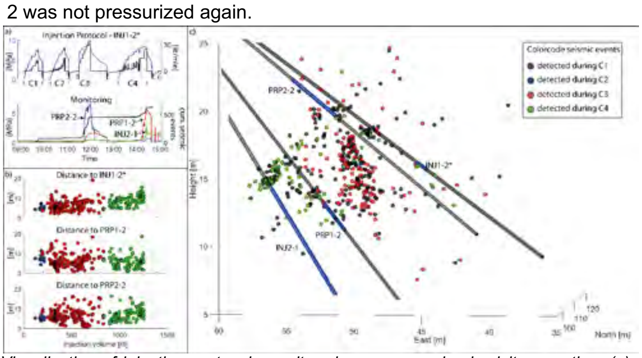

Visualization of injection protocol, monitored pressure and seismicity over time (a), and the relationship between injected fluid volume and distance between seismic event and pressure monitoring interval (b). View onto the target shear zone with pressure intervals and seismic events (including timing).

4. Schematic interpretation

Two different high pressure signals propagated along the target shear zone during the fluid injection. The first signal is characterized by a steep pressure front, mostly aseismic deformation and did not re-occur during the subsequent injection cycles (C4). This signal propagated upward towards east during C3. The stress field indicated that this pressure signal was coupled with normal opening (mode I) of the target shear zone. The second pressure signal consisted of a less steep pressure front during C3 and enhanced pressure signal during the subsequent injection cycle (C4). Based on the stress field, this pressure signal might be coupled with shear dislocation. This is consistent with the observed seismicity , which propagated in the same direction as the second pressure signal downwards towards east. Note that the peak pressure (P_{peak}) is higher for the first pressure signal, compared to the second one.

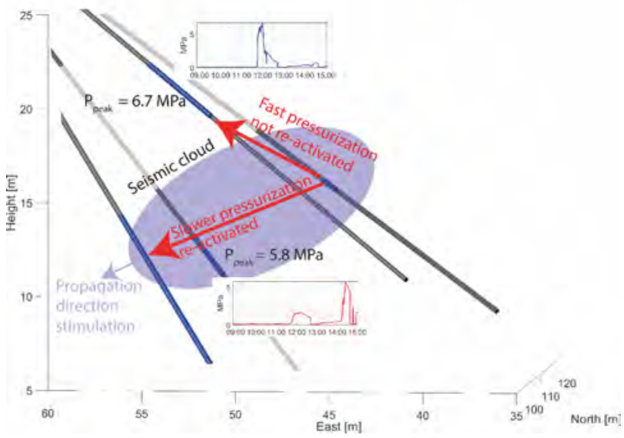

View onto the target shear zone. The pressure monitoring intervals are visualized with the obtained peak pressures. The pressure signals, the seismic cloud and the propagation direction of the stimulation direction are drawn schematically.

SCCER SoE
SWISS COMPETENCE CENTER for ENERGY RESEARCH
SUPPLY of ELECTRICITY

EPFL

SCCER-SoE Annual Conference 2019

Laboratory hydraulic fracturing tests in low-permeability rocks

Liu, D., Blum, T. & Lecampion, B.
Geo-energy Lab, Gaznat Chair on Geo-Energy, EPFL, Lausanne, Switzerland

Supported by:
Schweizerische Eidgenossenschaft
Confédération suisse
Confederazione Svizzera
Confederaziun svizra
Swiss Confederation
Innosuisse – Swiss Innovation Agency
GeoEnergyLab

1. Abstract

We aim to investigate the effect of grain size (corresponding to different process zone sizes) on the propagation of hydraulic fractures. We use active acoustic monitoring to track the evolution of the fracture radius and fluid thickness.We present preliminary results of a toughness-dominated experiment in Gabbro and a lag-viscosity dominated experiment in Marble.

2. Experimental set-up

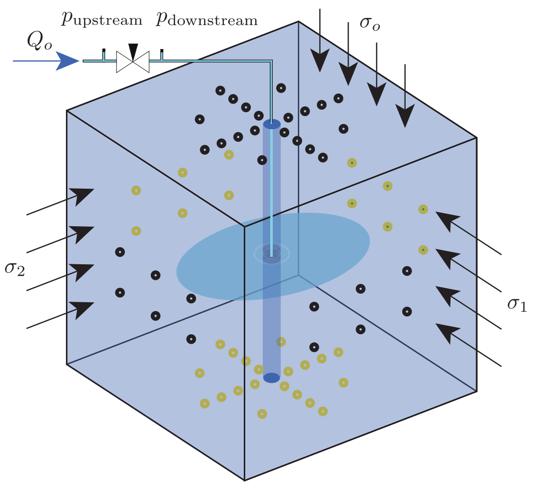

Fig. 1 Schema of the tested rock block (25x25x25 cm³) under true tri-axial confinement and fluid injection, along with the transducer disposition

3. Experimental Design

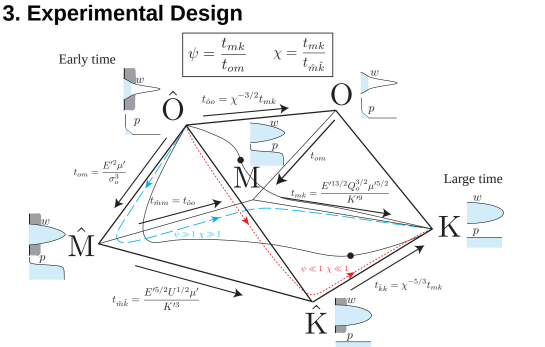

Fig. 2 Schematic evolution of the initiation and propagation of radial hydraulic fracture from a wellbore in dimensionless space [1].

$$\mu' = 12\mu \qquad E' = \frac{E}{1-\nu^2} \qquad K' = \sqrt{\frac{32}{\pi}} K_{Ic}$$

Table. 1 Material parameters for gabbro and marble

Rock	grain size (mm)	E(GPa)	ν	K_{Ic}(MPa.$\sqrt{\text{m}}$)	ρ(g/cm³)	V_p(km/s)
Gabbro	1-3	68.4	0.31	3.33	3.05	6.76
Marble	0.1-0.2	69.4	0.29	1.83	2.69	6.09

Table. 2 Sample configuration and tests parameters for different experiments

Rock	Wellbore radius (mm)	Initial defect length (mm)	σ_o(MPa)	$\sigma_1 = \sigma_2$(MPa)	μ(Pa.s)	Q_o (mL/min)	U (mL/GPa)
Gabbro	7.5	3	0.5	10.5	0.6	0.2	217.3
Marble	7.5	3	10	20	100	0.2	282.5

Table. 3 Viscosity-toughness transition time scales and dimensionless parameters

Rock	t_{mk}(s)	$\psi = \frac{t_{mk}}{t_{om}}$	$\chi = \frac{t_{mk}}{t_{\tilde{m}k}}$	$\mathcal{L} = \ell_o/(E'U)^{1/3}$	$\mathcal{A} = a/(E'U)^{1/3}$
Gabbro	7.34×10^{-4}	2.28×10^{-9}	1.72×10^{-4}	0.0118	0.029
Marble	6.32×10^{5}	9.18	12.5	0.0108	0.027

4. Preliminary results

4.1 Absolute Black Gabbro (Zimbabwei)

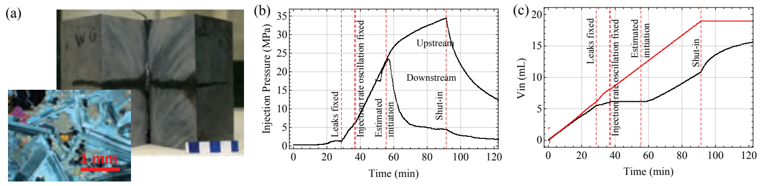

Fig. 3 a) Thin section of the gabbro and post mortem photo of the block (in the white-blue color bar, each square is 2x2 cm²), b) Evolution of the upstream and downstream injection pressure, c) Evolution of the volume injected by the pump (red) and the volume entering into the fracture (black).

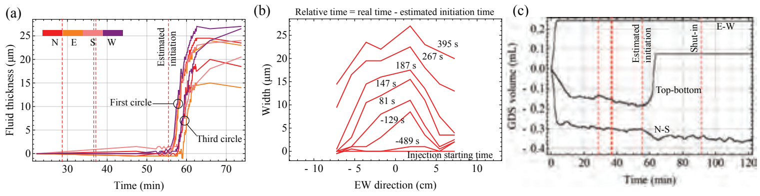

Fig. 4 a) Evolution of the fluid thickness corresponding to the transducers in the first and third circle nearest to the wellbore, b) Evolution of the fracture width profiles in the east-west direction at the relative time (real time substracted by the estimated intiation time using pressure and GDS data, c) Evolution of the GDS pump volume.

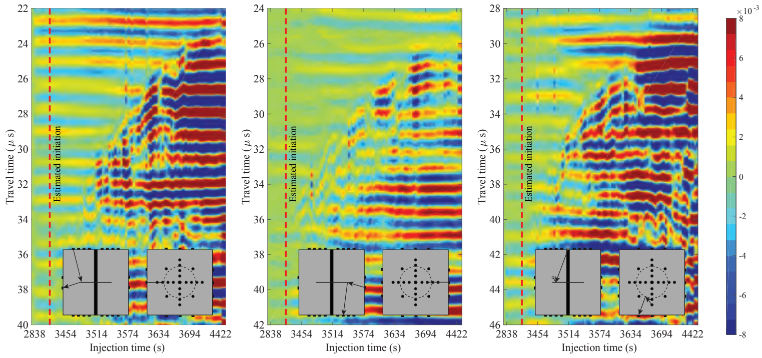

Fig. 5 Data in the difference domain for a pair of P-wave transducers (P-wave source to diffraction to P-wave receiver, PdP), along with the acquisition geometry.

4.2 Carrara Marble (Italy)

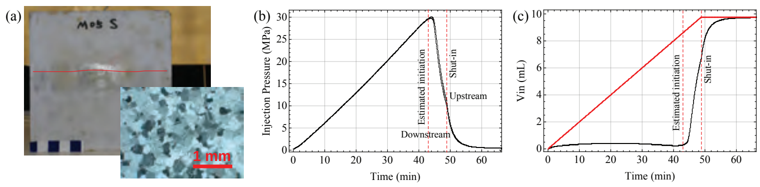

Fig. 6 a) Thin section of the marble and post mortem photo of the block (in the white-blue color bar, each block is 2x2 cm²), b) Evolution of the upstream and downstream injection pressure c) Evolution of the volume injected by the pump (red) and the volume entering into the fracture (black).

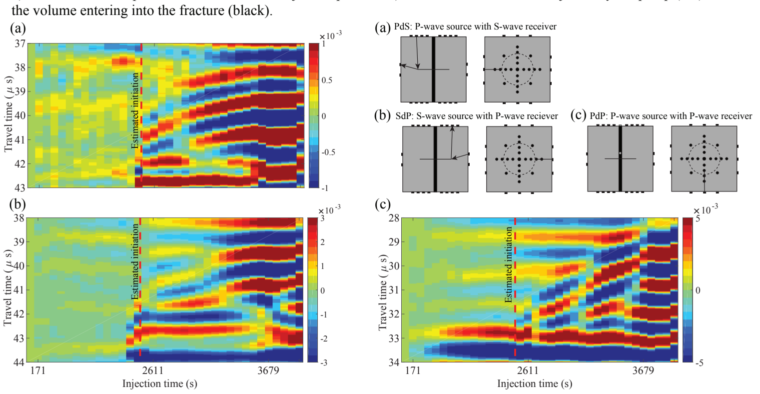

Fig. 7 Data in the difference domain for one P-wave transducer and one S-wave transducer (a, b), and a pair of P-wave transdu--cers (c), along with the acquisition geometry.

1. Lecampion, B., Desroches, J., Jeffrey, R. G., & Bunger, A. P. (2017). Experiments versus theory for the initiation and propagation of radial hydraulic fractures in low-permeability materials. Journal of Geophysical Research: Solid Earth, 122(2), 1239-1263.
2. J. Groenenboom, Acoustic monitoring of hydraulic fracture growth, PhD thesis, TU Delft, Delft Univeristy of Technology (1998).

d.liu@epfl.ch

Fluid injection driven, a-seismic fracture growth with remote nucleation on heterogeneous fault

Andreas Möri, Brice Lecampion* and Federico Ciardo
Geo-Energy Lab - Gaznat chair on Geo-energy, EPFL, Lausanne, Switzerland
*Contact: brice.lecampion@epfl.ch

Schweizerische Eidgenossenschaft
Confédération suisse
Confederazione Svizzera
Confederaziun svizra
Bundesamt für Energie BFE
Swiss Federal Office of Energy SFOE

1. Model and problem formulation

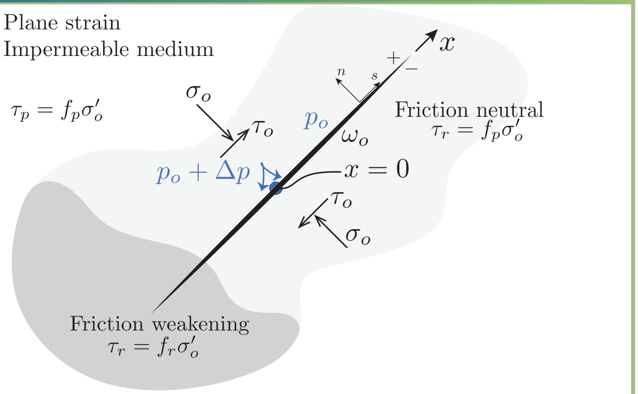

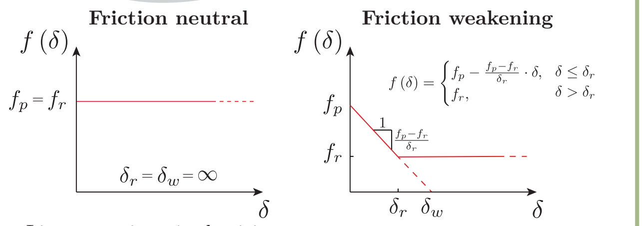

- Linear quasi-static elasticity

$$t_i(x,t) = t_i^o(x) + \int_{-a}^{a} K_{ij}(\xi, x) \cdot d_j(\xi, t) \mathrm{d}\xi, \text{ for } i,j = n,s \quad (1)$$

- Constant pressure injection condition / constant fault permeability case

$$p = p_o + \Delta p \quad (2)$$

We assume $p_o + \Delta p$ remains below fault opening pressure (σ^o).

2. Numerics

- Displacement discontinuity method for elasticity (BEM)
- Finite volume scheme for fluid flow
- Fully coupled implicit solver (HFPx2D) developed at EPFL
- Adaptive time stepping based on current crack velocity

3. Theoretical developments

A linear relation between the crack half length and the position of the fluid pressure front due to pore pressure diffusion along the fault exists. Defining the dimensionless half-crack length $\gamma = \ell / \sqrt{4\alpha t}$ (with α the fault diffusivity), using the solution for 1D diffusion and stating that $\tau(\xi) = \tau_p$ inside the crack, the elasticity equation reduce for a planar fault to:

$$\frac{\tau(\xi) - \tau_o}{f_p \Delta p} \overset{\tau(\xi)=\tau_p}{=} \underbrace{\frac{\tau_p - \tau_o}{f_p \Delta p}}_{T} = \mathrm{Erfc}|\gamma \xi| - \frac{1}{2\pi} \int_{-1}^{+1} \frac{\mathrm{d}\bar{\delta}}{\mathrm{d}\eta} \frac{\mathrm{d}\eta}{\xi - \eta} \quad (3)$$

Dimensionless parameter T balances stress criticality (prior to the injection) and magnitude of the over-pressure. Asymptotic solution following [Viesca R., pers. comm., September 2018] serve as benchmark for the numerical solvers.

6. Conclusions

- A-seismic crack tip and pore pressure front can significantly differ:
  - marginally pressurized (fluid pressure front $\gg$ aseismic crack front)
  - critically stressed (aseismic crack front $\gg$ fluid pressure front)
- Critically stressed faults with a weaker frictional weakening part can exhibit remote activation (far away from the pore-pressure disturbance), i.e. activation of a daughter crack with a possible subsequent nucleation of a dynamic rupture
- The dynamic nucleation lengthscale of the daughter crack scales as $a_w = \delta_w E' / (2\tau_p)$ following [Uenishi, K., and J.R. Rice (2003), Garagash, D. and Germanovich, L. (2012)] (linear frictional weakening).

4. Benchmark

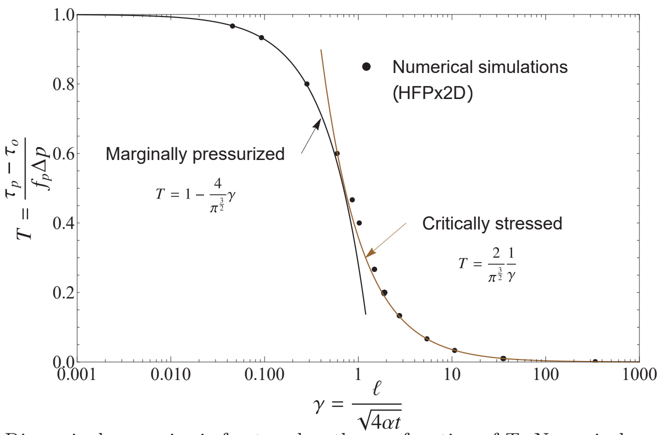

Dimensionless a-seismic fracture length γ as function of T. Numerical results are displayed as dots, analytical asymptotes for the marginally pressurized and critically stressed cases as continuous lines [Viesca, pers. comm., September 2018]

5. Remote activation on weaker part of fault

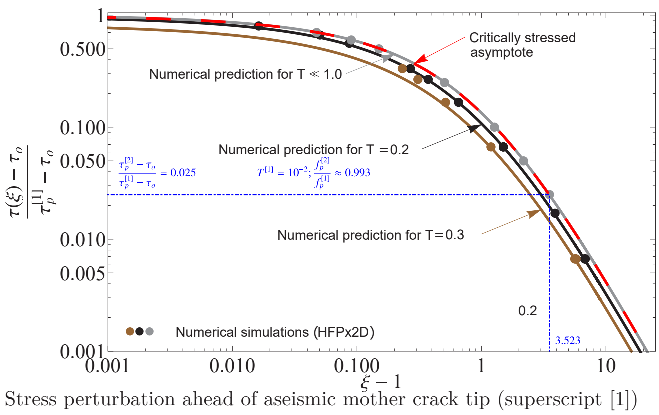

Stress perturbation ahead of aseismic mother crack tip (superscript [1]) for critically stressed cases, where $\xi = \frac{x}{\ell^{[1]}}$. This can lead to a remote activation of a daughter crack (superscript [2]), on a heterogeneity with lower strength, possibly nucleating dynamically (if frictional weakening occurs).

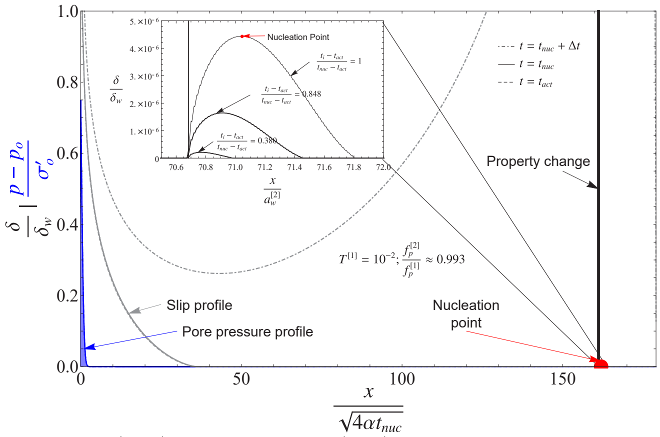

Slip profiles (gray) and pore pressure (blue) in function of normalized line coordinate. Inset shows slip evolution within the daughter crack. Nucleation in daughter crack scales with $a_w^{[2]}$.

- Friction neutral fault properties at injection
- Frictional weakening part with lower peak friction coefficient (i.e. $f_p^{[1]} > f_p^{[2]}$)
- Stress transfer dominated regime
- Remote activation of a-seismic slip with possible nucleation

Hydraulic fracture in transversely isotropic material: propagation perpendicular to the isotropy plane

Fatima-Ezzahra Moukhtari, Brice Lecampion
Geo-Energy Laboratory - Gaznat Chair on Geo-Energy (GEL),
Ecole Polytechnique Fédérale de Lausanne (EPFL)
fatima-ezzahra.moukhtari@epfl.ch, brice.lecampion@epfl.ch

Motivation

Transverse isotropy (TI) is an intrinsic characteristic of most sedimentary rocks, especially mudstones. We investigate here how TI anisotropy influence the growth & shape of planar 3D hydraulic fractures (HF). We focus on the case of propagation perpendicular to the plane of isotropy (i.e. bedding plane): a configuration encountered for normal / strike-slip stress regimes with horizontal bedding planes for which the normal stress to bedding or/and the bedding planes strength are sufficient to favor propagation perpendicular to the material isotropy plane. A practical situation for HF growth in unconventional reservoirs.

Near tip elastic modulus

Coupling between lubrication flow and LEFM yields a complex multiscale behavior near the tip of a hydraulic fracture [1]. The near-tip asymptotic solution is based on a plane-strain configuration which for a TI material depends on the local direction of propagation e_1' with: $\widehat{e_1, e_1'} \equiv \alpha$. In such a local plane-strain frame, the near-tip elastic relation is similar to the isotropic case, pending the use of a plane strain elastic modulus E'_α function of the local propagation direction.

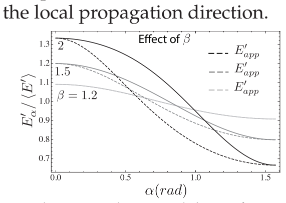

Figure 1: Local near-tip elastic modulus as function of propagation direction (α). E'_α also depends on 5 elastic constants: $\langle E' \rangle = (E'_\alpha(0) + E'_\alpha(\pi/2))/2$, $\beta = E'_\alpha(0)/E'_\alpha(\pi/2)$, Thomson parameters (ϵ, δ) and the ratio C_{13}/C_{11}. Approximation proposed by [3] in dashed lines. Other constants $\epsilon = 0.3$, $\delta = 0.2$, and $C_{13}/C_{11} = 0.5$.

Numerical scheme

We extend the implicit level set algorithm (ILSA) to account for anisotropy of both elastic properties and fracture energy [2]. This numerical scheme combines a finite discretization for the non-linear coupling of elasticity and lubrication flow (using boundary element method for elasticity discretization and finite volume method for fluid flow) and the near-tip hydraulic fracture asymptotes to evolve the fracture front. The extension to anisotropy notably requires the addition of an iterative loop to resolve the local propagation direction of the fracture all along its perimeter - i.e. in order to use the proper near-tip modulus (see Figure 1) and fracture toughness in the near-tip HF asymptote.

Problem formulation

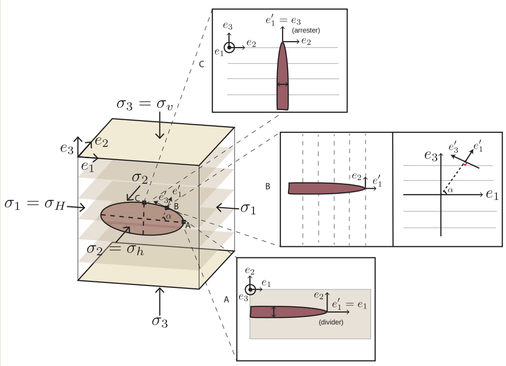

- TI Elasticity (mode I planar fracture)

$$p_f(y_1, y_3) - \sigma_h = -c_{22mn} \int_S \frac{\partial S^m_{22}(\boldsymbol{y}, \boldsymbol{x})}{\partial x_n} w(\boldsymbol{x})\, dx_1 dx_3$$

- Lubrication flow

$$\frac{\partial w}{\partial t} + \nabla \cdot \mathbf{q} = \delta(x_1, x_3) Q_o$$

$$\mathbf{q} = -\frac{w^3}{12\mu} \nabla (p_f - \rho_f g \delta_3)$$

- Propagation condition (along the front)

$$K_I = K_{Ic}(\alpha)$$

Planar hydraulic fracture propagating perpendicular to the isotropy plane (e_1, e_2) of a TI impermeable elastic media under constant point-source injection (rate Q_o). w denotes the fracture width, p_f the fluid pressure and $\mathbf{q}$ the fluid flux. Insets correspond to the variation of the near-tip plane-strain configuration along the fracture front as function of the angle α with the isotropy plane.

Viscosity regime

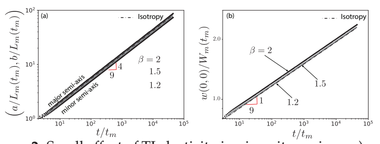

Figure 2: Small effect of TI elasticity in viscosity regime. a) semi-axis time evolution, and b) width at the injection function of time ($\epsilon = 0.3$, $\delta = 0.2$, $C_{13}/C_{11} = 0.5$). Penny-shaped HF M-scaling (L_m, W_m) [1].

Toughness regime / Elastic TI only

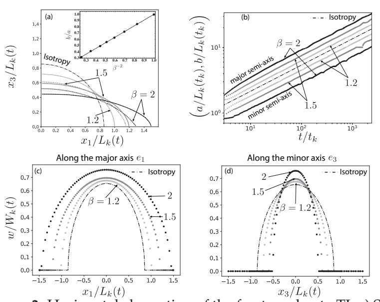

Figure 3: Horizontal elongation of the fracture due to TI. a) Self-similar (1/4) footprint, b) semi-axis time evolution, and c,d) self-similar width profiles along principal axis ($\epsilon = 0.3$, $\delta = 0.2$, $C_{13}/C_{11} = 0.5$). Penny-shaped HF K-scaling (L_k, W_k) [1].

Toughness regime / TI & Anisotropic K_{Ic}

"Elliptical" evolution of fracture toughness:

$$K_{Ic} = K_{Ic,3} \left(\frac{E'_\alpha}{E'_3}\right) \left(\sin^2\theta + \left(\frac{\kappa}{\beta}\right)^4 \cos^2\theta\right)^{1/4}$$

$$\theta = \arctan\left(\frac{\kappa \tan\alpha}{\beta}\right), \qquad \kappa = K_{Ic,1}/K_{Ic,3}$$

$$b(t) = \left(\frac{3tQ_oE'_3}{8K_{Ic,3}\sqrt{\pi}}\gamma\right)^{2/5}, \quad a(t) = \left(\frac{K_{Ic,3}}{K_{Ic,1}}\frac{E'_1}{E'_3}\right)^2 b(t).$$

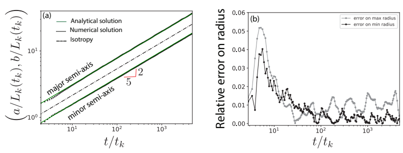

Figure 4: Verification - toughness dominated elliptical HF: $\kappa^{-1} = 1.2$, $\beta = 1.2$, $\epsilon = 0.3$, $\delta = 0.2$, and $C_{13}/C_{11} = 0.5$. (a) Time-evolution of the dimensionless minor and major axis, and (b) relative error compared to the toughness dominated analytical solution derived in [4].

References

[1] E. Detournay. Mechanics of hydraulic fractures. *Annual Review of Fluid Mechanics*, 48:311–339, 2016.

[2] H. Zia, B. Lecampion and W. Zhang Impact of the anisotropy of fracture toughness on the propagation of planar 3D hydraulic fracture. *Int. J. Frac.*, 211(1-2): 103-123, 2018.

[3] H. Laubie and F.J. Ulm Irwin's conjecture: Crack shape adaptability in transversely isotropic solids. *J. Mech. Phys. Sol.*, 68: 1-13, 2014.

[4] F.E. Moukhtari, B. Lecampion, and H. Zia Propagation of a planar hydraulic fracture perpendicular to the isotropy plane of a transversely isotropic material. No. CONF. 53rd US Rock Mechanics/Geomechanics Symposium, 2019.

SCCER-SoE Annual Conference 2019

Schweizerische Eidgenossenschaft
Confédération suisse
Confederazione Svizzera
Confederaziun svizra

Bundesamt für Energie BFE
Office fédéral de l'énergie OFEN

A fast 3D BEM solver for fracture mechanics

Carlo Peruzzo, Elizaveta Gordeliy, Dmitry Nikolskiy, Brice Lecampion, François Fayard

Geo-Energy Laboratory - Gaznat chair on Geo-Energy, EPFL, Lausanne, Switzerland

Motivation

Hydraulic fractures are mainly employed in geomaterials in order to increase the productivity of wells. They are used in geothermal energy and oil and gas production to increase the permeability of porous formation either for enhanced fluid production or storage (CO_2 storage).

They are created by engineering fluid injection from deep wellbores. The propagation of an hydraulic fracture is a coupled nonlinear problem where the elasticity of the rock is coupled with the fluid flow through the fracture channel and the porous formation. The coupling with the fluid flow requires the elasticity to be solved multiple times and so, a very fast and efficient solver for linear elastic fracture propagation is required.

Solver Description

The solver uses a displacement discontinuity Boundary Element Method (BEM) to solve for quasi-static elasticity. It allows to discretize only the 3D fracture surfaces avoiding the discretization of the surrounding 3D space required by other techniques such as Finite Element Method (FEM). On one hand this is an advantage because the resulting matrix, that has to be inverted to solve the linear problem, is much smaller compared to the one obtained via FEM (given the same goal error of the numerical solution). On the other hand, the major drawbacks of BEM are that the influence matrix is fully populated and, in the general case, non-symmetric. The first drawback leads to a large memory cost and the latter to an increase of the computational cost of the solution. The implementation described here tackle both problems by taking advantage from the spatial decay of the elastic kernel: the influence of a given displacement discontinuity (DD) at one source point on the traction at the observation point, decays as $1/d^2$, where "d" is the distance between them. We use a hierarchical matrix approach to approximate the original matrix [3-5]. This method can be summarized via two complementary methodologies: i) a cluster tree of the mesh (which depth is controlled by a parameter M) combined with an admissibility condition (controlled by a parameter η) decides which sub-block can be approximated as low-rank ii) the low-rank approximation is performed via adaptive cross approximation for speed (whose accuracy is controlled by ε).

Finally, the results presented here have been obtained using piece-wise quadratic triangular DDs element and ran on MacBook Pro (2017) i5 2.3GHz with 8GB of RAM.

Penny shaped crack

Uniform convergence studies

The numerical solution has been obtained for a penny shaped crack of a radius R=1.5, using a series of different meshes shown on the Figure 3. The elastic parameters used are G=1000 (shear modulus) and ν=0.1 (Poisson ratio). $\varepsilon=10^{-5}$ and M=500 has been assumed for all the computations. The figures below are showing the L_2 norm of the relative error in the crack width (Figure 5), the relative error of stress intensity factor (Figure 6), the creation time of the H matrix approximation (Figure 7) and the compression ratio achieved in each simulation vs. number of degrees of freedom (Figure 4). This result show that one can use a large value of η (e.g. η=10) without any reduction in the accuracy of the numerical solution. Beside that the computational cost and the storage requirements are significantly reduced.

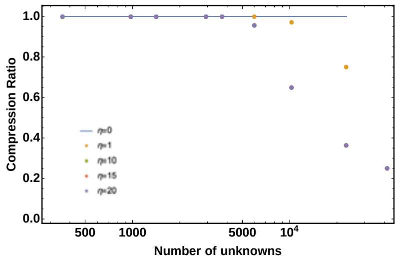

Figure 4: Compression ratio of the hierarchical matrix.

Stress verification

The numerical solution for the stress has been verified against the analytical solution for the stress around the penny shaped crack [1].

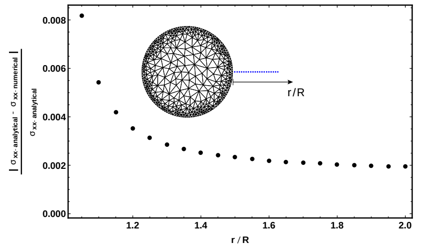

Figure 1: Comparison of the σ_{xx} with the analytical solution [1]. The inset of the figure is showing the location of the observation points (in blue) at which the stresses have been computed.

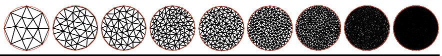

elements :	15	54	79	163	206	331	569	1276	2308
unknowns :	360	972	1422	2934	3708	5958	10242	22968	41544

Figure 3: series of different uniformly distributed meshes.

Crack opening verification

The numerical solution for the crack opening has been obtained for a uniform mesh and a non-uniform mesh refined at the crack front.

These results suggest that it is more efficient to use a non-uniform mesh refined at the crack front than a uniform mesh, for the same number of unknowns : 14220.

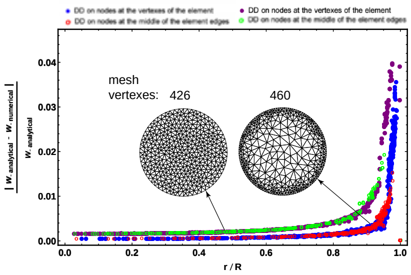

Figure 2: Relative error in crack width, obtained using a uniform and a non-uniform mesh refined at the crack front.

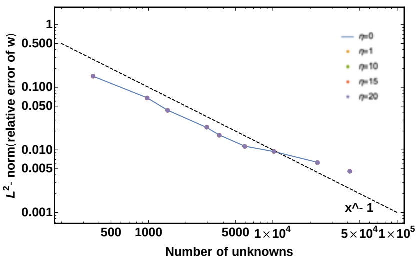

Figure 5: L_2 norm of the error of the crack opening.

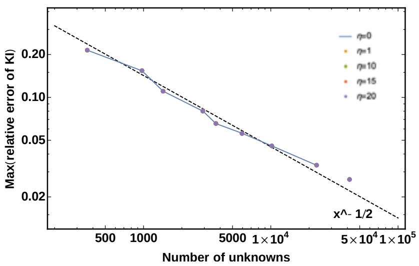

Figure 6: Max of the relative error on the stress intensity factor K_I

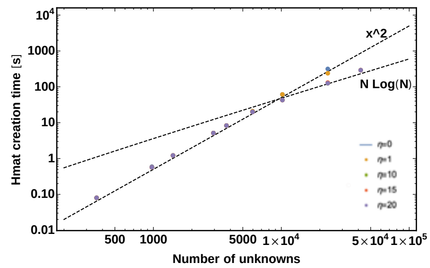

Figure 7: Hmat creation time vs. number of unknows.

Bowl-shaped crack (Mixed Mode Fracture)

A bowl-shaped crack of radius R = 1.5 and α=60º (see Figure 8) has been discretized with 890 triangular elements (see figure 9), leading to a system with 14760 unknowns. The elastic parameters that characterize the isotropic and elastic medium are G=1000 (shear modulus) and ν=0.1 (Poisson's ratio). The crack has been loaded with a uniform unit pressure. The solution obtained with the presented code, has been compared against a numerical solution obtained with an axisymmetric Displacement Discontinuity method. The comparison between the normal opening and the relative error is shown in figures 10 and 11 respectively.

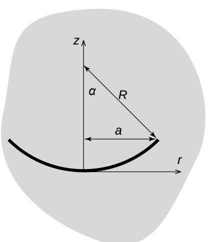

Figure 8: Cross-section of a bowl-shaped crack in an infinite space.

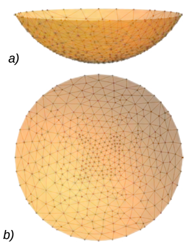

Figure 9: Lateral view a) and top view b) of the discretized bowl-shaped crack.

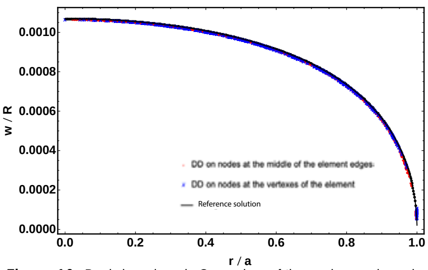

Figure 10: Bowl-shaped crack. Comparison of the crack normal opening (w) scaled with the crack radius R with a numerical solution obtained with an axisymmetric Displacement Discontinuity code [2].

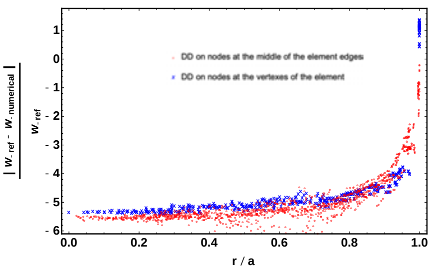

Figure 11: Bowl-shaped crack. Relative difference between the crack widths (w) obtained with the axisymmetric Displacement Discontinuity code [2] and the present code Hfp-3D.

References

[1] Nikolskiy, D.V., Mogilevskaya, S.G. & Labuz, J.F. (2013). *Complex variables boundary element analysis of three-dimensional crack problems.* Engineering Analysis with Boundary Elements, 37(11), 1532-1544.

[2] Gordeliy, E. & Detournay, E. (2011). *Displacement Discontinuity Method for Modeling Axisymmetric Cracks in an Elastic Half-Space.* International Journal of Solids and Structures, 48, 2614-2629.

[3] Hackbusch. W., (1999). *A sparse arithmetic based on H-Matrices. Part I: Introduction to H-Matrices.* Computing, 62, 89-108.

[4] Chaillat S., Desiderio L. & Ciarlet P. (2017).*Theory and implementation of H-matrix based iterative and direct solvers for Helmholtz and elastodynamic oscillatory kernels.* Journal of Computational Physics, 351, 165–186.

[5] Benedetti, L., Aliabadi, M.H. & Davi, G. (2008). *A fast 3D dual boundary element method based on hierarchical matrices.* International Journal of Solids and Structures, 45, 2355-2376.

SCCER SoE
SWISS COMPETENCE CENTER for ENERGY RESEARCH
SUPPLY of ELECTRICITY

SCCER-SoE Annual Conference 2019

Small Flex

Supported by:
Schweizerische Eidgenossenschaft
Confédération suisse
Confederazione Svizzera
Confederaziun svizra
Swiss Confederation
Innosuisse – Swiss Innovation Agency

Added value of smart storage operations on an alpine run-off-river HPP obtain from hydrological-hydraulic modelling

Maria Ponce, Jessica Zordan, Pedro Manso , Cécile Münch*
Laboratory of Hydraulic Construction (LCH), École Polytechnique Fédérale de Lausanne (EPFL), Switzerland
**Corresponding author: jessica.zordan@epfl.ch*
EPFL

Framework

Run-off-river hydro projects can create sustainable energy minimizing impacts to the surrounding environment. Among many advantages of these systems, whose development has in fact been largely supported during the past years by the confederation, their main limitation is that their functioning is dependent by the available discharge, as they do not have storage. In order to overcome this constrain and enhance their flexible use, the Smart Storage Operations (SSO) are introduced (Figure 1c). SSO consist on using temporarily some existed underground structures of the power plant, such as the settling basin, for water storage. This water can be used afterward to produce peak energy timed with the demand. This is particularly useful since it allows water accumulation in periods of the year when the discharge is too low for energy production, therefore minimizing water losses.

The aim of this study was to create a hydrological-hydraulic model in order to reproduce the HPP operations (both under normal use - Figure 1b - and SSO - Figure 1d). The elaborated framework was applied at the hydropower plant KW Gletsch-Oberwald (Figure 1a) located at Valais (Switzerland) but it can be applied to others HPP in the Alpine region with dominant glacier cover, or areas with an intermittent river. A validation of the model was possible thanks to the measurements which were collected at the HPP during one week of site tests.

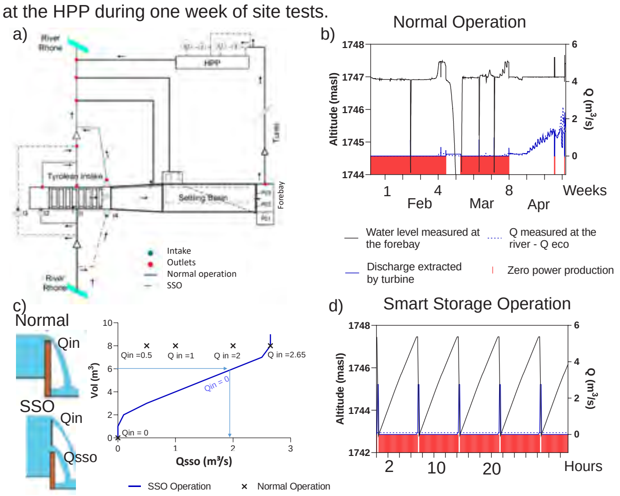

Figure 1: a) Schematic representation of the water infrastructure, and b) Measured water level at the forebay and turbine inflow during a normal operation at KW Gletsch-Obwerwald, c) Discharge and turbine inflow during the SSO operation, and d) Water level at the forebay and turbine inflow during a SSO.

Methods

RS Minerve was the computational selected tool. It allows to create a combined hydrologic and hydraulic model in a semi-distributed conceptual scheme. For the **hydrology model**, the snowmelt, glacier melt, snow accumulation and runoff process are reproduced by empirical models on daily base. The output was downscaled on an hourly basis, using climatic historical data of 28 years (Grimsel station). The **hydraulic model** was validated for normal operations and SSO using measured data.

These two models were joined to conform to a unique model. To evaluate the SSO, a yearly simulation was performed estimating the energy production and determining the economic revenues and the additional economic value of SSO with respect to normal operations.

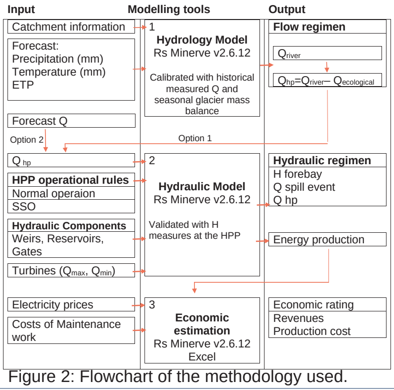

Figure 2: Flowchart of the methodology used.

Results and discussion

On this catchment of 39 km², the glacier (52% of the basin) and snowmelt have a direct influence in the hydrology. The final hourly calibration by the multi-objective function using 14 years (2005-2018) of measured discharge at Gletsch gave a performance indicator of Nash equal to 0.89 and a Relative Volume Bias of 1,1 e-3. The Figure 2b showed a good correspondence with the measured data.

The hydraulic model was validated with the measured water level inside the forebay tank, during normal operations, for winter 2017-2018 and the SSO for with the measurements collected during the site tests in November 2018. Both models showed a good correspondence with a Nash equal to 0.96 and 0.85 respectively.

With the validated simulations of the Normal and SSO, it was possible to reproduce in detail the SSO in a week of 2018 and for a complete year.

The simulation approach with the proposed framework proved an evident increment of power productions for the season with lower discharge (winter season), that goes from 50 to 100 %, depending on the inflow (when the inflow is less than the minimum discharge for one turbine, the HPP would need to switch off, therefore the gain goes up to 100%).

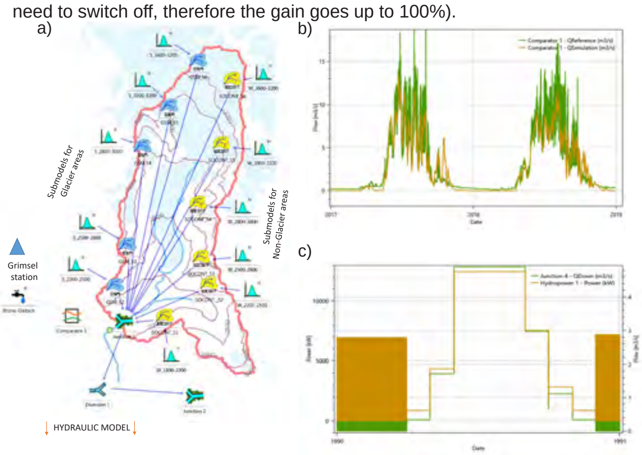

Figure 3: a) Schematic representation of the Gletsch catchment in the RS Minerve sotware, b) Observed and simulated discharge during 2017 and 2018, c) Power production simulated over one year using SSO operation.

Conclusion

- An integrated and numerically efficient hydrology-hydraulic model was developed in order to perform simulations of run-off-river HPP. The calibration of the hydrology model lead to the **accurate simulation** of the observations.
- The construction of a numerical model can easily reproduce different scenarios of energy production allowing for a good prediction of the HPP reaction for a certain inflow while adopting specific operational modes. It is therefore becoming a **relevant operational tool**.
- The **SSO benefit** was highlighted by comparing it with the power production resulted by normal operations. The simulations undertaken along a whole year have shown that the increment in power production during winter season doubles, reaching a gain of more than 700 MWh with respect to the adoption of normal operations.

References

- Farinotti, D. (2013) 'On the effect of short-term climate variability on mountain glaciers: insights from a case study', J. Glaciol., 59(217), pp. 992-1006.
- Gabbi, J., Carenzo, M., Pellicciotti, F., Bauder, A., & Funk, M. (2014). A comparison of empirical and physically based glacier surface melt models for long-term simulations of glacier response. J. Glaciol., 60(224), 1140-1154. doi:10.3189/2014JoG14J011
- Foehn, A., García Hernández, J., Roquier, B., Fluixá-Sanmartín, J. and Paredes Arquiola, J. (2018). Rs minerve – user's manual v2.11. In R. M. Group (Ed.). Switzerland.
- Morand G., Adam N., Manso P, Schleiss A. «« Augmentation de la flexibilité d'exploitation d'aménagements hydroélectriques à haute chute au fil de l'eau en Valais ». SCCER-SoE Science Report 2017.

SCCER-SoE Annual Conference 2019

PyFrac - A planar 3D solver for hydraulic fracture growth

Haseeb Zia, Brice Lecampion

Geo-Energy Laboratory - Gaznat chair on Geo-energy, EPFL, Lausanne, Switzerland

Motivations

Hydraulic fractures are a class of tensile fractures that propagate in response to fluid injection at sufficient pressure. At depth in the earth, rocks are under compressive stresses in-situ such that a hydraulic fracture propagates perpendicular to the minimum in-situ stress orientation (minimizing energy) at an injection pressure greater than minimum in-situ stress magnitude.

They are used to increase the permeability of porous formation either for enhanced fluid production (geothermal energy, oil and gas production) or storage (CO_2 storage). They are created by engineering fluid injection from deep wellbores. It is a very efficient process allowing to propagate fracture over large distance in a stable manner as the viscous fluid flows into the newly created fracture therefore driving it further as long as injection continues.

Hydraulic fractures also occur naturally in response to local fluid pressurization in the earth crust: for example in association with hydrocarbon generation (diagenesis) but also due to magma pressurization leading to very long vertical buoyant hydraulic fracture eventually reaching the earth surface (leading to so-called lava fissure – see figure 4).

The propagation of fluid-driven fracture exhibits strong non-linearities related to the coupling between mechanical deformation, the creation of new fracture surfaces and the flow of viscous fluid both inside the fracture and in the rock mass (leak-off). The relative balances between i) the energy dissipated in viscous flow versus the one dissipated in fracture creation and ii) the fluid volume stored inside the fracture versus the one lost in the rock mass ultimately control propagation. Numerical modeling of such a moving boundary problem is very challenging as it requires the resolution of multiple time and lengths-cales.

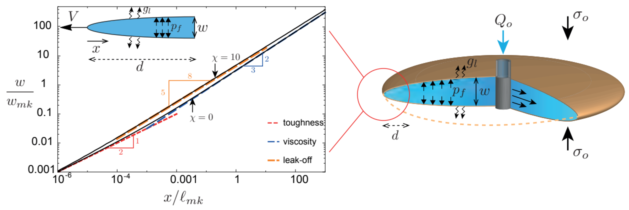

Figure 1: The near-tip behavior of a hydraulic fracture exhibit multiple asymptotic regions related to different physical processes (left). These asymptotes are valid locally close to the fracture front of a finite hydraulic fracture (right) and can be used to build a robust numerical scheme embedding the multiscale nature of the problem.

Code description

PyFrac is a Python implementation of an implicit level set algorithm originally developed by Peirce & Detournay (2008) to simulate planar Three-dimensional hydraulic fractures. Our implementation makes extensive use of Numpy and Scipy. The numerical scheme has the following features:

- Level set description of the fracture front atop a Cartesian mesh (rectangular elements)
- Multiscale resolution via the coupling of the semi-infinite hydraulic fracture tip solution (see figure 1) with the finite discretization
- Boundary element discretization for quasi-static elasticity
- Finite volume discretization for lubrication flow
- Fully coupled implicit hydro-mechanical solver
- Eikonal equation solved via fast-marching method for fracture front evolution
- Adaptive time-stepping
- Implicit/explicit fracture front advancing
- Remeshing

Current Capabilities

- Isotropic and transversely isotropic elastic infinite medium
- In-homogeneous and anisotropic fracture toughness
- In-homogeneousand leak-off properties
- In-homogeneous in-situ minimum stress
- Buoyant fluid
- Fracture closure and re-opening (multiple injection)
- Time dependent injection history
- Post processing and visualization routines

Verifications

The solver has been validated against all available reference solutions for hydraulic fracture growth. The figures below show the comparison of the solution computed by PyFrac against the semi-analytical solution for a penny shaped hydraulic fracture propagating in the viscosity dominated regime (case of negligible toughness and negligible leak-off).

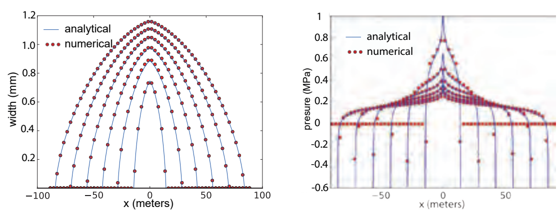

Figure 2: Penny shaped hydraulic fracture viscosity dominated regime benchmark. Fracture width (left) and net pressure (right) profiles at different time evaluated with PyFrac. The results are shown along a slice of the 3D fracture made at the x-axis. The semi-analytical solution is also shown for comparison.

References

- Peirce, A., & Detournay, E. (2008). An implicit level set method for modeling hydraulically driven fractures. *Comp. Meth. App. Mech. Engng*, 197(33), 2858-2885.
- Wu, R., Bunger, A. P., Jeffrey, R. G., & Siebrits, E. (2008). A comparison of numerical and experimental results of hydraulic fracture growth into a zone of lower confining stress. In the 42nd US rock mechanics symposium. American Rock Mechanics Association.
- Zia, H., Lecampion, B., & Zhang, W. (2018). Impact of the anisotropy of fracture toughness on the propagation of planar 3D hydraulic fracture. *Int. J. Frac.*, 211(1-2), 103-123.
- H. Zia and B. Lecampion (2019). Explicit versus implicit front advancing schemes for the simulation of hydraulic fracture growth. *Int. J. Numer. Anal. Meth. Geomech.* 43(6):1300–1315.

Validation against a laboratory experiment

We compare numerical predictions against optical measurement of the fracture front obtained in a laboratory experiment performed in a transparent PMMA block (Wu *et al.*, 2008) with three regions of different confining stress (see the figure below for schematics of the experiment). The fluid is injected in the middle layer. Due to the difference in confining stresses, the fracture herniates predominently in the layer having lower stress while being arrested at the boundary of the layer with higher confining stress.

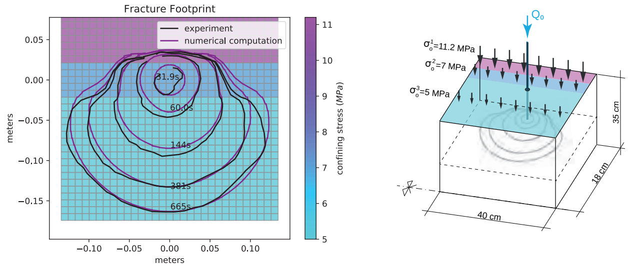

Figure 3: Schematics of the experimental setup showing the PMMA block with three levels of confining stress **(right)**. The fluid is injected into the middle layers and the fracture propagates in a plane at the half depth of the block (shown with a dotted line) perpendicular to the applied confining stresses. Fracture footprint at 31.9, 60, 144, 281 and 665 seconds after the start of injection. The numerical results obtained with PyFrac (magenta lines) compare well with the experimental results (black lines).

Dyke propagation

The buoancy contrast between magma and the surrounding rock drives fracture growth toward the surface. In this illustrative example, we simulate the propagation of a dyke due to a pulse release of magma from a point source at a depth of 6.4km.

Figure 4: Lava fissure appearing on Hawaii's Big Island on May 5, 2018. It corresponds to the emergence of a dyke propagating due to magma release from deep chambers (Kilauea volcano).

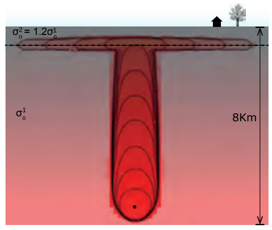

Figure 5: Time evolution of the footprint of the dyke. A pulse of magma is released at the injection point shown by the black dot. As time progresses, the magmatic dyke moves upward until it reaches a layer with 20% larger confining stress (dotted line), causing it to extend lateraly.

Figure 6: Fracture width of the dyke at different times. The head and tail structure, typical of buoyancy driven fractures can be observed on this 3D plot.

Anisotropy in fracture toughness

We simulate the growth of hydraulic fracture in an anisotropic medium having a higher fracture toughness in the vertical direction as compared to the horizontal direction.

Figure 8: Transition from a radial viscosity dominated hydraulic fracture to an elliptical toughness dominated hydraulic fracture case $K_{c,3}/K_{c,1}$ = 1.73. Fracture footprints obtained numerically at different times (black lines), with zooms for smaller times from top to bottom. The footprints of the analytical solution for radial viscosity dominated hydraulic fracture are also displayed in red at small times. The local propagation regime along the fracture front is represented by a color code in the cells just behind fracture front, with red being fully viscosity dominated and blue being fully toughness dominated.

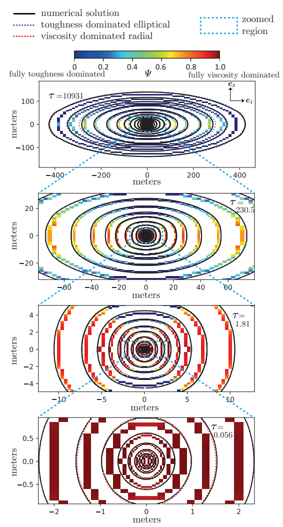

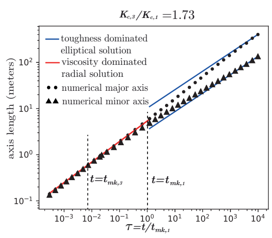

Figure 7: Lengths of the major and minor axes of the fracture with dimensionless time where $t_{mk,1}$ is the transition time scale from the viscosity to the toughness dominated regime in the horizontal direction.

Task 1.3

Title

Hydrothermal heat exploitation and storage

Projects (presented on the following pages)

Simulations of chemical processes during high-temperature aquifer thermal energy storage
Peter Alt-Epping, Daniela B. Van den Heuvel, Christoph Wanner, Larryn W. Diamond

Seismic stimulation of fractured reservoirs
Nicolás D. Barbosa, Santiago G. Solazzi, Matteo Lupi

Modeling Ground Surface Deformation at the Swiss HEATSTORE Underground Thermal Energy Storage Sites
Daniel T. Birdsell, Martin O. Saar

3-D Static Model to Characterize Geothermal Reservoirs for High-Temperature Aquifer Thermal Energy Storage (HT-ATES) in the Geneva Area, Switzerland
O. E. Eruteya, L. Guglielmetti, Y. Makhloufi, A. Moscariello

Reactive Flow Model for Porosity Reduction by Quartz Dissolution and Precipitation
Batoul Gisler, Boris Galvàn, Reza Sohrabi, Stephen A. Miller

Sensitivity Analysis of High Temperature Aquifer Thermal Energy Storage (HT-ATES) using TH Simulations
Julian Mindel, Thomas Driesner

Experimental Thermo-Hydro-Mechanical test site to quantify heat exchange characteristics of fractured limestone aquifers
Reza Sohrabi, Benoît Valley

Investigating mineral reactions during high-temperature aquifer thermal energy storage (HT-ATES)
D.B. van den Heuvel. Ch. Wanner, U. Mäder, P. Alt-Epping, L.W. Diamond

SCCER-SoE Annual Conference 2019

Simulations of chemical processes during high-temperature aquifer thermal energy storage

SCCER SoE
SWISS COMPETENCE CENTER for ENERGY RESEARCH
SUPPLY of ELECTRICITY

UNIVERSITÄT BERN

Peter Alt-Epping, Daniela B. Van den Heuvel, Christoph Wanner & Larryn W. Diamond
Rock-Water Interaction, Institute of Geological Sciences, University of Bern

Supported by:
Schweizerische Eidgenossenschaft
Confédération suisse
Confederazione Svizzera
Confederaziun svizra
Swiss Confederation
Innosuisse – Swiss Innovation Agency

1) Introduction

The aim of the Forsthaus heat storage project is to develop an aquifer thermal energy storage site at Bern, Switzerland where waste heat from various surface sources (e.g. municipal waste incinerators) is stored during the summer and recovered and fed into the district heating network during the winter months. The project, which is currently in the planning stage, is part of the Swiss contribution to the European GEOTHERMICA-Heatstore project. The target reservoir of the project is the Lower Freshwater Molasse (USM), a stratigraphic sequence of the Swiss Molasse Basin composed of several meters thick permeable sandstone aquifers surrounded by low-permeability shales.

Concept of typical injection (loading) and extraction (unloading) cycles during summer and winter, respectively, envisaged for the Forsthaus project.

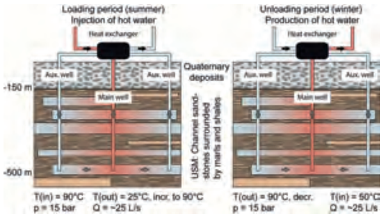

As part of the planning phase we developed reactive transport models to assess mineral scale formation in the installation and permeability changes of the aquifer material after repeated injection and extraction cycles. PFLOTRAN (*www.pflotran.org*) is used to carry out these simulations.

2) Constructing TH and THC models of the Forsthaus system

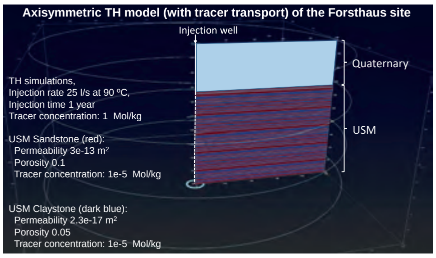

At the Forsthaus site the USM is about 350 m thick and overlain by 150 m of Quaternary unconsolidated sediments. The permeable sandstone layers constitute the target for fluid injection, heat will be stored within the entire USM rock sequence.

Axisymmetric TH models incorporating the entire stratigraphic sequence of the USM, reveal that within 1 year of injection at 25 l/s the thermal plume migrates < 50 m into the aquifer. The tracer plume migrates much faster.

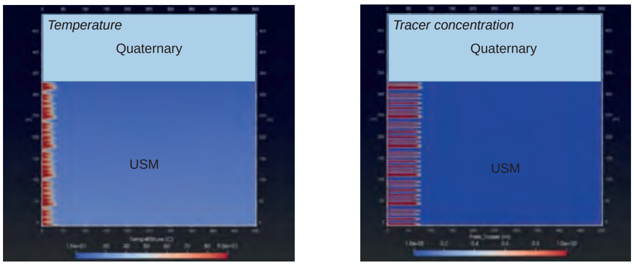

3) Chemical processes in the Forsthaus system: Implications of heating USM groundwater to 90 ℃

USM groundwater is heated from 15 ℃ to 90 ℃ in a simple 1D flowpath model 1) to assess the amount of mineral scaling to be expected upon extraction and 2) to compute the composition of the (re)injected hot water. The latter (2) is used in subsequent THC injection/extraction simulations.

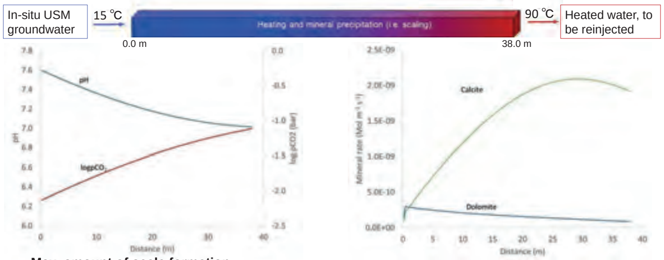

Max. amount of scale formation
A flow rate of 25 l/s yields **18.9 m³** of carbonate scales per year or **11.15 m³** per injection cycle (216 days)

4) Simulations of injection-extraction cycles over 10 years

The dimension of the TH model (Section 2) is reduced to a simple sequence of clay-ss-clay assuming symmetry at mid-depth. The composition of the injected fluid at 90 ℃ is taken from the 1D simulations (Section 3).

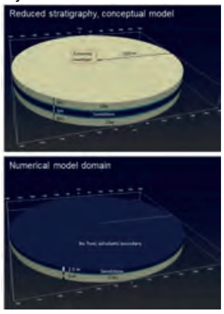

- Axisymmetric cylindrical domain
- 3 layers: clay-sandstone-clay, 5 m each, actual model domain is truncated at the horizontal plane of symmetry at mid-depth
- Injection and extraction along perforated borehole at center
- Dirichlet condition representing «undisturbed conditions» at r = 300 m
- Impermeable, adiabatic top and bottom boundaries assuming symmetry
- Pressure dependent CO_{2},g and carbonate mineral solubility
- Monitor possible CO_2 degassing in heat exchanger via «CO_2,s» precipitation
- Time-dependent material properties and chemical conditions to mimic processes in the well and heat exchanger

Annual injection/extraction cycle

Time [d]	Q [l/s]	T [℃]	Inject	Extract
0-216	25	90	+	
216-365	25	50		+

(total simulated time = 10 years)

Results

A) Time series of system aquifer properties (legend indicates distance from well in m)

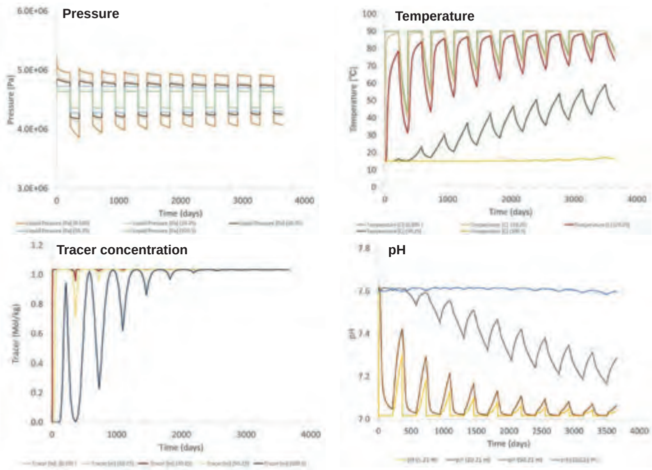

B) Spatial profiles of mineral reaction rates and pH during injection and extraction

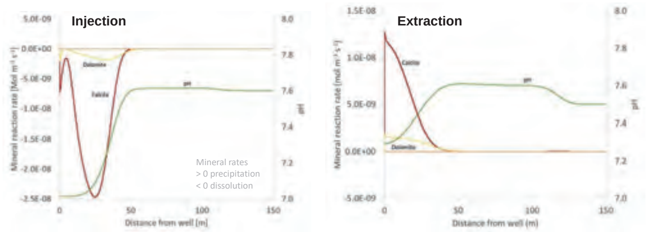

C) Time series of temperature and mineral scales in the well/heat exchanger during extraction

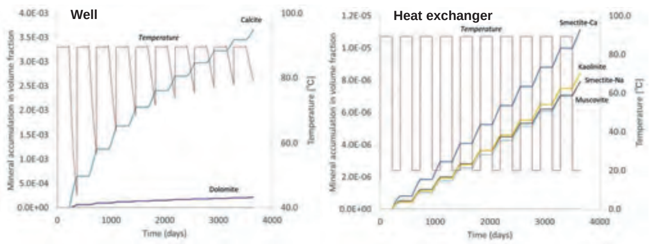

5) Conclusions

Reactive transport simulations of THC processes in the Forsthaus system suggest that carbonate scaling constitutes the greatest risk for a sustained operation. Simple heating of in-situ groundwater to 90 ℃ could clog the pipes of the surface installation. Minor scaling of clay minerals due to cooling occurs in the heat exchanger during operation. Mineral reactions in the aquifer following repeated injection extraction induce only small porosity changes and are not expected to affect the operation.

Contact: alt-epping@geo.unibe.ch

SCCER-SoE Annual Conference 2019

SCCER SoE
SWISS COMPETENCE CENTER for ENERGY RESEARCH
SUPPLY of ELECTRICITY

Supported by:
Schweizerische Eidgenossenschaft
Confédération suisse
Confederazione Svizzera
Confederaziun svizra
Swiss Confederation
Innosuisse – Swiss Innovation Agency

Seismic stimulation of fractured reservoirs

Nicolás D. Barbosa[1], Santiago G. Solazzi[2], and Matteo Lupi[1]

1. Department of Earth Sciences, UNIGE
2. Institute of Earth Sciences, UNIL

Summary

Experimental studies have shown that flow-driven mobilization of colloids can produce permeability changes in fluid-saturated porous media. Due to the well-known ability of seismic waves to induce transient fluid motion in porous media, this mechanism of permeability enhancement has been proposed to explain hydrogeological phenomena commonly associated with Earthquake events as well as a potential method for seismic stimulation of reservoirs (**Fig. 1**). We model the coupling between the dynamic strains imposed by a propagating seismic body wave and the development of oscillatory flow in porous media in the framework of Biot's theory of poroelasticity. We analyze the conditions (e.g., strain magnitude, frequency, wave mode) under which seismic waves may detach colloids from pores or fractures and, consequently, enhance permeability.

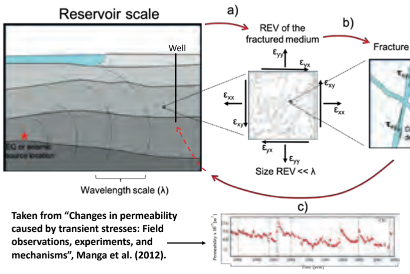

Figure 1: Illustration of permeability changes due to seismically induced fracture-unclogging. The plot in panel c) shows an example of permeability changes due to the action of seismic waves associated with Earthquake events (vertical dashed lines). Permeability is estimated from water level response to semidiurnal tides at a well.

Diffusive waves and colloidal mobilization

We follow Biot's theory of poroelasticity (Biot, 1962) to model seismic wave propagation in fluid-saturated porous rocks. The corresponding set of equations is given by

$$\tau_{ij}(\mathbf{u},\mathbf{w}) = 2\mu\varepsilon_{ij} + \delta_{ij}\left(\left(K_U - \frac{2\mu}{3}\right)\nabla\cdot\mathbf{u} + \alpha M\nabla\cdot\mathbf{w}\right), \quad (1a)$$

$$p_f(\mathbf{u},\mathbf{w}) = -\alpha M\nabla\cdot\mathbf{u} - M\nabla\cdot\mathbf{w}, \quad (1b)$$

$$-\omega^2\varrho_b\mathbf{u} - \omega^2\varrho_f\mathbf{w} = \nabla\cdot\boldsymbol{\tau}, \quad (1c)$$

$$-\omega^2\varrho_f\mathbf{u} + i\omega\frac{\eta}{\kappa}\mathbf{w} = -\nabla p_f, \quad (1d)$$

Symbols in Eqs. 1a-1d

- τ_{ij} and ε_{ij}: stress and strain tensors
- **u** and **w**: solid and fluid relative displacement
- p_f: fluid pressure
- K_U and μ: undrained bulk and shear moduli
- α and M: poroelastic parameters
- ϱ_f and η fluid density and viscosity
- ϱ_b, bulk density
- κ, permeability
- ω, angular frequency

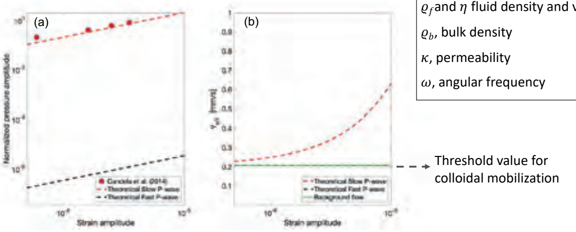

Figure 2: Assuming planar wave propagation, we compute the propagation characteristics of the slow and fast P-waves by solving the system of equations (1a)-(1d). a) Red dots show the ratio between imposed pressure oscillations and the background pressure drop driving flow as a function of the strain typically observed in laboratory stimulation experiments (Candela et al., 2014). Red and black dashed lines show the same relation predicted for propagating slow and fast P-waves, respectively. Panel b) shows the effective fluid velocity in the pores (v_{eff}= ẇ/φ, with φ being the porosity) generated by the slow and fast P-wave as well as by the background flow.

Relative permeability changes due to oscillatory fluid flow

Laboratory experiments showed that permeability changes associated with colloidal mobilization are correlated with the ratio between the pressure oscillations ($\nabla p_f(\omega)$) and the pressure gradient driving background flow (∇p_f^0) as

$$\frac{\Delta\kappa}{\kappa_0} = a\left(\frac{\nabla p_f(\omega)}{\nabla p_f^0}\right)^b. \quad (2)$$

In the following, we use **Eq. 2** with *a*=0.7 and *b*=1.7 (Elkhoury et al., 2011) to predict seismically-induced permeability changes. ∇p_f^0 is set to 1kPa/m, which produces a Darcy flow velocity ~10 m/day in a conductive fracture. We first consider a low porosity Berea sandstone embedding a set of highly conductive and compliant fractures. Then, we consider a two layer medium composed by an alternation of low and high porosity sandstones.

Seismically-induced permeability changes in porous media

To obtain the seismically-induced $\nabla p_f(\omega)$, we numerically solve Biot's equations neglecting inertial terms in **Eqs. (1c)-(1d)** and applying boundary conditions representative of the strain state of a seismic body wave (**Fig. 1a**). Then, we use the seismically-induced $\nabla p_f(\omega)$ in **Eq. 2** to predict permeability changes. Permeability changes are computed for the permeability of the medium parallel to the fractures or layers.

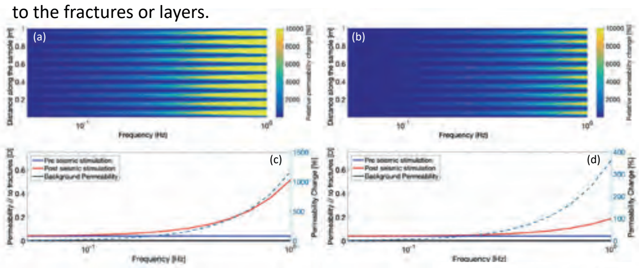

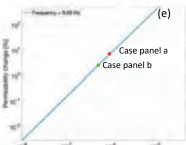

Figure 3: Predicted relative permeability change (**Eq. 2**) in a water-saturated fractured sandstone subjected to the action of a normally incident P-wave as a function of frequency. The P-wave strain is set to 1e−6 (a, c) and 5e-7 (b, d). Panel e) shows the strain dependence of the permeability changes for a frequency *f*=2πω=0.05 Hz.

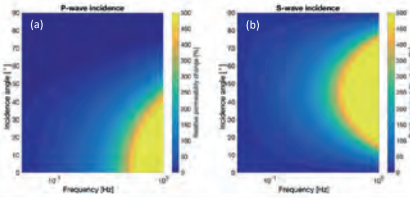

Figure 4: Angle and frequency dependence for (a) P- and (b) S-waves. Properties are the same as in **Fig. 3a**. Maximal permeability changes are expected at quasi-normal and ~45˚ incidence for P- and S-waves, respectively.

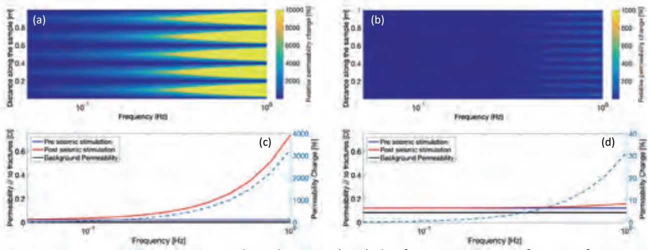

Figure 5: Same scenario as **Fig. 3a** but changing (a, c) the fracture intensity from 10 fractures per meter to 5 fractures per meter and (b, d) the background porosity from 0.035 to 0.1.

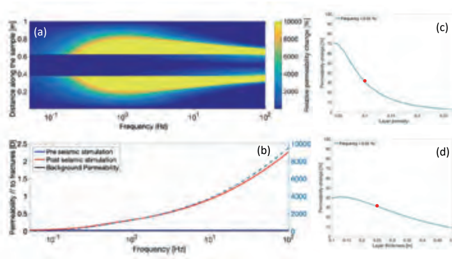

Figure 6: Predicted permeability change as a function of frequency in a water-saturated double porosity sandstone due to the action of a normally incident P-wave. The strain is set to 1e−6. Right panels show permeability changes for *f*= 0.05 Hz as a function of the porosity (c) and thickness (d) of the mid layer.

Conclusions

- We showed that only diffusive waves are able to induce flow rates in the pores that are in the order of those mobilizing fine particles (**Fig. 2**);
- In heterogeneous porous media (e.g., due to layering or fracturing), diffusive waves created as energy conversion from elastic waves at the interfaces separating two phases of the medium can induce permeability changes;
- For a medium containing conductive fractures, incident body waves of tenths of Hz and microstrains are able to induce hydrodynamic forces in the pores significantly larger than those associated with typical natural background flows, resulting in potential permeability increases >10% (**Fig. 3e**).

References: **Biot**, M. A., 1962, Mechanics of deformation and acoustic propagation in porous media. J. of App. Phys., 33; **Candela et al.**, 2014, Laboratory evidence for particle mobilization as a mechanism for permeability enhancement via dynamic stressing. Earth and Plan. Sci. Lett., 392; **Elkhoury et al.**, 2011, Laboratory observations of permeability enhancement by fluid pressure oscillation of in situ fractured rock. Journal of Geoph. Res.: Solid Earth, 116; **Manga et al.**, 2012, Changes in permeability caused by transient stresses: Field observations, experiments, and mechanisms. Rev. Geophys., 50.

SCCER SoE
SWISS COMPETENCE CENTER for ENERGY RESEARCH
SUPPLY of ELECTRICITY

SCCER-SoE Annual Conference 2019

heatstore High Temperature Underground Thermal Energy Storage

Supported by:
Schweizerische Eidgenossenschaft
Confédération suisse
Confederazione Svizzera
Confederaziun svizra
Swiss Confederation
Innosuisse – Swiss Innovation Agency

Modeling Ground Surface Deformation at the Swiss HEATSTORE Underground Thermal Energy Storage Sites

Daniel T. Birdsell[1] and Martin O. Saar[1]
[1]ETH Zürich - Geothermal Energy and Geofluids Group, Institute of Geophysics, Sonneggstrasse 5, 8092 Zürich (Switzerland)

Background and Motivation

- Storing summertime waste heat for wintertime heating of buildings offers potential environmental and economic benefits
- High Temperature (25 – 90 °C) Aquifer Thermal Energy Storage (HT-ATES) is promising, but offers new challenges
- The potential for geomechanical/geotechnical problems (e.g. surface uplift) in HT-ATES is poorly studied
- How is ground uplift affected by aquifer depth, rock properties, well spacing, and operational decisions?

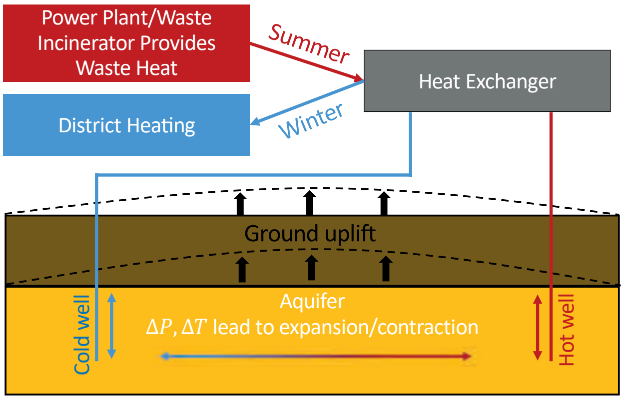

Adapted and expanded from Lu et al. (2019)

Partners

- HEATSTORE aims at developing subsurface storage techniques to reduce wasting heat.
- The Swiss contribution includes two HT-ATES pilot projects, industrial partners, and research institutions

Conceptual and Numerical Model

- Conceptual model based on simplified subsurface characterization and energy system scenario modelling at Geneva site
- Hydromechanical equations solved in MOOSE framework (Gaston et al., 2015)
- Base case uses push-pull injection; alternative scenarios also simulated

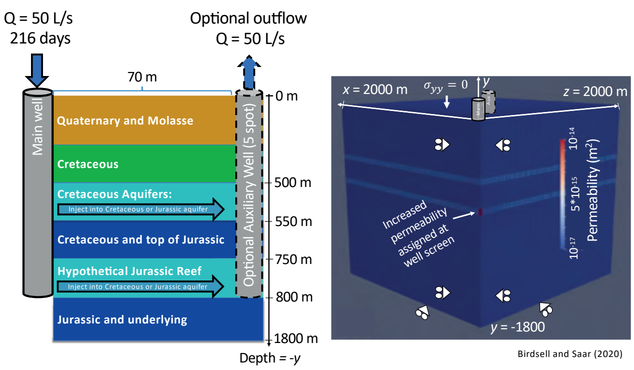

Birdsell and Saar (2020)

Results

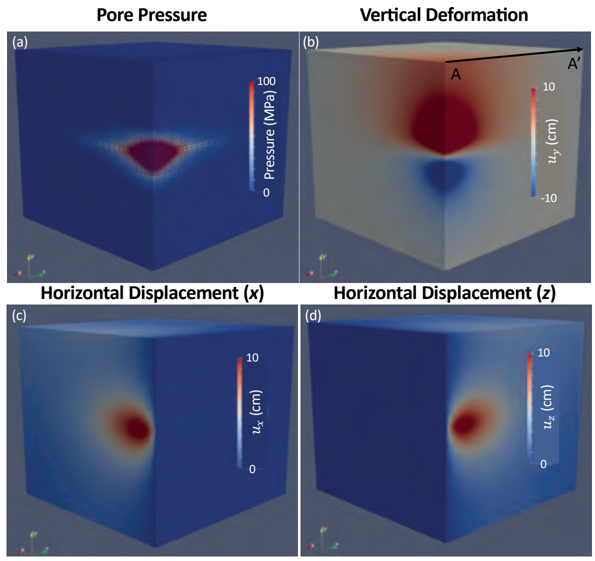

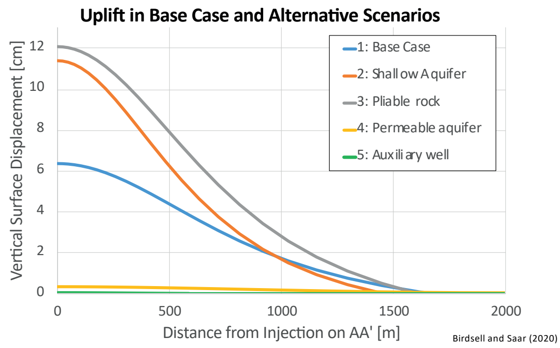

Birdsell and Saar (2020)

Conclusions and Future Work

- Auxiliary well to balance pressure and sufficient permeability are key to reducing pore pressure and uplift
- Future work will expand to thermo-hydro-mechanical modeling and investigate well spacing, operating temperature, and incorporate more complex, site-specific geological and energy system information

Acknowledgements

HEATSTORE (170153-4401) is one of nine projects under the GEOTHERMICA – ERA NET Cofund aimed at accelerating the uptake of geothermal energy in Europe. The project is subsidized through the ERANET cofund GEOTHERMICA (Project n. 731117) by the European Commission, RVO (the Netherlands), DETEC (Switzerland), FZJ-PtJ (Germany), ADEME (France), EUDP (Denmark), Rannis (Iceland), VEA (Belgium), FRCT (Portugal), and MINECO (Spain). More information is available via http://www.heatstore.eu

References

- Birdsell, D. T., & Saar, M. O. (2020). Modeling Ground Surface Deformation at the Swiss HEATSTORE Underground Thermal Energy Storage Sites. *World Geothermal Congress 2020*. Reykjavik, Iceland: Submitted for publication.
- Lu, H., Tian, P., Guan, Y., & Yu, S. (2019). Integrated suitability, vulnerability and sustainability indicators for assessing the global potential of aquifer thermal energy storage. *Applied energy*, 239, 747-756.
- Gaston, D. R., Permann, C. J., Peterson, J. W., Slaughter, A. E., Andrš, D., Wang, Y., ... and Zou, L.: Physics-based multiscale coupling for full core nuclear reactor simulation. Annals of Nuclear Energy, 84, (2015), 45-54.

SCCER SoE
SWISS COMPETENCE CENTER for ENERGY RESEARCH
SUPPLY of ELECTRICITY

SCCER-SoE Annual Conference 2019

Supported by:
Schweizerische Eidgenossenschaft
Confédération suisse
Confederazione Svizzera
Confederaziun svizra
Swiss Confederation
Innosuisse – Swiss Innovation Agency

3-D Static Model to Characterize Geothermal Reservoirs for High-Temperature Aquifer Thermal Energy Storage (HT-ATES) in the Geneva Area, Switzerland

UNIVERSITÉ DE GENÈVE
FACULTY OF SCIENCE
Department of Earth Sciences

Eruteya, O.E., Guglielmetti L., Makhloufi, Y., Moscariello A.
Department of Earth Sciences, University of Geneva, Switzerland | Email: Ovie.Eruteya@unige.ch

GE-RGBA

1. Background

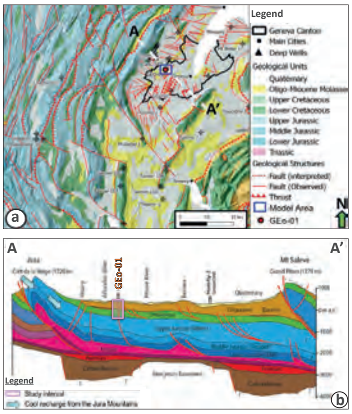

Figure 1a. Location of the study area. (b) Configuration of the Geneva Basin (Modified from Moscariello et al., 2020).

In the framework of the GEOTHERMICA ERA-NET co-funded project-HEASTORE, one of the main challenges related to assessing the technical feasibility and sustainability of High Temperature (~25°C to ~90°C) Aquifer Thermal Energy Storage (HT-ATES) is subsurface characterization.

In this study, we aim to develop a 3-D geologically robust static model in order to characterize the subsurface around the recently drilled GEo-01 geothermal exploration borehole in the Geneva Basin (Figure 1).

We focused on identifying possible candidate intervals suitable for HT-ATES within the Lower Cretaceous Carbonates in the Geneva Area. This was achieved by analyzing a suit of subsurface dataset (Figures 2 and 3).

2. Workflow

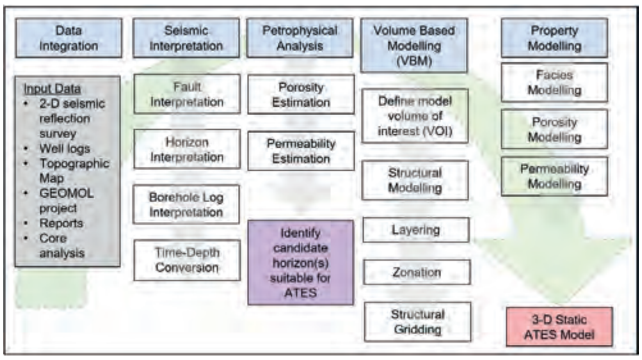

Figure 2. Workflow adopted to build the 3-D Static Model.

3. Seismic Interpretation

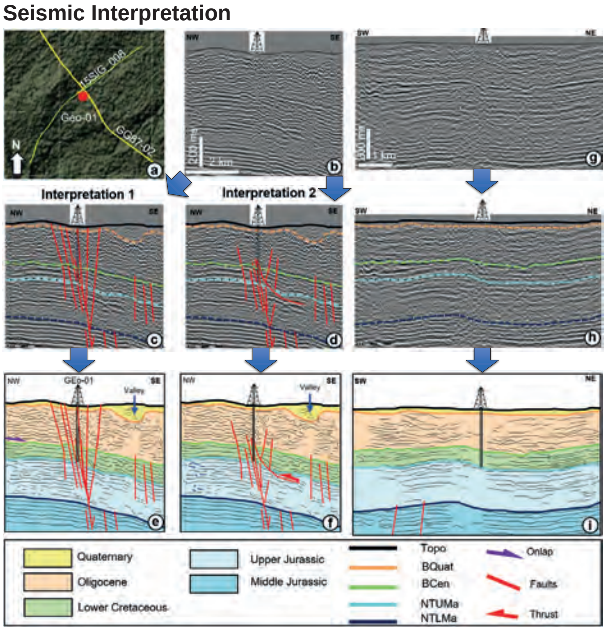

Figure 3. (a) Location of the seismic lines and Geo-01 well. (b - i) NW-SE and SE-NW seismic profile showing the subsurface structural situation around the Geo-01 borehole. Two plausible interpretations are presented for line GG 87-02 with a major difference being the introduction of a thrust fault in Interpretation 2.

Reference Moscariello A. et al. Heat production and storage in Western Switzerland: advances and challenges of intense multidisciplinary geothermal exploration activities, 8 years down the road. *Proceedings* World Geothermal Congress 2020, Reykjavik, Iceland, April 26 – May 2, 2020. 12 pp.

Acknowledgements
heatstore
Schlumberger

4. Potential Storage Interval in the Lower Cretaceous: CT 1-3★

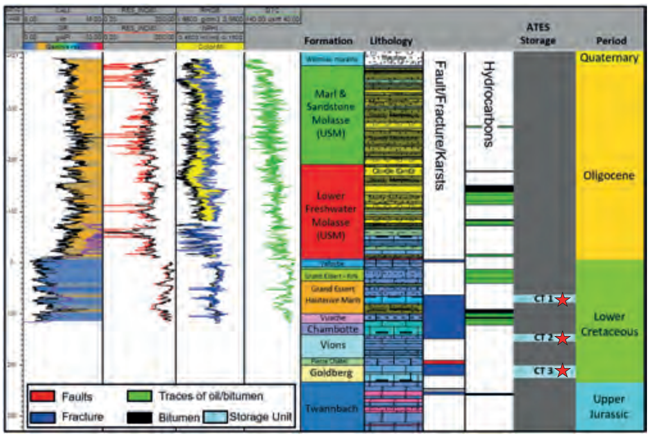

Figure 4. Well interpretation panel for GEo-01 borehole. Three candidate horizons have been identified as potential Lower Cretaceous targets (CT) suitable for HT-ATES in fractured intervals characterized by tested water outflows and devoid of hydrocarbon impregnation: (1) Grand Essert Fm / Pierre Jeune de Neuchatel + Marnes d'Hauterives Fm [CT1 – 10 m], (2) Vuache Fm - Chambotte- Chambotte inférieur [CT2 -12.5 m] and (3) Goldberg Fm [CT3 – 25 m].

5. 3-D Static Model Development (1.5 x 1.5 x 1 Km) – Interpretation 1

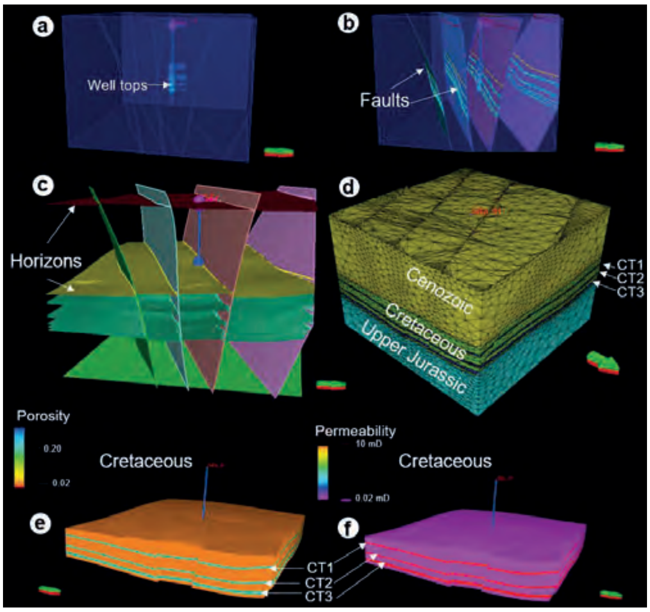

Figure 5. (a) Volume of interest (b) Faults interpreted (c) Fault and Horizons interpreted (d) Layering with the three candidate intervals for HT-ATES CT 1, CT2 and CT3. (e) Porosity model (f) Permeability model.

6. Outlook

- Uncertainties remain especially in the fault geometry and modelling and facies distribution which was assumed to be homogenous in this simplicist case presented here based on the low data density.
- The Lower Cretaceous unit are tight with low porosity and permeability values. The presence of karstified, faulted and fractured intervals locally enhance porosity and permeability. This permit large groundwater flows, making the well suitable for direct uses and only in a second instance favourable for storage.
- The 3-D static model presented here will be employed as input for numerical heat flow and predictive THMC models for the Geneva Basin.

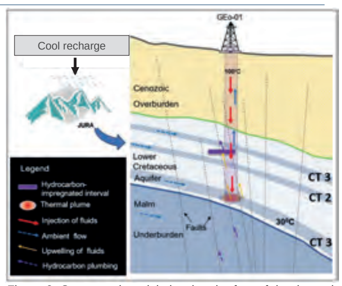

Figure 6. Conceptual model showing the fate of the thermal plume based on the GEo-01 well assuming high-temperature fluids are injected in the thickest and deepest aquifer CT3 in the Grand Essert formation. The natural recharge of the system here is from the Jura Mountain chains and circulation at depth is related to the hydraulic gradient. The presence of a highly conductive fault zone controlling the natural artesian flow observed at GEo-01 might reduce the likelihood for the development of an efficient HT-ATES system considering an extended period of thermal storage.

SCCER SoE
SWISS COMPETENCE CENTER for ENERGY RESEARCH
SUPPLY of ELECTRICITY

SCCER-SoE Annual Conference 2019

Supported by:
Schweizerische Eidgenossenschaft
Confédération suisse
Confederazione Svizzera
Confederaziun svizra
Swiss Confederation
Innosuisse – Swiss Innovation Agency

unine
UNIVERSITÉ DE NEUCHÂTEL

Reactive Flow Model for Porosity Reduction by Quartz Dissolution and Precipitation

Batoul Gisler, Boris Galvàn, Reza Sohrabi, Stephen A. Miller
Centre for Hydrogeology and Geothermics (CHYN), University of Neuchâtel, Switzerland
batoul.gisler@unine.ch

Introduction

Quartz dissolution and precipitation is an important pore reducing process in geothermal reservoirs. It also causes scaling, which affects the machinery and hinders the productivity of the geothermal energy project. Furthermore, permeability decrease due to quartz deposition has been proposed as an important factor in the temporal decay of aftershocks. In this work we present a reactive flow model to study the evolution of porosity, permeability and solute transport of the system. The geometry of the model assumes a porous medium block in which chemical reactions occur between the pore fluid and the rock matrix. The model assumes a coupling between heat and fluid mass transport. The Center for Hydrogeology and Geothermics has recently developed **“Efrack3D”**, a fully coupled 3D Thermo-Hydro-Mechanical (THM) model. We aim to ultimately integrate the reactive flow model with the THM model. Economic reservoir development requires a combined analysis of the thermo-hydro-mechanical and chemical processes.

Approach and model geometry

Quartz dissolution and precipitation is a surface controlled reaction, and is therefore highly temperature dependent. The solubility of silica increases rapidly with temperature, to almost double between 80°C and 110°C [1]. Fig.1 represents a road map of the **reactive flow** model. First, all temperature dependent parameters are calculated and initial and boundary conditions are defined. The REV of the system is a block composed of spherical shaped grains with an initial porosity. The change in contact area between the grains due to quartz precipitation and dissolution is calculated based on [2]. The solute transport equation includes both diffusion and advection terms, and is solved with finite difference method. Once the concentration is calculated, the porosity evolution is computed via the mass conservation equation. The new porosity is used to recalculate the contact surface area at each time step. Finally, the permeability is estimated as a function of time and space, allowing us to predict pore pressure evolution in the reservoir. In the beginning, to simplify the problem we assume no compaction of the grains, nevertheless, vertical stress and consolidation are controlling factors in the variation of the surface contact area.

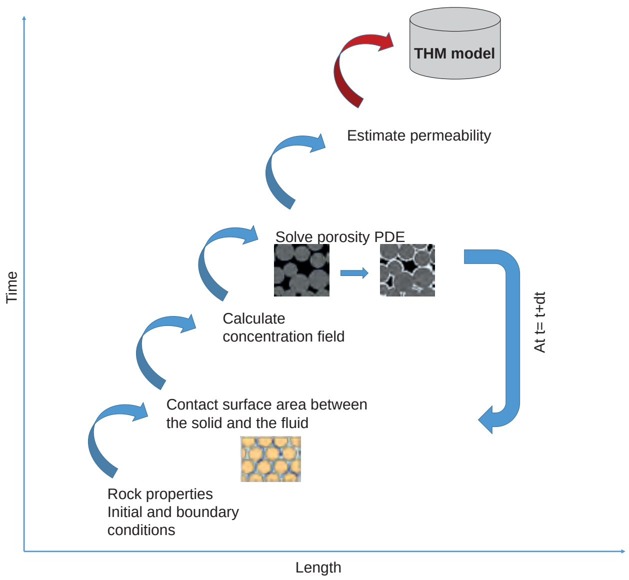

Figure 1: Road map for the reactive flow model as a function of time and length scales.

Mathematical model

$$H_4SiO_{4(aq)} = SiO_{2(s)} + 2H_2O_{(l)}$$

The precipitation rate constant k_- and the equilibrium quartz concentration c_{eq} are given by [3]:

$$\log k_- = -0.707 - \frac{2589}{T} \qquad \text{Eq. 1}$$

$$\log c_{eq} = -\left(\frac{1107}{T}\right) - 0.025 \qquad \text{Eq. 2}$$

Solute transport for quartz precipitation and dissolution in the rock matrix is described by the linear reaction equation:

$$\frac{\partial C'}{\partial t} = D_m \nabla^2 C' - \frac{K}{\emptyset} C' \qquad \text{Eq. 3}$$

We solve Eq.3 using total variation diminishing method, where $C' = c - c_{eq}$.The apparent precipitation rate constant K is given by:

$$K = \frac{A}{M} k_- \qquad \text{Eq. 4}$$

Where A is the interfacial area between the solid and the fluid of mass M [2]. Mass conservation of silica is governed by:

$$\frac{\partial(\emptyset c)}{\partial t} + \frac{\partial(uc)}{\partial x} = -\emptyset K\left(c - c_{eq}\right) \qquad \text{Eq. 5}$$

Assuming a constant flow rate, Eq. 5 represents porosity evolution and is solved using finite difference scheme.

Finally, permeability is estimated using the Cozeny-Carman Equation.

Outlooks

We ultimately aim to investigate the consequences of quartz dissolution and precipitation on the mechanical response of the rock matrix. It is essential for sustainable wellbore productivity and development. The porosity and permeability evolution terms may be integrated to the Efrack3D to visualize pore pressure development and analyze the geomechanics. Furthermore, this may allow us to visualize possible localized cracking due to pore pressure developement and better understand fluid driven aftershocks, as it has been stated that repeated fracturing events followed by crack healing are in connection with earthquakes [4].

References

[1] Giles, M.R., Indrelid, S.L., Beynon, G.V., Amthor, J. (2000). The origin of large-scale quartz cementation: evidence from large data sets and coupled heat-fluid mass transport modelling. Spec. Publs int. Ass. Sediment, No. 29, pp. 21-38.

[2] Canals, M. & Meunier, J.D. (1995). A Model for porosity reduction in quartzite reservoirs by quartz cementation. Geochimica et Cosmochimica Acta, Vol. 59, No. 4, pp. 699-709.

[3] Rimstidt, J.D. (2013). Geochemical Rate Models: An Introduction to Geochemical Kinetics.

[4] Walder, J. & Nur, A. (1984). Porosity reduction and crustal pore pressure development. Journal of geophysical research, Vol. 89, No. B13, pp. 11,539-11,548.

SCCER-SoE Annual Conference 2019

Sensitivity Analysis of High Temperature Aquifer Thermal Energy Storage (HT-ATES) using TH Simulations

Julian Mindel, Thomas Driesner, Institute of Geochemistry and Petrology, ETH Zurich

Supported by: Schweizerische Eidgenossenschaft, Confédération suisse, Confederazione Svizzera, Confederaziun svizra. Swiss Confederation. Innosuisse – Swiss Innovation Agency

Abstract / Background

The Geneva-section of the HEATSTORE project has set its goals on the assessment of the feasibility of an HT-ATES system to be operated in the Swiss Canton of Geneva. The studied area has been characterized as geologically and logistically challenging [1] as a result of its prospective aquifers being intersected and offset by faults and the relatively high population density. Given these challenges, using a numerical tool becomes essential to carry out a virtual exploration of possible scenarios. A sensitivity analysis can thus be performed and insight be obtained to characterize response, determine feasibility, and deliver fundamental understanding of the effects of geologic heterogeneities, operational strategies, and groundwater conditions on ATES efficiency. Such a study was carried out previously by [2], using a different numerical approach and addressing similar questions regarding the effects of possible parameters via the consideration of a doublet well pattern. It is our intent to contribute and compare to this previously-made analysis, by expanding the parameter space and introducing some of the advantages of simulating Discrete Fracture and Matrix models with a view towards the faulted/fractured complexity of the Geneva basin.

We present results and insights obtained during our first design iteration of TH simulations with particular focus on the geology of the Geneva Basin, although the insight obtained may be applicable elsewhere. By using a numerical tool to simulate a large number of scenarios we have worked towards a better understanding of an HT-ATES system response to variations in essential design factors.

Modelling approach

Through exploring a multi-dimensional parameter space composed of the terms explained in Tables 1 and 2, we produced a range of site-relevant scenarios to be numerically simulated. Well and fracture setup is described in Figure 2.

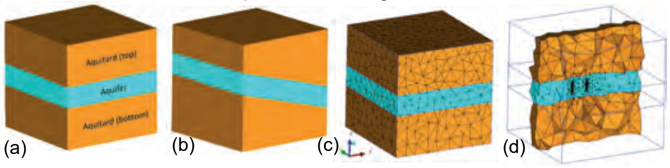

Figure 1 : *Geometrical/Geological model representing the basic elements of an ATES, depicting (a) a flat version of the model, (b) a version of the model possessing an aquifer with a 15º angle of dip, (c) the volumetric tetrahedral tesselation (i.e. mesh) of the flat geometrical model using the ICEMCFD software, and (d) mesh cutplane depicting variable resolution when approaching regions containing wells.*

Aquifer Permeability	Aquifer Thickness	Well Strategy	Groundwater	Fracture Configuration	Aquifer Dip
K13	L200	single	YGW	F0	FLAT
5K13	L300	doublet	NGW	FU	INCL
K12	L400	5spot		FD	

Table 1 : *Summary of sub-scenario variant codes. When combined, these codes produce the different simulation case names*

Parameter	Units	Aquitard (top)	Aquifer	Aquitard (bottom)
Density (r_r)	[kg/m³]	2450	2450	2680
Permeability (*k*) (original matrix)	[m²]	10^{-17}	10^{-15}	10^{-17}
Permeability K13 (*k*) (fractured, effective)	[m²]	10^{-17}	10^{-13}	10^{-17}
Permeability 5K13 (k) (fractured, effective)	[m²]	10^{-17}	$5 \cdot 10^{-13}$	10^{-17}
Permeability K12 (k) (fractured, effective)	[m²]	10^{-17}	10^{-12}	10^{-17}
Porosity (*f*) (matrix, effective)	[-]	0.01	0.2	0.01
Permeability (k) (fracture, effective)	[m²]	N/A	10^{-11}	N/A
Porosity (*f*) (fracture, effective)	[-]	N/A	0.5	N/A
Fracture thickness	[m]	N/A	0.1	N/A
Specific Heat Capacity ($c_{p,r}$)	[J/(Kg °K)]	860.2	832.9	849.9
Thermal Conductivity l_r (λ_r)	[W/(m °K)]	2.275	2.806	2.692
Thickness L200 (L)	[m]	400	200	400
Thickness L300 (L)	[m]	350	300	350
Thickness L400 (L)	[m]	200	400	400
Groundwater velocity (v_{gw}) (assumed)	[m/yr]	N/A	2	N/A

Table 2: *Summary rock material parameters [3]*

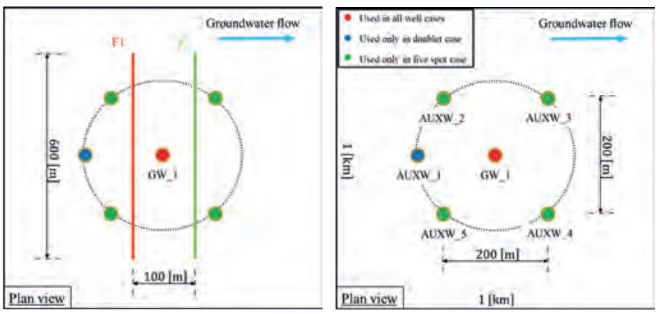

Figure 2: (left) Fracture locations with respect to wells, and (right) the specific x-y plane view of well locations and respective names .

Results

Having observed that system efficiencies increase monotonically over time, we found it practical to use the values at the end of the ATES lifetime (i.e. 15 years) for our analyses. A summary of exergy efficiency values at the end of life of the ATES for each of 324 simulations is presented in Figure 3. Snapshots of selected results are presented in Figures 4 and 5.

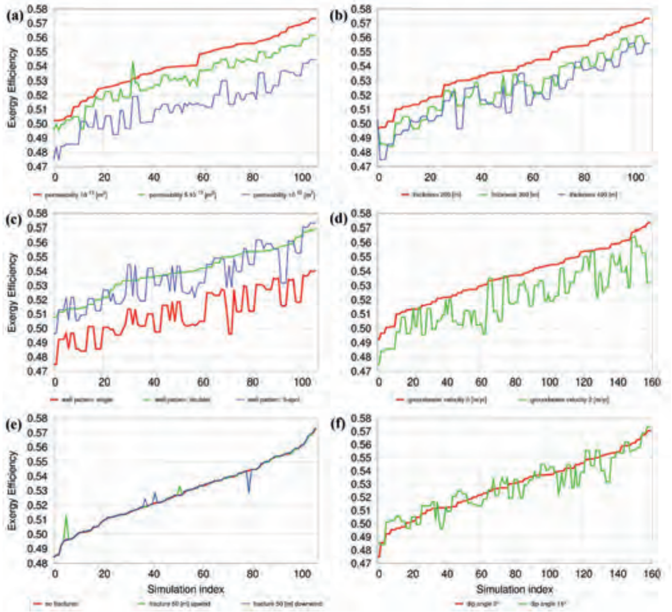

Figure 3: *Exergy efficiency measured at the end of the ATES lifetime. Each graph represents a particular horizontal ordering of the same set of results, sorted in increasing exergy efficiency w.r.t. a particular variant code (see Table 1). The simulation index is an arbitrary number guide pointing to a subset of otherwise identical simulations that only differ by one particular parameter: (a) aquifer permeability, (b) aquifer thickness, (c) well pattern, (d) groundwater velocity, (e) fracture configuration, and (f) aquifer dip angle.*

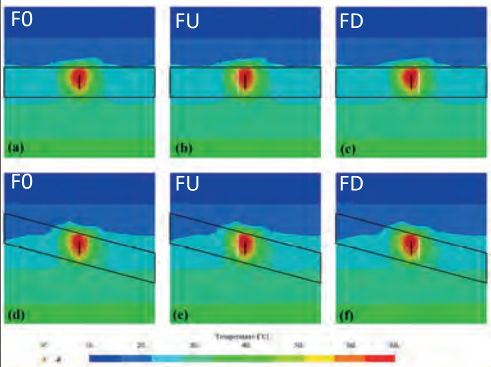

Figure 4: *Fracture and dip angle effects on the temperature signature at the end of the ATES lifetime in a full-domain middle x-z planar cross section for 6 simulations with equal permeability (K12), thickness (L200), well pattern (single), and no groundwater flow (NGW). Well GW_1 and aquifer perimeter are demarcated by black lines, while fractures are shown as white lines.*

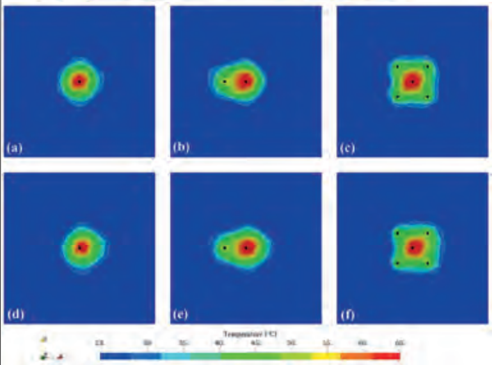

Figure 5: *Well pattern and groundwater effects on the temperature signature at the end of the ATES lifetime in a full-domain middle x-y planar cross section for 6 simulations with no inclination (FLAT), no fractures (F0), equal permeability (K12), and equal thickness (L200). Row-wise, NGW (a,b,c), and YGW (d,e,f), groundwater conditions have been applied to the top, and bottom rows respectively, while column-wise, single (a,d), doublet (b,e), and 5spot (c,f) have been applied to the left, middle and right columns of simulations, respectively.*

Conclusions & Outlook

Our study [4] further confirms some observations that have already been made in the literature, particularly with respect to groundwater drift and buoyancy effects present in high permeability aquifers. We have also observed that when active, auxiliary wells help mitigate pressure-peak related effects, improve the thermal front sweep, and also provide some measure of shielding against the drift due to the flow of groundwater.

Refrences

1. Nawtratil del Bono, C., Meyer, M. & Martin, F., 2019. GEothermie 2020: Avancée du programme et premiers succès. Presentation Journée Romande de Geothermie 2019, Lausanne: SIG.
2. Ingeneurs Résonance, 2017. Stockage de chaleur dans le Malm du bassin genevois., s.l.: Rapport technique TR-6001.031/NL.
3. Driesner, T. (ed.), 2019. Initial report on tools and workflows for simulating subsurface dynamics of different types of High Temperature Underground Thermal Energy Storage, Zurich: GEOTHERMICA – ERA NET Cofund Geothermal, unpublished report.
4. Mindel, J., Driesner, T., *Sub.,in review.* HEATSTORE: Preliminary Design of a High Temperature Aquifer Thermal Energy Storage (HT-ATES) System in Geneva Based on TH Simulations, Proc. WGC 2020.

SCCER SoE
SWISS COMPETENCE CENTER for ENERGY RESEARCH
SUPPLY of ELECTRICITY

SCCER-SoE Annual Conference 2019

Supported by:
Schweizerische Eidgenossenschaft
Confédération suisse
Confederazione Svizzera
Confederaziun svizra
Swiss Confederation
Innosuisse – Swiss Innovation Agency

Experimental Thermo-Hydro-Mechanical test site to quantify heat exchange characteristics of fractured limestone aquifers

Reza Sohrabi & Benoît Valley

Centre for Hydrogeology and Geothermics (CHYN), University of Neuchâtel, Switzerland

reza.sohrabi@unine.ch

Motivation

Providing to our societies greenhouse-gas free energy sources is a main challenge tackled by the energy turnaround initiated in many countries. Heat demand and supply are off-phase over seasonal cycles. Storing heat in time of surplus and providing it when needed is part of the tools required to reduced the energy footprint. Underground Thermal Energy Storage (UTES) [1] is one solution for this process. Various configuration of UTES are used including Aquifer Thermal Energy Storage (ATES). Until now many studies have shown the potential of ATES in shallow porous geological media. But conflict of use, aquifer availability and environmental regulations pushes for going to deeper, hard rock aquifers for which characterization approaches and suitability evaluation for heat storage need to be developed.

Methods

In hard rock aquifers and more specifically in limestone aquifers, fractures and karst (dissolution conduits) carry most of the flow. This results in complex flow geometry. The hydrodynamic characterization of such system is approached by coupling classic well tests analyses and geostatistical geo-structure distribution as Discrete Fractured Network (DFN) or conduit distribution (Karst) network.

The complexity of such systems make hard predicting the real shape of the reservoir and almost impossible to quantify the exchange area available for heat transfer between fractured or karstified structures and the rock matrix. The structures in the aquifer will control the flow geometry. At same bulk aquifer transmissivity, the flow geometry can differ significantly. This will have a large impact on heat exchange properties of the reservoir. Approaches needs to be further develop for heat storage application in order to assess heat transport and storage in fractured and karstified rock masses.

The methodology proposed is simple. We focus on the temperature that we can store in the reservoir via an injection test in satured condition and the thermal response of the push-pull experiment will allow us to determine experimentally and numerically, if the aquifer has the potential volume required considering simple structure (fractures or conduits) to store any heat demand (Figure 1).

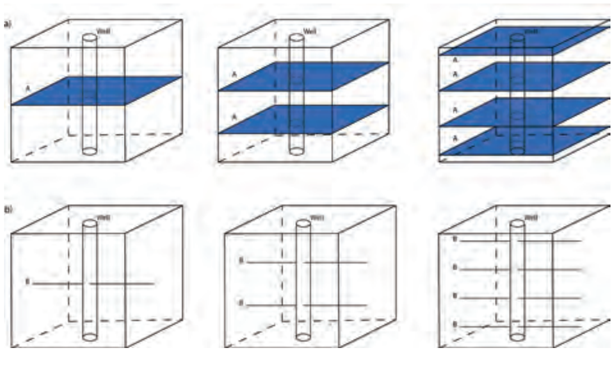

Figure 1: Simple conceptual model considering a) fractures network or b) conduits network.

Experimental site

The first ATES experiment in porous media was performed by the Centre of Hydrogeology and Geothermics (CHYN) at the University of Neuchâtel (Switzerland) in 1974 [2],[3],[4]. Further countries such as U.S.A, France, Japan, Germany, or Canada started participating in ATES research with their own experimental field sites.

Here, the idea is to develop a new experimental test site in fractured and karstified rocks in Concise (VD) Switzerland (Figure 2) and to perform hot water push-pull tests during several days in order to devise a thermo-hydraulic characterization approach for ATES in fractured media.

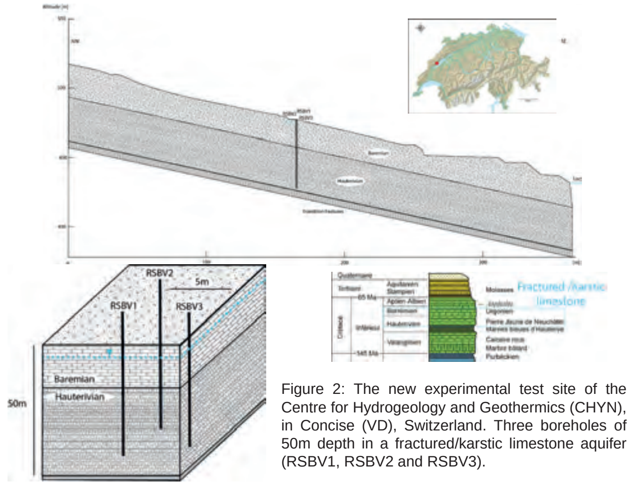

Figure 2: The new experimental test site of the Centre for Hydrogeology and Geothermics (CHYN), in Concise (VD), Switzerland. Three boreholes of 50m depth in a fractured/karstic limestone aquifer (RSBV1, RSBV2 and RSBV3).

In addition to thermo-hydraulic processes, we also consider the impact of thermo-hydro-mechanical (THM) response of the rock that in turn can impact the hydraulic characteristic of the aquifer. For example, thermo-elastic rock expansion could induce fracture closure and thus the transmissivity of the reservoir will decrease. It is required to measure the mechanical conditions in the reservoir (e.g. stress state) in order to assess the impact of such effects on an aquifer thermal storage system.

The thermal response will be different considering granular, fractured or karstic rock. Through analyses of the thermo-hydraulic field response with different numerical simulations, we will be able to better understand the flow and heat exchange geometry in the vicinity of the well. These is a requirement to assess the characteristics and predict the performance within local hydrogeological conditions of a given ATES site.

Conclusion and Outlooks

This research aims at developing thermo-hydro-mechanical tests in fractured / karstic rock that will enable characterization and design of the next generation ATES in such environments. The outcome of this research will include experimental protocols and analyses modelling tools required to predict performance and assess viability of ATES. This method include simple approach to make the link between storage capacity and real storage underground possibilities addressing a need of engineers and regulators for Heat Storage Projects. The research will provide improved approaches to quantify system connectivity, complex geo-structure, hydrogeology and storage volume, based on physical experiments. The proposed method will be tested and validated on a in-situ ATES analog test site in fractured and karstified rocks.

Advances from the program include:

- In-situ heat transport parameters determination
- Flow measurements and hydraulic: efforts to characterize and model flows at various scales will also be pursued
- Evaluation of thermo-hydro-mechanical coupled process in ATES
- Validation of numerical simulator against field data in order to improve the predictive capability of the simulation tools

Acknowledgements

This work was supported by the framework of the European Project HEATSTORE (170153-4401) under the GEOTHERMICA-ERA NET Grant (Nº 731117) supported by the European Commission, RVO (the Netherlands), DETEC (Switzerland), FZJ-PtJ (Germany), ADEME (France), EUDP (Denmark), Rannis (Iceland), VEA (Belgium), FRCT (Portugal), and MINECO (Spain), technological development and demonstration under agreement.

References

[1] Fleuchaus, P., Godschalk, B., Stober, I., & Blum, P. (2018). Worldwide application of aquifer thermal energy storage–A review. Renewable and Sustainable Energy Reviews, 94, 861-876.
[2] Saugy, B., Doy, R., Mathey, B., Aragno, M., Geister, M., Rieben, C., et al. (1984). Accumulateur de chaleur en nappe souterraine SPEOS - Bilan de deux ans d'exploitation. SEATU: Société des éditions des associations techniques universitaires.
[3] Saugy, B. (1992). Speos-dorigny and associated projects on aquifer thermal energy storage: Annex III des Programms der Internationalen Energieagentur: Energy conservation through energy storage.
[4] Tsang, C. F. and Hopkins, D.L. (1982). Aquifer thermal energy storage: a survey: Recent trends in hydrogeology. Geological Society of America. p. 427–42.

Investigating mineral reactions during high-temperature aquifer thermal energy storage (HT-ATES)

D.B. van den Heuvel (daniela.vandenheuvel@geo.unibe.ch), Ch. Wanner, U. Mäder, P. Alt-Epping & L.W. Diamond
Institute of Geological Sciences, University of Bern, Switzerland

Background

Industrial processes (e.g. waste incineration, manufacturing) generate **constant surplus heat** ⇒ **Heat demand strongly seasonal** → Excess energy to be **stored** during summer and fed into district heating network during winter to reduce wasting of energy/consumption of fossil fuels

Aquifer thermal energy storage (ATES) = using porous lithologies with little/no groundwater flow to seasonally store warm waters in the geosphere[1]

Low-T ATES (T_{inject} < 40 °C)
- Many successful systems installed in Europe (esp. NL) [1]

High-temp. ATES (T_{inject} > 40 °C, often > 70 °C)
- 5 operational + many failed systems around the world[1]

⇒ Challenges related to HT-ATES need to be overcome to increase contribution of ATES to the future heating energy supply

HT-ATES projects in Switzerland

Heat sources: waste-to-energy plants

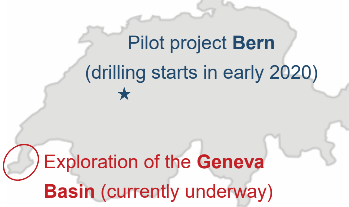

Target lithologies investigated for HT-ATES (porous but laterally constrained): Channel Sst (BE, GE), karstified Ls (GE), reef complex Ls/Dol (GE)

Geochemical challenges

Surface installations (during heating):
- Carbonate scaling[2]

Surface installations (during cooling):
- Silicate scaling

In the reservoir (during storage):
- Carbonate precipitation around injection well → Clogging[3]
- Dissolution of silicate/other minerals → Release of heavy metals[4] As Cd Pb
- Swelling of clay minerals → Surface uplift (up to 2.5 cm)[5]
- Microbial activity → Clogging (biofilms), scaling, MIC[6]
- Thermal stratification of aquifer → Reduced yield[7]

In the reservoir (during reinjection):
- Carbonate dissolution (cement) and release of fines → Clogging[4]

Investigations into the planned Bern HT-ATES pilot site

Planned system parameters

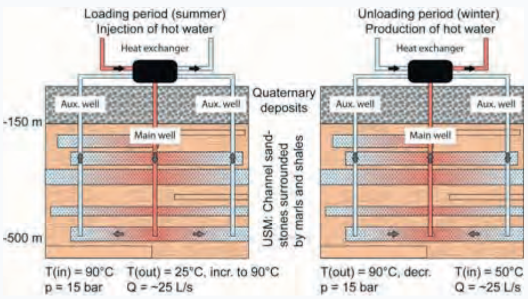

Characterisation of Sst & form. water

- Medium- to coarse-grained **channel Sst** (layers generally 2-8 m thick[8]) of the LFM
- **Composition**: Monomineralic and lithic grains cemented by Cc and clay minerals
- **Porosity**: 18 vol.%, **Permeability**: 370 mD
- **Water-type**: Na-Mg-Ca-Cl-SO_4-(HCO_3) TDS ~ 350 mg/L, pH 8.1 Temperature (in-situ) 13.7°C

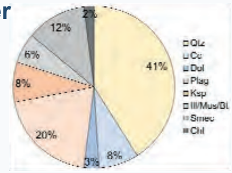

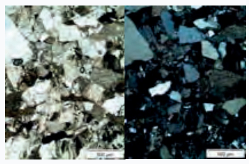

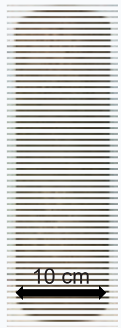

Simulation of loading – unloading cycle (PHREEQC, equilibrium approach)

① Equilibrate with aquifer minerals @ 20 °C
↓
② Heat solution to 90 °C in heat exchanger
↓
③ Equilibrate with aquifer minerals @ 90 °C
↓
④ Cool solution to 20 °C in heat exchanger

	SI > 0 (supersat.)	SI < 0 (undersat.)
①	Dol, Kaol, Musc, Qtz	Alb, Cc, Chl, Ill, Kspr, Montm
②	Cc, Dol	*Heat exch., ppt only*
③	Alb, Cc, Chl, Musc, Qtz	Dol, Ill, Kspr, Montm
④	Alb, Ill, Kaol, Kspr, Montm, Qtz	*Heat exch., ppt only*

Equilibrium approach ok for storage period ③ (lasts several months) but not for heating/cooling ②/④ (lasts a few minutes) → **Kinetics** to be taken into account

More soluble, less/non-crystalline polymorphs often precipitate instead of the least soluble mineral (e.g. Chal/$SiO_{2(am)}$ instead of Qtz)
- Kinetic data of such phases generally not well constrained

⇒ **Lab experiments to identify mineral reactions and quantify reaction rates**

⇒ **Use as input in reactive transport modelling of the site (PFLOTRAN)**

Precipitation experiments in Ti-vessels: monitoring of solution chemistry f(time) (ongoing)

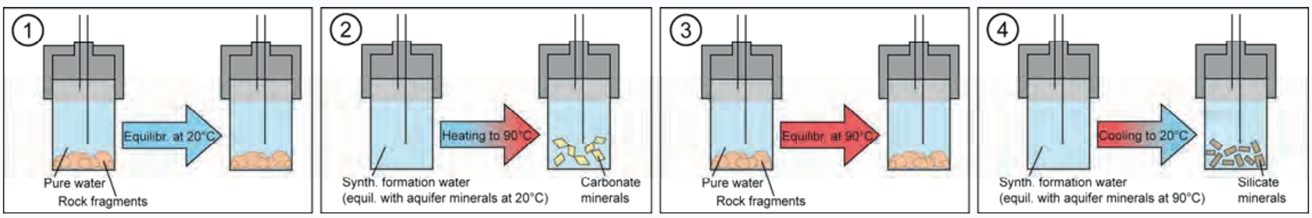

Testing of **different physicochemical parameters**: Temperatures, rock types, fluid chemistry, pCO_2… ⇒ Cover a range of possible conditions to **predict potential mineral reactions** and generate a dataset to allow predictions to be made for other sites (e.g. Geneva)

In collaboration with: Université de Genève, unine, ETH, Geo Energie Suisse, ewb, SIG
Funded by: Geothermica, heatstore, Schweizerische Eidgenossenschaft, Bundesamt für Energie BFE

References: [1] Fleuchaus et al. (2018). *Renew. Sust. Energ. Rev.* **94**; [2] Griffioen & Appelo (1993). *Appl. Geochem.* **8**; [3] Perlinger et al. (1987). *Water Resour. Res.* **23**; [4] Müller & Regenspurg (2017). *Geoth. Ener.* **5**; [5] Molz et al. (1979). *Water Resour. Res.* **15**; [6] Lerm et al. (2013). *Extremophiles* **17**; [7] Molz et al. (1983). *Water Resour. Res.* **19**; [8] Platt & Keller (1992). Sedimentology **39**

Task 1.4

Title

Geo-data infrastructure and analysis

Project (presented on the following page)

No posters

Work Package 2: Hydropower

According to the Energy Strategy 2050, the mean annual hydropower production has to be increased by 3.16 TWh/a. Considering more stringent environmental regulation that will reduce production by 1.4 TWh/a, the actual target is a plus of 4.56 TWh/a. Such increase is challenging and can be reached only by innovative and sustainable solutions for new large and small hydropower plants and by the extension and optimization of existing schemes. Especially new small hydropower plants require criteria for a careful site selection and strategies to optimize power production within a river network while at the same time minimizing the negative impacts on stream ecology. The effect of climate change will not only impact the availability of water resources in time but also the behavior of the catchment areas by an increased sediment yield and more frequent natural hazards, and thus considerably endanger hydropower production in the near future. The critical period of energy supply in Switzerland is still the winter half year, where 4 TWh had to be imported in average over the past 10 years. Therefore, Switzerland has to increase its storage capacity by new reservoirs where possible and to increase the volumes of existing ones.

Based on feedback from industry and on recent developments in Switzerland and Europe, WP2 focuses on five key objectives. The Highlights 2019 are structured accordingly. Note that a major part of the hydropower related work is reported under WP5, namely the three demonstrators for large hydropower (FLEXSTOR), small hydropower (SMALLFLEX), and the problem of reservoir sedimentation (SEDMIX).

Highlights 2019

Objective 1: To increase flexibility of HP production

Novel radar and observation based now-casting techniques have been developed and tested at the new HP-plant Gletsch-Oberwald, which allow the extrapolation of best estimates of the actual meteorological situation into the future for the next couple of hours. The potential of hydropower dams to mitigate water shortage during severe droughts in Switzerland has been assessed. It was found that mainly in the Aare catchment, existing or new HP reservoirs have the potential to alleviate summer droughts. Both model and prototype test series were conducted regarding aeration processes in bottom outlets. The governing parameters affecting air demand were combined in a new design equation to estimate the required air demand. A machine learning based framework was developed to automatically determine the optimal lead time for hydropower systems accounting for multiple operating objectives. Numerical analyses on the Visp valley hydropower system show that ideally the most valuable information to maximize hydropower production is a 3 month ahead streamflow forecast.

Objective 2: To assess the climate change impact on HP production

The energy potential of heightening existing dams in Switzerland was systematically investigated. It was estimated that about 2.3 TWh/a of electricity production could be additionally shifted from the summer to the winter semester, if 25 existing dams were heightened. This would correspond to about one quarter of the energy equivalent of the Swiss storage lakes today.

The impact of climate change on future hydro power operation was assessed by combining

1. the new CH2018 climate scenarios,
2. a new weather generator model at the local scale (sub-daily, sub-kilometre), and
3. a distributed physically explicit hydrological model (Topkapi-ETH).

The application of the framework to an ice-melt dominate hydropower system in the Visp valley shows a reduction of water availability due to climate change that may lead to a loss in electricity production of up to 27% in the next decades up to 2050.

Objective 3: To assess the risk of extreme natural events and hazards on HP operation

Field experiments in a gravel pit in Bülach were carried out in September 2018 in order to understand landslide-induced spatial impulse waves in lakes and reservoirs. The basin was 20 m wide 60 m long and had a water depth of 1.5 m. Rigid bodies with weights of up to 7 tons were slid down a 40 m long ramp and impacted the water body. The resulting wave heights along the wave propagation path and the wave run-up were visually determined using gauge poles and videometry. Identical model tests with a scale of 1:10 were carried out in the VAW laboratory and cross-compared to the field tests. The results help to (1) improve existing computational procedures, (2) determine possible scale effects; and (3) serve as calibration and validation data for numerical modelling of impulse waves.

Objective 4: To enable new projects under uncertainty

Novel reinforcement learning approaches have been tested to re-design the coordinated operation of multi-reservoir systems including pumping, explicitly accounting for the uncertain nature of the inflow process. The approach has been demonstrated on the Maggia Valley hydropower system to

1. assess the tradeoff between HP production and revenue;
2. develop a multiobjective analysis to explore the tradeoff between HP primary objectives (production and revenue) and river ecosystem services.

Numerical results obtained show a little conflict between hydropower production and revenue, while overemphasizing ecosystem preservation can lead to a rapid decrease of hydropower benefit.

Objective 5: To analyse reservoir sedimentation and enable sustainable use of storage HP

A new regulation has been recently approved in Canton Ticino, which constrains hydropower operators to release time-varying environmental flow releases for the benefit of the riparian ecosystems. We contrasted different minimum environmental flow regulations (past regulation, new regulation and a stipulated environmental objective) and analysed their impact on hydropower production in the complex hydropower system (OFIMA) of the Maggia valley, which is one of the few remaining natural alluvial rivers in Switzerland. Results show that the constraints posed by the newly approved regulation does not produce any significant benefit to the environment with respect to the past constraints, despite being more restrictive for hydropower operators. Explicitly including ecosystem preservation as operating objective rather than a constraint allows discovering win-win solutions for hydropower operators and the environment.

The temporal variation of fine suspended sediment transport in the power waterways of two run-of-river hydropower plants is being monitored in multi-year campaigns at a large scheme in Canton Valais and a small hydropower plant in Canton Grisons, respectively. In parallel, the development of the runners' geometries and the turbines' efficiencies are monitored to acquire important data for the development of a Pelton turbine abrasion model. The spatio-temporal development of invert abrasion is regularly monitored in three Swiss sediment bypass tunnels (SBTs) where a number of different high-resistant invert materials are used to study their erosion resistance in a pilot study.

At the Solis reservoir in Canton Grisons data of flow velocities, bathymetry and suspended sediment concentration are acquired for different inflow and operational conditions using ADCP technology, amongst others. Based on this data, the flow patterns and their effect on sedimentation processes are roughly evaluated in a first step. The data will serve for the calibration of a numerical model which shall be applied in a follow-up project to optimize reservoir drawdowns and sediment bypass operation accounting for both electricity production and sediment bypassing efficiency.

At a pilot hydropower plant on the Limmat river featuring a horizontal bar rack bypass system for fish downstream migration ADCP technology and numerical 3D modelling are used to analyse the hydraulic conditions in the vicinity of the rack and the bypass inlet. Together with fish monitoring data of an accompanying EU project conclusions on the fish guidance efficiency shall be drawn.

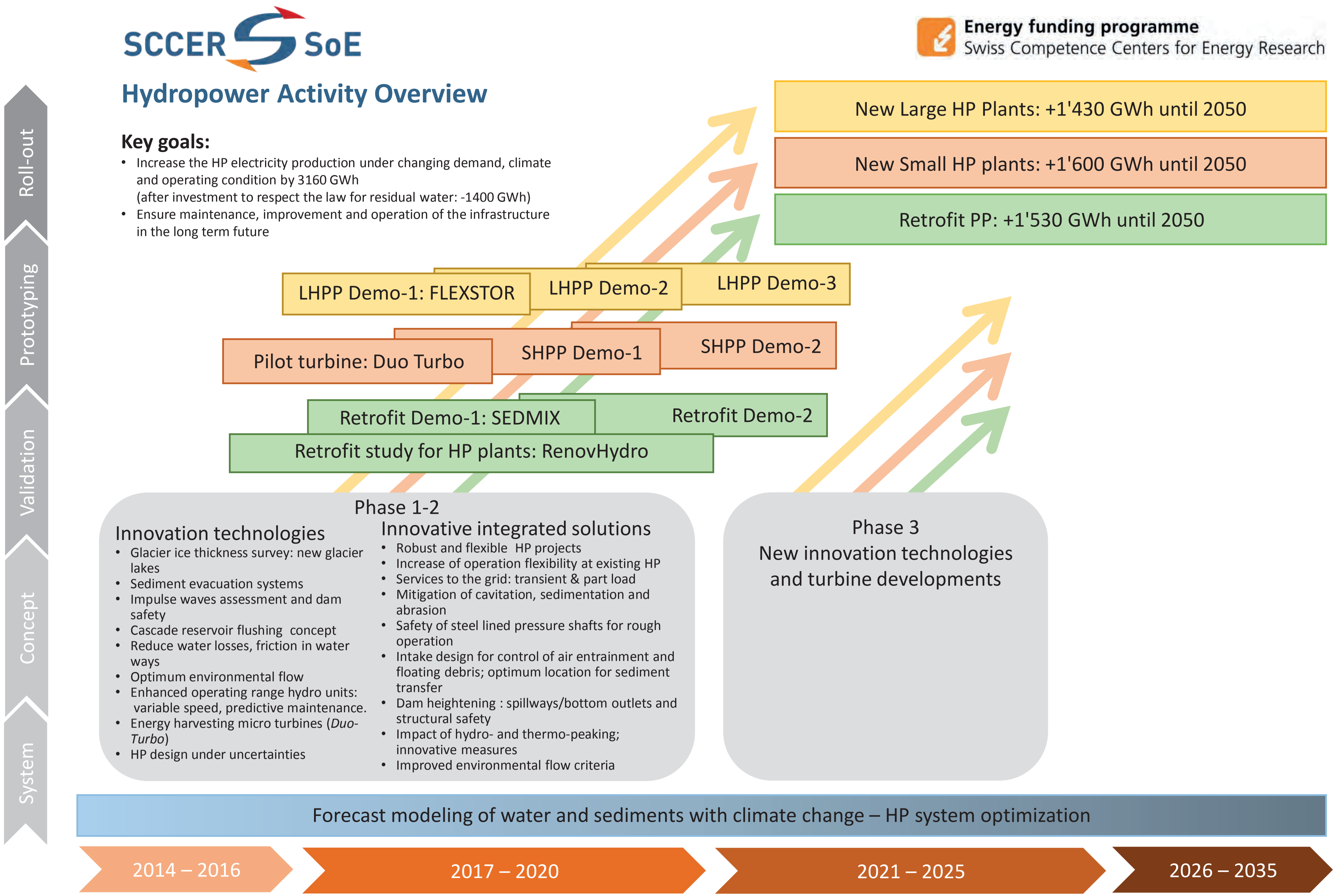
SCCER SoE
Energy funding programme
Swiss Competence Centers for Energy Research
Hydropower Activity Overview
Key goals:
• Increase the HP electricity production under changing demand, climate and operating condition by 3160 GWh (after investment to respect the law for residual water: -1400 GWh)
• Ensure maintenance, improvement and operation of the infrastructure in the long term future
New Large HP Plants: +1'430 GWh until 2050
New Small HP plants: +1'600 GWh until 2050
Retrofit PP: +1'530 GWh until 2050
LHPP Demo-1: FLEXSTOR
LHPP Demo-2
LHPP Demo-3
Pilot turbine: Duo Turbo
SHPP Demo-1
SHPP Demo-2
Retrofit Demo-1: SEDMIX
Retrofit Demo-2
Retrofit study for HP plants: RenovHydro
Phase 1-2
Innovation technologies
• Glacier ice thickness survey: new glacier lakes
• Sediment evacuation systems
• Impulse waves assessment and dam safety
• Cascade reservoir flushing concept
• Reduce water losses, friction in water ways
• Optimum environmental flow
• Enhanced operating range hydro units: variable speed, predictive maintenance.
• Energy harvesting micro turbines (Duo-Turbo)
• HP design under uncertainties
Innovative integrated solutions
• Robust and flexible HP projects
• Increase of operation flexibility at existing HP
• Services to the grid: transient & part load
• Mitigation of cavitation, sedimentation and abrasion
• Safety of steel lined pressure shafts for rough operation
• Intake design for control of air entrainment and floating debris; optimum location for sediment transfer
• Dam heightening : spillways/bottom outlets and structural safety
• Impact of hydro- and thermo-peaking; innovative measures
• Improved environmental flow criteria
Phase 3
New innovation technologies and turbine developments
Forecast modeling of water and sediments with climate change – HP system optimization
2014 – 2016
2017 – 2020
2021 – 2025
2026 – 2035
Roll-out
Prototyping
Validation
Concept
System

Task 2.1

Title

Morpho-climatic controls

Projects (presented on the following pages)

Predictability of Droughts using Monthly Forecasts
K. Bogner, M. Zappa

Glacier inventory for ice volumes from ice penetrating radar and glaciological modeling
Melchior Grab, Lisbeth Langhammer, Sebastian Hellmann, Gregory Church, Hendrik Pormes, Lino Schmid, Lasse Rabenstein, Andreas Bauder, Hansruedi Maurer

Climate change effects on reservoir inflows (Maggia valley, OFIMA)
Sebastian Moraga, Nadav Peleg, Daniela Anghileri, Simone Fatichi, Paolo Burlando

Calibrated Glacier Modelling – Correcting by Collecting
Hendrik Pormes, Lisbeth Langhammer, Melchior Grab, Andreas Bauder, Hansruedi Maurer

Change in Run-of-River Power Production Calculated with the New Climate Change Scenarios CH2018
Tobias Wechsler, Massimiliano Zappa, Manfred Stähli

SCCER SoE
SWISS COMPETENCE CENTER for ENERGY RESEARCH
SUPPLY of ELECTRICITY

SCCER-SoE Annual Conference 2019

Supported by:
Schweizerische Eidgenossenschaft
Confédération suisse
Confederazione Svizzera
Confederaziun svizra

Swiss Confederation

Innosuisse – Swiss Innovation Agency

Predictability of Droughts using Monthly Forecasts

K. Bogner and M. Zappa

70 NRP Energy Turnaround
National Research Programme

Motivation

Main questions:
Is it worth the effort to use monthly forecasts as an early indicator for upcoming dry periods?
Do they have skill, resp. are they reliable at all? When and where did they show the 2018 drought?

Data

In order to answer these questions tercile forecast have been produced for different variables indicating the likelihood of the forecast to be below, close to or above the long-term averages

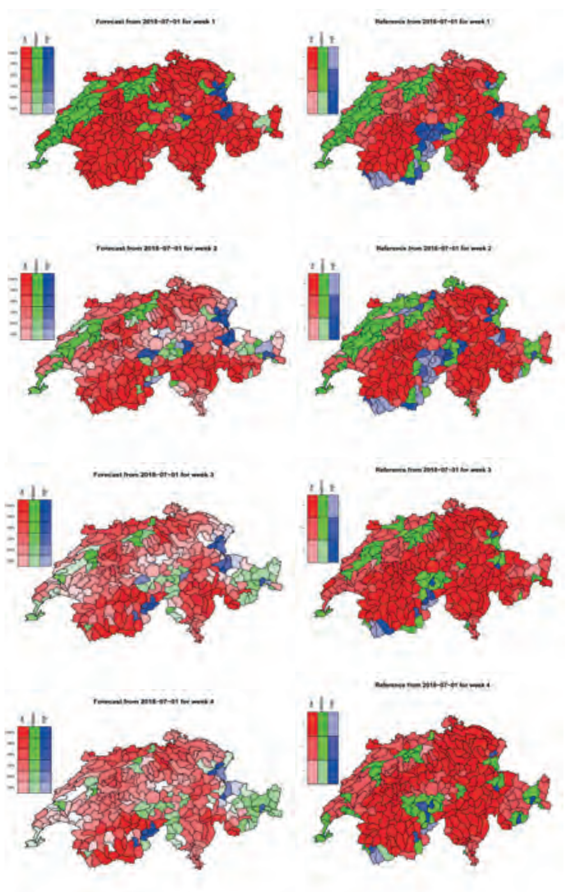

Figure 1: Example of a tercile forecasts end of June 2018 for the upcoming four weeks on the left. The right side shows the reference model simulation with measured meteorological input for the corresponding weeks.

Verification

Quality of the forecast expressed as Ranked Probability Score (RPS), with a perfect forecast shown in dark red (see below). The lighter red, the lower the skill in comparison to a climatological forecast. On the left side the results of the surface runoff are shown for the Summer 2018, on the right side the results for the baseflow R2) are shown after applying post-processing (quantile mapping) for the year 2018

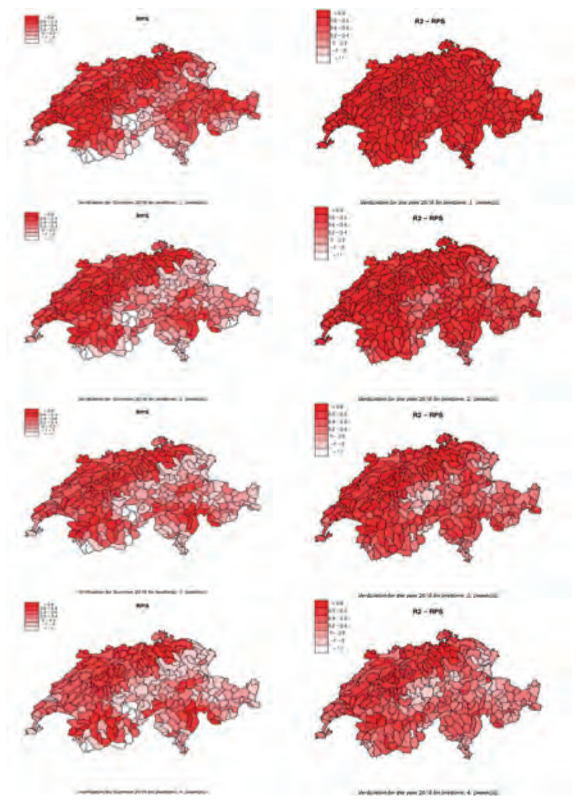

Figure 2: Results of the Ranked Probability Score (RPS) for the Summer period 2018 for the surface runoff (left) and the post-processed baseflow (right)

Results

The skill of the monthly forecasts shows some spatial variability. Especially catchments with glaciers are more difficult to predict.
Variables with short reaction times (surface runoff) are predictable for 1-2 weeks in advance, which can be enhanced using post-processing methods
For slower reacting variables (baseflow) the skill of the forecast lasts for up to 4 weeks
The skill of the Summer 2018 period was higher compared to the long-term predictability (with very stable atmospheric conditions)
Monthly forecasts are gainful! Already end of June the forecasts show some possibilities of dryness for the coming weeks (however site and variable dependent) and post-processing increase the forecast skill!

References

S. Monhart, M. Zappa, C. Spirig, C. Schär, and K. Bogner. Subseasonal hydrometeorologicalensemble predictions in small-and medium-size mountainous catchments: Benefits of the NWP approach. *Hydrology and Earth System Sciences*, (23):493–513, 2019.
K. Bogner, K. Liechti, L. Bernhard, S. Monhart, and M. Zappa. Skill of Hydrological Extended Range Forecasts for Water Resources Management in Switzerland. *Water Resources Management*, 2017.

Acknowledgment:
The authors would like to thank the WSL-Initiative: Drought for supporting this study

SCCER SoE
SWISS COMPETENCE CENTER for ENERGY RESEARCH
SUPPLY of ELECTRICITY

SCCER-SoE Annual Conference 2019

Supported by:
Schweizerische Eidgenossenschaft
Confédération suisse
Confederazione Svizzera
Confederaziun svizra
Swiss Confederation
Innosuisse – Swiss Innovation Agency

Glacier inventory for ice volumes from ice penetrating radar and glaciological modeling

Melchior Grab, Lisbeth Langhammer, Sebastian Hellmann, Gregory Church, Hendrik Pormes, Lino Schmid, Lasse Rabenstein, Andreas Bauder, Hansruedi Maurer

Introduction:
The ongoing melting of glaciers causes a large loss of ice volumes in the Alps: E.g. 75±22 km³ of ice have been estimated for the year 1973 and 65±20 km³ for 1999 (Linsbauer et al., 2012). This has consequences for the supply of electricity, for tourism, or with regard to natural hazards. Detailed knowledge of the bed topography is key for developing strategies to deal with risks and new opportunities arising from the glacier melt.

During the past years we have developed AIR-ETH (Airborne Ice Radar ETH Zurich), a helicopter-borne ground penetrating radar (GPR), and the data processing software package GPRglaz for surveying the ice thickness of Alpine glaciers. The acquired data is fed into the recently developed GlaTE algorithm to obtain maps of the ice thickness distribution and bedrock topography. The resulting map-data together with the GPR-data will be made accessible on public data base platforms.

Helicopter-borne Ice Penetrating Radar

- ~1500 km of older radar profiles from various data bases.
- ~1100 km of new radar profiles acquired in the framework of SCCER-SoE.
- Additional datasets, e.g. from seismics or boreholes.

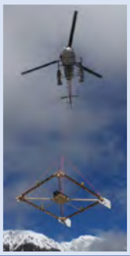

Geographic input data

- Digital elevation model from SwissTopo (currently 2008-2016)
- Glacier outline polygons (swissTLM3D, 2019-update in process)
- Manual picking of outlines across Swiss borders (for non-zero ice thickness models at the border)

Glacier Thickness Estimation (GlaTE)

- Glaciological modeling (Clarke at al., 2013)
- Optimized accounting for GPR-ice thickness using GlaTE inversion (Langhammer et al., 2019)

$$\begin{pmatrix}\lambda_1 \mathbf{G}\\ \lambda_2 \mathbf{L}\\ \lambda_3 \mathbf{B}\\ \lambda_4 \mathbf{S}\end{pmatrix}\mathbf{h}^{est} = \begin{pmatrix}\lambda_1 \mathbf{h}^{GPR}\\ \lambda_2 \nabla \mathbf{h}^{glac}\\ 0\\ 0\end{pmatrix} \xrightarrow{\text{invert for } \mathbf{h}^{est}\text{, until}} \left\| \mathbf{G}\mathbf{h}^{est} - \mathbf{h}^{GPR} \right\| < \varepsilon^{GPR}$$

- Calibrated glacier modeling for glaciers without GPR profiles (see poster of H. Pormes)

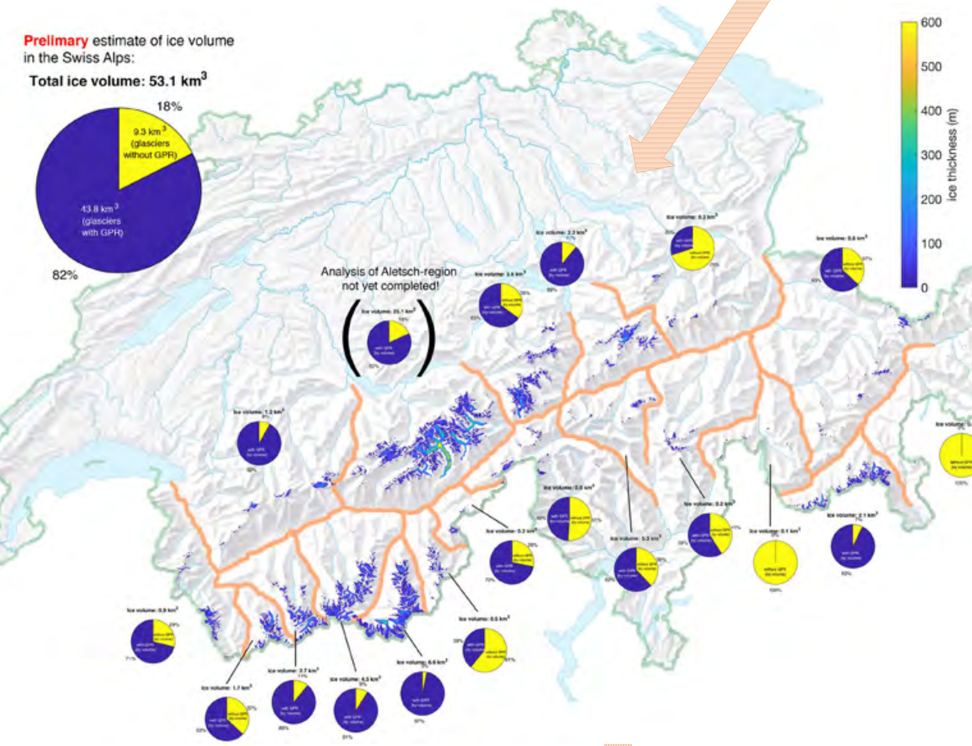

Dataset 1:

Surface elevation and ice thickness from new GPR profiles

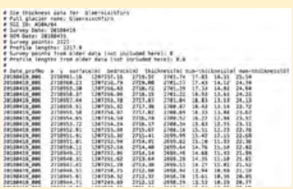

Dataset 2:

ESRI grid file with bedrock topography from GlaTE modeling

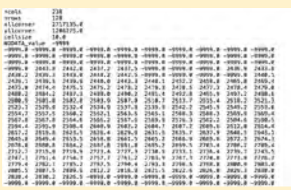

Dataset 3:

ESRI grid file with ice thickness distribution from GlaTE modeling

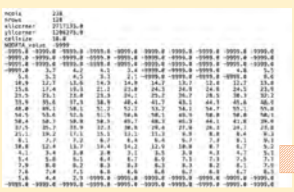

Final Steps:

1. Quality control of older GPR-input data (ice surface altitudes)
2. Optimizing weighting factors of the GlaTE inversion
3. Updating GlaTE inversion with the newest outlines and DEM's.
4. Uncertainty estimates
5. Publishing data on databases such as WGMS and/or GLAMOS

Acknowledgments:

We thank for the fruitful collaboration with P. Lathion, P. Schaer, K. Délèze (GEOSAT), B. Rinderknecht (BRTechnik), C. Bärlocher (ETH Zurich), AIR Glacier and Heli Bernina. Financial support was provided by ETH Zurich, the Swiss Geophysical Commission, and SCCER-SoE/Innosuisse.

References:

Clarke, G. K., Anslow, F. S., Jarosch, A. H., Radić, V., Menounos, B., Bolch, T., & Berthier, E, Ice volume and subglacial topography for western Canadian glaciers from mass balance fields, thinning rates, and a bed stress model. Journal of Climate, 26(12), 4282-4303, 2013.

Langhammer, L., M. Grab, A. Bauder, & H. Maurer, Glacier thickness estimations of alpine glaciers using data and modeling constraints. *The Cryosphere*, *13*(8), 2189-2202, 2019

Linsbauer, A., F. Paul, & W. Haeberli, W, Modeling glacier thickness distribution and bed topography over entire mountain ranges with GlabTop: Application of a fast and robust approach. Journal of Geophysical Research: Earth Surface, 117(F3), 2012.

SCCER SoE

SWISS COMPETENCE CENTER for ENERGY RESEARCH
SUPPLY of ELECTRICITY

SCCER-SoE Annual Conference 2019

Supported by:
Schweizerische Eidgenossenschaft
Confédération suisse
Confederazione Svizzera
Confederaziun svizra
Swiss Confederation
Innosuisse – Swiss Innovation Agency

Climate change effects on reservoir inflows (Maggia valley, OFIMA)

Sebastian Moraga, Nadav Peleg, Daniela Anghileri, Simone Fatichi, Paolo Burlando

Motivation

Climate change is expected to affect the hydrological system (e.g. modifying river flows, snow accumulation and melt), with consequences for the inflows to hydropower reservoirs and therefore their operation policies.

In the context of Task 2.4, we studied the effects of climate change on the three largest reservoir systems of the OFIMA hydropower system in the Maggia valley, Robiei-Zott, Cavgnoli-Naret, and Sambuco.

Objectives

- To estimate local climate change effects (precipitation and temperature) over the Maggia region for mid of the century and for a severe emission scenario (RCP8.5).
- To estimate the changes of the future inflows to the three reservoir systems.
- To provide inflows scenarios to Task 2.4 for the investigation of new hydropower operational policies, which account for uncertainties of changes in climate and hydrology.

Methods

- Changes in precipitation and temperature are estimated using 9 climate models that were post-proccessed in the official CH2018 climate change scenarios initiative.
- The AWE-GEN-2d stochastic weather generator model is used to produce local climate variables needed for the hydrological projections (present and future) at high-resolution of 2-km and 1-h.
- The Topkapi-ETH distributed hydrological model is used to simulate the basin hydrology and estimate the inflows to the reservoirs.

Climate change

- Temperatures in the Maggia valley are projected to increase during all seasons. The changes in precipitation are less pronounced, with most months showing small changes that are within the range of the natural variability (Fig. 1).

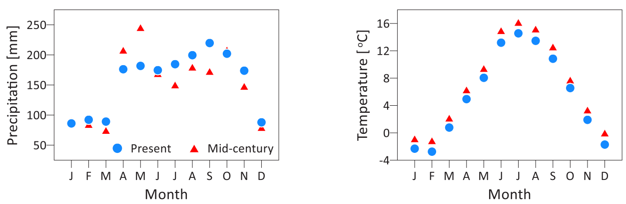

Fig 1. Example of changes in precipitation (left) and temperature (right) averaged over the Maggia valley, downscaled from the ECEARTH_CLMCOM-CCLM4 model using AWE-GEN-2d for the period 2030-2059.

- While the increase in temperature is projected to be relatively homogenous in space, precipitation is projected to change more in the central and southern areas than the northeast and southwest areas (Fig. 2).

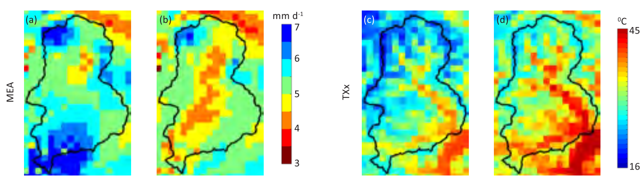

Fig 2. Comparison between present and future mean daily rainfall (left) and hottest day of the year (right) over the Maggia valley. Climate indices were computed from downscaled simulations driven by the IPSL_SMHI-RCA model.

Present inflows to the reservoirs

- Inflow data for the three reservoirs were obtained from OFIMA for the period of 2005-2015.
- Outputs (100 simulations, daily runs) from a preliminary set-up of the Topkapi-ETH model accounting only for the main diversions and intakes were compared with the observed data (Fig. 3).
- The seasonality and flow dynamics are reasonably reproduced by the model, while the absolute inflow values are either underestimated (for the peak season, Sambuco and Robiei-Zott) or overestimated (all seasons, Cavagnoli-Naret), due to the preliminary set-up.

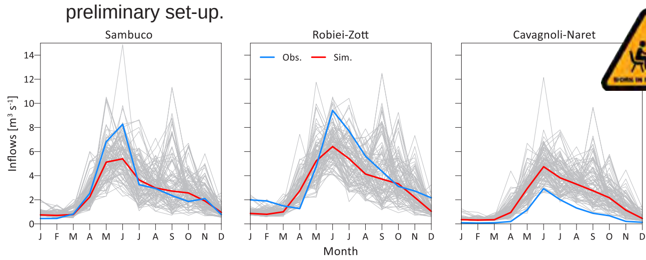

Fig 3. Comparison between the observed (blue lines) and 100 simulations (gray lines) of inflows to the three reservoirs. Red lines represent the median of the stochastic simulations.

Future inflows to the reservoirs

- 200 simulations were conducted to analyze the impacts of climate change on the hydrology for the mid of the century.
- The hydrological system is sensitive to the changes in climate, particularly with respect to the contribution of snow water equivalent, which declines significantly in all reservoirs in the future simulations (Fig. 4).
- Results point at a reduction in the total inflows into the reservoirs, with a clear seasonal pattern (increase during April-May and decrease between June and October, Fig. 5).

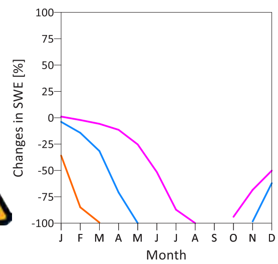

Fig 4. Relative change in snow water equivalent contributing to the flow between future and present climate.

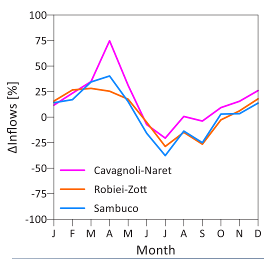

Fig 5. Relative change in inflows to the reservoirs between future and present climate.

Future work

This poster presents preliminary results from the project. For the next year, the following steps are planned:

- Finalizing the setup of the model – adding the missing contributions (e.g. Gries reservoir and Altstafel tunnel and Sfundau reservoir).
- Switching from daily simulations to hourly, in order to simulate sub-daily hydrological processes (e.g., radiation variability) and flow dynamics.
- Update the model parameterization to account for the new HP scheme and to improve the model performance.
- Providing the final set of inflow scenarios to be used for the investigation of future hydropower operation policies in Task 2.4.

SCCER SoE

SWISS COMPETENCE CENTER for ENERGY RESEARCH
SUPPLY of ELECTRICITY

SCCER-SoE Annual Conference 2019

Supported by:
Schweizerische Eidgenossenschaft
Confédération suisse
Confederazione Svizzera
Confederaziun svizra

Swiss Confederation

Innosuisse – Swiss Innovation Agency

Calibrated Glacier Modelling – *Correcting by Collecting*

Hendrik Pormes, Lisbeth Langhammer, Melchior Grab, Andreas Bauder, Hansruedi Maurer

1. How much ice is there left on the glaciers?

- The ice-thicknesses of glaciers can be estimated from surface measurements, such as *Ground Penetrating Radar* (GPR), in combination with glaciological modelling by using our **GlaTE** algorithm *(Langhammer et al.,2019)*
- For glaciers where no GPR data exists, glaciological modelling can be used *(Clarke et al., 2013).* The inputs then are:
  - The glacier boundary
  - The surface topography
- The glaciological model takes the conservation of mass and the physics of ice-flow into account, but there are still some **uncertainties**.
- These uncertainties cause the ice thickness estimations to be over- or under-estimated
- However, we can correct these uncertainties using the **Glacier Factor α_{GPR}**, obtain ... e GPR data exists

$$\mathbf{h}^{glac} = \alpha_{GPR}\hat{\mathbf{h}}^{glac}$$

- If the glacier-factor is >1, the ice-thickness is **under-estimated**
- If the glacier-factor is <1, the ice-thickness is **over-estimated**

Now the question is..

- *On wat does the value of this Glacier-Factor depend?*
  - Area? Altitude? Exposition? Slope?

2. Dataset Example

- To illustrate what the GlaTE model does, we take the one glacier, namely the **Huefifirn/Claridenfirn,** as an example:

- The black lines on the h^{glac} model indicate several GPR profiles, which eventually are used for the calibration of the glacier-model
- When we compare the $\hat{h}^{glac}$ and the h^{glac} model, we see that there is a **discrepancy**, which indicates that we need the **Glacier-Factor α_{GPR}**, in order to obtain the right results
- Using the Glacier-Factor the difference in what we model and what we measure gets smaller

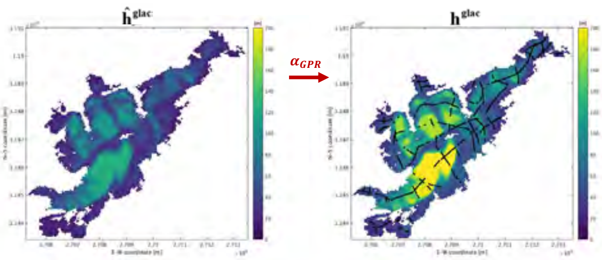

3. Testing the Glacier-Factor for multiple glaciers

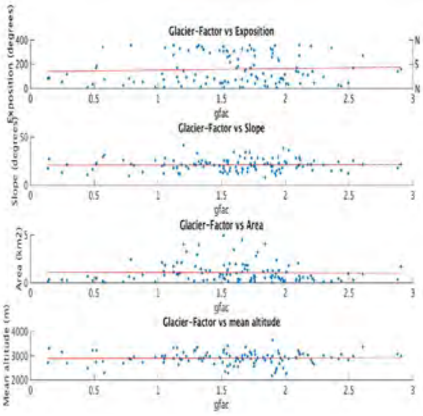

4. Turns out the Glacier-Factor …

- Does ***not*** have a strong correlation with any of the parameters
- Is often completely random

However ...

- The Glacier-Factor is almost always above 1!
- Which means most glaciers are **under-estimated**
- The average Glacier-Factor lies around **1.6** with a standard deviation of around 0.3
- This all means that for glaciers without GPR-data the calibration can be done with a Glacier-Factor *higher than 1* in order to minimize the discrepancy

References: - Langhammer, L., Grab, M., Bauder, A., and Maurer, H.: Glacier thickness estimations of alpine glaciers using data and modeling constraints, The Cryosphere, 13, 2189–2202, https://doi.org/10.5194/tc-13-2189-2019, 2019.,
- Clarke, G. K., Anslow, F. S., Jarosch, A. H., Radić, V., Menounos, B., Bolch, T., & Berthier, E, Ice volume and subglacial topography for western Canadian glaciers from mass balance fields, thinning rates, and a bed stress model. Journal of Climate, 26(12), 4282-4303, 2013

SCCER-SoE Annual Conference 2019

SCCER SoE

SWISS COMPETENCE CENTER for ENERGY RESEARCH
SUPPLY of ELECTRICITY

Supported by:

Schweizerische Eidgenossenschaft
Confédération suisse
Confederazione Svizzera
Confederaziun svizra

Swiss Confederation

Innosuisse – Swiss Innovation Agency

Change in Run-of-River Power Production Calculated with the New Climate Change Scenarios CH2018

Tobias Wechsler, Massimiliano Zappa, Manfred Stähli – Swiss Federal Research Institute WSL, Birmensdorf

Research question

How will run-of-river power production in Switzerland change with climate change?
This depends on the change in the **usable** water volume, which is controlled by the capacity/dimensions of the power plant and the residual flow regulations.

Method

We used the most recent climate change scenarios (CH2018) to calculate the change in water discharge of Swiss rivers (using PREVAH, a state-of-the-art hydrological model) for mid-century (2060) and the end of the century (2085).
Then, we determined for eleven selected RoR power plants the corresponding Flow-Duration Curve (FDC). In a FDC, all daily runoff values are ordered by size and frequency distribution, resulting in a concave shape. The shaded area represents the volume that can be used for power production and is limited by two parameters: 1) the maximum discharge that the power plant can use; 2) the volume that cannot be used for hydropower (HP) because the minimum turbine height is not reached or because discharge is used for residual flow or other purposes. FDCs can be used to estimate the yearly (or half-yearly) power production of a RoR power plant.

Example Wildegg/Brugg – Aare (a typical river of the Swiss plateau)

Flow-Duration Curve | Change in available water volume | Change in annual power production

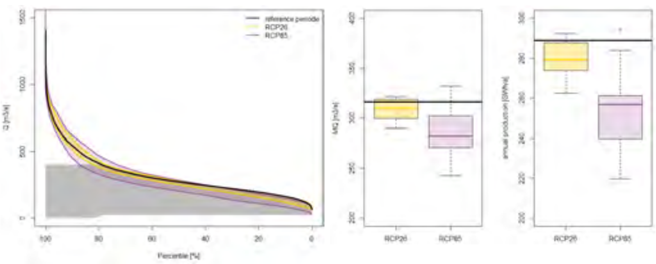

The water volume usable for HP production (shaded area) depends mainly on low and medium water ranges. For the RoR power plant Wildegg-Brugg, the hydrological predictions indicate that both the average water supply and the annual production will decrease in the future.

Example Davos Glaris - Landwasser (a typical alpine river)

Flow-Duration Curve | Change in available water volume | Change in annual power production

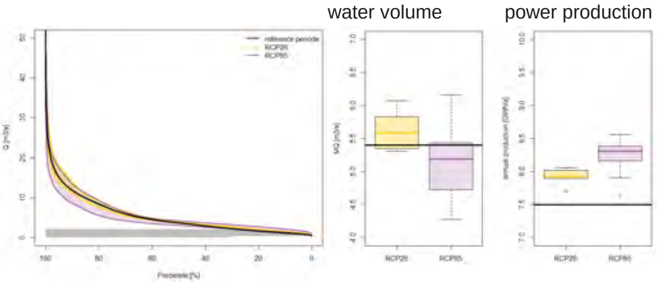

For the RoR power plant Davos Glaris, which is heavily influenced by snow, the total water supply will decline by the end of the century; still, HP production is likely to increase.

Change in mean annual production:

for eleven selected RoR power plants

for mid-century (2060) and the end of the century (2085) and
for two different emission scenarios (RCP2.6 – with the assumption of concerted mitigation efforts; RCP8.5 – with the assumption of no climate change mitigation)

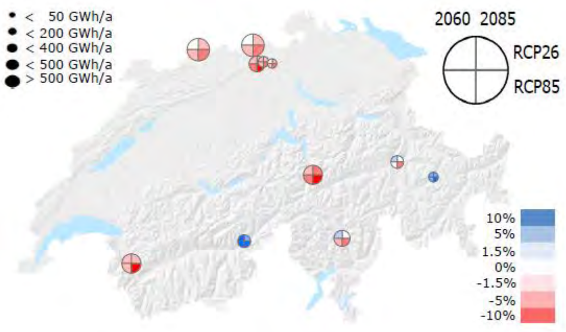

Change in mean winter production (Oct – Mar):

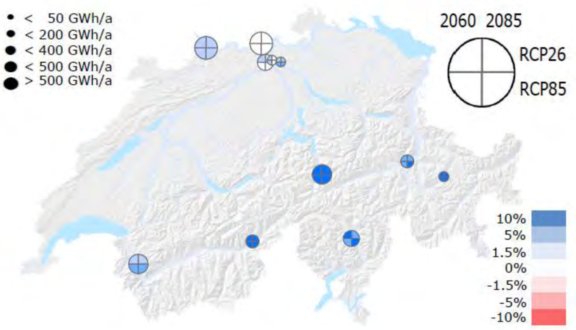

Overall projection for RoR power production in Switzerland

By mid-century (2045-2074):

- **Annual production** will remain roughly the same with concerted mitigation efforts (RCP2.6) as during the reference period. Production will slightly decrease (about -3%) without climate change mitigation (RCP8.5). Exceptions are those power plants that are influenced by strong melting processes.
- **Winter production** will increase at almost every RoR power plant considered in this study by mid-century, on average about +5%.

By the end of the century (2070-2099):

- **Annual production** will decline slightly (-1.5%), even with concerted mitigation efforts (RCP2.6). Without climate change mitigation (RCP8.5), production will even decrease by up to -7%.
- **Winter production** will increase at virtually all of the RoR power plants of this study. Depending on the emission scenarios, the average increases will be between +5% (RCP2.6) and +10% (RCP8.5). However, the increase in winter production will not be able to keep annual production at the same level.

Task 2.2

Title

Infrastructure adaption

Projects (presented on the following pages)

Alpine hydropower plants renewal : synergies between flexible production and hydropeaking mitigation
Mathieu Barnoud, Sabine Chamoun, Pedro Manso, Giovanni De Cesare

Suspended sediment in the turbine water of HPP Fieschertal in 2018
Matthias Eugster, David Felix, Robert Boes

Renewal of alpine hydroelectric plants according to the spatial and temporal scales of analysis
Vincent GAERTNER, Sabine CHAMOUN, Pedro MANSO, Giovanni DE CESARE

Comissioning of a new fatigue test rig based on pressure oscillations
A. Gaspoz, N. Gonçalves, L. Barras, V. Hasmatuchi, C. Nicolet, S. Rey-Mermet

Hydraulics of Horizontal Bar Rack-Bypass Systems: Field Study at HPP Stroppel
Roland Hagenbüchli, Ismail Albayrak, Mohammadreza Maddahi, Ricardo Mendez, Robert M. Boes

Two-phase flow hydraulics of low-level outlets
Benjamin Hohermuth, Lukas Schmocker, Robert Boes

Numerical investigation of HPP layouts and their effects on fish guidance racks
Andreas Huwiler

Run-up of Impulse Wave Trains
Maximilian Kastinger, Frederic Evers, Robert Boes

Assessing the acceptability of concrete dam submergence considering scour
L. Labrosse, S. Chamoun, P. A. Manso

Solving of a Lifting Problem in a Pumped Storage Power Plant
Daniel Pace, Giovanni De Cesare, Pedro Manso, Kaspar Vereide, Livia Pitorac, Leif Lia

Renewal of the Ritom hydropower plant
Jakob Siedersleben, Samuel Vorlet, Giovanni De Cesare, Nicola Tatti, Urs Müller, Graziano Sangalli

Hydro-abrasion at hydraulic structures
Damiano Vicari, Dila Demiral, Ismail Albayrak, Robert M. Boes

Seismic behavior of Pine Flat concrete gravity dam using microplane damage-plasticity model
Samuel Vorlet, Pedro Manso, Giovanni De Cesare

SCCER SoE
SWISS COMPETENCE CENTER for ENERGY RESEARCH
SUPPLY of ELECTRICITY

FMV

groupe e

SCCER-SoE Annual Conference 2019

RENOV Hydro

Supported by:
Schweizerische Eidgenossenschaft
Confédération suisse
Confederazione Svizzera
Confederaziun svizra
Swiss Confederation
Innosuisse – Swiss Innovation Agency

Alpine hydropower plants renewal : synergies between flexible production and hydropeaking mitigation

Mathieu Barnoud ; Sabine Chamoun ; Pedro Manso ; Giovanni De Cesare

EPFL

Motivation

Hydropeaking is the water flow or level variations in rivers caused by hydropower exploitation. This phenomenon have negatives impacts on fauna and flora. Mitigation measures can lead to producing less and reduce production at the times that are most economically attractive. In a context where renewable energy production wishes to be increased and where operators wish to maintain their revenues, these measures are not satisfactory. This work aims to propose mitigation solution which keep production and flexibility constant or even increase them.

Methodology and indicators

Several variants and operating scenarios will be evaluated on construction cost, energy production, revenues and hydropeaking.

Hydropeaking will be mainly evaluated with the indicators I_A. It will be considered problematic when its value is higher than 1.5.

$$I_A = \frac{Q_t}{Q_{min}}$$

Q_t : The hydropower plant exploitation discharge at time t

Q_{min} : The minimum discharge in the river on the period studied

Studied case

The case study is composed of 5 hydropower plants located in the Upper-Rhône Basin. Among these installations, Heiligkreuz is subject to an order of hydropeaking sanitation. **Hydropeaking have been detected between Heiligkreuz and Ze Binnen and also downstream Mörel power plant.** Two variant were preselected and three operating scenario were studied.

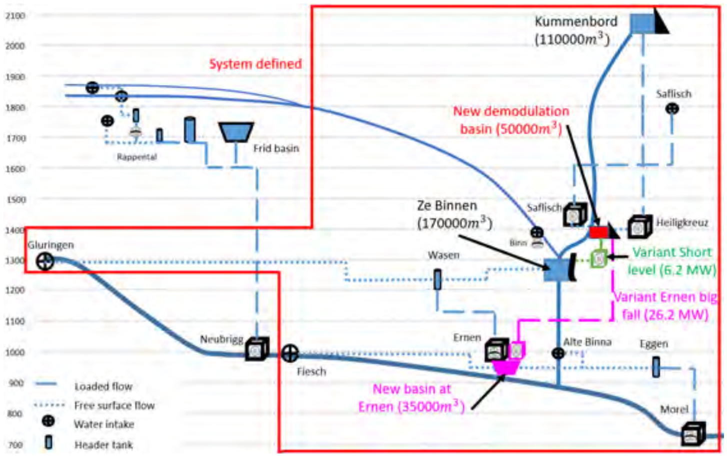

Figure 1 : Système and variants studied

Scenario Business as usual "BAU": The power plants operating modes try to be as close as possible to the reference state operating modes. The new plant operates in a similar way to Heiligkreuz one.

Scenario "Economic": The power plants use the maximum available volume when the price exceeds a threshold. The rest of the time, they operate on a run-of-river basis.

Scenario "Null Hydropeaking": The operating modes are similar to those of the "economic" scenario, but those which still causing hydropeaking are adapted in order to eliminate it completely.

Hydropeaking in Heiligkreuz river section

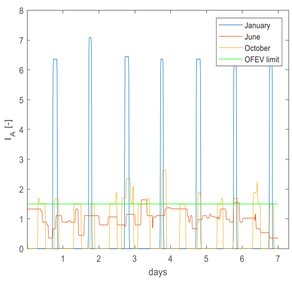

Figure 2 : I_A at the reference state

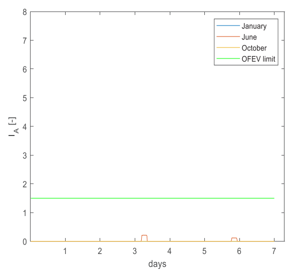

Figure 3 : I_A for both variants and all scenarios

Hydropeaking in Mörel river section

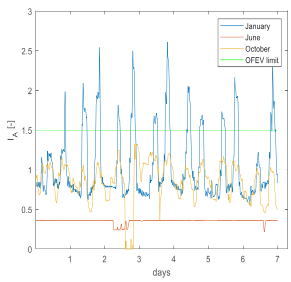

Figure 4 : I_A at the reference state

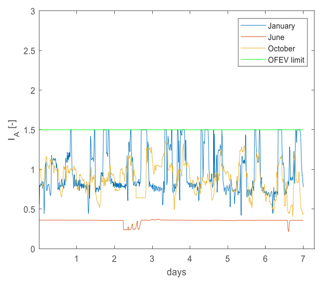

Figure 5 : I_A for the scenario null hydropeaking

Production and revenues

Table 1 : Production ($\Delta E[GWh/year]$) and revenues ($\Delta R[Mio\ CHF/year]$) differences with reference state(E_i, R_i)

Variants	Scenarios	ΔE	$\Delta E/E_i[\%]$	ΔR	$\Delta R/R_i[\%]$
Short level	BAU	10.4	2.31	0.41	2.23
	Economic	33.8	7.49	1.42	7.67
	Null Hydropeaking	23.6	5.23	0.84	4.55
Ernen Big Fall	BAU	24.4	5.39	0.94	5.07
	Economic	44.5	9.85	1.71	9.27
	Null Hydropeaking	35.2	7.80	1.19	6.46

Discussion

Variants studied allow to improve production and to mitigate hydropeaking on Heiligkreuz section but replace river section with hydropeaking by river section with residual flow. Ecological benefits induced by this replacement are not proved yet. The scenario "Null Hydropeaking" allow to delete hydropeaking on Mörel river section but cause a flexibility loss showed by a revenues reduction.

Conclusion

Based on a construction cost estimation, the short level variant appears about 6 time cheaper than the Ernen big fall variant. Solution with the smaller spatial scale and impact on the system is recommended.

References

[1] OFEV, « Assainissement des éclusées – Planification stratégique », 2012
[2] OFEV, « Eclusées – mesures d'assainissement », 2017
[3] D.Tonolla, A.Bruder, S.Schweizer. (2017), *Evaluation of mitigation measures to reduce hydropeaking impacts on river ecosystems – a case study from the Swiss Alps.*

SCCER SoE

SWISS COMPETENCE CENTER for ENERGY RESEARCH
SUPPLY of ELECTRICITY

SCCER-SoE Annual Conference 2019

Supported by:

Schweizerische Eidgenossenschaft
Confédération suisse
Confederazione Svizzera
Confederaziun svizra

Swiss Confederation

Innosuisse – Swiss Innovation Agency

Suspended sediment in the turbine water of HPP Fieschertal in 2018

Matthias Eugster, David Felix, Robert Boes; VAW, ETH Zürich

Introduction

Sediment particles transported in the water of mountain rivers (Fig. 1) cause hydro-abrasive erosion on turbines of medium and high-head Hydro-Power Plants (HPP). This reduces the turbine efficiency and electricity production while the costs for repairs and spare parts increase.
As a basis for economic optimizations, this study aimed at quantifying the Suspended Sediment Load (SSL) in the penstock of the high-head HPP Fieschertal in the Swiss Alps throughout the year 2018.

Fig. 1: Mountain stream with proglacial lake and high suspended sediment concentration approaching the intake of HPP Fieschertal (Photo: M. Eugster, 23.05.2019)

Set-up

The HPP Fieschertal is a run-of-river scheme (Fig. 2) downstream of the Fieschergletscher which is the second longest glacier in the Alps. In the valve chamber (Fig. 3), (1) an acoustic discharge measurement installation (ADM), (2) a Coriolis Flow and Density Meter (CFDM), (3) a Laser In Situ Diffractometer (LISST) and (4) an automatic water sampler were operated to measure the suspended sediment concentration (SSC). In addition, particle size distributions between 3 and 380 µm were measured by LISST every minute.

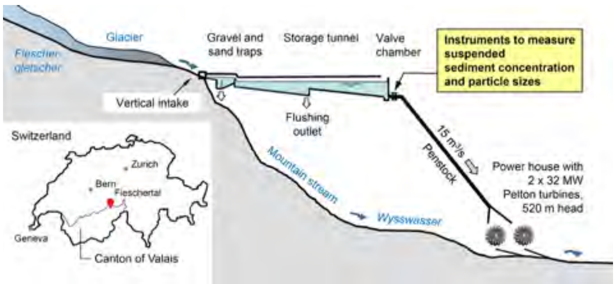

Fig. 2: Longitudinal profile of HPP Fieschertal with study site location (modified from Felix 2017)

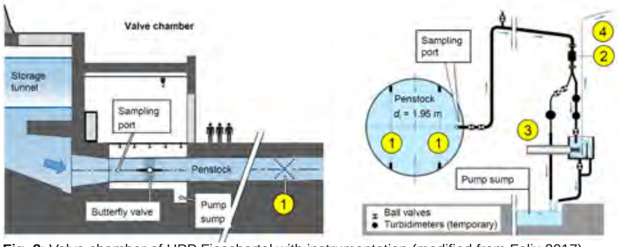

Fig. 3: Valve chamber of HPP Fieschertal with instrumentation (modified from Felix 2017)

Methods

From each water sample, the SSC was determined by weighing in the laboratory (gravimetrical method). Using these reference SSC and the median particle size d_{50} obtained from LISST, the SSC were evaluated from the raw data recorded by the other instruments. The SSC from the ADM were found to be most reliable for SSC < 0.5 g/l, whereas the data of the CFDM were preferred > 1 g/l. Between 0.5 and 1 g/l, a weighted average of SSC from ADM and CFDM was used.
The Suspended Sediment Load (SSL) in the penstock was calculated by integrating the product of SSC and discharge over time.

Results

Suspended sediment concentration (SSC)

Suspended sediment particles were mainly transported from mid April to mid November 2018 (Fig. 4). Some SSC peaks, e.g. on June 11 (day 161), are due to rain events, but no major flood occurred in 2018. The highest SSC in the penstock was caused by a re-suspension event in the storage tunnel (Fig. 2) on August 14 (day 225): When the water level in the tunnel was drawn down while the turbines were running, the flow velocity and the bottom shear stress in the tunnel increased. This led to the transport of more and coarser particles into the penstock compared to normal operating conditions in summer when the tunnel is completely filled with water and acts a secondary trap for fine sand.

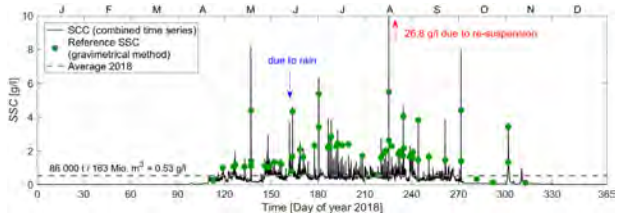

Fig. 4: Suspended sediment concentration (SSC) in the penstock of HPP Fieschertal in 2018

Suspended sediment load (SSL)

In 2018, about 86 000 t of mainly silt particles were transported through the penstock, corresponding to a specific fine-sediment yield of 0.6 mm per year in the catchment area of 58 km². While the average SSC was similar to previous years, a relatively high runoff volume due to the warm summer (glacier melt) led to a rather high SSL.
In contrast to the year 2012 with a major flood event, the sediment transport rate was quite uniform during the summer months of 2018. Hence there was no need to temporarily shutdown the HPP in this year.

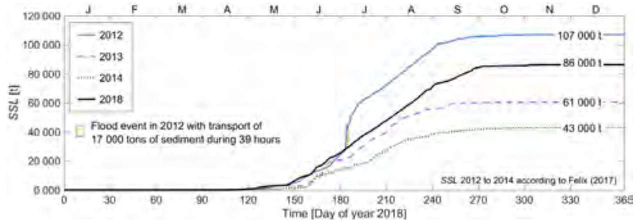

Fig. 5: Suspended sediment loads (SSL) in the penstock of HPP Fieschertal over the years

Conclusions

The SSC in the power waterway of HPPs depend not only on the weather conditions but also on the HPP operation. The annual sediment loads vary considerably mainly due to occasional flood events. Therefore, long-term data series are required to obtain reliable average values and to capture the full variability of the processes.
Real-time suspended sediment monitoring serves as a basis for economic and energetic optimizations of HPP operation. Thus it contributes to the sustainable and efficient use of the hydropower potential and hence to the implementation of the Energy Strategy 2050.

References

Abgottspon A., Felix D., Boes R., Staubli T. (2016). Schwebstoffe, hydro-abrasiver Verschleiss und Wirkungsgradänderungen an Peltonturbinen – Ein Forschungsprojekt am KW Fieschertal. *Wasser Energie Luft* 108(1), 9–24.

Felix D. (2017). Experimental investigation on suspended sediment, hydro-abrasive erosion and efficiency reductions of coated Pelton turbines. *VAW-Mitteilung* 238 (R. M. Boes, Ed.) and *Dissertation* 24145, ETH Zürich, Switzerland.

Felix D., Albayrak I., Boes R. M. (2018). In-situ investigation on real-time suspended sediment measurement techniques: Turbidimetry, acoustic attenuation, laser diffraction (LISST) and vibrating tube densimetry. *Intl. Journal of Sediment Research* 33, 3–17.

SCCER-SoE Annual Conference 2019

Renewal of alpine hydroelectric plants according to the spatial and temporal scales of analysis

Vincent GAERTNER, Sabine CHAMOUN[1], Pedro MANSO[1], Giovanni DE CESARE[1]
[1] Hydraulic Constructions Platform (PL-LCH), EPFL

Introduction

Since the adoption of the "Energy Strategy 2050" by the Federal Council in 2017, Switzerland has been looking for new energy alternatives to the nuclear sector and ways to reduce its greenhouse gas emissions, in particular by promoting the development of renewable energies. The national hydroelectric park, which represents 59% of total energy production, has an essential place in this context of upheaval in electricity supply. In the coming years, more and more existing power plants will come to the end of the concession. In this transitional period, they must be the subject of interventions to adapt their installations and operations to future economic, energy, legislative and environmental contexts. The main objective of the project is the development of a methodology to identify and promote technical solutions to increase winter energy production and operating flexibility. It consists of a first step of diagnosing the installations reference state and then a second step of generating and analysing renewal variants. It is then applied to the case study of the Forces Motrices de Conches (GKW) and the Forces Motrices Valaisannes (FMV) power plants in Haut-Valais.

Methodology

The general methodology followed in this work consists of three main steps. First of all, the establishment of the existing system reference state aims to study the existing power plants and their environment in order to choose the spatial and temporal scales of analysis and to identify the potential for optimising operation. Renewal variants are generated according to the identified intervention possibilities. These variants are then compared using multi-criteria analysis, modelling and pre-dimensioning to produce final recommendations.

The choice of the spatial scale of analysis is intended to limit the scope of investigations for the generation of renewal variants. The approach of choice proposes to evaluate at different scales the additional potential of existing facilities and their environment in order to achieve the project objectives. If large-scale surveys are required, a simplified cost calculation of an extension of storage capacity should allow for a comparison of construction costs and potential winter production gains.

Preselection is carried out to evaluate and compare the variants using criteria on energy, technical, environmental and social aspects. Finally, a second comparison based on the results of this in-depth analysis should lead to recommendations for final solutions.

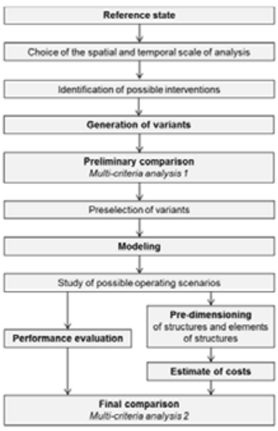

Figure 1: General approach for a hydroelectric facilities renewal project

Case study

The project applies to the Heiligkreuz (GKW), Ernen and Mörel (FMV) power plants located on the left bank of the Rhône in Haut-Valais, Switzerland.

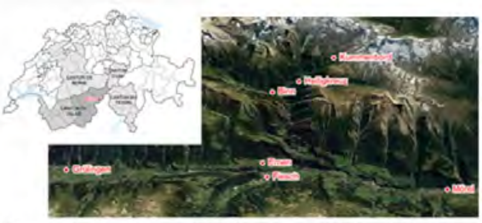

Figure 2 : Geographical location and topography of the case study region

The system has an installed capacity of 119.5 MW for an annual production of 448 GWh. Seasonal transfer of inputs is not feasible in the current state of the facilities and winter production represents between 1/10 and 1/4 of the annual production depending on the plant.

Rivers and intakes in the study area are not instrumented and the required hydrological data are only partially available. The operating data from the Heiligkreuz, Ernen and Mörel power plants and the Rhone flow measurements at Reckingen provided by the FOEN are therefore used to reconstitute the water inflow curves at the intakes.

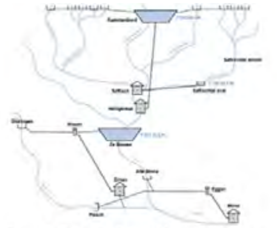

Figure 3: General scheme of the current facilities

Results

The procedure for generating adaptation concepts enables the development of 18 local variants and sub-variants based on the intervention types identified in the previous step. They can be divided into two main groups according to whether they aim to specifically optimize the use of Lengtalwasser inflows or whether they propose to exploit the potential of the Saflischtal. The three of them that are preselected provide an increase in production thanks to two new power plants and seasonal storage possibilities thanks to a large capacity reservoir upstream of Kummenbord and new pumping systems between Ze Binnen and Kummenbord.
Hydraulic modelling of operating scenarios and energy performance assessment show an increase in the annual production of the three main power plants.

	Variant n°2		Variant n°4		Variant n°6	
	Scenario 1	Scenario 2	Scenario 1	Scenario 2	Scenario 1	Scenario 2
Heiligkreuz	+8.53%	+8.53%	+6.65%	+5.40%	+4.29%	+1.46%
Ernen	+6.78%	+6.71%	+6.55%	+6.47%	+6.47%	+5.82%
Mörel	+6.12%	+6.16%	+5.81%	+6.07%	+5.77%	+5.69%

Figure 4: Rate of increase in annual production from existing plants

The development of scenarios based on the seasonal transfer of inputs also provides an opportunity to rebalance the annual distribution of production by increasing winter supply.

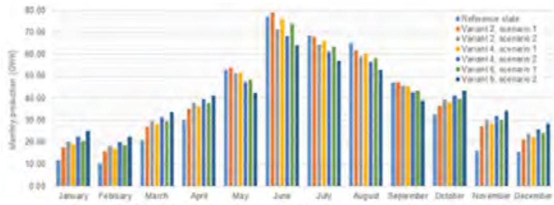

Figure 5: Monthly total production of the system in the different scenarios

The economic evaluation of the variants shows a decrease in the profitability of the largest variants due to high construction costs. A balance must therefore be found between the advantages of winter supply and the expected financial benefits.

Conclusions

The application of the methodology to a case study in Upper Valais provided different variants to achieve the objectives of increasing energy production and developing operational flexibility and seasonal storage for winter supply. It has been established that the GKW and FMV power plants in the Conches Valley have a real potential for optimization. Variants with large storage capacities have been selected and submitted for further study. Finally, modelling and pre-dimensioning steps demonstrated their relevance to the project objectives.
One of the avenues for continuing the project could be the instrumentation of strategic points of the system in order to ensure better monitoring of the available hydrological inflows and to consider optimising operation up to the limits of the current and future concession.

References

GIOVANNI, Marco, 2017. *Rénovation d'aménagements hydroélectriques alpins*. Lausanne : Ecole Polytechnique Fédérale de Lausanne. Travail de Master.

Guide pratique pour la réalisation de petites centrales hydrauliques. Programme d'action PACER – Energies renouvelables, Office fédéral des questions conjoncturelles, septembre 1992.

SCHLEISS, A.J. *Aménagements Hydrauliques*. Section de Génie Civil, Laboratoire de Construction Hydrauliques, Ecole Polytechnique Fédérale de Lausanne (EPFL). Edition 2015.

SCCER SoE
SWISS COMPETENCE CENTER for ENERGY RESEARCH
SUPPLY of ELECTRICITY

SCCER-SoE Annual Conference 2019

Hes·so VALAIS WALLIS School of Engineering

Supported by:
Schweizerische Eidgenossenschaft
Confédération suisse
Confederazione Svizzera
Confederaziun svizra
Swiss Confederation
Innosuisse – Swiss Innovation Agency

Comissioning of a new fatigue test rig based on pressure oscillations

A. Gaspoz[1], N. Gonçalves[1], L. Barras[1], V. Hasmatuchi[1], C. Nicolet[2], S. Rey-Mermet[1]
[1]HES-SO Valais, School of Engineering, powder technologies and advanced materials Group, CH-1950 Sion, Switzerland, samuel.rey-mermet@hevs.ch
[2]Power Vision Engineering Sàrl, Chemin des Champs Courbes 1, CH-1024 Ecublens, Switzerland

Context

Hydraulic power plants are an important part of the electricity production. Most of installations have been build before the 80's. The maintenance and the research of defects are the base to ensure their security. Fatigue phenomenon appears faster when the parts contain defects.
To study the behavior of a defect under pressure oscillation, a special test rig was build in the HES-SO laboratory in Sion. The idea consists to create periodically water hammer with a rotating valve and use the resonance (sum) phenomenon in the middle of the pipe. The oscillations are comparable to those present in a penstock and responsible of a fatigue break.

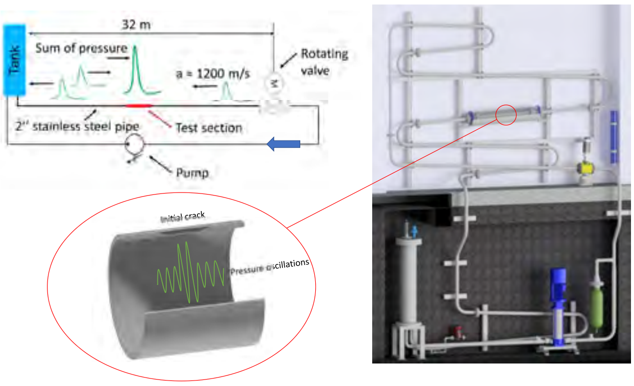

Methods

The commissioning started at the end of 2018 and the characterisation of the test rig was realized whit pressure sensors during spring 2019. Numerical simulation have permit to design and chose the different operating point. Simulation were realised with the software Simsen [1] marketed by Powervision Engineering in Ecublens, Switzerland.

Characterisation Results

Curves of energy losses in function of the flow and the valve's position.

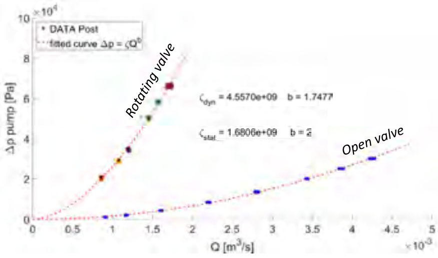

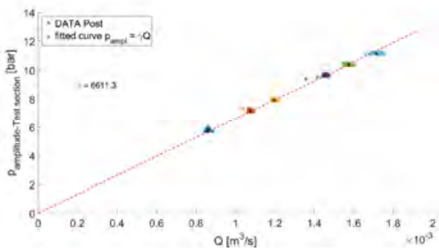

Pressure oscillation amplitude at the test section which is considerate as the half of the peak to peak difference.

Numerical Results

Pressure amplitude on the test section, directly upstream of the valve and the pump normalized by the values of the main operating point.

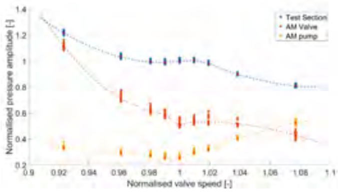

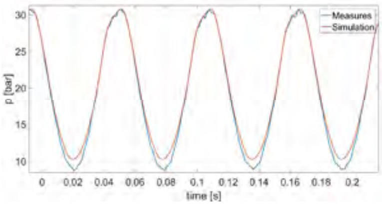

Pressure on the test section with a 88.9 x2 mm pipe that correspond to an stress oscillation between 22 and 66 MPa.

The pressure amplitude directly upstream of the valve is equal to half that present in the test section.

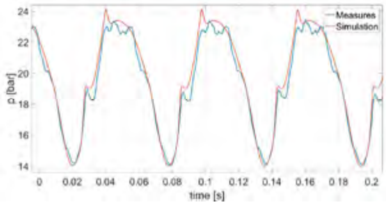

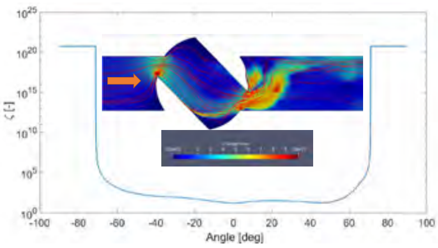

The transient characteristic of the valve was simulated with the open source software OpenFOAM. The result is used in Simsen for the global transient simulation.

Conclusion

- ✓ The test rig is in function and the last corrections are planned for the end of 2019.
- ✓ The principle of cyclic water hammer in resonance was measured and corresponds to the transient simulations.
- ✓ The installation of a crack sensor has started this year. The sensor is marketed by Sensima and uses the Foucault current effect to measure the depth and the length of a crack [2]
- ✓ The first break of pipe should be realized by the end of 2019.

Acknowledgements

SCCER SoE
SENSIMA inspection
Power Vision Engineering

References

[1] Nicolet, C., Béguin, A., Bollaert, E., Boulicaut, B., & Gros, G. (2015). Real-time simulation monitoring system for hydro plant transient surveys Int. *Journal on Hydropower & Dams*, *22*(5), 62-69.
[2] http://www.sensimainsp.com/

SCCER SoE
SWISS COMPETENCE CENTER for ENERGY RESEARCH
SUPPLY of ELECTRICITY

SCCER-SoE Annual Conference 2019

Supported by:
Schweizerische Eidgenossenschaft
Confédération suisse
Confederazione Svizzera
Confederaziun svizra
Swiss Confederation
Innosuisse – Swiss Innovation Agency

Hydraulics of Horizontal Bar Rack-Bypass Systems: Field Study at HPP Stroppel

Roland Hagenbüchli, Ismail Albayrak, Mohammadreza Maddahi, Ricardo Mendez, Robert M. Boes

Introduction

Horizontal bar rack-bypass systems (HBR-BS) are widely used for fish protection and guidance at hydropower plants (HPP). In 2014 a HBR-BS was installed at Stroppel HPP located on River Limmat in Switzerland. Axpo Power AG as the HPP operator and Aquarius [1] conducted an extensive fish monitoring campaign at this HPP in 2015 – 2017. In the present study, the hydraulics of the HBR-BS were investigated and linked to the results from the fish monitoring campaigns.

Study Site HPP Stroppel

Stroppel HPP is the most downstream power plant on the River Limmat before its confluence with the River Aare. Table 1 list the main characteristics of the HPP and its HBR-BS system.

Tab. 1: Main characteristics of Stroppel HPP and its HBR-BS

HPP Stroppel			HBR-BS		
Design discharge	[m³/s]	33	Bar opening	[mm]	20
Installed power	[kW]	840	Length of the rack	[m]	25.3
Installed turbines		1 Francis, 2 Kaplan	Horizontal rack angle	[°]	38
Fish region		Grayling and Barbel	Discharge in the bypass	[m³/s]	0.69

During the fish monitoring campaign, 28 fish species were detected. 86% of the fish had a body length < 10 cm and 98% of them were smaller than 20 cm. Moreover, the monitoring results indicated that the HBR-BS performed well independent of fish size and species and the delay in downstream migration was short. However, some small fishes < 10 cm were observed behind the rack using an ARIS sonar system (1.6 to 3.2% of the small fishes that migrated via bypass), whereas fish with a body length larger than 10 cm were not detected behind the rack. Furthermore, no fish impingement on the rack was observed during the monitoring.

Methods

An Acoustic Doppler Current Profiler (ADCP) mounted on a remote controlled boat with RTK-GPS was used to investigate the hydraulics of the HBR-BS (Fig. 1). Velocity measurements were conducted in 13 cross-sections normal to the flow direction in the headrace channel and in two sections parallel to the rack (Fig. 2). In addition, six stationary measurements were conducted at selected positions as shown with red crosses in Fig. 2.

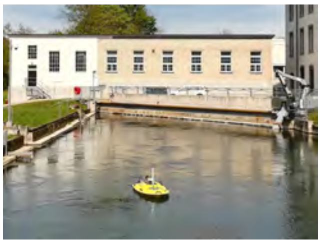

Fig. 1: Measurement device in the headrace channel of HPP Stroppel.

Fig. 2: Positions of velocity measurements (ortophoto [2])

Results and Discussion

Figure 3 shows the depth-averaged velocity magnitudes along the headrace channel. The vectors indicate longitudinal and transverse velocity directions. The velocity field shows that the main flow has the tendency to shift towards the left side, where the bypass entrance is located. Furthermore, due to the low ratio of channel width to flow depth ≈ 4, the flow is 3D and the maximum velocities are concentrated at the channel center and below the water surface (Figs. 3 and 4).

Figure 4a shows the distribution of the velocity component normal to the rack (v_n) in a cross-section along the rack measured at 1.7 m upstream of the rack. $y = 0$ indicates the left bank of the channel. Close to the surface at the centre of the rack, the flow velocities exceed the general design criteria of 0.5 m/s [3] with the maximum value of 0.7 m/s.

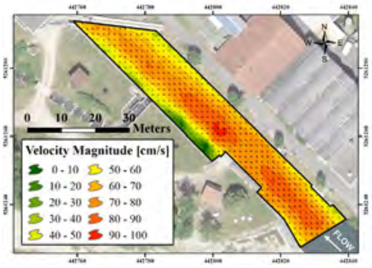

Fig. 3: Depth-averaged velocity magnitude along the headrace channel of HPP Stroppel (ortophoto [2]).

Fig. 4b shows the ratio of the rack-parallel (v_p) to the normal (v_n) velocity components. A ratio of $v_p/v_n > 1$ is recommended in order to guide approaching fish towards the bypass [3, 4]. From the center to the left channel side, where the bypass entrance is located, the ratio is uninterruptedly higher than 1 and therefore indicating a well-guiding flow field.

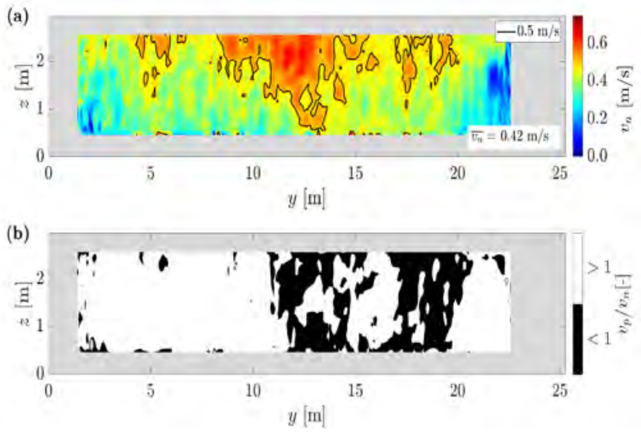

Fig. 4: Cross-sectional distributions of the velocity normal to the rack (v_n) **(a)** and the ratio of the rack-parallel to the rack-normal velocities (v_p/v_n) **(b)**.

Conclusion

The hydraulics of HBR-BS at Stroppel HPP were investigated. The results show that the HBR-BS creates favorable flow conditions for fish protection and guidance at a large portion of the rack area and up to the bypass. Even though small fish with a body length < 10 cm could physically pass the rack, only a small fraction of them was observed behind the rack. Such results indicate that the rack and bypass are well designed and positioned. Overall, Stroppel HPP is a promising example of a good implementation of a HBR-BS for protection and guidance of downstream migrating fish and hence the restoration of the longitudinal connectivity in riverine systems.

References

[1] Zaugg, C. and Mendez, R. (2018). Kleinwasserkraftwerk Stroppel - Wirkungskontrolle Fischabstieg am Horizontalrechen mit Bypass. Axpo Kleinwasserkraft AG.
[2] map.geo.admin.ch (2019). Kartenserver der Schweiz.
[3] Courret, D. and Larinier, M. (2008). Guide pour la conception de prise d'eau ichtyocompatibles pour les petites centrales hydroélectriques.
[4] Raynal, S., Chatellier, L., Courret, D., Larinier, M., and David, L. (2013). An experimental study on fish-friendly trashracks – part 2. angled trashracks. *Journal of Hydraulic Research*, 51(1): 67–75.

SCCER SoE
SWISS COMPETENCE CENTER for ENERGY RESEARCH
SUPPLY of ELECTRICITY

SCCER-SoE Annual Conference 2019

Supported by:
Schweizerische Eidgenossenschaft
Confédération suisse
Confederazione Svizzera
Confederaziun svizra

Swiss Confederation

Innosuisse – Swiss Innovation Agency

Two-phase flow hydraulics of low-level outlets

Benjamin Hohermuth, Lukas Schmocker, Robert Boes – VAW, ETHZ

Introduction

Low-level outlets are key safety elements of high-head reservoir dams. The load on low-level outlets will likely increase in the near future due to more frequent sediment flushing and dam heightening. Therefore, an improved understanding of their hydraulic properties is necessary.
A common outlet configuration uses a high-pressure vertical slide gate discharging into a free-flow tunnel. The high-speed water jet in the outlet tunnel leads to considerable air entrainment and transport resulting in negative air pressures, which can aggravate problems with gate vibration, cavitation, and slug flow. Sufficient air supply via an air vent mitigates such problems. However, current methods for estimating the required air demand do not incorporate all factors affecting design of air vents for low-level outlets. Additionally, information on two-phase flow hydraulics regarding e.g. flow pattern or mixture flow depth is almost inexistent.
The hydraulics of low-level outlets were investigated in a doctoral thesis using hydraulic model tests, prototype measurements and numerical simulations. The main findings are summarized herein.

Results

Air-water flow pattern

Four different air-water flow pattern were observed in the model and prototype tests:

- Spray flow; for relative gate openings ≤ 0.12 and contraction Froude numbers $F_c \geq 40$
- Free-surface flow; significant shockwave formation due to detachment of corner vortices was observed for 0.3 ≤ relative gate opening ≤ 0.7 (Fig. 1a).
- Slug flow; strong counter-current air flow can trigger the formation of slugs. A novel flow pattern map allows to identify and consequently avoid slug flow (Fig. 1b).
- Pressurized flow; for relative tunnel fillings ≥ 0.8 the downstream tunnel end was pressurized.

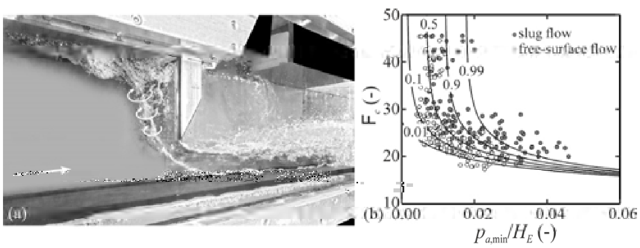

Figure 1: (a) gate vortices observed in model tests; pressurized air added for visualization. (b) Flow pattern map to identify slug flow; lines denote different probabilities of slug formation. H_E=energy head at gate, $p_{a,min}$=minimum air pressure in gate chamber.

Air demand

The influence of air vent, tunnel length L_t and tunnel slope S_t on the relative air demand β of low-level outlets was studied in extensive model tests. The air demand is primarily a function of F_c and the air vent properties. Increasing L_t leads to an increase in air demand, the effect of S_t is small. Prototype measurements were used to validate and extend the model-based results leading to a new predictive equation:

$$\beta = \frac{Q_{a,o}}{Q_w} = 0.08\mathrm{F}_c^{1.3}\left(\frac{A_v}{A_t\left(\zeta+1\right)^{0.5}}\right)^{0.8}\left(\frac{L_t}{h_t}\right)^{0.25} \qquad (1)$$

where A_t=tunnel area, A_v=air vent area, h_t=tunnel height, $Q_{a,o}$=air discharge through air vent, Q_w=water discharge, ζ=air vent loss coefficient.
Equation 1 captures the available prototype data roughly within ±50%, thus considerably improving air demand predictions compared to order of magnitude errors of existing approaches.

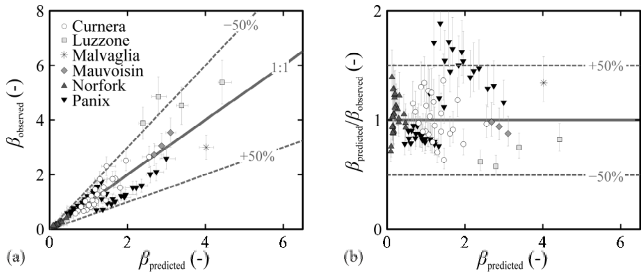

Figure 2: Comparison of (a) observed prototype air demand versus predicted β (Eq. 1). (b) relative error versus predicted β.

Hydraulics air-water flow

High velocities of up to 22 m/s in model tests allowed to gather data at prototype like conditions leading to the following results:

- Void fraction c; the void fraction profile can be described by an advection-diffusion equation (Fig. 3a). The mean void fraction C_m reaches a maximum after the gate and decreases from thereon.
- Interfacial velocity u; a wall-jet like profile was observed close to the gate, whereas a velocity-dip profile occurred further downstream. The latter can be described with a novel modified power law (Fig. 3b).
- Mixture flow depth h_{90}; the development of h_{90} can be described with a novel empirical approach based on a simplified backwater calculation (Fig. 3c).

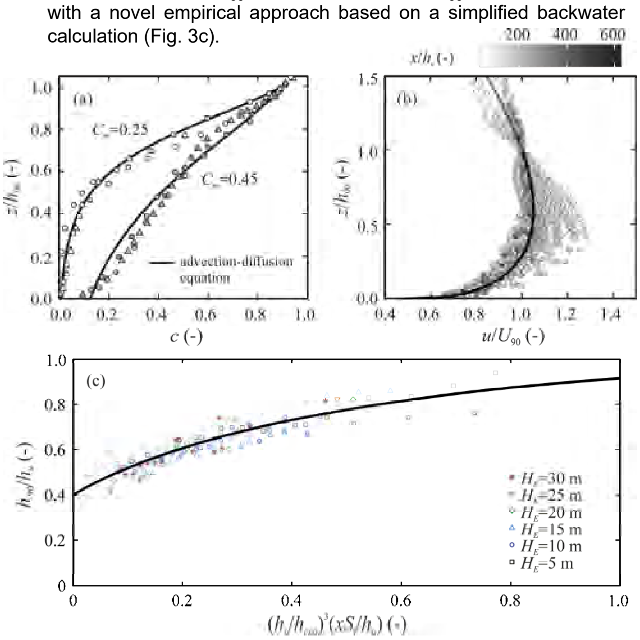

Figure 3: (a) c-profile for different C_m. (b) u-profile at different dimensionless distances, h_c=contraction flow depth. (c) Simplified backwater curve h_{90}, h_{crit}=critical flow depth, h_u=uniform (non-aerated) flow depth, S_t=tunnel slope.

Conclusions

A detailed model study on air-water flows in low-level outlets was conducted. The results were complemented by prototype measurements. The findings presented herein allow for an improved design of low-level outlets for future infrastructure adaptions.

Acknowledgement
This project is financed by the SNF Grant No. 163415 and is embedded in the SCCER-SoE framework. The prototype tests were financially supported by the Lombardi Engineering Foundation and conducted in cooperation with Ofible.

SWISS COMPETENCE CENTER for ENERGY RESEARCH
SUPPLY of ELECTRICITY

SCCER-SoE Annual Conference 2019

Supported by:
Schweizerische Eidgenossenschaft
Confédération suisse
Confederazione Svizzera
Confederaziun svizra

Swiss Confederation

Innosuisse – Swiss Innovation Agency

Numerical investigation of HPP layouts and their effects on fish guidance racks

Andreas Huwiler

Introduction

Hydro power plants (HPP) inhibit downstream fish migration. Fish guidance structures (FGS) can be used to improve this situation. The goal of this study was to analyze the upstream flow fields at different HPP layouts. The analyses were conducted with computational fluid dynamics (CFD). The effect of different measures at the HPP layouts to fish guidance structures were investigated.

Background

There are different concepts to ensure downstream fish migration. One criterion for good fish guidance efficiency is the ratio between the velocity parallel (v_p) and the velocity normal to the rack (v_n). This ratio (R_v) should be higher than one [1]. In this study, horizontal bar racks (HBR) were investigated since HBRs have little influence on the flow field. Different physical studies were conducted at the VAW to investigate HBR [2]. At HBRs, the ratio depends mostly on the HPP layout. The layout influences the approach flow to the turbines and to the rack, as can be seen in figure 1. The pillar at the bay unit HPP layout (1b) improves the ratio in front of the rack.

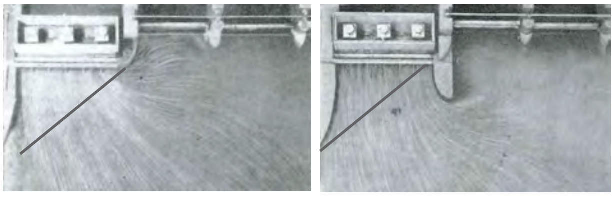

a): without pillar **b):** with pillar

Fig. 1: Flow field at a bay unit HPP [3]. The rack is simplified as a line.

Methodology

Using CAD Software a block unit HPP, a bay unit HPP and a HPP with side intake were built (fig. 2). Based on this layouts different simulations were conducted with the CFD Software FLOW-3D. The HBR was substituted as a baffle. The analysis of the approach flow of the rack was of particular interest. Furthermore, the influence of different discharges over the weir and different angles of the rack to the fish guidance were examined.

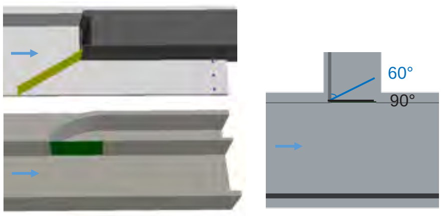

Fig. 2: The three investigated geometries: a block unit HPP, a bay unit HPP and a HPP with a side intake.

For the block unit HPP layout, observed data was available from a physical model of the VAW laboratory. With this data, the results of the simulation could be validated.
The settings of the validated simulation could be used to test the other two layouts for which no laboratory analyses were carried out. The steps are shown in the scheme in figure 3.

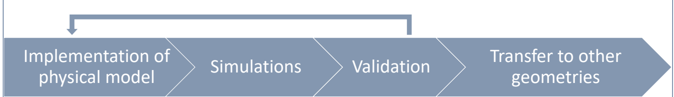

Fig. 3: Schema of the conducted work

Results and Discussion

The flow field was analyzed with horizontal planes of the flow velocity in x-direction (U) and different cross sections (CS). The most important CS was the one along the rack where the R_v was plotted. Figures 4 and 5 of the simulated and measured results of the block unit HPP are shown as examples. The simulated data represents the measured data in a high agreement. Differences in the horizontal flow field are direct in front of the weir and after the rack. At the CS along the rack, the biggest differences can be identified direct at the weir on the left side of the plot. The plot illustrates how the fish guidance worsens along the rack towards the weir (R_v <1).

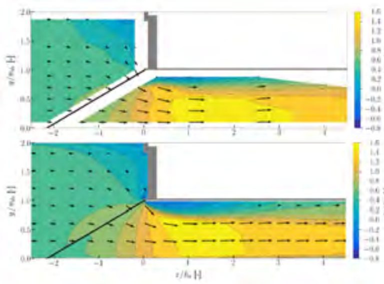

Fig. 4: Horizontal plane at z=0.5h_0 of U/U_{th}

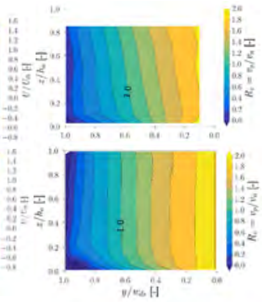

Fig. 5: Cross Section of R_v along rack

In figure 6, the cross sections of the HPP with side intake are shown. In the two pictures, R_v is shown at different rack angles.

With smaller horizontal angle the fish guidance effect increases.
In figure 7, the same CS is shown with a 90° angle. Here, the discharge over the weir is changed. By increasing discharge over the weir better fish guidance efficiency can be achieved.

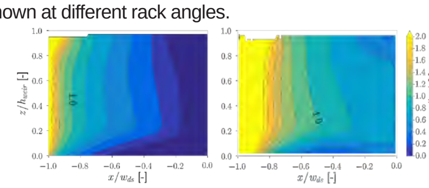

Fig. 6: CS at rack of Rv. The left rack has an angle of 90°, the right rack one of 60°.

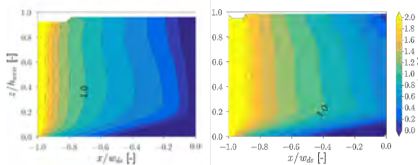

Fig. 7: CS at rack of Rv. On the left, the weir discharge is 40% of Qin and 60% on the right.

Conclusion

The results of different CFD simulations at a block unit HPP could be verified with measurements from a physical model. Thus, the HBR could be well implemented as a baffle in FLOW-3D. Additional HPP layouts were analyzed. There, the influence of different rack angles and discharges on the FGS could be quantified. Both measures can be used to improve the R_v. Which measure should be implemented depends on the studied layout and existing restrictions.
Because this works includes an approach how a HBR can be implemented in CFD studies, the head loss caused by the rack can be included in the evaluation.

References

[1] U.S. Department of Interior Bureau of Reclamation (USBR) (2006). Fish protection at water diversions: a guide for planning and designing fish exclusion facilities. Denver, CO: USBR.
[2] Meister, J., Fuchs, H., Albayrak, I., Boes, R.M. (2018). Horizontal bar rack bypass systems for fish downstream migration: state of knowledge, limitations and gaps. In Proc. 12th International Symposium on Ecohydraulics, Tokyo, Japan.
[3] Mosonyi, E. (1987). Water Power Development, volume one: Low-head power plants. Akadémiai Kiadó, Budapest.

SCCER-SoE Annual Conference 2019

SCCER SoE
SWISS COMPETENCE CENTER for ENERGY RESEARCH
SUPPLY of ELECTRICITY

Supported by:
Schweizerische Eidgenossenschaft
Confédération suisse
Confederazione Svizzera
Confederaziun svizra
Swiss Confederation
Innosuisse – Swiss Innovation Agency

Run-up of Impulse Wave Trains

Maximilian Kastinger, Frederic Evers, Robert Boes

Introduction

Very rapid gravity-driven mass movements including landslides, rockfalls, avalanches and glacier calvings can cause large water waves in open oceans, bays, natural lakes and reservoirs. Resulting impulse wave trains propagate away from the impact location and can run up several meters high on the shore. Possible consequences are damages to settlements and infrastructure or overtopping of dams, as shown by numerous historic events in Switzerland and abroad. Reservoirs are of particular interest, as there is usually a freeboard of just a few meters between the still water level and the dam crest.

While the run-up of single and periodic waves has already been extensively researched, there is only few knowledge about the multiple run-up of irregular wave trains. Therefore, the aim of this master's thesis was to investigate the run-up behavior of impulse wave trains and to develop an approach in order to estimate their run-up heights.

Methodology

Physical model tests were carried out in a 2D wave channel. The waves were generated by mesh-packed granular material sliding into the water body. First, the unconfined wave propagation was measured with ultrasonic distance sensors (UDSs). Then, the experiments were repeated with a barrier of different slope angles β, which was installed at the location of one of the sensors. The run-up was recorded with cameras. Fig. 1 shows the test setups for unconfined and run-up experiments.

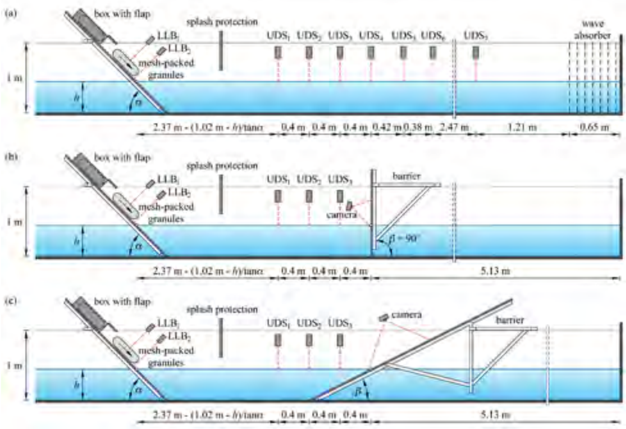

Fig. 1: Test setup for (a) unconfined wave propagation, (b) wave run-up at a vertical barrier and (c) wave run-up at an inclined barrier, exemplarily being installed at the location of UDS_4

Different wave characteristics were achieved by varying the water depth h, slide angle α, impact velocity V_s, sliding mass m_s and grain density ρ_g. Target wave properties include the wave crest and trough amplitudes a_{ci} and a_{ti}, respectively, wave heights H_i, wave celerities c_i, wave periods T_i and wave lengths L_i. The wave run-up R_i refers to the still water table, as shown in Fig. 2.

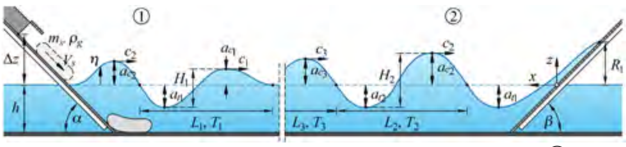

Fig. 2: Definition scheme with the governing parameters for ① wave generation and ② wave run-up

Results and Discussion

Breaker types

A different run-up behavior of the waves was observed. It was divided into non-breaking (NO), surging breaker (SU) and plunging breaker (PL). Fig. 3 illustrates these three types for an exemplary experiment.

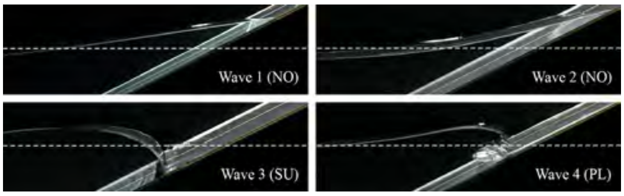

Fig. 3: Run-up behavior of the first four waves for a barrier slope angle β = 26.6°, the first two waves are non-breaking (NO), the third wave is a surging breaker (SU) and the fourth wave is a plunging breaker (PL)

As the breaker type influences the run-up height significantly, a predicttion criterion based on the surf similarity parameter $\xi_i = \tan\beta/(H_i/L_i)^{1/2}$ (Iribarren and Nogales, 1949) and the relative wave height H_i/h is proposed (Fig. 4).

Non-breaking waves (NO):

$$\xi_i > 2.1\left(\frac{H_i}{h}\right)^{-0.15} \quad (1)$$

Surging breakers (SU):

$$1.5\left(\frac{H_i}{h}\right)^{-0.15} \leq \xi_i \leq 2.1\left(\frac{H_i}{h}\right)^{-0.15}$$

Plunging breakers (PL):

$$\xi_i < 1.5\left(\frac{H_i}{h}\right)^{-0.15} \quad (2)$$

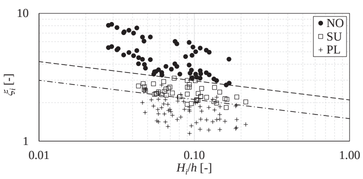

Fig. 4: Surf similarity parameter ξ_i versus relative wave height H_i/h for the different breaker types and the proposed criteria (– – –) Eq. (1) and (– · –) Eq. (2)

Run-up heights

A new prediction equation for the run-up heights is proposed (Eq. (3)). Fig. 5 shows the measured over predicted run-up heights. While non-breaking waves and surging breakers are represented well, plunging breakers are overestimated.

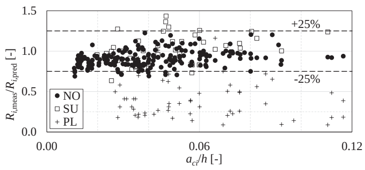

Fig. 5: Measured over predicted (Eq. (3)) run-up height $R_{i,\mathrm{meas}}/R_{i,\mathrm{pred}}$ versus relative wave crest amplitude a_{ci}/h

$$\frac{R_i}{h} = 2\frac{a_{ci}}{h}e^{0.4\frac{a_{ci}}{h}}\left(\frac{c_i}{\sqrt{gh}}\right)^{-0.25}\left(\frac{90°}{\beta}\right)^{0.2\left(\frac{a_{ci}}{H_i}\right)^{-0.9}\left(\frac{c_i}{\sqrt{gh}}\right)^{-1.25}} \quad (3)$$

Conclusion

A new data set with run-up heights of impulse wave trains for later reuse was created. Based on this, a new breaker type criterion and run-up prediction equation are proposed. Tests with additional barrier slope angles and further data analysis are required in order to develop a well founded, practicable run-up equation for impulse wave trains.

References

Iribarren, C. R., Nogales, C., 1949. "Protection des ports (Harbour protection)". *17th International Navigation Congress*, Lisbon, Section 2, Communication 4, 31-80. (In French)

SCCER SoE
SWISS COMPETENCE CENTER for ENERGY RESEARCH
SUPPLY of ELECTRICITY

SCCER-SoE Annual Conference 2019

EPFL

Supported by:
Schweizerische Eidgenossenschaft
Confédération suisse
Confederazione Svizzera
Confederaziun svizra

Swiss Confederation

Innosuisse – Swiss Innovation Agency

Assessing the acceptability of concrete dam submergence considering scour

Labrosse L., Chamoun S. and Manso P. A.
Plateforme de Constructions Hydrauliques, Ecole Polytechnique Fédérale de Lausanne,
labrosse.lucas@gmail.com sabine.chamoun@epfl.ch pedro.manso@epfl.ch

Why ?

For many dam operators, their assets are aging in a context that evolves both with new flood assessment methods and new legal or normative frameworks. Building new outlet structures to ensure enough flood release capacity can be expensive and limited. Figure 1 presents the reason for submergence acceptability assessment for a generic case, based on a real dam [1].

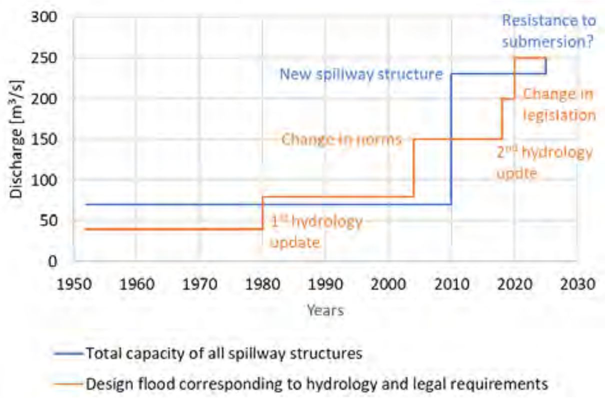

Fig. 1 Hypothetic dam history regarding flood release capacity

Submergence can be an alternative, but the dam stability has to be guaranteed and therefore it raises a few questions:

- Can the dam withstand higher reservoir levels above the crest?
- Which flood events can be accepted?
- What is the acceptable residual risk?
- To which extent is dam toe scour acceptable, considering the dam's or the abutment's instability?

This last question can be the most challenging one.

The proposed method

Divided in four modules, the method offers a framework to consider the different inputs necessary to assess the risk of dam instability due to scour following dam submergence (Fig. 2), due to insufficient conventional spilling capacity. The vulnerability to scour formation is assessed based on the duration of the submergence events, on the geometry of the falling nappes, on the downstream tailwater levels and on dam foundation & riverbed rock conditions. Then, scour evolution is assessed through different methods, considering to some extent the complexity of the processes taking place during scour progress by the interaction of air, water and rock.

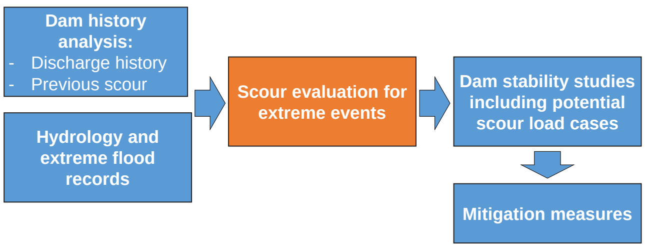

Fig. 2 Simplified chart of the proposed method for risk assessment

One of the most challenging issues in rock scour assessment is to account for the effect of time [1]. **Ultimate scour methods (USM)** allow estimating scour extent for a given discharge assuming it last long enough to reach an equilibrium configuration. **Energy-based methods (EBM)** [7,8] focus on scour progress as function of a chronological sequence of spillage discharges, varying in intensity and duration.

EPFL's **Comprehensive Scour Model** (CSM) [1] illustrates a possible way to sequentially link several physical processes, one of them being time-dependent. Rock fracture propagation under hydrodynamic loads is modelled using the Paris-Erdogan fatigue law and hydrodynamic loads defined according [2,3,4,6]. Recently, a novel EBM model was proposed by [5] considering only the E**xcess Energy** [EEBM] available for scour at each given moment. The four previous methods allow having multiple truncated entries to inform decisions and risk assessment. Figure 3 graphically shows the required data to properly calibrate such methods.

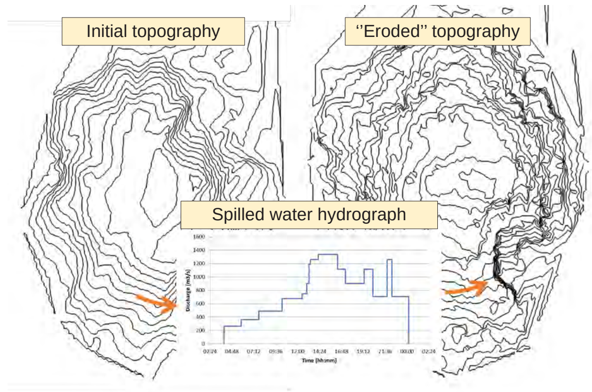

Fig. 3 Calibrating scour computation with passed spill events

Results

The general method was applied to two different dams. The first one is a dam located at a high altitudes with a fairly small reservoir and ungated crest overflow spillway. A Piano Key Weir spillway was added recently to ensure enough capacity for the revised millennial flood. The second dam is quite different, situated at intermediate altitudes and equipped with a three-bay gated spillway with ski-jumps for a total capacity of 5800 m^3/s. The study of the first dam revealed that no scour had occurred yet in over 50 years. The scour analysis with USM methods showed that some erosion could occur for extreme flood events with a return period of 5000 years or more. However, the EEBM time-accounting method [5], based on the potentially available energy for scour, showed that the flood event duration was too short for any serious erosion to occur. For the second case study, with gated spillways, the available plunge pool bathymetries and spillage records allowed obtained site constants of scour progression (according [8]) and estimating scour from extreme events. The application of the EEBM showed interesting results as well, indicating that instead of using site constants to calibrate Spurr's scour evolution function, one should rather use event-related constant for calibration of such function (i.e. the same event might not produce the same scour increase if occurring at different chronological moments in the spillage records).

Further application of these methods could help to better assess how rock quality, discharge intensity and duration are linked to the equilibrium state of a scour pool. Indeed, better knowledge of possible scour evolution can help with assessing the acceptability of dam submergence.

References

[1] Blancher, B., Laugier, F., & Leturcq, T. (2015). Méthodes d'évaluation du risque d'érodabilité des fondations soumises à déversement. Colloque CFBR. Chambéry.
[2] Bollaert, E., & Schleiss, A. (2005). Physically based model for evaluation of rock scour due to high-velocity jet impact. Journal of Hydraulic Engineering, 131(3).
[3] Duarte, R., Pinheiro, A., & Schleiss, A. (2016). An enhanced physically based scour model for considering jet air entrainment. Engineering, 2, pp. 294-301.
[4] Federspiel, M. (2011). Response of an embedded block impacted by high-velocity. Thèse de doctorat, EPFL, Lausanne.
[5] Labrosse L. (2019) Résistance ultime au déversement des barrages en béton, EPFL Master thesis (Supervisors: Manso, Chamoun, De Cesare).
[6] Manso, P., Bollaert, E., & Schleiss, A. (2009). Influence of plunge pool geometry on high-velocity jet impact pressures and pressure propagation inside fissured rock media. ASCE J. Hydraulic Engineering, 135(10):783-792. DOI: 10.1061/ ASCE HY.1943-7900.0000090
[7] Manso, P., Marques, M., Almeida, F., Canellas, A., & Botelho, M. (2007). Rock scour downstream ski-jumps : comparison of prototype observations with analytical and physical-model estimates. 32nd IAHR Congress. Venice.
[8] Spurr, K. (1985). Energy approach to estimating scour downstream of a large dam. Water Power and Dam Construction, 37(11).

SCCER SoE
SWISS COMPETENCE CENTER for ENERGY RESEARCH
SUPPLY of ELECTRICITY

SCCER-SoE Annual Conference 2019

EPFL NTNU

Supported by:
Schweizerische Eidgenossenschaft
Confédération suisse
Confederazione Svizzera
Confederaziun svizra

Swiss Confederation

Innosuisse – Swiss Innovation Agency

Solving of a Lifting Problem in a Pumped Storage Power Plant

Daniel Pace, Giovanni De Cesare, Pedro Manso, Kaspar Vereide, Livia Pitorac, Leif Lia
Email: daniel.pace@alumni.epfl.ch

Motivation

The construction and upgrading of pumped storage hydropower plants (PSHP) will be very beneficial in the years to come in order to regulate the power systems. They are very flexible and allow covering peak demands and storing energy on a large scale.
In this work, the Duge PSHP in Norway is used as a case study. The power plant has two Francis reversible pump-turbines (RPT) with a total installed capacity of 200 MW. In 2017, however, the turbines were refurbished and since then, a lifting problem occurs at the rotor of one of the turbines (Unit 1) when generating at a high load. As a consequence of this problem, the generation has to be restricted to 80% of the maximal load, i.e. 160 MW. The aim of this work is to understand the causes of the lifting and to find a civil engineering solution to this problem by modifying the waterway of the power plant.

Trash rack in the Duge power plant

Results

In order to solve the lifting problem, three solutions have been selected. The first aims to avoid any problems in the worst load case and to be able to run the power plant at 200 MW again. The second aims to avoid any problems in a normal load case and to run at 200 MW as well. Finally, the third solution aims to be lighter on a technical and economic point of view and to be able to run the power plant at 185 MW. For each solution, the downstream pressure is compared to the unmodified power plant.

Solution 1

- Addition of a downstream air cushion surge tank
- Addition of a 6 km parallel tunnel in the tailrace

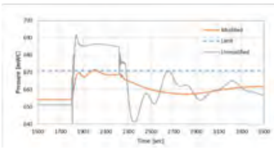

Solution 2

- Increase of volume in the surge tank upper chamber
- Addition of a 6 km parallel tunnel in the tailrace

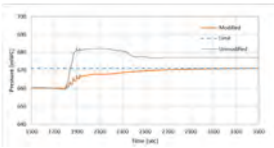

Solution 3

- Addition of a 6 km parallel tunnel with smaller section in the tailrace

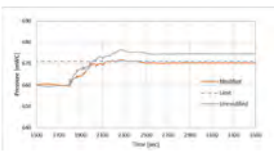

After an economic analysis is made, the final costs for each solution are estimated considering the construction works (new access tunnels, excavation, draining of tailrace tunnel, etc.) and the losses due to the power plant outage. The costs are given in different currencies (1 NOK = 0.1177 CHF and 1 NOK = 0.1008 EUR):

	Solution 1	Solution 2	Solution 3
Norwegian kroner [NOK]	275 million	215 million	162 million
Euros [EUR]	27.7 million	21.7 million	16.3 million
Swiss francs [CHF]	32.3 million	25.3 million	19.0 million

Methods and materials

The Duge PSHP has a very long tailrace tunnel (12 km) in comparison to the headrace tunnel (650 m). The high friction losses due to the long tailrace give a high downstream pressure rise at the RPT units in generating mode.

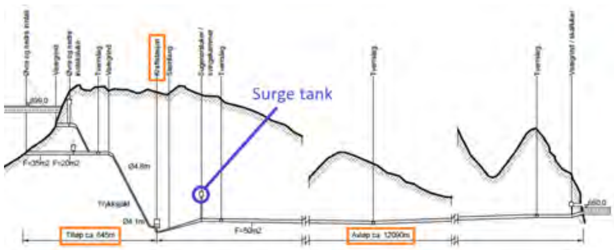

Duge power plant layout

In order to propose modifications of the power plant, a model is made on LVTrans, a numerical modelling freeware allowing to calculate transients in a loaded pipe system [1]. To simulate the real behaviour of the prototype, the model is calibrated against downstream pressure measurements, done at the draft tube wall for a turbine shutdown.

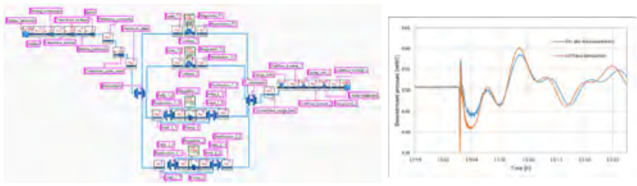

LVTrans model of the Duge power plant (left) and calibration (right)

The calibration is considered satisfactory, since only the first pressure peaks, which are the worst, are of interest for the lifting problem. The lifting of the rotor (246 tons) at Unit 1 occurs when the resulting vertical force acting on the runner is directed upwards; the downstream pressure is therefore the significant factor to consider.
Norconsult, a Norwegian consulting company, calculated that 1 [mWC] downstream pressure change = 4.1 [tons] of lifting force. This is obtained by multiplying the pressure by the surface of the outlet. Moreover, the maximal lifting force acting on the runner should be no more than 75 tons [2]. Considering this, it is possible to have a threshold that the downstream pressure should not exceed in order to safely run the power plant without the lifting problem.

Discussion

As showed in the results, the modifications of the power plant improve both the steady and unsteady states and allow the downstream pressure at Unit 1 to remain under the critical threshold. However, the solutions seem to be disproportionate, considering the total amount of the required investments and construction works. A limitation of the economic analysis is that only the total costs are considered, but not the associated benefits of having more power available.
Finally, the Duge power plant will receive new runners in the future, which means that the problem may be solved in a few years. Considering all these conclusions, it seems that it is probably better to not opt for a civil engineering solution to solve this lifting problem.

References

[1] **Svingen, B., 2016.** *LVTrans manual*. Sintef & NTNU, Trondheim
[2] **Norconsult, 2014.** *Aksialkrefter - måleresultater og gjennomgang av tiltak.* Sira Kvina Power Company, restricted access

SCCER SoE
SWISS COMPETENCE CENTER for ENERGY RESEARCH
SUPPLY of ELECTRICITY

SCCER-SoE Annual Conference 2019

Supported by:
Schweizerische Eidgenossenschaft
Confédération suisse
Confederazione Svizzera
Confederaziun svizra
Swiss Confederation
Innosuisse – Swiss Innovation Agency

Renewal of the Ritom hydropower plant

Jakob Siedersleben, Samuel Vorlet, Giovanni De Cesare(, Nicola Tatti, Urs Müller, Graziano Sangalli)

Context

On the basis of the Water Protection Act of 2013, a new generation of regulating reservoirs is under construction across Switzerland. It requires that all Swiss operators of hydroelectric power plants must eliminate within 20 years all severe issues caused by the rapid change of water discharge, called hydropeaking, due to the exploitation of hydrodynamic power. In Tessin, the hydroelectric power plant constructed in 1921 will be modernized. In the framework of this modernisation a new powerhouse with three machine groups will be constructed. In order to minimize the effects of hydropeaking, a regulating reservoir with a volume of 100.000 m³ is planned. The discharge exiting the reservoir can be controlled by a regulating structure which leads the water via an outlet in the Ticino. Due to the new reservoir, the course of the river Foss has to be changed and four sills will be installed. Fig. 1 shows the current and the planned situation.

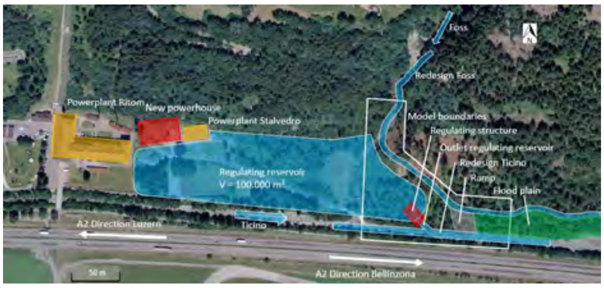

Fig. 1: Scheme of the modeled area

Objectives

The Laboratory of Hydraulic Constructions of the EPFL was mandated to execute experiments on a physical model. The following objectives were determined for the project:

- Concept validation of the planned geometry of the Ticino, the regulating reservoir and the Foss
- The investigation of the influence of the regulating structure on the Ticino
- The behaviour of the whole system under flooding up to an EHQ (extreme flood)
- The analysis of floating debris and debris flow in the Ticino and the Foss

Physical Modelling

The modelled area is 215.2 m long in flow direction of the Ticino and 181.2 m wide perpendicular to the flow direction. The modelled area is illustrated in Fig. 1. The model was constructed with a scale of 1:40 according to the Froude similitude.

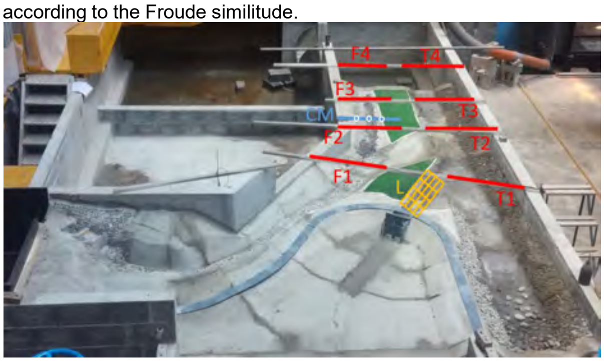

Fig. 2: The model and the eight ultrasound sensors (red), three current meter locations (blue) and the twenty-five laser locations (yellow)

In order to analyse the model, the water heights are measured at eight locations with ultrasound sensors. The height of the riverbed is measured with a red laser on a grid of twenty-five points. The flow velocities are measured with a current meter at three points. The physical model and the measuring positions are illustrated in Fig. 2. Furthermore, visual observation and colorant was used to determine dead and recirculation zones and determine possible locations prone for deposition of sediments.

Results

The tests showed a well-functioning of the whole system. But the course of the Foss had to be adapted. Furthermore, rock sills were installed and the roughness of the riverbed was increased. With these adaptations the desired maximum capacity of Q_{Foss} = 60 m³/s is exceeded. Dependent on the discharge combination of the Ticino and the outlet of the regulating structure, one must expect sediment accumulation either at the outlet of the regulating reservoir or at the embouchure. Furthermore, one must expect a scour hole dependent on the discharge at the outlet of the regulating reservoir and the discharge of the Ticino as illustrated in Fig. 3. However, the main influence on the depth of the scour hole is the discharge in the outlet of the reservoir.

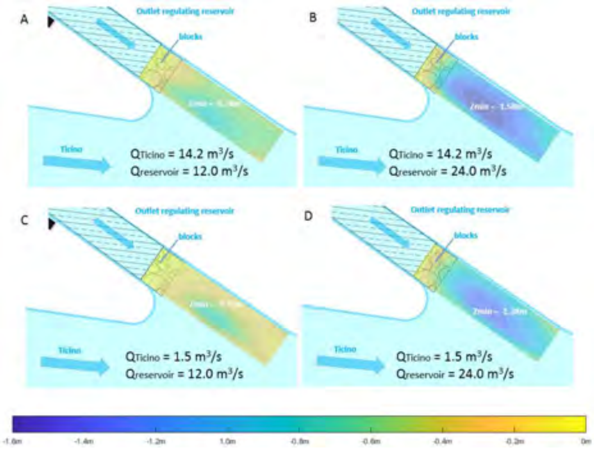

Fig. 3: The scour hole depth after the outlet of the regulating reservoir

The investigation of the floods showed that the Foss will overflow in the regulating reservoir. The regulating reservoir will overflow over the southern bank in the Ticino and the Ticino will overflow at an HQ100 over the southern bank in direction of the high way. Although the Foss overflows already significantly earlier, it inundates only the flood plain and the ramp, which does not pose any problems.

The experiments with debris flow in the Foss show that it will be transported until the ramp were it accumulates. However, if the discharge of the Foss is sufficient enough, the debris flow can overflow in the regulating reservoir as well. On the other hand, floating debris did not pose any problems in the Foss, on the contrary to the Ticino, where there can be accumulations at the outlet of the reservoir observed.

References

- Bassin de démodulation des rejets d'une centrale hydroélectrique : Barrage de Ritom ; Cédric Egolf ; 2019
- Erneuerung des Wasserkraftwerkes Ritom; Hydraulische Modellversuche; LCH Offerte 11/2017; 31.08.2017
- Auslaufbauwerk Demodulationsbecken – Verlegung Fossbach – Pflichtenheft für physikalische Modellversuche; Ritom SA (Bauherr); 02.08.2017
- Wasserkraftanlage Ritom; 28.06.2019; Retrieved from https://www.aet.ch/DE/Impianto-idroelettrico-del-Ritom-ba89fd00#.XRXZFuszZaQ

SCCER-SoE Annual Conference 2019

SCCER SoE
SWISS COMPETENCE CENTER for ENERGY RESEARCH
SUPPLY of ELECTRICITY

Supported by:
Schweizerische Eidgenossenschaft
Confédération suisse
Confederazione Svizzera
Confederaziun svizra
Swiss Confederation
Innosuisse – Swiss Innovation Agency

Hydro-abrasion at hydraulic structures

Damiano Vicari, Dila Demiral, Ismail Albayrak, Robert M. Boes
ETH Zurich, Switzerland

Motivation and objectives

Sediment transport from glacier basins, rivers and waterways have strongly increased under the effect of climate change. As a consequence, high sediment transport rates combined with high flow velocities cause severe hydro-abrasion at hydraulic structures such as Sediment Bypass Tunnels (SBTs) and bedrock incision in high-gradient mountainous streams. A better understanding of the physical processes of turbulent flow characteristics, bedload particle motion, and hydro-abrasion and their interrelations is of prime importance for both sustainable use of hydraulic structures and landscape evolution. Therefore, this study aims at (1) investigating turbulence characteristics of supercritical open-channel flows, (2) conducting hydro-abrasion experiments at the same flow conditions as in (1) to determine the abrasion depths and patterns, and (3) data evaluation and calibration of the abrasion prediction model.

Experimental setup and test program

The experiments were conducted in a b = 0.2 m wide, h = 0.5 m deep and l = 13.5 m long glass and wood-sided laboratory flume with S_b = 1% bed slope (Fig. 1). The first 5 m of the flume is covered with a non-erodible concrete followed by 6.6 m erodible foam.

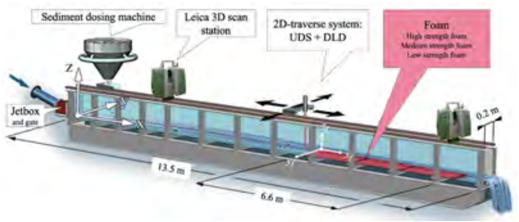

Figure 1. Experimental flume and measuring instruments

Three types of foams with different tensile strengths (f_{st}), compressive strengths (f_c) and Young's modulus (Y_M) were used as bed lining materials (Table 1). The supercritical open channel flow conditions were provided by a gate controlled jetbox system that converts the pressurized conduit flow into the free surface channel flow. The experiments were conducted with flow depths h_o = 10 and 20 cm with F_o = 2, 3 and 4 at four different sediment supply rates Q_s = 100, 200, 400 and 800 g/s (Table 2). Polyurethane foams were placed to the flume bottom with decreasing material strength in the flow direction (Fig. 1). Flow depths were measured using an Ultrasonic Distance Sensor (UDS) and a Distance Laser Device (DLD) mounted on a traverse system consisting. The surfaces of the foams were scanned using a 3D Leica P15 laser scanner after each run with 1 ton of sediment supplied to the flow. The obtained data were used to determine the development of hydro-abrasion pattern and rates.

Table 1. Bed lining material properties

	ρ_s [t/m^3]	f_{st} [MPa]	f_c [MPa]	Y_M [MPa]
Low-strength foam	0.064	0.32	0.36	3.92
Medium-strength foam	0.096	0.50	0.60	5.38
High-strength foam	0.128	0.84	0.92	10.33

Table 2. Experimental matrix

	F_0	b/h_0	S_b	D [mm]	particle	Q_s	material
E1	3	1	1	7.1	sandstone	100, 200, 400, 800	foam 1+2+3
E2	2	2	1	7.1	sandstone	200	foam 1+2+3
	3	2	1	7.1	sandstone	200	foam 1+2+3
	4	2	1	7.1	sandstone	200	foam 1+2+3

Results and discussion

Figure 2 presents the contour maps of final surfaces for the experiments E1 and E2. It shows that hydro-abrasion pattern is dominated by an incision channel along the flume center, growing and enlarging in time. Such pattern is triggered by saltation of bed load particles transported by the flow at the flume center where the bed shear stresses are higher compared to flume side walls. Results also show that for the same amount of sediment transport i.e. 1 ton, the abrasion depths are similar in the two test runs, independent from the sediment supply rate, Froude number, and aspect ratio.

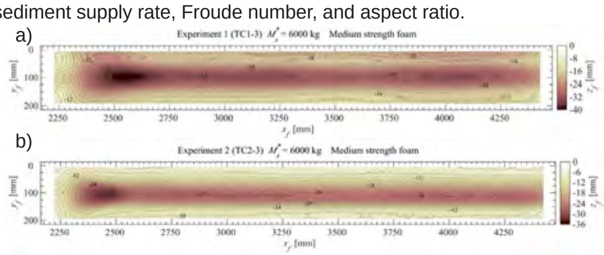

Figure 2. Abrasion pattern on the medium strength foam for a) E1, b) E2

Figure 3a shows the specific gravimetric bedload rate q_s versus the vertical abrasion rate A_r for E1. The abrasion linearly increases with increasing supply rate and it does not reach at a threshold. Fig. 3a also reveals that the abrasion rates decrease with increasing bed lining material strength. The Froude number effect on the abrasion rate A_r is shown in Fig. 3b. A_r increase up to a limit F number and then decreases with increasing F. This behavior is attributed to the reduced energy transfer to the bed per unit meter due to the longer particle hops caused by higher bed shear stresses at high F.

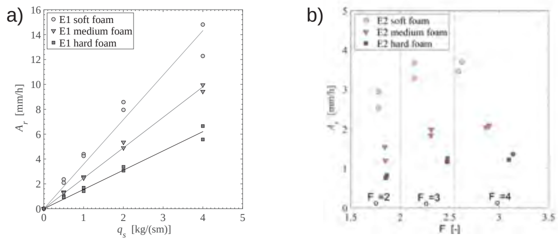

Figure 3. Vertical abrasion rate A_r versus a) bed load mass transport rate per unit width q_s and b) Froude number

Conclusions and outlook

An experimental investigation was conducted to understand the bed abrasion mechanism in supercritical narrow open channel flows existing in hydraulic structures and steep bedrock rivers. Results show that hydro-abrasion develops in the flume center creating a continuous incision channel and such pattern is independent from the Froude number and aspect ratio in the range of b/h < 2. Vertical abrasion rate A_r linearly increases with increasing bedload rate, whereas it decreases with increasing bed lining material strength. The Froude number affects the abrasion rate. The findings of this study provide knowledge basis to better understand on hydro-abrasion mechanism and hence lead us to develop a hydro-abrasion prediction model.

References

Auel, C. (2014). Flow characteristics, particle motion and invert abrasion in sediment *bypass tunnels*. *PhD Thesis, VAW-Mitteilung 229* (R. M. Boes, Ed.) Laboratory of Hydraulics, Hydrology and Glaciology, ETH Zürich, Switzerland.
Auel, C., Albayrak, I., Sumi, T., Boes, R.M. (2017). Sediment transport in high-speed flows over a fixed bed: 2. Particle impacts and abrasion prediction. *Earth Surface Processes and Landforms, 42(9), 1384-1396.*
Müller-Hagmann, M. (2017). *Hydroabrasion by High-Speed Sediment-Laden Flows in Sediment Bypass Tunnels. VAW-Mitteilung 239* (R.M. Boes, Ed.), Laboratory of Hydraulics, Hydrology and Glaciology, ETH Zürich, Switzerland.
Scheingross, J.S., Brun, F., Lo, D.Y., Omerdin, K., Lamb, M.P. (2014). Experimental evidence for fluvial bedrock incision by suspended and bedload sediment. *Geology, 42(6).;* **Sklar, L.S., Dietrich, W.E. (2001).** Sediment and rock strength controls on river incision into bedrock. *Geology, 29(12).*

SCCER SoE

SWISS COMPETENCE CENTER for ENERGY RESEARCH
SUPPLY of ELECTRICITY

SCCER-SoE Annual Conference 2019

Supported by:

Schweizerische Eidgenossenschaft
Confédération suisse
Confederazione Svizzera
Confederaziun svizra

Swiss Confederation

Innosuisse – Swiss Innovation Agency

Seismic behavior of Pine Flat concrete gravity dam using microplane damage-plasticity model

EPFL

Samuel Vorlet, Pedro Manso, Giovanni De Cesare

Platform of Hydraulic Constructions (PL-LCH), Ecole Polytechnique Fédérale de Lausanne (EPFL)

Introduction

The response of gravity dams under seismic loads is a major concern of dam safety assessment in earthquake-prone areas. The dynamic response of the dam body depends to some extent on the binding foundation conditions as well as on the interaction with the reservoir. During earthquakes, gravity dams are subject to strong horizontal and vertical motions inducing stresses with peaks that may be greater than the maximal strength and consequently lead to damage in the dam body, mainly in tension state. Currently, most dam safety evaluations with finite elements (FE) analysis of reservoir-dam-foundation systems consider a linear elastic model for mass concrete with failure criteria based on maximal tensile strength [1,2], in particular for the non-extreme load combinations. First assessments of extreme load combinations using linear analyses allow preliminary estimates of the location and extent of tensile stress peaks greater than the maximal concrete tensile strength but cannot inform on stress and stiffness redistribution during an earthquake (damage time evolution). This study concerns linear and nonlinear analyses with damage model in order to assess the dam safety under seismic loads resulting with stress peaks leading to damage in the dam body. It presents the seismic analysis of Pine Flat Dam for the 15th International Benchmark Workshop on Numerical Analysis of Dams to be held in Milan in September 2019. It focuses on the tallest non-overflow monolith of Pine Flat concrete gravity dam located on King's River, east of Fresno, California (USA).

Methods

Numerical simulations were performed using the finite element code ANSYS (M-APDL) to discretize the governing equations on the computational domain. A two-dimensional finite elements (FE) model of the reservoir-dam-foundation system is considered. The dam is composed of 37 monoliths and its crest is 561 m long. The tallest non-overflow monolith is 121.91 m high with a 95.8 m base length. The dam body and rock foundation (700 m x 122 m) are modeled with quadrilateral structural plane strain elements. The reservoir is modeled using acoustic elements with inviscid and compressible.

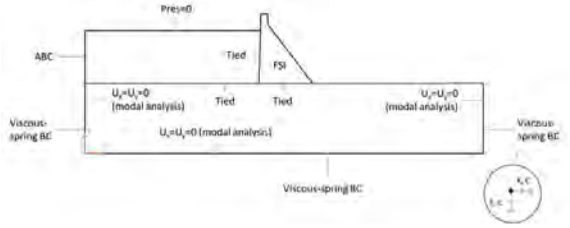

Figure 1: *Reservoir-dam-foundation FE model boundary conditions and interfaces*

For damage modeling in the dam body, a coupled damage-plasticity model for concrete [3] based on microplane formulation [4, 5] is used. The model has the ability to define different damage initiation criteria and damage evolution laws between tension and compression states. The model can additionally represent cyclic loading conditions, where stiffness lost during cracking is recovered due to crack closure during transition from tension to compression state, while damage sustained under compression remains upon transition to tension state [3].

Dynamic properties

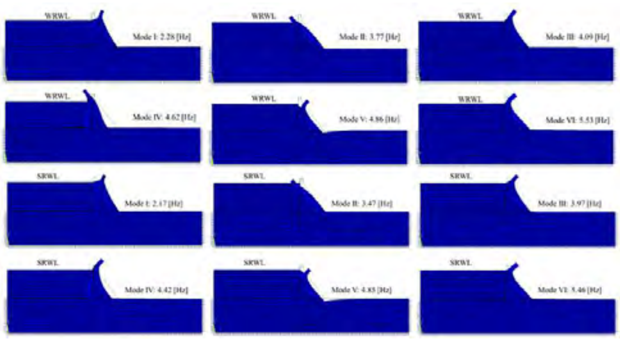

Figure 2: *Natural frequencies and mode shapes; Winter Reservoir Water Level (WRWL); Summer Reservoir Water Level (SRWL)*

Linear analysis

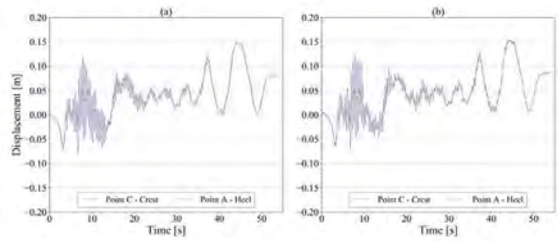

Figure 3: *Computed horizontal displacements at crest and heel of the dam; (a) WRWL; (b) SRWL; Taft Record acceleration*

Nonlinear analysis

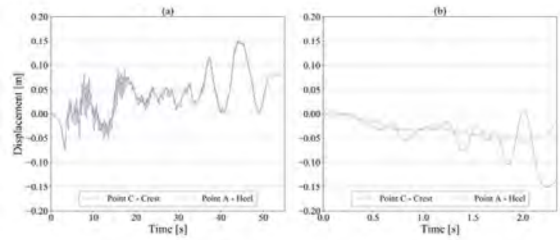

Figure 4: *Computed horizontal displacements at crest and heel of the dam; (a) Taft Record acceleration, no failure; (b) artificially designed ETAF acceleration, failure*

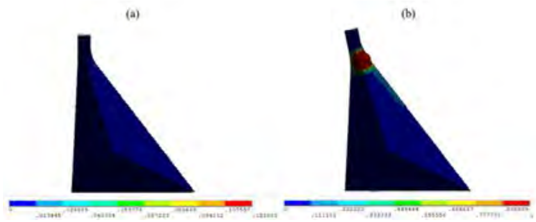

Figure 5: *Computed damage parameter DMG; (a) Taft Record acceleratoin, no local dam failure; (b) artificially designed ETAF acceleration, failure of the dam body*

Conclusions

Results show the ability of the numerical models to: (i) reproduce adequately the dynamic properties of the reservoir-dam-foundation system and (ii) conduct dynamic linear and nonlinear analysis. Results of nonlinear analyses show the ability of the model to represent cyclic loading conditions, with recovery of the stiffness lost during cracking in the transition from tension to compression state, and subsequent failure of the dam body near the crest.

References

[1] Calayir Y., Karaton, M. (2005). A continuum damage concrete model for earthquake analysis of concrete gravity dam-reservoir systems. Soil Dynamics and Earthquake Engineering, Vol. 25(11), pp. 857-869.
[2] Brühwiler E., Wittmann F. (1990). Failure of dam concrete subjected to seismic loading conditions. Engineering Fracture Mechanics, Vol. 35(11/2/3), pp. 565-571.
[3] Zreid I., Kaliske M. (2018). A gradient enhanced plasticity-damage microplane model for concrete. Computational Mechanics, Vol. 62(15).
[4] Bazant Z., Bambarova P. (1984). Crack shear in concrete: crack band microplane model. Journal of Structural Engineering, Vol.10(19), pp.201-2035
[5] Bazant Z., Oh B. (1985). Microplane model for progressive fracture of concrete and rock. Journal of Engineering Mechanics, Vol.11(115), pp.559-582

Task 2.3

Title

Environmental impacts of future operating conditions

Projects (presented on the following pages)

Ecological Impacts of Small-Flexible Hydropower:Macroinvertebrate Resilience to Varying Frequency Hydropeaking
Claire Aksamit, Davide Vanzo, Mauro Carolli, Nathalie Friese, Kate Mathers, Christine Weber, Martin Schmid

Sediment Flushing Downstream Dams a Study on the Clogging by Fine Sediments
Romain Dubuis, Giovanni De Cesare, Christophe Ancey

Optimizing of Coanda screen for Swiss bodies of water
Imad Lifa, Max Witek, Barbara Krummenacher, Seraina Braun

Integrated Sediment Management of Alpine Rivers
Christian Mörtl, Giovanni de Cesare

Hydropower thermal effects on the early life stages of brown trout
Kunio Takatsu, Martin Schmid, Davide Vanzo, Jakob Brodersen

Numerical modelling of river thermal heterogeneity under hydropeaking conditions
Davide Vanzo, Martin Schmid

SCCER SoE
SWISS COMPETENCE CENTER for ENERGY RESEARCH
SUPPLY of ELECTRICITY

SCCER-SoE Annual Conference 2019

Supported by:
Schweizerische Eidgenossenschaft
Confédération suisse
Confederazione Svizzera
Confederaziun svizra
Swiss Confederation
Innosuisse – Swiss Innovation Agency

Ecological Impacts of Small-Flexible Hydropower:

Macroinvertebrate Resilience to Varying Frequency Hydropeaking

Claire Aksamit[1], Davide Vanzo[1], Mauro Carolli[2], Nathalie Friese[1], Kate Mathers[1], Christine Weber[1], and Martin Schmid[1]

1. Eawag: Swiss Federal Institute of Aquatic Science and Technology, Surface Waters – Research and Management 2. IGB: Leibniz-Institute of Freshwater Ecology and Inland Fisheries

Introduction

- Hydropower plants play an important role in providing a stable power network
- Switzerland is phasing out nuclear energy
- Small hydropower plants are expected to aid in compensation of this power loss, including flexible (intermittent) production from run-of-the-river schemes

Motivation

- Understand ecological impacts of a flexible hydropower schedule
  - Producing power in winter months and/or when energy demand is high (i.e., mornings and evenings)
  - Use of settling basin as water storage
  - More frequent fluctuations of water flow (hydropeaking)
  - Run as run-of-the river in summer months
- Abrupt changes from hydropeaking can negatively impact aquatic habitats, organisms, and river ecosystem processes (e.g., Tonolla et al. 2017)

Context

- Impacts of small run-of-the-river schemes on **natural flow regimes** are **poorly understood**
- **Drift** is a key aspect of macroinvertebrate population dynamics in rivers
- **Macroinvertebrate drift is** commonly used for assessing hydropeaking impacts
- Field measurements were performed in an alpine stream at a **small hydropower plant without previous hydropeaking**
- Study is part of the **SmallFLEX** project

Research Question

How does a varying hydropeak frequency affect drifting macroinvertebrates in a small alpine river in winter?

Experiment Site

- Canton of Valais
- Upper Rhône River (1377 m a.s.l)
- Unregulated until 2018

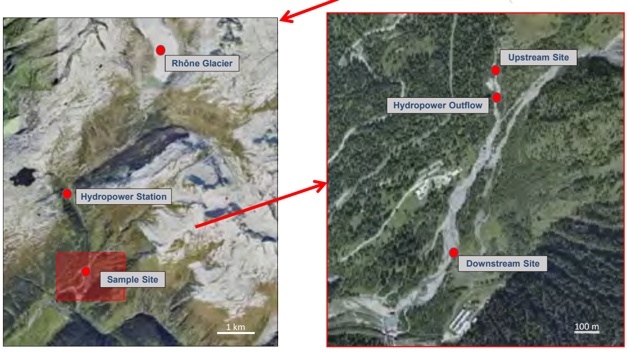

Methods

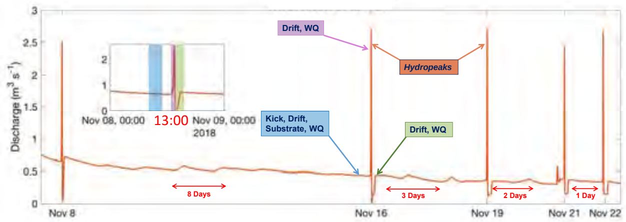

- Five hydropeaks with decreasing recovery intervals in between
- Sampling locations upstream and downstream of the outflow
- Two habitats (riffle and pool) with three drift nets per habitat
- Measured: Invertebrate drift, benthos (kick sample), temperature, water quality (WQ), substrate composition, and velocity

Preliminary Results

Riffle Habitat – Net 3, Density of drifting invertebrates

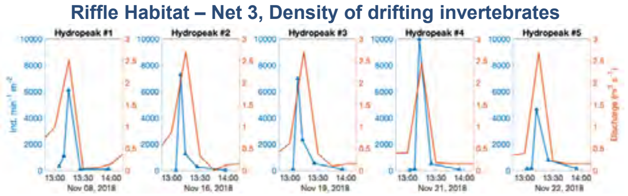

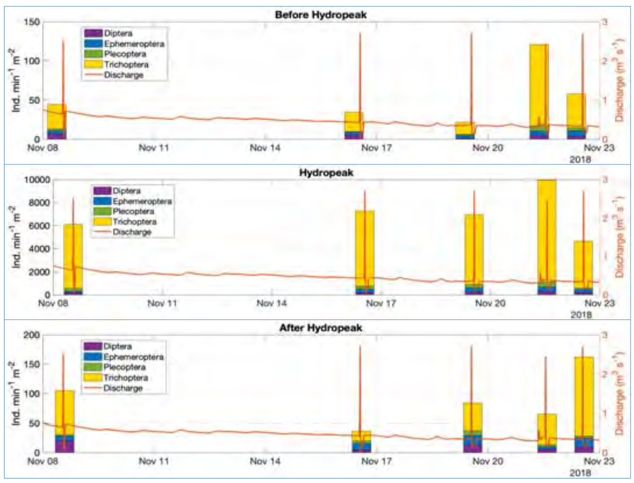

Outlook & Status

Initial Findings: In a realworld setting, **hydropeak frequency, duration,** and **environmental variables** are all important drivers of macroinvertebrates drift.

Other Initial Findings

Composition of drifting communities was different during hydropeaks compared to before and after hydropeaks

To Be Completed

Contrast of riffle and pool habitats

Validate and confirm factors driving different behaviour on Nov 21 and Nov 22

Future Contributions

Help inform hydropower strategies for the Swiss Energy Strategy 2050 that minimize ecological damage while still meeting societal energy demand

References

Tonolla D, Bruder A, Schweizer S. 2017. Evaluation of mitigation measures to reduce hydropeaking impacts on river ecosystems – a case study from the Swiss Alps. Science of The Total Environment **574**: 594-604.
Site Maps: Federal Office of Topography swisstopo: map.geo.admin.ch

Contacts:
Martin Schmid
martin.schmid@eawag.ch

eawag aquatic research

SEDIMENT **FLUSHING** DOWNSTREAM DAMS
A STUDY ON THE **CLOGGING** BY **FINE SEDIMENTS**

A sub-project of : Wasserbau & Ökologie

Funded by :

Romain Dubuis, Dr. Giovanni De Cesare, Prof. Christophe Ancey
E-mail : romain.dubuis@epfl.ch

Plateforme de construction hydraulique, EPFL

Introduction

Water reservoirs used to produce electricity have an impact on the environment and durability by :

- stopping the natural sediment flux
- changing the flow regime downstream of the reservoirs
- storing (fine) sediments that reduce the storage volume

Those 3 issues have been leading to the development of strategies in order to improve the equilibrium of the ecosystem downstream such structures, with solution such as sediment flushing and simple water flushing reproducing flood events.

Those operations produce excessive sediment inflow on certain river sections, which can lead to the clogging of the gravel bed. River construction work, soil erosion, emergency actions and natural river bank erosion can also bring similar problematic.

For example, a dramatic event happened in 2013 on the Spöl River in Eastern Switzerland. Due to some operations on a Punt dal Gall dam, important amounts of fine sediments were flushed downstream the reservoir and resulted in significant damages to the river ecosystem[1]. A strong clogging of the river bed was noted (see fig. 1). A clean water flushing a few months later led to a cleaning of the clogged areas (fig 2.).

Fig. 1 : Clogged bed of the Spöl river after the release of fine sediments, from De Cesare, G et al. 2015 (1)

Fig. 2 : River-bed at the same location as fig. 1 after the clean water flushing, from De Cesare, G et al. 2015 (1)

Clogging and hyporheic layer

The hyporheic layer represent the interface between groundwater and surface flow, and play an important role in the vertical connectivity of rivers. It is also a decisive zone for the life and reproduction of aquatic fauna. Many studies[2] concluded on the impact of clogging by fine sediments on the development of fish spawns and benthos. In order to understand the clogging of rivers, numerous on-field, flume and numerical experiments were undertaken in the last 50 years[3].

However, the influence of factors such as up- and downwelling (exchange with the groundwater) and the self-cleaning process remain hard to quantify and poorly documented. A better understanding of the physical processes and influences of the different parameters is needed in order to assess new solutions to prevent the damaging of river bed ecosystems.

Thesis research goals

Degree of clogging of benthic habitats and fish spawns depending on:
- bed composition
- size and distribution of suspended fine sediments
- flow conditions (surficial and interstitial)

Capacity of the surface flow to reduce the fine sediment suspension under the various conditions

Consequence of clogging on the river-bed and flood plain permeability, considering case studies.

Flume experiments with gravel composition based on river-bed size distributions

Analysis of vertical flux using PIV-RIMS technology and spatial development of clogging

Influence of **upwelling** and **downwelling** on the clogging, induced by the gradient between surface flow and groundwater. Main concern regarding the transport of:
- oxygen
- nutrients
- water temperature
- removal of metabolic wastes

Conditions needed for a **self-cleaning** of clogged fine sediment under different flow conditions - effectiveness of the process (depth of cleaning)

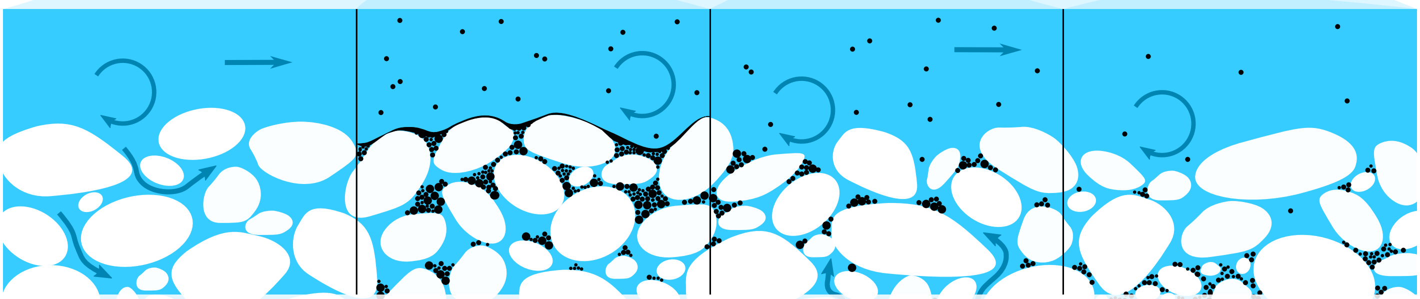

References

1. De Cesare, G., Altenkirch, N., Schleiss, A., Roth, M., Molinari, P., Michel, M., (2015), Störfall vom 30. März 2013 bei der Staumauer Punt dal Gall, «Wasser Energie Luft» – 107. Jahrgang, 2015, Heft 1, CH-5401 Baden.
2. For example : Boulton, A., Findlay, S., Marmonier, P., Stanley, E., Valett, M., (1998) The functional significance of the hyporheic zone in streams and rivers. Annu Rev Ecol Syst 1998, 29:59–81.
3. A good summary of the general state of the research can be found in : Wharton, G., Mohajeri, S. H., & Righetti, M. (2017). The pernicious problem of streambed colmation: A multi-disciplinary reflection on the mechanisms, causes, impacts, and management challenges. Wiley Interdisciplinary Reviews: Water, 4, e1231.

SCCER-SoE Annual Conference 2019

SCCER SoE
SWISS COMPETENCE CENTER for ENERGY RESEARCH
SUPPLY of ELECTRICITY

SCCER-SoE Annual Conference 2019

Supported by:
Schweizerische Eidgenossenschaft
Confédération suisse
Confederazione Svizzera
Confederaziun svizra

Swiss Confederation

Innosuisse – Swiss Innovation Agency

Optimizing of Coanda screen for Swiss bodies of water

Imad Lifa, Max Witek, Barbara Krummenacher, Seraina Braun (HTW Chur, Switzerland)

Motivation

Coanda screens help to clean mountain water for turbines in hydropower plants. There are problems with the abrasion of their sharp-edged profiles, so that the screens often have to be replaced, or have limited swallowing ability. Isolated scientific studies on Coanda screens can be found in the literature. However, comprehensive hydraulic investigations under natural boundary conditions do not exist.

Methods

We constructed a 1:1 scale model at the VAW (Versuchsanstalt für Wasserbau, Hydrologie und Glaziologie, ETH Zurich), where we were able to run different flow rates from 50 l/s – 300 l/s with or without debris.

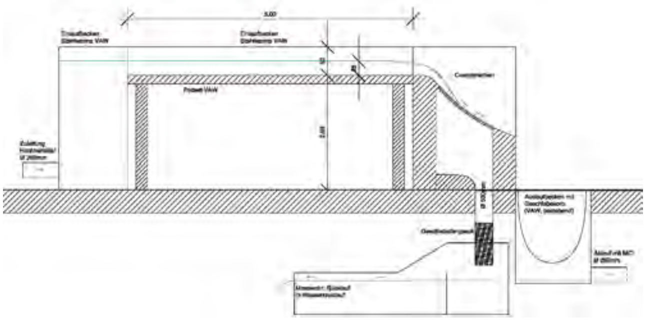

Fig. 1: longitudinal section of the model

We used in total seven screens whereas six screens were constructed by Wild Metal, Italy. They showed a gap width of 0.4 mm, 0.6 mm, 1.0 mm, 1.5 mm, 2.0 mm and 3.0 mm, respectively. The seventh screen was constructed by Höhenergie, Switzerland, and showed a gap width of 1.05mm.
In a first step, we performed clear water tests to analyse the intake capacity of each screen. In a second step, we inserted defined debris at different flow rates, both, broken material and grounded gravel. We then examined the material passing through the screen in weight and granulometry.

Fig. 2: flow rate of 300 l/s over the screen with 0.8 mm gap width

Results

<u>Intake capacity</u>
The intake capacity is high for all the tested screens. Even the maximum of 300 l/s could be swallowed by all the screens. Only the two screens with the widest gaps of 2 mm resp. 3 mm showed 1 – 2 % of overflow. Figure 3 ist showing the gravel sticking in the gaps as seen in every screen tested so far. This leads as well to lower intake capacity over time.

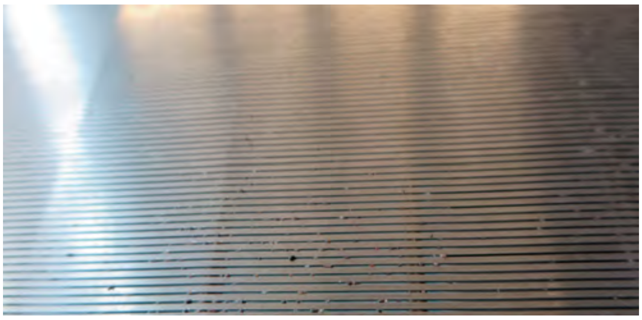

Fig. 3: screen with sticking gravel in the gaps

<u>Rejection rate</u>

Following the manufacturer specifications, 90 % of the debris with a size of at most 50 % of the gap width should be rejected. Our investigations showed, that only a few screens reached this aim. These are shown in the following tables 1a and 1b.

ROUNDED GRAVEL 0 - 8 MM	
gap width	rejection rate
1.5 mm	90 %
2.0 mm	97 %
3.0 mm	98 %

BROKEN MATERIAL 0 – 4 MM	
gap width	rejection rate
2.0 mm	88 %
3.0 mm	93 %

Tab. 1a and 1b: screens following the manufacturer specifications

Discussion

Following the unexpected results, we discuss the shape of the screen in general as well as the different possibilities to form the gaps between the single metal rods.
We also sealed part of the screen with tape to simulate growth of moss or glaciation.
Furthermore, we narrowed the channel above the screen to simulate flow rates above 300 l/s.

Outlook

Hydropower plants are in general competing against natural wildlife, particularly fish downstream migration. We are therefore interested in proofing or denying the fish friendliness of the Coanda screen. Therefore, we are currently working on further investigations to gain more information about the behaviour of fishes. We focus on their probable loss of scales and the mortality rate.

SCCER SoE
SWISS COMPETENCE CENTER for ENERGY RESEARCH
SUPPLY of ELECTRICITY

SCCER-SoE Annual Conference 2019

Supported by:
Schweizerische Eidgenossenschaft
Confédération suisse
Confederazione Svizzera
Confederaziun svizra

Swiss Confederation

Innosuisse – Swiss Innovation Agency

Integrated Sediment Management of Alpine Rivers

Christian Mörtl, Giovanni de Cesare

Ecole Polytechnique Fédérale de Lausanne, Plateforme de Constructions Hydrauliques

Motivation

Sediment management of alpine rivers is crucial to ensure sustainable hydropower production.

Dams inhibit not only biological consistency but also drastically restrain natural sediment dynamics.
Upstream of the dam, coarse material is accumulated, leading to a progressive *sedimentation* of the reservoir. This causes a reduction in the effective water head and can even lead to the blockage of lower-lying operation organs.
Downstream of the dam, reduced flow velocities promote the settling of suspended sediments, causing the *clogging* of open pore spaces in the bed material that naturally serve as fish spawning ground. The lack of coarse sediment also provokes extended *streambank erosion* and the *channeling* of the river, leading to a less altered river morphology and reduced living space for a large biodiversity.

An integrated sediment management helps to optimize ecological, economical and social effects linked to hydropower.

State of Science

Understanding sediment dynamics of alpine rivers and its sequential effects is subject to ongoing interdisciplinary research.

Field studies quantify the effects of *reservoir flushing* combined with *sediment replenishment* on short-term morphologic [1] and ecologic changes [2].
Laboratory experiments provide insights on optimization potential for *replenishment techniques* [3] as well as reference for *sediment transport theories* [4].
Computational Models deliver *predictions of altered sediment dynamics* based on high-level numerical [5], morphodynamical [6] or statistical modelling [7].

Due to the complexity and variability of alpine rivers, research is generally performed based on specific study conditions.

Practical Application in Switzerland

In Switzerland, about 140 hydropower and 360 non-hydropower plants have been identified to require remediation.

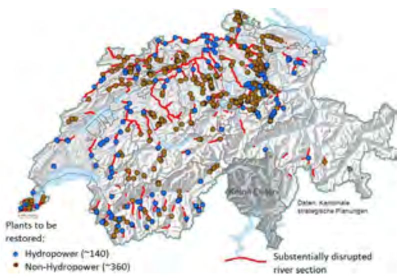

The procedure and responsibilities are regulated by the Swiss Water Protection Law (GSchG).

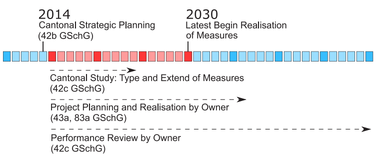

This project is part of a PhD Thesis on the **Eco-Morphological Assessment of Sediment Replenishment** (E.ASSERT).

It is conducted in the framework of the research program **Hydraulic Engineering and Ecology** from a joint initiative of the Swiss Federal Office for the Environment (BAFU) and four research institutions:

- Swiss Federal Institute of Aquatic Science and Technology (Eawag)
- Swiss Federal Institute of Forest, Snow and Landscape (WSL)
- Platform of Hydraulic Constructions (PL-LCH) of the EPFL
- Laboratory of Hydraulics, Hydrology and Glaciology (VAW) of the ETH

The objectives are to outline the state of science and practical applications of **Integrated Sediment Management of Alpine Rivers** in Switzerland and to identify key research questions for future investigation.

The approach is based on comprehensive literature research, contact of officials and the analysis of the latest national statics.

A comprised source of information on integrated sediment management will outline its importance for sustainable hydropower production. It can deliver key aspects for strategic decision making in the framework of the **Energy Strategy 2050.**

Research Gaps

The following research questions are addressed:

- Influence of hydrographs and duration of artificial floods on alternating gravel banks
- Durability of gravel banks with regard to natural flood events
- River morphological structures formed by debris from different water morphologies
- Influence of bedload cover on sole stability in channel widenings
- Characterization of the ecological value of the resulting habitat structures

Artificial Flooding at the Sarine underneath the Rossens Dam [8]

Ongoing Field-Work at the Sarine River

Scheduled Laboratory Work at the EPFL PL-LCH

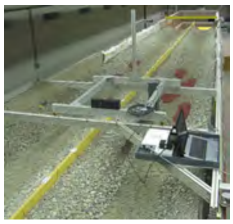

Experimental channel with sediment replenishment in the PL-LCH [3]

References

[1] R. Loire, L. Grosprêtre, J. R. Malavoi, O. Ortiz, and H. Piégay, “What discharge is required to remove silt and sand downstream from a dam? An adaptive approach on the selves River, France,” Water (Switzerland), vol. 11, no. 2, 2019.
[2] S. Stähly, M. J. Franca, C. T. Robinson, and A. J. Schleiss, “Sediment replenishment combined with an artificial flood improves river habitats downstream of a dam,” Sci. Rep., vol. 9, no. 1, pp. 1–7, 2019.
[3] E. Battisacco, M. J. Franca, and A. J. Schleiss, “Sediment replenishment: Influence of the geometrical configuration on the morphological evolution of channel-bed,” Water Resour. Res., vol. 52, no. 11, pp. 8879–8894, 2016.
[4] C. Juez, I. Bühlmann, G. Maechler, A. J. Schleiss, and M. J. Franca, “Transport of suspended sediments under the influence of bank macro-roughness,” Earth Surf. Process. Landforms, vol. 43, no. 1, pp. 271–284, 2018.
[5] C. Escauriaza, C. Paola, and V. R. Voller, “Computational models of flow, sediment transport and morphodynamics in rivers,” in Gravel-Bed Rivers: Process and Disasters, 2017, pp. 1–31.
[6] L. Vonwiller, D. F. Vetsch, and R. M. Boes, “Modeling streambank and artificial gravel deposit erosion for sediment replenishment,” Water (Switzerland), vol. 10, no. 4, pp. 1–23, 2018.
[7] F. Neugirg et al., “Using terrestrial LiDAR data to analyse morphodynamics on steep unvegetated slopes driven by different geomorphic processes,” Catena, vol. 142, pp. 269–280, 2016.
[8] M. Döring et al., “Künstliches Hochwasser an der Saane – Eine Massnahme zum nachhaltigen Auenmanagement,” Wasser Energ. Luft, vol. 2, pp. 119–127, 2018.

SCCER SoE
SWISS COMPETENCE CENTER for ENERGY RESEARCH
SUPPLY of ELECTRICITY

SCCER-SoE Annual Conference 2019

Supported by:
Schweizerische Eidgenossenschaft
Confédération suisse
Confederazione Svizzera
Confederaziun svizra
Swiss Confederation
Innosuisse – Swiss Innovation Agency

Hydropower thermal effects on the early life stages of brown trout

Kunio Takatsu[1†], Martin Schmid[2], Davide Vanzo[2], Jakob Brodersen[1]

[1] Eawag, Swiss Federal Institute of Aquatic Science and Technology, Department of Fish Ecology and Evolution, Kastanienbaum, Switzerland,
[2] Eawag, Swiss Federal Institute of Aquatic Science and Technology, Surface Waters - Research and Management, Kastanienbaum, Switzerland
† Contacts: Kunio Takatsu (kunio.takatsu@eawag.ch)

1. Research background

Hydropower induced temperature change

In general, hydropower plants cause water temperatures to decrease during summer and increase during winter.

Wüest (2010) *Downstream Relevance of Reservoir Management. In: Bundi (eds) Alpine water*

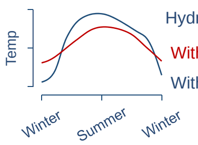

Riverine organism; ectotherms

e.g., Fish, aquatic invertebrate…

Riverine ecosystem is probably sensitive to the hydropower thermal alterations

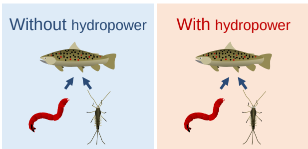

2. Motivation

Energy strategy 2050 of Swiss government: Increase hydropower production

Our knowledge of how hydropower plants may thermally affect river communities is still limited

3. Objective

Study organism: **brown trout**…

- ecologically and commercially important species

To examine how hydropower thermal alterations affect the early life stages of brown trout

Early life stages

- Most vulnerable life stage
- Play a key role in shaping population dynamics

Einum et al. (2000) *Evolution*
Skoglund et al. (2012) *Funct Ecol*

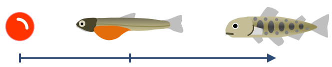

- Hydropower increases temperature during early life stages

Winter → **Spring**

4. Methods

- **Egg collection**

We collected eggs from 14 sites from 5 drainages (altitude 343 – 2073 m)

Each local population might be adapted to each local environment

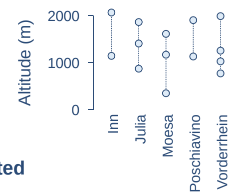

canton Graubünden

- **Laboratory experiment**

Eggs were divided between two temperature treatments and many traits were measured throughout the early life stage

Without hydropower
Cold (3 ºC)

With hydropower
Warm (6 ºC)

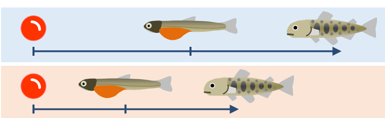

5. Results

Statistical analysis 1

To examine how early life history traits are affected by
1. rearing temperature (thermal effects in ecological time scale)
2. altitudinal origin (thermal effects in evolutionary time scale)
3. drainage

Linear mixed model

Traits = Altitude + Treatment + Drainage
"Altitude x Treatment" + "Altitude x Drainage"
"Treatment x Drainage" + "Altitude x Treatment x Drainage"
+ Random effects (Family, Incubator)

Trait	A	T	D	A*T	A*D	T*D	A*T*D
Hatch timing		-	*			*	*
Metabolic rate	+	+					
Size at hatching	-	-				*	
Yolk sac volume	-				*		
Yolk absorption timing	-	-			*		
Size at yolk absorption	-				*		

- **Increase in rearing temperature enhanced embryonic development** (probably due to increased metabolic rates)
- **Trout from high altitude (i.e., cold environment) developed faster than that from low altitude (i.e., warm environment)**
(faster development might be achieved by higher metabolic rate)
- **Embryonic traits differed among drainage**

Ecological and evolutionary effects of hydropower thermal alterations could differ in direction

Statistical analysis 2

- Egg size reduced with altitude
- Egg size is a well known factor affecting early life history traits

Hutchings. (1991) *Evolution*;
Einum et al. (1999) *Proc R Soc B*

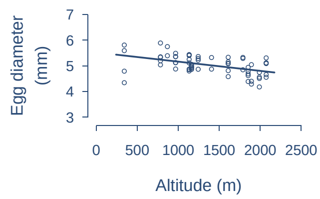

We considered egg size as explanatory variable

- Significant effects of egg size were found in almost all traits
- Except yolk sac volume, effects of altitude were no longer significant

The observed altitude effects on life history traits can be explained by the altitude-dependent egg size

6. Future research

Develop mathematical models to predict how hydropower thermal alterations affect each local population

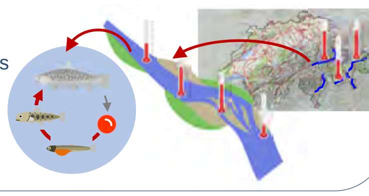

SCCER SoE

SWISS COMPETENCE CENTER for ENERGY RESEARCH
SUPPLY of ELECTRICITY

SCCER-SoE Annual Conference 2019

Supported by:

Schweizerische Eidgenossenschaft
Confédération suisse
Confederazione Svizzera
Confederaziun svizra

Swiss Confederation

Innosuisse – Swiss Innovation Agency

Numerical modelling of river thermal heterogeneity under hydropeaking conditions

Davide Vanzo[1] and Martin Schmid[1]

1. Eawag, Swiss Federal Institute of Aquatic Science and Technology, Surface Waters - Research and Management, Kastanienbaum, Switzerland

Introduction

- River water temperature is a fundamental physical property of flowing waters.
- **Alterations** of the natural thermal regime can adversely affect the river biota (e.g. Caissie 2006).
- Artificial **reservoirs** and **hydropower plants** cause thermal alterations on a broad spectrum of temporal and spatial scales (e.g. Vanzo *et al.* 2016a).
- The **modelling** and **quantification** of local thermal heterogeneity alterations is still a challenge (Carrivick *et al.* 2012).

Motivation

- Further **exploitation** of hydropower (HPP) sector (Swiss Energy Strategy 2050).
- Need for scenario-based **predicting tools** of future climate-change and anthropogenic effects on river hydro- thermodynamics.

Research questions

- How is river **thermal heterogeneity** affected by hydropower production?
- Does **river morphology** play a relevant role in the thermal dynamics of hydropeaking rivers?
- Which are the **dominant heat fluxes** at different seasons under **hydropeaking** conditions?

Fig. 1 – Average water depth per hour of the day recorded at the beginning of the study reach (Moe_10_w). Hydropeaking events are concentrated in the morning (7 to 11) and in the late afternoon (16-20) .

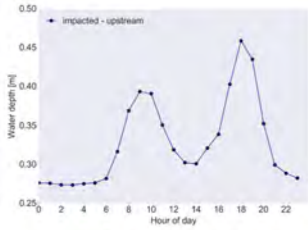

Challenges

A tool to simulate river thermal heterogeneity under hydropeaking conditions requires several features:

- **two dimensional, unstructured** grid: to properly describe morphological feature in shallow rivers, as for Alpine and headwater streams;
- **shock-capturing** methods (e.g. Toro 2001): to ensure the proper simulation of hydro-thermal waves that propagate in the investigated reach;
- robust **wet-and-dry** and **advection-diffusion** strategy (Vanzo *et al.* 2016b): to simulate the wetting and drying and dispersion processes during hydropeaking rising and falling limbs;
- computational **efficiency** and **parallelization** strategies: to allow high-resolution thermodynamic simulations on standard workstations.

Modelling workflow

Hydrological INPUTS

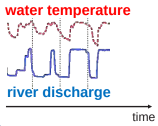

Meteorological INPUTS

Novel 2D Numerical MODEL

Temperature module in BASEMENT

- coupled solution of hydrodynamic and thermodynamic variables
- GPU-accelerated computation
- currently in testing phase

Complementary DATA

Measurement campaign of **river water temperature:**

- 13 sensors in total
- 5 min sampling rate
- Dec 2018 – Nov 2019

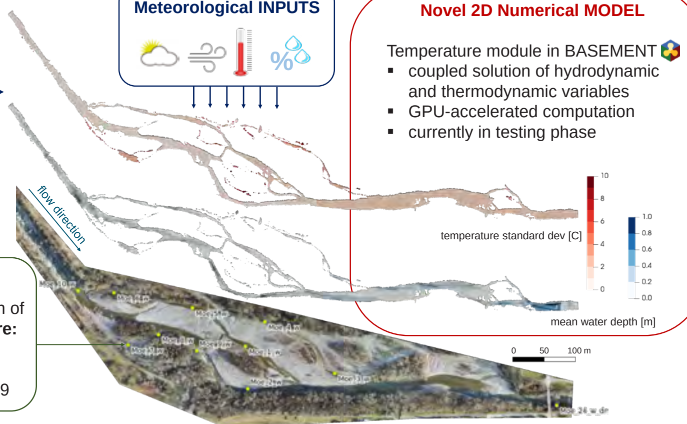

Fig. 2 – Study site in Moesa River with location of the thermal sensors.

Study case

Moesa River at Lostallo, Graubünden (CH) (Fig. 2)

- **Sharp hydraulic alterations** at sub-daily scale due to HP production (Fig. 1).
- Winter records (Dec-Jan-Feb) show differences of about 3 °C compare to unaltered water temperature, with a variability of about 0.5 °C within the floodplain (Fig. 3).
- **Magnitude** of sub-daily thermal variation (TP1, Fig. 4) lies outside the range of natural variability.

Outlook

- The full measurement campaign will allow the comparison of thermal dynamics among different seasons.
- Remote-sensing (UAV) surveys will be used to further test and calibrate the numerical model.
- Preliminary tests suggest the model is robust and can well reproduce hydro-thermopeaking events.
- After the testing phase, scenario-based simulations will be conducted.

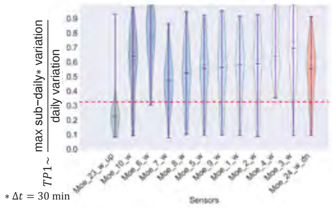

Fig. 4 – Magnitude of sub-daily* thermal alterations (TP1, Vanzo *et al.* 2016a); the red dashed line is the threshold between natural (below) and altered (above) thermal fluctuation. First and last violin represent the most upstream (before HP release) and most downstream sensor, respectively (see Fig. 2).

Fig. 3 – Winter (Dec-Jan-Feb) water temperature: first and last violin represent the most upstream (before HP release) and most downstream sensor, respectively (see Fig. 2).

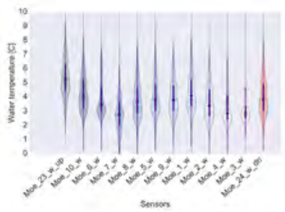

References

BASEMENT – Basic Simulation Environment for Computation of Environmental Flow and Natural Hazard Simulation. Version 3pre. © ETH Zurich, VAW, 2006-2019. http://www.basement.ethz.ch.
Caissie, D. (2006) 'The thermal regime of rivers: A review', Freshwater Biology, 51(8).
Carrivick, J. *et al.* (2012). 'Numerical Modelling of Spatio-Temporal Thermal Heterogeneity in a Complex River System.' Journal of Hydrology 414–415.
Swiss Energy Strategy 2050. https://www.uvek.admin.ch/uvek/en/home/energy/energy-strategy-2050.html
Toro, E. F. (2001). 'Shock-capturing methods for free-surface shallow flows'. John Wiley.
Vanzo, D. *et al.* (2016a) 'Characterization of sub-daily thermal regime in alpine rivers: Quantification of alterations induced by hydropeaking', Hydrological Processes, 30(7).
Vanzo, D. *et al.* (2016b). 'Pollutant Transport by Shallow Water Equations on Unstructured Meshes: Hyperbolization of the Model and Numerical Solution via a Novel Flux Splitting Scheme.' JCP 321.

Contacts:
Dr. Davide Vanzo
davide.vanzo@eawag.ch

Task 2.4

Title

Integrated simulation of systems operation

Projects (presented on the following pages)

No posters

Work Package 3: Innovation Agenda

The objective of WP3 is to provide innovations both on the technical and the computational sides for hydropower and geoenergies to reach the energy strategy 2050 targets.

Technical Highlights 2019

Refurbishment of large hydropower plants

RENOVHydro is a multidisciplinary research project targeting the development of a methodology – and its implementation into EPFL SIMSEN software – to assist the decision making for hydropower projects and refurbishments by automating the investigation of civil and electro-mechanical engineering scenarios and their performance in terms of energy generation, installed capacity and ancillary services to the grid. Numerous scenarios for the hydraulic structures, hydraulic machinery and electrical equipment have been evaluated by an automated engine. The provided scenario explorer highlights the synergies between the different fields of engineering involved. This high level of support for the decision-making process of the stakeholders will drastically reduce the risks of selecting a suboptimal solution.

Small hydropower plants

The aim of the SMALLFlex project is to demonstrate the capacity of small hydropower to provide clean, sustainable and renewable energy while delivering ancillary service. A first campaign to investigate the flexibility of this run-off-river power plant was carried out in Fall 2018 with success lasting three weeks. Several production peaks have been generated from 15 min to two hours and from 1.5 MW to 6.5 MW with different recovery intervals. The two first weeks were dedicated to the hydropeaking events monitoring in the alluvial area whilst during the last week, daily programs of production to follow the energy demand and thus the spot price have been provided. An increase of the electricity produced by up to 40% has been observed by operating the power plant with production peak at high power with a higher efficiency.

Development of new turbines for existing infrastructure

A first 5 kW product (DuoTurbo) of a new axial turbine for drinking water networks has been successfully tested and commissioned on a pilot site in May 2019, to assess the long-term behaviour of the system. The monitoring of the first 16 weeks of operation shows a satisfying behaviour in terms of stability, operating regulation, efficiency and vibration. No significant drifts of the efficiency or vibration levels have been observed. Before the end of 2019, a second pilot site will be equipped. Further investigations are ongoing in urban drinking water distribution networks.

Improvements in borehole drilling

Regarding geoenergies, the work on borehole stability conducted at UNINE in collaboration with Geo-energieSuisse is now close to completion and includes a systematic parameter estimation approach in order to produce robust optimal drilling directions. In order to circumvent the lack of data to calibrated our failure prediction model, we investigate systematically the parameter space in order to find potential but not unique set of adequate parameters and then use them to make predictions and assess the uncertainty on the predictions. We will now speed up this process as the decision has to be taken rapidly in order to minimize cost associated with rig downtime and test our approach on synthetic and real case study.

Computational Highlights 2019

New Coupling Tools for Multi-Physics Simulation

The simulation of turbines and fracture networks has one thing in common: fluid-structure interaction. In fact, different physical models for the fluid flow and for the elastic behavior of the structure have to be coupled. Within “Computational Energy Innovation”, we have developed a new coupling library, which is based entirely on modern variational transfer approaches. Moreover, we have extended this modern transfer

approaches to multi-dimensional models. For example, fracture networks can now be modeled as 2D-manifolds in a 3D-volume or as full 3D-fractures in a 3D volume. Our library MoonoLith implements this functionality in a robust and efficient way. MoonoLith is designed for parallel computations on modern supercomputers, e.g. the machines at the Swiss supercomputing center CSCS.
Using MoonoLith, we have realized simulations of fluid flow in fracture networks as well as fluid flow in turbines. The library is available for download and is used in several energy related projects in SCCER and in the PASC (Platform for Advanced Scientific Computing) initiative.

New Modeling Approaches for Fracture Networks

To predict how fracture networks grow when a reservoir is stimulated is a highly challenging task: complex and non-linear processes govern the growth if fractures, and the numerical simulation of fracture growth has been at the forefront of computational mechanics for decades. In “Computational Energy Innovation”, we have developed a new multi-scale solution method, which allows to use so called phase filed models highly efficiently for simulating fracture growth. Our new method is based on techniques from optimization and from multigrid techniques. Using our method, simulation times can be reduced drastically, and fracture evolutions can be computed not only faster than before, but also on massively parallel machines. We hve implemented our new method in our simulation library Utopia, which is being developed together with the Swiss Supercomputing Center CSCS for the work in SCCER SoE.

Task 3.1

Title

Innovative technologies

Projects (presented on the following pages)

DuoTurbo : Pilot Plant Commissioning and Monitoring
D. Biner, V. Hasmatuchi, C. Münch-Allligné

Prediction of unstable full load conditions in a Francis turbine prototype
J. Gomes Pereira Jr., E. Vagnoni, A. Favrel, C. Landry, S. Alligné, C. Nicolet, F. Avellan

RENOVHydro: Methodology to determine the parameters of the hydraulic turbine governor for primary control
Christian Landry, Christophe Nicolet, João Gomes Pereira Junior, François Avellan

Numerical modelling of fish guidance structures
Claudia Leuch

SCCER SoE
SWISS COMPETENCE CENTER for ENERGY RESEARCH
SUPPLY of ELECTRICITY

SCCER-SoE Annual Conference 2019

Hes·so VALAIS WALLIS School of Engineering

Supported by:
Schweizerische Eidgenossenschaft
Confédération suisse
Confederazione Svizzera
Confederaziun svizra
Swiss Confederation
Innosuisse – Swiss Innovation Agency

DuoTurbo : Pilot Plant Commissioning and Monitoring

D. Biner [1], V. Hasmatuchi [1], C. Münch-Allignè [1]

[1]HES-SO Valais//Wallis, School of Engineering, Hydroelectricity Group, Sion, cecile.muench@hevs.ch

Context

- Recovering hydraulic energy lost in **drinking water networks**
- Modular in-line "plug and play" turbine from **5 to 25 kW**
- No environmental impact
- Low investment costs

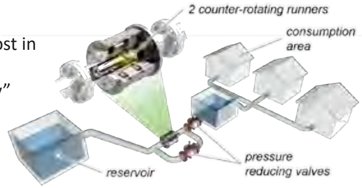

Project

DUO TURBO

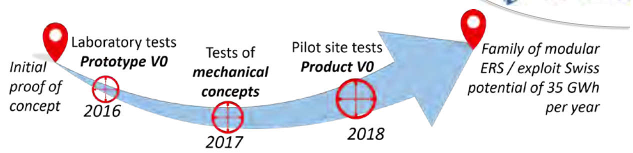

Pilot plant installation

The first DuoTurbo product has been installed in the drinking water supply network of Savièse, VS. Various hydraulic, mechanical and electrical parameters are monitored to study the long term behaviour of the DuoTurbo pilot plant. The installation was commissioned on 15th May 2019.

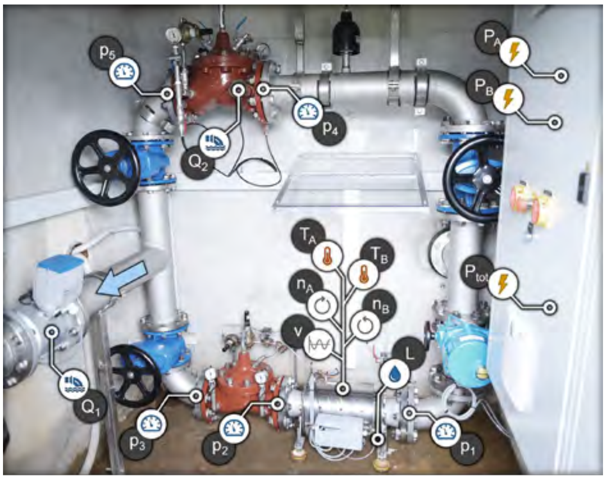

Automation flow chart

The realized micro-hydropower installation operates completely autonomously. The operator's intervention is required only in case of errors, failure and maintenance.

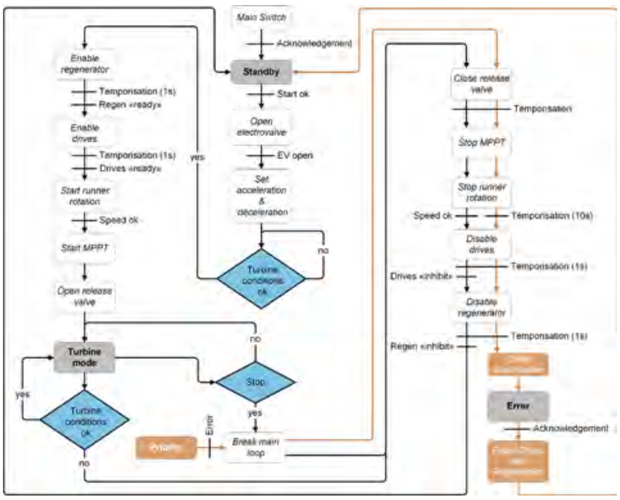

Monitoring results

The monitoring of the first 12 weeks of operation (15th May to 7th August 2019) shows a satisfying behaviour in terms of stability, operating regulation, efficiency and vibration. No significant drifts of the efficiency or vibration levels have been observed at this state.

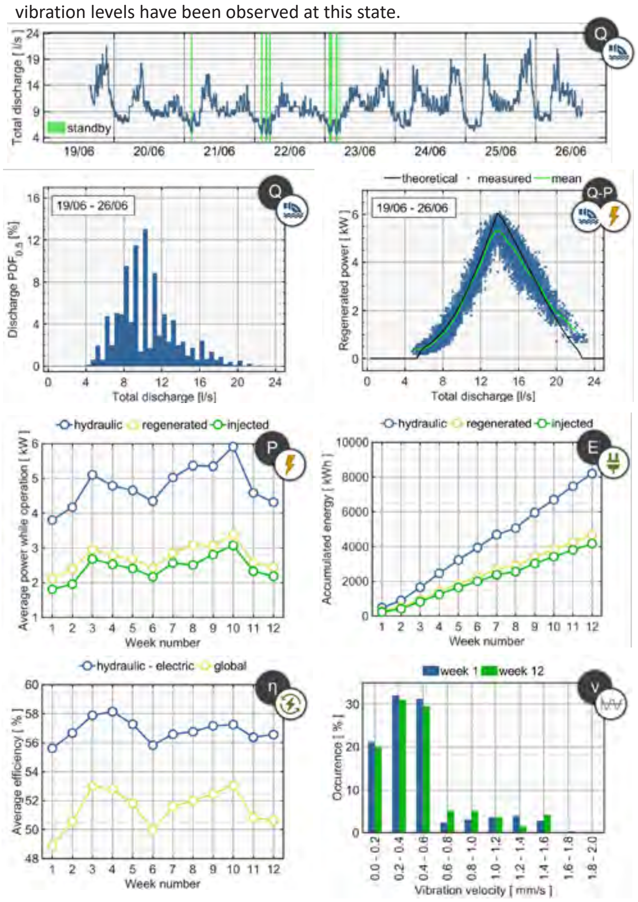

Conclusion

The DuoTurbo pilot plant has successfully been installed and commissioned in May 2019. The turbine has recovered about 4.2 MWh of electrical energy during its first 12 weeks of operation. Furthermore, a very satisfying behavior in terms of system stability could be observed. Long term tests are ongoing for the final proof of the product's capability.

References

Biner, D., Andolfatto L., Hasmatuchi, V., Rapillard, L., Chevailler, S., Avellan, F. and Münch-Alligné, C., **"DuoTurbo: A New Counter-Rotating Microturbine for Drinking Water Facilities"**, Proceedings, International Conference on Innovative Applied Energy (IAPE'19), Oxford City, United Kingdom, March 14-15, 2019

Development team of Duo Turbo (CTI Nr. 17197.1 PFEN-IW)

HES-SO Valais//Wallis:
D. Biner, S. Luisier, S. Martignoni, D. Violante , V. Hasmatuchi, S. Richard, C. Cachelin, L. Rapillard, S. Chevailler, C. Münch-Allignè

EPFL LMH:
L. Andolfatto, V. Berruex, F. Avellan

Industrial partners:
Telsa SA, Jacquier-Luisier SA, Valelectric Farner SA

Hes·so VALAIS WALLIS – Haute Ecole d'Ingénierie – Hochschule für Ingenieurwissenschaften
LMH Laboratory for Hydraulic Machines – EPFL
VALELECTRIC FARNER SA
TELSA ELECTROTECHNIQUE
Jacquier & Luisier SA Atelier mecanique

SCCER SoE
SWISS COMPETENCE CENTER for ENERGY RESEARCH
SUPPLY of ELECTRICITY

SCCER-SoE Annual Conference 2019

Supported by:
Schweizerische Eidgenossenschaft
Confédération suisse
Confederazione Svizzera
Confederaziun svizra
Swiss Confederation
Innosuisse – Swiss Innovation Agency

Prediction of unstable full load conditions in a Francis turbine prototype

J. Gomes Pereira Jr., E. Vagnoni, A. Favrel, C. Landry, S. Alligné, C. Nicolet, F. Avellan

Introduction

Francis turbines operating in full load conditions feature an axisymmetric vortex rotating in the opposite direction of the turbine runner. This vortex rope may enter in an unstable self-exciting process, leading to large pressure pulsations and oscillations in the generating unit power output. In this research work, prototype on-site and reduced scale model test results are presented where the turbine changes from a stable to an unstable full load condition due to an increase in discharge. Measurements are compared in the frequency and time domain, where similarities are evidenced between model and prototype. Using the measurements on the reduced scale model and 1-D numerical models of both the reduced scale model and the turbine prototype, eigenvalue calculations are performed to predict the discharge value of transition from stable to unstable conditions. The transition point on the prototype is then predicted with a small deviation. Transient simulations in the time domain are performed replicating the self-exciting behavior of the unstable full load condition

Predicting unstable full load conditions on the prototype

Hill chart with measurements results:

Reduced scale model measurements: *defining the stability limits*

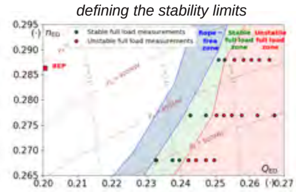

Comparing the reduced scale model and the *prototype measurements*

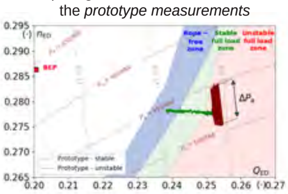

Eigenvalue calculations:

- *Pipes bulk viscosity [1]* $R_{\mu'} = \dfrac{\mu'}{\rho g A dx}$
- *Cavitation vortex bulk viscosity [2]* $R_{\mu''} = \dfrac{\mu''}{\rho g A dx}$
- *Mass flow gain factor (quantified by a new method)* $\chi = -\dfrac{\partial V_{Cav}}{\partial Q_1}$
- *Cavitation compliance [3]* $C_c = -\dfrac{\partial V_{Cav}}{\partial h}$

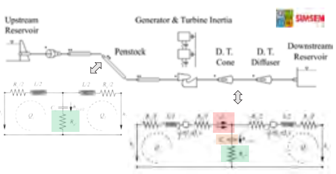

Stable and unstable conditions on the *reduced scale model*, predicted by eigenvalue calculations

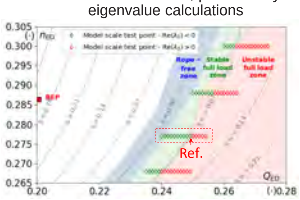

Stable and unstable conditions on the *turbine prototype*, predicted by eigenvalue calculations

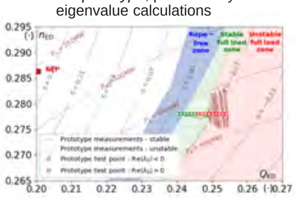

Transient simulation in time domain

Hydroacoustic parameters are *updated at each simulation time step*

$$a_{Cone(t)} = \left[\frac{\Pi}{\rho}\cdot\left(\bar{p}_{Cone} + \Delta p_{(t)} - p_{Vap}\right)\right]^{0.5}$$

$$\mu''_{(t)} = M''\cdot\frac{\bar{p}_{Cone} + \Delta p_{(t)} - p_{Vap}}{f_0}$$

Self-excited behaviour of unstable full load conditions *are simulated*

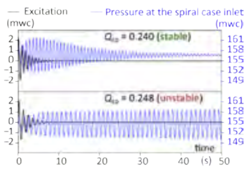

Reduced scale model measurements

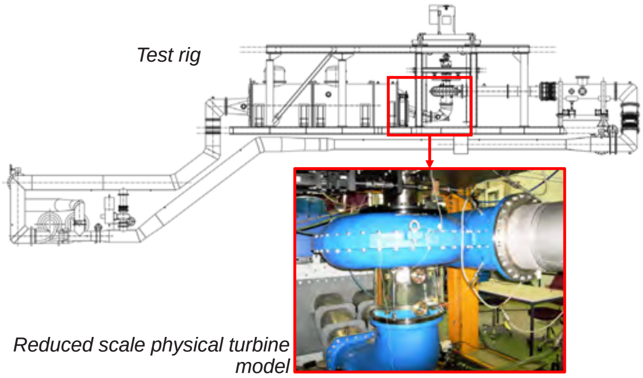

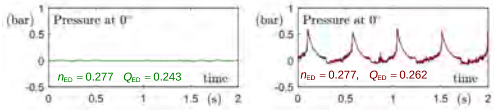

IEC speed & discharge factors
$n_{ED} = nD/\sqrt{E}$
$Q_{ED} = Q/D^2\sqrt{E}$

Hydropower plant featuring the full-scale Francis turbine prototype

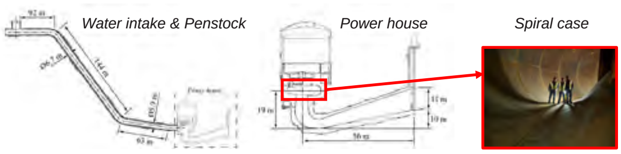

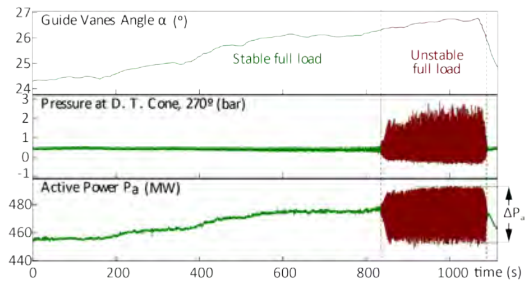

Conclusions and future works

The occurrence of unstable full load operating conditions on the prototype was predicted by reduced scale model measurements and eigenvalue calculations on this specific test case. Further measurements for different test cases are expected to further validate the new methodology.

References

[1] P. K. Dörfler, Pressure wave propagation and damping in a long penstock, in: 4th International Meeting on Cavitation and Dynamic Problems in Hydraulic and Systems, Serbia, 2011 (2011).
[2] C. Landry, A. Favrel, A. Müller, C. Nicolet, F. Avellan, Local wave speed and bulk flow viscosity in Francis turbines at part load operation, Journal of Hydraulic Research 54 (2) (2016) 185–196 (2016). doi:10.1080/00221686.2015.1131204.
[3] C. Brennen, A. Acosta, Theoretical, quasi-static analysis of cavitation compliance in turbopumps., Journal of Spacecraft and Rockets 10 (3) (1973) 175–180 (1973). doi:https://doi.org/10.2514/3.27748.

HYPERBOLE ERC/FP7-ENERGY-2013-1-Grant 608532
HYdropower plants PERformance and flexiBle Operation towards Lean integration of new renewable Energies
LMH Laboratory for Hydraulic Machines
EPFL ECOLE POLYTECHNIQUE FEDERALE DE LAUSANNE

SCCER SoE
SWISS COMPETENCE CENTER for ENERGY RESEARCH
SUPPLY of ELECTRICITY

SCCER-SoE Annual Conference 2019

RENOVHydro

Supported by:
Schweizerische Eidgenossenschaft
Confédération suisse
Confederazione Svizzera
Confederaziun svizra
Swiss Confederation
Innosuisse – Swiss Innovation Agency

RENOVHydro: Methodology to determine the parameters of the hydraulic turbine governor for primary control

Christian Landry, Christophe Nicolet, João Gomes Pereira Junior, François Avellan

Motivation

The RENOVHydro project is dedicated to the **renovation** of an existing hydroelectric power plant with a systematic assessment of a **high number of civil and electromechanical potential modifications**. In order to automatically assess the primary control potential of the renovated hydroelectric power plant, it is necessary to have a **simple** and **robust** methodology to deduce the **parameters of a PID controller**.

1. Application to 40 different Francis turbine

- 40 Francis turbines are selected with head from 30 to 500 mWC.
- Mechanical power is fixed arbitrary to 50MW or 300MW.
- The Francis turbine is connected to electrical grid (f_{grid} = 50 Hz)
- The layout of the generic hydraulic power plant are defined by the following rules.

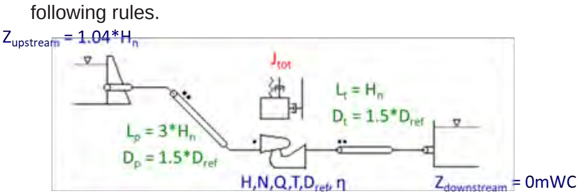

Fig. Dimensioning rules defining the layout of the hydraulic power plant

Dimensioning:

- The dimensioning of the turbine (spiral casing, runner and draft tube) are derived from statistical laws.
- A realistic performance hill chart are obtained with the new SIMSEN library.

$$\begin{cases} T_m = \dfrac{J_{tot}\omega^2}{P} = [5.5-9.6] \\ T_w = \dfrac{Q}{H}\sum\dfrac{L}{gA} = [0.9-2.6] \\ Hadley = \dfrac{T_m}{T_w} = [2.35-9.36] \end{cases}$$

2. Block diagram of the PID controller

The control system is a PID turbine governor with both speed and power control loops combined with the permanent droop Bs.

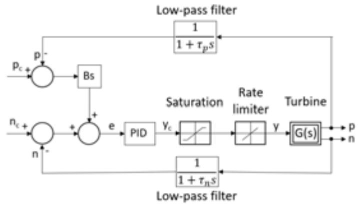

Fig. SIMSEN model of the control system

The PID controller is in series, where K is the proportional gain, *Ti* is the integral time constant and *Td* is the derivative time constant.

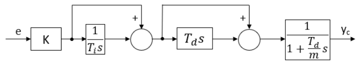

Fig. Block diagram of the PID controller in SIMSEN software

3. Primary control capability defined by Swissgrid

For each Francis turbine, the test defined by Swissgrid for primary control capability is based on a frequency linear variation of 200 mHz in 10 seconds. The output power variation must be delivered within 30 s and remain between minimum and maximum threshold. The permanent droop Bs is fixed to 4%, leading to ΔP/Pn = 10%.

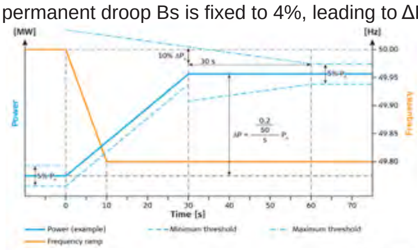

$$Bs = \frac{\dfrac{\Delta f}{f_n}}{\dfrac{\Delta P}{P_n}} = 4\%$$

Fig. Test for primary control capability defined by Swissgrid (2011)

4. Methods to define the PID controller parameters

A. Ziegler-Nichols Method

Limit of stability → Kc and Tc → Parameters for PID controller

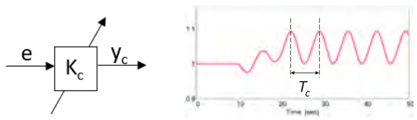

$$\begin{cases} K = 0.3\cdot K_c \\ T_i = 0.5\cdot T_c \\ T_d = 0.114\cdot T_c \end{cases}$$

B. Time constant Method

Tm and Tw → Parameters of PID controller in parallel → Parallel to series

$$\begin{cases} T_m = \dfrac{J_{tot}\omega^2}{P} \\ T_w = \dfrac{Q}{H}\sum\dfrac{L}{gA} \end{cases}$$

$$\begin{cases} K_p = 0.0193\cdot\dfrac{T_m^3}{T_w} + 3.8126 \\ K_I = 0.4362\cdot\dfrac{T_m}{T_w} + 0.3983 \\ K_d = 1.6356\cdot T_m - 6.6442 \end{cases}$$

$$\begin{cases} K = \dfrac{K_p + \sqrt{K_p^2 - 4K_iK_d}}{2} \\ T_i = \dfrac{K}{K_i} \\ T_d = \dfrac{K_d}{K} \end{cases}$$

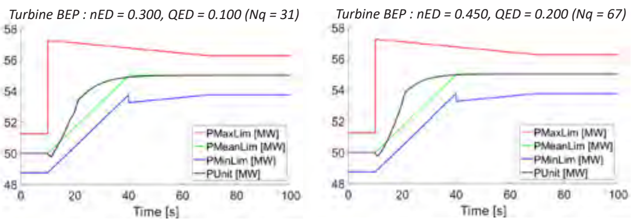

Fig. Time response to the frequency variation of 200 mHz (Pm = 50MW)

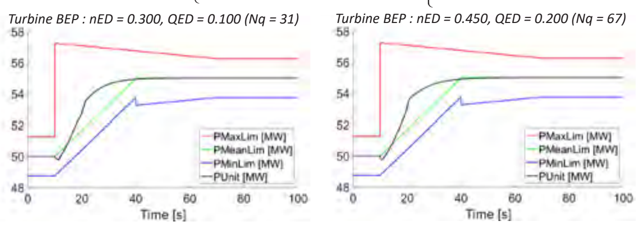

Fig. Time response to the frequency variation of 200 mHz (Pm = 50MW)

5. Conclusion

- The Ziegler-Nichols method is robust and can be applied regardless of the mechanical power of the Francis turbine.
- The time constant method is based on the geometric quantities of the layout and avoids a search for the limit of stability. A correction constant must be applied depending on the power of the hydraulic turbine ($K_{300MW} = 0.6*K_{50MW}$)

Acknowledgments

The RENOVHydro project is granted by CTI, Commission for Technology and Innovation (Grant funding 19343.1 PFEN-IW) and by SFOE, Swiss Federal Office of Energy (Grant funding SI/501436-01).

EPFL · LMH Laboratory for Hydraulic Machines · HES-SO · Power Vision Engineering · groupe E · FMV

SCCER SoE
SWISS COMPETENCE CENTER for ENERGY RESEARCH
SUPPLY of ELECTRICITY

SCCER-SoE Annual Conference 2019

Supported by:
Schweizerische Eidgenossenschaft
Confédération suisse
Confederazione Svizzera
Confederaziun svizra
Swiss Confederation
Innosuisse – Swiss Innovation Agency

Numerical modelling of fish guidance structures

Claudia Leuch, VAW, ETH Zürich

Introduction

Fish guidance structures (FGS) are implemented at hydropower plants to reduce fish mortality during downstream migration. Their design is crucial for their guidance efficiency and the losses caused to the power production. The objective of this thesis was to set up and test a numerical model. The model was then used to analyse FGS configurations.

Background

Fish Guidance Structures

Vertical FGS consist of a bar rack implemented at an angle to the flow. The bars create hydraulic cues, which trigger an evasive behavior of the fish. Traditionally, rectangular, angled bars are used. However, they cause high hydraulic losses and an asymmetric admission flow to the turbines. Curved bars are currently tested at VAW, ETH, as an alternative design to mitigate these issues. Two additional bar shapes were also analyzed numerically (Fig. 1).

Fig. 1: Analyzed bar shapes: angled bar, curved bar, slim bar and fish bar

Numerical modelling

Numerical simulations can be used as an alternative to expensive and laborious physical experiments. Turbulent flow is often modelled using Reynolds averaging on the flow equations to reduce computational costs. As this leads to an under-determined set of equations, a turbulence model is needed as a closure relation (Fig 2). Several different models exist, and it is difficult to know a priori which one is suitable for a given problem.

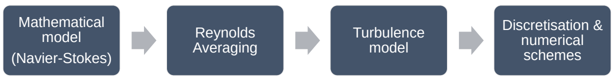

Fig. 2: Schematic approach of the numercial modelling of turbulent flow

Turbulence model evaluation

Five common turbulence models (*standard k-ε*, *realizable k-ε*, *RNG* k-ε*, *standard k-ω* and *k-ω SST***) were analysed for their applicability on the FGS set-up. In a preliminary assessment, the performance of the turbulence models was tested on standard scenarios (flow over flat plate, flow around a cylinder). Grid convergence was studied on a single bar and a 10-bar set-up for the drag coefficient and the overall pressure difference. The *k-ε* models could not capture well the boundary layer behaviour (Fig. 3). The *k-ω* SST model showed the best performance and was chosen for the FGS model set-up.

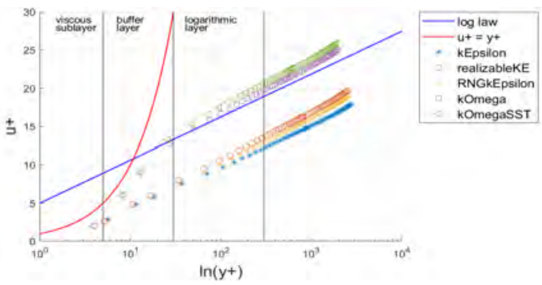

Fig. 3: Boundary layer behavior of the tested turbulence models displayed by the dimentionless parameters for velocity (u+) and wall distance (y+)

Bar rack simulation

2D Set-Up

Loss coefficient (ξ_{FGS}) and flow distribution downstream of the rack of the numerical model were determined for two approach velocities. They were compared to empirical data for the angled and the curved bar to validate the model. The model proved to depict both parameters well. The deviation of the loss coefficient was 12 % for the angled bar and 7 % for the curved bar set-up (Fig. 4).

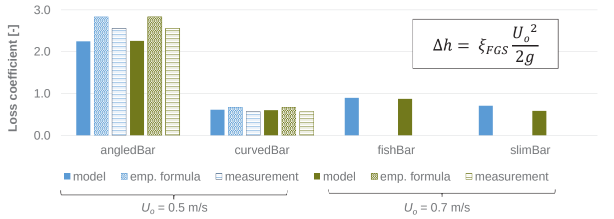

Fig. 4: Comparison of loss coefficients of the numerical model, empirical formula and physical measurement for the different bar shapes and two different approach flow velocities

Both additionally tested bar shapes performed much better than the original angled bar and indicated to be comparable alternative designs to the curved bar layout.

The numerical simulation was used to analyze the flow field in close vicinity of the bars where physical measurements were not possible. Regions of flow detachment or high shear stress can thus be detected (Fig. 5), and flow features might then be correlated to observed fish behavior.

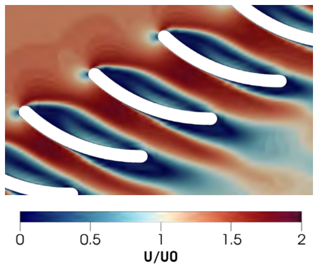

Fig. 5: Flow field around the bars of the curved bar rack set-up. The velocity U is normalised by the approach velocity U_o

3D Set-Up

To assess the flow variation in vertical direction, the model was extended to a 3D setting. Near the bottom, the flow was influenced by wall friction. In the water column, however, there was only small variation of the vertical flow field.

Conclusions

The choice of a fitting turbulence model is a crucial part of numerical flow simulations. It could be shown that the *k-ω* SST turbulence model was suitable for the numerical simulation of the bar rack configuration. Both flow field and loss coefficient could be reproduced well. A 2D model seems to be appropriate for a simple bar rack set-up. Further analysis should be done on the use of 3D models for simulations of FGS with additional structures such as overlays, which introduce stronger vertical flow components.

References

Kriewitz, C. R. (2015): Leitrechen an Fischabstiegsanlagen: Hydraulik und fischbiologische Effizienz, Dissertation, Laboratory of Hydraulics, Hydrology and Glaciology (VAW), ETH Zurich

Beck, C. (2019): Hydraulic performance of fish guidance structures with curved bars – part I: head loss assessment and part II: flow fields, Laboratory of Hydraulics, Hydrology and Glaciology (VAW), ETH Zurich (in review)

Moukalled et.al (2016): The Finite Volume Method in Computational Fluid Dynamics, Springer International Publishing

Task 3.2

Title

Computational energy innovation

Projects (presented on the following pages)

GPU-accelerated Finite Volume Particle simulation of multi-jet Pelton Turbine Flow
S. Alimirzazadeh, S. Leguizamón, T. Kumashiro, K. Tani, F. Avellan

Turbulence modeling for extendedoperating-range of hydraulic machines
A. Del Rio, E. Casartelli, L. Mangani, D. Roos Launchbury

Multiscale Simulation of Prototype-Scale Pelton Turbine Erosion
Sebastián Leguizamón, Siamak Alimirzazadeh, François Avellan

Simulations of transport phenomena in porous media on non-conforming meshes
Maria Giuseppina Chiara Nestola, Marco Favino, Patrick Zulian, Klaus Holliger, Rolf Krause

Fictitious domain methods for HMprocesses in fractures
Cyrill von Planta, Daniel Vogler, Xiaqing Chen, Maria Nestola, Martin O. Saar, Rolf Krause

Non-conforming mesh models for flow in fractured porous media using the method of Lagrange multipliers
Patrick Zulian, Philipp Shäddle, Daniel Vogler, Maria Nestola, Liudmila Karagyaur, Sthavishtha Bhopalam, Anozie Ebigbo, Martin Saar, Rolf Krause

SCCER SoE
SWISS COMPETENCE CENTER for ENERGY RESEARCH
SUPPLY of ELECTRICITY

SCCER-SoE Annual Conference 2019

LMH Laboratory for Hydraulic Machines

EPFL

In cooperation with the CTI
Energy
Swiss Competence Centers for Energy Research
Commission for Technology and Innovation CTI

GPU-accelerated Finite Volume Particle simulation of multi-jet Pelton Turbine Flow

S Alimirzazadeh, S Leguizamón, T Kumashiro, K Tani, F Avellan

GPU-SPHEROS

GPU-SPHEROS is a GPU-accelerated particle-based versatile solver based on Arbitrary Lagrangian Eulerian (ALE) Finite Volume Particle Method (FVPM) which inherits desirable features of both Smoothed Particle Hydrodynamics (SPH) and mesh-based Finite Volume Method (FVM) and is able to simulate the interaction between fluid, solid and silt [1]. With GPU-SPHEROS, the goal is to perform industrial size setup simulations of hydraulic machines.

Multi-jet Pelton Simulation

Multi-jet Pelton turbines are popular for their flexibility in covering a wide operating range including high specific speeds. However, with by increasing the number nuzzles, there is a higher risk of jet interference which can cause a sudden efficiency drop. GPU-SPHEROS, as particle-based solver is used to simulating a six-jet Pelton turbine flow in a wide operating range including the Best Efficiency Point (BEP) and off-design conditions. The jet interference inception range is then predicted and validated by the experiments performed by Hitach-Mitsubishi Hydropower systems.

Geometry

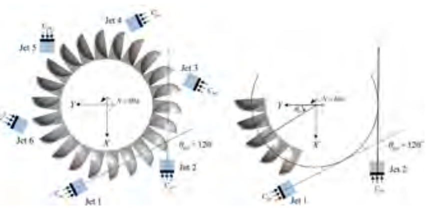

Six-jet simulation setup

Validation for Turbulent Impinging Jet on a Flat Plate

- A turbulent fluid jet impinging on a flat plate has been validated for pressure and free surface elevation against available experimental data for non-uniform jet velocity profile. As a case study with close hydrodynamics to Pelton turbine.
- The validated solver has been then used for multi-jet Pelton flow simulation.

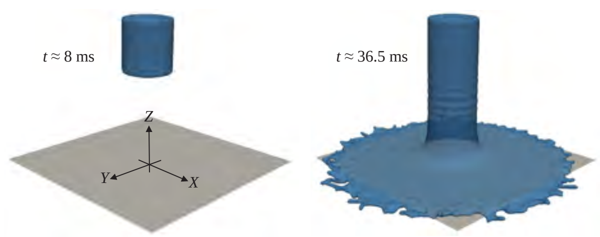

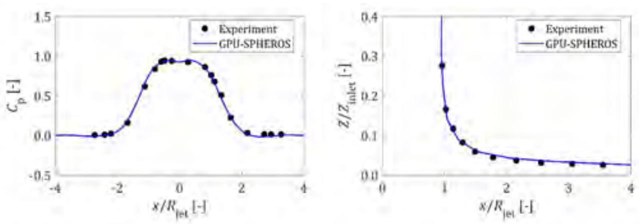

Dual-jet Simulation Setup

- A dual-jet simplified simulation setup is used to investigate the interaction between the adjacent jets at eight different operating points N/N_{BEP} = $\{0.89, 0.94, 1.0, 1.05, 1.11, 1.16, 1.22, 1.31\}$ where N is the runner rotational speed in min^{-1} and BEP is the Best Efficiency Point.
- The free surface has been reconstructed and visualized in Paraview open source data analysis software.
- Even though the torque is underestimated, the trend is in a very good agreement with the experiment.

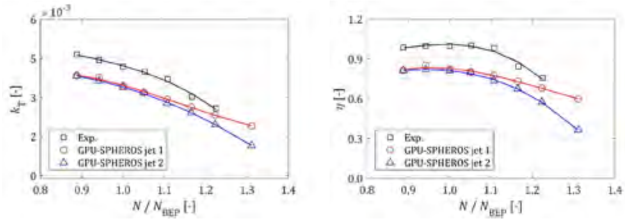

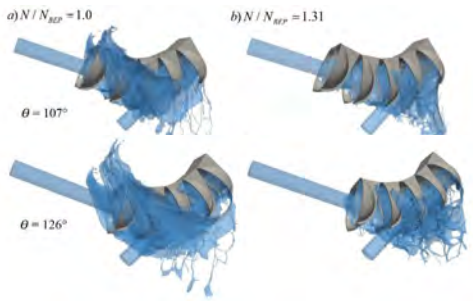

Six-Jet Full Pelton Flow Simulation

- A six-jet full Pelton flow has been simulated with GPU-SPHEROS on 12 GPUs to investigate and track the free surface and jet interactions.
- The solver is able to robustly handle industrial size problems with a violent free surface.

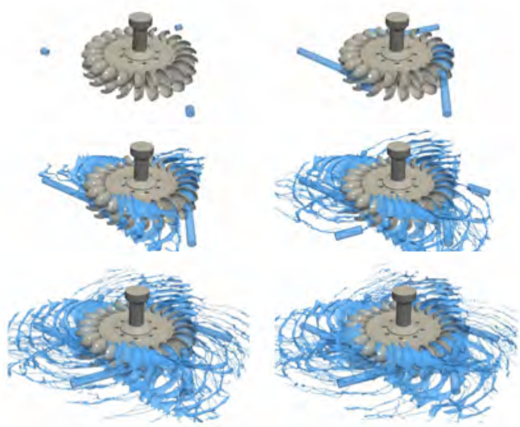

References

S Alimirzazadeh, E Jahanbakhsh, A Maertens, S Leguizamon, F Avellan, GPU-Accelerated 3-D finite volume particle method, *Computers & Fluids*. 171 (2018) 79–93

Experimental data is provided by "Kvicinsky S. Kvicinsky, Methode d'analyse des Ecoulements 3D a Surface Libre: Application aux Turbines Pelton, École Polytechnique Fédérale de Lausanne, doctoral Thesis N° 2526 2002»

SCCER-SoE Annual Conference 2019

SCCER SoE
SWISS COMPETENCE CENTER for ENERGY RESEARCH
SUPPLY of ELECTRICITY

Supported by:
Schweizerische Eidgenossenschaft
Confédération suisse
Confederazione Svizzera
Confederaziun svizra
Swiss Confederation
Innosuisse – Swiss Innovation Agency

Lucerne University of Applied Sciences and Arts
HOCHSCHULE LUZERN
Technik & Architektur

Turbulence modeling for extended operating-range of hydraulic machines

A. Del Rio, E. Casartelli, L. Mangani, D. Roos Launchbury

Introduction

Hydropower plants are very well suited for the modern electricity market which depends on high flexibility and storage capabilities. In order for pump turbines to fulfill todays requirements, favorable stable behavior over a large range of guide vane openings (GVO's) is necessary. This includes operation points (OP's) from turbine start (GVO3°) and synchronization (GVO6°) all the way to regular operation and part/over-load (GVO ~ 20°).

Simulations of unstable off-design conditions are difficult to perform, because the conditions are dominated by turbulent vortex structures in the vaneless space, which often cannot be accurately predicted using conventional turbulence models. This is due to the fact that the most commonly used models, such as k-epsilon and the Shear Stress Transport (SST) model assume *isotropic turbulence*. This assumption is not valid for many flow problems but seems to have an especially large influence in pump turbine instability simulations.

The goal of the current efforts is to investigate and compare the performance of various turbulence models at off-design conditions over a broad range of GVO's. The standard eddy viscosity models SST k-omega and k-epsilon are thereby compared with more advanced turbulence models.

CFD Setup

- Full-size pump-turbine prototype
- Computational domain includes Volute & Stay Vanes (A), Guide Vanes (GV, B), Runner (C) and Draft Tube (D) shown in Fig. 1
- In-house, coupled, unsteady solver with efficient moving-mesh Capabilities
- Investigated Turbulence models: k-epsilon, SST k-omega, Explicit Algebraic Reynolds Stress Model (EARSM)

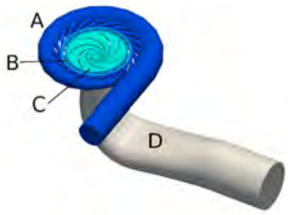

Figure 1: Computational domain

EARS models do not solve for additional transport equations but try to reconstruct the unknown stress tensor through an algebraic equation based on the strain rate, vorticity and the turbulent time-scale [1]. The implemented model is based on [2][3] and uses the baseline (BSL) k-omega model to calculate the turbulent time-scale.

Results

Fig. 2 shows the four quadrant characteristic for load rejection, a sort of emergency shutdown of the pump-turbine. The GVO are thereby decreased from 24° to 6°, which leads to oscillations in the operation mode between turbine-brake and reverse-pump.

As can be seen from Fig. 2 all three turbulence models are in good agreement with the reference curve for large GVO's (~20°). For GVO6° only k-epsilon and BSL EARSM are capable of capturing the positive slope in the S-shape according to the reference curve.

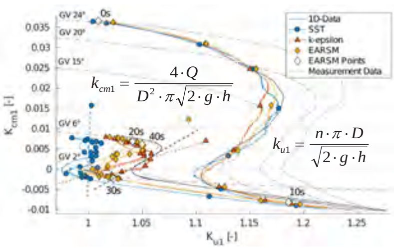

Figure 2: Influence of the turbulence model on the simulated stability characteristic for large GVO angles (~20°) and for the synchronisation angle of 6°

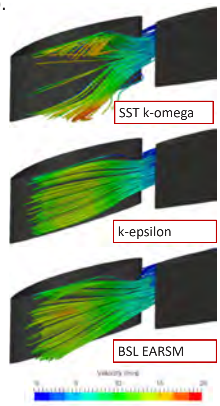

Figure 3: 3D Velocity-streamlines for GVO6°

SST k-omega produces almost a stable characteristic. Fig. 3 shows the flow behavior in the GV channel and vaneless space for all three turbulence models. The SST k-omega model overestimates the separation behavior on the GV blades, which leads to horseshoe type vortices. These structures seem to have a stabilizing effect on the simulation. BSL EARSM and k-epsilon on the other hand produce less separation.

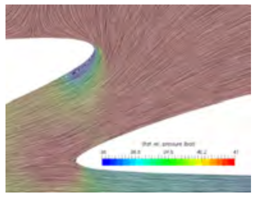

Figure 4: LIC velocity plot through the GV channel for GVO6°

During the process of turbine-start (Fig. 5) the GVO is increased from 1° to a final value of 3°. For these small openings operates the pump-turbine in a stable way, which can be reproduced with SST k-omega and BSL EARSM. The k-epsilon model on the other hand produces still and instability as can be seen from Fig. 5. The smaller GVO leads to more incidence at the GV LE (Fig. 4), which produces strong horseshoe type vortices for the SST k-omega and BSL EARSM simulations (Fig. 6). These vortices seem again to have a stabilizing effect on the simulation.

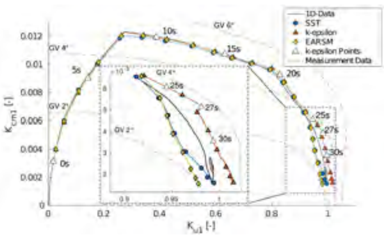

Figure 5: Influence of the turbulence model on the simulated stability characteristic for a small GVO angle of 3°

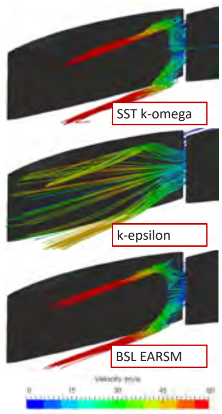

Figure 6: 3D Velocity-streamlines for GVO3°

Discussion

The benefits of the anisotropic BSL EARSM turbulence model have been presented for pump-turbine simulations under unstable off-design conditions. Although for certain GVO's it is possible to produce good results with k-epsilon and/or SST k-omega, only BSL EARSM guarantees consistently good results for all investigated GVO's. In addition, the better numerical performance can be partly explained physically. The higher complexity of BSL EARSM allows for example the capturing of turbulence driven secondary flow, which provides the low-energy boundary layer flow with momentum and prevents the flow from separation. This effect is one of the main causes, why BSL EARSM produces better results for the load rejection case (Fig. 2) compared to SST k-omega. K-epsilon on the other hand provides no physical explanation for its superiority compared to SST k-omega in this case.

In the upcoming research additional operating cases will be considered and further turbulence models will be investigated. Of special interest are the full Reynolds-Stress model (RSM) and 4-equation models with focus on elliptic blending. The available RS-model is implemented in coupled form in the in-house code of the CC FMHM. The coupling improves the stability behavior drastically, which makes the model suitable for the challenging pump-turbine simulations.

References

[1] Wallin, S., and Johansson, A., "An explicit algebraic Reynolds stress model for incompressible and compressible turbulent flows." Journal of Fluid Mechanics 403 (2000): 89-132.

[2] Hellsten, A., "New Advanced k-omega Turbulence Model for High-Lift Aerodynamics", AIAA Journal, Vol. 43, No. 9, 2005, pp. 1857-1869.

[3] Menter, F. R., Garbaruk, A.V., and Egorov, Y., "Explicit Algebraic Reynolds Stress Models for Anisotropic Wall-Bounded Flows", Progress in Flight Physics, Vol. 3, 2012, pp. 89-104

SCCER SoE
SWISS COMPETENCE CENTER for ENERGY RESEARCH
SUPPLY of ELECTRICITY

SCCER-SoE Annual Conference 2019

LMH Laboratory for Hydraulic Machines

EPFL

Supported by:
Schweizerische Eidgenossenschaft
Confédération suisse
Confederazione Svizzera
Confederaziun svizra
Swiss Confederation
Innosuisse – Swiss Innovation Agency

Multiscale Simulation of Prototype-Scale Pelton Turbine Erosion

Sebastián Leguizamón, Siamak Alimirzazadeh, François Avellan

Motivation and Problem Description

The hydro-abrasive erosion of turbomachines is a **significant problem** worldwide. In the context of the Energy Strategy 2050, it is a problem that will become **more severe in the future** due to the retreat of glaciers and permafrost caused by **climate change**.

The project objective is to deliver a numerical **simulation tool** with predictive power that may become **advantageous** for the **design** and the **operation** of the machines.

The erosion of hydraulic turbomachines is an **inherently multiscale process**; its simulation is therefore very complicated. It requires a multiscale modeling approach.

Case Study Description

The model has been previously validated on a laboratory-scale case [1] and on a fixed Pelton bucket [2]. Now, a **prototype-scale Pelton turbine** case study is used for further **validation**.

The 84 MW turbine has a pitch diameter D_1 = 2.87 m, and features 21 buckets and 6 jets.

The study period lasts 21 months during which characterizations of the sediments and the turbine erosion have been performed.

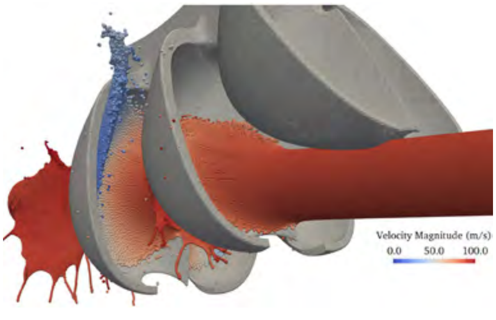

Discretization of the jet impinging on the Pelton turbine.

Multiscale Erosion Model

A multiscale model has been recently formulated by the authors [1]. It encompasses two submodels to tackle the multiscale character of the problem.

Microscale output
- Erosion ratio $f(\alpha_i, C_j)$
- Restitution coefficients $f(\alpha_i, C_j)$

Sequential coupling

Macroscale output
- Impact condition distributions
- Sediment flux against the surface
- Erosion distribution
- Global erosion rate

In the **Microscale Model**, detailed impact simulations are performed taking into consideration all the important physical effects. These simulations result in the **erosion ratio** for each impact condition studied.

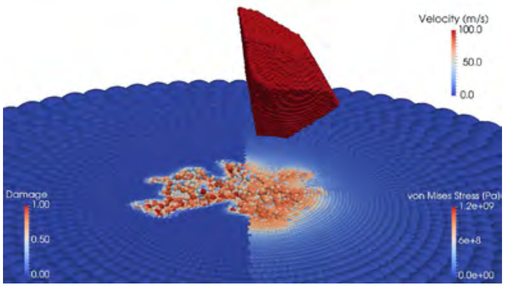

Microscale simulation: Sediment impacting a solid specimen.

In the **Macroscale Model**, the turbulent sediment transport is computed; each time a sediment impact is detected, the results of the microscale simulations are interpolated, resulting in the macroscopic **erosion accumulation**.

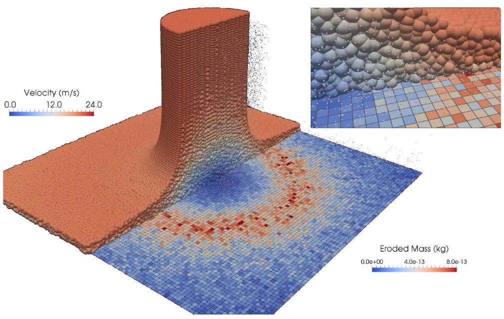

Macroscale simulation: Slurry jet eroding a flat plate.

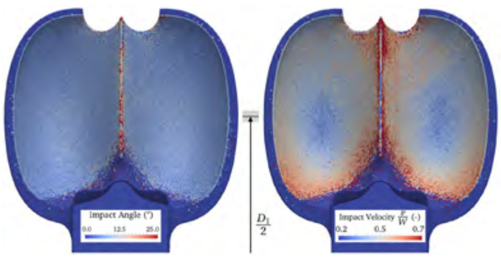

Average impact angle and velocity distributions.

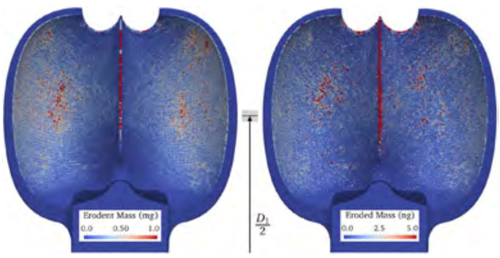

Impacted sediment mass and eroded mass distributions.

Simulation Results

The macroscale simulation yields important information that may be used to understand the erosion process.

For instance, the average **impact conditions** shown on the left, namely the sediment impact **angle** and **velocity**, are directly related to the material-dependent erosion magnitude.

Similarly, the **sediment flux** against the bucket wall, shown on the left, is determined by the sediment characteristics such as its size distribution, and by the local bucket curvature.

These three distributions are the culprit of the **eroded mass** distribution, also presented on the left, and may therefore shed some light on the erosion phenomenon.

Validation of the Erosion Predictions

The simulation results were validated with the experimental **erosion depth** available for each bucket, at the points D_i, O_i and sections S_i shown on the right, and with the experimental **total eroded mass**.

As shown below, the **average relative error** is 35% for the pointwise comparisons, 14% for the sectional comparisons, and only 4% for the total eroded mass.

The **modeling error** has been estimated at **26%±24%** based on these results and the experimental uncertainty.

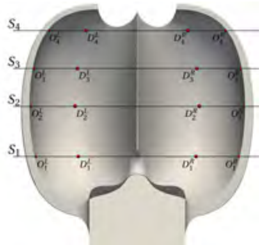

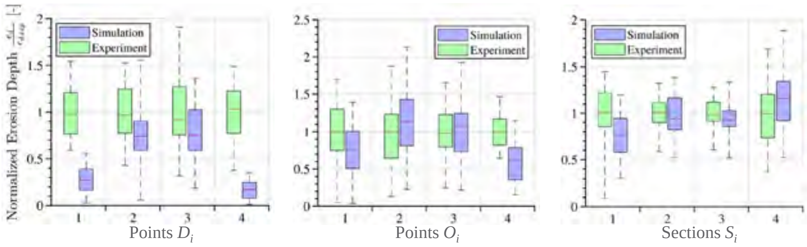

Comparison of simulated and measured erosion depth at eight points and across four sections.

References

[1] S. Leguizamón, E. Jahanbakhsh, A. Maertens, S. Alimirzazadeh, F. Avellan, A multiscale model for sediment impact erosion simulation using the finite volume particle method, *Wear* 392-393 (2017).

[2] S. Leguizamón, E. Jahanbakhsh, S. Alimirzazadeh, A. Maertens, F. Avellan, Multiscale simulation of the hydroabrasive erosion of a Pelton bucket: Bridging scales to improve the accuracy, *International Journal of Turbomachinery, Propulsion and Power* 4 (2019) 9.

SCCER SoE
SWISS COMPETENCE CENTER for ENERGY RESEARCH
SUPPLY of ELECTRICITY

SCCER-SoE Annual Conference 2019

ETH zürich · Unil UNIL | Université de Lausanne · Institut des sciences de la Terre · Università della Svizzera italiana, Institute of Computational Science ICS

Supported by:
Schweizerische Eidgenossenschaft
Confédération suisse
Confederazione Svizzera
Confederaziun svizra

Swiss Confederation

Innosuisse – Swiss Innovation Agency

Simulations of transport phenomena in porous media on non-conforming meshes

Maria Giuseppina Chiara Nestola, Marco Favino, Patrick Zulian, Klaus Holliger, Rolf Krause

Introduction

Numerical simulations of fluid flow and transport **in fractured porous media** is a challenging problem due to the different scales involved. In fact, the fracture width tends to be **orders-of-magnitude** smaller than the characteristic size of the embedding matrix. Due to this difference, the creation of computational meshes that explicitly resolve fractures remains an immensely complicated and tedious task, which, so far, is possible only for small numbers of fractures.

In order to allow for the numerical simulation of complicated fracture networks, hybrid-dimensional approaches have been developed [1]. In contrast to equi-dimensional ones, where fractures are **three-dimensional objects**, fractures, due to their aspect ratio, are described as **lower-dimensional objects**, whose width is modeled as a coefficient in the equations and suitable coupling conditions between the fractures and the embedding matrix are imposed.

Although, hybrid-dimensional approaches have been widely employed for the simulation of rather complicated media, a comparison with equi-dimensional approaches has never been performed for **transport problems** in fractured media. In this work, we consider the case of a regular fracture network, whose computational mesh for the hybrid model can be generated employing an adaptive mesh refinement technique [2]. For both approaches, we compare the results of the simulations of fluid flow and transport.

Methods

Equi-dimensional model

The matrix and the fractures have the same spatial dimension, thus allowing for a full characterization of the geometrical features.

Fluid flow

$$\begin{aligned} -\nabla\cdot K\nabla P &= 0 \ \text{in}\,\Omega \\ P &= \bar{p}\ \text{on}\,\Gamma^D \\ -K\nabla P\cdot n &= \bar{J}\ \text{on}\,\Gamma^N \end{aligned}$$

Transport

$$\phi\frac{\partial c}{\partial t}+\nabla(c\tilde{u}) = 0 \ \text{in}\,\Omega \qquad c = \bar{c}\ \text{on}\,\Gamma^c$$

$$\tilde{u} = -K\nabla P$$

$$\int_\Omega K\nabla P^h\cdot\nabla v^h\,dV - \int_{\Gamma^N}\bar{J}v^h\,dS = 0 \qquad \int_\Omega \phi\frac{\partial c^h}{\partial t}w^h\,dV + \int_\Omega \tilde{u}\cdot\nabla c^h w^h\,dV = 0$$

The embedded fractures are defined as subsets of the domain, for which different values of the permeability and porosity are assigned.

Hybrid-dimensional model

The fractures have a lower spatial dimension than the matrix. The equations for the fractures are obtained by averaging across the fractures.

Fluid flow

$$\begin{aligned} -\nabla\cdot K_i\nabla P_i &= 0 \ \text{in}\,\Omega_i \\ P_i &= \bar{p}_i\ \text{on}\,\Gamma_i^D \\ -K_i\nabla P_i\cdot n_i &= \bar{J}_i\ \text{on}\,\Gamma_i^N \end{aligned}$$

Transport

$$\phi_i\frac{\partial c_i}{\partial t}+\nabla(c_i\tilde{u}_i) = 0 \ \text{in}\,\Omega_i \qquad c_i = \bar{c}_i\ \text{on}\,\Gamma_i^c$$

i={m,f}, with m referring to the matrix and f to the fractures

$$\begin{aligned} &\int_\Omega K_m\nabla P_m^h\cdot\nabla v_m^h\,dV - \int_{\Gamma^N}\bar{J}_m v_m^h\,dS - \int_\gamma \lambda^h v_m^h\,dS = 0 \\ &\int_\omega K_f\nabla P_f^h\cdot\nabla v_f^h\,dV - \int_{\gamma_N}\bar{J}_f v_f^h\,dS + \int_\gamma \lambda^h v_f^h\,dS = 0 \\ &\int_\gamma (P_f^h - P_m^h)\mu^h\,dS = 0 \end{aligned}$$

$$\begin{aligned} &\int_\Omega \phi_m\frac{\partial c_m^h}{\partial t}w_m^h\,dV + \int_\Omega \tilde{u}_m^h\cdot\nabla c_m^h w_m^h\,dV - \int_\gamma \lambda^h w_m^h\,dS = 0 \\ &\int_\omega \phi_f\frac{\partial c_f^h}{\partial t}w_f^h\,dV + \int_\omega \tilde{u}_f^h\cdot\nabla c_f^h w_f^h\,dV + \int_\gamma \lambda^h w_f^h\,dS = 0 \\ &\int_\gamma (c_f^h - c_m^h)\mu^h\,dS = 0 \end{aligned}$$

Lagrange multipliers are used to apply **coupling conditions** at the interfaces between the matrix and the fractures [3]. These additional equations are denoted in red.

Discretization and stabilization Technique

For both approaches, we employed first-order finite element methods. To ensure the stability of the discretization and the positivity of the solution, we employed a Flux Correction Transport technique [4].

Results

For both approaches, we compare
- pressure distribution for the flow problem,
- concentration for the transport problem.

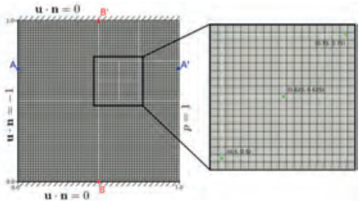

The considered domain is a unitary square with 6 fractures [1], whose width is four orders-of-magnitude smaller of the domain size. For the hybrid-dimensional model, we employ a fine mesh with 0.6 millions of elements, while for the equi-dimensional approach, we consider four different mesh resolutions.

Fluid flow **Transport**

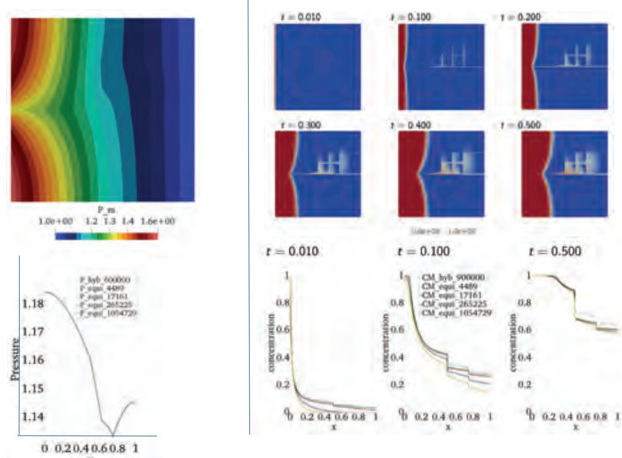

Top row: **pressure distribution** of the flow problem (left) and **concentration** at six different time-steps for the transport problem (right). Both solutions have been computed using the equi-dimensional model. Bottom row: comparison of **pressure distribution** (left) and **concentration** at three different time steps (right) between hybrid- and equi-dimensional approaches along the line y=0.5.

Discussion

Flow problem: No relevant differences between hybrid- and equi-dimensional approaches. Both are able to reproduce the reference solution [1].

Transport problem: Hybrid-dimensional approach reproduces the reference solution. In particular, the vertical drop in the concentration at x=0.5 is bounded. On the other hand, in the equi-dimensional approach the vertical drop increases over time. At the final simulation time, we observe that the two approaches have converged to different solutions. This may be due to lower cross-fracture transport for the hybrid-dimensional model, which, in turn, would suggest that the equi-dimensional approach **allows to describe features,** which a hybrid-dimensional **one doesn't account for.**

References

[1] Odsæter, Lars H., Trond Kvamsdal, and Mats G. Larson. *A simple embedded discrete fracture matrix model for a coupled flow and transport problem in porous media*. Computer Methods in Applied Mechanics and Engineering 343 (2019): 572-601.
[2] Hunziker, Jürg, et al. *Seismic attenuation and stiffness modulus dispersion in porous rocks containing stochastic fracture networks.* Journal of Geophysical Research: Solid Earth 123.1 (2018): 125-143.
[3] Schädle, Philipp, et al. *3D non-conforming mesh model for flow in fractured porous media using Lagrange multipliers*. arXiv preprint arXiv:1901.01901 (2019)
[4] Kuzmin, Dmitri. *Algebraic Flux Correction I. Scalar conservation laws.* Flux-corrected transport. Springer, Berlin, Heidelberg, 2005. 155-206. APA

SCCER SoE
SWISS COMPETENCE CENTER for ENERGY RESEARCH
SUPPLY of ELECTRICITY

SCCER-SoE Annual Conference 2019

Supported by:
Schweizerische Eidgenossenschaft
Confédération suisse
Confederazione Svizzera
Confederaziun svizra
Swiss Confederation
Innosuisse – Swiss Innovation Agency

Fictitious domain methods for HM-processes in fractures

Cyrill von Planta[1], Daniel Vogler[2], Xiaqing Chen[2], Maria Nestola[1], Martin O. Saar[2], Rolf Krause[1]
[1]Institute of Computational Science, Università della Svizzera Italiana
[2]Institute of Geophysics, ETH Zurich

Introduction

Fluid flow in rough fractures and the coupling with the mechanical behaviour of the fractures pose great difficulties for numerical modelling approaches, due to complex fracture surface topographies, the nonlinearity of hydromechanical processes and their tightly coupled nature.

Fictitious Domain Method

We have adapted a fictitious domain method to simulate hydromechanical processes in fracture-intersections. The solid is immersed in the fluid. The solid and fluid are simulated on separately and coupled with L²-projections which can transfer information between non-conforming meshes. We use finite elements, linear elasticity, and the incompressible Navier-Stokes equations.

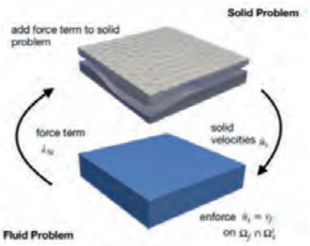

Figure: Schematic FD method. The full problem is solved in a fixed point iteration.

Figure: Contact surfaces within the fracture. Simulating contact is highly complex because nonmatching surfaces meshes must be properly related to each other.

Dual Mortar Method for Contact

Within the solid problem we simulate a two-body contact problem. We developed a dual mortar method to resolve the non-matching surfaces at the contact boundaries.

2D Intersection

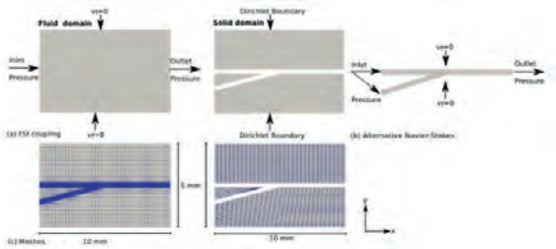

Figure: Setup of the benchmark meshes.

With the 2D intersection benchmark we validated our FD approach against a fluid simulation using only the Navier Stokes equations but with the same fluid-solid boundary.

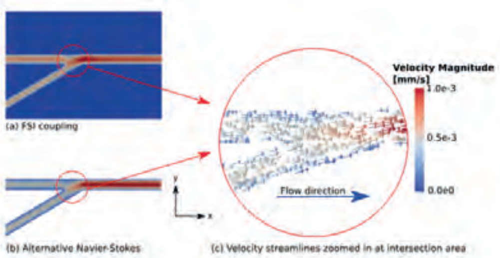

Figure: Left: Fluid velocity of FD approach is the same as in the alternative setup. Right: Acceleration of fluid velocities at channel intersection.

Governing equations

Solid: $\rho_s \ddot{u}_s - \mathrm{div}\sigma(u_s) = f_s \quad \text{on } \Omega^t_{s,1} \cup \Omega^t_{s,2},$

$$u_s = 0 \quad \text{on } (\Gamma^t_s)^D,$$

$$\sigma(u_s)\cdot n_s = h_s \quad \text{on } (\Gamma^t_s)^N,$$

Contact conditions: $\sigma_n \leq 0 \quad \text{on} \quad (\Gamma^t_{s,2})^C,$

$$\sigma_n(u_{s,1}\circ\Phi) = \sigma_n(u_{s,2}) \quad \text{on} \quad (\Gamma^t_{s,2})^C,$$

$$[u] \leq g \quad \text{on} \quad (\Gamma^t_{s,2})^C,$$

$$([u]-g)\sigma_n(u_{s,2}) = 0 \quad \text{on} \quad (\Gamma^t_{s,2})^C,$$

$$\sigma_T = 0 \quad \text{on} \quad (\Gamma^t_{s,2})^C.$$

Fluid: $\rho_f \dot{v}_f + \rho_f(v_f\cdot\nabla)v_f - \mu_f \nabla\cdot\sigma_f(p_f, v_f) = f_{\mathrm{fsi}} \text{ on } \Omega_f$

$$\nabla\cdot v_f = 0 \quad \text{on } \Omega_f$$

Coupling: $\dot{u}_s = v_f$

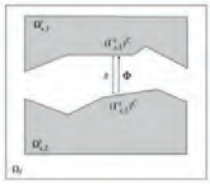

Fluid Flow in intersecting fracture

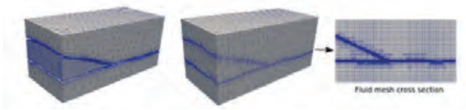

Figure: Setup of the meshes. In the fluid mesh, the area within the fracture has been refined.

We created a realistic intersecting fracture using SynFrac and used the FD approach to simulate fluid flow under increasing normal load. The simulations results show, that increasing closure of the fracture planes coincides with increasing fluid flow channeling.

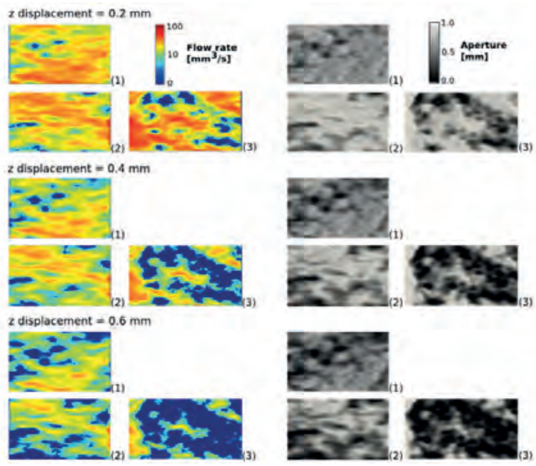

Figure: Left: flow rate under increasing load, measured in displacement of the top side of the fracture. Right: Aperture fields within the fracture.

Outlook

Fictitious domain methods combined with L² –projections are a highly promising tool to simulate geophysical processes. Next steps include the extension of the approach to nonlinear materials, thermal and other physical processes.

References

[1] Planta et. al. Simulation of hydro-mechanically coupled processes in rough rock fractures using an immersed boundary method and variational transfer operators. 2019. Comp. Geosciences.
[2] Planta et. al. Fluid-Structure Interaction with a parallel transfer operators to model hydro-mechanical processes in heterogeneous fractures. 2019. Special Issue Comp. Geosciences, submitted.
[3] Nestola et. al. An immersed boundary method for fluid-structure interaction based on variational transfer. J. of Comp. Phys. 2019

SCCER SoE
SWISS COMPETENCE CENTER for ENERGY RESEARCH
SUPPLY of ELECTRICITY

SCCER-SoE Annual Conference 2019

Supported by:
Schweizerische Eidgenossenschaft
Confédération suisse
Confederazione Svizzera
Confederaziun svizra

Swiss Confederation

Innosuisse – Swiss Innovation Agency

Non-conforming mesh models for flow in fractured porous media using the method of Lagrange multipliers

Patrick Zulian, Philipp Shäddle, Daniel Vogler, Maria Nestola, Liudmila Karagyaur, Sthavishtha Bhopalam, Anozie Ebigbo, Martin Saar, Rolf Krause

Motivation

- Flow through fracture networks is governed by **3D effects**
- **Mesh generation** of 3D fracture **networks** with conforming matrix **mesh** is very **challenging**

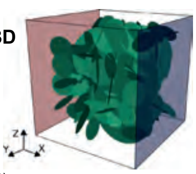

Our embedded non-conforming mesh approach

- Method of Lagrange multipliers (Köppel M. et al. 2018)
- **Variational transfer** operator (Krause R. & Zulian P. 2016)

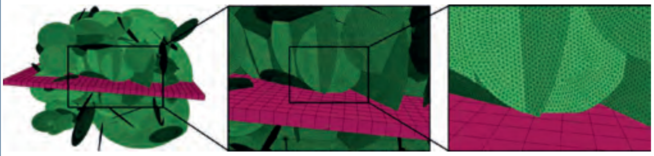

Article: Schädle P., Zulian P., Vogler D., Bhopalam S., Nestola M., Ebigbo A., Krause R., Saar M. **3D non-conforming mesh model for flow in fractured porous media using Lagrange multipliers**, *Computers & Geosciences*, 2019.

Method

Lagrange multiplier formulation

Flow in the porous-medium matrix, Ω

$$\begin{aligned} \nabla\cdot(-\mathbf{K}\nabla p) - \lambda = f \quad & \text{in} \quad \Omega\,, \\ p = 0 \quad & \text{on} \quad \Gamma = \partial\Omega \end{aligned}$$

Flow in the fracture, γ

$$\begin{aligned} \nabla_\gamma\cdot(-\mathbf{K}_\gamma\nabla_\gamma p_\gamma) + \lambda = f_\gamma \quad & \text{in} \quad \gamma\,, \\ p_\gamma = 0 \quad & \text{on} \quad \Gamma = \partial\gamma \end{aligned}$$

Find $(p, p_\gamma) \in \mathbf{V}$ and $\lambda \in \Lambda$, such that

$$\int_\Omega \mathbf{K}\nabla p\cdot\nabla q + \int_\gamma \mathbf{K}_\gamma\nabla_\gamma p_\gamma\cdot\nabla_\gamma q_\gamma - \int_\gamma \lambda(q - q_\gamma) = \int_\Omega fq + \int_\gamma f_\gamma q_\gamma\,, \qquad \forall(q, q_\gamma) \in \mathbf{V}$$

and

$$\int_\gamma (p - p_\gamma)\mu = 0\,, \qquad \forall\mu \in \Lambda$$

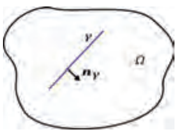

Matrix domain Ω with an embedded fracture domain γ and normal vector $\mathbf{n}$ on γ

The Lagrange multiplier represents the fluid pressure gradient $\lambda = \mathbf{K}\nabla p\cdot\mathbf{n}_\gamma$

Köppel, M. et al. (2018). *Computational Geosciences*, 1–15

Results: 2D validation

2D benchmarks from

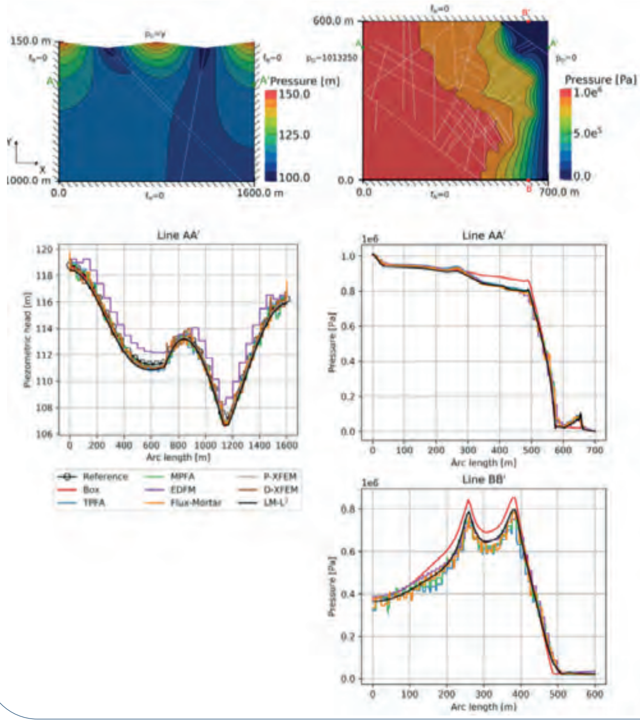

Results: 3D experiments

- Heterogeneous fracture network, error of embedded discretization

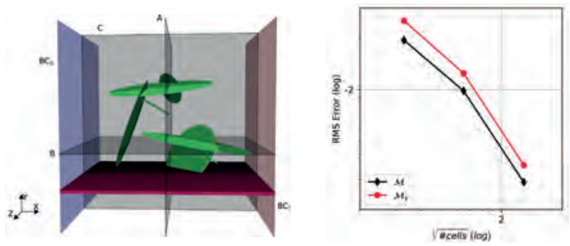

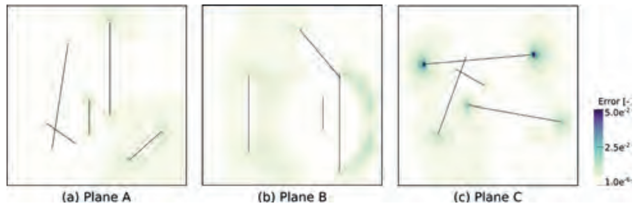

- Example with 150 randomly oriented fractures

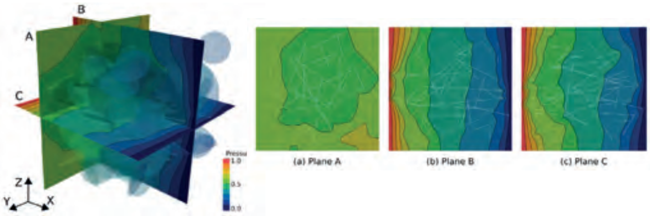

General information

- Simulation of fracture network for geothermal energy extraction
- Tool for automated generation of flow and transport in fracture networks
- Current status: equi- and hybrid-dimensional discretization for flow in 3D using the finite element method
- Simplification of the study of stochastic discrete fracture networks (DFN).
- DFNs necessary whenever the actual fracture network is not known

Conclusion

- Robust method with expected behaviour of the L^2—error
- Results in agreement with benchmarks present in the literature
- Suitable for **large-scale, realistic fracture network realizations in 3D**

Limitations of current state

- Discretization of the model is not locally mass conservative
- Method of Lagrange multiplier

Open source software

- **Utopia** bitbucket.org/zulianp/utopia
- **ParMOONoLith** bitbucket.org/zulianp/par_moonolith

Institutions

Università della Svizzera italiana | Institute of Computational Science ICS

ETH zürich

CSCS Centro Svizzero di Calcolo Scientifico Swiss National Supercomputing Centre

Work Package 4: Future Supply of Electricity

Work package 4 (WP4) takes a systemic view on the transformation of the Swiss energy system to support the implementation of the Energy Strategy 2050. Therefore, it significantly broadens and complements the other work packages that focus primarily on the technological challenges of hydropower and deep geothermal energy. In particular, WP4 also considers a range of overarching aspects such as: sustainability, energy security, risk cost benefit analysis, societal concerns and stakeholder interactions, long-term scenario modeling, socio-economic and political drivers, and Multi-Criteria Decision Analysis (MCDA) to systematically evaluate trade-offs and conflicting objectives. These interconnected thematic areas are addressed in four dedicated tasks, for which the following, key achievements are reported for 2019.

Risk, safety and societal acceptance for geoenergy and hydropower

The assessment of accident risks for deep geothermal systems by PSI-LEA has been substantially expanded by:

1. introducing additional hazardous materials potentially used as part of the matrix acidizing in the stimulation phase;
2. consideration of further hazardous materials potentially used as working fluids in the operational phase, and
3. a comprehensive update of historical accidents for the period 1990-2017.

The focus of the hydropower risk assessment has been on the finalization of the framework for uncertainty quantification (UQ) in the modelling of dam-break consequences, particularly the assessment of uncertainties in the life loss (LL) estimates in a hypothetical downstream area in Switzerland due to a hypothetical dam break. Furthermore, results indicate that the global sensitivity analysis applied in this study can help in understanding how the variability of each model input affected variability of the LL-estimates.

The algorithmic geo-energy seismic risk governance framework developed by ETHZ-SED has been published in Applied Energy, and is now being converted into a R package (with tutorial) for wider use. Guidelines for seismic risk mitigation have been given in the form of risk re-ports for operators and authorities. This includes the risk analysis of the Bedretto lab experiments, the Haute Sorne EGS planned project and the Geldinganes EGS project, Iceland The anomalous (outlier) characteristics of the Pohang event has been added in our a-priori risk model (regarding the ratio of possible earth-quake size, which has an impact on the adaptive TLS, requiring improved seismic data for taking a decision in time, prior to crossing a fixed safety criterion).

Global observatory of electricity resources

As a follow-up analysis of the previous evaluation of potentials, costs and environmental impacts of electricity generation technologies in the Swiss context for SFOE (Bauer et al. 2017), PSI-LEA has carried out an update of electricity generation costs (levelized costs of electricity, LCOE) of solar photovoltaic roof-top installations, wind turbines, biomass conversion technologies, natural gas combined cycle power plants and cogeneration units as well as fuel cells. This new cost assessment has been performed in order to appropriately reflect latest developments and take into account recent technology cost reductions (mainly for PV systems and offshore wind turbines) and new estimates for future natural gas prices. In line with the previous analysis, LCOE have been estimated for today (reference year 2018) and up to year 2050.

The spatial Multi Criteria Decision Analysis (sMCDA) tool to assess the sustainability of potential areas for deep geothermal energy (DGE) systems in Switzerland has been extended during the last reporting period. In particular, marginal distributions for uncertain impact categories have been added to the Stochastic Multi-criteria Acceptability Analysis (SMAA-TRI). Furthermore, indicators of the social sustainability dimension have been updated and extended (e.g. non-seismic accident risk, induced seismicity, and proximity to major cities). Finally, the application of spatial MCDA based on a stochastic method with GIS capabilities demonstrates its suitability as decision-making making tool for deep geothermal energy in Switzerland.

Energy economic modeling of PSI-LEA focused on further developments in the following activity areas. First, price formation on the Swiss wholesale electricity markets and long-term price development under energy policy scenarios of Switzerland and the EU, with emphasis on a fundamental model of reasonable size and complexity that can approximate today's prices. Second, hydropower dispatch optimization against electricity prices, focusing on models that take into account the probability distribution, but that are still numerical tractable for sensitivity analyses. Third, long-term investment and electricity dispatch for Switzerland and EU. Finally, nonlinear inverse demand curves in electricity market modeling were developed to provide a more accurate demand curve estimation which is close to real biding case, and reduces the model bias of Nash Cournot electricity market models with linear demand curves, which usually have higher prices and lower volumes than observed.

Socio-economic-political drivers

The ETHZ-TdLab further worked on the case study GEothermie2020 to analyze stakeholder and public engagement and developed decision support tools. It conducted focus group research and participant observation, and also analyzed visions of participation of the general public and of program managers. Results showed that project developers idealize co-productive participatory formats that give the public possibilities to influence projects. However, such formats require participants to invest time, and developers want to be able to participants. In the wider public, formats of participation that are self-organized and that can be blended in everyday activities (such as energy consumption) are favored. We are developing a tool to assess and choses participatory formats based on these results.

The media analysis on media discourse on deep geothermal energy has been expanded. Further studies on UK local media, Chile and South Korea have been conducted. A comparative analysis will be done in 2020 to identify global trends in reporting on deep geothermal energy.

A social network analysis combined with qualitative interviews was conducted to analyze the controversy around the reconcessioning of the Lago Bianco hydropower dam. The study highlighted the role of trustable brokers to enable collaboration between conflicting parties.

Joint activities

Work within the Joint Activity IDEA (Integrated Development Processes for Hydropower and Deep Geothermal Projects: Regulatory, Political and Participatory Perspectives) focusses on the “less-technical” aspects of the energy transition such as the challenges experienced by the various actors in the energy arena. Media analysis and stakeholder interviews revealed that despite the current difficulties of hydropower, the economic situation is not seen as a long-term threat. Within the Joint Activity Scenarios & Modelling (JASM) the modelling teams of the eights SCCER work together to generate scenarios for a Swiss energy system in 2050 that cuts CO2 emissions from todays 38 MTCO2/a to near-zero. First results are available and confirm the importance of sector coupling for achieving the Swiss climate targets.

Task 4.1

Title

Risk, safety and societal acceptance

Projects (presented on the following pages)

Induced seismicity risk analysis of the planned geothermal hydraulic stimulation in Geldinganes, Iceland
M. Broccardo, F. Grigoli, D. Karvounis, A. Mignan, A.P. Rinaldi, L. Danciu, S. Wiemer

Risk Assessment of Accidents in the Energy Sector for Selected Long-Term Scenarios
P. Burgherr, M. Spada, L. Vandepaer, A. Kalinina, W. Kim, P. Lustenberger

Geothermal Exploration Chance Of Success
L. Guglielmetti, L. Perozzi, A. Moscariello, F. Martin, M. Meyer, C. Nawratil De Bono

Public perception of hydrogen technologies combined with CCS in Switzerland
Lisa Hämmerli, Michael Stauffacher

The spatial diffusion of solar PV in Switzerland: an interdisciplinary approach
Léon F. Hirt, Marlyne Sahakian, Evelina Trutnevyte

Uncertainty quantification and global sensitivity analysis in life loss estimates due to an instantaneous dam-break
Anna Kalinina, Matteo Spada, Peter Burgherr, Christopher T. Robinson

A tool to visualize different participation formats
Franziska Ruef, Michael Stauffacher, Olivier Ejderyan

Quantitative risk assessment for Deep Geothermal Energy (DGE) systems in Switzerland
Matteo Spada, Peter Burgherr

Using GIS to discuss place factors for CCS projects siting
Juanita von Rothkirch, Olivier Ejderyan, Michael Stauffacher

SCCER SoE
SWISS COMPETENCE CENTER for ENERGY RESEARCH
SUPPLY of ELECTRICITY

SCCER-SoE Annual Conference 2019

Schweizerischer Erdbebendienst
Service Sismologique Suisse
Servizio Sismico Svizzero
Swiss Seismological Service

ETH
Eidgenössische Technische Hochschule Zürich
Swiss Federal Institute of Technology Zurich

Supported by:
Schweizerische Eidgenossenschaft
Confédération suisse
Confederazione Svizzera
Confederaziun svizra
Swiss Confederation
Innosuisse – Swiss Innovation Agency

Induced seismicity risk analysis of the planned geothermal hydraulic stimulation in Geldinganes, Iceland

M. Broccardo, F. Grigoli, D. Karvounis, A. Mignan, A.P. Rinaldi, L. Danciu, S. Wiemer

Motivation

The rapid increase of energy demand in Reykjavik has posed the need for additional supply of geothermal energy. The deep hydraulic (re-)stimulation of the well RV-43 in the peninsula of Geldinganes (north of Reykjavik) is an essential component of the plan implemented by Reykjavik Energy to increase the geothermal supply of energy. Hydraulic stimulation are often associated with fluid-induced seismicity, which can cause damage to the nearby building stock and nuisance to population. This study presents a pre-drilling preliminary probabilistic induced-seismic hazard and risk analysis for the site of interest. The induced-seismic hazard and risk analyses are based on a fully probabilistic framework, with focus on inherent epistemic and aleatory variability. We provide full probabilistically estimated of peak ground accelerations, European Microseismicity intensity, damage, and individual risk for the area of interest.

Site description and planned operations

The well RV-43 is located in the Geldinganes geothermal field in the northeastern part of the city of Reykjavik, Figure 1. Reykjavik Energy (OR) is the main supplier of heat in Reykjavik and has drilled several wells in Geldinganes. OR aims producing hot water from RV-43 to be directly utilized for heating purposes and to meet the increasing energy needs of Reykjavik. RV-43 was drilled in 2001, it is 1832 m long, where the deeper 924 m long are uncased (8½ inches open hole). The well is oriented towards the northeaster of Geldinganes, an area speculated to be exceptionally warm, since it is closer than the rest of the Geldingane's wells to the extinct central volcanic system north of Reykjavik.The locations of both Geldinganes, its wells, its shallow temperature gradient and RV-43 are shown in Figure 1.

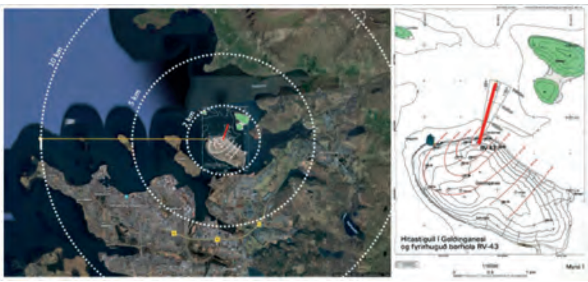

Figure 1 Map view of the Geldinganes island in Reykjavik. On the right, the Geldinganes area is plotted with all its wells, the temperature gradients measured at shallow depths and with the solid red line representing RV-43 at different measured depths (figures extracted from OR's report for the drilling of RV-43).

Probabilistic fluid-induced seismicity seismic hazard and risk analysis in a nutshell

- Classical PSHA analysis, Intensity measures PGA, and EMS-98 scale
- Sources: fixed point source at injection points (data driven, S1) and *Karvounis et al.* physical based model (synthetic catalogue, S2)
- Frequency-magnitude distribution: Truncated Gutenberg Richter
- Epistemic Uncertainties, logic tree (Figure 2): 2 rate models, 7 Ground Motion Predictive Equations (GMPE), 2 Ground Motion Intensity Conversion Equation (GMICE). Number of brunches 120
- Results Hazard curves Figure 3 show larger uncertainty for data driven source model
- Risk computation computed as classical convolution of hazard vulnerability and exposure
- Output Individual Risk (IR), and Damage Risk (DR)
    - IR is defined as frequency at which a statistically person is expected to experience death or a given level of injury
    - DR is defined as frequency at which a statistically average building class is expected to experience light non-structural damage
- Vulnerability models: Macroseismic intensity approach for IR and local mechanical fragility function for DR
- IR threshold 10^{-6} (one micromort), DR threshold 10^{-2}. Figure 4 and 5
- Results of the a-priory risk analysis shows IR and DR bellow the safety limits.
- It is mandatory to update hazard and risk computations during stimulation

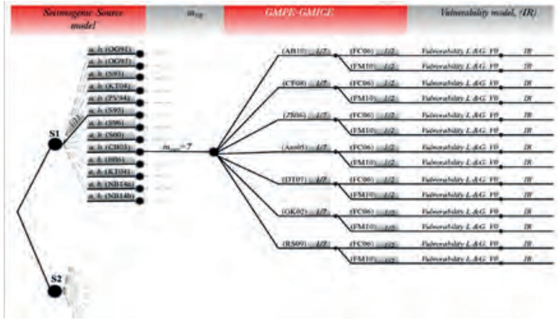

Figure 2 Full logic tree for hazard and risk computation

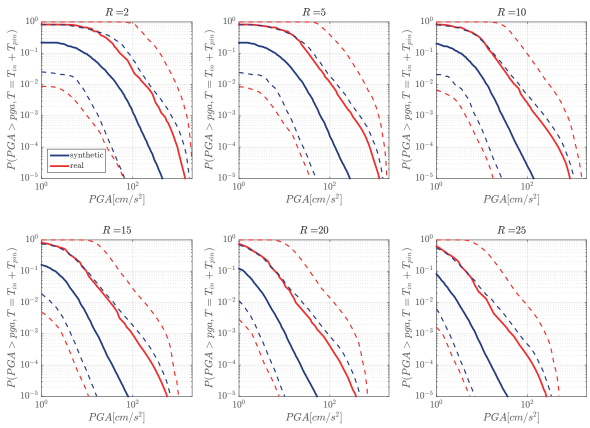

Figure 3 PSHA analysis comparison between source model S1 (Data driven) and S2 (synthetic catalogue). Solid lines: medians; dashed lines 10% and 90% quantiles.

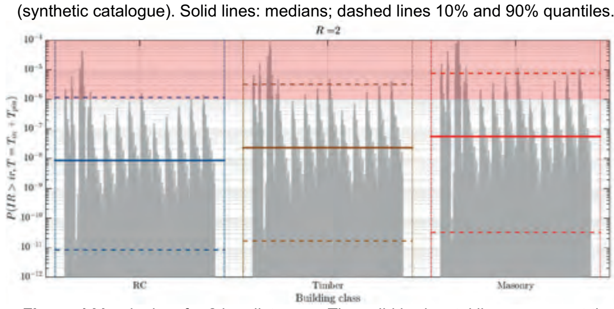

Figure 4 Marginal $\boldsymbol{IR}$ for 2 km distances. The solid horizontal lines represent the weighted median values of the vertical gray lines. The dashed horizontal lines represent the 10 and 90% epistemic quantiles.

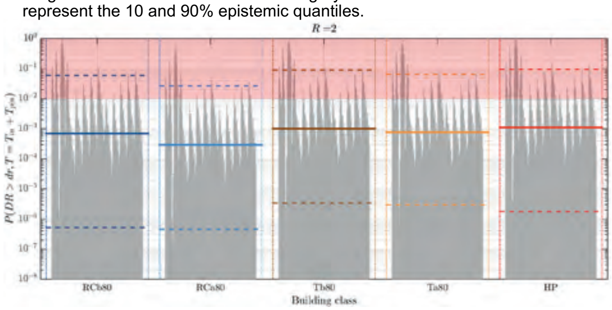

Figure 5 Marginal $\boldsymbol{IR}$ for 2 km distances. The solid horizontal lines represent the weighted median values of the vertical gray lines. The dashed horizontal lines represent the 10 and 90% epistemic quantiles.

References

Broccardo et al. (2019). *A-priori seismic risk study for the stimulation of well RV-43 in Geldinganes, Iceland.* Internal risk report

SCCER SoE

SWISS COMPETENCE CENTER for ENERGY RESEARCH SUPPLY of ELECTRICITY

PAUL SCHERRER INSTITUT PSI

(FRS) FUTURE RESILIENT SYSTEMS 未来韧性系统

SCCER-SoE Annual Conference 2019

Risk Assessment of Accidents in the Energy Sector for Selected Long-Term Scenarios

P. Burgherr[1], M. Spada[1], L. Vandepaer[1,3], A. Kalinina[1], W. Kim[2], P. Lustenberger[2]

[1]Laboratory for Energy Systems Analysis (LEA), Paul Scherrer Institut, Villigen PSI, Switzerland

[2]Future Resilient Systems (FRS) , Singapore-ETH Centre, Singapore, [3]Sherbrooke University, Sherbrooke, Québec, Canada.

Supported by:

Schweizerische Eidgenossenschaft
Confédération suisse
Confederazione Svizzera
Confederaziun svizra

Swiss Confederation

Innosuisse – Swiss Innovation Agency

UNIVERSITÉ DE SHERBROOKE

Introduction

The comparative risk assessment of accidents in the energy sector is well established to evaluate the performance of technologies [1]. In recent years, it has become an essential component within the broader concepts of sustainability, energy security and resilience [2].

This study focuses on how the overall accident risk of a country's electricity supply mix is affected by long-term energy projections like the World Energy Outlook (WEO) scenarios [3]. It includes several novel elements: (1) average and marginal electricity supply mixes for today and 2030; (2) updated accident risk indicators until 2016; and (3) coverage of 11 country groups / countries (three shown here).

PSI's ENSAD Database

The Energy-related Severe Accident Database (ENSAD) comprises a comprehensive global coverage of full energy chains, and focuses on severe accidents (e.g. ≥5 fatalities) that are a major concern to industry, authorities and the public. Recently, it has been transformed in a spatial database with comprehensive GIS functionality, running on a Platform as a Service (PaaS) cloud environment [4].

Normalized fatality risk indicators were calculated for fossil energy chains (coal, oil, natural gas), hydropower, nuclear power and new renewable technologies. Figure 1 shows fatality rates per energy chain and country group (i.e. OECD, EU28, non-OECD). Generally, OECD and EU28 countries perform better than non-OECD for fossil and hydropower energy chains. Compared to the 1990s, the Chinese coal chain is only slightly higher than the rest of non-OECD. Hydropower is most deadly in non-OECD countries, but the difference becomes substantially smaller if the most extreme dam failure in China (Banqiao/Shimantan, 1975, 26'000 fatalities) is excluded. For nuclear, fatality rates are among the lowest, particularly for the new generation III reactors. Finally, new renewables have clearly lower fatality rates than fossil chains (except biogas).

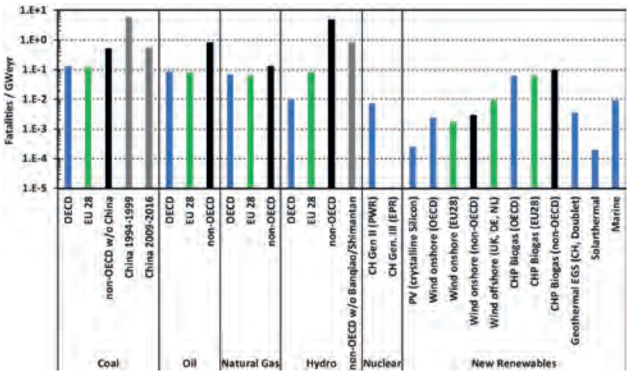

Figure 1: Severe (≥5 fatalities) fatality rates for fossil, hydro, nuclear and new renewables in OECD, EU28 and non-OECD countries for the period 1970-2016. PWR: Pressurized Water Reactor, EPR: European Pressurized Reactor, CHP: Combined Heat and Power, EGS: Enhanced Geothermal Systems.

Risk Indicators in Long-Term Scenario Modeling

Three core scenarios from the WEO were considered [3]:

- **Current Policies Scenario** (CPS) takes into account only those policies and measures that are confirmed and legally consolidated.
- **New Policies Scenario** (NPS) illustrates the general direction in which the most recent policy ambitions could lead the energy sector.
- **Sustainable Development Scenario** (SDS) is fully aligned with the goal of the Paris Agreement to keep global average temperature rise well below 2 °C above pre-industrial levels.

The current mix (2017) for each scenario is compared against the corresponding 2030 average (attributional) electricity mixes, and the 2017 and 2030 marginal (consequential) mixes (see [5] for details). Fatality rates for 2030 were approximated using data for the period 1990-2016 as presented in [6].

Figure 2 shows the overall accident risk for the current and future average and marginal electricity supply mixes per scenario for OECD, EU28 and non-OECD countries. The former two country groups clearly perform better, but all three groups exhibit a similar pattern: (1) overall accident risk becomes smaller for scenarios with increasingly ambitious climate targets; (2) improvements become larger for 2030 compared to 2017; (3) the overall accident risk is consistently lower for the marginal mix than the corresponding average mix, indicating that renewable technologies increasingly replace large, centralized power plants, especially coal and to a large extent also natural gas.

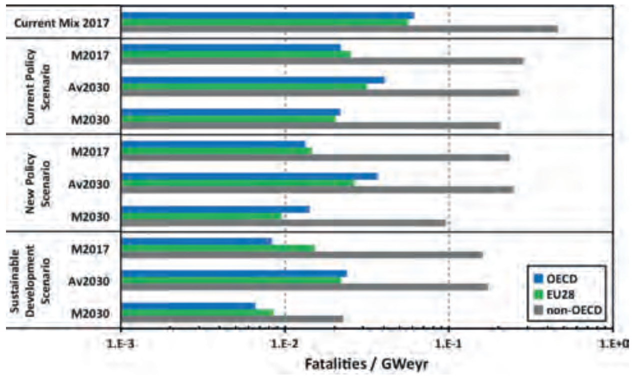

Figure 2: Overall accident risk for the current mix (2017) and scenario-specific average (Av) and marginal (M) electricity supply mixes in 2017 and 2030 for OECD, EU28 and non-OECD.

Conclusions

Among centralized, large-scale technologies, fossil energy carriers have the highest fatality rates, whereas hydro and nuclear perform best in industrialized countries. Decentralized, new renewables are less sensitive to the issue of severe accidents, and geothermal is clearly better than natural gas and biogas.

The implementation of more stringent climate policies often leads to a reduced overall accident risk as exemplified by the current scenario analysis. Furthermore, results showed the impact of the increasing penetration of new renewables on the average electricity supply mixes, but also reflected their growing importance for marginal mixes, replacing particularly coal and to a lesser extent natural gas until 2030, which further reduces overall accident risks.

Acknowledgements

This work has been carried out within the **Swiss Competence Center for Energy Research (SCCER) – Supply of Electricity** (concept, data management and scenario analysis), and the **Future Resilient Systems (FRS) program** of the Singapore-ETH Centre (SEC) (database development and implementation).

References

[1] Burgherr, P., Hirschberg, S. (2014) Comparative risk assessment of severe accidents in the energy sector. Energy Policy, 74, S45-S56.

[2] Gasser, P., Lustenberger, P., Cinelli, M., Kim, W., Spada, M., Burgherr, P., Hirschberg, S., Stojadinovic, B., Sun, T.J. (2019) A review on resilience assessment of energy systems. Sustainable and Resilient Infrastructure 1-27.

[3] International Energy Agency (2018) World Energy Outlook 2018. Paris, France: IEA.

[4] Kim, W., Burgherr, P., Spada, M., Lustenberger, P., Kalinina, A., Hirschberg, S. (2019) Energy-related Severe Accident Database (ENSAD): cloud-based geospatial platform. Big Earth Data 2(4), 368-394.

[5] Vandepaer, L., Treyer, K., Mutel, C., Bauer, C., Amor, B. (2019) The integration of long-term marginal electricity supply mixes in the ecoinvent consequential database version 3.4 and examination of modeling choices. The International Journal of Life Cycle Assessment, 24, 1409-1428.

[6] Burgherr, P., Spada, M., Kalinina, A., Vandepaer, L., Lustenberger, P., Kim, W. (2019) Comparative risk assessment of accidents in the energy sector within different long-term scenarios and marginal electricity supply mixes. Proceedings of the 29th European Safety and Reliability Conference (ESREL), Hannover, Germany.

GECOS

Geothermal Exploration Chance Of Success

Supported by:
Schweizerische Eidgenossenschaft
Confédération suisse
Confederazione Svizzera
Confederaziun svizra
Swiss Confederation
Innosuisse – Swiss Innovation Agency

UNCERTAINTY REDUCTION

Acquisition of cost-effective, quick and high resolution geophysical data such as 3D DAS VSP, S-waves seismic and high resolution gravity can help to improve the understanding of the subsurface.

RISK MITIGATION

Stochastic and machine learning approach are perfectly shaped to integrate and analyse different types of geodata to mitigate the risk of developing geothermal project projects.

EXPLORATION COST REDUCTION

High-resolution acquisition and integration of data from different sources using machine learning allow improving the probability of success of new geothermal projects.

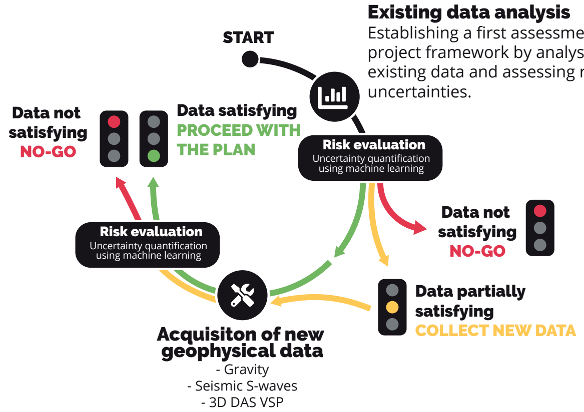

GECOS WORKFLOW

This workflow can be replicated at any stage of a geothermal project. From the early stages when only scarce data are available, during exploration when new data will be collected and when large new investments (i.e. 3D seismic and drilling) need to be planned, and during production to monitor the reservoir and eventually design new drilling operations. Predictive machine learning models are updated as far as new data are available.

Gravity Data

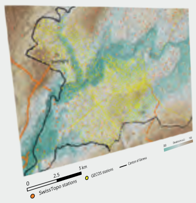

Location of the survey area and the Gravimetric Atlas of Switzerland stations and the stations collected in the framework of the GECOS project. The survey was carried in 71 days adopting an approach aimed at optimizing at most the quality and the time of the acquisition. This was achieved by running cycles between control stations and by using the Geneva Canton cadastral points as reference for the coordinates XY of each station and the DPGS or the Geneva Canton LiDAR DTM for the Z coordinate.

One objective of the new acquisition campaign is to improve the knowledge of the subsurface density and better quantify its uncertainty. Starting from a gravity survey, we are able to produce a map of the complete Bouguer anomaly (CBA) that is a result of an interpolation of the observed anomaly at each survey location. However, since the distribution of the acquisitions stations could be more or less dense, we need to quantify the uncertainty related to the resulting interpolated map realizations.

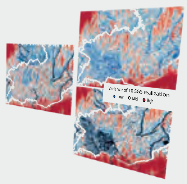

For this purpose, we propose a stochastic approach to produce several sequential Gaussian simulation of the CBA over the studied area, before and after the new gravimetric acquisition. First order statistics are then applied to estimate the variance at each pixel of the interpolated grid to evaluate uncertainty of the resulting interpolated map. Adding the new GECOS stations allowed to reduce the uncertainty on the CBA map.

3D density model resulting after inversion processing. The inversion processing allows to reconstruct the density distribution in the subsurface according to gravity data observed on the field. The GM-SYS 3D toolset in Geosoft Oasis Montaj was used in this task. The inversion processing can provide accurate results when geometrical constraints (i.e. from a 3D geological model) and/or density data for the lithology of interest are available, therefore reducing the uncertainty of the resulting density model

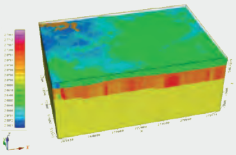

Machine learning on seismic en borehole data

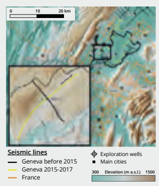

About 200 km of 2D seismic lines are available over the Geneva Basin, corresponding principally to 4 acquisition campaigns undertaken from 1987 to 2015, as well as a selection of unitary lines issued from earlier acquisition campaigns (1972-1977) to complete the seismic dataset toward the Northeast of the studied area.

Two time-migrated, 2D seismic reflection profiles intersecting the well GEo-01 have been retained to apply the proposed methodology, highlighted in the bottom left box of the left figure. Lines GG87-02 and SIG 2015-L08 are oriented NW-SE and NE-SW, covering approximately a distance of 4630 m and 8039 m, with a trace spacing of 15 m and 10 m respectively. Vertically, the profiles were recorded down to 4000 ms and 2000 ms respectively.

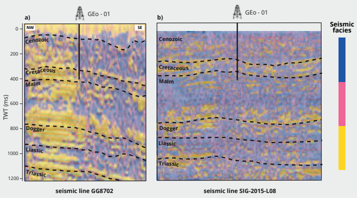

Machine learning allows classifying the seismic data into 3 facies that can be interpreted as unfractured intervals zone (yellow facies), especially visible in the left part of the GG8702 section; a likely occurrence of fractures zone (blue facies), which cover the most of the seismic line SIG-2015-L08 and a region of likely occurrence of fractures and small offset faults (pink facies).

Automatic classification of facies in GEo-01 well, using a K-means algorithm that allows to identify similar group of clusters (or facies) within a dataset of different wireline logs measurements. Figure (a) shows the 14 the geophysical logs used with the proposed approach, figure (b) shows the result of K-means algorithm with the number of clusters fixed to 7 for the lithofacies classification compared to the original litholog (c).

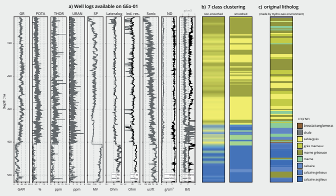

Geophysics for Geology
Dupuy D
Métraux V
Mijic G
Radogna PV

GE-RGBA
GEOENERGY RESERVOIR GEOLOGY AND BASIN ANALYSIS GROUP
Guglielmetti L
Perozzi L
Moscariello A

UNIVERSITÉ DE GENÈVE
FACULTY OF SCIENCES
Department of Earth Sciences

Martin F
Meyer M
Nawratil De Bono C
SIG

The present study is part of GECOS (Geothermal Exploration Chance Of Success), a project (no. 26728.1 PFIW-IW) co-funded by INNOSUISSE and by Services Industriels de Genève and GEO2X SA.

SCCER SoE
SWISS COMPETENCE CENTER for ENERGY RESEARCH
SUPPLY of ELECTRICITY

SCCER-SoE Annual Conference 2019

Supported by:
Schweizerische Eidgenossenschaft
Confédération suisse
Confederazione Svizzera
Confederaziun svizra

Swiss Confederation

Innosuisse – Swiss Innovation Agency

Public perception of hydrogen technologies combined with CCS in Switzerland

Lisa Hämmerli, Michael Stauffacher

Limiting global warming and technology perception

- A majority of the climate scenarios considers negative emission technologies (NET) to reach a long-term climate stabilization under 2°C (Fuss et al., 2014)
- Bioenergy with carbon capture and storage (BECCS) is a NET
- There are few economic driver for the commercial deployment of carbon capture and storage (CCS). The introduction of hydrogen (H_2) as a low-carbon fuel for transport, industrial processes, heating and cooling could be a driver for the development of CCS or BECCS.

→ **How does the public perceive the options fossil fuel to H_2 and biogas to H_2 with carbon storage in Switzerland, abroad or no storage?**

→ **Is CCS more accepted when it is used in combination with hydrogen for the mobility sector?**

Quantitative Online Survey (N = 923)

- April to May 2019, quota on gender & age
- Audience segmentation: climate change view
- Vignettes design study

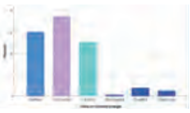

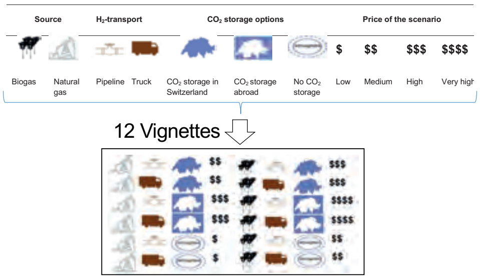

Results

- Subjective knowledge of hydrogen and CCS (N = 923)

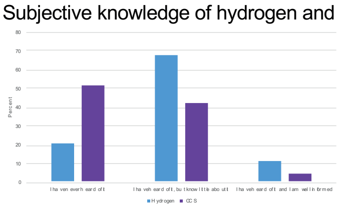

- Affective perception of different end-use options

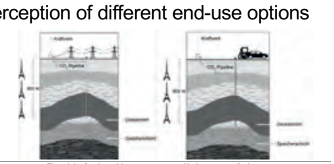

Affective perception (1 = very negative to 7 = very positive)	Electricity for the grid Mean value (SE)	Hydrogen as a fuel Mean value (SE)
Biogas	4.41 (.064)	4.40 (.065)
Natural gas	4.16 (.060)	4.14 (.065)

- Preferences of the vignettes

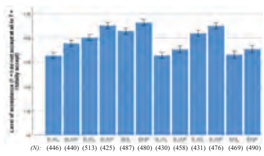

Legend of vignette labels:

B = Biogas
J = CO_2 storage
A = Storage abroad
S = Storage in Switzerland
L = Truck
P = Pipeline
E = Natural gas
N = No storage

1. *Biogas without CO_2 storage & H_2 transportation via pipeline*
2. *Biogas with CO_2 storage in Switzerland & H_2 transportation via pipeline*
3. *Natural gas with CO_2 storage in Switzerland & H_2 transportation via pipeline*

- Perception regarding storage

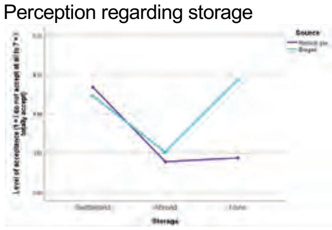

- Climate change view on different emission options

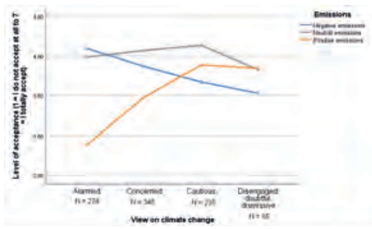

- Affect of h-mobility and e-mobility

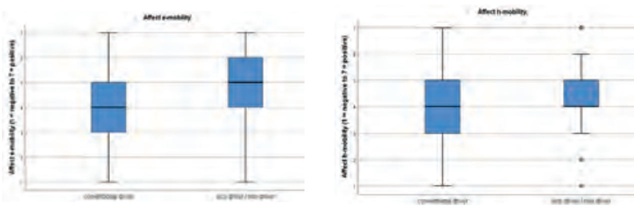

Summary and Discussion

- Affective response to hydrogen is more positive than to CCS.
- Affective response to both end-uses (hydrogen in the mobility sector or electricity for the grid) is similar.
- To accept negative emission technologies (BECCS in this case), you need to be alarmed by climate change.
- The study showed no clear preference towards scenarios with negative emissions.
- There is a significant preference of pipelines over transport by trucks. But rresults from Wallquist et al. (2012) suggest, that options without pipeline are preferred over options with a (CO_2) pipeline.
- There is a preference towards storing CO_2 in Switzerland compared with storing options abroad. There is also a clear preference using biogas in comparison with natural gas.
- There is no significant difference in the perception of h-mobility between conventional drivers and eco- and non-drivers.

References

Chryst, B., Marlon, J., van der Linden, S., Leiserowitz, A., Maibach, E., & Roser-Renouf, C. (2018). Global warming's "six americas short survey": Audience segmentation of climate change views using a four question instrument. *Environmental Communication*, 12(8), 1109-1122.

Fuss, S., Canadell, J. G., Peters, G. P., Tavoni, M., Andrew, R. M., Ciais, P., Jackson, R. B., Jones, C. D., Kraxner, F., Nakicenovic, N., Le Quéré, C., et al. (2014). Betting on negative emissions. *Nature Climate Change*, 4, 850.

Wallquist, L., L'Orange Seigo, S., Visschers, V. H. M., & Siegrist, M. (2012). Public acceptance of CCS system elements: A conjoint measurement. *International Journal of Greenhouse Gas Control*, 6, 77-83.

UNIVERSITÉ DE GENÈVE
INSTITUT DES SCIENCES DE L'ENVIRONNEMENT

UNIGE RES

The spatial diffusion of solar PV in Switzerland:
an interdisciplinary approach

Léon F. Hirt[1], Marlyne Sahakian[2], Evelina Trutnevyte[1]

[1]Renewable Energy Systems group, Faculty of Science, Department F.-A. Forel for Environmental and Aquatic Sciences, Institute for Environmental Sciences, University of Geneva, Switzerland
[2]Institute of Sociological Research (IRS), Institute for Environmental Sciences (ISE), University of Geneva, Switzerland

INTRODUCTION

Solar photovoltaic (PV) systems and spatial technology diffusion approaches

Switzerland is seeking to increase its share of renewable electricity to meet its Energy Strategy 2050 targets. Due to its high technical potential, solar PV could have an important role to play [1, 2, 3]. Cumulative installed capacity of solar PV has been increasing in the last decade (Fig. 1), but in a spatially uneven way (Fig. 2 and 3) [1, 2]. Therefore, a better understanding of how solar PV diffused in the past could help define measures to increase the uptake of this technology.

The literature on solar PV diffusion has focused on finding quantitative socio-technical/economic variables (e.g. feed-in tariffs) to predict the uptake of solar PV, whereas theoretical frameworks have only rarely been used [4]. Transitions studies more broadly have studied transitions using theoretical frameworks [5,6] but they were only rarely quantified [7].

Aim and approach

Our overall aim is to contribute to a better retrospective understanding of solar PV diffusion in Switzerland by linking the *Multi-level perspective (MLP)* on socio-technical transitions framework [5, 6] with quantitative indicators (n=36, e.g. population density). More specially, we aim to gain a better understanding of the spatial diffusion of solar PV which may contribute to helping Switzerland meet its energy targets.

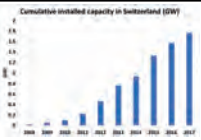

Figure 1. *Cumulative installed capacity in Switzerland (GW). Temporal perspective. Source: own analysis of the Pronovo dataset of registered solar PV projects [8]*

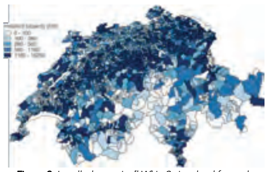

Figure 2. *Installed capacity [kW] in Switzerland for each municipality in 2017. Source: own analysis of the Pronovo dataset of registered solar PV projects [8]*

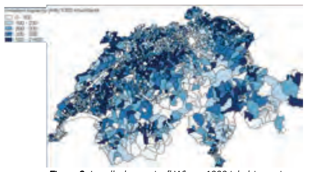

Figure 3. *Installed capacity [kW] per 1000 inhabitants in Switzerland for each municipality in 2017. Source: own analysis of the Pronovo dataset of registered solar PV projects [8]*

METHODOLOGY

The *Multi-level perspective (MLP)*

The MLP framework is a heuristic tool to study long-term socio-technical transitions. A transition is conceptualised as the destabilisation of a socio-technical regime, triggered by interactions between 3 hierarchical levels: a *Landscape* level (macro), a *socio-technical regime* level (meso) and a *niche-innovation* level (micro) level [5, 6] (Fig.3). The MLP has predominantly been used to study transitions at the national level [9]; here, we apply it to the municipality scale (N=2212) and focus on the regime level. Broadly speaking, a regime can be defined as the rules and regulations embedded in institutions and infrastructures which characterize a society's trajectory.

Theory and quantitative indicators

We selected quantitative indicators (n=36) based on the literature on solar PV uptake and the MLP framework (Fig. 3). We aimed to select indicators that quantitatively describe regimes of municipalities.

Statistical methods

We use a dataset of PV systems in Switzerland (includes projects e.g. that received federal subsidies, are on a waiting list; M=76'587). We used *cluster analysis* and *principal component analysis (PCA)* to identify and analyse clusters of municipalities which have similar regimes. We statistically described the growth of solar PV in each of these clusters and linked the findings to broader qualitative insights from the MLP framework.

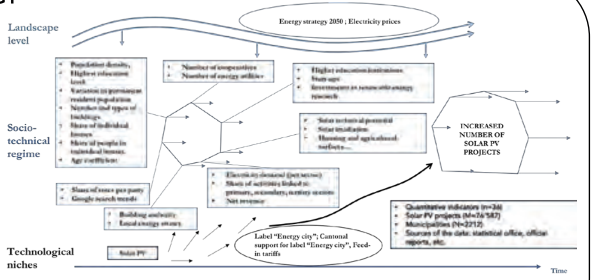

Figure 3. *The MLP framework is used to explore solar PV uptake in Switzerland. Quantitative indicators are defined based on the theory of the MLP [5, 6] and the existing literature on solar PV uptake (see examples of indicators in blue boxes). Indicators have municipality-level resolution and are chosen as to identify different socio-technical regimes across Switzerland.*

PRELIMINARY RESULTS

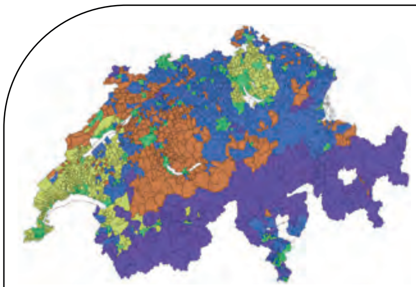

Figure 4. *Using the MLP and quantitative indicators, we did cluster analysis and PCA and identified five main clusters of regime configurations in Switzerland. Cluster of municipalities names: see legend.*

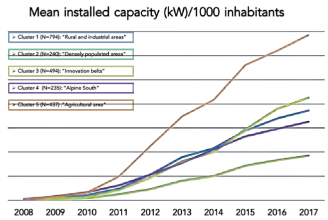

Figure 5. *Growth of solar PV in each cluster measured here using the mean installed capacity (kW) per 1000 inhabitants. Cluster of municipalities names: see legend.*

"Regimes" across Switzerland

- At least 5 main types of different regimes across Switzerland were identified (Fig. 3) . For example, a higher share of agricultural and primary sector activities (values above the national average) characterize cluster 5 (orange).
- Growth rates of solar PV are different between clusters: the mean installed capacity per capita is highest in cluster 5 (orange, "Agricultural activities") and lowest in cluster 2 (blue, "Densely populated areas") (Fig. 5). The 3 remaining clusters have similar growth rates (Fig. 5). We obtained similar results using other metrics (e.g. number of projects per capita).

Analysis of clusters of municipalities with similar regimes

- We identify outliers (municipalities) in most clusters that drive the growth of solar PV. For example, in cluster 5 (orange, "Agricultural activities"), 27 municipalities show a faster growth of solar PV (Fig. 6, 7 and 8).
- The 27 municipalities show in particular, a higher electricity demand than the other municipalities in the same cluster, stemming from the agricultural activities. Similar results (i.e. a small number of municipalities driving solar PV growth) are found in other clusters.
- Further analysis should determine whether these municipalities are front-runners or perhaps benefited from more favourable conditions facilitating PV growth.

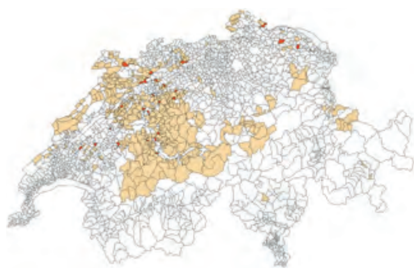

Figure 6. *In-depth analysis of each cluster identified in Fig. 4. Here, the example of cluster 5 (N=437, "Agricultural area"). Twenty-seven municipalities (red) were identified as outliers and show faster-growing solar PV in terms of installed capacity (kW) per capita.*

Installed capacity (kW)/1000 inhabitants, N=410

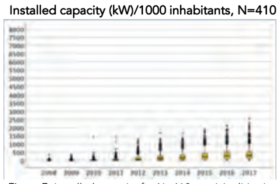

Figure 7. *Installed capacity for N=410 municipalities in cluster 5 (see Fig. 6).*

Installed capacity (kW)/1000 inhabitants, N=27

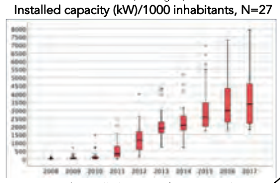

Figure 8. *Installed capacity for N=27 outlier municipalities in cluster 5 (see Fig. 6).*

Summary

We carried out a spatial analysis of solar PV uptake in Switzerland :

- In terms solar PV diffusion, we find that specific regimes may influence solar PV uptake.
- In terms of methodological findings, we suggest that an MLP analysis may be refined using quantitative methods by providing more quantitative context-driven indications. Correspondingly, we can place quantitative analysis into a broader context using the MLP.
- Finally, our results may potentially provide helpful insights to local governments to elaborate tailored policies for solar PV diffusion according to the dominant regime identified in their area.

References

[[1] Carattini, S., Péclat, M., Baranzini, A., 2018. Social interactions and the adoption of solar PV: evidence from cultural borders (No. 339/305). Centre for Climate Change Economics and Policy Working Paper 339/Grantham Research Institute on Climate Change and the Environment Working Paper 305. London: London School of Economics and Political Science.
[2] Thormeyer, C., Sasse, J.-P., Trutnevyte, E., 2020. Spatially-explicit models should consider real-world diffusion of renewable electricity: Solar PV example in Switzerland. Renew. Energy 145, 363–374. https://doi.org/10.1016/J.RENENE.2019.06.017
[3] Bundesamt für Energie (BFE), 2019. Sonnendach.ch und Sonnenfassade.ch: Berechnung von Potenzialen in Gemeinden. Ittigen: Switzerland.
[4] Ford, R., Walton, S., Stephenson, J., Rees, D., Scott, M., King, G., Williams, J., Wooliscroft, B., 2017. Emerging energy transitions: PV uptake beyond subsidies. Technol. Forecast. Soc. Change 117, 138–150. https://doi.org/10.1016/J.TECHFORE.2016.12.007
[5] Geels, F.W., Schot, J., 2007. Typology of sociotechnical transition pathways. Res. Policy 36, 399–417. https://doi.org/10.1016/j.respol.2007.01.003
[6] Geels, F.W., 2002. Technological transitions as evolutionary reconfiguration processes: a multi-level perspective and a case-study. Res. Policy 31, 1257–1274. https://doi.org/10.1016/S0048-7333(02)00062-8
[7] Bento, N., Wilson, C., Anadon, L.D., 2018. Time to get ready: Conceptualizing the temporal and spatial dynamics of formative phases for energy technologies. Energy Policy 119, 282–293. https://doi.org/10.1016/J.ENPOL.2018.04.015
[8[Pronovo (2019), Repository of solar PV projects in Switzerland, electronic dataset. Frick, Switzerland.
[9] Hirt, L. F., Schell, G., Sahakian, M., Trutnevyte, E., 2019. Working towards energy and climate solutions: Insights from a systematic review on linking models and socio-technical transitions theories. Environ. Innov. Soc. Transitions. *Under review.*

SCCER-SoE Annual Conference 2019

SWISS COMPETENCE CENTER for ENERGY RESEARCH
SUPPLY of ELECTRICITY

Energy Turnaround
National Research Programme

PAUL SCHERRER INSTITUT

Supported by:

Schweizerische Eidgenossenschaft
Confédération suisse
Confederazione Svizzera
Confederaziun svizra

Swiss Confederation

Innosuisse – Swiss Innovation Agency

Uncertainty quantification and global sensitivity analysis in life loss estimates due to an instantaneous dam-break

Anna Kalinina[1], Matteo Spada[1], Peter Burgherr[1] & Christopher T. Robinson[2]

[1]Technology Assessment Group, Paul Scherrer Institut, Villigen PSI, Switzerland;
[2] Department of Aquatic Ecology, Eawag, Dübendorf, Switzerland

Research objectives

1. Application of the HEC-LIFESim life-loss (LL) modeling software to a case study with conditions relevant for Switzerland;
2. Application of metamodeling for quantification of uncertainties in the estimation of life loss provided by HEC-LIFESim;
3. Global analysis of the model sensitivities.

Framework for uncertainty quantification (UQ) & global sensitivity analysis (GSA)

Modeled input uncertainty is propagated through the surrogate model created using Polynomial Chaos Expansion (PCE) (Figure 1):

$$M^{PCE} \stackrel{\text{def}}{=} \sum_{\alpha \in N^M} y_\alpha \Psi_\alpha (X_j)$$

M^{PCE}: PCE response, X_i: input vector, y_α: coefficient, Ψ_α: polynomials.

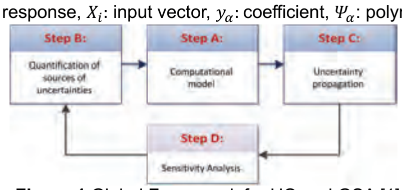

Figure 1 Global Framework for UQ and GSA [1]

Global Sensitivity Analysis is performed in this study by calculating two indices for comparative reasons:

- Sobol' indices, S_i, define individual contributions of each model input to the total variance D. Sobol' indices are calculated from the coefficients of the PCE-metamodel [2], such that:

$$S_i = \sum_{\alpha \in A_i} y_\alpha^2 / D,\ A_i = \{\alpha \in N^M\colon \alpha_i > 0, \alpha_{j \neq i} = 0\}$$

- Borgonovo index [3], δ_i, which is a measure of the expected shift in the probability distribution of the model output when a random input variable X_i is set to a fixed value. If the expected shift is close to zero, then the variable is not important, otherwise for more important variables it takes a larger value:

$$\delta_i = \frac{1}{2} E_{X_i}\left[\int \left| f_Y - f_{Y|X_i} \right| dy\right]$$

Where f_Y is the probability distribution of the model output and $f_{Y|X_i}$ is the conditional distribution of X_i.

Step A: Computational model

The HEC-LIFESim software [4] is a spatial dynamic system for modeling LL of a flood event. It is a modular system consisting of four modules (Red boxes in Figure 2). These modules are built around databases and exchange data through geo-layers. HEC-LIFESim estimates the number of LL by redistributing the initial Population At Risk (PAR), i.e., the number of people living in the inundated area, based on different information, e.g. flood severity, warnings, etc..

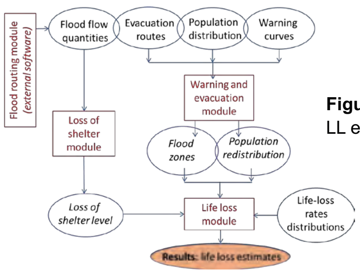

Figure 2 HEC-LIFESim approach for LL estimation (modified from [5])

In this study, the LL is estimated for a generic locality downstream of a large concrete arch dam over 100 m height located in Switzerland.

Step B: Marginal distributions for uncertain model inputs

Parameter	Name	Unit
	Inhabited locality	
P_{tot}	Total population	[people]
P_{o65}	Population over 65	[fraction]
H	Building foundation height	[m]
	Flood and Warning process	
F_{chance}	Fatality rate in the chance zone	[fraction]
F_{compr}	Fatality rate in the compromised zone	[fraction]
T_{hcd}	Hazard communication delay	[hour]
T_{wid}	Warning issuance delay	[hour]

Table 1 The marginal distributions modeled in this study for the Swiss case used as input for the metamodel

Swiss Data on demographics (P_{tot}, P_{o65}), structural inventory (H), etc. collected from [6-8], data on Warning issuance delay (T_{wid}) provided by [9] and Swiss specific fatality rates (F_{chance}, F_{compr}) estimated in [10].

Step C: Example results for uncertainty propagation

PCE of different degrees are built on the experimental design of 550 samples for the parameter of the model output for 6 different scenarios, based on 3 different flood inflow severity and 2 times in a day (2 a.m. and 2 p.m.) (Figure 3).

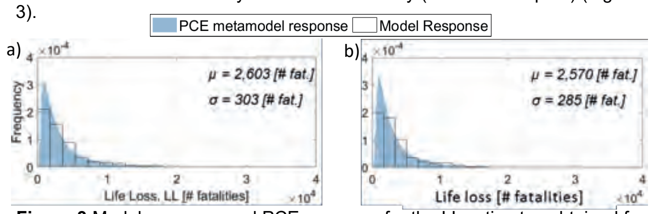

Figure 3 Model response and PCE response for the LL estimates obtained for two selected scenarios. a) daytime – mean flood inflow; b) nighttime – mean flood inflow

Step D: Example results for global sensitivity analysis

Sobol' and Borgonovo indices indicate that the total population, the fatality rate in the chance zone and the warning issuance delay contributed most to the variability of the model output for both day and nighttime (Figure 4). Discrepancies between Sobol' and Borgonovo indices (e.g. T_{hcd}) are related to the fact that the latter provides a relative ranking with respect to the most important parameter (P_{tot}), while Sobol' indices provide absolute values.

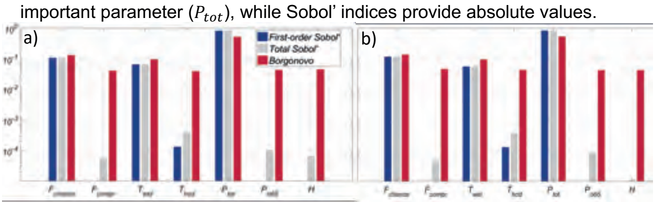

Figure 4 Results for global sensitivity for the LL estimates obtained for two selected scenarios. a) daytime – mean flood inflow; b) nighttime – mean flood inflow

Conclusions

- The applied metamodeling approach is in good agreement with the physical model;
- Application of the constructed metamodel enables reducing computational effort with respect to, for example, Monte Carlo approaches;
- Global sensitivity analysis can help to understand how the variability of each model input affected variability of the LL-estimates;
- The constructed metamodel can support inform ed risk management and reliability-based design for typical Swiss hydropower dams.

Acknowledgements

This research project is part of the National Research Programme "Energy Turnaround" (NRP 70) of the Swiss National Science Foundation (SNSF). Further information on the National Research Programme can be found at www.nrp70.ch. It is also integrated with the activities of the Swiss Competence Center on Energy Research – Supply of Electricity (SCCER SoE). The authors express their sincere thanks to Prof. Dr. Bruno Sudret and Dr. Stefano Marelli, ETHZ, Dr. David Vetsch, ETHZ, and to Dr. Calvin Whealton, PSI, for valuable comments and assistance.

References

[1] Sudret, B. 2007. Uncertainty propagation and sensitivity analysis in mechanical models: Contributions to structural reliability and stochastic spectral methods., Report: Habilitation `a diriger des Recherches, Universite Blaise Pascal.
[2] Sudret, B. 2008. Global sensitivity analysis using polynomial chaos expansions. Reliability Engineering & System Safety, 93: 964-979.
[3] Borgonovo, E. 2007. A new uncertainty importance measure. Reliability Engineering and System Safety 92, 771-784. 14, 15.
[4] USACE 2017. HEC-LifeSim 1.0. U.S. Army Corps of Engineers, Hydrologic Engineering Center.
[5] Bowles, D. S. 2007. Life Loss Estimation for RAMCAP, Appendix D,. Conventional Dams and Navigation Locks, Sector-Specific Guidance (SSG), Risk Analysis and Management for Critical Asset Protection (RAMCAP)
[6] Bowles, D. S. & Aboelata, M. 2007. Evacuation and life-loss estimation model for natural and dam break floods.
[7] McClelland, D. M. & Bowles, D. 2000. Estimating life loss for dam safety and risk assessment: Lessons from case histories.
[8] SFSO, 2017a. Regionalporträts 2017: Kennzahlen aller Gemeinden, Rep. No. je-d-21.03.01: Swiss Federal Statistical Office.
[9] Kalinina A., 2019. Risk Assessment of hydropower in Switzerland. Uncertainty Quantification in the modelling of dam-break consequences.
[10] Kalinina, A., Spada, M. & Burgherr, P. 2018. Alternative life-loss rates for failures of large concrete and masonry dams in mountain regions of OECD countries. In: Haugen S, Barros A, Gulijk Cv, Kongsvik T, Vinnem J, editors. Safety and Reliability – Safe Societies in a Changing World. London, UK: CRC Press.

SCCER-SoE Annual Conference 2019

SCCER SoE
SWISS COMPETENCE CENTER for ENERGY RESEARCH
SUPPLY of ELECTRICITY

Supported by:
Schweizerische Eidgenossenschaft
Confédération suisse
Confederazione Svizzera
Confederaziun svizra
Swiss Confederation
Innosuisse – Swiss Innovation Agency

A tool to visualize different participation formats

Franziska Ruef, Michael Stauffacher, Olivier Ejderyan – D-USYS TdLab, ETH Zürich

Context of a geothermal energy program – GEothermie2020

The context of our study is the geothermal program GEothermie2020 funded by the public utilities SIG and the canton of Geneva. Launched in 2014, the program started with an extensive prospection and exploration campaign. We accompany the program in its different steps to work on participation and the public. With the program transgressing different phases of development, we adapt our research questions and priorities in order to stay in line with the pressing issues and questions at hand.

GEOTHERMIE 2020 · RÉPUBLIQUE ET CANTON DE GENÈVE · SIG

►► Need for a new conception of participation…

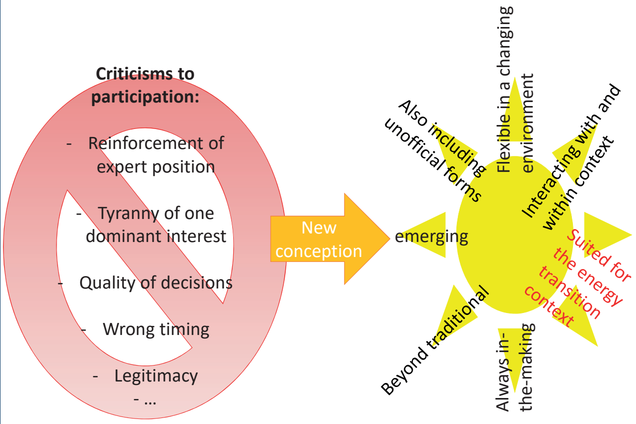

Research Questions and Method

1. How does structuring different formats of participation allow to identify blind spots in a participation context?
2. Which are these blind spots and how do they highlight different understandings of participation?

Two perspectives: the project managers and residents

Aim: grasp participation seen and understood from different perspectives through the lenses of the 2 central actors:
- The ones initiating a participative format: PROJECT MANAGERS
- The ones participating (or not) in it: RESIDENTS


© SIG


© Olivier Ejderyan, 2017

Data

Core findings are based upon a detailed analysis of in-depth qualitative data elicited through **focus groups** with residents and **participant observation** in strategic management meetings of the geothermal project managers in Geneva.

References

- Chilvers, J., & Kearnes, M. (2016). Remaking Participation: Science, Environment and Emergent Publics. (J. Chilvers & M. Kearnes, Eds.). Abingdon and New York: Routledge.
- Chilvers, J., Pallett, H., & Hargreaves, T. (2018). Ecologies of participation in socio-technical change: The case of energy system transitions. Energy Research & Social Science, 42(March), 199–210. https://doi.org/10.1016/j.erss.2018.03.020
- GEothermie 2020 (2018). Documents et Médias. http://www.geothermie2020.ch/ressources/categorie/3 (31.08.2018)

Results

Project Managers' view

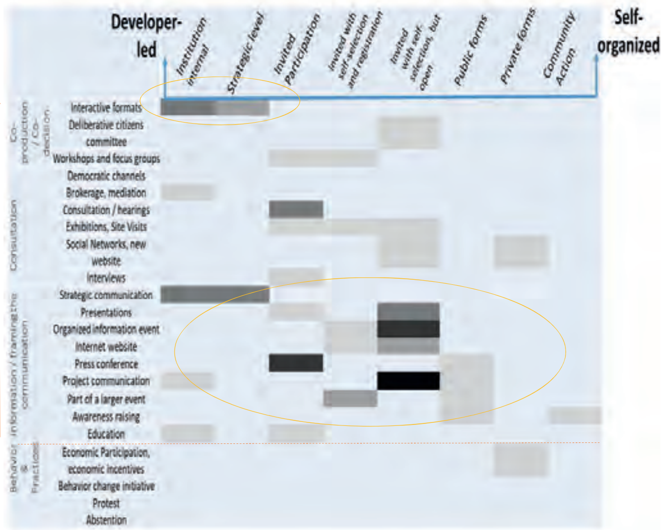

The distribution for project managers' references shows that they see participatory formats mostly in the classical sense, ranging from information over consultation to co-production. Rather common governance schemes, as through information provision for example. Lesser-theorized top-down participative models deployed internally or within an invited group were also part of their view.

Residents' view

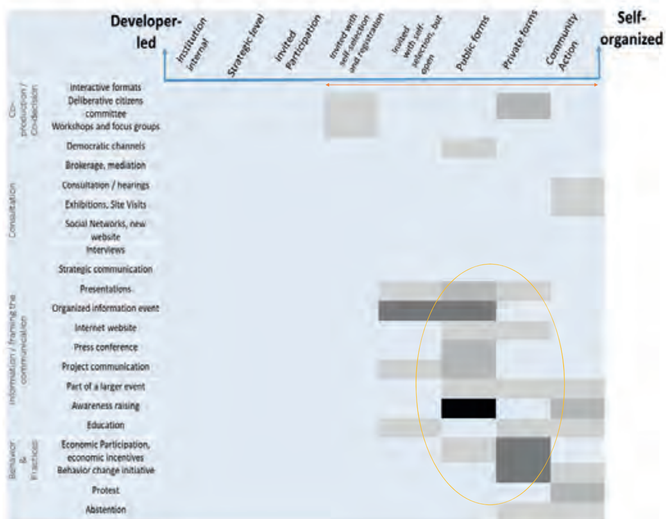

For residents, information provision is also very important. However, more references to self-organized than to institution-led forms of participation. Private forms of participation such as buying responsibly and investing in renewable energy installations came up often.

Discussion – the following blind spots were identified:

- Untypical participation forms are just as important! Such as forms linked to behaviour and practices, abstention and protest.
- What's hot in literature, doesn't need to be relevant on the ground! One example: highly discussed consultative participation, rare in practice.
- "Just" transparent information, please! Residents not necessarily wish for ideal-type participation, but rather transparent information.
- What *exactly* is behind the format? Implicit definitions of different formats are important to use them well!

SCCER-SoE Annual Conference 2019

SCCER SoE
SWISS COMPETENCE CENTER for ENERGY RESEARCH
SUPPLY of ELECTRICITY

PAUL SCHERRER INSTITUT

Supported by:

Schweizerische Eidgenossenschaft
Confédération suisse
Confederazione Svizzera
Confederaziun svizra

Swiss Confederation

Innosuisse – Swiss Innovation Agency

Quantitative risk assessment for Deep Geothermal Energy (DGE) systems in Switzerland

Matteo Spada, Peter Burgherr

Technology Assessment Group, Laboratory for Energy Systems Analysis, Paul Scherrer Institut (PSI)

Introduction

This work is built upon the approach developed in the TA Swiss study [1], which is significantly extended since SCCER-SoE Phase 1. Deep geothermal energy (DGE) systems are, like all energy technologies, not risk free. Although the risk of induced seismicity is frequently pointed out, geothermal systems present additional potentially risky aspects such as borehole blowouts or chemical related incidents. In this study, different technological risks associated with deep geothermal energy systems are identified, characterized and quantitatively analyzed. In particular, two major updates have been achieved in this phase:

- the introduction of additional hazardous materials potentially used as working fluids in the operational phase and as part of the matrix acidizing in the stimulation phase;
- the update of historical accidents in the period 1990-2017.

Results are shown in terms of normalized risk indicators (e.g. fatality rate, injury rate, etc.) in order to compare risks of blowouts in the drilling and stimulation phases and the use of hazardous substances in drilling, stimulation and operational phases.

Data

Since DGE systems have not been yet installed at many sites, historical experience in terms of accidents is rather limited. Therefore, the estimation of risk indicators is based on historical experience of other industries that can be considered a meaningful proxy for DGE systems. In all considered cases, accident data for the time period 1990-2017 from OECD countries were used because they can be considered sufficiently representative for Switzerland. However, when dealing with hazardous substances, it was necessary to focus on the chemicals that could be possibly used in Switzerland. In addition to PSI's Energy-related Severe Accident Database (ENSAD) several other databases were used in order to collect accidents related to the use of hazardous substances (Table 1) and blowouts (Table 2), i.e. ERNS, ARIA, FACTS, etc..

Table 1: Summary of the numbers of accidents and associated consequences for the Hazardous Substances analyzed in this study.

Phase	Hazardous Substance	Accidents/Fatalities	Accidents/Injuries
Drilling	Caustic Soda	13/30	142/1149
Stimulation	Hydrogen Chloride (HCl)	2/4	94/697
	Hydrogen Fluoride (HF)	3/3	26/83
	Ammonium Persulphate	2/2	8/76
	Boric Acid	1/1	10/43
Operational	Benzene	3/4	33/562
	Toluene	16/20	66/679
	Methanol	18/43	15/103
	n-Hexane	11/25	20/205
	o-Xylene	8/24	27/415
	Ammonia	16/20	136/1191

Table 2: Summary of onshore blowout accidents in the natural gas industry, collected for USA and Alberta, since no specific historical experience for deep geothermal systems is available.

Blowouts	Accidents/Fatalities	Accidents/Injuries
	5/5	11/25

Method

The risk indicators are normalized to the unit of energy production (i.e. Gigawatt-electric-year, GWeyr) using specific normalization factors for each substance and blowout.

$$NF_{Caustic\ Soda} = \frac{CS_{Well} * WD * NW}{total\ production\ 1990 - 2017} * \frac{1}{P_{GWeyr}}$$

$$NF_{Stimulation} = \frac{HS_{Well} * NW}{total\ production\ 1990 - 2017} * \frac{1}{P_{GWeyr}}$$

$$NF_{Working\ Fluid} = \frac{WF_{Year1} + (kg\ of\ substance\ refilled * LT)}{total\ production\ 1990 - 2017} * \frac{1}{P_{GWeyr}}$$

$$\mathrm{NF_{Drill+Stim}} = \frac{\mathrm{NW}}{\text{total number of natural gas drilled wells 1990} - 2017} * \frac{1}{\mathrm{P_{GWeyr}}}$$

$NF_{Caustic\ Soda}$, $NF_{Stimulation}$, $NF_{Working\ Fluid}$ and $NF_{Drill+Stim}$ are the normalization factors for Caustic soda, Stimulation Fluids, Working Fluids, Blowouts, respectively. P_{GWeyr} is the production of the plant in Gweyr. Table 3 summarizes the key physical parameters considered in this study for normalization purposes.

Table 3: Key physical parameters of the capacity cases for DGE plants considered in this study.

		SCCER-SoE/BFE/GEOTHERM-2 Doublets			SCCER-SoE/BFE/GEOTHERM-2 Triplets		
Capacity cases		**High**	**Base**	**Low**	**High**	**Base**	**Low**
Net plant power		3.28 Mw_e	1.45 MW_e	1.18 MW_e	5.21 MW_e	2.73 Mw_e	2.27 MW_e
Production in GWeyr (P_{GWeyr})		6.56e-2 Gweyr	2.99e-2 GWeyr	2.36e-2 GWeyr	1.04e-1 GWeyr	5.46e-2 GWeyr	4.54e-2 GWeyr
Well depth (WD)		5 km					
Number of wells (NW)		2			3		
Surface plant life time (LT)		20 years					
Caustic Soda as additive in the drilling mud per Well (CS_{Well})		1 kg/m					
Additives in Hydraulic Stimulation (total average) per Well (HS_{well})		HCl:3.4E7 kg HF:7.1E6 kg; Ammonium Sulphate: 3.1E5 kg; Boric Acid: 1.2E5 kg					
Working Fluids used at the power plant at year 1 (WF_{Year1})	**Ammonia**	1415 kg	863 kg	740 kg	1716 kg	1369 kg	1179 kg
	Benzene	1208 kg	737 kg	632 kg	1465 kg	1169 kg	1007 kg
	Toluene, Methanol, n-Hexane, o-Xylene	1197 kg	730 kg	626 kg	1452 kg	1158 kg	998 kg
Yearly losses of the working fluids (YLWF)		8%					

Results: Example for Fatality Rates

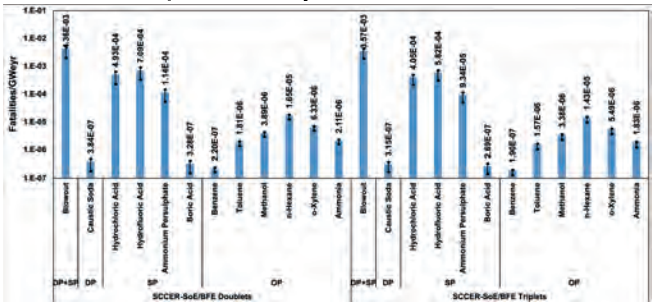

Figure 1: Fatality rate for the drilling, stimulation and operational phases based on accident data for the period 1990-2017. Blue bars: Base Case; Error bars: High and Low Capacity plants (See Table 3). DP: Drilling Phase; SP: Stimulation Phase; OP: Operational Phase.

- Accident risks of blowouts are significantly higher than the risk related to the use of hazardous substances.
- Among hazardous substances, HF exhibits the highest risk followed by the use of HCl and Ammonium Persulphate at the geothermal site.
- In the operational phase, n-Hexane performs worst with respect to the other potential working fluids.
- Doublets (2 production wells) and triplets (3 production wells) plant types show similar results in terms of risk related to the considered phases.

Conclusions

- Results for the use of hazardous substances in drilling, stimulation and operational phases point towards low risk levels.
- Based on these results, the drilling and stimulation phases in deep geothermal systems exhibit higher risks compared to the operational phase.
- Deep geothermal systems compare favorably to, for example, natural gas (7.19E-2 fatalities/GWeyr for OECD countries, according to [2]).

References: [1] Spada, M., Burgherr, P. (2015). Chapter 6.1: Accident Risk. In Hirschberg S., Wiemer S. and Burgherr P.: Energy from the Earth. Deep Geothermal as a Resource for the Future? TA-SWISS Study TA/CD 62/2015, vdf Hochschulverlag AG, Zurich, Switzerland, pp. 229-262. http://dx.doi.org/10.3218/3655-8
[2] Burgherr, P. & Hirschberg, S. (2014) Comparative risk assessment of severe accidents in the energy sector. *Energy Policy*, 74 (S1), S45-S56.

SCCER SoE
SWISS COMPETENCE CENTER for ENERGY RESEARCH
SUPPLY of ELECTRICITY

SCCER-SoE Annual Conference 2019

Supported by:
Schweizerische Eidgenossenschaft
Confédération suisse
Confederazione Svizzera
Confederaziun svizra
Swiss Confederation
Innosuisse – Swiss Innovation Agency

Using GIS to discuss place factors for CCS projects siting

Juanita von Rothkirch, Olivier Ejderyan, Michael Stauffacher

Motivation

Geological CO_2 storage is a key technology for facilitating the removal of carbon dioxide from the atmosphere. However, the progression of CO_2 storage has been hindered by public opposition to some proposed projects, once storage sites had been selected. As numerous experiences on contested technologies have shown, public participation processes determine whether communities become a door or barrier for the emplacement of projects in local contexts. Yet there is much literature on the importance of early public engagement for normative, substantive and instrumental reasons, there are no tools for integrating social aspects early on in the site selection process.
This poster presents an exploratory study of the upstream inclusion of social characteristics and concerns in the site selection process for CO_2 storage in Switzerland.

Methods

Relevant place factors were identified through a literature review. These factors were mapped for potential CO_2 storage sites. A cluster analysis was conducted to identify categories of sites for which similar public engagement procedures might apply.

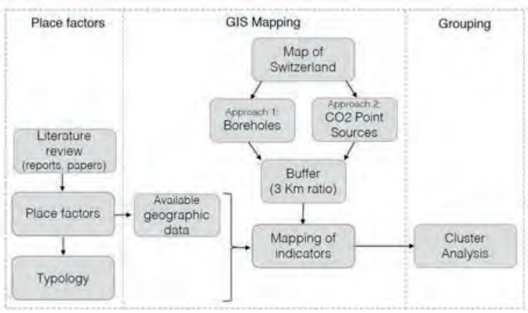

Results

Place factors are the social characteristics and concern linked to specific places (Peterson et al, 2015). The table below lists the relevant place factors for CO_2 storage projects and the indicators used to map them in the Swiss context.

Place factor	Indicator	Unit
Industrial zone	Industrial areas. Land use statistics NOAS04 2013-2018. (FSO, 2018b)	ha
Employment	Employment rate per district 15- 64 years old. (FSO, 2018a)	% (mean)
Tourism	Hotel industry: supply and demand of open establishments in 100 municipalities in 2018. (FSO, 2019)	Number
Natural Parks	Swiss National Park and parks of national importance. (FOEN, 2019)	m2
Geothermal energy	Present and future projects of geothermal energy. (Swisstopo, 2019)	Number
Landscape	Federal Inventory of Landscapes and Natural Monuments. (FOEN, 2019a)	m2
Groundwater	Groundwater protection zones. (Swiss Cantons, 2019)	m2
Private housing	Private housing. (FSO, 2017)	Number (median)
Cultural Areas	Heritage sites of national importance. (FOC, 2019)	Number
CO2 from a different political unit	Cantonal boundaries. (Federal Office of Topography (Swisstopo), 2019a)	Number
CO2 emission points	Industrial CO2 emissions > 10 Mtonnes. (PRTR, 2017)	-
Oil and gas extraction or storage	Energy raw materials: Deposits. (Swisstopo & SGTK, 2019)	-

Mapping place factors relevant for CO2 storage sites


Map based on existing boreholes as proxy for potential sites


Map based on CO2 emission point sources (≥ 10 Megatons) as proxy for potential sites

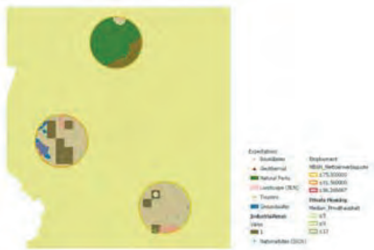

After mapping all the factors in the buffers using the first approach (Boreholes), the statistics of the different indicators per location were extracted to conduct cluster analyses to group sites with similar place factors into categories.

Cluster Analyses
The cluster analyses presented in this section show that there are no clusters of locations, according to the indicators used. Therefore, it is not possible to structure the discussion based on a systematic classification of locations.

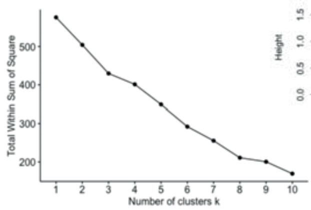

Elbow method for identifying the optimal number of clusters, using K-means.

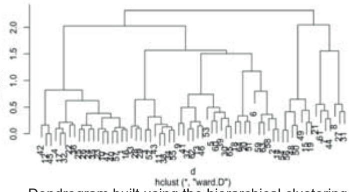

Dendrogram built using the hierarchical clustering method Ward.

Discussion

The typology of place factors allows to understand the logic behind the success or failure of projects in relation to the locations. Our typology indicates that benefits and familiarity can contribute to the positive response to a project. Negative experiences, conflicting expectations, technology-related concerns, status-quo bias and distributive fairness issues can contribute to a negative response.

Our results indicate that maps can help to get a first approximation to place characteristics and people's concerns in potential CO_2 storage sites. We found that several geographical indicators exist which partially or completely represent place factors. Therefore, visualization of place factors on maps allows to cope with complex information and make non-technical aspects of sites explicit.

The clustering analyses conducted show that our data does not contain distinct groups of locations with the same set of indicators. Therefore, it is not possible to design strategies to approach locations according to categories. This is the result of having a small ratio of observations and variables: there are only few observations and several variables

References

Peterson, T. R., Stephens, J. C., & Wilson, E. J. (2015). Public perception of and engagement with emerging low-carbon energy technologies: A literature review. MRS Energy & Sustainability, 2, E11. https://doi.org/10.1557/mre.2015.12

Task 4.2

Title

Global observatory of electricity resources

Projects (presented on the following pages)

Modelling of dispatch of stored hydropower
Martin Densing

Electricity Prices Under Energy Policy Scenarios and Profitability of Hydropower
Martin Densing, Evangelos Panos

How will geothermal energy transform the environmental performance of Geneva's heating and cooling mix from a life-cycle perspective?
Astu Sam Pratiwi, Evelina Trutnevyte

A stochastic method for spatial Multi-Criteria Decision Analysis: Application to Deep Geothermal Energy in Switzerland
Matteo Spada, Marco Cinelli, Peter Burgherr

Energy system pathways with low environmental impacts and costs
Laurent Vandepaer, Panos Evangelos, Christian Bauer, Ben Amor

Nonlinear Inverse Demand Curves in Electricity Market Modeling
Yi Wan, Martin Densing

The potential & levelized cost of solar PV in Switzerland
Xiaojin Zhang, Christian Bauer

SCCER SoE

SWISS COMPETENCE CENTER for ENERGY RESEARCH
SUPPLY of ELECTRICITY

SCCER-SoE Annual Conference 2019

Supported by:

Schweizerische Eidgenossenschaft
Confédération suisse
Confederazione Svizzera
Confederaziun svizra

Swiss Confederation

Innosuisse – Swiss Innovation Agency

PAUL SCHERRER INSTITUT PSI

Modelling of dispatch of stored hydropower

Martin Densing (martin.densing@psi.ch),
Energy Economics Group, Laboratory for Energy Systems Analysis, Paul Scherrer Institute (PSI)

Motivation

- Traditional modeling of dispatch of stored energy, that is, when to release energy for generation and when to charge (e.g. in case of pumped-storage hydropower plants) faces **issues:** E.g., the **time horizon**: The dispatch decision is hourly (or sub-hourly), but the time horizon for price-driven dispatch is a year because of the seasonality of electricity prices and of natural water inflow. Moreover, several markets may investigated (ancillary services).
- **Model of a single plant vs. aggregated Swiss hydropower**: Commercial dispatch software is usually tuned to a specific set of plants. E.g., it is not well known how "academic" hydropower dispatch can approximate aggregated Swiss hydro storage.
- **Research directions:** ***(i)*** *Theoretical model of ancillary services;* ***(ii)*** *Change in optimal dispatch under price scenarios 2050;* ***(iii)*** *Model comparison for aggregated Swiss hydropower*
- Partners in (i) + (ii): **Karlsruhe Institute of Technology (KIT)** and **SFOE (Project *PowerDesign*) [1,2]**.
- Application of linear optimization model with exogenous stochastic prices, deterministic inflow, and reservoir constraints in expectation

I. Lower bound on secondary spinning reserve entry [1]

- A linear maximization problem has always an associated maximization problem (the "dual"). It can be shown: the dual yields necessary conditions to enter spinning reserve service: **Capacity payment (per time unit, per MW)** >= **Mean absolute deviation from the median (MAD) of electricity prices**.

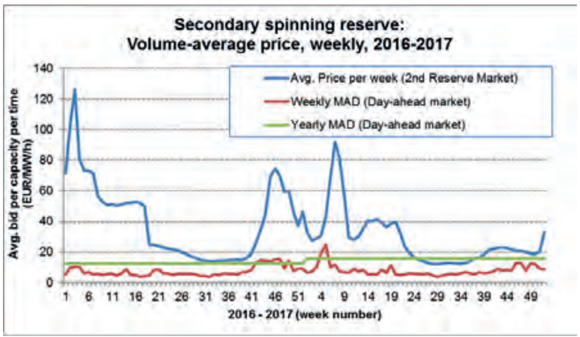

- Result: Price data of spinning reserve in Switzerland (Swissgrid, 2018) and MAD of power prices (EPEX, 2018) validate the analytically derived lower bound of spinning reserve price

II. Future scenarios of electricity prices: Profit & Cycling [2]

- Model input: Swiss power price scenarios, driven by large deployment of renewables in neighboring countries and CH, and calculated by **Karlsruhe Institute of Technology:** (i) **EOM 2050** ("energy-only-market"): has no market mitigation measures against price peaks (capacity scarcity); (ii) **CRM 2050** ("capacity remuneration mechanisms"): such measures are in place.

Validation and scenario analysis for the example of aggregated Swiss stored hydropower:

- Scenarios for 2050 (EOM and CRM) have high price levels
- → hydropower, as a price-taker, has higher profits.
- Storage volume in relation to today's generation capacity seems to be properly sized.

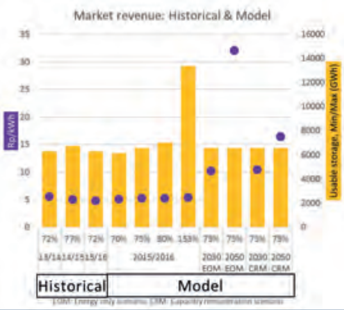

Example of **Muttsee:**
1GW pump-storage,
~0 natural inflow,
large lower reservoir

Price distribution of years 2015-16 | **Price distribution of 2050 Scenario: Energy-only-Market**

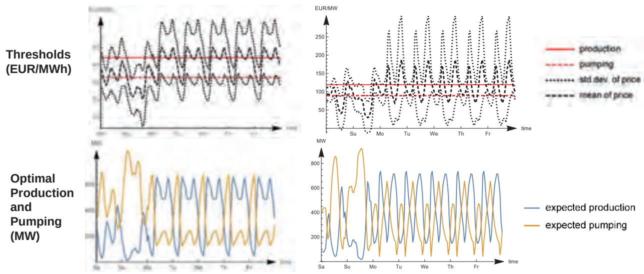

- Result: More volatile electricity prices having different patterns in the considered scenarios in 2050 leads to more cycling over a week → more turbine wear-down

III. Modelling Comparison [3]

- Example: **Aggregated Swiss stored hydropower** (pumps are neglected) over two years (Apr 2014 - Mar 2016). Input: electricity prices, natural inflow; output: storage levels, dispatch.
- **Comparison:** Models with *deterministic* prices (mean of prices), with different time steps: (i) monthly, (ii) daily, (iii) hourly; and (iv) monthly *stochastic* model with reservoir constraints in expectation

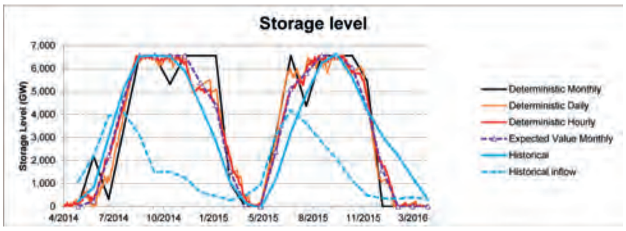

- Result: Monthly stochastic model can outperform monthly deterministic model. To keep in mind: The (many) plant owners of the 100+ different plants dispatch in reality by idiosyncratic rules.

Conclusions

- A stochastic model approach is presented based on the statistical properties of electricity prices. Based on this model, a first analytical treatment of spinning reserve provision can be provided.
- Because boundary conditions by the power markets will likely change for Swiss stored hydropower (e.g. see the 2050 scenario of dispatch above), we focus modeling of stochastics and seasonality.

References

[1] **M. Densing.** The value of flexible selling: Power production with storage for spinning reserve provision. *European Journal of Operational Research*, 2019. doi: 10.1016/j.ejor.2019.08.012.

[2] F. Zimmermann, **M. Densing**, D. Keles, J. Dehler, F. Hack, and W. Fichtner. *Impact of different market designs in the CWE market area on electricity prices and on the competitiveness of Swiss hydropower (PowerDesign)*. SFOE-EWG research programme, final project report, Swiss Federal Office of Energy (SFOE), *ARAMIS Swiss Federal Research Database, 2018*. https://www.aramis.admin.ch/Dokument.aspx?DocumentID=50031.

[3] **M. Densing**. Explicit solutions of stochastic energy storage problems, *29th European Conference on Operational Research (EURO2018),* Valencia, Spain, 8-11 July 2018.

SCCER SoE
SWISS COMPETENCE CENTER for ENERGY RESEARCH
SUPPLY of ELECTRICITY

SCCER-SoE Annual Conference 2019

Supported by:
Schweizerische Eidgenossenschaft
Confédération suisse
Confederazione Svizzera
Confederaziun svizra

Swiss Confederation

Innosuisse – Swiss Innovation Agency

PAUL SCHERRER INSTITUT PSI

Electricity Prices Under Energy Policy Scenarios and Profitability of Hydropower

Martin Densing (martin.densing@psi.ch), Evangelos Panos
Energy Economics Group, Laboratory for Energy Systems Analysis, Paul Scherrer Institute (PSI)

Within Task 4.2 "Global Observatory of Electricity Resources" the Energy Economics Group investigates:

1. *Price formation on the Swiss wholesale electricity markets* and long-term price development under energy policy scenarios of Switzerland and the EU. Emphasis is on a fundamental model of reasonable size and complexity that can approximate today's prices
2. *Hydropower dispatch optimization against electricity prices*. Emphasis is on models that take into account the probability distribution, but that are still numerical tractable for sensitivity analyses (hence no modeling with a scenario tree, which grows exponentially in time steps)
3. *Long-term investment and electricity dispatch for Switzerland and EU*

Scenario modeling with BEM – Cross-Border Electricity Market model

- Understanding price-formation and investments on electricity markets
- Day-ahead wholesale electricity prices (which are usually above marginal production costs) are calibrated by using a game-theoretic model of Switzerland and surrounding countries

Regions in BEM

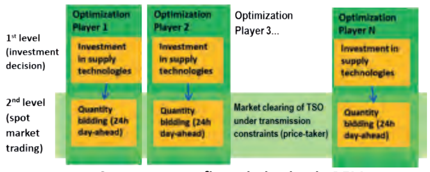

Concurrent profit optimization in BEM

Results for **two core scenarios** for year 2030 are presented:

	Base	Low Carbon
Description	Reference scenario, based on EU TRENDS 2016 Scenario of EC	Climate scenario -40% reduction of CO_2 in 2030 from 1990 levels ("Clean Energy for All Europeans")
Fuel prices in 2030 [1]	Gas: 28 €/MWh, Coal: 12 €/MWh (in EUR_{2015})	
CO_2 price in 2030	30 €/tCO_2	80 €/tCO_2 [2]

[1] IEA World Energy Outlook 2017, New Policies Scenario [2] IEA World Energy Outlook 2017, Sustainable Scenario
Today's gas price (2015/6) 14 €/MWh, today's coal price 9 €/MWh

Two **additional variants**:

a) Enabling investment in batteries (transmission level) for additional flexibility
b) Maintaining the fuel costs and CO_2 prices of today ("TodayCost")

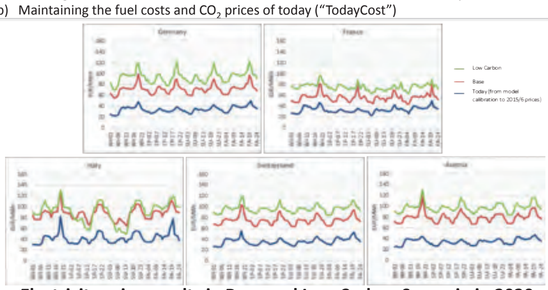

Electricity price results in Base and Low Carbon Scenario in 2030
→ Germany: Prices driven by CO_2 and gas prices (despite more PV+Wind)

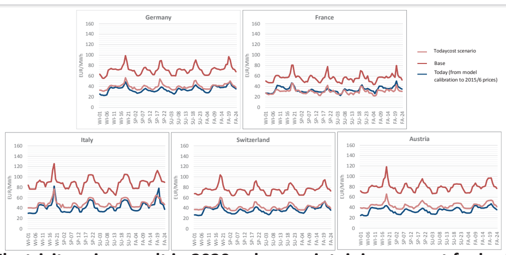

Electricity price result in 2030, when maintaining current fuel prices
→ Electricity price increase key factors (in order of magnitude):
(1) Fossil fuel price, especially gas (indirectly CO_2 prices), (2) Load levels, (3) penetration of wind & solar, (4) decommissioning (mainly nuclear power)

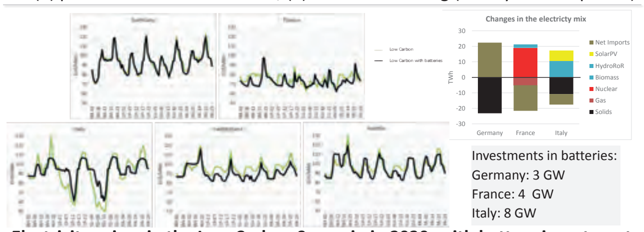

Investments in batteries:
Germany: 3 GW
France: 4 GW
Italy: 8 GW

Electricity prices in the Low Carbon Scenario in 2030, with battery investments allowed
→ Additional (relatively small) storage can help to shave price-peaks

Hydropower Dispatch Modeling

Linear stochastic multi-period control model that optimizes expected profit under expected water constraints. Input: Price-distributions over time steps.
Reduced example of a single-period model:

- Constraint on water-level in expectation
- $S \in L^1_+$ electricity spot price (EUR/MWh), continuous distribution function
- $u^{\pm}: \mathbb{R}_+ \to \mathbb{R}_+$ control function, $u^{\pm}(S)$: turbined/pumped water (MWh)
- Maximal capacity, available water per period: $u^{+}_{\max} > l > 0$
- $\eta \in (0,1)$ efficiency of pumping

$$\max_{u^{\pm}} \mathbb{E}\Big[Su^{+}(S) - \frac{1}{\eta}Su^{-}(S)\Big]$$
$$\text{s.t.} \begin{cases} l - \mathbb{E}[u^{+}(S) - u^{-}(S)] \geq 0 \\ 0 \leq u^{\pm}(S) \leq u^{\pm}_{\max} \end{cases}$$

Optimal solution:

$$\hat{u}^{+}(S) = u^{+}_{\max}1_{\{S \geq \hat{q}\}}, \quad \hat{u}^{-}(S) = u^{-}_{\max}1_{\{S \leq \eta\hat{q}\}}, \quad \hat{q} \text{ given by}$$
$$u^{+}_{\max}\mathbb{P}[S \geq \hat{q}] - u^{-}_{\max}\mathbb{P}[S \leq \eta\hat{q}] = l$$

1. Example: Stored hydropower (Switzerland aggregated into 1 plant):

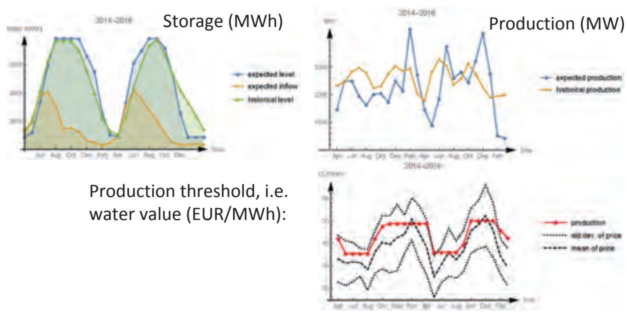

2. Example: 1 GW Pumped-storage over a week:

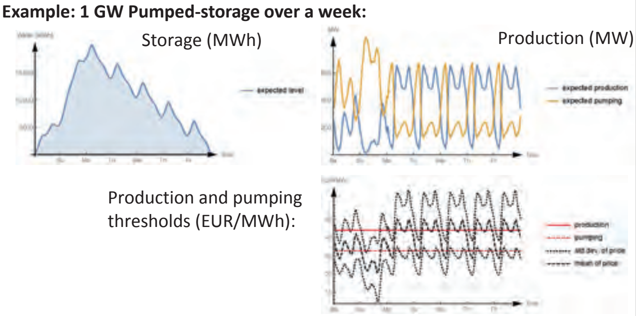

Hydropower Profitability by using scenario prices from BEM [3]

Swiss Hydropower is analyzed under different scenarios in target years 2025 and 2035: (i) Annual imports allowed (yes/now); (ii) Low carbon scenario (high CO_2 price of Swiss NEP scenario); today's fuel costs

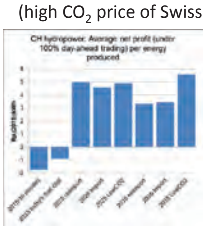

- **Preliminary** results (VSE-PSEL project [3]):
  - Hydropower plants will not be profitable if today's fuel costs prevail (e.g. CO_2 price < 10 EUR/tCO2 in European ETS)
  - Hydropower can become more profitable under high gas (and CO_2) prices

References

[1] **Panos, E, Densing, M.** The future developments of the electricity prices in view of the implementation of the Paris Agreements: Will the current trends prevail, or a reversal is ahead? *Energy Economics*, 2019. doi: 10.1016/j.eneco.2019.104476

[2] **Panos, E., Densing, M., Schmedders, K.** (2017): OCESM- Final Report for SFOE, https://www.aramis.admin.ch/Default.aspx?DocumentID=46075

[3] **Densing, M., Ramachandran, K., Panos, E., Kober, T.** (2018): Final Report, VSE PSEL project, Aargau

SCCER-SoE Annual Conference 2019: 3 & 4 September 2019

How will geothermal energy transform the environmental performance of Geneva’s heating and cooling mix from a life-cycle perspective?

Astu Sam Pratiwi[1], Evelina Trutnevyte[1]

[1]Renewable Energy Systems group, Faculty of Science, Department F.-A. Forel for Environmental and Aquatic Sciences, Institute for Environmental Sciences, University of Geneva, Switzerland

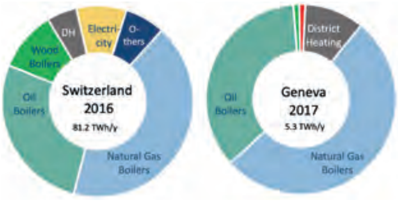

Figure 1. Heat delivery to buildings by source. *Adapted from Narula et al., 2019 and Quiquerez et al., 2020*

Background

- In Geneva, like Switzerland, fossil fuels dominate the heating sector [1] (Figure 1).
- A combination of geothermal heating applications in Geneva could potentially cover 75% of the heating demand by 2030 [2].
- GEothermie 2020 program [3] aims to comprehend Geneva’s subsurface characteristics better and to develop new geothermal projects.
- The environmental impacts of geothermal energy inclusion in the heating and cooling mix need to be evaluated to ensure their sustainable deployment.
- Life Cycle Assessment (LCA), as an widely used component of sustainability assessments, is the suitable methodology to analyze the environmental performance of geothermal energy in the heating and cooling sector.

Research questions

1. How do different standalone geothermal heating and cooling systems perform environmentally in the context of the Canton of Geneva?
2. What are the key parameters that influence this performance and how this performance could be improved?
3. How could the deployment of geothermal heating and cooling change the environmental performance of the current heating and cooling mix in Geneva?

Methodology

- Literature review of LCA studies on geothermal heating
- Define base scenarios of relevant geothermal heating systems in Geneva
- Collect new life cycle inventory and develop approaches to estimate unknown parameters (documents, interviews, literature)
- Carry out case-specific LCA analyses, taking into account uncertainty and sensitivity analysis (Open LCA)
- Carry out spatial analysis or build parameterized model (yet to be defined)

First results

- Out of 28 LCA-based studies on geothermal heating systems in the literature, 20 cover Ground Source Heat Pump (GSHP).
- A comparison between LCA studies and existing installations shows a lack of LCA studies on medium-enthalpy geothermal systems involving extraction of groundwater, despite their popular deployment in Europe (Figure 2).
- The impacts of GSHP depend on the electricity mix and COP [4-6], thus have a large spread and are not always better than individual oil boilers (Figure 3).
- Groundwater systems are reported to perform relatively better than oil boilers (Figure 3).

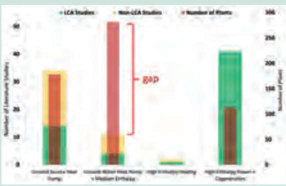

***Figure 2.** Identified research gap in LCA for open the geothermal systems*

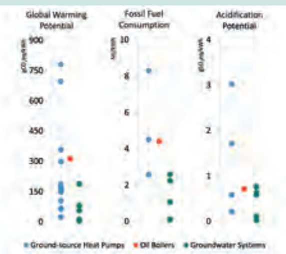

***Figure 3.** Summary of the reported impacts in the literature and the comparison to the impacts of individual oil boilers (except for GWP, only CML-based calculations are plotted)*

- LCA on groundwater geothermal systems is needed to strengthen the literature, as well as to support GEothermie 2020 program.

	HP INDIVIDUAL OR DECENTRALIZED (A)	HP + DISTRICT HEATING (B)	NO HP + DISTRICT HEATING (C)
SMALL DEPTH (I) < 100 m	Scenario IA-1 (*EMS La Plaine) / Scenario IA-2 (*Jargonnant)	Scenario IB	
MEDIUM DEPTH (II) < 1500 m	Scenario IIA	Scenario IIB	Scenario IIC
LARGE DEPTH (III) >1500		Scenario IIIB	Scenario IIIC

***Table 1.** Scenarios of groundwater extraction geothermal systems that could be relevant in Geneva and their installation references. *The case studies analyzed so far are presented in the next section.*

- Several scenarios are defined to represent the probable configurations of subsurface and surface systems in Geneva (Table 1).
- Existing installations (written in green in Table 1) are the identified references to collect life cycle inventory, to develop LCA models, and to validate the models.

- LCA studies were carried out for EMS La Plaine (Scenario IA-1) and Jargonnant (Scenario IA-2) for a lifetime of 30 years. Table 2 presents the differences between the two.
- Operation stage is the major contributor to almost all environmental impacts (Figure 4).
- Compared to oil boilers, the two systems have lower climate change impact, emit less particulate matter, and depend less on fossil fuel (Figure 5).

	Scenario IA-1 EMS La Plaine	Scenario IA-2 Jargonnant
Well diameter / depth	0.18 m / 10 m	1 m / 30 m
Flowrate	5.5 l/s	30 l/s
Cooling	Passive	Active
Solar Thermal	Yes	No

***Table 2.** Main differences between Scenario IA-1and IA-2*

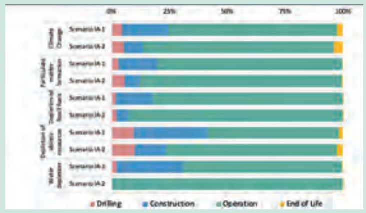

***Figure 4.** Preliminary results on the contribution of different life-cycle stages of Scenario IA-1 and Scenario IA-2 towards five selected environmental impacts*

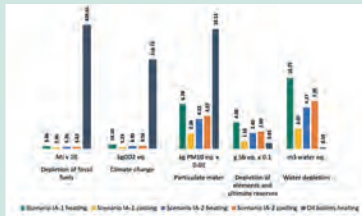

***Figure 5.** Preliminary results on environmental impacts by Scenario IA-1 and Scenario IA-2 as compared to oil boilers*

- The high impacts on water and abiotic resources are mainly due to the use of reservoir hydro electricity and the metal-based materials (Figure 5).

Acknowledgement

The work was carried out in the framework of GEothermie 2020 program, a collaboration between Services industriels de Genève (SIG) and the State of Geneva. The authors gratefully acknowledge SIG for their support.

References

[1] Quiquerez, L., Lachal, B., Monnard, M., & Faessler, J. (2017). The role of district heating in achieving sustainable cities: Comparative analysis of different heat scenarios for Geneva. *Energy Procedia*, *116*, 78–90. https://doi.org/10.1016/j.egypro.2017.05.057

[2] Groupe de Travail PGG. (2011). *Évaluation du potentiel géothermique du canton de Genève (PGG). Vol. 1: Rapport Final, GADZ 5753/1*. Retrieved from http://www.crege.ch/download/rapports/PGG_vol1_Rapport_final_v3.pdf

[3] Geothermie 2020. Un potentiel géothermie important. (2019, August 22). Retrieved from https://www.geothermie2020.ch/geothermie2020/enjeux-et-objectifs-du-programme/2

[4] Bayer, P., Saner, D., Bolay, S., Rybach, L., & Blum, P. (2012). Greenhouse gas emission savings of ground source heat pump systems in Europe: A review. *Renewable and Sustainable Energy Reviews*, *16*(2), 1256–1267. https://doi.org/10.1016/j.rser.2011.09.027

[5] Saner, D., Juraske, R., Kuebert, M., Blum, P., Hellweg, S., Bayer, P. (2010). Is it only CO2 that matters? A life cycle perspective on shallow geothermal systems. *Renewable and Sustainable Energy Reviews*, *14*(7), 1798–1813. https://doi.org/10.1016/j.rser.2010.04.002

[6] Greening, B., & Azapagic, A. (2012). Domestic heat pumps: Life cycle environmental impacts and potential implications for the UK. *Energy*, *39*(1), 205–217. https://doi.org/10.1016/j.energy.2012.01.028

[7] Narula, K., Chambers, J., Streicher, K. N., & Patel, M. K. (2019). Strategies for decarbonising the Swiss heating system. *Energy*, *169*, 1119–1131. https://doi.org/10.1016/j.energy.2018.12.082

etc.

SCCER SoE

SWISS COMPETENCE CENTER for ENERGY RESEARCH
SUPPLY of ELECTRICITY

PAUL SCHERRER INSTITUT

SCCER-SoE Annual Conference 2019

A stochastic method for spatial Multi-Criteria Decision Analysis: Application to Deep Geothermal Energy in Switzerland

Matteo Spada[1], Marco Cinelli[2], Peter Burgherr[1]

[1]Technology Assessment Group, Laboratory for Energy Systems Analysis, Paul Scherrer Institut (PSI)
[2] Institute of Computing Science, Poznan University of Technology, Poznan, Poland

Supported by:

Schweizerische Eidgenossenschaft
Confédération suisse
Confederazione Svizzera
Confederaziun svizra

Swiss Confederation

Innosuisse – Swiss Innovation Agency

Introduction

The aim of this study is to develop a Multi-Criteria Decision Analysis (MCDA) Tool for Deep Geothermal Energy (DGE) systems in Switzerland. In particular, the tool aims to help decision makers to identify the most sustainable area for DGE plants using spatial MCDA, which combines Geographical Information Systems (GIS) capabilities with MCDA frameworks. The proposed approach uses a stochastic approach to combine spatial information from both explicit data (e.g., heat flow) and calculated ones (e.g., risk indicators, environmental impact indicators, etc.). For each indicator, marginal distributions for uncertain model inputs are generated based on specific *a priori* defined plant characteristics (e.g., capacities, number of drilled wells over lifetime). The marginal distributions are then used as input to the model to assess the sustainability of DGE in different areas of the Molasse basin, Rhine Graben, and Jura mountains regions.

Method

The spatial MCDA (sMCDA) framework consists of different steps. First, the characteristics of the technology to be used in the sustainability assessment have been selected. In this study, since no running DGE plants exist in Switzerland, a set of hypothetical power plants based on SCCER-SoE Phase 1 activities are considered (Table 1).

Table 1: Selected key physical parameters of DGE plant capacity cases considered in this study

Model Assumption	Unit	Doublet Plant			Triplet Plant		
		Poor	Base	Good	Poor	Base	Good
Net Plant Capacity	MWe	1.19	1.47	3.34	2.31	2.81	5.27
Life Time	years	20	20	20	20	20	20
Number of Wells	integer	2	2	2	3	3	3
Well Depth	km	5	5	5	5	5	5
Well Life Time	year	20	20	20	20	20	20

Next, criteria are established to cover all 3 pillars of sustainability (environment, economy and society). Furthermore, indicators are chosen for each criterion based on availability and potential spatial variability (Table 2).

Table 2: Selected criteria and indicators used in this study.

Criteria	Indicators	Unit
Environment	Climate Change	kg CO2 eq to air
	Human Toxicity	kg 1,4-DCB eq to urban air
	Particulate Matter Formation	kg PM10 eq to air
	Water Depletion	m3 (water)
	Metal Depletion	kg Fe eq
Economy	Average Generation Cost	Rp/kWhe
Society	Non-seismic Accident Risk	Fatalities/kWh
	Natural Seismic Risk	Ordinal Scale [1-3]
	Induced Seismicity	Flow Rate [l/sec]
	Proximity to Major Cities	Distance [km]

Indicators are then quantified for the hypothetical plants in Table 1 and for a set of 32 potential areas defined using Heat Flux (HF) and Natural Seismic Risk maps (https://map.geo.admin.ch). Environmental and economic indicator values have been estimated based on the temperature gradient (ΔT) in the area of interest, since ΔT is the ratio between the HF and the thermal conductivity of rocks (on average 3 W/m*ºC in Switzerland [1]). On the other hand, the non-seismic accident risk indicator considers blow out risk and release of selected hazardous chemicals, which are related to the number of drilled wells [2]. The Natural Seismic Risk and the Proximity to Major Cities (> 100000 inhabitants) indicators are considered in this study as a proxy of social acceptance, meaning that high risk(scale 3)/short distance are associated with lower social acceptance of a DGE system. The Induced Seismicity Indicator is estimated based on the flow rate expected for the stimulation (i.e. higher the flow rate, the higher the risk of induced seismicity) for each of the plant capacities considered in this study.

Marginal distributions for uncertain model in each area have been generated by fitting the indicator values estimated for each hypothetical plant. In general, uniform distributions fitted best each indicator in Table 2, except for the Proximity to Major Cities (lognormal distribution) and Natural Seismic Risk, where no variation among plants is considered, i.e. no marginal distribution has been further considered.

The generated marginal distributions have been used as input for the Stochastic Multi-criteria Acceptability Analysis (SMAA-TRI) [3] applied to the spatial case. The SMAA-TRI algorithm is a classification method, which does not allow compensation between criteria and the weights are considered independent from the measurement scales. The SMAA-TRI assigns a class of sustainability (e.g., high, medium-high, medium, medium-low, low) to an area in probabilistic terms (Figure 1). It estimates the Class Acceptability Index (CAI), which measures the stability of the assignment to a class in terms of probability for membership in the class. The CAI is driven by the weights (if considered) of the indicators and according to the cutting level (λ), which gives a measure on how demanding the decision maker is (i.e., lower λ implies that a better class is easier to be reached). In this study, λ and the marginal distribution of each indicator are arbitrarily distributed parameters analyzed using 10000 Monte Carlo simulations.

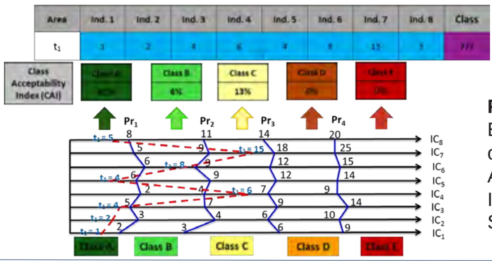

Figure 1: Evaluation steps of the Class Acceptability Index (CAI) in SMAA-TRI

Results

In this study, no stakeholder elicitation has been performed to assess weighting profiles, instead two approaches have been applied and compared:

- Missing information, where the indicator weights are sampled 10000 times using a Monte Carlo approach
- Four artificial preference profiles have been defined:
  - equal weights at all levels (both criteria and indicators in Table 2), which corresponds to the spirit of sustainability, where all pillars have the same weight.
  - three weighting profiles that strongly favor one of the sustainability pillars (weight 80%), whereas the two other are both weighted 10%, and all indicators are equally weighted.

As an example, the results based on sampling are presented in Figure 2. It clearly shows that DGE in Switzerland is considered from medium to highly sustainable, with the most sustainable areas being in North-East Switzerland.

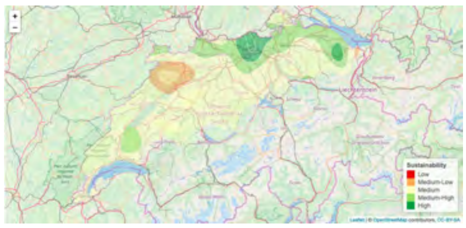

Figure 2: Sustainability map for DGE in Switzerland

Conclusions

- The application of a spatial MCDA based on a stochastic method with GIS capabilities, demonstrates its suitability as decision-making tool for deep geothermal energy in Switzerland.
- Results from the missing information profile, and the profiles representing equal weighting and focusing on environment are quite similar. Generally, areas in NE Switzerland perform best.
- Results focusing on the economic dimension strongly differ, with the Western part of Switzerland achieving Low and Medium-Low sustainability.
- When focusing on social indicators, results for most areas fall into the Medium-High and High sustainability categories.

References

[1] Bodmer Philippe H., (1982): Beiträge zur Geothermie der Schweiz. Diss. Naturwiss. ETH Zürich, Nr. 7034, 210 p.

[2] Spada, M., Burgherr, P. (2015). Chapter 6.1: Accident Risk. In Hirschberg S., Wiemer S. and Burgherr P.: Energy from the Earth. Deep Geothermal as a Resource for the Future? TA-SWISS Study TA/CD 62/2015, vdf Hochschulverlag AG, Zurich, Switzerland, pp. 229-262. http://dx.doi.org/10.3218/3655-8.

[3] Tervonen T., Lahdelma R., Almeida Dias J., Figueira J., Salminen P. (2007) SMAA-TRI. In: Linkov I., Kiker G.A., Wenning R.J. (eds) Environmental Security in Harbors and Coastal Areas. NATO Security through Science Series (Series C: Environmental Security). Springer, Dordrecht

SCCER SoE
SWISS COMPETENCE CENTER for ENERGY RESEARCH
SUPPLY of ELECTRICITY

SCCER-SoE Annual Conference 2019

PAUL SCHERRER INSTITUT PSI

Supported by:
Schweizerische Eidgenossenschaft
Confédération suisse
Confederazione Svizzera
Confederaziun svizra
Swiss Confederation
Innosuisse – Swiss Innovation Agency

Energy system pathways with low environmental impacts and costs

Laurent Vandepaer[1,2], Panos Evangelos[2], Christian Bauer[2] and Ben Amor[1]
[1]Université de Sherbrooke, Civil Engineering Department, Sherbrooke, Quebec, Canada,
[2]Laboratory for Energy Systems Analysis, Paul Scherrer Institute, CH-5232 Villigen PSI, Switzerland
E-Mail: laurent.vandepaer@psi.ch
Website Technology Assessment Group PSI : https://www.psi.ch/en/ta

Introduction

Energy systems cause substantial environmental impacts, spanning climate change, air pollution, resource depletion and ecosystem degradations.

Energy system models (ESM) that guide energy policies by generating future energy pathways, at the national and regional level, offer limited insights into such environmental issues.

Solution: environmental indicators based on the life cycle assessment (LCA) methodology are integrated into an (ESM).

Methods

Swiss TIMES energy model is used to represent the Swiss energy system: electricity, heat, and transport.

19 environmental categories are assessed: IPCC Global Warming Potential (GWP 100) and the ReCiPe method.

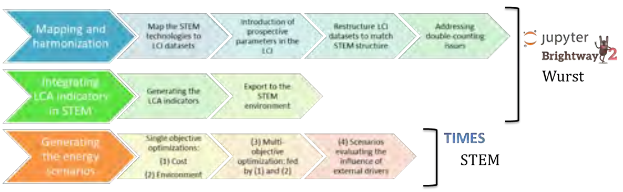

Fig. 1 integration LCA indicators into STEM and generating the energy scenarios, tools used per stage.

Energy pathways are generated for Switzerland up to the year 2050, resulting from the single- and multi-objective optimization of cost and environmental impacts.

Table 1 List of scenarios presented in the study, full name, primary objective, secondary objective(s), abbreviation, type and family

Energy scenario name	Primary objective	Secondary objective(s)	Abbreviation	Type	Family + (Background LCI databases)
Cost-optimized climate scenario	Cost	-	Clim, cost opt.	Single-objective optimization	Least-cost scenarios (BAU)
Cost-optimized Business as usual scenario	Cost	-	BAU, cost opt.	Single-objective optimization	Least-cost scenarios (BAU)
Least climate change scenario	Climate change	-	CC opt.	Single-objective optimization	Least-LCIA scores scenarios (BAU)
Least metal depletion scenario	Metal depletion	-	MDP opt.	Single-objective optimization	Least-LCIA scores scenarios (BAU)
Least human toxicity scenario	Human toxicity	-	HT opt.	Single-objective optimization	Least-LCIA scores scenarios (BAU)
Least climate change scenario, with σ % cost increase from optimal value	Climate change	Cost (relax. fac.: σ= 5%, 30 % and 50%)	CC opt., + σ % least cost	Multi-objective optimization	Least-LCIA scores scenarios with constraints based on the single-objective optimal value (BAU)
Least metal depletion scenario, with σ % cost increase from optimal value	Metal depletion	Cost (relax. fac.: σ = 5%, 15% and 30 %)	MDP opt., + σ % least cost	Multi-objective optimization	Least-LCIA scores scenarios with constraints based on the single-objective optimal value (BAU)
Least human toxicity scenario, with σ % cost increase from optimal value	Human toxicity	Cost (relax. fac.: σ = 5% and 30 %)	HT opt., + σ % least cost	Multi-objective optimization	Least-LCIA scores scenarios with constraints based on the single-objective optimal value (BAU)
Least climate change scenario, with σ % cost increase and μ % increase of metal depletion level from optimal values	Climate change	Cost (relax. fac.: σ = 5% and 30 %), Metal depletion (relax. fac.: μ = 5% and 30%)	CC opt., + σ % least cost & + μ % least MDP	Multi-objective optimization	Least-LCIA scores scenarios with constraints based on the single-objective optimal value (BAU)
Cost-optimized climate scenario, without additional investments on energy storage	Cost	-	Clim, cost opt., no battery	Single-objective optimization	Scenarios evaluating the influence of external drivers (BAU)
Least climate change scenario, without DAC and CCS technologies	Climate change	-	CC opt., no DAC & CCS	Single-objective optimization	Scenarios evaluating the influence of external drivers (BAU)
Cost-optimized climate scenario, with climate background LCI database	Cost	-	Clim, cost opt., Cli.DB	Single-objective optimization	Scenarios evaluating the influence of external drivers (Climate)
Least climate change scenario, with climate background LCI database	Climate change	-	CC opt., Cli.DB	Single-objective optimization	Scenarios evaluating the influence of external drivers (Climate)
Cost-optimized climate scenario, with climate background LCI database and least climate change value	Cost	Climate change (relax. fac.: μ = 0%)	Clim, cost opt., Cli.DB and least CC value	Multi-objective optimization	Scenarios evaluating the influence of external drivers (Climate)

Results

It is possible to generate energy pathways with low life cycle greenhouse gas (GHG) emissions with moderate increase in the costs (e.g. CC opt, +5% least cost).

Fig. 2 Cumulative cost (x-axis) against cumulative LCIA scores in terms of climate change (y-axis), metal depletion (size of the bubbles), and human toxicity (color scale) for the different scenarios between the years 2010 and 2050. The cost shown as relative to the cost-optimized climate scenario ('Clim, cost opt.', red circle). The metal depletion shown as relative to the optimal value from least metal depletion scenario ('MDP opt').

Minimization of the life cycle impacts on climate change generates:
(i) Trade-offs, increasing the impacts of metal depletion (i.e. large bubble) and human toxicity (i.e. color scale toward yellow) caused by the upstream extraction and manufacturing stages.
(ii) Substantial environmental co-benefits with regards to air pollution, ozone depletion, acidification, and land transformation (not in Fig.2).

Ambitious reduction targets of direct GHG emissions of 95% for the year 2050 might still result in substantial climate change impacts if emissions embodied in the infrastructure and upstream supply chain are not mitigated jointly (see red circle in Fig.2 cost-optimized climate scenario, and Fig.3.a)

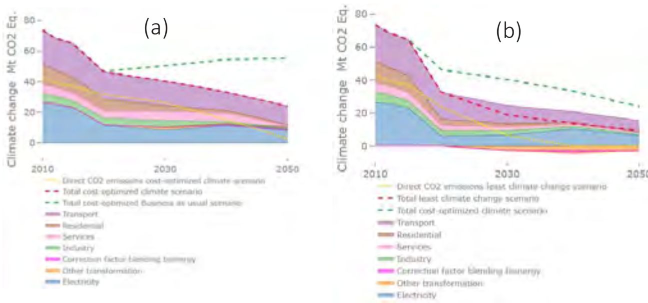

Fig. 3 Life cycle climate change impacts of the (a) cost-optimized climate scenario from 2010 to 2050, total, distribution per sector and comparison with the total impact of the cost-optimized business as usual scenario; (b) least climate change scenario from 2010 to 2050, total, distribution per sector and comparison with the total impact of the cost-optimized climate scenario.

Contributions

Multi-objective optimization allows to create pathways with minimized impacts at moderate cost.

The integration of the environmental impact minimization as an objective gives access to additional part of the solution space.

The environmental indicators consider the future evolution of the environmental performance of energy processes represented in the ESM, through prospective LCA including foreground and background LCI changes

This work is replicable to perform similar integration of LCA indicators either into other ESM or Integrated Assessment Models.

Acknowledgements : The authors received financial contribution from Wallonie-Bruxelles International (WBI) through the WBI-World Excellence Scholarship, and from the Natural Sciences and Engineering Research Council of Canada through the Discovery Grants Program. This work was partially funded by the Commission for Technology and Innovation in Switzerland (CTI) within the Swiss Competence Center for Energy Research in Heat and Electricity Storage, the Swiss Competence Center for Energy Research in Supply of Electricity and the Swiss Competence Center for Energy Research Joint Activity Scenario and Modelling.

SCCER SoE

SWISS COMPETENCE CENTER for ENERGY RESEARCH
SUPPLY of ELECTRICITY

SCCER-SoE Annual Conference 2019

Supported by:
Schweizerische Eidgenossenschaft
Confédération suisse
Confederazione Svizzera
Confederaziun svizra

Swiss Confederation

Innosuisse – Swiss Innovation Agency

Nonlinear Inverse Demand Curves in Electricity Market Modeling

Yi Wan, Martin Densing
Energy Economics Group, Laboratory for Energy Systems Analysis, Paul Scherrer Institute (PSI)

Motivations

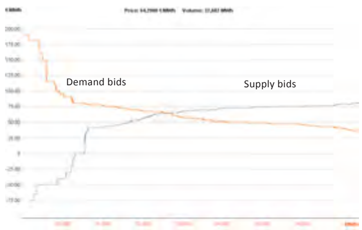

- Provide a more accurate demand curve estimation which is close to real biding case
- Reduce the model Bias of Nash Cournot electricity market models with linear demand curves, which usually have higher prices and lower volumes than observed
- Give a proper estimation for the parameter in the conjectural variation mechanism in equilibrium models and improve the basic electricity market modeling for other scenarios

Numerical Implementation of Nonlinear Demand Curves

In order to implement nonlinear demand curves into electricity market modeling, a technology detailed model, the Cross-Border Electricity Market Model (BEM) and a new computational tool, EMP are combined.

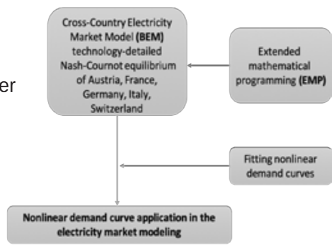

- BEM is an equilibrium model with market power where a Nash Cournot mechanism is implemented as well.
- EMP is a generalization framework that can derive optimality conditions automatically and allows multiple format models' reformulation, including MCP.

Results

Elasticity analysis of Germany and Austria day-ahead market:

- Nonlinear curves give lower price elasticity estimation
- The absolute value of elasticity decreases over time:
- In 2010, the elasticity decreases due to renewable generation expansion
- After 2013, one of the reasons for the elasticity increase is the improved price forecast of players [preliminary]

Price Elasticity and Average Hourly Volume of Germany & Austria Day-ahead Market, 2006 - 2015

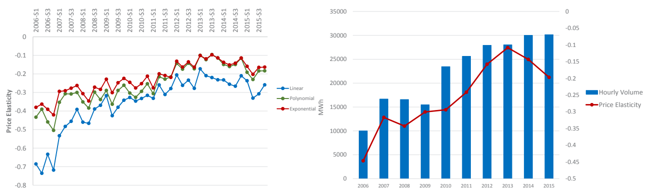

Impacts of the nonlinear inverse demand curves on electricity market modeling:

Using one representative nonlinear demand curve for 4 seasons × 24 day hours:

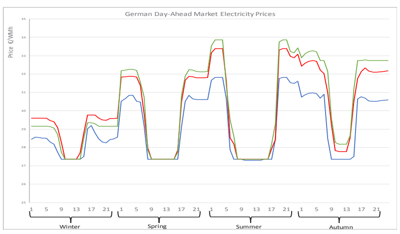

Results (cont.)

Using corresponding hourly fitted nonlinear demand curves for four seasons × 24 day hours:

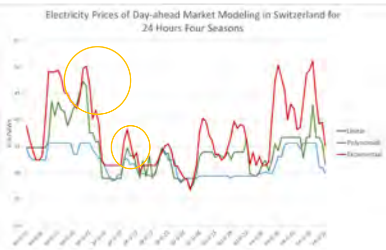

Market prices with nonlinear demand curves are more volatile. In the low supply case prices with nonlinear demands are higher than in the high supply case, where prices between nonlinear and linear demand curves are close.

Improved conjectural variation parameter (θ) estimation:

The Conjectural variation parameter is estimated to be lower by using nonlinear than by using linear demand curves.

Using the estimated θ, modeling results are close to the historical real market prices.

Conjectural Variation:

$$P(d) + \mathrm{d} \cdot \theta \frac{\partial P(d)}{\partial d} - C = 0$$

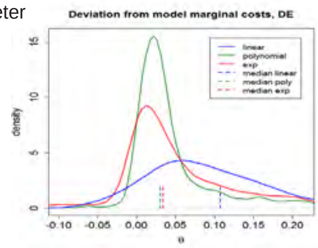

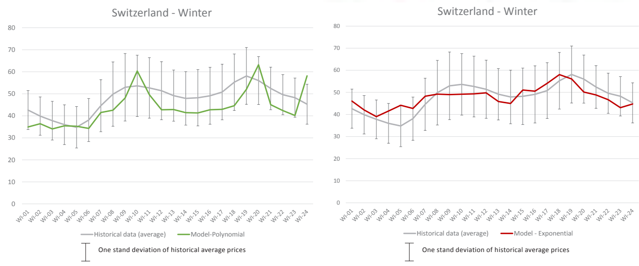

Θ scaled by 60%

Conclusions

- Polynomial demand curves perform best in fitting the day-ahead electricity market data compared with linear and exponential ones.
- Nonlinear fitting inverse demand curves suggest lower elasticity estimations.
- Nonlinear inverse demand curves can be implemented to improve the electricity market modeling especially when market supply is low.
- Better explanation for large price deviations between market prices and marginal cost-based prices can be provided by models with nonlinear demand curves, even under the assumption of small market distortions.

References

- Panos, E., Densing, M. "The future developments of the electricity prices in view of the implementation of the Paris Agreements: will the current trends prevail, or a reversal is ahead?." *Energy Economics,* 2019.
- Wan, Y., "Non-linear demand curves", Msc Thesis, ETH Zurich, 2019.
- Youngdae, K., Ferris. M. "Solving equilibrium problems using extended mathematical programming". *Math Prog Comp*, 2019.
- Panos, E., Densing, M., Schmedders, K. "Oligopolistic capacity expansion with subsequent market bidding under transmission constraints (OCESM)", 2017.

SCCER SoE
SWISS COMPETENCE CENTER for ENERGY RESEARCH
SUPPLY of ELECTRICITY

more about us

SCCER-SoE Annual Conference 2019

Supported by:
Schweizerische Eidgenossenschaft
Confédération suisse
Confederazione Svizzera
Confederaziun svizra
Swiss Confederation
Innosuisse - Swiss Innovation Agency
Swiss Federal Office of Energy

The potential & levelized cost of solar PV in Switzerland

Xiaojin Zhang[1](xiaojijn.zhang@psi.ch), Christian Bauer[1]
[1]Technology Assessment Group, Laboratory for Energy Systems Analysis, Paul Scherrer Institute, Switzerland

Introduction

- Update of levelized cost of electricity (LCOE) for solar PV in Switzerland with most recent data available
- Calculated:
  - Current & future LCOE
  - System size 6 -1000 kWp
  - Uncertainty ranges of LCOE
  - Sensitivity analysis for key parameters
- Associated for the first time the LCOEs for all the roofs in Switzerland with the potential of national annual generation

Methodology

$$\text{LCOE}=\frac{\sum_{t=1}^{n}\frac{I_t+M_t+D_t}{(1+r)^t}}{\sum_{t=1}^{n}\frac{E_t}{(1+r)^t}}$$

LCOE Levelized Cost Of Electricity
I_t capital investment in the year t
M_t operations and maintenance cost in the year t
D_t decommissioning expenditures in year t
E_t annual electricity generation in year t (including degradation)
r discount or interest rate
n system lifetime

Related assumptions	Key source of reference
System investment cost	Solar offer check tool
Area, solar irradiance of roofs in Switzerland	Sonnendach
Annual O&M cost, Replacement cost	Toggweiler et al. 2018
System investment cost breakdown	Heiniger and Perret. 2017
General methodology, decommissioning cost	Bauer. et al. 2017

Results

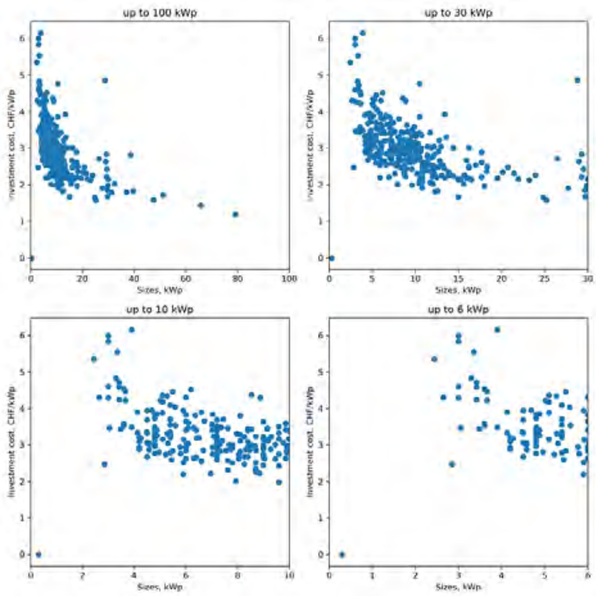

Figure 1: System investment costs of various system sizes in Switzerland, 2018; from top left to bottom right: size up to 100 kW_p, 30 kW_p, 10 kW_p and 6 kW_p.

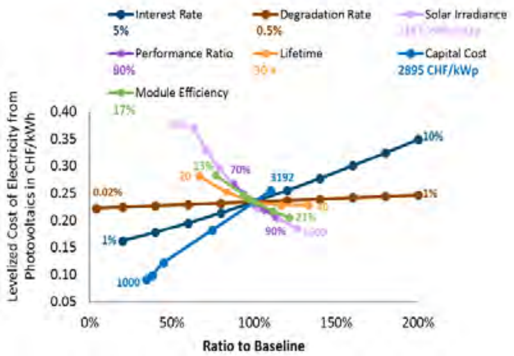

Figure 2: Sensitivity analysis for LCOE of a 10 kW_p system in 2018.

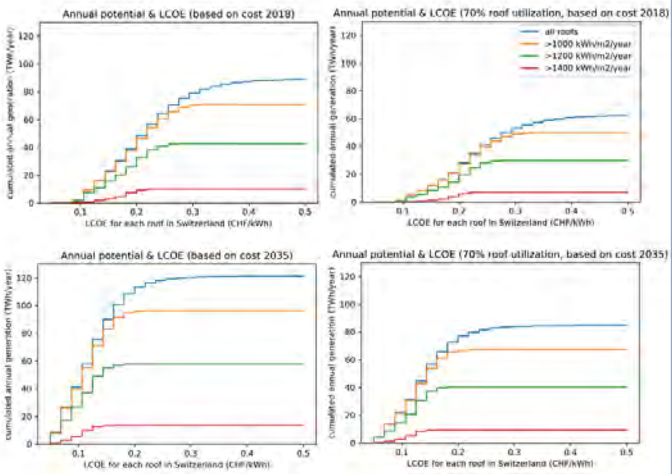

Figure 3: Annual electricity generation potential and LCOE for all roofs and solar irradiance of more than 1000, 1200 and 1400 kWh/m2/year, considering system investment cost in 2018 and 2035

Discussion & Conclusions

- Most of the installed PV systems in Switzerland are small-scale (less than 20 kW_p).
- LCOE is most sensitive to the solar irradiance, followed by system lifetime.
- The total generation potential in Switzerland is high (given the national annual consumption of 60 TWh of electricity), especially considering further cost reduction in the future.
- However, considering the actual utilization rate of roof and socially-acceptable LCOE will reduce the potential
- Future research should focus on investigating daily and seasonal generation pattern, local electricity tariff and consumption mix to better understand the possible potential

References

- Solar offer check tool, SFOE: https://www.energieschweiz.ch/page/de-ch/solar-offerte-check
- Sonnendach: SFOE swisstopo, MeteoSchweiz: https://www.uvek-gis.admin.ch/BFE/sonnendach/
- Toggweiler, P. (2018) Betriebskosten von Photovoltaikanlagen – Update der Analyse zu den Betriebskosten von PV-Anlagen aus dem Jahr 2015.
- Heiniger., L-P. and Perret, L. (2017) IEA PVPS, National Survey Report of Photovoltaic Applications in Switzerland 2017.
- Bauer, C., S. Hirschberg (eds.), et al. Potentials, costs and environmental assessment of electricity generation technologies." PSI, WSL, ETHZ, EPFL. Paul Scherrer Institute, Villigen PSI, Switzerland.

Task 4.3

Title

Socio-economic-political drivers

Projects (presented on the following pages)

Spillover dynamics in energy controversies
Eefje Cuppen, Olivier Ejderyan, Udo Pesch, Shannon Spruit, Elisabeth van de Grift, Aad Correljé, Behnam Taebi

Geothermal direct use and electricity in Chilean media discourse
Amanda Martinez Reyes, Sofia Vargas Payera, Olivier Ejderyan

The power of collaboration: Case study of two pumped storage hydropower projects
Fabienne Sierro, Selma L'Orange Seigo, Olivier Ejderyan, Johan Lilliestam, Patricia Zundritsch

SCCER SoE
SWISS COMPETENCE CENTER for ENERGY RESEARCH
SUPPLY of ELECTRICITY

SCCER-SoE Annual Conference 2019

TUDelft

Supported by:
Schweizerische Eidgenossenschaft
Confédération suisse
Confederazione Svizzera
Confederaziun svizra
Swiss Confederation
Innosuisse – Swiss Innovation Agency

Spillover dynamics in energy controversies

Eefje Cuppen[1], Olivier Ejderyan[2], Udo Pesch[1], Shannon Spruit[1], Elisabeth van de Grift[1], Aad Correljé[1], Behnam Taebi[1]
[1]Delft University of Technology, [2]ETH Zürich

Motivation

Energy controversies have been widely studied. Such studies are, however, generally based on either single case studies, providing rich and in-depth understanding of (local) dynamics of planning processes, or they focus on understanding responses to a specific technology (not bounded to a location). These studies tend, therefore, to overlook a key dynamic in controversy, namely that publics respond to projects by drawing on earlier experiences.
Spillovers occur when actors' explicit reference to experiences with a similar technology elsewhere, or with earlier experiences with other technologies at the same location, determine the discursive space of the controversy, and thereby the dynamics of the controversy.
Spillovers are usually considered to be contextual factors and as such ignored as part of the policy debate
The objective of this paper is to conceptualize spillover as an important dynamic in controversies and to develop a research agenda.

Methods

The paper is based on a review of the literature from social science and humanities on energy controversies and on the analysis of three specific cases to understand the mechanisms of spillover.

Three types of spillover

We identify different types of spillovers in energy controversies.

- Spillovers may be spatial: a controversy in one place may spill over to another place. We refer to this type of spillover as *geographical spillover*.
- Spillovers may concern technologies: a controversy on one technology may spill over to another technology, as the example above on geothermal energy and fracking illustrates. We label this type of spillover as *technology spillover*.
- Spillover may also be temporal: it may arise from earlier controversies about other policy issues within a region. We label this type of spillover as *historical spillover*.

Geographical spillover in the Dutch shale gas debate
In 2009 the first plans were made for exploration of shale gas in the Netherlands, when the British oil company Cuadrilla requested exploration permits for two areas in the Netherlands. In 2011, Cuadrilla received the permit to start exploration in Boxtel, a small town in the south of the Netherlands. From that moment onwards, the controversy rapidly expanded. What started as a local debate on safety and risks of shale gas exploration, soon erupted to a fierce national debate on the role of shale gas in the energy transition. In these dynamics, spillover from controversies on shale gas in the US and the UK played an important role. References were made to the movie Gasland and to earthquakes in Blackpool, UK. The case is therefore an illustration of geographical spillover.

Technology spillover in the Swiss deep geothermal energy debate
The Swiss Energy Strategy 2050 supports the development of deep geothermal energy (DGE) production. This triggered debates in the national and local parliaments about whether authorising DGE in Switzerland would open the way to fracking for the exploitation of shale oil and gas. In the town of Haute-Sorne in the Canton of Jura in western Switzerland, residents have opposed a project by drawing on arguments against fracking for shale-gas. Opponents argue that DGE is just like fracking and that it will cause repeated induced earthquakes and groundwater pollution like in US regions that have experienced a shale boom, even suggesting that DGE projects might be a cover-up to develop shale gas exploitation.

Historical spillover in the Dutch Peat Colonies
In 2011 the formal planning procedures for two onshore wind farms in the north-east of the Netherlands were initiated. Both plans triggered fierce local opposition. In addition to common arguments against wind power like the impact of sound and shadow flicker and impact on landscape, opponents also drew from pre-existing sources of contention on the region's past. As renewable energy production has become more and more prominent, the north-east of the Netherlands has been faced with several initiatives for large-scale wind-farms. This has triggered an existing sentiment that renewable energy production is yet another way for the rest of the country to profit from the region's resources. Public debates and issues triggered by preceding energy (related) projects spilled over in this northern Dutch context and (negative) experiences from the past are being projected onto current or proposed projects.

Outlook for a research agenda

Compared to other notions such as "context" or "environment" that are used to describe the effects of site-specific features on energy controversies, the notion of spillover presents several advantages:

1. it emphasizes the agency (intentional or not) needed to "make" something become a context;
2. the notion of geographical spillover points to the possible discursive connections that shape the space of a controversy by linking remote locations;
3. historical spillovers highlight that the relevant past for a project is not limited recent events or other project related controversies.

Our conceptual and empirical explorations of spillover as an important dynamic in energy controversies raise several questions that seem worthwhile to explore. We will propose here four lines of research that support a more detailed understanding of the workings of spillovers in controversies. These lines of research relate to:

1. the empirical analysis of arenas, actors and strategies;
2. the influence of conventional and new forms of media;
3. meta-analysis of the dynamics of controversies, and
4. to normative questions about the political and democratic repercussions that come with spillovers.

SCCER SoE
SWISS COMPETENCE CENTER for ENERGY RESEARCH
SUPPLY of ELECTRICITY

SCCER-SoE Annual Conference 2019

CEGA
CENTRO DE EXCELENCIA EN GEOTERMIA DE LOS ANDES

Supported by:
Schweizerische Eidgenossenschaft
Confédération suisse
Confederazione Svizzera
Confederaziun svizra
Swiss Confederation
Innosuisse – Swiss Innovation Agency

Geothermal direct use and electricity in Chilean media discourse

Amanda Martinez Reyes,† Sofia Vargas Payera,Ψ and Olivier Ejderyan†
†Swiss Federal Institute of Technology Zurich, ΨAndean Geothermal Center of Excellence.

Motivation

- Media coverage helps understand public opinion of geothermal energy **[1]**, which is important for the realization of projects.
- Chile is a country with growing geothermal development.
- In Chile, lack of information about successful cases of geothermal projects has been linked to the shaping of negative opinions among local stakeholders. However, opinions tend to be more positive for geothermal direct use because it is seen as an opportunity to meet local needs **[2]**.
- Analyzing media coverage may shed light on public opinion of geothermal energy in Chile, and to identify ways to effectively promote it.

Method: collection and analysis of data

We are conducting a media analysis of the most read National newspapers from Chile: El Mercurio (2002-2018) and La Tercera (2009-2018). The first insights presented only cover findings form El Mercurio's articles.

Article were analyzed through a thematic content analysis using Nvivo 12 Plus. Statements were coded to identify their content. Then they were grouped into thematic categories. Some categories had been predefined based on literature on geothermal energy while others emerged through the grouping of statements. For this poster, we compared the attributes between geothermal end uses to identify differences and similarities.

First insights

Statements were grouped into the following themes, and their frequency is show in the bar chart below:

- Social impact: the involvement of the public in energy projects/development
- Environment: the impact of energy projects/development in the environment
- Governance: the way of running the energy sector
- Technology: energy technologies (power plants, grid, greenhouses, etc.)
- Financing: economic aspects of projects and technologies
- Energy sector: general statements about energy, but not specific to projects
- Energy projects: identified projects

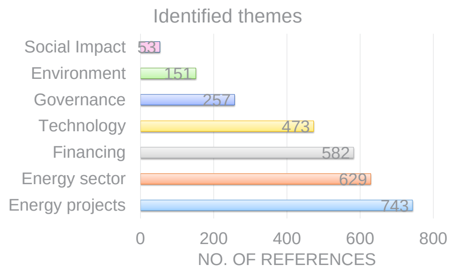

The number of references about direct-use and electricity-generation statements per year are shown in the following histogram. Geothermal direct use was considerably less mentioned than geothermal electricity generation, and started to gain coverage from 2009.

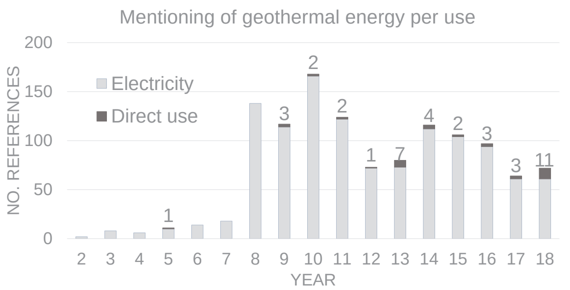

Attributes of geothermal direct use and electricity generation were grouped in the described themes. The later covered mostly positive environmental and technological attributes such as "respectful to the environment", and "efficient technology", respectively. The former was mainly described by: its relation with the energy sector, for example "base-load supply"; and its environmental impact, for example "low-CO2 emissive". In contrast, financing attributes for electricity generation referred to the high investment cost, whereas for direct use to the low investment cost of projects.

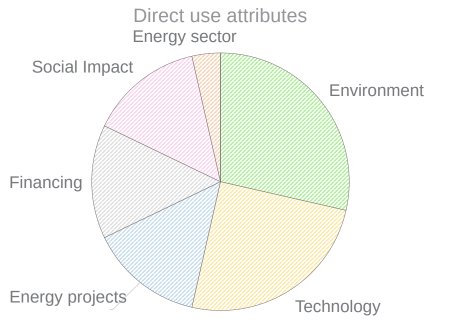

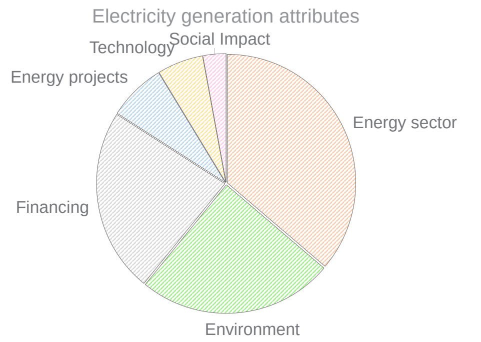

Discussion

- The most dominant theme among El Mercurio's articles was energy projects, followed by energy sector, and financing. This shows that this press medium communicates geothermal energy as specific projects and energy sector development, and less focus is given to the environmental and social implications.
- Geothermal direct use was described only positively, whereas electricity generation additionally covered critical attributes in reference to its costs and complexity. This implies such electricity-related challenges are not perceived for direct use projects.
- Energy sector was the most dominant theme for electricity generation, whereas the second least dominant (after governance) for direct use. This suggests that geothermal electricity generation is discussed in relationship to national issues related to energy provision (energy security, development, decarbonization…). Direct-use in contrast is discussed more in terms of its local impacts. This is signalled by the highest share of statements on specific projects as well as the focus on social impact and potential environmental benefits.

References

[1] Stauffacher, Michael, Nora Muggli, Anna Scolobig, and Corinne Moser. 2015. "Framing Deep Geothermal Energy in Mass Media: The Case of Switzerland." *Technological Forecasting and Social Change* 98 (September): 60–70. https://doi.org/10.1016/j.techfore.2015.05.018.
[2] Vargas Payera, Sofía. 2018. "Understanding Social Acceptance of Geothermal Energy: Case Study for Araucanía Region, Chile." *Geothermics* 72 (March): 138–44. https://doi.org/10.1016/j.geothermics.2017.10.014.

SCCER SoE
SWISS COMPETENCE CENTER for ENERGY RESEARCH
SUPPLY of ELECTRICITY

SCCER-SoE Annual Conference 2019

Supported by:
Schweizerische Eidgenossenschaft
Confédération suisse
Confederazione Svizzera
Confederaziun svizra
Swiss Confederation
Innosuisse – Swiss Innovation Agency

The power of collaboration: Case study of two pumped storage hydropower projects

Fabienne Sierro, Selma L'Orange Seigo, Olivier Ejderyan, Johan Lilliestam, Patricia Zundritsch

Background

The Energy Strategy 2050 calls for an increase of hydropower production capacity. Pumped storage hydropower (PSH) projects willplay an important role to reach this goal.

However PSH projects often conflict with protection of landscape and environment and lead to legal opposition from environmental NGOs. We examine two successful cases: Linth Limmern in Canton Glarus & Lagobianco in Canton Graubünden.

- Linth Limmern: extension of existing PSH plant (including a dam raise + and new high-voltage transmission line). A collaborative approach to include stakeholders was chosen from beginning
- Lagobianco: initial project to expand existing dam. Initial project abandoned due to opposition from environmental NGOs. Operators and NGOs searched collaboratively for a new solution and agreed to have a new PSH plant

Aim of paper: Look at success factors, as perceived by involved actors. Results can be used for planning of future projects (in paper we want to make it relevant for outside Swiss context – here the opposite?)

Method

In both case studies, data on the perception of the collaborative process was collected through semi-structured, in-depth interviews (n=14) with involved actors (working group members and decision makers from involved organizations).

Interview transcripts were analysed through thematic content analysis to identify what interviewees perceived key elements in making the collaboration successful. These could be stated explicitly or inferred through the description they made of the process.

Results

The situation in both cases corresponds to what Covey & Brown (2001) have identified as critical cooperation (Tab.1). Operators wanted to develop solutions to maximise electricity production which conflicted with the NGOs and residents wish to protect the environment and landscape. However all actors saw the necessity to have a sustainable energy production system that minimizes impacts on environment and landscape.

	Converging Interests Low	Converging Interests High
Conflicting Interests Low	Non-engagement	Cooperation
Conflicting Interests High	Conflict	Critical Cooperation

Tab. 1: Types of engagement of actors in function of interest conflicts and convergence (adapted from Covey & Brown 2001),

Interviewees highlighted the role of trustable and competent persons that enabled the parties to collaborate. These are brokers who connect organizations or people that would not otherwise be connected (term from social network theory). The importance of their role has been recognized for critical cooperation (Long et al. 2013). Our paper looks at conditions that help brokers to exercise their function successfully.

We identified that the factors enabling good collaboration were not limited to the direct interactions between the actors during the workshops or the meetings. They also related to the situation within the organisation/group to which individual actors belonged too, as well as the cooperation between these organisation.

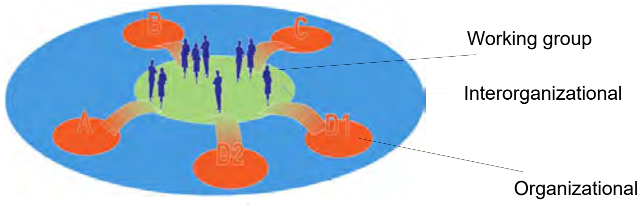

Fig. 1: The 3 spheres of collaboration.

We identify 3 spheres of collaboration that are related to each others (Fig 1.). "Working group" refers to the group of stakeholders meeting to discuss the project. "Organizational" refers to the organization (or group, or community) to which the members of the working group belong, et to whom they have to refer about the process. "Interorganizational" refers to the relationships between the organizations. By considering these 3 spheres, we identified the success factors for collaboration listed in table 2.

Sphere	Perceived success factors
Interorganizational	• Commitment of top-level individuals of each organization • Clear definition of working group mission (outcome left open) • Delegation of negotiation to technical experts • Irregular but sustained involvement of top-level management
Organizational	• Delegation of negotiation to internal experts • Continuous support of and trust in delegated expert • Resource allocation to delegated broker
Working group	• Common definition of rules • Openness of outcome • Transparent knowledge and data sharing • Regular validation within own organization • Focus on particular project at hand, balancing it as a whole

Tab. 2: Perceived success factors in each of the 3 spheres of collaboration

Discussion

- Important to look at all 3 different spheres, not just concentrate on working group, or involved organizations
- Working group members act as brokers between the group and their organizations
- Conditions can be shaped such that brokers can fill their role well
- Commitment has to come from top-level, but actual negotiations should happen between experts in the field
- Focus on project at hand important, no discussion of energy politics in general
- Full disclosure of information within group, commitment not to disclose information to the public/media

Selected References

Covey, J., & Brown, L. D. (2001). Critical Cooperation: An Alternative Form of Civil Society-Business Engagement. *JDR Reports*, *17*(1), 21.

Long, J. C., Cunningham, F. C., & Braithwaite, J. (2013). Bridges, brokers and boundary spanners in collaborative networks: A systematic review. *BMC Health Services Research*, *13*(1), 158. https://doi.org/10.1186/1472-6963-13-158

Task 4.4

Title

Joint Activity Scenarios & Modeling (JA-S&M)

Project (presented on the following page)

Joint Activity Scenarios & Modelling
JASM-team

Distributional trade-offs of renewable electricity generation, transmission and storage in Europe
Jan-Philipp Sasse, Evelina Trutnevyte

Models on the wrong track: Model-based electricity supply scenarios in Switzerland are not aligned with the perspectives of energy experts and the public
Georgios Xexakis, Ralph Hansmann, Sandra P. Volken, Evelina Trutnevyte

SCCER-SoE Annual Conference 2019

Supported by:

Schweizerische Eidgenossenschaft
Confédération suisse
Confederazione Svizzera
Confederaziun svizra

Swiss Confederation

Innosuisse – Swiss Innovation Agency

Joint Activity Scenarios & Modelling

JASM-team (contact: Adriana Marcucci, madriana@ethz.ch)

JASM-structure: How do the models fit?

Modelling groups of 8 SCCERs work together to analyse scenarios for the realization of the Swiss Energy Strategy 2050

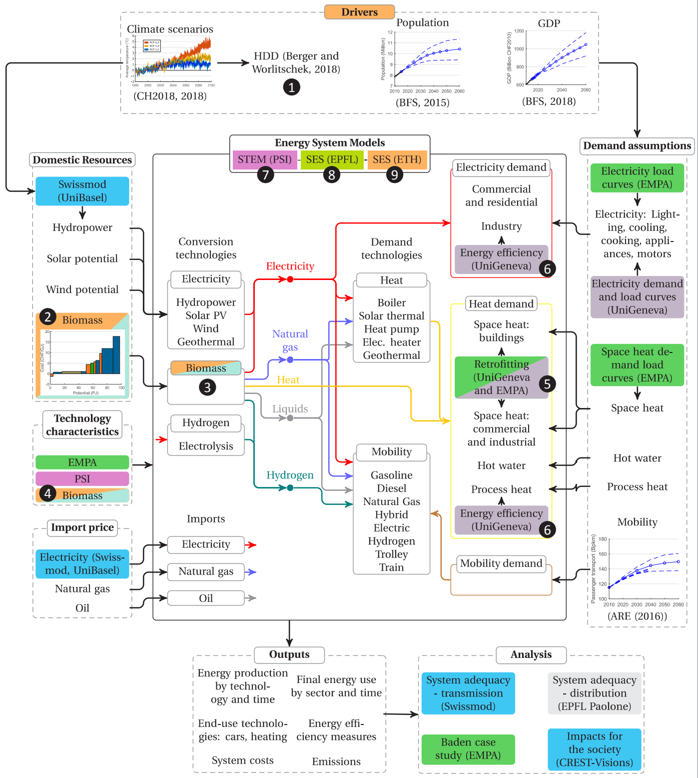

Universität Basel · SCCER CREST · Empa · Université de Genève · IPESE · biosweet · ETH zürich · SCCER SoE · DESL, EPFL · PSI · SCCER FURIES · Heat & Electricity Storage · SCCER mobility

Modelling Highlights

Impact of climate change

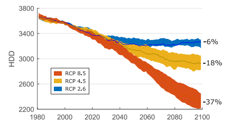

1. Heating and cooling demand (Berger and Worlitschek, 2018)

Biomass

2. Updated assessment of biomass and waste resources
3. Biomass roadmap
4. Expert elicitation on biomass technologies

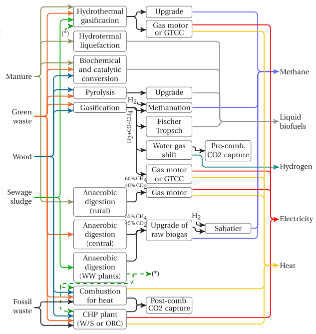

Energy efficiency

5. Buildings: Investment cost for building retrofitting (Streicher et al., 2018, 2019)
6. Industry: Energy efficiency for heat and electricity demand (Zuberi et al., 2017, 2018)

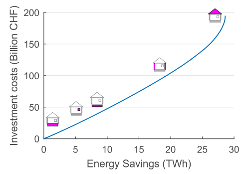

STEM 7

→ Updated costs of Mobility technologies

→ Detailed model of industrial subsectors

→ Model of demand-side management mechanisms

SES

8. Industry: Detailed model of chemicals and plastics

8 9 Integration of new biomass technologies (from JASM roadmap)

Selected results

STEM-PSI

Alternative policy scenarios

Electricity supply 2020-2050 pathways

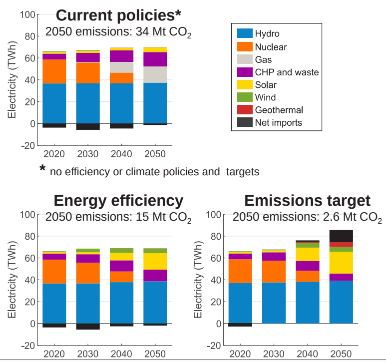

* no efficiency or climate policies and targets

SES-EPFL

2050 electricity production and carbon flow for climate scenario

→ Electricity technologies with the increase in the share of renewables

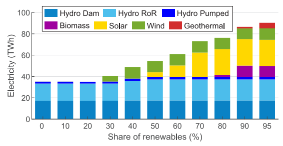

→ 2050 Carbon flow in climate scenario with 1.5 t CO_2 per capita

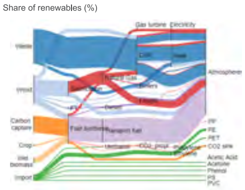

SES-ETHZ

Role of SCCER-SoE technologies

Pareto frontiers of scenarios for 2050 with or without certain technologies

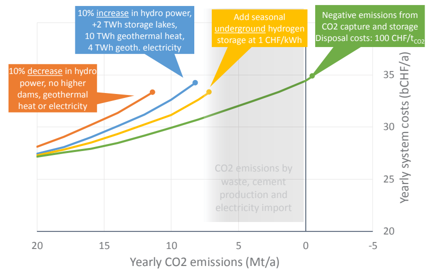

References

- Berger, M., Worlitschek, J., 2018. A novel approach for estimating residential space heating demand. Energy 159, 294-301.
- CH2018, 2018. CH2018 – Climate Scenarios for Switzerland. National Centre for Climate Services
- Streicher, K.N., Padey, P., Parra, D., Bürer, M.C., Patel, M.K., 2018. Assessment of the current thermal performance level of the Swiss residential building stock: Statistical analysis of energy performance certificates. Energy and Buildings 178, 360-378.
- Streicher, K.N., Padey, P., Parra, D., Bürer, M.C., Schneider, S., Patel, M.K., 2019. Analysis of space heating demand in the Swiss residential building stock: Element-based bottom-up model of archetype buildings. Energy and Buildings 184, 300-322.
- Zuberi, M.J.S., Bless, F., Chambers, J., Arpagaus, C., Bertsch, S.S., Patel, M.K., 2018. Excess heat recovery: An invisible energy resource for the Swiss industry sector. Applied Energy 228, 390-408.
- Zuberi, M.J.S., Tijdink, A., Patel, M.K., 2017. Techno-economic analysis of energy efficiency improvement in electric motor driven systems in Swiss industry. Applied Energy 205, 85-104.

Distributional trade-offs of renewable electricity generation, transmission and storage in Europe

Jan-Philipp Sasse[1], Evelina Trutnevyte[1]
[1]Renewable Energy Systems group, Faculty of Science, Department F.-A. Forel for Environmental and Aquatic Sciences, Institute for Environmental Sciences, University of Geneva, Switzerland

Introduction

- Expansion of decentralized renewable electricity generation (DREG) is the key requirement for climate protection, energy security and economic growth [1].
- To reach net-zero emissions by 2050 in the EU, the share of electricity supply from renewables has to increase from 21% (2010) to 57% (2050) [2] (Fig. 1).
- Previous research showed that such clean energy transition risks creating new patterns of spatially uneven regional development, e.g. clustering of renewable energy investments to few locations and regionally uneven impacts on emissions, electricity generation costs, health and employment [3, 4, 5].
- The appropriate spatial allocation of renewable electricity generation and potentially emerging inequities is a new and recently noticed policy challenge [4, 6, 7].

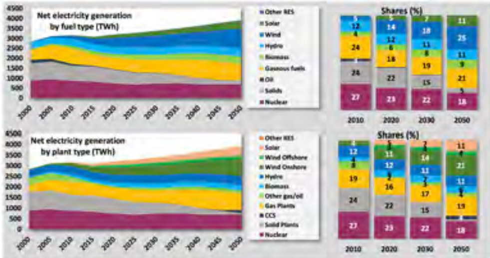

Figure 1. *Share (%) of DREG net electricity generation by fuel type and by plant type. This figure is reproduced from [2]*

Research questions

1. What are the distributional impacts (i.e. additionally installed renewable capacity, storage, transmission infrastructure, and its impact on electricity generation cost) for reaching net-zero emissions in Europe at NUTS-3 level by 2050?
2. How do these distributional impacts vary when increasing levels of regional equity (i.e. equitable spatial allocation of DREG) compared to the cost-efficient spatial allocation?
3. How do NUTS-3 regions in Europe (today and in future scenarios) compare in terms of regional equity of DREG spatial allocation?

Methods and materials

- Study region: Europe at high NUTS-3 spatial resolution (Fig. 2).
- We setup the model by hard-linking the PyEXPANSE and PyPSA models (Fig. 3):
  - PyEXPANSE to assess long-term capacity expansion requirements by generating equitable scenarios with Modeling to Generate Alternatives (MGA) method [4,8].
  - PyPSA [9] to assess short-term economic dispatch, storage and transmission requirements and costs.
- Each scenario is compared in terms of distributional impacts for multiple levels of regional equity, which we measure with an adapted concept of the Gini coefficient [4,10].

Figure 2. *Study regions (Switzerland in red)*

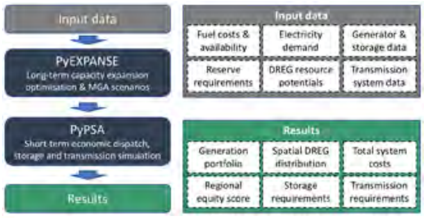

Figure 3. *Overview of the modelling methodology*

- We develop an energy justice framework in which we embed our equity analysis [4] (Fig. 4).
- We include multiple equity or "effort-sharing" principles to assess the equitable spatial allocation of renewable electricity generation as proposed by Höhne et al. [11].
  - Equality: e.g. equal per capita renewable capacity allocation.
  - Cost-efficiency: e.g. least-cost allocation by total system cost (generation, storage & transmission).
  - Capability: e.g. allocation of renewable capacity weighted by GDP.
  - Responsibility: e.g. allocation of renewable capacity weighted by historic emissions.

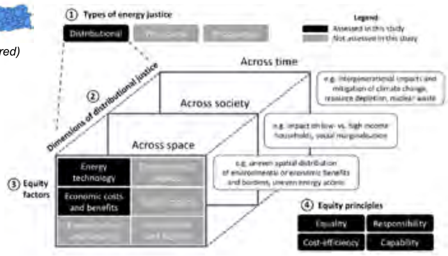

Figure 4. *Energy justice framework. This figure is reproduced from [4]*

Preliminary results for one country (Switzerland)

- Least-cost DREG allocation leads to highest electricity storage and net import costs; but still has low total system costs (Fig. 5).
- Most regionally equitable scenarios lead to high total system costs (Fig. 5 & 6).
- There is a significant trade-off between equity, levelized cost of electricity (LCOE) and total system cost found in Switzerland: 100% increase in regional equity when allocating DREG leads to 20% higher LCOE and 35% higher total system costs (Fig. 6).
- Existing transmission line capacity is sufficient to achieve Swiss 2035 DREG capacity targets (n-1 security approximation) (Fig. 5).
- Pumped hydro and battery storage plants are able to balance high solar PV power supply and demand (Fig. 7 & 8).

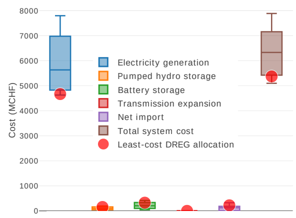

Figure 5. *Boxplot of total system cost components (annualized) for least-cost DREG allocation and 200 MGA scenarios*

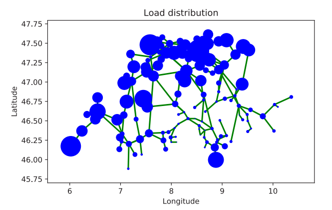

Figure 7. *Hourly load distribution with ENTSO-E transmission grid infrastructure extracted with GridKit model [12]*

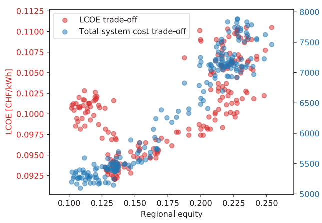

Figure 6. *Equity trade-off between LCOE and total system costs for 200 MGA scenarios*

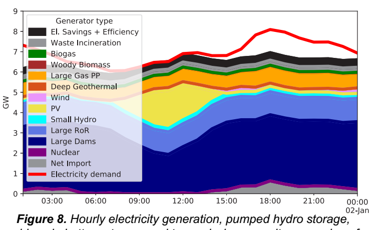

Figure 8. *Hourly electricity generation, pumped hydro storage, grid-scale battery storage and transmission capacity expansion of least-cost DREG allocation scenario*

Next steps

- Expand analysis to further 4 countries: France, Germany, Netherlands and Austria, and later to all regions from Fig. 2.
- Assess distributional trade-offs of total system cost for varying degrees of regional equity for these regions.
- Assess distributional trade-off for a range of equity principles: equality, cost-efficiency, responsibility and capability (Fig. 4).

References

[1] Directorate-General for Climate Action (European Commission). Going climate-neutral by 2050 - A strategic long-term vision for a prosperous, modern, competitive and climate-neutral EU economy. Luxembourg: 2019.
[2] Directorate-General for Climate Action (European Commission). EU reference scenario 2016. Energy, transport and GHG emissions Trends to 2050. Luxembourg: 2016.
[3] Bridge G, Bouzarovski S, Bradshaw M, Eyre N. Geographies of energy transition: space, place and the low-carbon economy. Energy Policy 2013;53:331–40. doi:10.1016/j.enpol.2012.10.066.
[4] Sasse J-P, Trutnevyte E. Distributional trade-offs between regionally equitable and cost-efficient allocation of renewable electricity generation. Appl Energy 2019. doi:10.1016/j.apenergy.2019.113724
[5] Drechsler M, Egerer J, Lange M, Masurowski F, Meyerhoff J, Oehlmann M. Efficient and equitable spatial allocation of renewable power plants at the country scale. Nat Energy 2017;2:17124. doi:10.1038/nenergy.2017.124.
[6] Balta-Ozkan N, Watson T, Mocca E. Spatially uneven development and low carbon transitions: insights from urban and regional planning. Energy Policy 2015;85:500–10. doi:10.1016/j.enpol.2015.05.013.
[7] Thormeyer C, Sasse J-P, Trutnevyte E. Spatially-explicit models should consider real-world diffusion of renewable electricity: solar PV example in Switzerland. Renew Energy 2020;145:363–74. doi:10.1016/j.renene.2019.06.017.
[8] Trutnevyte E. Does cost optimization approximate the real-world energy transition? Energy 2016;106:182–93. doi:10.1016/j.energy.2016.03.038.
[9] Brown T, Hörsch J, Schlachtberger D. PyPSA: Python for Power System Analysis. Journal of Open Research Software 2018; 6(1). doi: 10.5334/jors.188
[10] Gini C. Variabilità e mutabilità. Rome: Libreria Eredi Virgilio Veschi; 1912.
[11] Höhne N, den Elzen M, Escalante D. Regional GHG reduction targets based on effort sharing: a comparison of studies. Clim Policy 2014;14:122–147. doi:10.1080/14693062.2014.849452
[12] Wiegmans B. (2016). GridKit extract of ENTSO-E interactive map [Data set]. Zenodo. doi:10.5281/zenodo.55853

UNIVERSITÉ DE GENÈVE
FACULTÉ DES SCIENCES

ETH zürich

SCCER SoE
SWISS COMPETENCE CENTER for ENERGY RESEARCH
SUPPLY of ELECTRICITY

FNSNF
This study was part of a SNSF Ambizione Energy project (Grant No.160563)

UNIGE RES

Models on the wrong track: Model-based electricity supply scenarios in Switzerland are not aligned with the perspectives of energy experts and the public

Georgios Xexakis[1,2], Ralph Hansmann[2], Sandra P. Volken[2], Evelina Trutnevyte[1,2]

[1]Renewable Energy Systems group, Faculty of Science, Department F.-A. Forel for Environmental and Aquatic Sciences, Institute for Environmental Sciences, University of Geneva, Switzerland
[2]Institute for Environmental Decisions, Transdisciplinarity Lab, Department of Environmental Systems Science, ETH Zurich, Switzerland

Introduction

- Model-based scenarios have become the key method to explore uncertainties and decision alternatives in the electricity supply transition of many countries [1-3].
- In Switzerland, such scenarios have been developed by many different organisations, including public administration (e.g. Swiss Federal Office of Energy [4]), research institutes (e.g. Paul Scherrer Institute [5]), universities (e.g. ETH Zurich [6]), and non-governmental organizations (e.g. Cleantech [7]).
- Combining scenarios in multi-organization, multi-model scenario ensembles increases the diversity of considered uncertainties [3].
- However, it is unclear whether such ensembles align with the perspectives of stakeholders, including the wider public [8-9].

Methods and Materials

- We collected model-based scenarios by reviewing published scenario studies that provided electricity supply results for 2035 (Table 1).
- We elicited preferred scenarios using the interactive web-tool Riskmeter (Figure 1) from three samples of participants in Switzerland:
  1. non-experts ("citizens", N=61)
  2. non-experts that received balanced information and participated in informational workshops about the electricity supply topic prior to giving their preferred scenarios ("informed citizens", N=46)
  3. participants that were mainly working in or studying about energy topics in Switzerland ("energy experts", N=60)
- We compared model-based and preferred scenarios in terms of technology-specific electricity supply and the whole supply system.

Pub. year	Organisation	Study	Cost-optimization used?	Scenario diversity method used?	Uncertainties explored: Related to nuclear, fossil fuels or imports	Uncertainties explored: Related to domestic renewable sources	Electricity supply excl. hydro (TWh/year)
2019	PSI	[11]	✓				
2018	EPFL - LEURE	[12]	✓		✓		
2017	VSE	[13]		✓			
	ETHZ - TD	[2]		✓			
	ETHZ - FEN & PSI	[14]	✓		✓	✓	
	ETHZ - CP	[15]			✓	✓	
2016	PSI	[16]	✓		✓	✓	
	PSI	[17]	✓		✓		
2015	Econability & PSI & EPFL - LEURE	[18]	✓		✓		
	ETHZ - CP	[19]			✓		
2014	PSI	[20]	✓		✓		
2013	PSI	[21]	✓		✓		
	Cleantech	[7]				✓	
	Greenpeace	[22]				✓	
2012	VSE	[23]	✓			✓	
	PSI	[5]	✓		✓		
	SFOE	[4]			✓		
2011	ETHZ - ESC	[6]					

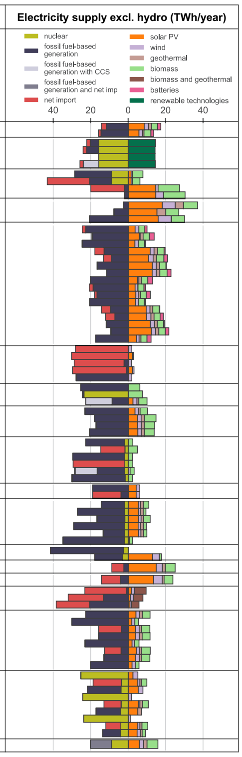

__Table 1.__ Scenario development details for all studies included in the review. Acronyms used: PSI (Paul Scherrer Institute), LEURE (Laboratory of Environmental and Urban Economics), VSE (Verband Schweizerischer Elektrizitäts-unternehmen), FEN (Research Center for Energy Networks) CP (Climate Policy group), TD (Transdisciplinarity lab), SFOE (Swiss Federal Office of Energy), ESC (Energy Science Center).

Aim and research questions

We compare a multi-organization, multi-model ensemble of 80 Swiss electricity supply scenarios for 2035 from 18 studies between 2011-2018 with the preferred scenarios from three samples of stakeholders: citizens (N=61), informed citizens (N=46), and energy experts (N=60). Our study aims to answer the following questions:

1. How does an ensemble of multi-organization, multi-model electricity scenarios compare to the preferred scenarios from citizens, informed citizens, and energy experts?
2. What are the key factors of scenario development that may explain the alignment or misalignment between the model-based scenarios and the preferred scenarios?
3. Does the difference in energy knowledge level of the three samples result in differences in preferred scenarios?

Figure 1. *The interactive web-tool Riskmeter for building Swiss electricity supply scenarios for 2035 [10]*

Results

- Most informed citizens and experts preferred an almost 100% domestic renewable electricity supply in Switzerland in 2035 (Figure 2).
- Most model-based scenarios relied significantly more on fossil fuel-based generation and net electricity imports (Figure 2).
- Possible reasons for this misalignment are the lack of broad stakeholder participation in scenario development, the wide use of cost-optimization models that are known to underrepresent renewable electricity [8], and the limited diversity due to a focus on specific uncertainties (Table 1).
- The energy knowledge level affected preferred scenarios. Citizens preferred statistically significantly lower supply from domestic renewable electricity than informed citizens and experts (Figure 2).

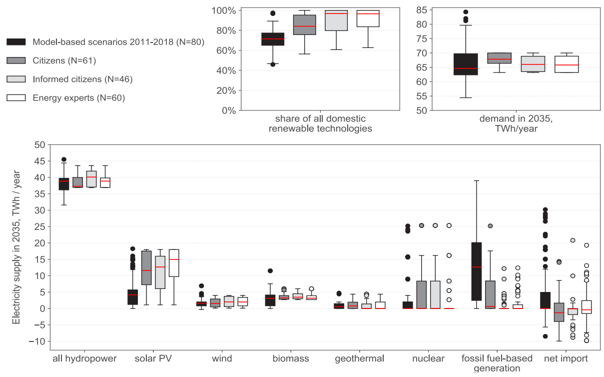

Figure 2. *Comparison of annual electricity supply for 2035 between model-based and preferred scenarios. The boxplots depict median, 25th and 75th quartiles, and 1.5 interquartile range.*

Implications

- For scenario developers and users: even multi-model scenario ensembles can focus on alternatives that are not preferred by stakeholders; diverse stakeholder and public perspectives can enrich scenarios.
- For the electricity supply transition in Switzerland: more scenarios with large-scale deployment of renewable electricity before 2035 should be modelled in the future.

References

[1] Maier HR, Guillaume JHA, van Delden H, Riddell GA, Haasnoot M, Kwakkel JH. An uncertain future, deep uncertainty, scenarios, robustness and adaptation: How do they fit together? Environ Model Softw 2016;81:154–64.
[2] Berntsen PB, Trutnevyte E. Ensuring diversity of national energy scenarios: Bottom-up energy system model with Modeling to Generate Alternatives. Energy 2017;126:886–98.
[3] Trutnevyte E, McDowall W, Tomei J, Keppo I. Energy scenario choices: Insights from a retrospective review of UK energy futures. Renew Sustain Energy Rev 2016;55:326–37.
[4] Prognos. Die Energieperspektiven für die Schweiz bis 2050 [The energy perspectives for Switzerland until 2050]. Basel, Switzerland: Swiss Federal Office of Energy; 2012.
[5] Kannan R, Turton H. Swiss Electricity Supply Options - A supplementary paper for PSI's Energie Spiegel. Villigen PSI, Switzerland: Paul Scherrer Institute; 2012.
[6] Andersson G, Boulouchos K, Bretschger L. Energiezukunft Schweiz [Energy future Switzerland]. Zurich, Switzerland: ETH Zurich; 2011.
[7] Bolliger R, Zeyer C. Cleantech Energiestrategie [Cleantech energy strategy]. Bern, Switzerland: Swiss Cleantech; 2012.
[8] Blok K, Sharma R, Jager D de, Bruinderink RG, Cihlar J. The socio-political merit order. Developing energy strategies that can be rapidly deployed. Utrecht, the Netherlands: ECOFYS; 2018.
[9] Shaw CJ. Reframing climate risk to build public support for radical emission reductions: The role of deliberative democracy. Carbon Manag 2014;5:349–60.
[10] Xexakis G, Volken S, Trutnevyte E. Riskmeter - Portfolio builder 2017. https://portfolio-builder.riskmeter.ch/basic/ (accessed May 5, 2019).
[11] Panos E, Kannan R. Challenges and Opportunities for the Swiss Energy System in Meeting Stringent Climate Mitigation Targets. Limiting Glob. Warm. to Well Below 2 °C Energy Syst. Model. Policy Dev., vol. 64, Springer International Publishing; 2018, p. 155–72.
[12] Babonneau F, Thalmann P, Vielle M. Defining deep decarbonization pathways for Switzerland: an economic evaluation. Clim Policy 2018;18:1–13.
[13] Verband Schweizerischer Elektrizitätsunternehmen. Energiewelten [Energy worlds]. Aarau, Switzerland: Verband Schweizerischer Elektrizitätsunternehmen; 2017.
[14] Fuchs A, Demiray T, Panos E, Ramachandran K, Kober T, Bauer C, et al. ISCHESS – Integration of stochastic renewables in the Swiss electricity supply system. Switzerland: Competence Center for Energy and Mobility (CCEM) and Swisselectric Research; 2017.
[15] Díaz P, Van Vliet O, Patt A. Do we need gas as a bridging fuel? A case study of the electricity system of Switzerland. Energies 2017;10.
[16] Panos E, Kannan R. The role of domestic biomass in electricity, heat and grid balancing markets in Switzerland. Energy 2016;112:1120–38.
[17] Pattupara R, Kannan R. Alternative low-carbon electricity pathways in Switzerland and it's neighbouring countries under a nuclear phase-out scenario. Appl Energy 2016;172:152–68.
[18] Maire S, Pattupara R, Ramachandran K, Vielle M, Vöhringer F. Electricity markets and trade in Switzerland and its neighbouring countries (ELECTRA). Mühlethurnen, Switzerland: Econability, Paul Scherrer Institut, École Polytechnique Fédérale de Lausanne; 2015.
[19] Redondo PD, Van Vliet O. Modelling the Energy Future of Switzerland after the Phase out of Nuclear Power Plants. Energy Procedia 2015;76:49–58.
[20] Kannan R, Turton H. Switzerland Energy Transition Scenarios – Development and Application of the Swiss TIMES Energy System Model (STEM). Villigen PSI, Switzerland: Paul Scherrer Institute; 2014.
[21] Weidmann NO. Transformation strategies towards a sustainable Swiss energy system: An energy-economic scenario analysis. ETH Zurich, 2013
[22] Teske S, Heiligtag G. Energy [r]evolution. Greenpeace International, Greenpeace Schweiz; 2013.
[23] Verband Schweizerischer Elektrizitätsunternehmen. Wege in die neue Stromzukunft - die drei Szenarien [Paths to the new future of electricity - the three scenarios]. Aarau, Switzerland: Verband Schweizerischer Elektrizitätsunternehmen; 2012.

Work Package 5: Pilot & Demonstration Projects

The key objective of the SCCER-SoE in Phase II is the initiation and in some case completion of pilot & demonstration (P&D) projects, which will be executed in close collaboration with industrial partners. The new WP5 combines the integrated approaches developed for geo-energies (WP1), hydropower (WP2), and the innovative technologies of WP3 in a series of seven P&D projects. The successful completion of these projects is a key milestone to deliver a portfolio of tested solutions, which shall enable Switzerland to reach the targets of the Energy Strategy 2050. Status and highlights are summarized below.

The seven demonstrator projects are:
Demo-1: Flagship stimulation experiment in the Deep Underground Laboratory
Demo-2: Reservoir engineering for heat exchange in Haute Sorne
Demo-3: Geneva basin-scale hydrothermal play for heat extraction and storage
Demo-4: CO_2 geological storage pilot
Demo-5: Small Hydro-Power Plant
Demo-6: Controlled fine sediment release from a reservoir by a hydrodynamic mixing device
Demo-7: Complex large hydropower scheme

Demo-1: Flagship stimulation experiment in the Deep Underground Laboratory

Continued analysis of the stimulation experiments at the Grimsel underground laboratory has (1) led to significant advances in our ability to characterize the hydraulic properties and architecture of complex fracture-fault networks, (2) advanced our understanding of the stimulation physics in complex fracture-fault networks, (3) identified a potential technique for direct remote monitoring of fluid pressure propagation, and (4) made progress in integrating results towards quantifying the connection between stimulation protocol and seismicity. Three projects are combined to advance soft, multi-stage hydraulic stimulation techniques in the Bedretto Lab. The experimental program is a logical continuation of the work in Grimsel, and a pathway towards industrial electricity generation. The Bedretto Lab was inaugurated in May 2019. First monitoring wells are being drilled in Aug-Sep 2019. Stimulation experiments are planned to start mid of 2020.

Demo-2: Reservoir engineering for heat exchange in Haute Sorne

GeoEnergie Suisse AG is developing a pilot and demonstration project for deep petrothermal electricity generation in the village of Haute-Sorne (Jura). The system aims at depths of 4000 – 5000 m and is projected to deliver up to 5 MW electricity and/or heat for industrial processes as well as district heating. The project will implement the so-called multi-fracture system in a granitic environment. Many activities within the SCCER are targeted towards enabling the technology but also using the data for calibration, upscaling and validation of methods and results, such as strategies for adaptive traffic light seismic monitoring systems, underground heat exchanger design, construction, and optimization, as well as research on optimal fluid circulation and associated heat extraction strategies.

Demo-3: Geneva heat storage and utilization project enters the exploration phase

The prospection phase of Geneva’s “Geothermie 2020” program is fully running with wells (production and storage) being drilled at progressively increasing depths. The first GEo-01 exploration well in the NE sector of the Canton successfully reached Mesozoic fractured carbonate reservoirs at 775 m depth yielding an artesian flow at 35 °C at 3 bars. The well is being tested for a long period in order to assess well deliverability and reservoir connectivity. Drilling of a second well will start late 2019 aiming at deeper stratigraphic intervals. The encouraging preliminary results will provide the opportunity to test and validate the effectiveness of exploration concepts and models developed within WP1 as well as proof the feasibility of direct heat production and subsurface storage potential in sedimentary basins at relatively shallow depths.

Demo-4: CO_2 Geological Storage Pilot

According to IEA, IPCC and COP21, (Carbon Capture & Storage) CCS has to be implemented to keep global warming within 2 °C. ELEGANCY, an SFOE funded P&D project, embedded in a larger European framework, has the mission to provide clean hydrogen for heat and mobility based on steam-methane-reforming. CCS is an essential part of this concept. Underground experiments at the Mt Terri Lab study the potential CO_2 migration through a fault in the caprock and the effects of fault activation. The objectives are to investigate how the exposure to CO_2-rich brine affects sealing integrity of a caprock, hosting a fault system (permeability changes, induced seismicity), to observe directly the fluid migration along a fault and its interaction with the surrounding environment, and to test instrumentation and methods for monitoring and imaging fluid transport. The installation of all equipment is completed as well as the pre-characterization (core interpretation, geophysical baseline measurements, injection tests). Currently, long-term injection tests are ongoing with constantly low flow rates accompanied with repeated geophysical measurements.

Demo-5: Small Hydro-Power Plant

The project aims at demonstrating the feasibility of the smart use of available infrastructure and equipment for increased electricity production and revenues. A first campaign has been carried out in November 2018 on the selected pilot, the KWGO power plant commissioned in July 2018. A specified program has been imposed to the power plant to generate peaks of production with different amplitudes and durations during 3 weeks using partially the identified storage volume. The monitoring of the power plant has been ensured to assess the different models developed concerning the forecast, the available storage, the power plant and the turbines while measurements of the discrete hydropeaking events in the alluvial area have been performed. A second campaign is planned in March 2020 using this time all the storage volume including part of the headrace pressurized pipe.

Demo-6: Controlled fine sediment release from a reservoir by a hydrodynamic mixing device

The project aims to demonstrate the effectiveness of technologies to artificially stir the water stored in a dam reservoir to prevent fine sediment from settling and allow for the sediment to be conveyed downstream at acceptable rates through the turbines during their normal operation. The mobile mixing device will be tested at a few dams to show its efficiency in different conditions. The expected outcome is (i) to validate the flushing efficiency as compared to laboratory development conditions; (ii) to characterize the dependence from local conditions; (iii) to identify practical difficulties and shortcomings of field implementation; (iv) to control the modifications to the sediment regime in the river downstream of the powerhouse as well as in the residual flow strength, and the resulting environmental impacts. A workshop with potential implementation partners from industry has been held in 2018. Discussions with potential collaboration partners from industry are ongoing. The current funding commitment of industry partners is still insufficient to start the envisaged Innosuisse and or BFE proposal.

Demo-7: Complex large hydropower scheme

FLEXSTOR comprises testing a set of innovative tools for flexible operation of storage hydropower plants in changing environment and market conditions. This demonstrator is motivated by the need to allow for flexible operation targeting premium remuneration hours, for which comprehensive methodologies for hydropower upgrading projects are still missing. It started at the end of Q3'2016; it is composed of six complementary research projects. Two projects are now completed, one related with hydropeaking, another with the optimization of storage use. The first project provides tools for validation of discharge demodulation basins, such as that of KWO at Innertkirchen. The second provided tools to assess the operation of complex hydropower systems with cascading reservoirs and multiple plants over several decades, in a way to support operational management and strategic planning. The other four project are up and running, as illustrated by preliminary results and conclusions. They concern (i) management of reservoir sedimentation across a cascade of alpine reservoirs, (ii) address mountain slope instability risks in glacier-liberated zones, avoiding non-optimal “preventive reservoir lowering”, (iii) mitigation of turbine abrasion; (iv) extend the operating range of hydraulic machinery, whilst avoiding instabilities. These issues are being addressed in the complex system of KWO Oberhasli, for later replication in other hydropower schemes in Switzerland.

WP 5 Projects

Title

Pilot & Demonstration projects

Projects (presented on the following pages)

Analysis of the Nowcasting System INCA-CH at Gletsch (VS)
Konrad Bogner, Matteo Buzzi, Massimiliano Zappa

In-situ stress and rock mass characterisation via mini-frac tests at the Bedretto Underground Laboratory
Kai Bröker, Xiaodong Ma and the Bedretto Lab Team

Heightening of very high gravity dams: the case study of the Grande Dixence
Basile Clerc, Giovanni De Cesare, Pedro Manso

Hydro-structural investigation of a 100 MW Francis turbine based on experimental tests and numerical simulations
J. Decaix, V. Hasmatuchi, M. Titzschkau, L. Rappilard, P. Manso, F. Avellan, C. Münch-Alligné

Control of sediment transport on an alpine catchment basin for the safe application of smart storage operations on an run-off-river HPP
Rafael Casimiro de Figueiredo, Jessica Zordan, Pedro Manso, Cécile Münch

Monitoring of small hydropower plants with a digital clone
Matthieu Dreyer, Christophe Nicolet, Anthony Gaspoz, Steve Crettenand, Cécile Münch Alligné

First insights on the production flexibility at the KWGO Power Plant
A.Gaspoz, V. Hasmatuchi, J. Decaix, C. Nicolet, M. Dreyer, J. Zordan, P. Manso, S. Crettenand, C. Münch-Alligné

HEATSTORE SWITZERLAND: New Opportunities for District Heating Network Sustainable Growth by High Temperature Aquifer Thermal Energy (HT-ATES) Storage
L. Guglielmetti, P. Alt-Epping, D. Birdsell, F. De Oliveira Filho, L. Diamond, T. Driesner, O. Eruteya, P. Hollmuller, M. Koumrouyan, Y. Makhloufi, F. Martin, P. Meier, M. Meyer, J. Mindel, A. Moscariello, C. Nawratil de Bono, L. Quiquerez, M. Saar, R. Sohrabi, U. Spring, B. Valley, D. Van den Heuvel, C. Wanner

Atténuation dans l’espace cours d’eau des éclusées résiduelles d’un bassin de démodulation: cas d’étude de Piotta
Marie Loverius, Pedro Manso, Giovanni De Cesare, Samuel Vorlet

Directional-dependence of Mode I fracture toughness in Grimsel Granite
Morteza Nejati, Ali Aminzadeh, Martin Saar, Thomas Driesner

Computational Modelling of Fine Sediment Release Using SEDMIX Device with Thrusters
A. Onate-Paladines, A. Amini, G. De Cesare

Assessment of a turbine model to predict cost effectively the far wake of a hydrokinetic farm
O. Pacot, D. Pettinaroli, J. Decaix, C. Münch-Alligné

Large-scale Field Tests on Impuse Waves
Eva Sauter, Yuri Prohaska, Lukas Schmocker, Helge Fuchs, Robert Boes, Axel Volkwein

High Resolution Snow Melt and Runoff Modelling
Michael Schirmer, Massimiliano Zappa, Tobias Jonas

Multipurpose water reservoirs : a necessity for future irrigation?
J. Schmid, J. Decaix, C. Münch-Alligné, A. Gillioz

Set-up and configuration of an ensemble Kalman filter for an operational flood forecasting system
Anne Schwob, Alain Foehn, Javier Fluixa, Giovanni de Cesare

GPR imaging of fractures in the Bedretto Lab
Alexis Shakas, Peter-Lasse Giertzuch

Tracing the CO2 pathway in a faulted caprock: the Mont Terri Experiment of the ELEGANCY-ACT project
Alba Zappone, Melchior Grab, Anne C. Obermann, Claudio Madonna, Christophe Nussbaum, Antonio P. Rinaldi, Clément Roques, Quinn C. Wenning, Stefan Wiemer

SCCER SoE
SWISS COMPETENCE CENTER for ENERGY RESEARCH
SUPPLY of ELECTRICITY

SCCER-SoE Annual Conference 2019

70 NRP Energy Turnaround
National Research Programme

Supported by:
Schweizerische Eidgenossenschaft
Confédération suisse
Confederazione Svizzera
Confederaziun svizra

Swiss Confederation

Innosuisse – Swiss Innovation Agency

Analysis of the Nowcasting System INCA-CH at Gletsch (VS)

Konrad Bogner, Matteo Buzzi** and Massimiliano Zappa**

*WSL, Zürcherstrasse 111, CH-8903 Birmensdorf ; **Federal Office of Meteorology and Climatology MeteoSwiss

Motivation

One objective of the **SmallFlex** project is **to increase the flexibility of the management** of the Small Hydropower Plant (SHP) by coupling the high resolution **now-cast system INCA-CH** and **COSMO-1** forecasts to predict the **inflow** for the next hours to days. This combined forecast system is implemented now at WSL and runs operationally since March 2018.

Study site

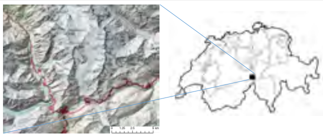

Gletsch catchment:
Area: 39.8 km²
Glaciation: 52%
Mean elevation: 2719 m a.s.l

Example of INCA forecasts

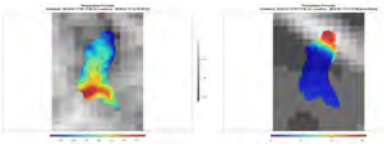

1 km resolution of the INCA – CH model output (in grey) and the forecast downscaled to 100m by fitting Thin Plate Splines (TSP) to the surface taking the elevation as covariate.

Operational forecast chain

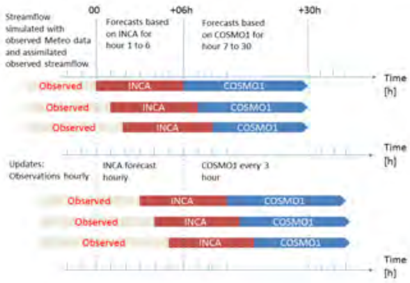

Combination of the INCA-CH and the COSMO-1 based forecasts of the inflow having different initialization times and update intervals.

Data

The forecast system runs operationally since March 2018, but during the first year the runoff at Gletsch was mainly driven by glacier and snow melt processes. Thus, the analysis concentrates on June and July 2019, when two precipitation events have been predicted.

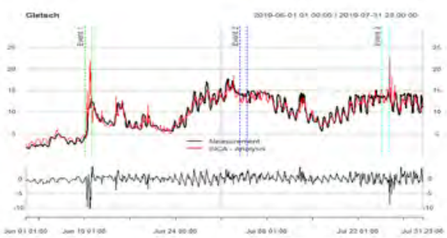

Series of the observed (black) and the analysis (lead time zero) of the INCA-CH predictions (red). The vertical lines indicate the three periods, which have been analysed in detail. At the bottom the error is shown.

Methods

Events driven by convective rainfall are highly localized and small deviations in the predicted direction and amount of the rain cells could lead to big errors. Therefore two machine learning (ML) based post-processing methods have been tested in order to reduce such error.

The methods used are[1]:

Gradient Boosting Method (GBM),
Multivariate Adaptive Regression Splines (MARS).

Additionally the different forecasts (raw, GBM, MARS) have been optimally combined by fitting a **Nonhomogeneous Gaussian Regression (NGR)**, which assigns more weight to the best performing forecast in the calibration period (i.e. previous 20 days).

Results

At first the Nash-Sutcliffe Efficiency has been estimated for June and July 2019 (see below). All post-processing methods show some significant improvements; the best results were achieved with NGR.

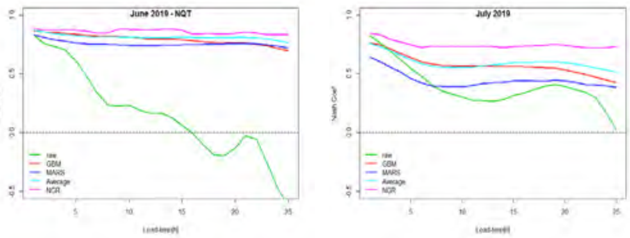

Nash Sutcliffe Coefficient for June and July 2019 for the raw and the post-processed forecasts

At next the three events are analysed in more details.

Event 1:

The timing of the beginning of the event is predicted very well, but the amount of rain was to high[2] resulting in overestimates of the runoff. Only after applying the post-processing the predicted inflow is within the range of the observed runoff.

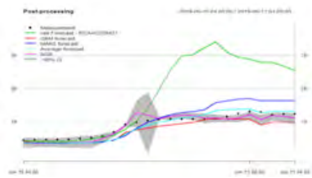

Event 2:

In order to test whether the post-processing is correcting the inflow always in the same direction a period is chosen, where the raw forecasts were lower than the observations.

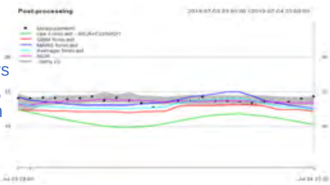

Event 3:

This event is a false alarm, where the forecast showed quite a big event and nothing was happening in reality. The ML post-processor would have been able to identify this mistake and reduce the false peak accordingly.

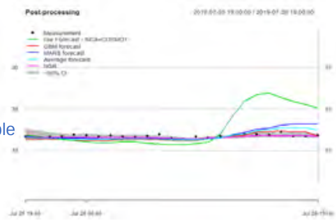

Conclusions

The application of the INCA-CH system to such a small mountainous catchments reveals the sensibility of small shifts in the temporal and spatial evolution of thunder storms reflected by large errors. Thus it will be necessary to work with ensembles of such high resolution forecasts[3] and to apply post-processing methods. First results of testing machine learning based error correction methods are shown highlighting the potential of such methods for improving the inflow forecasts.

References

[1]Bogner, K., Pappenberger, F. and Zappa,M.: Machine learning techniques for predicting the energy consumption/production and its uncertainties driven by meteorological observations and forecasts. *Sustainability*, 11(12), 2019.

[2]See also the Poster of Michael Schirmer, et al. for more details.

[3]Pulkkinen, S., Nerini, D., Pérez Hortal, A. A., Velasco-Forero, C., Seed, A., Germann, U., and Foresti, L.: Pysteps: an open-source Python library for probabilistic precipitation nowcasting (v1.0), Geosci. Model Dev. Discuss., in review, 2019.

ETH zürich

SCCER-SoE Annual Conference 2019

SCCER SoE
SWISS COMPETENCE CENTER for ENERGY RESEARCH
SUPPLY of ELECTRICITY

Supported by:
Schweizerische Eidgenossenschaft
Confédération suisse
Confederazione Svizzera
Confederaziun svizra
Swiss Confederation
Innosuisse – Swiss Innovation Agency

In-situ stress and rock mass characterisation via mini-frac tests at the Bedretto Underground Laboratory

Kai Bröker[1,2], Xiaodong Ma[1,2] and the Bedretto Lab Team

[1]*Swiss Competence Center for Energy Research – Supply of Electricity (SCCER-SoE)*
[2]*Geothermal Energy and Geofluids Group (GEG)*

INTRODUCTION AND MOTIVATION

- Investigation of in-situ stress state (principal stress directions + magnitudes) and its variation around the **Bedretto Underground Laboratory for Geoenergies (BULG)** → located inside Bedretto tunnel, Canton Ticino
- Stress filed determines hydraulic fracture initiation pressure + propagation direction
- Knowledge of stress state important for future creation of geothermal reservoir via **hydraulic stimulation**, especially for reactivation of pre-existing fractures linked to **induced seismicity**
- experiments carried out in crystalline rock (**Rotondo granite**), overburden ≥ 1 km

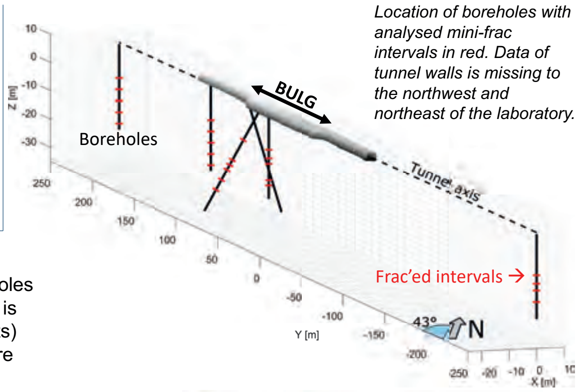

Location of boreholes with analysed mini-frac intervals in red. Data of tunnel walls is missing to the northwest and northeast of the laboratory.

METHODS

1. **Mini-frac tests**: performed in four 30 m-long vertical + two 40 m-long inclined boreholes → estimation of formation breakdown (P_b) and fracture closure pressure (P_{cl}), which is ≈ minimum horizontal stress (S_{hmin}), on different diagnostic plots (e.g. G-function plots)
2. **Extended shut-in times** (20 min, 1 hr, to 12 -14 hr): estimation of local pore pressure (P_p), when pressure derivative approaches zero
3. **Dry packer reopening test**: calculation of rock mass stiffness and evaluation of fracture reopening pressure (P_r) without interfering fluid flow effects due to residual aperture of fracture

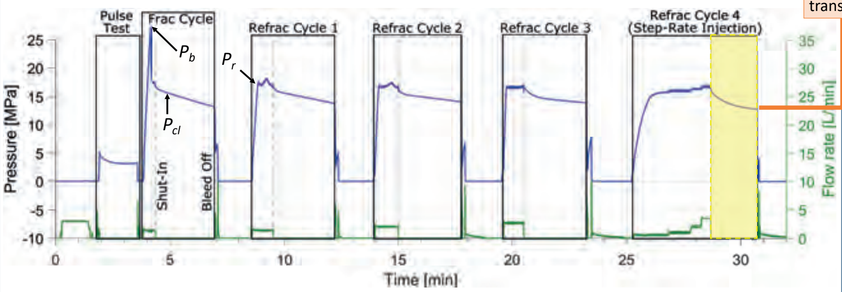

Injection protocol of a mini-frac test. Flow rate shown in green and interval pressure in blue. P_b is obtained from the initial frac cycle, P_{cl} from the transient after pump shut-in of every cycle and P_r from the refrac cycles.

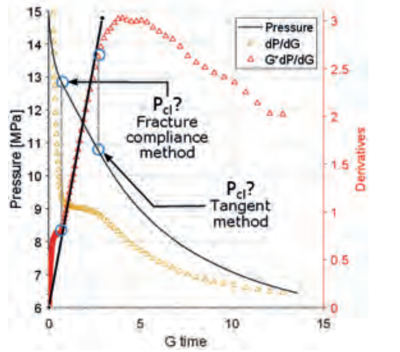

Data analysis example with pressure transient, its derivative and Bourdet derivative on a G-function plot to estimate fracture closure pressure according to two common picking methods.

RESULTS

- **Fracture compliance method** by *McClure et al.* (2014, 2016) is applicable to crystalline rock mass to pick P_{cl} as estimate for S_{hmin}.
- G-function plots show comparable pressure transients between intervals, often two peaks visible in Bourdet derivative.
- **Intra- and inter-borehole variations** of pressure values and stress magnitudes are identified.
- Proximity to **natural fractured zones** (identified using borehole logs) influences stress state.
- Dry reopening tests give higher P_r values than mini-frac tests.
- P_p between 2.4 – 5.3 MPa (below hydrostatic) indicates tunnel drainage effects.

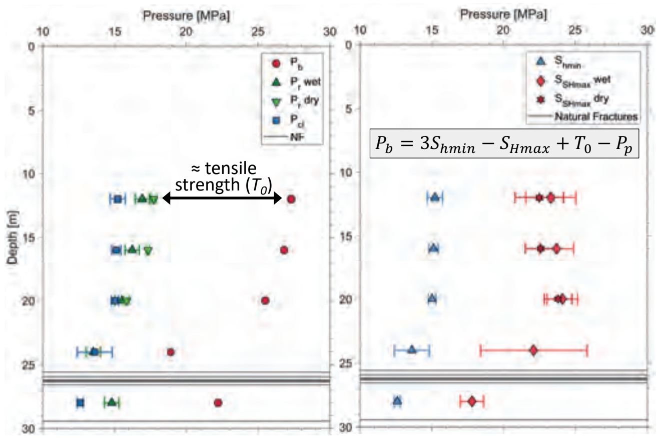

Results of vertical borehole SB3.1. Estimation of maximum horizontal stress (S_{Hmax}) is based on the formula by Hubbert and Willis (1957). Variations of the stress magnitudes are visible on tenth of meters scale and the fractured zone around 26 m seems to decrease the stress magnitudes.

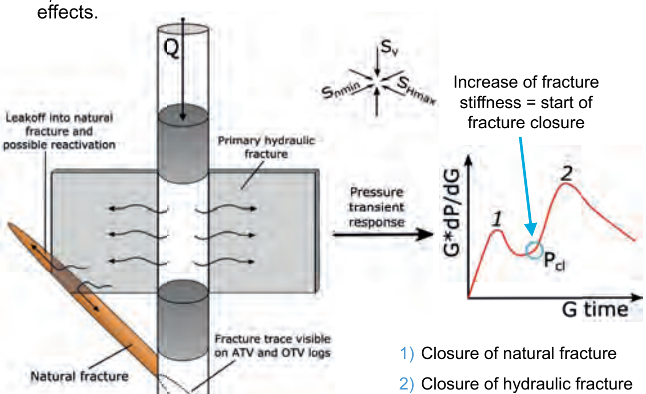

Hydraulic fracture is likely to intersect natural fractures. Slip tendency analysis showed that pressure increase is sufficient for reactivation. → creation of **complex fracture network**

OUTLOOK

- Calculate matrix permeability from overnight shut-in pressure transients
- Estimate stiffness from wet- and dry- packer reopening tests → calibration of equipment needed
- Analyze remaining boreholes and intervals to characterize larger scale spatial variations (stress heterogeneity)

References

M. Hubbert and D. Willis. Mechanics of hydraulic fracturing. Petroleum Transactions, AIME, 210:153-168, 1957.
M. McClure, C. A. Blyton, H. Jung, and M. M. Sharma. The effect of changing fracture compliance on pressure transient behavior during diagnostic fracture injection tests. In SPE Annual Technical Conference and Exhibition. Society of Petroleum Engineers, 2014. doi: 10.2118/170956-MS.
M. McClure, H. Jung, D. D. Cramer, and M. Sharma. The fracture-compliance method for picking closure pressure from diagnostic fracture-injection tests. SPE Journal, 21(4):1321-1339, 2016. doi: 10.2118/179725-PA.

Contact: broekerk@ethz.ch; xiaodong.ma@sccer-soe.ethz.ch

SCCER SoE

SWISS COMPETENCE CENTER for ENERGY RESEARCH
SUPPLY of ELECTRICITY

SCCER-SoE Annual Conference 2019

Supported by:

Schweizerische Eidgenossenschaft
Confédération suisse
Confederazione Svizzera
Confederaziun svizra

Swiss Confederation

Innosuisse – Swiss Innovation Agency

Heightening of very high gravity dams: the case study of the Grande Dixence

Basile Clerc, Dr. Giovanni De Cesare, Dr. Pedro Manso

E-Mail: basile.clerc17@gmail.com; giovanni.decesare@epfl.ch; pedro.manso@epfl.ch

EPFL

Motivation

Dam heightening can provide large incremental positive impacts on storage with minimum incremental negative impacts, but requires deep knowledge of the structure and its foundation. Very high gravity dams are usually well studied and documented due to their importance and complexity. Such profound knowledge of the dam-reservoir-foundation system considerably reduces the uncertainty about site conditions already at an early stage of design. Furthermore, the availability of monitoring data and safety assessment tools (FE models, predictive behaviour models) strongly reduce the preparation time to reach feasible design solutions.

The Grande Dixence dam, located in the Canton of Valais, creates the largest reservoir in Switzerland, providing 10% of the country's storage energy. If heighten this dam could be used to transfer a larger share of the summer inflows to produce electricity in winter.

Top view of the Grande Dixence dam

Methods

The methodology consists of two main steps. The first step evaluates the reference state of the studied hydroelectric scheme to identify major constraints, while the second step consists of analysing and generating heightening solutions. The analysis of the results obtained during both prior stages should allow an assessment of the developed variants to determine the optimal solution.

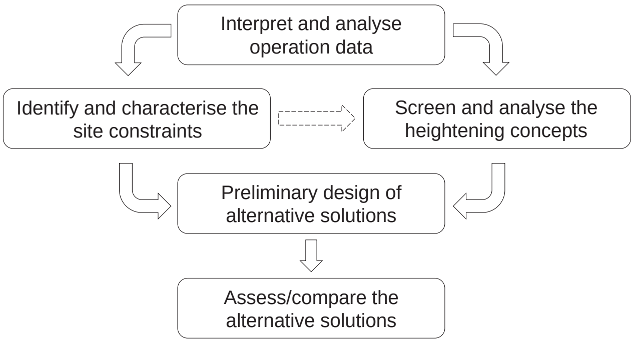

Methodology flow chart

Results

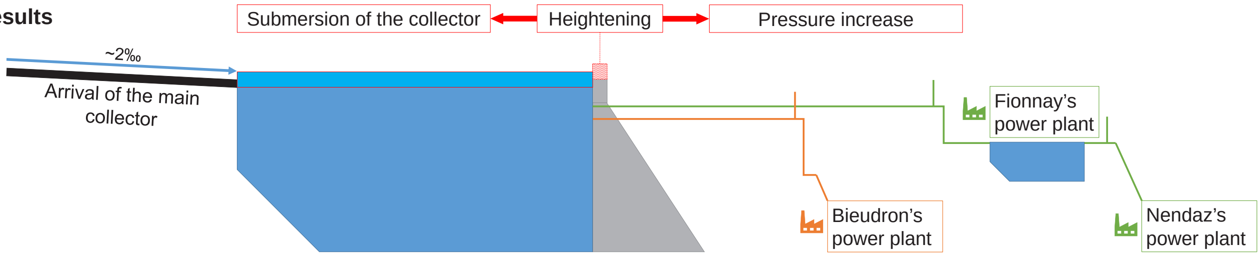

Grande Dixence simplified scheme (not to scale)

Screening of heightening concepts

Several heightening solutions were considered, but constraints were quickly acknowledged [1]. The plan shape of the dam crest strongly limits the integration of an arch and the presence of joints every 16 m is a strong constraint to any solution of buttress or multiple-arch heightening concepts.

Considering building artificial abutments and/or using post-stressed anchors was also investigated. However, the use of 300 m long anchors is technically unheard off and challenging and has been discarded.

In summary, due to its easier implementation and higher flexibility in regards to the geometry of the actual dam, a similar structural concept was preferred from inception when considering joint behaviour of the original and heightened structures.

This concept lead to retaining four alternative solutions for comparison, all with a new crest width of 5 m. Investigations cover height increase solutions from few meters up to maximum 30 m (~10% of the existing dam height). Key differences are the water column over the upstream face of the height increase and the location of its gravity centre with regards to the main structure.

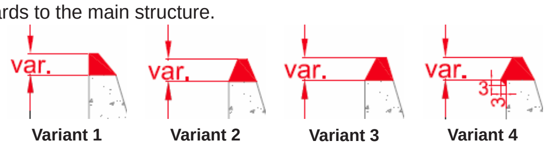

2D cross-section of the four alternative dam heightening solutions

Verification results analysis

The verification analysis shows satisfactory results as all variants meet the design criteria.

Major constraints

As seen on the simplified diagram above, the height increase solutions would submerge the main conveyance tunnel outlet and the backwater effects modify pumping and aeration conditions farther upstream. Moreover, the water pressure increases on the waterways leading to both powerplants downstream: although Bieudron's surge tank can withstand the increase, Fionnay's cannot without adaptation measures.

Economic analysis

A preliminary analysis of the Levelized Cost of Electricity (LCOE) indicates a remarkably low cost price and point out that a height increase within 10 to 15 m would likely be optimal.

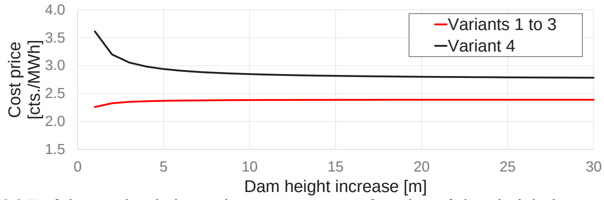

LCOE of the retained alternative concepts as a function of dam height increase

References

[1] Clerc, B., Manso, P., De Cesare, G. (2019) Heightening of very high gravity dams: the case study of the Grande Dixence. International Benchmark Workshop on Numerical Analysis in Dams, Open Theme, Milan (in press).

[2] Office fédéral de l'énergie OFEN. (2015). Directive sur la sécurité des ouvrages d'accumulation, Parties A à E.

[3] Schleiss, A. J., Pougatsch, H. (2011). Traité de Génie Civil volume 17 : Les barrages. Presses polytechniques et universitaires romandes, Lausanne.

[4] Schaefli, B., Manso, P., Fisher, M., Huss, M., & Farinotti, D. (2019). The role of glacier retreat for Swiss hydropower production. Renewable Energy, Volume 132.

SCCER-SoE Annual Conference 2019

SCCER SoE
SWISS COMPETENCE CENTER for ENERGY RESEARCH
SUPPLY of ELECTRICITY

FlexSTOR

Hes·so VALAIS WALLIS School of Engineering

Supported by:
Schweizerische Eidgenossenschaft
Confédération suisse
Confederazione Svizzera
Confederaziun svizra
Swiss Confederation
Innosuisse – Swiss Innovation Agency

Hydro-structural investigation of a 100 MW Francis turbine based on experimental tests and numerical simulations

J.Decaix[1], V. Hasmatuchi[2], M. Titzschkau[3], L. Rappilard[2], P. Manso[4], F. Avellan[5], C. Münch-Allignê[2]

[1] Institute of Sustainable Energy / [2] Institute of Systems Engineering, School of Engineering, HES-SO Valais-Wallis, Rawil 47, Sion, Switzerland
[3]Kraftwerke Oberhasli AG, Grimsel Hydro, Innertkirchen, Switzerland
[4] PL-LCH / [5] LMH, EPFL, Lausanne, Switzerland

Motivation

- Pumped-storage power plants: key components in a successful integration of renewable energies
- Hydraulic turbines and pump-turbines:
  - Operation in a wide range to offer power regulation flexibility;
  - Undergo frequent start-up and/or stand-by operating regimes;
  - Facing to harsh structural loadings with impact on their lifetime.

Objectives

- Achievement of a hydrodynamic instability level hill-chart of the machine;
- Investigation of the harmful conditions using experimental and numerical resources;
- Proposal of an alternative less-harmful start-up path and stand-by position with direct effect on the long-term maintenance costs;
- Elaboration of a diagnosis protocol to redraw hydrodynamic instability level hill-charts on different hydropower units using only a simplified instrumentation set.

Hydrodynamic instability hill-chart

- Puts in evidence the high level of strain fluctuations observed on the runner blades at the Speed No-Load (SNL) operating condition characterized by a small opening angle of the guide vanes.

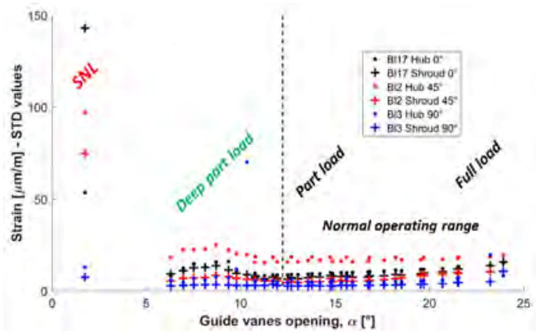

Investigation of harmful conditions

- Combining the experimental data with CFD and FEM simulations as well as the theoretical works, an origin for the high level of strain fluctuations has been proposed:
  - At the SNL operating condition, an Eigen mode of the runner is excited by an external source;
  - After several years of operation, the fatigue limit of the material is reached and cracks are observed at the trailing edge of the runner close to the hub.

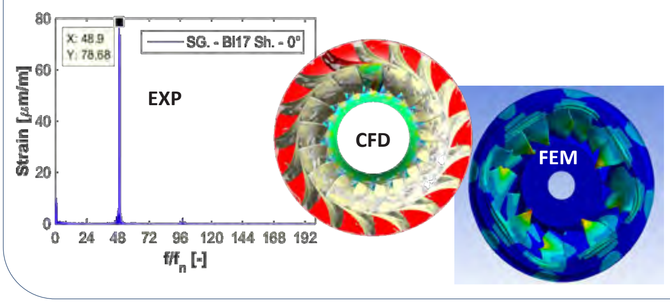

Alternative start-up path

- Three alternative slower start-up procedures have been tested:
  - No beneficial effect noticed since the synchronization process remains unchanged.
- Synchronization procedure with the pump filled seems to be safe for the turbine.

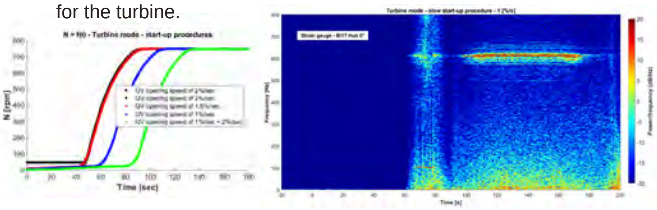

Diagnosis protocol with a simplified instrumentation set

Main achievements

References

[1] J. Decaix, V. Hasmatuchi, M. Titzschkau, L. Rapillard, P. Manso, F. Avellan & C. Münch-Alligné, 2019, "**Experimental and numerical investigations of a high-head pumped-storage power plant at speed no-load**", IOP Conf. Ser. Earth Environ. Sci., 240(8).

[2] M. Titzschkau, V. Hasmatuchi, J. Decaix & C. Münch-Alligné, 2018, "**On-board measurements at a 100MW high-head Francis turbine**", Vienna Hydro 2018, Vienna, Austria.

[3] V. Hasmatuchi, J. Decaix, M. Titzschkau & C. Münch-Alligné, 2018, "**A challenging puzzle to extend the runner lifetime of a 100 MW Francis turbine**", Hydro 2018, Gdansk, Poland.

Acknowledgements

Supported by:
Schweizerische Eidgenossenschaft
Confédération suisse
Confederazione Svizzera
Confederaziun svizra
Swiss Confederation
Innosuisse – Swiss Innovation Agency

FlexSTOR

Partners of the FLEXSTOR - WP6 project (17902.3 PFEN-IW-FLEXTOR)

Hes·so VALAIS WALLIS School of Engineering
EPFL ECOLE POLYTECHNIQUE FÉDÉRALE DE LAUSANNE
KWO GRIMSELSTROM

SCCER-SoE Annual Conference 2019

SCCER SoE
SWISS COMPETENCE CENTER for ENERGY RESEARCH
SUPPLY of ELECTRICITY

Small Flex

Supported by:
Schweizerische Eidgenossenschaft
Confédération suisse
Confederazione Svizzera
Confederaziun svizra
Swiss Confederation
Innosuisse – Swiss Innovation Agency

Control of sediment transport on an alpine catchment basin for the safe application of smart storage operations on an run-off-river HPP

Rafael Casimiro de Figueiredo; Jessica Zordan; Pedro Manso, Cécile Münch*
Plateforme en Constructions Hydrauliques (PL-LCH), École Polytechnique Fédérale de Lausanne (EPFL)
**Corresponding author: jessica.zordan@epfl.ch*

EPFL

Objectives

Smart storage operations (SSO) have been implemented on an alpine run-off-river HPP (case study: KW Gletsch-Oberwald HPP) in order to enhance the flexibility of the power plant (ref poster SmallFlex). SSO operations consist on the use of available space underground, such as the settling basin, in order to store the water, particularly in periods of the year with low inflow, which can afterward be used for energy production when the demand and the remuneration tariffs are higher and at a discharge close to the optimum of the turbine to have the best efficiencies[1].

The aim of efficiently implementing the SSO operations on the settling basin requires sediment management in order to assure a safe use of this part of the system whose function is temporarily changed. In order to understand the amount of sediment inflow into the settling basin, the following actions were undertaken:

- Determine the amount of potential mobilized sediments at the catchment scale with the use of Beyer-Portner (1998) and Gavrilović (1990) formulas;
- Determine the maximum sediment transport capacity of the river Rhone upstream the intake with the use of Beyer-Portner (1998) formula.

This will allow to verify in which periods of the year the sediment basin can be used for water storage with no risk related with sediment conveyance into the waterways and therefore at the turbines.

Study Area

Gletsch catchment[6]

- Surface area: 40.34 km^2
- Average altitude: 2691m a.s.l.
- River principal watercourse length: 3450m
- River secondary watercourse length: 3870m
- River discharge: 2.93m^3/s
- Average slope along the course: 13.7%

Procedure

Soil coverage analysis

The map was created to display the land use of the case study. The values produced for calculating the erosion models and sediment transport model.

Land use[6]:

- Vegetation: 5.1 km^2
- Open spaces with little or no vegetation: 15.9 km^2
- Lakes and rivers: 0.2 km^2
- Glaciers and perpetual snow: 18.8 km^2
- Artificial surfaces: 0.3 km^2
- Erodible soils: 15.5 km^2

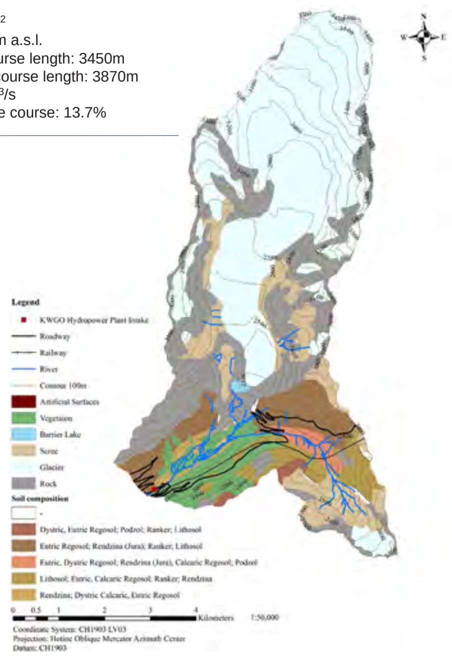

Pebble count

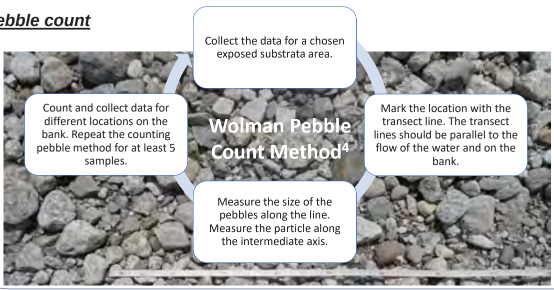

Results

Grain size discribution

The analysis of the measurements following the Pebble count method resulted in the compilation of the following grain size distribution:
d_{90} = 5.8cm, d_{84} = 3.8cm, d_{65} = 4.2cm, d_{50} = 3.6cm and d_{30} = 1.0cm.

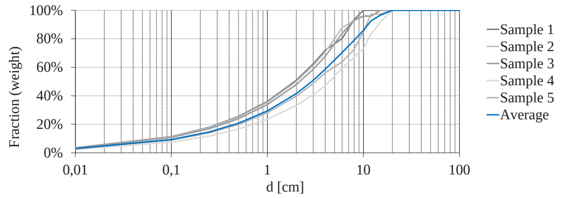

Erosion Model Calculations

Beyer-Portner formula[2]

$$V_A = 93 \cdot 10^{-15} \cdot H_{été}^{0.052} \cdot SE^{0.091} \cdot SV^{8.108} \cdot \Delta L_G^{0.082} + 274$$

$$V_A = 93 \cdot 10^{-15} \cdot 323.8^{0.052} \cdot 38.54^{0.091} \cdot 39.38^{8.108} \cdot 0.44^{0.082} + 274$$

$$V_A = 275.41 \text{ m}^3 \text{ km}^{-2} \text{ an}^{-1}$$

$$V_A = 11\,110 \text{ m}^3/\text{year}$$

V_A	Specific volume of annual sediment input [m^3 km^{-2} an^{-1}]
$H_{été}$	Average rainfall between June and September [mm]
SE	Percentage of the catchment area made up of erodible soils [%]
SV	Percentage of watershed area without vegetative cover [%]
ΔL_G	Annual change in glacier length relative to total length [%]

Gavrilović method[3]

$$W_a = T \times P_a \times \pi \times \sqrt{Z^3} \times A$$

$$W_a = 0.8 \times 323.8 \times \pi \times \sqrt{0.5^3} \times 40.3$$

$$W_a = 11\,915.4 \text{ m}^3/\text{year}$$

W_a	Total annual volume of detached soil [m^3/year]
T	Temperature coefficient
P_a	Average annual precipitation [mm]
Z	Erosion coefficient
F	Study area [km^2]

Sediment Transport Model Calculations

Smart and Jaeggi formula[5]

$$q_B = \frac{4}{(s-1)} \cdot \left(\frac{d_{90}}{d_{30}}\right)^{0.2} \cdot q \cdot J^{1.6} \cdot \left(1 - \frac{\theta_{cr}(s-1)d_{50}}{h_m \cdot J}\right)$$

$$q_B = \frac{4}{(2.65-1)} \left(\frac{0.058}{0.010}\right)^{0.2} 0.74 \cdot 0.14^{1.6} \left(1 - \frac{0.05(2.65-1)0.036}{0.2 \cdot 0.14}\right)$$

$$q_B = k \cdot q = 0.13 \cdot q \;\; \text{m}^3/\text{s m}$$

q_B	Specific sediment discharge (net sediment volume per time per unit width) [m^3/s m]
$s = \frac{\sigma}{\rho}$	Relative density of sediment to water [-]
d_{30}, d_{90}	Characteristic grain sizes, 30% or 90% (by weight) of the bed material are smaller [m]
d_{50}	Mean grain size [m]
q	Specific water discharge per unit width [m^3/s m]
J	Slope
θ_{cr}	Critical Shields factor at beginning of motion
h_m	Mixture (water and sediment) flow depth [m]
K	sediment transport model linearization between specific water and sediment discharges

Discussion

A detailed analysis of the catchment characteristics, in terms of **soil coverage** and **grain size,** has allowed to investigate the potential sediment input to the KWRO hydropower plant. It has been found that the sediments volume available at the catchment scale is limiting the effective sediment inflow i.e. the sediments transport capacity is reduced by the sediments availability.

The sediment transport formula has been used to calculate the sediment discharge as a function of the water discharge and linearly distributing estimated sediment availability. The hourly sediment volume at the intake can therefore be calculated as:

$$V_{sed}(h) = \frac{k\,Q_w(h)}{(325 * 24)/W_a}$$

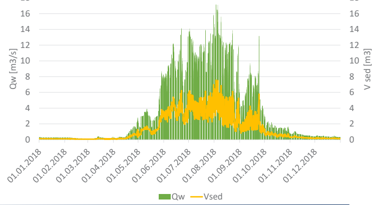

References

1. First insights on the production flexibility at the KWGO Power Plant, Smallflex Project, SCCER-SoE Annual Conference 2019
2. Beyer Portner, N. (1998). *Communication: Erosion des bassins versants alpins par ruissellement de surface.* Lausanne: Communications de Laboratoire de constructions hydrauliques, Ecole Polytechnique Federale de Lausanne.
3. Dragičević, N., Karleuša, B., & Ožanić, N. (2017). *Erosion Potential Method (Gavrilović Method) Sensitivity Analysis.* Rijeka: Soil.
4. Harrelson, C., Rawlins, C., & Potyondy, J. (1994). *"Bed and Bank Material Characterization" in Stream Channel Reference Sites: An Illustrated Guide to Field Technique. .* Colorado: United States Department of Agriculture.
5. Smart, G., & Jaeggi, M. (1983). *Sediment Transport on Steep Slopes.* Zürich: Mitteilungen der Versuchsanstalt für Wasserbau, Hydrologie und Glaziologie.
6. Swiss Confederation. (2019, July 15). *Maps of Switzerland.* Retrieved from map.geo.admin.ch: https://map.geo.admin.ch/

SCCER SoE
SWISS COMPETENCE CENTER for ENERGY RESEARCH
SUPPLY of ELECTRICITY

SCCER-SoE Annual Conference 2019

Small Flex

Supported by:
Schweizerische Eidgenossenschaft
Confédération suisse
Confederazione Svizzera
Confederaziun svizra
Swiss Confederation
Innosuisse – Swiss Innovation Agency

Monitoring of small hydropower plants with a digital clone

Matthieu Dreyer, Christophe Nicolet, Anthony Gaspoz, Steve Crettenand, Cécile Münch-Allingé

SmallFlex motivation

- To show how small-hydropower plants (SHP) can provide winter peak energy and ancillary services, whilst remaining eco-compatible.

Overarching research question

- *What are the consequences of enlarging the operational range of the Pelton turbines in case of large head variations ?*

Hydro-Clone® contributions

- Monitoring of the power plant
- Estimation of the available power/energy for ancillary services

Demonstrator site : the Gletsch-Oberwald SHP

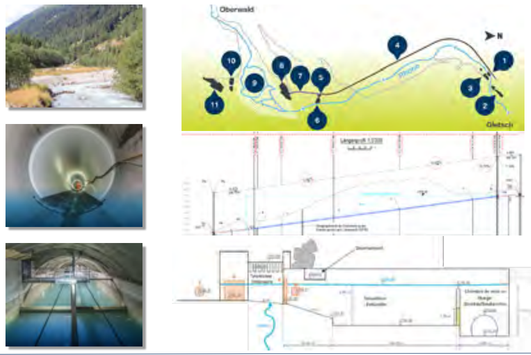

Digital clone implementation

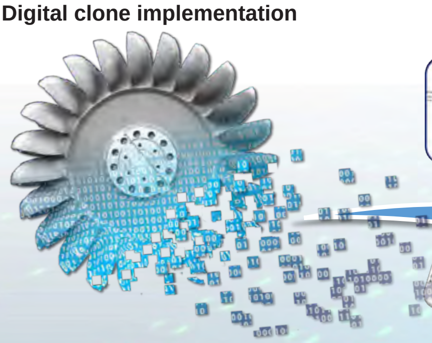

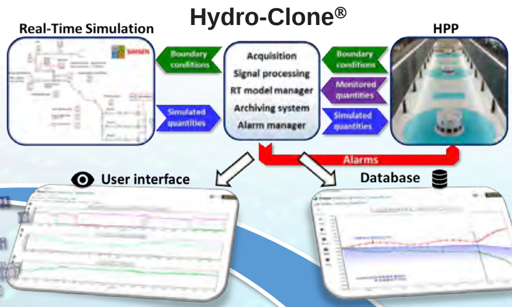

Live monitoring and data archiving

- Monitoring of non-measurable quantities
- Detection of abnormal pressure transients prior to reach admissible limit
- Detection of Hydraulic/Electrical anomalies
- Anticipation of power plant damages

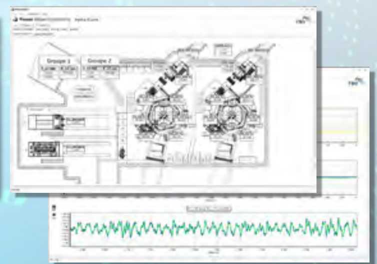

Numerical modeling of the power plant

- Complete 1D-model of the power plant with *SIMSEN*
- Calibration of the model based on powerplant real operating sequences

Hydro-Clone real-time simulation

- Real-Time numerical “cloning” using the complete 1D-model of the power plant
- Boundary conditions measured in-situ and fed to the model in real-time
- Data processing and diagnosis of the power plant health

Benefits and outcomes from real-time simulation monitoring

1. Commissioning follow-up

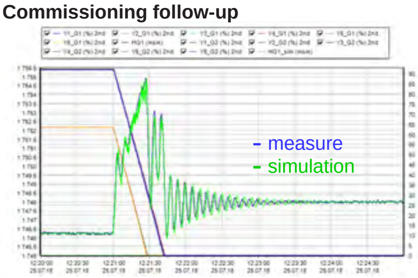

- Comparison of the measured and simulated pressure at the penstock bottom during an emergency shutdown

2. Monitoring of the power plant during hydropeaking

- Recording of the time evolution of the sandtrap water level and discharge during hydropeaking operating mode

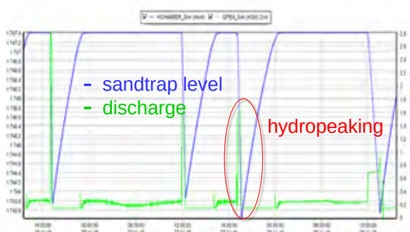

3. Available power/energy assessment for ancillary services

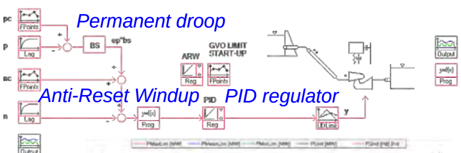

- Calibrated numerical model used to explore the behavior of the power plant ➔assessment of the primary control potential

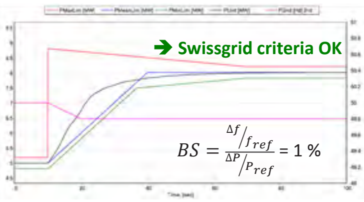

$$BS = \frac{\Delta f / f_{ref}}{\Delta P / P_{ref}} = 1\ \%$$

Contributors

Power Vision Engineering
Hes·so VALAIS WALLIS School of Engineering
FMV

Acknowledgments

This work is funded by SFOE, Swiss Federal Office of Energy (grant funding SI/501636-01), within the framework of the project «*Demonstrator for flexible Small Hydropower Plant*»

Schweizerische Eidgenossenschaft
Confédération suisse
Confederazione Svizzera
Confederaziun svizra
Office fédéral de l'énergie OFEN

SCCER SoE
SWISS COMPETENCE CENTER for ENERGY RESEARCH
SUPPLY of ELECTRICITY

SCCER-SoE Annual Conference 2019

Small Flex

Supported by:
Schweizerische Eidgenossenschaft
Confédération suisse
Confederazione Svizzera
Confederaziun svizra
Swiss Confederation
Innosuisse – Swiss Innovation Agency

First insights on the production flexibility at the KWGO Power Plant

A.Gaspoz, V. Hasmatuchi, J. Decaix, C. Nicolet, M. Dreyer, J. Zordan, P. Manso, S. Crettenand, C. Münch-Allingé

Contact : HES-SO Valais, School of Engineering, Hydroelectricity Group, CH-1950 Sion, Switzerland, cecile.muench@hevs.ch

Context

The aim of the SMALLFLEX project is to investigate how small-hydropower plants (SHP) can provide **winter peak energy** and **ancillary services**, whilst remaining **eco-compatible.** The 15 MW Gletsch-Oberwald Power Plant, owned by FMV and commissioned at the end of 2017, has been selected as pilot site.

Project organization

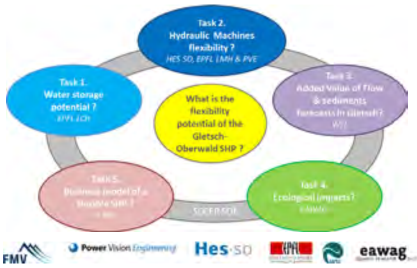

Source : Bulletin Electrossuisse, 02.2019, "Acceptation de l'énergie hydraulique alpine».

Available storage for the first campaign

For the first campaign of this project, the settling basin and the forebay tank, connected by two gates, have been used providing a storage volume of **3'700 m³**. This part of the identified storage allows to maintain a minimum available net head of 282 m required for a comfortable operation of the Pelton turbines.

Settling Basin of KWGO

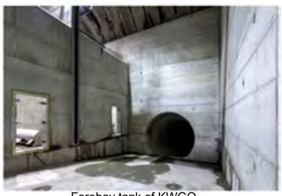

Forebay tank of KWGO

First campaign objectives & method

In November 2018, during three weeks, the competences of the research team have been gathered to explore experimentally the flexibility of KWGO. The first two weeks have been dedicated to induce 5 hydro-peaking events to monitor the impact in the downstream alluvial area. The last week was devoted to generate **several production peaks** taking into account the **energy demand** and the available storage.

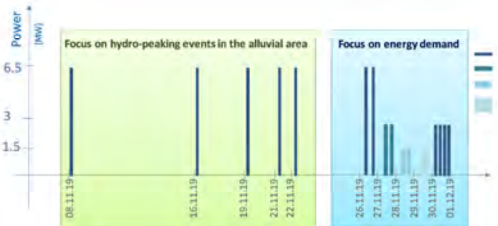

Program of the first campaign

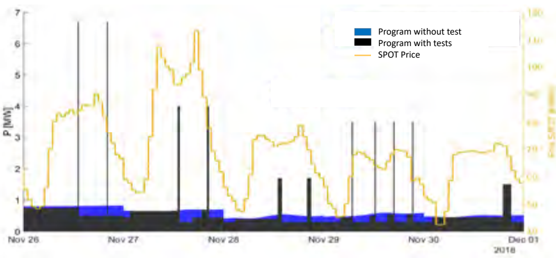

Focus on the program of the 3rd week of the 1st campaign with/without the test & SPOT price.

According to the discharge forecast and the available storage, a schedule for each day of test has been systematically prepared by the research team and sent to FMV.

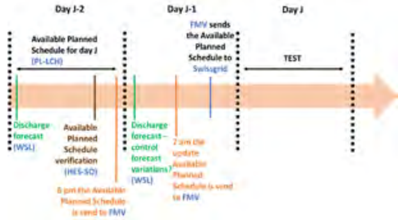

Workflow for the 3rd week of test during the 1st SmallFLEX campaign

Monitoring in the power plant during the tests

Since the acceptance tests of the turbines in July 2018, the HydroClone developed by PVE, partner of the project, is installed in the power plant. This monitoring system records all operating parameters of the power plant and provides access, from numerical simulation, to non-measured quantities. In parallel, a turbidimeter to monitor the sediments in the settling basin, a camera to supervise the free surface level in the forebay tank and several sensors on the turbine casing have been installed by HES-SO and EPFL PL-LCH.

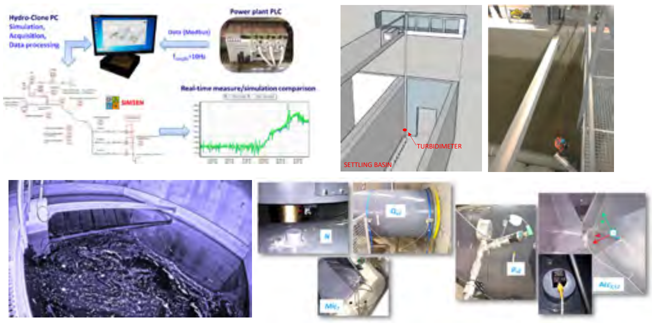

Monitoring in the power plant : Hydroclone, turbidimeter, camera and several sensors.

Analysis

During the five days, the planned and effective productions show a minimum difference of around 1%. Through the use of the storage, the energy production has been increased of more than 40% for the five days considered[1].

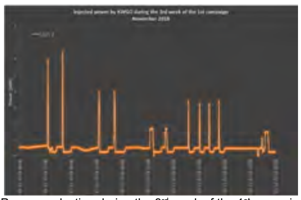

Power production during the 3rd week of the 1st campaign

1. Zordan et al., Introducing flexibility in small hydropower plants, HYDRO 2019, Porto, Portugal

Conclusion and perspective

This first campaign demonstrated the possibility to use the settling basin and the forebay tank as a storage during periods of low discharge to maximize the energy production and the income adjusting the peak according to the SPOT price.
A second campaign is planned in 2020, doubling the available storage using part of the headrace tunnel of the power plant.

Acknowledgements

This project, developed in the framework of the SCCER-SoE, is financially supported by SFOE and FMV.

Contributors

Hes-so EPFL Power Vision Engineering SCCER SoE FMV

SCCER SoE
SWISS COMPETENCE CENTER for ENERGY RESEARCH
SUPPLY of ELECTRICITY

SCCER-SoE Annual Conference 2019

heatstore
High Temperature Underground Thermal Energy Storage

Supported by:
Schweizerische Eidgenossenschaft
Confédération suisse
Confederazione Svizzera
Confederaziun svizra
Swiss Confederation
Innosuisse – Swiss Innovation Agency

HEATSTORE SWITZERLAND: New Opportunities for District Heating Network Sustainable Growth by High Temperature Aquifer Thermal Energy (HT-ATES) Storage

Guglielmetti L., Alt-Epping P. +, Birdsell D. ^^, De Oliveira Filho F.**, Diamond L+., Driesner T. ++, Eruteya O.*, Hollmuller P.**, ^ Koumrouyan M., Makhloufi Y.*, Martin F.˚, Meier P., Meyer M.˚, Mindel J. ++, Moscariello A.*, Nawratil de Bono C.˚, Quiquerez L.˚, Saar M. ^^, Sohrabi R^, Spring, U. ˚˚, Valley B.^, Van den Heuvel D. +, Wanner C+.*

Motivation

- Industry uses about 92% of their total energy requirement for generating process heat
- 50% of the total energy consumed in Switzerland is used to supply heat
- 86% of the required heat is generated by the burning of fossil fuel
- Households and services use about 92% of their total energy needs for heating applications
- Waste heat generated is continuously discharged into the environment

Let's convert waste heat into a resource

HEATSTORE

HEATSTORE aims at developing subsurface storage techniques to reduce wasting heat. A key technology is High Temperature (~25°C to ~90°C) Underground Thermal Energy Storage (**HT-UTES**). HEATSTORE is a European GEOTHERMICA ERA-NET co-funded project, with 24 contributing partners from 9 countries, composing a mix of scientific research institutes and private companies.

THE SWISS CONTRIBUTION

- 2 Industrial partners
- 4 Research institutions
- 2 **HT-ATES** study sites

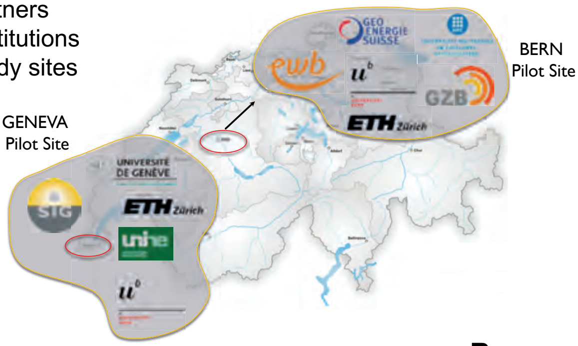

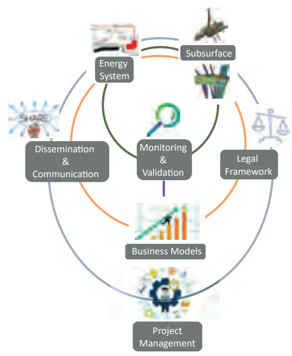

Geneva:

- Seasonal storage of waste heat from the Chenevier incinerator
- Two potential reservoirs at depths between 500m and 1100m
- Heatstore contribution: subsurface characterization constrained by drilling and testing at two different locations (GEo-01 and GEo-02); Energy system integration modelling, which will be coupled to economical, regulatory, and social constraints, to potentially lead to a commercial implementation of the system in a following stage.

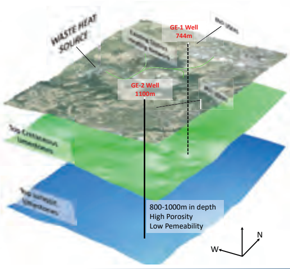

Bern:

- Seasonal storage of waste heat from the Bern-Forsthaus power plant.
- Three wells will be drilled to a depth of <500 m deep, into sandstone layers of the Lower Freshwater Molasse (USM)
- Assess the feasibility of an HT-ATES system and, if the results are encouraging, more wells will be drilled after the HEATSTORE project, to realize a fully functional heat storage system

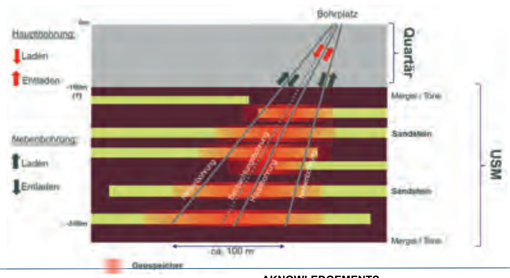

**Department of Earth Sciences, University of Geneva. Rue des maraichers 13, 1205 Geneve (Switzerland) +University of Bern. Baltzerstrasse 3 3012 Bern (Switzerland)*
^^ETH Zürich - Geothermal Energy and Geofluids Group, Institute of Geophysics, Sonneggstrasse 5, 8092 Zürich (Switzerland)
***Department of F.-A. Forel for environmental and aquatic sciences, University of Geneva. Bvd. Carl Vogt 66, 1205 Geneva (Switzerland)*
++ETH Zürich - Institute of Geochemistry and Petrology. Clausiusstrasse 25, 8092 Zürich (Switzerland) ˚Energie Wasser Bern (EWB). Monbijoustrasse 11, 3001 Bern (Switzerland)
˚˚Services Industriels de Genève. Chemin du Château-Bloch 2, 1219 Le Lignon (Switzerland) ^University of Neuchâtel. Rue Emile Argand 11 2000, Neuchâtel (Switzerland)
luca.guglielmetti@unige.ch

AKNOWLEDGEMENTS
HEATSTORE (170153-4401) is one of nine projects under the GEOTHERMICA – ERA NET Cofund aimed at accelerating the uptake of geothermal energy in Europe. The project is subsidized through the ERANET cofund GEOTHERMICA (Project n. 731117) by the European Commission, RVO (the Netherlands), DETEC (Switzerland), FZJ-PtJ (Germany), ADEME (France), EUDP (Denmark), Rannis (Iceland), VEA (Belgium), FRCT (Portugal), and MINECO (Spain). More information is available via http://www.heatstore.eu

SCCER-SoE Annual Conference 2019

SWISS COMPETENCE CENTER for ENERGY RESEARCH
SUPPLY of ELECTRICITY

Supported by:
Schweizerische Eidgenossenschaft
Confédération suisse
Confederazione Svizzera
Confederaziun svizra
Swiss Confederation
Innosuisse – Swiss Innovation Agency

Atténuation dans l'espace cours d'eau des éclusées résiduelles d'un bassin de démodulation: cas d'étude de Piotta

Marie Loverius, Pedro Manso, Giovanni De Cesare, Samuel Vorlet
Platform of Hydraulic Constructions (PL-LCH), Ecole Polytechnique Fédérale de Lausanne (EPFL)

Introduction

L'aménagement hydroélectrique de Ritom se situe dans le canton du Tessin. Actuellement, l'aménagement turbine les eaux du lac de Ritom (CFF) et du bassin d'Airolo (AET) essentiellement pour l'approvisionnement électrique du réseau électrique CFF et AET. Dans le cadre du renouvellement de l'aménagement hydroélectrique de Ritom, la construction d'un bassin de démodulation d'un volume de 100'000 m^3 est prévue à l'aval des centrales de Ritom (CFF) et de Stalvedro (AET) avec pour objectif l'atténuation des éclusées. Le projet comprend l'augmentation de la production à 60 MW impliquant un débit turbiné maximal de 29.3 m^3/s.

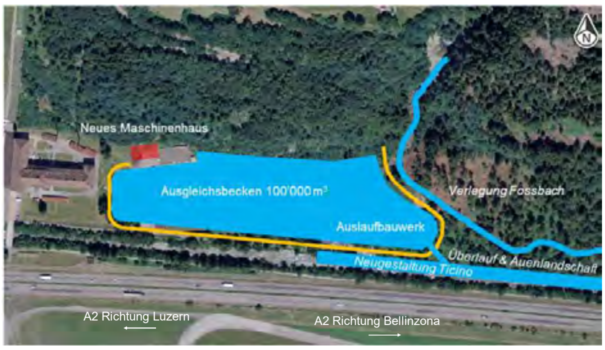

Figure 1: *Aménagement hydroélectrique de Ritom*

De par la demande spécifique du réseau CFF, de fortes variations du débit turbiné infra-journalier sont à prévoir. Ces pics de production influenceront l'efficacité du bassin de démodulation et des éclusées résiduelles dans le Ticino sont à prévoir. Ce projet vise à étudier l'atténuation des éclusées résiduelles du bassin de démodulation dans l'espace cours d'eau.

Méthodes

Divers variantes on tété testées. La solution retenue consiste en la création d'une zone tampon sous forme de plaine alluviale par l'élargissement du cours d'eau aval. Cette zone tampon est délimitée du cours d'eau par une marche de 35 cm et a une rugosité plus élevée que le cours d'eau naturel.

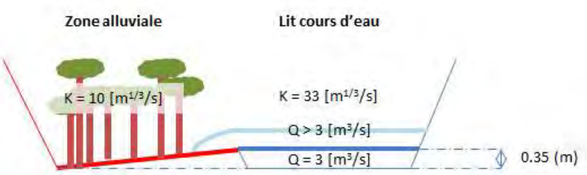

Figure 2: *Plaine alluviale et cours d'eau naturel*

Des simulations numériques sont réalisées à l'aide du logiciel Basement v.2.8 sur le tronçon aval du cours d'eau pour vérifier l'efficacité de la solution. Une modélisation 2D tu tronçon est réalisée pour résoudre les équations de conservation de la masse et de la quantité de mouvement sur le domaine computationnel. Deux hydrogrammes de sortie du bassin de démodulation sont utilisés pour la modélisation hydraulique.

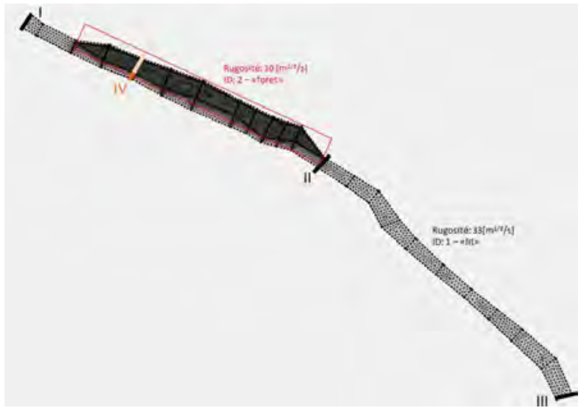

Figure 3: *Domaine computationnel: cours d'eau naturel et élargissement*

Résultats

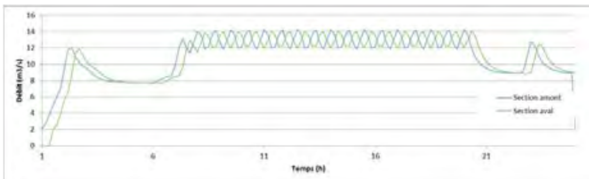

Figure 4: *Evolution du débit en fonction du temps, hydrogramme de sortie du bassin de démodulation considérant des pics au débit maximum toutes les 30 min entre 6h et 19h, toutes les 3h entre 19h et 1h et pas de turbinage entre 1h et 6h; section amont (I) et section avale (III)*

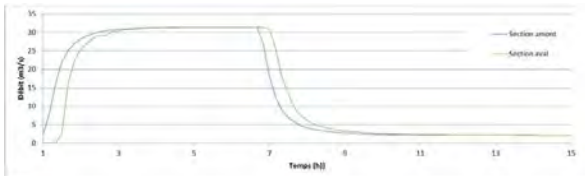

Figure 5: *Evolution du débit en fonction du temps, hydrogramme de sortie du bassin de démodulation considérant un turbinage au débit maximum jusqu'au vidage complet du bassin (durée de 6h) ; section amont (I) et section avale (III)*

Conclusion

Les résultats montrent que la solution proposée est relativement efficace pour les faibles débits (c.f. Figure 4). En effet, on observe une atténuation du débit de pointe à la zone avale ainsi qu'une atténuation des gradients pour les débits inférieurs à 15 m^3/s. Pour les débits supérieurs (c.f. Figure 5), on n'observe aucune atténuation de l'hydrogramme. En effet, l'espace de stockage limité représente moins de 1% du volume à atténuer pour des débits importants. Une solution possible consisterait à activer l'espace de stockage avec une section critique contrôlée située à la fin de la plaine alluviale.

Références

[1] Bieri, M., Zünd, B., Gasser, M., & Schleiss, A. (2016). 'Intervention strategies to mitigate hydropeaking: Two case studies from Switzerland. In HYDRO 2016 (No. EPFL-CONF-222964).
[2] Hager, W. H. & Schleiss, A. J. (2009). Constructions hydrauliques: écolouements stationnaires. Lausanne : Presses polytechnique et universitaires romandes.
[3] Pisaturo, G. R., Righetti, M., Dumbser, M., Noack, M., & Cavedon, V. (2017). The role of 3D-hydraulics in habitat modelling of hydropeaking events. Science of The Total Environment, 575, 219-230. doi: 10.1016/j.scitotenv.2016.10.046.
[4] Schleiss, A. J. (2012). Aménagements de cours d'eau. Lausanne : Presses polytechnique et universitaires romandes.
[5] Walter H. G. & Altinakar, M. S. (2011). Hydraulique fluviale: écoulement et phénomène de transport dans les canaux à géométrie simple. Lausanne : Presses polytechnique et universitaires romandes.

SCCER-SoE Annual Conference 2019

SCCER SoE
SWISS COMPETENCE CENTER for ENERGY RESEARCH
SUPPLY of ELECTRICITY

In cooperation with the CTI

Directional-dependence of Mode I fracture toughness in Grimsel Granite

Morteza Nejati[1], Ali Aminzadeh[2,3], Martin Saar[2], Thomas Driesner[3]
[1] Department of Earth Sciences, ETH Zurich, Switzerland
[2] Geothermal Energy and Geofluids, Department of Earth Sciences, ETH Zurich, Switzerland
[3] Institute of Geochemistry and Petrology, Department of Earth Sciences, ETH Zurich, Switzerland

Introduction

Many rock types behave anisotropic in their elastic and inelastic properties due to their complex micro-structure. Gischig et al. (2018) has recently demonstrated that rock anisotropy plays a critical role in the in-situ stimulation and circulation experiments in the deep underground laboratory at the Grimsel test site in Switzerland. It was concluded that the anisotropy of the mechanical properties such as elasticity, strength and fracture toughness must be taken into account to accurately predict the rock mass deformation and failure in those experiments (Dutler et al., 2018, Dambly et al., 2019). In this research, we present the experimental results on the directional-dependency of Mode I fracture toughness in Grimsel Granite.

Methodology

The stress intensity, or K-based approach, postulates that a crack extends when the stress, strain or a linear combination of the two, reaches a critical value in the region near the crack tip. Fracture growth criteria, such as maximum tangential stress and maximum tangential strain are based on the value of K_{Ic} to predict the crack growth under Mixed-Mode I/II conditions. The two energy-based fracture growth criteria, maximum energy release rate and minimum strain energy density, predict the onset of the crack growth using the critical values of the energy release rate (G_{Ic}) and the critical strain energy density (S_{Ic}). G_{Ic} and S_{Ic} are related to to K_{Ic} through the elastic constants.

We point out that the measurement of K_{Ic} requires crack extension in a self-similar manner. While this typically happens in isotropic solids, it is likely that a Mode I crack in an anisotropic solid kinks towards the direction in which crack extension requires less fracture energy. This normally happens when K_{Ic} exhibits a strong directional dependency.

We recently modified the semi-circular bend (SCB) test to incorporate the elasticity anisotropy in the determination of the fracture toughness (Nejati at al., 2019a). The schematics of this test is shown in Figure 1a. This new test scheme allows to determine the fracture toughness at any orientation with respect to the principal directions (see Figure 1b).

In order to prepare the SCB samples, the original rock core, with the diameter of 120mm, was sub-cored in the direction normal to its axis in such a way that the foliation plane is parallel to the axis of the sub-core. A meter of the original core produced eight sub-cores with a diameter of 95 mm, each being cut to yield four SCB samples that have identical angles between the SCB base and the foliation. The SCB specimens from each sub-core were then notched with a thin cutting blade, so that all have the same angle, β, between the crack plane and the foliation. In total, a set of 29 samples with seven different angles, β = 0º; 15º; 30º; 45º; 60º; 75º and 90º, were prepared. Once the peak load is measured for each experiment, the fracture toughness, K_{Ic}, is calculated using the geometry and material factors given in Nejati et al. (2019a). These values are then corrected if the fracture has not extended in a self-similar manner.

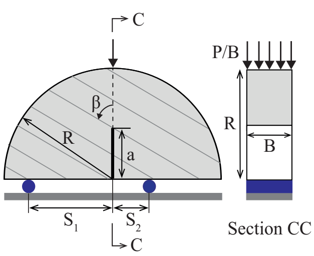

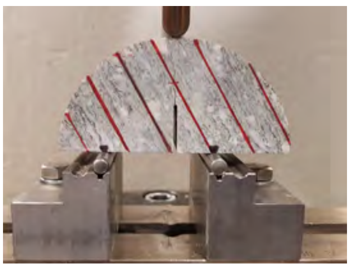

Figure 1. a) Schematics of the modified SCB test with asymmetric loading. b) Modified SCB test of Grimsel Granite with S_1/R=0.6.

Results and Discussion

Figure 2 illustrates the variations of the different measures of fracture toughness, K_{Ic}, G_{Ic}, and S_{Ic}, versus the angle β. The K_{Ic} data are obtained by correcting the apparent fracture toughness for the kink angle. The solid lines in K_{Ic} results represent the least-squares fit to the shown sinusoidal fit. It can be seen that the experimental data are fitted well using this sinusoidal variation. This gives supporting evidence for that yields a suitable type of variation of the critical SIF in an anisotropy plane. One can therefore use the two principal values of fracture toughness, measured along the two principal material directions, to determine the fracture toughness in any other direction.

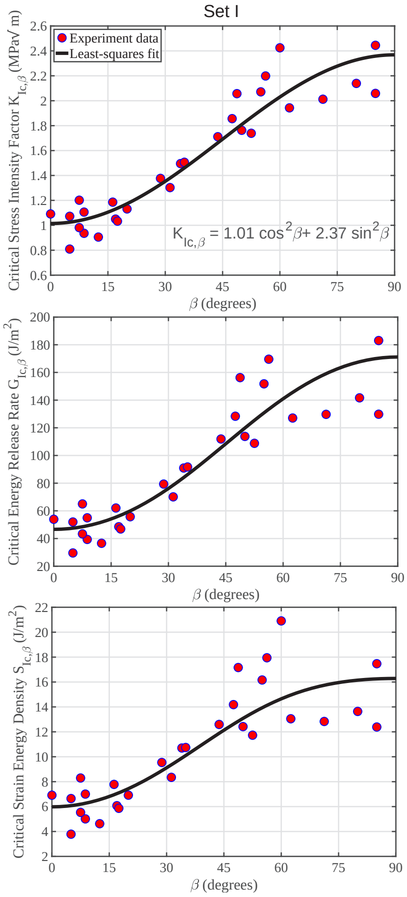

Figure 2. Variations of different measures of Mode I fracture toughness against β for a set of experiments on Grimsel Granite samples.

References

Gischig, V., Doetsch, J., Maurer, H., et al., (2018). On the link between stress field and small-scale hydraulic fracture growth in anisotropic rock derived from micro-seismicity. *Solid Earth* 9 (1), 39–61.
Dutler, N., Nejati, M., Valley, B., Amann, F., Molinari, G., (2018). On the link between fracture toughness, tensile strength, and fracture process zone in anisotropic rocks. *Engineering Fracture Mechanics* 201, 56–79.
Dambly, M., Nejati, M., Vogler, D., Saar, M. O., (2019). On the direct measurement of the shear moduli in transversely isotropic rocks using the uniaxial compression test. *International Journal of Rock Mechanics and Mining Sciences* 113, 220–240.
Nejati, M., Aminzadeh, A., Saar, M. O., Driesner, T. (2019a). Semi-circular bend test designed for mode I fracture toughness experiments in anisotropic rocks. *Engineering Fracture Mechanics 213*, 153-171.

SCCER-SoE Annual Conference 2019

Computational Modelling of Fine Sediment Release Using SEDMIX Device with Thrusters

Onate-Paladines, A., Amini, A., De Cesare, G.*
Platform of Hydraulic Constructions (PL-LCH), EPFL. *Corresponding author: onatari8@aquacloud.net

Introduction

- ***Problem:*** Reservoir sedimentation occurs in dams worldwide, reducing the live storage available in the reservoirs.
- ***Possible solution:*** Jenzer-Althaus (2011) tested a water stirring device (called SEDMIX) that keeps sediments in suspension, enhancing its release through the power intakes of the dam reporting a high efficiency.
- ***Background studies:*** Numerical simulations for a prototype for the Trift reservoir have been carried out in the past by Amini et al. (2017) and Chraibi et al. (2018), obtaining good results for sediment evacuation and determining the optimal location and dimensions of the device.
- ***Objective of the current work***: Numerically test the performance of SEDMIX at the Trift reservoir implementing thrusters instead of the previous configuration with water jets using ANSYS 2019 R1 software .

Methodology

1. Compare the flow patterns in a regular tank obtained through numerical modelling (figure 1) with the experimental ones obtained by Jenzer-Althaus (2011).
   - Considering various bottom clearances and a single phase flow, using the k-ε turbulence model and assuming a steady state flow.
   - The jets were modelled as inner sources and the thrusters as a combination of inner sinks and sources to avoid refining elements.

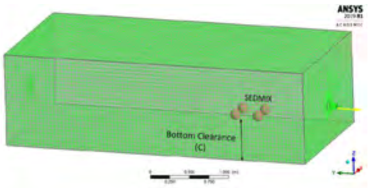

Figure 1: Numerical model of regular tank.

2. Determine the sediment release at Trift reservoir and compare it with the one obtained with jets.
   - The geometrical dimensions and location of the device were the optimal found by Chraibi et al. (2018) (figure 2).
   - A constant inflow Q_{in} of 21 m³/s, a relative pressure of 0 at the water intake and a multiphase flow were considered.
   - It was assumed a concentration of 0.7 g/L of sediments, with a mean particle diameter (D_s) of 0.1 mm, and a density (ρ_s) of 2600 kg/m³.
   - Three diameters of thrusters were considered. Each has its own thrust force (T) and rotational speed (n) that determined its maximum efflux velocity (U_0) as proposed by Albertson et al (1948) and its thrust coefficient (K_t) as suggested by Blaauw & Van de Kaa (1978):

$$U_0 \approx 1.60 \cdot n \cdot D \cdot \sqrt{K_t} \qquad K_t = \frac{T}{\rho \cdot n^2 \cdot D^4}$$

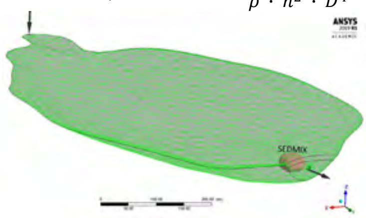

Figure 2: Numerical model of Trift reservoir

Results And Analysis

- The flow patterns obtained through numerical simulation of SEDMIX with water jets (figure 3a) are similar to the ones obtained by Jenzer-Althaus (2011) (figure 3b).
- With thrusters maintaining the same induced flow as the one considered for the jets, the flow velocity provided by them is too small to reproduce the flow patterns expected (figure 3c).
- Adjusting the thrusters to a higher velocity, a similar flow pattern was obtained (figure 3d).

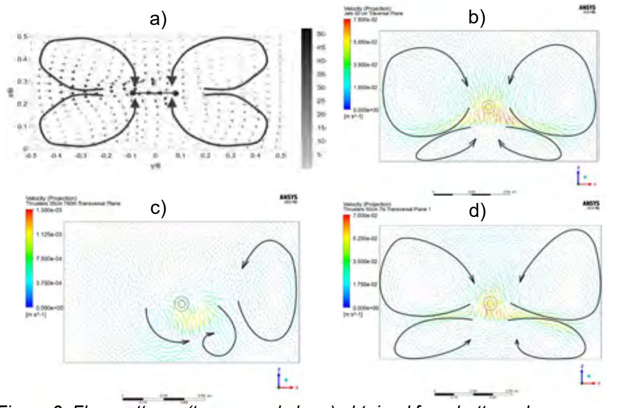

Figure 3: Flow patterns (transversal plane) obtained for a bottom clearance of 0.5 m: a) Experimentally (jets). b) Numerically (jets). c) Numerically (thrusters 760 l/h). d) Numerically (thrusters 7.2 l/s).

- The set of thrusters of 0.42 m were successfully calibrated to obtain the optimum sediment release (73 % of increment in evacuation), with a global induced flow of ~ 12.8 m³/s (3.2 m³/s per thruster) (figure 4). With this flow, the variation of the sediment velocity along the water column located at the vortex center resembles the one obtained for water jets, as shown in figure 5.

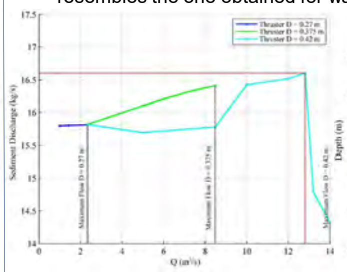

Figure 4: Sediment discharge with SEDMIX using thrusters of various diameters.

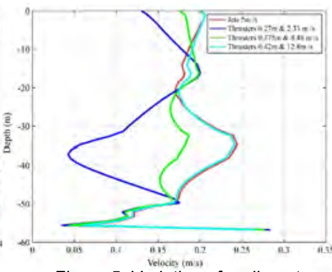

Figure 5: Variation of sediment velocity with depth for jets and thrusters.

Figure 6: SEDMIX to the 3D Dredger's™ floating platform

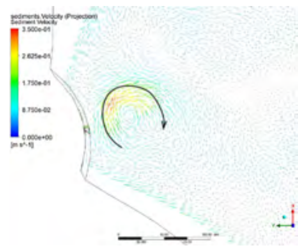

Figure 7: Rotational flow generated when using SEDMIX with thrusters.

Conclusion

- The numerical simulations showed similar patterns when using jets and thrusters, however, a higher induced flow is needed by the thrusters to be able to replicate the recirculation flow generated by the jets.
- For the Trift reservoir, the optimal thruster had a diameter of 0.42 m with a induced flow of 3.2 m³/s.
- Since the use of thrusters means no dealing with head losses, the power requirements could be less and the operational costs could be lower compared to the use of water jets.
- The experimental study of the device using thrusters is highly advised and the hydrodynamic behaviour in the reservoir should be further studied.

References

- Jenzer-Althaus, J. Sediment evacuation from reservoirs through intakes by jet induced flow. PhD thesis, Ecole Polytechnique Fédérale de Lausanne: Switzerland, 2011.
- Amini, A.; Manso, P.; Venuleo, S.; Lindsay, N.; Leuipi, C.; Schleiss, A. Computational hydraulic modelling of fine sediment stirring and evacuation through the power waterways at the Trift reservoir.; Hydro 2017, Seville, Spain.
- Chraibi, A. Amini, A. Manso, P. Schleiss, A.J. Controlled fine sediment release through the power waterways by using a mixing device. SCCER-SoE Annual Conference. Switzerland, 2018.
- Albertson, M., Dai, Y., Jensen, R., & Rouse, H. Diffusion of submerged jets. ASCE Transactions, 1948. 648-697.
- Blaauw, H., & Van de Kaa, E. Erosion of bottom and sloping banks caused by the screwrace of maneuvering ships, publication 202. Delft: Delft Hydraulics laboratory, 1978.

SCCER SoE
SWISS COMPETENCE CENTER for ENERGY RESEARCH
SUPPLY of ELECTRICITY

SCCER-SoE Annual Conference 2019

Hes·so VALAIS WALLIS
School of Engineering

Supported by:
Schweizerische Eidgenossenschaft
Confédération suisse
Confederazione Svizzera
Confederaziun svizra
Swiss Confederation
Innosuisse – Swiss Innovation Agency

Assessment of a turbine model to predict cost effectively the far wake of a hydrokinetic farm

O. Pacot, D. Pettinaroli, J. Decaix, C. Münch-Alligné

Institute of Sustainable Energy, School of Engineering, HES-SO Valais-Wallis, Sion, Switzerland, olivier.pacot@hevs.ch

Context

- To maximize the energy harvest from rivers, several hydrokinetic turbines [1,2] are assembled to form a farm, which requires to investigate the influence of the machines between each other and their influences on the local flow.
- To study theses influences, numerical simulations are used. However, it requires to compute the free surface flow and all the interfaces between the stationary and rotating parts, which is time and computational expensive.

Objective

- To implement a simplified hydrokinetic model to save computational resources.

Hydrokinetic Turbine Model

The hydrokinetic turbine model (similar to the actuator disk) mimics the pressure drops experienced by the fluid from the runner [3]. The model requires a loss coefficient as parameter, which is obtained numerically using steady state simulations with a simplified computational domain.

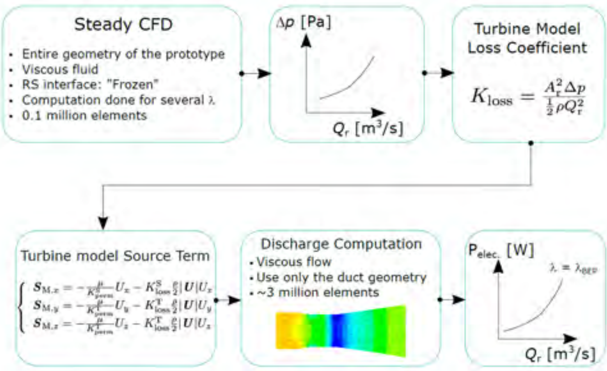

Numerical setup

Two different computational domains were designed using ANSYS ICEM CFD. The first one (**case 1**) uses a rectangular domain and was used to define the turbine model by steady and single phase simulations. The second one uses a trapezoidal domain and was used to simulate the flow field through a farm using once the full geometry of the machine (**case 2**) and once the turbine model (**case 3**). These simulations were unsteady and multiphase.

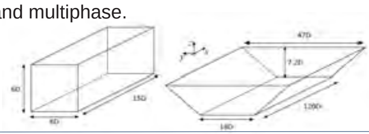

Computed performance and loss coefficient

To establish the performance characteristic and the model parameter of the hydrokinetic turbine, several combination of the tip speed ration λ were computed using ANSYS CFX R17.2. The Best Efficiency Point is reached for a Cp=0.87 [-] and a λ=2.54 [-]. Based on these simulations, the coefficient of resistance K can be computed and corresponds to 0.71 [-] at BEP [4].

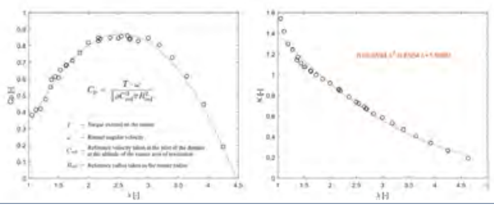

Results

- Case 3 required approximately 15 time less CPU hours and mesh resources compared to case 2.
- Case 2 shows a qualitative faster wake recovery, which might be attributed to the difference of mesh type and the lack of flow rotation in case 3.
- However, the quantitative comparison between case 2 and 3 shows that the difference in the horizontal velocity profile at x/D=99.0 is only of -13%.

Case	1	2	3
Mesh size [Millions of elements]	0.1	45.6	2.9
Computation time [CPU hours]	24	25'000	1'500

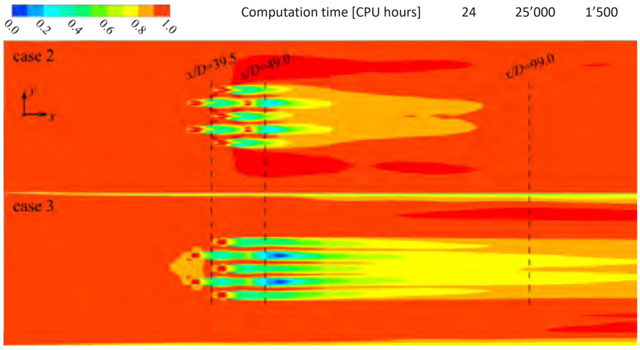

Comparison of the instantaneous normalized streamwise velocity on the Oxy plane (z/D=2.6)

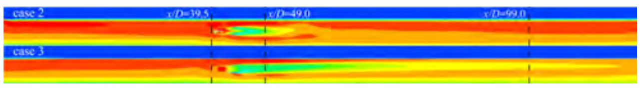

Comparison of the instantaneous normalized streamwise velocity on the Ozx plane (y/D=0.0)

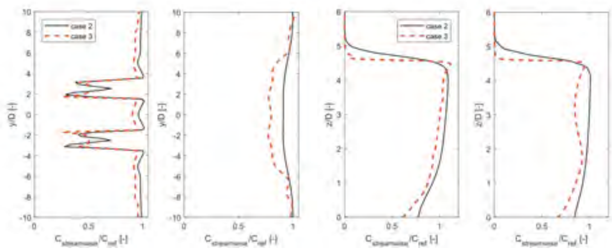

Comparison of the instantaneous normalized velocity profiles. (a) horizontal profile at z/D=2.6. Left : x/D= 39.5. Right: x/D= 99.0. (b) vertical profile at y/D=0.0. Left : x/D= 39.5. Right: x/D= 99.0.

Conclusions

- A methodology was proposed to investigate faster the flow field passing through a hydrokinetic turbine farm.
- The comparison between the high resolution simulation (case 2) with the simplified one (case 3) showed acceptable discrepancies but a significant gain in mesh size and computation time.
- This methodology is well suited for an initial investigation on where to place hydrokinetic turbines in a river to get the maximum power output.

References

[1] C. Münch, S. Richard, A. Gaspoz, V. Hasmatuchi, N. Brunner, "New Prototype of a Kinetic Turbine of Artificial Channels" Advances in Hydroinformatics, Springer, Singapore, 2018, pp. 981-996.

[2] C. Münch, J. Schmid, S. Richard, A. Gaspoz, N. Brunner, V. Hasmatuchi, "Experimental Assessment of a New Kinetic Turbine Performance for Artificial Channels" Water 2018, Volume 10, Issue 3, 311.

[3] Batten W M J, Harrison M E and Bahaj A S 2013 *Phil Trans R Soc A* 371 20120293-20120293

[4] O. Pacot, D. Pettinaroli, J. Decaix and C. Münch, "Cost-effective CFD simulation to predict the performance of a hydrokinetic turbine farm". To be presented at the IAHRWG2019, 9-11 October 2019, Stuttgart, Germany.

SCCER SoE
SWISS COMPETENCE CENTER for ENERGY RESEARCH
SUPPLY of ELECTRICITY

SCCER-SoE Annual Conference 2019

FlexSTOR

Supported by:
Schweizerische Eidgenossenschaft
Confédération suisse
Confederazione Svizzera
Confederaziun svizra
Swiss Confederation
Innosuisse – Swiss Innovation Agency

LARGE-SCALE FIELD TESTS ON IMPULSE WAVES

Eva Sauter, Yuri Prohaska, Lukas Schmocker, Helge Fuchs, Robert Boes - VAW, ETHZ; Axel Volkwein - WSL

Motivation

Impulse waves, generated by avalanches, ice- or rockfalls, may seriously impair the reservoir of a hydropower plant. In some cases they even overtop or damage the dam and trigger hazardous flood waves (Fig. 1). Examining their potential impact is therefore an inevitable part of a comprehensive hazard assessment for hydropower reservoirs in alpine areas.

Fig 1: Impulse wave generation at Grindelwald Glacier Lake (Photo: Hans-Ruedi Burgener)

Field and laboratory tests

Within the CTI project FlexSTOR, both laboratory tests at VAW and prototype field tests at a gravel pit in Bülach were carried out to investigate the impulse wave generation and propagation. A test site was established in a 30 m deep gravel pit. The artificial reservoir was 15 m wide, 55 m long and had a still water depth of 1.5 m. A 40 m long steel ramp along the pit slope (37°) provided a sliding surface. The sliding mass was represented by a steel sledge (3 to 7 tons). The sledge could be released from different ramp positions to vary the impact velocity between 6 and 17 m/s. The resulting wave heights along the wave propagation path and the wave run-up were visually determined using gauge poles. A total of 13 tests were carried out in both field and model scale.

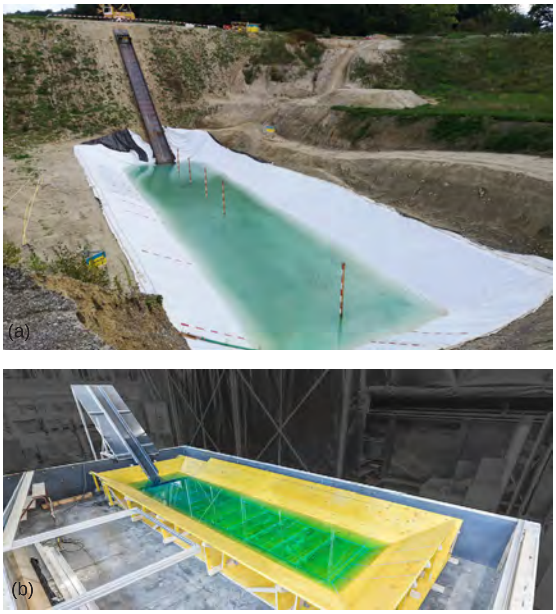

Fig 2: (a) Impulse wave field test site in gravel pit; (b) 1:10 scale model at VAW

Results

Due to the high sledge impact velocity in the field tests, a large splash is created, reaching up to 3/4 of the basin length. The maximum wave height occurs when a maximum of the sledge's energy has been transferred to the water body and the wave has propagated a certain distance from the impact location. The first and second waves are very steep and therefore start to break shortly after generation such that they finally propagate as long waves with reduced wave height.

Fig 3: Impact of sledge and splash generation in the field test

The maximum wave amplitudes were evaluated at the 5 gauges for all tests. Figure 4 compares the wave profiles measured for test V11 (maximum weight and impact velocity). Field and laboratory tests are in good agreement and the maximum wave amplitudes agree within ±30%. Larger amplitudes show generally a better correlation, whereas smaller amplitudes may be partially affected by the measurement accuracy. The correlation however changes with the propagation distance as the amplitudes decrease. Overall, no significant scale effects have been determined and laboratory tests are consequently a feasible option to investigate slide induced impulse waves and the acquired results may be classified as robust and reliable.

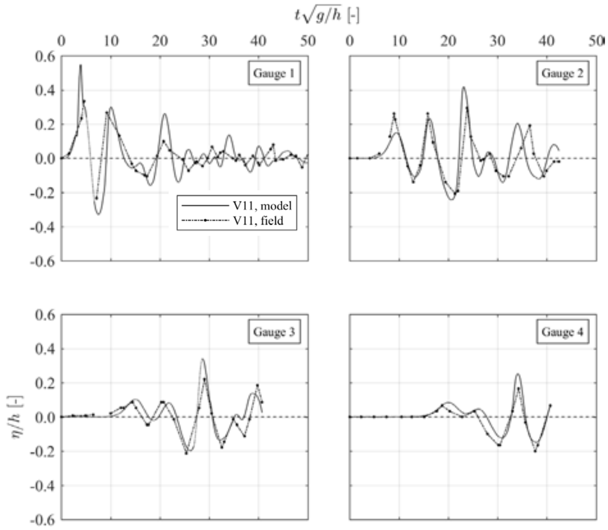

Fig 4: Comparison of relative wave amplitude at relative times measured in field (dotted line) and laboratory for tests (solid line)

Acknowledgement

This project is financially supported by Innosuisse with the industrial partner Kraftwerke Oberhasli (KWO). It is part of the FlexSTOR project and is embedded in the Swiss Competence Centre for Energy Research - Supply of Energy (SCCER-SoE) framework.

SCCER-SoE Annual Conference 2019

SWISS COMPETENCE CENTER for ENERGY RESEARCH
SUPPLY of ELECTRICITY

Supported by:
Schweizerische Eidgenossenschaft
Confédération suisse
Confederazione Svizzera
Confederaziun svizra

Swiss Confederation

Innosuisse – Swiss Innovation Agency

High Resolution Snow Melt and Runoff Modelling

Michael Schirmer, Massimiliano Zappa, Tobias Jonas

Motivation

The role of WSL and SLF within the SCCER-SoE is to develop and provide state-of-the-art snow cover and hydrological models suitable to predict inflow at the intake of hydropower plants as a basis for sediment management and for a flexible power production scheme. A high-resolution energy-balance-type snow model is applied enabling a realistic representation of small-scale processes in alpine terrain. Accounting for spatial variability is key to accurately assess changes in the distribution and frequency of runoff in small mountain catchments.

Methods

We used the state-of-the-art snowcover model JIM to describe the spatially variable water input at the soil surface. We recently refined the model to allow applications at very high spatial resolution by specifically accounting for small-scale processes relevant in mountainous environments. This model upgrade integrates developments such as a dynamically downscaling of radiation input delivered by Numerical Weather Prediction (NWP) models from 1 km to 250 m resolution and a subgrid-paramerization of snow covered fraction. Measured snow and air temperature data were assimilated in the model in order to initialize realistic start conditions for forecast values. Modelled surface water input was provided to the hydrological model PREVAH to simulate the intake to a hydropower plant. This model setup was applied to the demonstrator project "SmallFlex" (Task 5.1) in Gletsch, VS.

Results and Discussion

Shortwave radiation (SWR) was dynamically downscaled from coarser NWP models and include shading from the terrain.

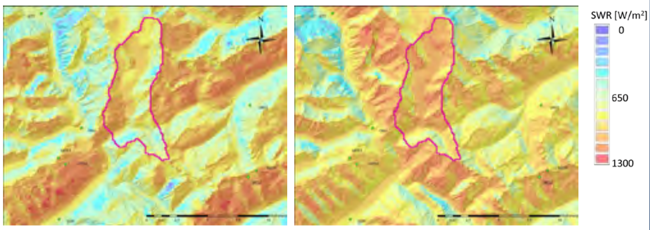

Figure 1: Modelled shortwave radiation for a clear day in June 2019 at 10 am (a) and 1 pm (b), respectively.

The resulting surface water input reacts on the spatial difference in shortwave radiation, but is also dependent on other factors as the current states of snow amount, snow covered fraction and snow wetness (next block) as well as other energy fluxes (Discussion).

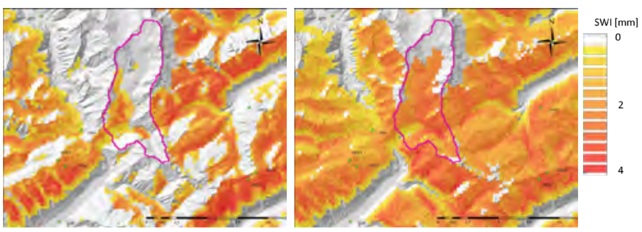

Figure 2: Modelled surface water input for one hour on a clear day in June 2019 starting at 10 am (a) and 1 pm (b), respectively.

Snow covered fraction (SCF) is dependent on modelled snow depth and terrain variables to account for snow depth variability. It is an important state variable since it strongly influences modelled surface water input (SWI). SWI is also dependent on the ability of snow to retain melt or rain water.

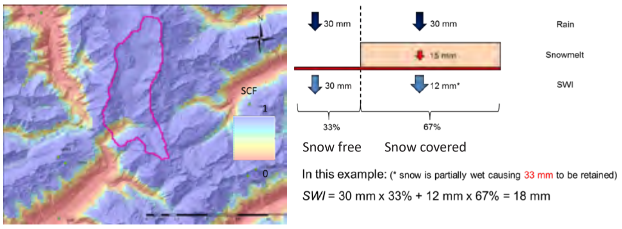

Figure 3: Modelled snow covered fraction for a day in June 2019 (a) and an example of the effect of SCF and snow retention capacity on surface water input (SWI) (b).

Surface water input (SWI) is provided to the hydrological model PREVAH, a high resolution semi-distributed model. This model chain is able to forecast the intake of the small hydropower plant of up to five days. A first analysis of the quality shows that the largest uncertainty is due to the input data. For example, the model receives too little precipitation at June 10. Ensemble of precipitation input may improve the forecast value significantly, especially for small alpine catchments where the localisation of high intensity precipitation is difficult to forecast correctly.

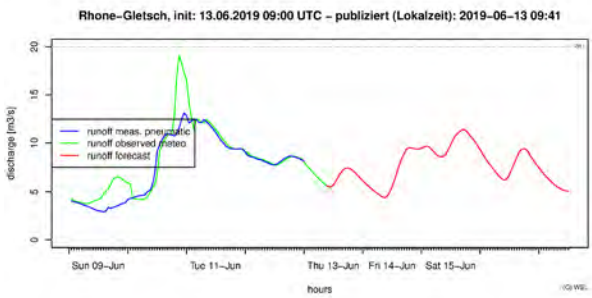

Figure 4: Intake of the small hydropower plant, in blue are observations, in green hindcast intake and in red forecast intake.

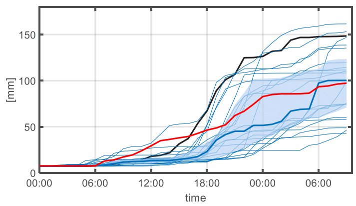

Figure 5: Accumulated precipitation this catchment for June 9 and 10. Observation in red, deterministic forecast in black, and ensemble forecast in blue (median in bold and innerquartile range shaded)

Discussion

Snow melt depends only indirectly on air temperature, while shortwave radiation is known to be the main driver for most situations. However, in most hydrological models snow melt is calibrated based on air temperature. This works fine for most situations, however, snow melt during rain-on-snow events can hardly be modelled correctly. Also for extreme situations, which are not well represented in the calibration data set, the less calibration-based energy balance model approach has a strong advantage.
This is also true for future climate scenarios, for which the empirical relation between air temperature and runoff may change substantially.

SCCER SoE
SWISS COMPETENCE CENTER for ENERGY RESEARCH
SUPPLY of ELECTRICITY

SCCER-SoE Annual Conference 2019

Hes·so VALAIS WALLIS
School of Engineering

Supported by:
Schweizerische Eidgenossenschaft
Confédération suisse
Confederazione Svizzera
Confederaziun svizra

Swiss Confederation

Innosuisse – Swiss Innovation Agency

Multipurpose water reservoirs : a necessity for futur irrigation?

J. Schmid, J. Decaix, C. Münch-Allligné, A. Gillioz

HES-SO Valais, School of Engineering, Hydroelectricity Group, CH-1950 Sion, Switzerland, jeremy.schmid@hevs.ch

Context and Motivation

Switzerland, considered as the water tower of Europe, will not escape the problems related to water in the next years. Several causes indicate that such as fluctuating water supplies, local water shortages and also local geopolitical conflicts between the resources users.

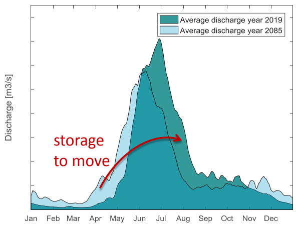

Climate variations will change the hydrological regimes of alpine regions in the next years (2050-2100). The glaciers will slowly disappear inducing changes in the water regime by moving the peak earlier in the year [1]. So it is necessary to be able to store the water when we do not need to reuse it later in the year.

The challenges are the storage of winter water for the summer and that all users of the region are equitably supplied with water [2]. The multipurpose reservoir are part of the solution.

Multipurpose reservoirs:

- Significant contribution to having enough water available in the future
- Can compensate for the disappearance of glaciers
- Coordinate the multiple users of water
- Available for flood protection

Objective and Method

The project is divided into 4 distinct parts. The project aims to define the future hydrological regime of the region, to monitoring a part of the current network to make a numerical model that will allow to set up a master plan by the municipality of Val de Bagnes.

- Know the needs and future water resources in Val de Bagnes (VS)
- Develop a decision support for the management of water reservoirs
- Develop a general planning of the irrigation network

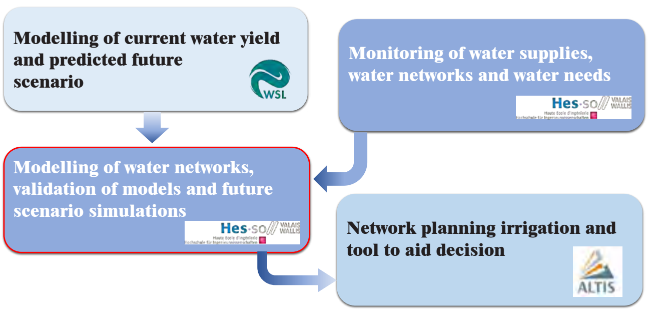

Water Network Modelling

- The numerical model is initially divided into two part. On the one hand the water adduction network (open channel flow (A)) and on the other hand the irrigation network distribution (pipe flow (B)).

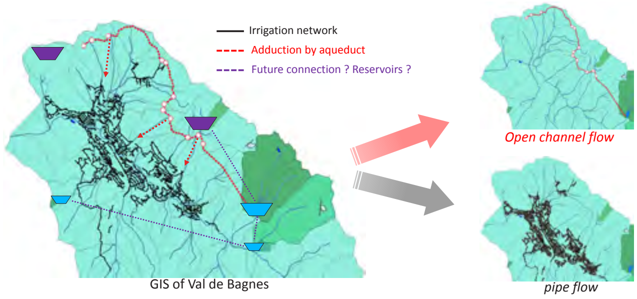

A) Macro level of the network

- *Reservoirs modelling (H-V)*
- *Lag-time river modelling*
- *Level-discharge relation (spillway)*
- *Time-series of flow discharge*
- *Overall consumption of users*
- ➢ *Keywords : **flow - volume - level***

B) Specific level of the network

- *Reservoir modelling (infinity volume)*
- *Junction (with demand)*
- *Pipe (head losses : Hazen-Williams)*
- *Cane and valve (more than 2500)*
- *Irrigation consumption*
- ➢ *Keywords : **pressure - flow***

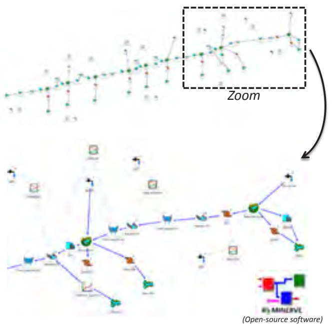

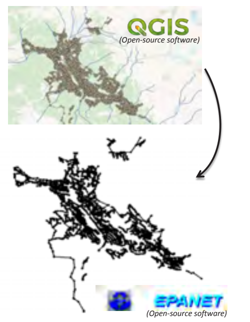

Perspectives and illustrative simulation

- Identify critical section of the network according to future scenario simulations
- Connecting the two numerical models
- Develop a holistic approach to water use in these watersheds
- Participate in the development of the master plan (connection - new reservoirs)

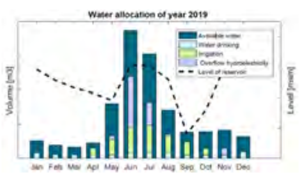

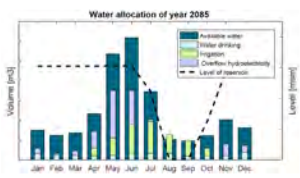

- Volume over the year is sufficient
- No drought condition in ***average*** year
- Spring period of filling the reservoir

- Volume over the year is sufficient
- More availability in winter (early)
- Drought condition in late summer

➢ New reservoir for storage in winter could reduce the drought period.

Acknowledgements

ALTIS WSL Pôle Innovation blueark Entremont

References

[1] PNR 61. (2013). MontanAqua. Anticiper le stress hydrique dans les Alpes - Scénarios de gestion de l'eau dans la région de Crans-Montana-Sierre (Valais). Université de Berne.
[2] Thut, W., Weingartner, R., & Schädler, B. (2016). Des réservoirs à buts multiples assurent l'alimentation en eau et en énergie. Université de Berne.
[3] Manuela I. Brunner, hydrological simulation and products of Val de Bagnes (hydrological data)

SCCER SoE
SWISS COMPETENCE CENTER for ENERGY RESEARCH
SUPPLY of ELECTRICITY

SCCER-SoE Annual Conference 2019

crealp EPFL LCH

Supported by:
Schweizerische Eidgenossenschaft
Confédération suisse
Confederazione Svizzera
Confederaziun svizra
Swiss Confederation
Innosuisse – Swiss Innovation Agency

Set-up and configuration of an ensemble Kalman filter for an operational flood forecasting system

Anne SCHWOB[1], Alain FOEHN[1], Javier FLUIXA[2], Giovanni DE CESARE[1]
Contact: anne.schwob@epfl.ch
[1]Laboratoire de Constructions Hydrauliques (LCH-EPFL), [2] Centre de Recherche sur l'Environnement Alpin (CREALP)

INTRODUCTION:

To forecast riverine floods, short-range forecasts are normally provided. In such cases the initial hydrological conditions highly influence the predictability of a flood event.
The study evaluates the potential of an **ensemble Kalman filter (EnKF)** for the operational flood forecasting system in the Upper Rhone River basin (Fig 1). **Observed discharge data is used to update the initial conditions of the hydrological model.** Past flood events in the Reckingen subbasin (Fig. 1) are modelled to assess the robustness of the methodology and the quality of flood predictions.

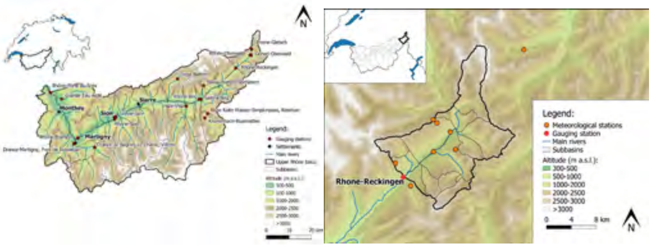

Figure 1: Maps of the Upper Rhone River basin (left) and the Reckingen subbasin (right) showing gauging stations and meteorological stations.

METHODOLOGY:

- Simulations are computed with the semi-distributed hydrological model RS MINERVE (Crealp, 2019).
- Three different discharge predictions are computed and compared:
  - **Control simulation**: Open-loop scenario where discharge observations are not used to correct model initial conditions.
  - **Volume based update (VBU) simulation**: Iterative approach correcting the initial soil saturation in order to generate the modelled water volume which has been observed over the 24 h before the forecast.
  - **EnKF simulation**: Data assimilation (DA) method where the initial conditions of the model are updated based on the covariance matrices of the discharge observations and the model prediction (Fig. 2) (Evensen 1994).
- Forecast quality is evaluated based on the Kling-Gupta-efficiency (KGE) calculated for different lead times (Gupta et al., 2009):

$$KGE = 1 - \sqrt{(r-1)^2 + (a-1)^2 + (b-1)^2}$$

where r is the correlation coefficient, a is measure of variability and b is a measure of bias.

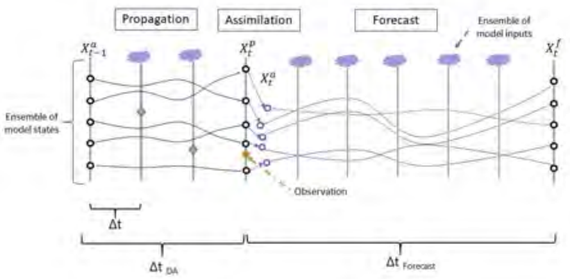

Figure 2: Schematic of the investigated EnKF where perturbed inputs are applied to an ensemble of model states (adapted Noh 2013).

RESULTS:

Figure 3 shows the streamflow prediction of the EnKF in comparison with the Control and VBU simulation as well as the observed discharge during an event in Reckingen in 2012. Figure 4 shows the KGE of the different simulation methods for four flood events in the Reckingen subbasin.

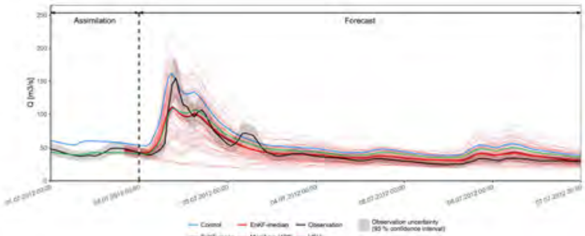

Figure 3: Example hydrograph during an event in Reckingen, July 2012.

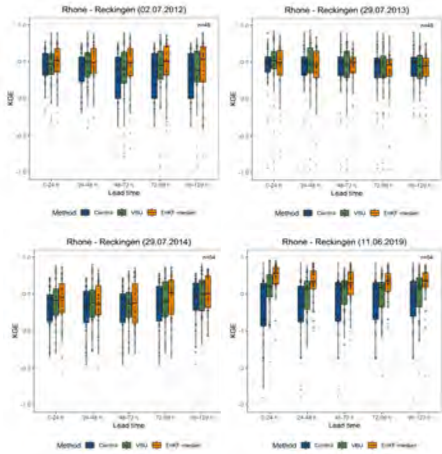

Figure 4: KGE of the three simulation methods for flood events in Reckingen in 2012, 2013, 2014 and 2019.

DISCUSSION AND CONCLUSION:

- **For short lead times, the EnKF simulation outperforms the other two simulations.** With an increased lead time the results depend on the event and the model calibration.
- To achieve good results with the EnKF, **an appropriate model calibration and high-quality input data is needed.**
- A DA method which specifically **accounts for the time lag needed for streamflow routing could increase the robustness** of the framework.

REFERENCES:

Crealp, 2019. Available versions of RS MINERVE installers. URL https://www.crealp.ch/down/rsm/install2/archives.html (accessed 24.06.19).

Evensen, G., 1994. Sequential data assimilation with a nonlinear quasi-geostrophic model using Monte Carlo methods to forecast error statistics. Journal of Geophysical Research 99, 10143.

Gupta, H.V., Kling, H., Yilmaz, K.K., Martinez, G.F., 2009. Decomposition of the mean squared error and NSE performance criteria: implications for improving hydrological modelling. Journal of Hydrology 377, 80–91.

Noh, S.J., Tachikawa, Y., Shiiba, M., Kim, S., 2013. Ensemble Kalman filtering and particle filtering in a lag-time window for short-term streamflow forecasting with a distributed hydrologic model. J. Hydrol. Eng. 18, 1684–1696.

SCCER-SoE Annual Conference 2019

SWISS COMPETENCE CENTER for ENERGY RESEARCH
SUPPLY of ELECTRICITY

GPR imaging of fractures in the Bedretto Lab

Alexis Shakas and Peter-Lasse Giertzuch

Motivation

The Bedretto Tunnel is located in Bedretto Valley (Ticino). Within the tunnel, at 2 km length (from a total of 5.2 km) there exists the Bedretto Underground Laboraty for Geosciences (BULG) - a research facility where the ETH Zurich and external partners are conducting experiments that focus on the safe and efficient extraction of geothermal heat from engineered geothermal systems within crystalline rock reservoirs.

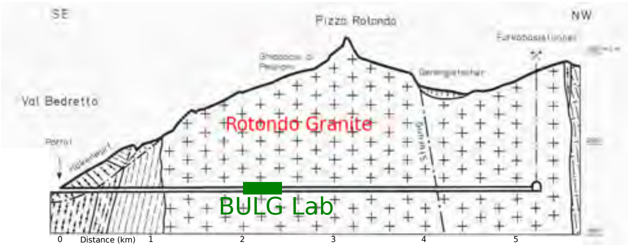

Figure 1. Geologic map of the Bedretto tunnel and the location of the BULG. This figure has been modified from Keller and Schneider (1982).

Fracture Detection using Ground Penetrating Radar (GPR)

Various geophysical techniques are used in the BULG to characterize the granitic rock mass and the presence of fractures along with their spatial properties. These properties, including the fracture density, aperture, length scale and orientation allow us to characterize processes such as fluid flow, heat dissipation and rock meachanical aspects such as hydraulic shearing and fracturing. One of the most promising methodologies for remote sensing of fractures (and associated processes) is ground penetrating radar; a technique that uses high-frequency (100 to 250 MHz) electromagnetic wave propagation and scattering.

.

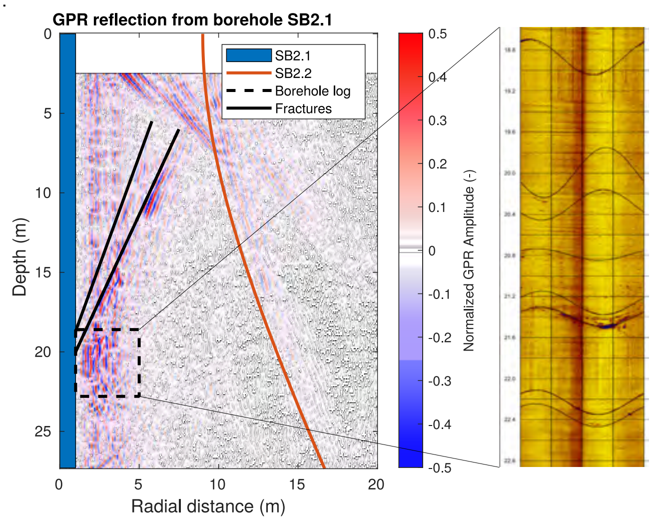

Figure 2. *Left*: Processed single-hole GPR reflection data from borehole SB2.1 (the borehole configuration is shown in the next figure). The first few meters are muted because strong reflections from the metal casing saturate the signal. The location of borehole SB2.2 is shown in red (computed from borehole trajectory alone). Two fractures are interpreted and shown in solid black lines. A region of the data where strong reflections arise is shown with a dashed rectangle. *Right*: The acoustic televiewer log reveals 8 fractures that intersect the borehole in the region identified by the GPR reflection image.

Forward Modeling of GPR reflections

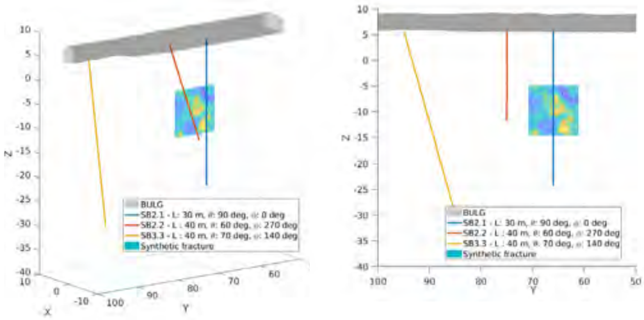

Figure 3. *Top*: Model showing the location and orientation of the three boreholes in the BULG. A synthetic fracture is also shown, of 10 m by 10 m extend and 4 m radially away from SB2.1. Color changes along the fracture plane correspond to aperture variations (blue to yellow corresponds to small to large apertures respectively - apertures vary in the sub-mm range=

Right: Simulated GPR reflection data corresponding to the fracture plane shown in the model above. The data were computed using the forward modeling scheme introduced by Shakas and Linde (2015). The dashed line reveals the real location of the fracture plane.

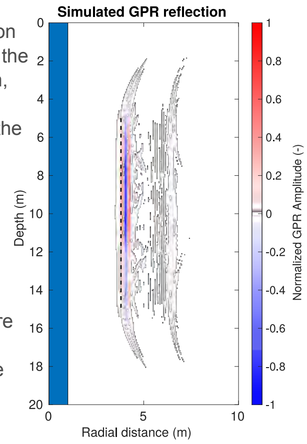

Discussion and Outlook

The Bedretto Underground Lab for Geosciences has been developing since 2017. Geophysical characterization of the granitic rock mass that surrounds the underground laboratory is of primary importance, prior, during and after any stimulation experiments, which can alter the natural state of the fracture network. Geophysical tools such as GPR offer a promising technology to delineate geometrical properties of fractures. This can be done in boreholes, as is presented here, but also along the tunnel wall.

Additionally, several geophysical imaging techniques can be combined in order to reduce the uncertainty in the measured properties by providing complementary information. For example, GPR uses electromagnetic waves to detect fracture aperture using the dielectric properties of the host rock and water (for water filled fractures). Additionally, active seismic methods will be used in a similar geometry to detect fracture aperture, while being sensitive to the density and elastic properties of the host rock and water. Such information can then be used in a joint modeling and inversion framework to constrain fracture permeability and assess permeability enhancement as a result of stimulation experiments.

Acknowledgements

The work presented here is part of the Bedretto project for Geo-energies (http://www.bedrettolab.ethz.ch/). The Bedretto team is to thank for all their individual contributions and effort in the project.

References

Keller, F. & Schneider, T. R. (1982). Geologie und Geotechnik. Schweizer Ingenieur und Architekt, Heft 24.

.

Shakas, A. & Linde, N. (2015). Effective modeling of GPR in fractured media using analytic solutions for propagation, thin-bed interaction and dipolar scattering. *Journal of Applied Geophysics*(116), 206-214

SCCER SoE
SWISS COMPETENCE CENTER for ENERGY RESEARCH
SUPPLY of ELECTRICITY

SCCER-SoE Annual Conference 2019

Supported by:
Schweizerische Eidgenossenschaft
Confédération suisse
Confederazione Svizzera
Confederaziun svizra
Swiss Confederation
Innosuisse – Swiss Innovation Agency

Tracing the CO_2 pathway in a faulted caprock: the Mont Terri Experiment of the ELEGANCY-ACT project

Alba Zappone, Melchior Grab, Anne C. Obermann, Claudio Madonna, Christophe Nussbaum, Antonio P. Rinaldi, Clément Roques, Quinn C. Wenning, Stefan Wiemer

1. Aims of the Experiment:

- Understanding how exposure to CO2-rich water affects sealing integrity of faults in caprock (permeability changes; mechanical changes; induced seismicity);
- Imaging fluid migration along a fault and its interaction with the surrounding environment;
- Testing instrumentation and methods for monitoring fluid transport;
- Validate Thermo - Hydro - Mechanical - Chemical (THMC) simulations.

2. CS-D Experiment

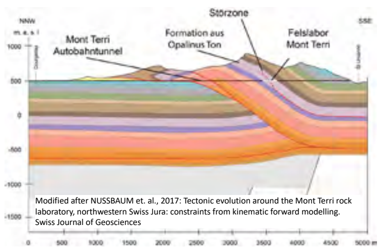

Fig 1: The Mont Terri laboratory, in NW Switzerland, is an international research underground facility for hydrogeological, geochemical geotechnical characterization of a clay formation (Opalinus Clay).

The CS-D experiment is located in a niche in the shaly facies of the clay. We inject CO_2-saturated water into the fault and monitor changes in pressure, pH and electrical conductivity in nearby wells. The portable mass spectrometer Miniruedi (cooperation with EAWAG) is used to monitor the chemical composition in the monitoring well. Seismic sensors in boreholes and along the walls of the niche will detect microseismicity, if any. Strain is measured through FO and SIMFIB (cooperation with LBNB).

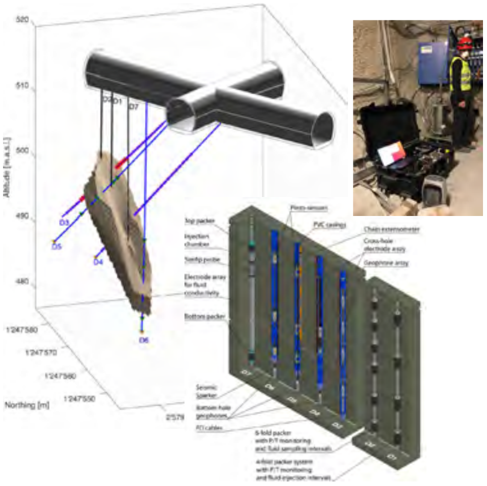

Fig 2: Layout of the experiment. The fault, c.a. 3 m thick, is at 12 to 30 m depth, and dips 60° towards SE. 7 boreholes are intersecting the fault and have been equipped with various instruments.

3. Injection tests

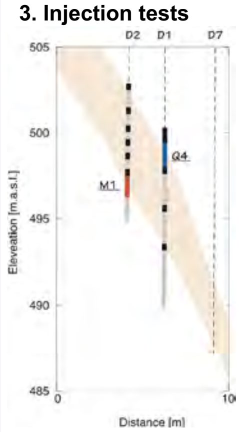

Fig 4: Injection borehole D1 (with interval Q4 highlighted) and monitoring well D2 (with interval M1 highlighted). Fault zone is shown in brown.

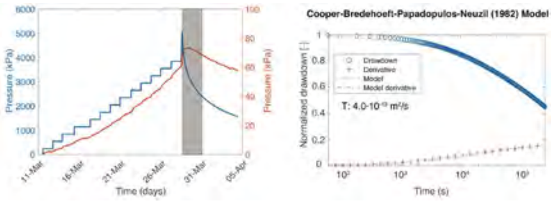

Fig 3: Right: Injection pressure in blue (injection into interval Q4) and observed fluid pressure in interval M1 (see Fig 4). Left: Analysis of constant head test with the Jacob and Lohman analytical solution provides an estimate of transmissivity in the order of 10^{-9} m²/s.

Several injection tests were performed to understand the system response to pressurization. The test shown in Fig. 3 is a prolonged step test in interval Q4. The pressure was increased by steps of 300 kPa, up to 4800 kPa. Each step was about 28-30 hours long. Analysis of pressure decay (3 days) with the Neuzil model provides an estimate of transmissivity in the order of 10^{-13} m^2/s (~10^{-21} m^2 permeability).

4. Geophysical monitoring

The experiment is monitored using active and passive seismic methods. Two sets of sensors consisting of piezoelectric transducers and grouted geophones were installed for this purpose (Fig. 2). During the pumping tests, no induced seismicity was detected. Further analysis of data, including also recordings during gallery excavation activities (Fig. 5), is ongoing.

Active seismic measurements have been performed with hammer sources in the gallery and a P- and S-wave sparker sources in the boreholes. During the injection test and the long-term injection, these measurements are repeated.
In Fig 6. an example trace is shown, which has been recorded during injection tests. Variations in arrival times were detected which are larger than the variability within repeated shots (Fig 6. left). The data is currently processed for tomographic travel time imaging.

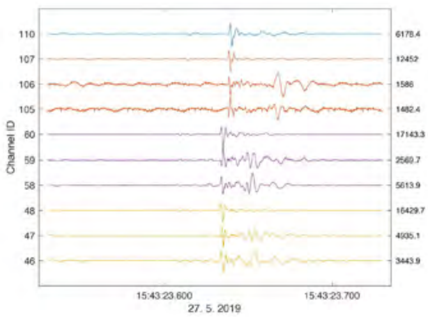

Fig 5: Microseismic event recorded with geophones during drilling activities in the laboratory. Traces of the same color are recorded with different components of the same geophone.

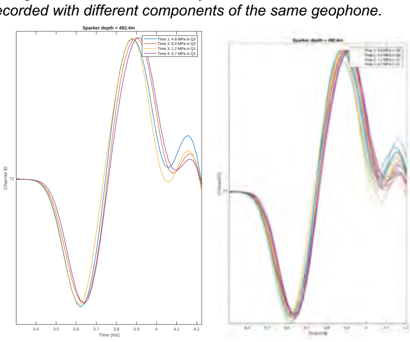

Fig 6: Example trace from time-lapse active seismic monitoring during injection tests after (right) and before(left) stacking.

5. Start of the long term injection of CO_2 saturated water

Mid June 2019, the long-term injection of CO_2 saturated water was started, together with repeated active seismic and ERT measurements. Since then, the injection takes place under constant pressures of 4500 kPa. The injection rates are small (< 0.1 ml/min) and up to now slightly decreasing with time.

Acknowledgements: We thank Christoph Bärlocher, David Jaeggi, Edgar Manukyan, Hansruedi Maurer, Linus Villiger, Marija Lukovic, Nils Knornschild, Nima Gholizadeh, Paul Bossart, Semih Demir, Senecio Schefer, Thierry Theurillat, and Thomas Mörgeli for technical support, scientific advice, and/or on-site assistance. ACT ELEGANCY, Project No 271498, has received funding from DETEC (CH), FZJ/PtJ (DE), RVO (NL), Gassnova (NO), BEIS (UK), Gassco AS and Statoil Petroleum AS, and is cofunded by the European Commission under the Horizon 2020 programme, ACT Grant Agreement No 691712.

ELEGANCY Accelerating CCS Technologies Chevron BERKELEY LAB Mont Terri Project eawag aquatic research TOTAL

Academic Research Partners

Cooperation Partners